Pore pressure and moisture migration in concrete at high and non uniform temperatures.

Khan, Saadat Ali

PORE PRESSURE AND MOISTURE MIGRATION IN CONCRETE AT HIGH AND NON UNIFORM TEMPERATURES

A Thesis submitted to
The University of London
for the Degree of Ph.D.
in the
Faculty of Engineering

by

Saadat Ali Khan
B.Sc. (Honours), Eng.

King's College May 1990

ABSTRACT

The influence of temperatures and temperature gradients on the time-dependent moisture behaviour of concrete has been studied, for concretes containing Sulphate Resisting Portland Cement (SRPC) and Blast Furnace Slag (BFS).

Firstly, sealed specimens of concrete were uniformly heated to known elevated temperatures, and pore pressures, temperatures and time were recorded. Moisture was periodically released in a controlled manner and weight was monitored to obtain relationships between pore pressure, temperature, weight loss and weight remaining. The quantity and state of water held in concrete after exposure to temperature and pressure was studied to derive moisture content relationships for drying concrete, applicable to numerical analysis. Morphological and pore pressure changes of the hydrate structure of cementitious materials are inferred from these tests.

Secondly, tests were staged to simulate the thermal shock problem caused by an accident situation to a Fast Breeder Reactor (FBR) in which hot sodium coolant makes contact with the metal liner of concrete containment. Sealed and partially sealed cylindrical concrete specimens cast inside thick steel tubes were constructed with a stainless steel diaphragm at one end. This diaphragm was heated with molten lead (up to 675^{o}C) and time varying records were made of concrete temperatures and pressures at various distances from the simulated liner. Central deflection readings from the calibrated diaphragm end plates provided a check on liner/concrete interface pressure. Moisture movement within the concrete was determined from gravimetric tests at the end of the experiment.

Finally, the influence of temperatures, temperature gradients, pore pressures and moisture movement on the physical and chemical properties of concrete are highlighted.

ACKNOWLEDGEMENTS

I am indepted to many people who helped me throughout the execution of the research work, however I would especially like to express my most sincere gratitude to the following:-

Professor G.L. England for his help, guidance, suggestions, patience, encouragement and interest at all stages of the research project.

All the staff of Civil Engineering department in general and workshop staff, past and present and the technicians of other laboratories of the department in particular for their suggestions, assistance and help in designing and construction of the experimental apparatus and coordination during the performing of the experiments and willingness to help in all aspects of practical work.

Mr. R. Hunt and Mr. M. Collins for taking, developing and printing the photographs for this thesis.

My parents, my wife (Mina) and my children for their patience and understanding throughout and especially to Mina for typing this thesis.

Finally to Nuclear Installations Inspectorate of the Health and Safety Executive for the sponsorship of the research of this thesis under contract NUC 56/62A, and for financial support during the experimental phase of the work. The work was carried out under the general direction of Mr. J.S. Macleod, Superintending Inspector of NII.

This thesis is dedicated to my parents,

my wife and my children.

CONTENTS

DEFINITIONS OF SOME IMPORTANT TERMS

"EXPERIMENTAL" RESULTS: These are the results obtained from the experiments and are presented without any corrections.

"EXPERIMENTALLY DEDUCED" RESULTS: These are the results which were obtained during the main experiments and then corrected by using the calibration factors from calibration tests described in Appendix III or Appendix IV.

"THEORETICAL" RESULTS: These are the results where one or more of the experimental parameters were used in the appropriate equation and the calculations were performed.

"INTERPOLATED" RESULTS: These are the results where one of the main experimental result parameter was used to interpolate the values of the second parameter from the calibration test results of Appendix III or Appendix IV.

NOTE: The remaining abbreviations and the glossary of terms are given in Appendix V.

CHAPTER 1

INTRODUCTION AND BACKGROUND TO THE THESIS

1.1 INTRODUCTION

Concrete is an effective and economical shielding material against nuclear radiation. Hydrogen (a lighter element in concrete), which is predominantly available in the form of water slows down and absorbs fast neutrons. The heavier constituents in concrete (i.e. aggregates etc.) attenuate gamma rays and also partially slow down very high energy neutrons.

If concrete is used as a shield for a reactor core, then the water contents of the concrete shield must be maintained within the mass of the concrete. On the other hand the large quantity of water vapour generated upon heating the concrete would produce significant pore pressures, particularly when the temperatures are in excess of 100 ^{o}C. The total pressure is the sum of partial pressure of air and water vapours, and the pore pressures are generally greater than the saturation vapour pressure of water for corresponding temperatures (Chapter 6, Section 6.4.1). One of the controlling factors for the generation of pore pressure is the degree of pore filling (percentage of air and water in the pores).

The application of a thermal gradient can produce a pore pressure gradient inside the concrete shield of the reactor vessel. The pore pressure and temperature gradients would produce moisture migration and pressure changes through the concrete. Depending on the sealing conditions of concrete the moisture movement may cause eventual drying of concrete (i.e. escape of water to atmosphere), rendering the concrete less useful for shielding purposes. However, when concrete is effectively sealed pore pressure generation can be large and may result in hydraulic fracture of the shielding material.

Movement of moisture through concrete contributes to the alteration of heat transfer properties (i.e. thermal conductivity). The generation of pore pressures and movement of moisture under thermal gradient should be considered in predicting the service life behaviour of prestressed concrete reactor vessels (PCRV).

1.2 BACKGROUND

Many workers (Chapter 2) have been involved in the study of thermal properties of concrete in general, and moisture and pressure migration under thermal gradient in particular. Several investigations into moisture migration in concrete under thermal gradient have been carried out experimentally at King's College, University of London by Ross, Illston and England (1965), Parkinson (1966), Sharp (1971) and Chapman (1976). The investigations carried out for this thesis were the continuation of the programmes discussed above.

Sharp and Chapman also studied experimentally the variations of pore pressures in heated concrete. Sharp tested gravel aggregate concrete at temperatures up to 150 ^{o}C and Chapman used limestone aggregate at temperatures between 105 ^{o}C and 200 ^{o}C. These investigations are discussed further in Chapter 2.

1.3 OBJECTIVES

The objectives of this project are to study:

1. In a simulated way the existence and generation of pore pressure in concrete behind a steel liner of a fast reactor containment vessel under the influence of thermal shock.

2. The establishment of thermal gradients in mass concrete.

3. Moisture migration caused by pore pressure and temperature.

4. The effects of pore pressure and temperature on the behaviour of the steel liner (principally deflection).

5. The influence of various sealing conditions of concrete upon the magnitude of pore pressures and movement of moisture in heated concrete.

6. The relationship between pore pressure and water content, when concrete is uniformly heated to a steady-state condition and moisture is periodically released.

7. The state and quantity of water in concrete before heating and after heating to temperatures up to 400 ^{o}C.

8. Predictions of pore pressure adjacent to the steel liner by knowing (measuring) the deflection of the liner.

The engineering significance of these parameters is studied for a certain hypothetical core disruptive accident, when liquid sodium coolant comes into contact with the steel liner of a Fast Breeder Reactor (FBR), causing sudden heating of the concrete behind the liner. Pore pressures develop and moisture migrates into cooler regions away from heated zones. If the pore pressures are not allowed to dissipate, they could become of significant magnitude to affect the stability of the steel liner. The stresses induced in the liner may deflect, buckle or possibly cause rupture of the liner.

The movement of moisture into the central region of the concrete mass would cause swelling of concrete and the creation of an impermeable concrete effectively sealing the pore structure. On further heating the pore pressures would increase and exert force against the liner resulting in deformation and possible damage. Therefore, deliberate venting to atmosphere of the pressurised zone behind the liner may be desirable.

If concrete is allowed to dry it would be less effective as a nuclear shield. The drying of concrete and the movement of moisture due to pore pressures and temperature would also affect other concrete properties, e.g. creep, shrinkage, swelling, cracking, thermal conductivity, mechanical strength, and pore structure of the cement paste.

It was the aim of this study to show the existence and importance of pore pressures and moisture movement under uniform, non-uniform and time varying temperatures. The effects of different sealing conditions were also examined. An experimental programme was carried out to determine the effects of temperature and moisture on concrete, and obtain data on these parameters which would be of use to researchers and designers alike for predicting moisture migration in concrete.

1.4 PROJECT

The initial period was spent on carrying out the design, construction, experimental set up, testing and calibration of the test rig, before casting concrete into the test cells. Experiments were performed on concrete which was at least one year old at the time of test.

The mix specification for concrete was supplied by the sponsors and its details are given in Chapter 3, Section 3.2. The concrete cementitious materials were a blend of Sulphate Resisting Portland Cement (SRPC) and Blast Furnace Slag (Cemsave) with a water cement ratio of 0.39. Cormix P1 was used as a workability agent. The aggregate used was quartz dolerite (basalt) and sand was calcareous quartz.

The project has two main themes.

1. To investigate the effects that rapid heating of the liner of a FBR would have on the development and time-dependent dissipation of pore vapour pressures in the concrete adjacent to the liner. Simulated Liner Tests or the "Liner Test Series" ("LTS") were performed. These are described in Chapter 5.

2. To determine the relationships between pore vapour pressure, temperature and water content at temperature up to 400 ^{o}C, for use in numerical analysis. Sealed samples heated to uniform temperatures and subjected to periodical release of moisture were used in this part of the work. Details of release tests are given in Chapter 6 under the heading the "Release Test Series" ("RTS").

Additionally, a number of subsidiary experiments needed to be performed, e.g. pilot studies, calibration tests etc. These are described in Appendix III and Appendix IV.

1.5 THESIS

The thesis consists of seven chapters and five appendices; cross reference is made whereever possible to avoid repetition.

Chapter 2 is devoted to the study of the literature relating to the

project and it is divided into sections appropriate to the various subjects discussed in the thesis.

Chapter 3 describes the design of experimental equipment and testing techniques employed. The detailed description of equipment is presented in Appendices I and II.

Chapter 4 discusses the instrumentation, measurement techniques and various methods used for the analysis of the experimental results.

Chapters 5 and 6 contain the main experimental results of the thesis: Simulated Liner Tests ("Liner Test Series") and Release Tests ("Release Test Series"). Conclusions are drawn from the results of each test category.

Chapter 7 highlights the conclusions and contains suggestions for future work.

Appendix I describes the design of the equipment of "Liner Test Series"

Appendix II contains the design of the equipment of "Release Test Series".

Appendix III discusses the pressure/deflection calibration test of the stainless steel diaphragm for hydraulic pressure.

Appendix IV describes the pressure/deflection separation from the deflection due to the temperature correction of the stainless steel diaphragm.

Appendix V lists the abreviations and terms used in this thesis.

CHAPTER 2

LITERATURE REVIEW

2.1 INTRODUCTION

Concrete may be defined as a compound formed by mixing together aggregate, cement and water. When these constituents are mixed, they first form a semi-plastic viscous material. A chemical reaction takes place between the cement and water forming a solid matrix (cement paste) due to the reaction of the constituents. The cement paste forms a gel around the aggregates and the final product is known as concrete.

The use of cementing material as a constituent of concrete is a very old and well established practice. The ancient Egyptians used calcined gypsum. The Greeks and Romans used calcined limestone as the cementing material. Later on they added sand, crushed stones or bricks and broken tiles to lime and water, which was the first concrete in history (Neville, 1977). Some buildings constructed in those times are still standing today.

The story of the invention of Portland cement is not easy to disentangle. Lea (1970) suggests that the usual attribution to Joseph Aspdin, who in 1824 took out a patent for the manufacture of Portland cement, is partly true. His cement was prepared by heating a mixture of finely divided clay and hard limestone in a furnace until carbon dioxide had been driven off. This temperature was much lower than that necessary for clinkering. Isaac Johnson in 1845 modified the process of manufacturing Portland cement used by Aspdin, when he burned a mixture of clay and chalk until clinkering. This process is still the basic way of manufacturing cement today.

Cement is probably the most widely used cementitious material in the world today and an extensive amount of literature is available on this material. However, in recent years many other materials like Blast Furnace Slag (BFS) or Pulverised Fuel Ash (PFA) have been used, blended with cement for the achievement of better properties of the final product. The concrete mix design discussed in Chapter 3, Section 3.2, used BFS with Sulphate Resisting Portland Cement (SRPC) with 50:50 ratio by weight. Therefore the origin and the properties of the BFS are also discussed in this chapter along with cement.

BFS is a by-product obtained in the manufacture of pig-iron in the blast furnace and is formed by the combination of the earthy constituents of the iron ore with the limestone flux. The molten by-product is rapidly quenched in high volume cold water jets and forms Granulated Blast Furnace Slag. Granulated BFS is then ground to the required size grading for using it as a cementing material.

BFS can be used blended with cement up to a replacement level of 90% to reduce heat of hydration, increase long term strength, achieve better workability and produce concrete with enhanced chemical resistance.

The cementing property of Granulated Blast Furnace Slag has been known for over a hundred years. In 1862 Emil Langens discovered that the process of water granulation of slag yielded a material which, when used with lime had good cementing properties. BFS alone has a negligible cementing action but if some suitable activator is present, it shows marked cementitious properties. The activator may be lime, Portland cement, alkalis such as caustic soda or sodium carbonate, or the sulphates of the alkalis, lime or magnesia. It is this property which has led to the use of the material in various forms.

BFS has been extensively used for the production of Portland-Blast furnace cements since the early part of the century. First production of a Portland blast furnace type of cement was achieved by grinding together Portland cement clinker and granulated slag in Germany in 1892 (Lea, 1970).

Although concrete is perhaps the most widely used construction material in the world, its complex nature and the chemical and physical make up of the cementitious materials is still not completely understood. However, since the advances in physical and chemical techniques have progressed, the intricate nature of cement paste and interaction between the paste and aggregate is much better understood.

In this chapter the chemistry and physics of cementitious materials is surveyed, the use of a water reducing agent is discussed and the pore pressure and moisture migration in heated concrete are studied.

2.2 PROPERTIES AND CHEMISTRY OF CEMENTITIOUS MATERIALS

All the experimental work described in this thesis was carried out using SRPC and BFS (50% by weight). A brief description of the properties and the chemistry of cement and BFS is given below.

2.2.1 CEMENT CHEMISTRY

The cements of interest in the making of concrete have the property of setting and hardening under water by virtue of a chemical reaction with it. These cements, called hydraulic cements consist mainly of silicates and aluminates of lime and can be classified broadly as natural cements. Several types of cement exist and these fall into two groups, namely Portland cements and Non-Portland or aluminous cements.

The most commonly used Non-Portland cement is High-Alumina cement. This cement is not used for structural purposes any more, following collapses of a number of buildings containing High-Alumina cement. However, it is still used for refractory concrete and in concrete which is cast under sea water.

All the Portland cements are of similar form, but vary slightly in the relative proportions of each compound. Some of the more common members of Portland cement group are given below:

Ordinary Portland Cement
Rapid Hardening Portland Cement
Low Heat Portland Cement
Sulphate Resisting Portland Cement
White Portland Cement.

The raw materials used in the manufacture of Portland cement consist mainly of lime, silica, alumina and iron oxide. These compounds react with one another in the kiln and the four major compounds considered as the constituents of Portland cement are given in Table 2.1. The shortened notations, used by cement chemists (used repeatedly in this thesis), describe each oxide by one letter, viz:

CaO = C; SiO_2 = S; Al_2O_3 = A; Fe_2O_3 = F; H_2O in hydrated cement by H.

Name of Constituents	Constituent Composition	Abbreviation
Tricalcium silicate	$3CaO.SiO_2$	C_3S
Dicalcium silicate	$2CaO.SiO_2$	C_2S
Tricalcium aluminate	$3CaO.Al_2O_3$	C_3A
Tetracalcium aluminoferrite	$4CaO.Al_2O_3.Fe_2O_3$	C_4AF

Table 2.1: Four major constituents of Portland cement.

In reality, these constituents are not pure compounds. However, these may be represented by the formulae given in Table 2.1.

In addition to the major compounds listed in Table 2.1, minor compounds, such as MgO, TiO_2, Mn_2O_3, K_2O and Na_2O, also exist, amounting to not more than a few percent of the weight of cement.

The oxide and the calculated compound composition of a typical cement is reproduced from Neville (1977) in Table 2.2.

Typical oxide Composition per cent		Hence, calculated compound composition percent	
CaO	63.0	C_3A	10.8
SiO_2	20.0	C_3S	54.1
Al_2O_3	6.0	C_2S	16.6
Fe_2O_3	3.0	C_4AF	9.1
MgO	1.5	Minor compounds	-
SO_3	2.0		
K_2O, Na_2O	1.0		
Other	1.0		
Loss on ignition	2.0		
Insoluble residue	0.5		

Table 2.2: Oxide and compound composition of a typical cement.

All the compounds present in cement are anhydrous, but when brought into contact with water they are all attacked or decomposed, forming hydrated compounds. These products of hydration increase the viscosity of the paste in time, prevent reactants coming together freely and produce a firm and hard mass, thus slowing down the rate of reaction.

Although significant strengths are not developed (Double, 1980) during the first few hours of cement hydration, the chemical reactions that occur at this time, establish the pattern for subsequent hydration and provide the initial microstructural framework (i.e. during setting) upon which the final strength of the cement paste is developed. The progressive hardening takes place over weeks, months and even years.

Whatever the mode of precipitation of the products of hydration, the rate of hydration decreases continously, so that even after a long time an appreciable amount of unhydrated cement remains in the system.

The rate of reaction after adding water to the cement varies considerably between various major constituents, and the final product of hydration (Lea, 1970 and Neville, 1977) are:

(a) Tricalcium Silicate (C_3S)

$$2C_3S + 6H \longrightarrow C_3S2H_3 + 3Ca(OH)_2$$

(b) Dicalcium Silicate (C_2S)

$$2C_2S + 4H \longrightarrow C_3S_2H_3 + Ca(OH)_2$$

(c) Tricalcium Aluminate (C_3A)

$$2C_3A + 21H \longrightarrow C_4AH_{13} + C_2AH_8$$

(d) Tetra Calcium Aluminoferite (C_4AF)

$$C_4AF + 16H \longrightarrow 2C_2(AF)H_8$$

$$C_4AF + 16H \longrightarrow C_4(AF)H_{13} + (AF)H_3$$

The main source of strength is derived from the hydration of two principal silicates phases in the clinker, namely C_3S (alite) and C_2S (belite). The 'alite' reacts fairly quickly and gives the cement paste its early strength. The reaction of 'belite' takes place more slowly and it is probably responsible for the longer term hardening processes. In spite of this difference in reactivity, the hydration of

the two silicates is essentially similar. The product in both cases, is a cohesive matrix consisting primarily of calcium-silicate-hydrate (C-S-H) gel along with $Ca(OH)_2$ as a by-product. The (C-S-H) gel is called Tobermorite gel because the crystal structure resembles that of the natural mineral tobermorite.

The aluminate phases C_3A and C_4AF contribute very little to the strength of the cement paste, but influence the setting and act as flux during the manufacture of cement. The reaction between C_3A and water is the faster reaction. According to Neville (1977), the reaction of pure C_3A with water is very violent and leads to immediate stiffning of the paste, known as 'flash set'. To prevent the stiffening, gypsum ($CaSO_4.2H_2O$) is added to cement clinker as a retarder. Gypsum reacts with C_3A and forms insoluble calcium sulpho-aluminate ($3CaO.Al_2O_3.3CaSO_4.31H_2O$), but eventually tricalcium aluminate hydrate is formed.

The reaction between the C_4AF and the saturated solution of calcium hydroxide (Brunauer and Copeland, 1964) produces calcium aluminoferrite hydrate, which resembles a class of natural mineral called hydrogarnet. The above mentioned reaction is faster than that between C_2S and water, although it is considerably slower than those between C_3S and C_3A with the free water shown in Figure 2.1 reproduced from Brunauer et al (1964).

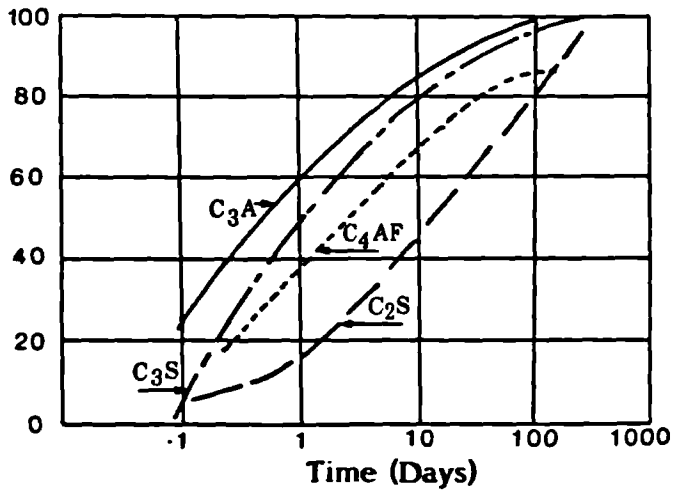

Figure 2.1:

Speed of hydration of the four major components in normal Portland cement, (Brunauer et al, 1964).

Neville (1977) suggests that C_4AF hydrates into tricalcium aluminate hydrate and an amorphous phase, probably $CaO.Fe_2O_3$. aq. It is also possible that some Fe_2O_3 is present in solid solution in the tricalcium aluminate hydrate.

The mechanism of hydration has been under investigation for a considerable period of time and many research workers have contributed towards this. In studying the chemical reactions that occur in the setting of cement, Bogue and Lerch (1934) observed that the products of hydration of cement are chemically the same as the product of hydration of the individual compounds under similar conditions. However, these products can also interact with one another in the system and may produce some variations in the final products.

2.2.2 PROPERTIES AND HYDRATION OF BLAST FURNACE SLAG (CEMSAVE)

Blast furnace slags have hydraulic properties, although the rate of reaction with water is slow. Blending of finely ground granulated blast furnace slag with Portland cement is a much used technology in several parts of the world. As explained in Chapter 3, Section 3.2 'Cemsave' was blended with Portland cement (50% cement, 50% cemsave) and is used throughout the experimental programme described in this thesis. One of the main reasons for blending cemsave with cement was to reduce heat generation.

Some of the properties of BFS (when it is blended with cement and used in concrete) are discussed below, and slag-cement hydration is described in Section 2.2.3.

2.2.2.1 STRENGTH

Roy and Idorn (1982) suggest that the early age strengths of slag-cement blends hydrated at 23 ^{o}C are lower than for pure Portland cement (Figure 2.2). However, by three days the strength of the blends are found to be equal to or greater than those of pure Portland cement. Slag-cements have a favourable long term strength gain over cement alone. Hogan and Meusal (1981) reported that increased strength developes by steam curing of mortars containing slag.

2.2.2.2 HEAT OF HYDRATION

As the proportion of slag in slag-cement blends increases, the rate of heat generation decreases. Roy et al (1982) investigated the rate of

heat evolution using various percentages of slag, cured at temperatures of 15 °C, 27 °C, 38 °C and 60 °C. They found that the cumulative heat liberated for both pure cement and slag-cement in 24 hours varies with temperature (Figure 2.3). The heat liberation of pure cement is higher than that of slag cement at 27 °C, which is consistent with the observation that the early compressive strength of pure cement is higher than that of slag cement at normal temperatures. However, the heat liberation of slag cement is more than that of pure cement at 60 °C and this elucidates the benefit that slag cement realises from thermal activation. In practical terms the characteristics of curing at normal temperatures is of considerable advantage, since cement rich or thick sectioned pours can be undertaken with less risk of thermal movement (or differential thermal movement) which could cause cracking where there is external restraint.

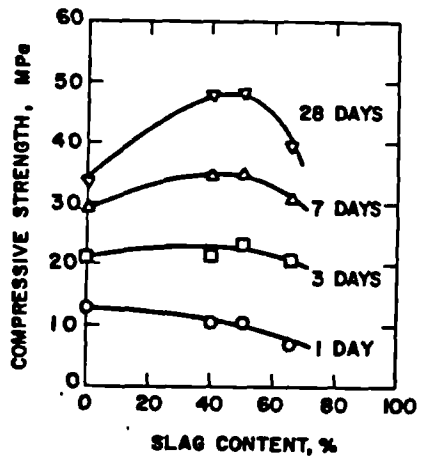

Figure 2.2:
Strength of Slag-Cement at 23 °C (Roy et al, 1982)

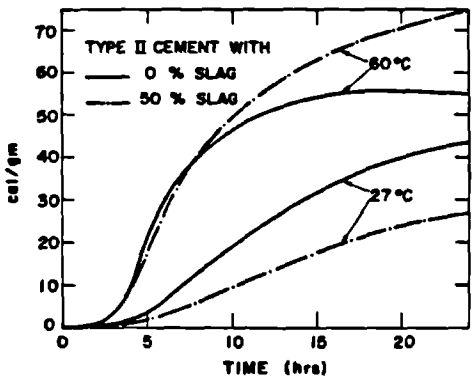

Figure 2.3:
Cumulative heat libration of cements (Roy et al, 1982)

2.2.2.3 CHEMICAL RESISTANCE

Good chemical resistance properties of slag-cement have been known and successfully used for many years and its sulphate-resisting property in particular compares well in performance with Sulphate Resisting Portland Cement. Slag-cement can resist aggressive weathering and chemical action. Figure 2.4 (taken from Civil & Marine Ltd; Data Sheet 1) shows sulphate resistance of slag-cement.

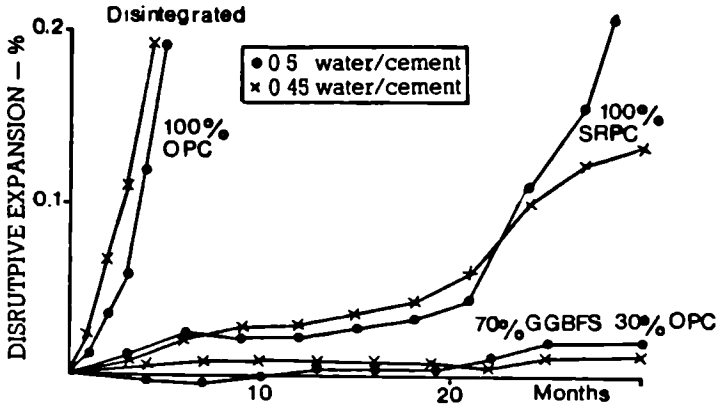

Figure 2.4:
Sulphate Resistance
(Civil & Marine Ltd;
Data Sheet 1)

2.2.2.4 VOLUME SHRINKAGE

Roy et al (1982) investigated early stage (chemically conditioned) volume shrinkage of pure cement paste and a 50:50 slag-cement paste at room temperature (23 °C). They suggested that this phenomenon (Figure 2.5 and 2.6) parallels the effects of heat liberation, i.e. the higher the heat liberation, the higher the shrinkage.

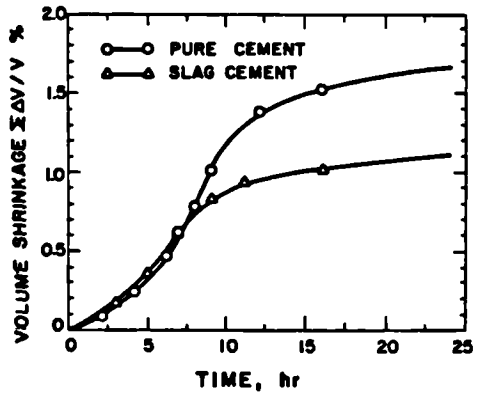

Figure 2.5:
Cumulative Chemical Shrinkage
at 23 °C (Roy et al, 1982)

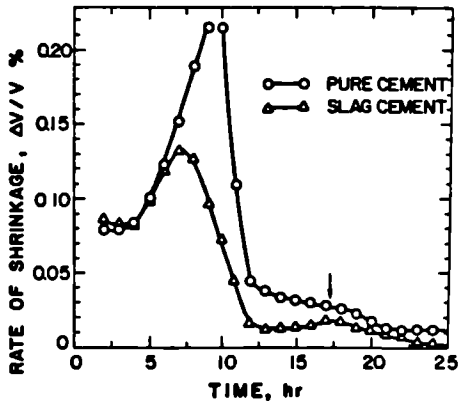

Figure 2.6:
Rate of Shrinkage
(Roy et al, 1982)

2.2.2.5 DURABILITY

Slag-cement concrete is acknowledged to be more durable than that made with Portland cements. This is because the permeability is lower and the chemical structure is more stable.

Slag-cement mortars attain much lower ionic diffusivity (Table 2.3) and permeability than equivalent portland cement mortars (Baker, 1981). The permeability of slag-cement mortars was measured to

be 10 to 100 fold less than for equivalent portland cement mortar and the reduction of permeability for slag-cement mortars continued during storage times.

Slag-cement concrete is considerably more resistant to ingress of salts than Portland cement concrete, as shown in Figure 2.7 (Civil & Marine Ltd, Data Sheet 1) and it can be used to provide protection against salt induced corrosion.

Hardening time of mortars	Diffusion ion	Dm in. 10^{-8} cm^2/s	
		OPC	BFS
3	Na^+	7.02	1.4
	K^+	11.38	2.10
14	Na^+	2.38	0.10
	K^+	3.58	0.21

Table 2.3: Diffusion coefficients (Roy et al, 1982)

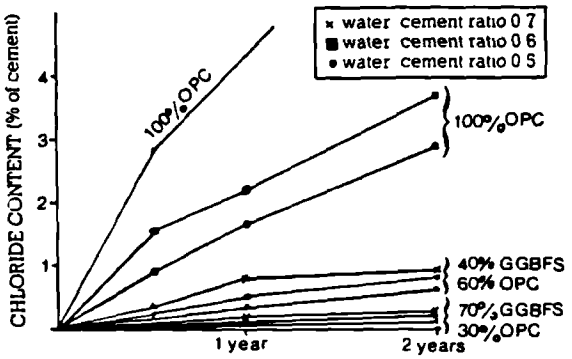

Figure 2.7: Chloride diffusion (Civil & Marine)

2.2.2.6 WORKABILITY

Concrete made with slag-cement has excellent flow characteristics, particularly where vibration is employed. For a given slump it is easier to place and compact slag-cement concrete than Portland cement concrete. Workability of slag-cement concrete is maintained relatively longer than Portland cement concrete, which is an advantage on large pours or where there may be delays. The cohesive nature of slag-cement concrete aids production of good surface finish.

2.2.2.7 ALKALI-AGGREGATE REACTION

It has been established by Baker (1981), Roy et al (1982), Langton and Roy (1980) and many other research workers that alkalis from cement can react with certain types of aggregate and disrupt concrete. There is more than one form of alkali-aggregate reaction. However, the major reaction comes from aggregate-silica reaction, as shown in Figure 2.8 reproduced from Civil & Marine Ltd, (1985).

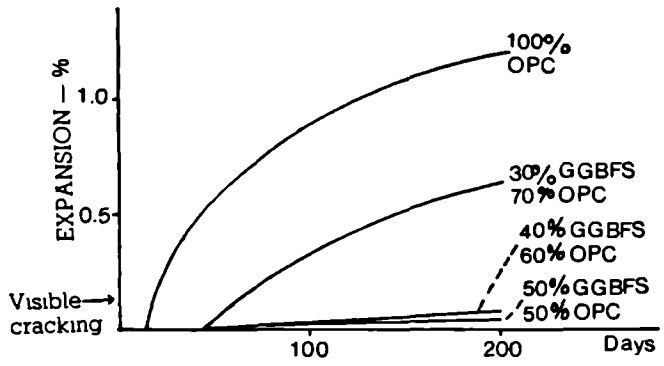

Figure 2.8: Potential Alkali-Aggregate Reactivity (Civil & Marine Ltd, 1985)

One simple and effective precaution against aggregate-silica reaction is to use an appropriate proportion of slag with cement. The effectiveness of slag-cement, as a precaution against aggregate-silica reaction is due to a combination of various factors.

The alkalis in cement may be retained by the C-S-H gel during cement hydration and hence not be available for alkali-silica reactions in aggregate particles (Bhatty and Greening, 1978 referred to by Roy et al, 1982). Alkalis work as slag-activators, and therefore these apparently contribute to the "densification" of slag-cement paste during its hardening, later described in this section.

2.2.3 SLAG-CEMENT HYDRATION

In the previous section cement and slag hydration was discussed separately, but in this section the hydration of slag-cement blend is outlined. The slag hydration reaction can be activated by several methods, but the end product is always C-S-H. The conventional concept of hydration in blended cement assumes that slag is activated by lime made available during hydration of the Portland cement fraction.

The hydration products of slag-cement are similar to those of Portland cement, i.e. C-S-H, AF_t phases (ettringite) and AF_m phases. The C-S-H around slag grains is lower in calcium and richer in aluminium and magnesium, than C-S-H surrounding Portland cement grains (Regourd, 1980).

The rate of hydration of slag can be just as fast as that of Portland cement (Regourd et al, 1983). However, as chemical composition and the glass content of the slag affect the hydraulic reactivity, the rate of hydration varies from one slag to another.

Smolczyk (1975) examined slag in the cement paste of concrete, and found a strong bonding effect on Na^+-ions. He concludes that the slag content does not merely limit the mobility of the alkalis in the pore liquid, it also reduces its alkali concentration. He also reports the formation of hydrated compound with NaOH.

Daimon (1980) reports the activation of slag during hydration with $Ca(OH)_2$, $Na(OH)_2$, $CaSO_4.2H_2O$ and $CaSO_4.2H_2O$ (10 %) plus $Ca(OH)_2$, by measuring the amount of combined water. According to his findings gypsum and lime are principal reactants, but he explains that NaOH is a simple catalyst.

Regourd (1980) explains that the alkaline activation can either be soda or lime activation. If slag is activated by soda it gives C-S-H, C_4AH_{13} and C_2ASH_8. In lime activation the hydrate phases compatible with $Ca(OH)_2$ are C-S-H and C_4AH_{13}. The sulphate activation produces ettringite, with high slag content. The later phase forms primarily as short needles, possibly acting as binders. The ettringite converts to various complex tricalcium aluminate sulphate phases and C_4AH_{13}.

The particular hydration mechanism with alumina is not very clear (Roy et al, 1982). However, some of the mechanisms of slag hydration are given below.

1. $Ca(OH)_2$ content of high slag concrete is low, and the material is very resistant to chemical attack.

2. Slag hydration gives the same reaction products as Portland cement.

3. Slag hydration is much slower than Portland cement hydration.

4. Slag hydration is activated chemically (alkalis, lime, sulphate), mechanically (fine grinding), or thermally.

5. Slag generally produces a denser structure of the hardened paste in slag-cement paste and the final product is less permeable.

Figure 2.9 (a) and (b) reproduced from Roy et al (1982) show models

for early and for long term hydration of slag-cement, respectively.

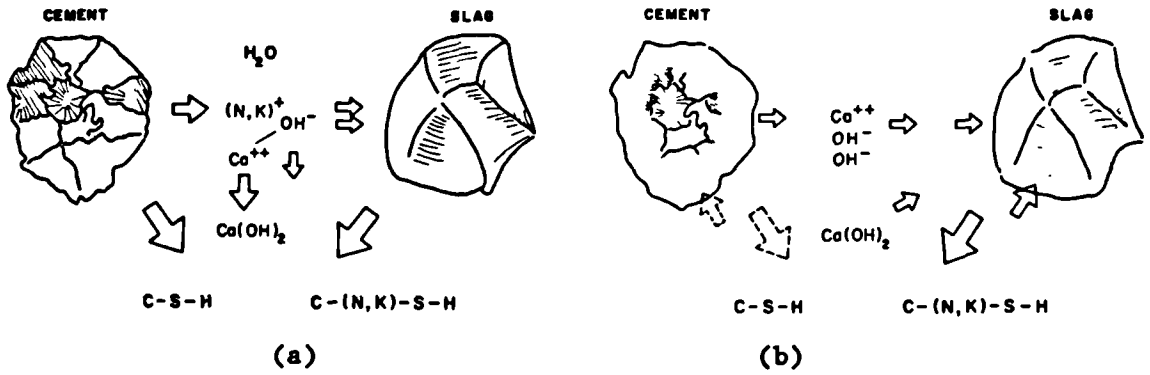

Figure 2.9: (a) Early and (b) long term hydration of slag-cement (Roy et al, 1982).

2.3 CEMENT PHYSICS

Hardened cement paste is a mixture of various compounds (Section 2.2) and it is an essential ingredient of ordinary concrete. Cement paste in hardened form is composed mostly of solid reaction products and spaces that are penetrable by water. In the hardened state cement paste is not simply a chemical product, it is a rigid structure formed by solid reaction products.

2.3.1 STRUCTURE OF CEMENT PASTE

The hardened cement paste comprises hydrates of various compounds, referred to collectively as gel, some minor components, unhydrated cement, and capillary pores (Powers, 1960). Figure 2.10 shows the simplified model of the paste structure.

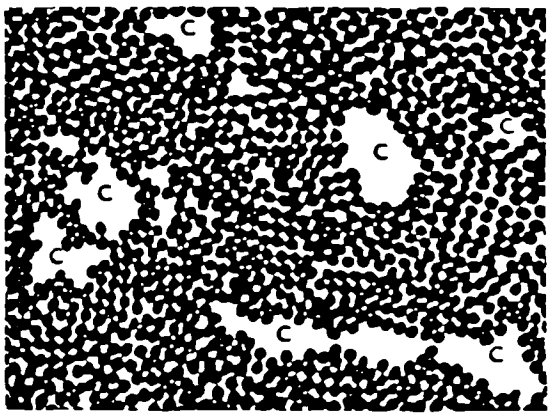

Figure 2.10:
Simplified model of cement paste structure (Powers, 1960).

2.3.1.1 CEMENT GEL, GEL PORES

The cement gel mainly consists of colloidal substances although it also contains some non-colloidal particles. The gel is made up of the products of reaction, consisting of cement and water of hydration and interspaced with gel pores. The gel holds large quantities of evaporable water which shows the gel is porous, and the gel pores are interconnected interstitial spaces between the gel particles (Neville, 1977). The gel pores are filled with water.

The porosity of gel was reported to be 28% by Powers (1960) and Neville (1977). Gel pores are much smaller than the capillary pores and their size has been estimated both by Powers (1960) and Neville (1977) as 15-20 Å, which is about five times the diameter of a water molecule.

The specific volume of cement gel is about 0.567 cm^3/g of dry weight according to Powers, as reported by Taylor (1964).

2.3.1.2 CAPILLARY PORES

The capillary pores represent that part of the gross volume of cement paste which has not been filled by the products of hydration. Since these products of hydration occupy more than twice the volume of the original solid phase (i.e. cement) alone, the volume of the capillary system is reduced with the progress of hydration (Neville, 1977). The actual time for this to occur depends upon the water/cement ratio and the fineness of the cement along with other factors.

The size of the capillary pores is estimated to be at least a thousand times larger than gel pores. They vary in shape but form an interconnected system randomly distributed throughout the cement paste (Verbeck, 1955 referred to by Neville, 1977). He has estimated the size of capillary pores from vapour pressure measurement to be of the order of 5×10^{-5} inch. These pores are mainly filled with water, water vapour and air, if no drying has taken place from the concrete.

The high porosity of gel is regarded by most workers to have little influence on the permeability of concrete, as the pores are so small. It is the capillary porosity (i.e. 30-40%), that is regarded as

important when considering the concrete permeability (Powers, 1960).

When concrete is freshly mixed all the spaces between cement particles and aggregate exist as capillary pores, but as the hydration of cement progresses, cement gel gradually replaces capillary pores. It is very important for achieving good concrete to eliminate the continuity of capillary pores, or in other words the relative volume occupied by the gel, the unhydrated cement and the capillaries determine the quality of the cement paste and hence the concrete.

2.4 BLAST FURNACE SLAG PHYSICS

Although the hydration of slag (activated by the lime from Portland cement) is slower than the hydration of Portland cement in the initial stages, its final products of hydration are the same as the cement. In the long run the slag-cement blend exhibits better properties than the cement on its own (Section 2.3). The structure of slag-cement is described in the following section.

2.4.1 STRUCTURE OF SLAG-CEMENT

Once again the hydration products consist of cement and slag gel, capillary pores, and unhydrated cement and slag. Hence the structure of slag-cement is similar to cement structure. The difference in pore sizes of slag-cement and cement are discussed below.

Portland cement developes more capillary pores (greater than 300 Å) than slag-cement paste, which develops more gel pores (Smolczyk, 1980). The capillary porosity can be reduced from 30 to 22.5 percent, by increasing slag content in cement from 0 to 76%.

Gjorv and Vennesland (1979) evaluated 80:20 slag-cement paste and showed that 79% of the total porosity was made up of the pores smaller than 200 A, while for Portland cement the corresponding number was only 29%.

Parker and Roy (1982) have investigated 60:40 slag-cement paste for the effect of water-cement ratio and curing temperature on the porosity and critical pore radius of the paste. They reported that the paste achieved very fine pore structure and also showed that curing

temperatures up to 60 ^{o}C did not significantly increase the coarseness of the pore structure at water-cement ratios less then 0.5.

Baker (1981) and other workers (Section 2.2.2.5) have shown that slag-cement mortars have lower permeability and ionic diffusivity than equivalent Portland cement mortars.

Smolczyk (1975) investigated the penetration of Na^{+} from NaCl solution into Portland cement concrete and concrete made with slag-cement (40:60% and 70:30%). He measured smaller penetration depths for both the slag-cement samples than for the Portland cement concrete.

The early retention of alkali and the compactness of slag-cement paste structure together produce a physico/chemical barrier against later stage alkali-silica reactions (Roy et al, 1982). This phenomenon cannot be achieved by pure Portland cement.

It is evident from the discussion above that good concrete can be cast more efficiently by using a slag-cement blend, which achieves better compactness, smaller capillary pores, denser gel and sound structure of hydration products.

2.4.2 TYPES OF WATER IN SLAG-CEMENT PASTE AND THEIR PHYSICAL PROPERTIES

In considering the types of water in the paste, reference will be made only to slag-cement paste. It has been established in the previous section that the structure of slag-cement paste is similar to the structure of cement paste with certain differences in their physical properties.

The water in the paste can be divided into three physical states as described below (Powers and Brownyard, 1947):

1. Chemically combined, or water of hydration, or water of crystallisation: In this state the water is chemically combined to, and forms a definite part of, the hydrated compound.

2. Adsorbed water, or gel water: The water contained in the pores of the gel, and physically adsorbed on the gel surface, falls in

this category of water. The gel pores are so small that most, if not all, of the gel water is within the range of the Van der Waal surface forces of the solid phase.

3. Capillary water or free water: This is the water which occupies the capillary space in the paste, and it is beyond the range of the surface forces of the solid phase.

It seems there is no definite boundary between each state of water and each type blends gradually into the next. There is a zone at the interface between the two types of water, within which the properties of water lie between the two types. Considering the water at the interface between the gel and the capillary water, there is a zone which cannot strictly be termed as either gel or capillary water. The water molecules controlled by the physical forces acting between the water and the cement molecules form the gel water, whereas the free water molecules form the capillary water. The physical forces acting on the molecules within the zone vary depending on their distance from the cement molecules. In this way the orientation of the molecules is partially controlled.

Although water may be classified in the manner described above, it is not easy to determine how much water is present in each state. However, the following arbitrary definitions of the water in the cement paste have been formulated.

Powers et al (1947) arbitrarily divided the water into two types: evaporable water, and non-evaporable water. Evaporable water was defined as the water which is lost on drying to constant weight at 23 ^{o}C in a vacuum dessicator with anhydrous magnesium perchlorate. The evaporable water approximately equals the gel plus capillary water. The gel water is defined by Neville (1977) as the water which fills the gel pores, assuming that the porosity of the gel is 28%.

The non-evaporable water or chemically combined water was defined by Powers et al (1947) as the water which is retained by the concrete when subjected to the above drying technique but which is lost on heating to 1000 ^{o}C.

Later on, the definitions of these arbitrary types of water were

modified by many research workers. Copeland and Hayes (1953), firstly, dried the cement paste at the vapour pressure of water over ice at 79 ^{o}C (equal to a pressure of 0.5 x 10^{-3} mm of mercury), and then using the same method of ignition, as used by Powers et al (1947), determined the evaporable and non-evaporable water contents. According to them, their method was an improvement on the method described by Powers et al (1947), as it was quicker, more reliable and measured the value of non-evaporable water nearly equal to the chemically combined water.

The evaporable water is defined (Hilsdorf (1967) and Neville (1977)), as the water which is given up when concrete is dried to constant weight at 105 ^{o}C. Hilsdorf suggests this is approximately equal to the amount given up when the concrete is dried at 20 ^{o}C and zero relative vapour pressure. He defined the the non-evaporable water as before. This definition of evaporable water has been adopted in the experimental work described in this thesis, because its simplicity of measurement has a distinct advantage over other methods that require elaborate apparatus.

The disadvantage of this technique is that a temperature rise can increase the hydration and hence the amount of chemically combined water. However, all the concrete used for tests reported in this thesis was over a year old. Hence the errors due to this phenomenon were very small.

The gel water exists in pores with an average diameter of about 20 Å and that at relative humidities of less than 40% all the evaporable water exists in this form (Hilsdorf, 1967). He reports the weight of non-evaporable water per unit weight of hydrated cement as 0.24.

The most comprehensive and one of the earliest research work, for the physical properties of the different types of water in cement paste was reported by Powers et al (1947). Many other workers have since carried out work in the same field.

The paper of Powers et al (1947) was published in nine parts. In part 2 of the paper, they proposed the arbitrary definitions of water previously described in this section (i.e. evaporable and non-evaporable water). They studied the relationship between relative

vapour pressure and the amount of evaporable water in concrete, using sorption curves for concrete at various vapour pressures and found that:

1. As the relative vapour pressure increases the evaporable water content also increases.

2. Hysteresis occurs in the relationship between these two parameters. The evaporable water content is lower at a given relative vapour pressure, if the vapour pressure has increased to reach the given value than if it has decreased.

3. As the length of curing time increases, that the total water held at any vapour pressure, as well as the amount of non-evaporable water increases.

4. For humidities below 40% the amount of evaporable water is proportional to the amount of non-evaporable water in the paste

5. Under saturation conditions, however, the amount of evaporable water decreases as the amount of non-evaporable water increases.

6. Below 40% humidities, all the evaporable water occupies the gel spaces, while at humidities above 40%, the gel pores are full and water collects in the capillary pores.

7. The volume occupied by the larger capillary pores decreases as the volume of hydration products increases.

In part 5, entitled 'Studies of Hardened Paste', by means of specific volume measurements, Powers et al (1947) divided total water in a saturated specimen into two categories: that which had specific volume less than unity and that which had specific volume equal to 1.0. All the water having a specific volume less than 1.0 was called compressed water. This water comprised the non-evaporable water and a part of the evaporable water. The mean specific volumes of the gel water was calculated by them as 0.90 and that of capillary water as 1.0. The mean specific volumes of non-evaporable water and gel water reported by them were 0.86. They proposed the maximum amount of non-evaporable water in concrete to be approximately 50% of mix water.

Powers (1949) found that the amount of non-evaporable water in hardened cement paste depends on the curing conditions and fineness of cement and suggested the weight of non-evaporable water was about 26% the weight of cement for completely hydrated normal Portland cement. Powers (1960) in a later paper adjusted this value to 22.7%, Hilsdorf (1967) suggests 24% and according to Neville (1977) the value is 23%, which is now the generally accepted value.

Powers (1949) reports that hydration stops when the capillary pores are filled, which normally occurs when the original weight of water is less than 39% of the weight of cement; where the capillary pores contain no water, which is known as self dessication, or when all the cement has hydrated. The strength of the paste depends upon the degree of hydration and upon the volume of the capillary pores.

Copeland (1956) investigated the specific volume of the evaporable water in cement paste by measuring the apparent specific volume of the total water (W_t) at various non-evaporable water contents (W_n). He reported that the specific volume of evaporable water compared with free water was 0.99 after extrapolating the results to a value of W_n/W_t of zero. Then using the same results and extrapolating to W_n/W_t of one, he found that the specific volume of non-evaporable water was 0.74. Neville (1977) gives a value of 0.746.

2.5 WATER REDUCING AGENT

As explained in Chapter3, Section 3.2, a water-reducing agent (Cormix P1) was used in the concrete mix for this thesis. Cormix P1 is a high grade lignosulphonic acid derative. The sugar contents of this agent are low, hence the rate of hydration is neither accellerated nor retarded (Field, 1979 and 1980).

The effects of the addition of the water-reducing agent can be summarised as follows.

1. It forms adsorbed layers on the grain surface and modifies the short range Van der Walls attraction and longer range cat-ionic electrical repulsion between the particles.

2. It reduces the viscosity of the paste and changes the rheological properties of concrete.

3. It acts as a plasticizer and improves the workability of concrete.

4. Generally it results in better mixing and compaction, resulting in reduced permeability and improved concrete quality.

2.6 PORE PRESSURE IN HEATED CONCRETE

The pores in concrete contain liquid water, water vapour and air. With a rise in temperature, the water vapour and air can generate increased pressure in the pores in the concrete. The total pore pressure inside concrete is the sum of the partial pressures exerted by water vapour and air. The magnitude of pore pressures caused by heating of concrete is of considerable importance for predicting the response of prestressed concrete nuclear reactor vessels. If the concrete is sealed, or the mass is so large that it is effectively sealed, so that the contents of the pores cannot escape, the application of temperature should produce a significant increase in pore pressures.

If concrete is heated non-uniformly a thermal gradient is established inside the concrete, which generates a pressure gradient similar in shape to the temperature gradient. Many research workers have investigated the pore pressures in heated concrete e.g. Bremer (1967), England and Ross (1970), Sharp (1971), England and Sharp (1972), Chapman(1976), Bazant and Thonguthai (1978), Bazant et al (1979) and Schneider and Herbst (1989).

Bremer (1967) was possibly the first person to measure pore pressures inside a sealed specimen of concrete. His apparatus shown in Figure 2.11, consisted of a sealed block of concrete with a thermocouple and two mercury-filled pipes connected to manometers for measuring pressure. One of the measuring pipes was perforated so that the pressure in the mercury was equal to the pressure in the concrete, whereas the other pipe was sealed. Bremer reported that pressure in the concrete capillaries varied between 40% and 60% of the saturated pressure of steam for various temperatures (Figure 2.12).

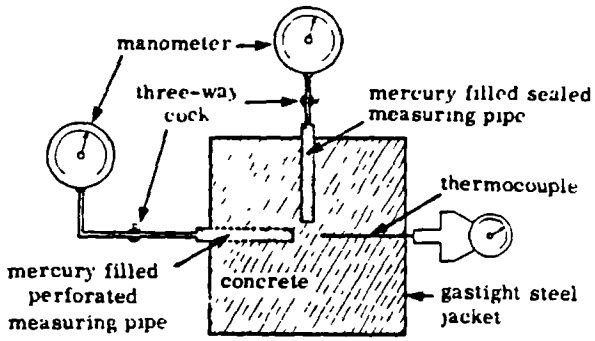

Figure 2.11: Pressure measuring system (Bremer, 1967)

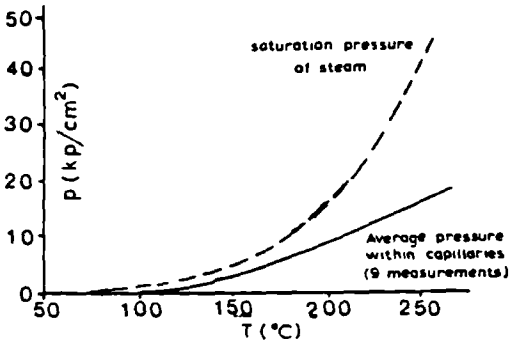

Figure 2.12: Pressure v Temp. (Bremer, 1967)

England et al (1970) experimentally recorded the pore pressures in the concrete by connecting six manometer tubes to the porous inclusions in the concrete (Figure 2.13). These were simply used to maintain conditions of constant volume. The pore pressure was obtained by applying the back pressure to the porous inclusions and by maintaining the mercury level in the manometer tubes.

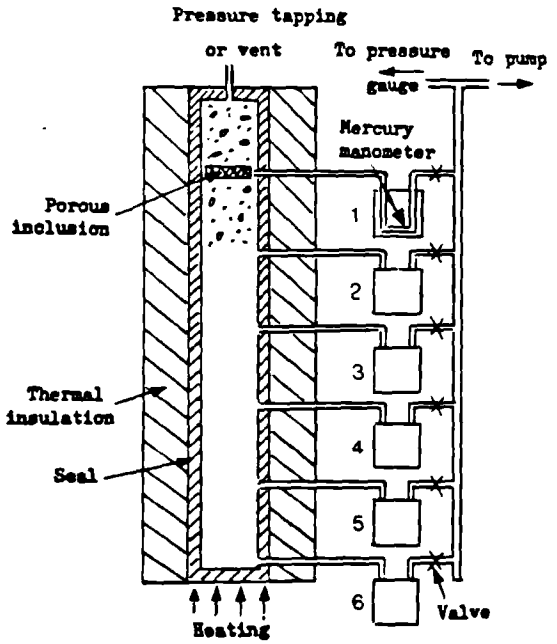

Figure 2.13:
Pressure measuring system used by England and Ross (1970).

Sharp (1971) measured pore pressures in two separate test series with heated concrete specimens. His method of measuring pore pressure is described in Chapter 4, Section 4.2.1. In the first series, specimens (4 inches long and 4 1/8 inches diameter) of various ages from 2 days to 260 days were tested and the temperature of the specimen was

increased from room temperature to 150 °C. In order to investigate whether the pore pressures were affected by the previous temperature history of the specimen, many of the specimens underwent several temperature cycles. The ageing effect on pore pressures was investigated by re-testing specimens after several months. Sharp concluded that:

i. The pore pressure was temperature dependent.

ii. The pore pressure values for any given temperature were greater than the saturated vapour pressures of steam at the same temperature, provided the specimen remained sealed from the time of casting.

iii. The degree of hydration was a function of the age of concrete and had a small effect on the pore pressure.

iv. The previous history had no appreciable effect on the recorded pore pressures.

Sharp predicted the pore pressures inside his specimens, by taking into account the relative volumes of capillary water and air in the concrete. He found that the predicted pore pressures were higher than those measured experimentally, when the volumes of non-evaporable water, gel water and their expansions were taken into account.

Sharp (1971) heated a specimen (similar to the one described earlier in this section) to a constant temperature of 150 °C and allowed the fluid to escape periodically. He recorded the pore pressure and after it reached steady conditions, fluid was released from the specimen. The amount of fluid loss was monitored by weighing (Figure 2.14). The variation in pore pressure with weight loss was divided into the following three areas.

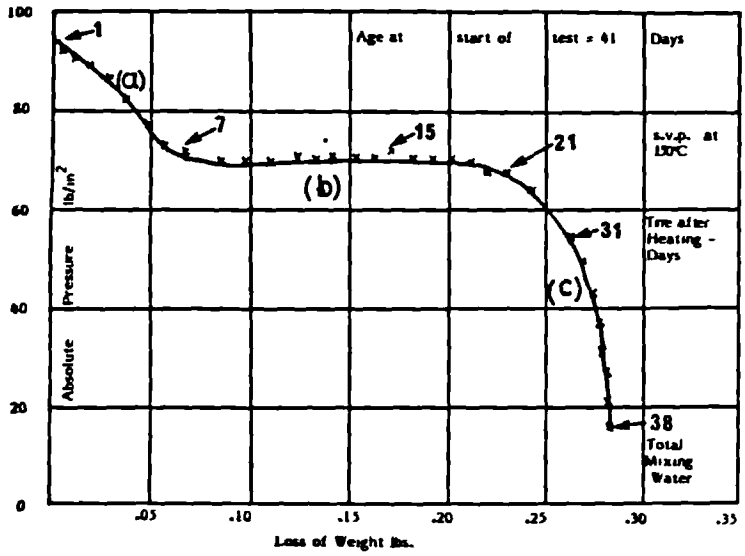

Figure 2.14: Pore pressure against weight loss reproduced from Sharp (1971).

1. The part (a) of the curve, when pressure is dropping with weight loss, corresponds to the loss of the entrapped air.

2. The pore pressure values represented by the flat portion of the curve correspond to the saturated vapour pressure of steam at 150 ^{o}C. These values were maintained while the gel pores in the concrete were full of water.

3. When the gel pores began to empty, the pressure curve begins to fall rapidly and becomes zero when all the evaporable water had escaped from the concrete.

These points are relevant in the discussion of the "Release Test Series" results (Chapter 6).

In the second series of tests, Sharp (1971) monitored pore pressures, temperatures and moisture movement in both sealed and one-end sealed specimens (2 feet long and 3 1/2 inches diameter), under the effects of a thermal gradient. The specimens were tested at various ages from 28 to 200 days, for a duration of 110 to 540 days, and the bases having a fixed temperature level in the range 130 ^{o}C to 175 ^{o}C. He observed the following points in his experiments.

a. The temperature gradient produced a pressure gradient and caused uniaxial migration of fluid along the specimen.

b. The pore pressures slowly dissipated in the hot region as water

migrated to the cooler part of the specimen.

c. In the early stages, the sealed specimens and one-end sealed specimens exhibited similar pore pressure behaviour.

d. In sealed specimens, the pressure values at the top increased rapidly until these were higher than at points lower down the specimen, and an accumulation of water was detected.

e. The unsealed end of the specimen remaining at atmospheric pressure did not show the above trend; however, liquid collected on the surface of the concrete.

The results of the "Liner Test Series" described in Chapter 5 are discussed in the light of the points given above.

Chapman (1976) recorded the pore pressure of heated concrete experimentally in three separate test series. The method used by him to measure the pore pressure is explained in Chapter 4, Section 4.2.1.

In the first series, he investigated the relationship between the pore pressure developed inside a concrete specimen (4 inches long and 4 1/8 inches diameter) under a constant temperature and the loss in weight of that concrete specimen when fluid was permitted to escape. Tests were carried out at two average ages of 49 days and 365 days and at temperatures of 105 ^{o}C, 125 ^{o}C, 150 ^{o}C and 175 ^{o}C. The following conclusions were drawn by Chapman from his results.

i. The maximum recorded pore pressure depends upon the initial ratio of the volume of liquid to gas inside the pores.

ii. The pore pressure is temperature dependent.

iii. The recorded pore pressure was higher than the saturation vapour pressure of steam at any given temperature, as seen in Figure 2.15 reproduced from his thesis.

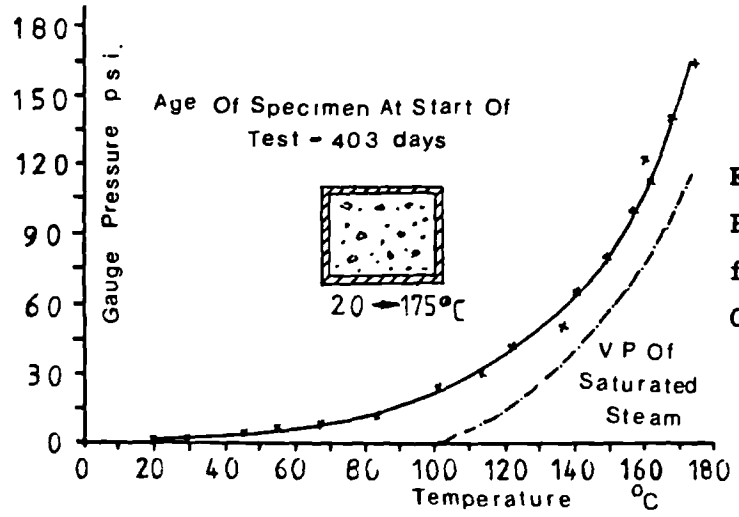

Figure 2.15:
Pore pressure v temperature for heated concrete from Chapman (1976).

iv. The pore pressure at a given temperature can be depressed or elevated by dissolved salts and gases respectively.

The second test series was further divided into two categories.

The aim of the first category of tests (Migration Series) was to monitor the variation of pore pressure and water content with time by the application of a thermal gradient to the cylindrical concrete specimens (5 feet and 10 feet long, and 6inches diameter). The specimens were sealed along their base and sides. The test temperatures were 105 ^{o}C, 125 ^{o}C, 150 ^{o}C, 175 ^{o}C and 200 ^{o}C, and heating was applied at the base and the sides of the specimens. The findings from the experimental work are described below.

1. The application of a temperature gradient created a pressure gradient in each specimen.

2. The pressure gradient was responsible for the movement of moisture inside the concrete and caused the moisture to be lost from the open end of the specimen.

3. Pore pressure values drop in the region below the drying front as the drying front progresses up the specimen.

4. In the region below the drying front, the pressure values, as well as the water content values become virtually uniform.

5. Pore pressure values were generally higher than the saturated

vapour pressure for the temperature of the section.

The specimens of the second category of the second test series (Venting Series) were designed and constructed in exactly the same manner as the first category (Chapman, 1976). One of the objects of these tests was to see the effects of breaking the pressure seal at various points along the specimen at various times, and observing the dissipation of the pore pressure in concrete. The conclusions drawn by Chapman are given below.

a. The effect of venting was to lower the pore pressure and water content values.

b. The mechanism of moisture migration was temperature and pressure dependent.

In the third series of tests (Pore Pressure/Shrinkage Test), Chapman (1976) monitored the pore pressures and shrinkage in the cylindrical limestone concrete specimens (5 feet long and 10 inches diameter), which were sealed along the sides and bottom, and were heated from the sealed end. Each specimen consisted of twenty slices of 3 inches length, and a P.T.F.E. ring was placed between the adjacent slices for separation. Once again a thermal gradient was set up in the concrete.

He concluded from these tests that moisture migrated from hot zones to the cooler areas as seen before, and that the pore pressure and water content results exibited similar behaviour to that seen in the second test series (Migration Series), as described earlier in this section.

The "Liner Test Series" (Chapter 5) and the "Release Test Series" (Chapter 6) tests will be discussed in the light of these findings.

Bazant et al (1978) suggest that, 'for non-saturated concrete, pore pressure must be regarded as the pressure in vapour rather than in capillary water'. They based their calculations on the following two assumptions and proposed that calculated pressures would be far higher than observed without these two hypotheses.

i. The pore volume available to free water (capillary porosity)

increases in proportion to the amount of chemically combined water that is released by dehydration due to heating.

ii. Above the saturation pressure, the pore space available to free water must increase with increasing pressure.

Although moisture migration is generally controlled by both moisture concentration gradient and temperature gradient, it can be shown that for concrete it is possible to use the gradient of a single potential i.e. the pore pressure (Bazant et al, 1978).

In another paper Bazant et al (1979) predicted that the application of thermal shock (rapid uniform heating) on one face of a thick wall produces pore pressure peaks inside the concrete. Their calculations show that these peaks are much higher than those for slow heating. In the region where the pressure gradient is opposite to the temperature gradient, the calculated moisture movement is rather irregular, and the moisture movement tends to give oscillation in the pore pressures.

Schneider and Herbst (1989) suggest that the influencing factors for the pressure development in a porous system like concrete are: the strength and the dimensions of the concrete member, kind of temperature elevation and heating, the water content in the porous system, the evaporability and the permeability of the porous system. The development of pressure in concrete will lead to the formation of microcracks and therefore strongly increase the coefficient of permeability.

2.7 MOISTURE MIGRATION IN CONCRETE

Concrete is a material containing extremely fine pores and water exists in concrete in both liquid and vapour form. The movement of moisture inside the thick walls of a prestressed concrete pressure vessel, is not of great significance in its early life. The only moisture loss occurs from, and near, the surface of the wall (McDonald 1970) at ambient temperature. However, after the commissioning of the reactor, thermal gradients exist inside the wall, and moisture migrates within the wall and some of it is lost from the external surface. The moisture migration and the loss of moisture caused by the heating of concrete is of considerable concern for the designers of

prestressed concrete reactor vessels (Kordina and Schneider (1979), Kamp, Roelfstra, Wittmann and Mehashi (1987), Schneider and Herbst (1987), Takeda, Nakane and Nagao (1989) and Zangle, Sadouki and Wittmann (1989)).

The mechanism that causes the migration of moisture and the factors influencing the rate of moisture movement are reviewed in this section.

The laws of diffusion have been applied to moisture movement and drying of concrete. The transfer of fluid matter from one region to another within a porous solid may take place by either random motion of the molecules of fluid or by a definite force acting on the fluid. The concentration gradient within the fluid will result in diffusion. The movement of moisture which may be considered to be caused by a 'force' derived from the difference in concentration of the fluid can be expressed in the form of Fick's Law, and this, for uniaxial diffusion, is:

$$\partial c/\partial t = k \cdot d^2c/dx^2$$

c = concentration of free water.
t = time elapsed after start of the diffusion process.
k = coefficient of diffusion.
x = distance from the exposed face.

The coefficient of diffusion increases with temperature and the value of the coefficient of diffusion decreases with moisture loss at normal temperature (Browne, 1967). The diffusion coefficient varies with the type of cement, mix proportion of concrete and the degree of hydration.

A single constant diffusion coefficient could be used to describe the drying at any particular temperature, provided that the drying conditions at the surface were adequate (Hughes et al, 1966).

Harmathy (1970) has theoretically investigated moisture and heat transport with particular reference to concrete. He suggested the following theories for the movement of moisture in a porous medium.

1. The diffusion theory.
2. The capillary flow theory.
3. The evaporation - condensation theory.

The drying of a wet porous solid actually consists of at least three phases. During the capillary and funicular states (i.e. at relatively high pore saturation), the moisture moves by a convective transport mechanism, and the rate of moisture movement is relatively insensitive to the properties of the solid matrix. However, the movement of moisture depends mainly on the external factors (i.e. temperature, water vapour concentration in the ambient air, and air velocity), which affect the coefficients of heat and mass transfer at the surfaces. During the pendular state (i.e. the falling rate period of drying), the internal characteristics are of primary importance.

Huang, Siang and Best (1979) also reported that three theories (as discussed above) explain the physical phenomenon of moisture transfer in porous media.

Moisture transfer in concrete is limited to water and vapour movement through the porous system of hardened cement paste and along the interface (Wittmann, Roelfstra and Kamp, 1988). They suggest subdividing the structure of concrete into three different levels, called the 3L-approach:

i. Micro-level to describe moisture transfer mechanism.

ii. Meso-level to take the composite structure of concrete into consideration.

iii. Macro-level to formulate realistic material laws.

A similar approach (i.e. 3L-approach as described above) could be adopted to predict time-dependent moisture and pressure distribution in concrete, under various effects, e.g. different temperatures, thermal gradients, and humidity contents of the environment.

The steam transport in concrete may not be described by diffusion formula but only by a vapour flow model, i.e. the driving potential must be considered to be steam pressure (Kordina et al, 1979).

According to them the evporation rates at high heating rates are 3 powers of 10 higher than the evaporation rates obtained from diffusion calculations at ambient temperatures.

The rate at which the drying front progresses into the concrete is dependent upon the difference in temperature, and relative humidity in the pores of concrete (Chapman, 1976). He also reports that the rate of moisture movement is dependent upon temperature, pressure and the initial permeability coefficient of concrete in the heated region.

The capillary water dries out first even if the capillary pores are not interconnected (Powers, 1960). He explains this by the theory of hydrostatic tension; as the relative humidity drops, air comes out of the solution in the capillary pores and the water is pushed through the gel towards the surface of the concrete , and it evaporates into the atmosphere. According to Powers if the humidity is above ~45% all the gel pores are full and there is some capillary water; however, below this value there is no capillary water and the gel begins to empty.

Takeda et al (1987) experimentally studied the characteristics of concrete members subjected to high temperature. In the moisture migration tests they monitored moisture movement in two ways. Firstly, by venting the heated end, and secondly, by not venting the heated end. According to them the portion of concrete close to the heated lining of the specimen with venting system was in an almost absolute dry state from the initial stage of heating. The dry zone gradually moved upwards and the open surface dried as time passed. The moisture content in the specimen without a venting system decreased at a slower rate. They report that the moisture content distribution after 91 days of heating showed almost the same pattern in both types.

Chapman (1976) in his experimental work also found that the rate of moisture loss increased considerably in a vented specimen compared with the corresponding results from non-vented specimens.

These findings support the point made in Chapter 5, Section 5.3.6, where it is suggested that the build-up of pressure inside the concrete behind the steel liner should be avoided.

Concrete which contains a considerable amount of water and hydrate in its porous system, when heated to high temperatures results in accelerated mass transport in consequence of dehydration and decomposition effects (Schneider et al, 1989). Their findings agree with the results of the "Liner Test Series" discussed in Chapter 5.

It is shown by many studies (e.g. Schneider et al, 1987 and others reported in this and the following sections) that high pore pressures generated in heated concrete are responsible for moisture transport. The "Liner Test Series" results (Chapter 5) are in agreement with this point.

2.7.1 ROLE OF CONCRETE PERMEABILITY ON MOISTURE MIGRATION

As concrete is a porous material its permeability plays an important role in the moisture movement through it.

Powers et al (1947) in part 7 of their paper (permeability and absorptivity) explain that water movement through hardened cement paste takes place according to Darcy's Law and can be written as:

$$dq/dt = AK' \Delta H/L$$

dq/dt = volumetric rate of flow through porous medium.
A = area of the porous medium.
ΔH = drop in hydraulic head.
L = thickness of the porous medium.
K' = coefficient of permeability (having units of length per unit time); it depends on the properties of the porous medium and the permeating fluid.

Muskat (1937) expressed this expression in more general form as:

$$dq/dt = AKg/\eta \ \Delta P/L$$

η = viscosity of the permeating liquid.
g = acceleration due to gravity.
ΔP = pressure drop across the medium.
K = coefficient of permeability (having units of area) and depends only on the properties of porous medium.

Powers (1958) reports the permeability of cement gel as

7×10^{-14} cm/sec. The permeability of cement paste as a whole is 20 to 100 times more than the gel itself, because cement paste consists of capillary pores as well as gel pores, and water can flow more easily through the capillary pores than the gel pores.

The permeability of cement paste varies with both water/cement ratio and degree of hydration (Powers et al, 1954). Table 2.4 reproduced from their work shows the reduction in permeability of cement paste of water/cement ratio 0.7, with the progress of hydration. The permeability of concrete as a whole is much higher than the permeability of hardened cement paste itself, due to the weak bond between aggregate and cement paste and fissures and pores in the aggregates. Table 2.5 taken from Powers (1958) gives the permeability of some common rocks; alongside the figures is a list of water/cement ratios of mature paste of the same permeability.

Age Days	Coefficient of Permeability cm/sec
Fresh	2×10^{-4}
5	4×10^{-8}
6	1×10^{-8}
8	4×10^{-9}
13	5×10^{-10}
24	1×10^{-10}
Ulti-mate	6×10^{-11} (Calculated)

Table 2.4: Permeability of cement paste for 0.7 w/c ratio.

Type of rock	Coefficient of Permeability cm/sec	Water/cement ratio of paste of same Permeability
Dense trap		
Quartz	2.47×10^{-12}	0.38
Dolorite	8.24×10^{-12}	0.42
Marble	2.39×10^{-11}	0.48
Granite	5.35×10^{-9}	0.70
Sandstone	1.23×10^{-8}	0.71
Granite	1.56×10^{-8}	0.71

Table 2.5: Permeability of some common rocks and the cement pastes.

As seen in the preceding text, the coefficient of permeability of concrete is a controlling factor in the rate of moisture migration in concrete. The movement of moisture in concrete is affected by elevated temperatures and thermal gradients, and the temperature also influences the permeability of concrete. When the temperature of concrete is raised all the constituents of concrete will expand. If

the cement paste and the aggregate have dissimilar coefficients of thermal expansion, microcracks may appear between the cement paste and the aggregate, thus increasing the permeability of concrete. Crispino (1970) reported that the difference in the coefficients of thermal expansion is enhanced by an increase in temperature.

The effect of thermal gradient on concrete is complicated and depends on the moisture conditions at the point considered. The temperature gradient imposes a pressure gradient inside the concrete mass as described in Section 2.6, and results in the movement of moisture away from hot zones.

"Free" or capillary water is first to be removed from the hot zones and the removal of this water causes little or no shrinkage of the cement paste (Neville, 1977). This would have very little effect on the permeability. However, as the moisture is continously lost from the hot zones, the gel shrinks, and increases the cement paste permeability. The increase in permeability would eventually stop, when the gel stops shrinking. The permeability in heated zones may increase further, due to the change in the hydration products.

In the cooler zones, into which the moisture moves from hotter zones, the inflow of moisture in the form of water will cause a slight swelling of the paste. The permeability would be decreased slightly due to this effect.

The movement of water from the hot zones produces a local leaching effect and subsequently hydration products are deposited in cooler regions (England and Skipper, 1973). However, Chapman (1976) suggests that there is no experimental evidence to support that.

Cambell-Allen et al (1967) and Bertero et al (1970) show that thermal cycling decreases the bond between the cement paste and aggregate and this will increase the permeability. The first thermal cycle is mainly responsible for the damage and the increase in permeability diminishes as the number of thermal cycles increase.

Chapman and England (1977) report that the permeability of concrete is lower in the regions of high water content and raised temperature, due to enhanced cement hydration. However, the permeability is

higher in more severely heated zones, due to impeded hydration or degeneration. They report permeabilities approximately one hundred times greater in hotter zones than those in the excess water zones.

Bazant et al (1978) also reported the dependence of permeability on temperature, which they say exibits an upward jump by two orders of magnitude when the temperature passes 100 ^{o}C. They suggest that up to about 100 ^{o}C, the temperature dependence of permeability appears to be determined by activation energy and the moisture is controlled by the transfer of water molecules along adsorbed water layers. Their explanation for the jump in permeability at 100 ^{o}C is:

i. The moisture flow is possibly governed by 'necks' of negligible volume (in cement paste) in the flow passages.

ii. At room temperature, these 'necks' are assumed to be of subcapillary size and the flow consists of adsorbed water migration.

iii. As temperature increases above 100 ^{o}C, the 'necks' become much wider, allowing rapid flow of steam and liquid.

Greathead (1986) carried out extensive experimental work on the permeability of concrete containing Blast Furnace Slag and looked at temperature, moisture and time effects. Some of his conclusions are as follows.

a. The ability of concrete to transmit moisture when heated to 200 ^{o}C falls by a factor of ~10 as vapour phase (unsaturated) flow displaces liquid phase (saturated) flow.

b. To predict the permeability of concrete within a factor of 2-3, Darcy's law may be applied at temperatures and pressures up to the point where liquid-vapour phase change occurs in concrete with fine pores.

c. Concrete made with blended cement (i.e. BFS-OPC) reduces permeability as compared with only Portland cement concrete, due to a fine microstructure achieved by the blended cements.

Greathead (1986) used similar concrete mix design as described in this thesis and his findings confirm the experimental results described in (Chapters 5 and 6).

Khoury, Grainger and Sullivan (1985) report that sharply increased rate of moisture loss above 100 ^{o}C markedly increases the concrete permeability.

Schneider, Herbst and Diederichs (1985) found that the permeability of concrete increases beneath the vapourisation region of water by a factor of 10-100 in temperature range of 100 ^{o}C to 300 ^{o}C, as compared to concrete below 100 ^{o}C.

Kamp, Roelfstra and Wittmann (1987) while theoretically studying the mechanism of moisture transfer through porous materials reported a permeability coefficient roughly 40 times larger at 100 ^{o}C than at 20 ^{o}C at the same relative humidity.

All the literature surveyed on the effects of temperature on the permeability of concrete, unanimously highlights the fact that temperatures in excess of 100 ^{o}C result in increased concrete permeability. These factors are taken into account when discussing the results of the "Liner Test Series" (Chapter 5).

2.7.2 THERMAL AND PORE PRESSURE GRADIENT EFFECTS ON MOISTURE MIGRATION

McDonald (1975) investigated the moisture distribution in a pie-shaped specimen representing the flow path through a cylindrical wall of a prestressed concrete reactor vessel subjected to a temperature gradient. The lateral surfaces were sealed and thermally insulated, one of the two ends being left open and the other closed after casting until the heat was applied. After casting, the temperature, shrinkage and moisture distribution were monitored for approximately 17 months while the specimen matured. A thermal gradient of 44 ^{o}C was applied after 17 months. McDonald (1975) reports that the concrete temperatures within the specimen continued to increase, but at a decreasing rate until 43 days after heating commenced, and no significant changes were observed in the local temperatures. He explains that with the exception of those zones nearest the ends of the specimen, moisture contents were fairly constant. He also observed

that moisture contents in the intermediate zone were higher than would normally be expected. He concluded from his results that moisture migration in thick sections of concrete, such as PCRV, is a slow process and is not likely to be a significant factor with temperature differences of 44 ^{o}C or less.

Poitevin (1970) tested concrete cylinders 80mm in diameter and 300mm long under sustained temperature gradients and monitored the moisture migration. Three types of specimen were tested:

1. A sealed specimen left at room temperature.
2. A partially sealed specimen left at room temperature.
3. A partially sealed and laterally insulated specimen subjected to a longitudinal temperature gradient of 20 ^{o}C.

All the specimens were cured for 3 months and then left for periods of 9 months under their specific thermal gradients. He observed that the non-evaporable water content of the sealed specimen after 9 months was 0.30 per unit weight of mix water, while the value for partially sealed specimens was 0.36. His conclusions were as follows:

i. The hydration process was slowed down in the concrete in sealed conditions.

ii. The sealing conditions and temperature gradient influenced the rates of moisture loss.

iii. The highest loss was for the partially sealed specimen under thermal gradient, while the lowest loss was for the sealed specimen at room temperature.

iv. The water distribution in sealed specimens and the partially sealed specimen at room temperature was fairly constant throughout.

v. The moisture migration away from the higher temperature zone was detected in the partially sealed specimen under a thermal gradient.

Hundt and Schimmelvitz (1973) tested a beam of dimensions 40cm x 40cm x 240cm. The open end was exposed to a climate of 20 ^{o}C and 50%

relative humidity, while the other end was kept at a temperature of 80 ^{o}C. After 80 days of heating the biggest changes in moisture content were noticed in the area adjoining the heated face. They report that the area of high moisture loss extended to about 30cm from the heated face. The area between 30cm and 200cm from the heated face showed an approximately constant moisture distribution. They also noticed an area with a small increase in moisture between 60cm and 80cm from the heated face.

Sharp (1971) reports similar results; however, the heating period for his tests was not so long. The last 40cm of the beams to the open end (Hundt et al 1973) showed a slight decrease in moisture content, which was probably due to evaporative drying.

England and Sharp (1972) suggest that migration of water in concrete at a temperature above 100 ^{o}C is affected by the pore pressures which develop as a result of the entrained air and the rapid increase of saturated vapour pressure with increase of temperature. They concluded that, although simple diffusion theories may be adequate for specifying drying at ambient temperature they do not provide adequate representation in regions of high temperature and recognition must be given to other more influential factors such as pore pressures in these regions.

Chapman and England (1977) suggest that moisture migration is caused by a state of non-uniform temperature, resulting in drying and shrinkage in hot areas and possible physical saturation and swelling in cooler region far removed from a free boundry.

Khoury et al (1985) while investigating the transient thermal strain of concrete, show that 'the temperature gradient can initially drive some moisture inwards, causing moisture and pore pressure build-up in the central region at the same time as free capillary water escapes from the surface layer.

Bazant et al (1978) state that although moisture transport is generally controlled by the gradients of both moisture concentration and temperature, the gradient of a single potential (i.e. the pore pressure) appears to be responsible for the moisture movement in concrete, and this potential alone can be used for predicting the

moisture migration in concrete.

Bazant et al (1981) in a later paper reported that the heating of concrete produces significant pore pressures which cause migration of moisture through concrete resulting in eventual drying. The significance of pore pressures can also be noticed in explosive spalling of concrete due to rapid heating during a fire. The major factor in the above phenomena is no doubt the thermal stress produced by rapid heating in a restrained concrete. An important factor may also be the rise of the pore pressure caused by heating. They point out that explosive spalling is generally observed only in concrete of high moisture content.

Huang and Siang (1983) analysed moisture migration in a cylindrical concrete vessel under the effects of thermal gradient and reported that:

1. A considerable amount of moisture loss takes place in both the hot and the cold zones, during the stage of high pore saturation (or the funicular saturation stage).

2. The rate of moisture loss locally is dependent on the intensity of heat flux.

3. The higher intensity of heat flux imposed on the inner surface of the cylinder, shows a higher drying rate in the heated surface zone only.

4. A steep temperature gradient provides a large thermal driving force to transport the moisture in the hot inner zone outward into the middle zone.

5. The moisture loss on the outer unheated surface is caused by moisture diffusion.

6. The drying rate of moisture is dependent upon the parameters characterizing the surroundings of the system and it is relatively independent of the properties of the porous concrete and the properties of fluid moisture.

7. A small amount of moisture loss has been observed in the middle zone between two surfaces, and both diffusion and thermal driving force are inactive in this region. England et al (1970) and McDonald (1975) also reported similar phenomena.

8. In the pendular stage, capillary action and evaporation condensation occur in the pore spaces.

9. The moisture migration at this stage depends on internal and topological characteristics of porous concrete and the intensity of heat flux.

10. The rate of moisture loss is faster near the heated end than that at the outer exposed surface.

11. The moisture in the hot zone travels outward in the negative direction of temperature gradient.

12. An increase in heat flux generally increases the mobility of the water molecules.

13. Finally the drying rate and moisture loss at any time are functions of temperature and the drying rate increases rapidly with temperature.

The reasons cited by Huang et al (1983) all seem reasonably justified, but they do not take into account the development of pore pressure in heated concrete, which contributes towards the moisture migration under thermal gradient as shown by many research workers and described in this section previously.

The dependence of moisture migration on thermal and pore pressure gradients has been reported by many authors e.g. Kordina et al (1979), Schneider et al (1987), Kamp et al (1987), Takeda et al (1987) and Schneider et al (1989). Reference is made to these and other studies when discussing the results in Chapter 5.

The comments on literature reviewed in this chapter are further highlighted in Chapter 5 and Chapter 6, when the results of experimental work are discussed.

3.1 INTRODUCTION AND OBJECTIVES

The experimental programme (Table 3.1) was divided into two main groups, "Liner Test Series" ("LTS") and "Release Test Series" ("RTS").

Type of Test	Abreviations Used	Test Temperature ^{o}C	Sealing Conditions
Liner Test Series	LTS	400	One-end sealed Partially sealed Sealed
Release Test Series	RTS	250, 275, 300, 325, 342, 350.	Sealed

Table 3.1: The experimental programme of the "LTS" and the "RTS".

The objects of the "Liner Test Series" were to investigate:

i. The pore pressure developed inside the heated concrete behind the liner of a Fast Breeder Reactor (FBR).

ii. The movement of moisture through the length of concrete under temperature and pressure gradient with different sealing conditions.

iii. The relationship between the pore pressure and the deflection of the liner under the combined effects of pressure and temperature.

The variation of pore pressures and water contents of concrete under thermal gradients was also investigated. Therefore, experimental work was carried out to study in a simulated way, the effects of rapid heating applied to the steel liner of a Fast Breeder Reactor. The existence and influence of pore pressures in the concrete adjacent to and behind the liner, caused by heat transmission through the liner were monitored. The temperature of the stainless steel diaphragm (simulated steel liner) and the temperature distribution inside the concrete were recorded.

In the "Release Test Series" the aim was to monitor the pore pressures, the temperature and the weight loss, in concrete heated at

a constant temperature. The relationship between the pore pressure and temperature was investigated. Finally to understand the effects of rapid heating applied to a moist and dry (or patially dry) concrete, a relationship was studied between the pore pressure developed inside a sealed concrete specimen under a constant temperature and the loss in weight of that concrete specimen, when the fluid was allowed to escape. The concrete mix used for "RTS" was identical to the one used for "LTS". Table 3.1 shows the test temperatures.

3.2 THE CONCRETE MIX

The concrete mix throughout the experimental programme was the same. The maximum size of aggregate was 3/4 inch (20mm) and the Sulphate Resisting Portland Cement (SRPC) was blended with Ground Granulated Blast Furnace Slag (Cemsave) to reduce heat generation. To increase the workability of the mix a water reducing agent was used. The mix proportions were as below.

Cement	(SRPC)	= 0.5		
Cemsave	(BFS)	= 0.5		
Sand		= 1.463		
3/8 inch	Aggregate	= 0.873		
3/4 inch	Aggregate	= 1.633		
Water		= 0.39	Water/Cement Ratio	0.39
Plasticizer (Cormix Pl)		= 0.0057	Aggregate/Cement Ratio	3.969

The cement used was from Ribblesdale Cement Ltd; and Cemsave was from Frodingham Cement Company at Scunthorpe. The properties and chemical analysis of cement and Cemsave used are given in Table 3.2.

		CEMENTITIOUS MATERIAL		AGGREGATES	
		CEMENT	CEMSAVE	AGGREGATE	SAND
Lime	CaO	63.90	43.60	9.35	12.74
Silica	SiO_2	20.66	34.16	51.98	67.83
Alumina	Al_2O_3	3.22	14.10	15.00	3.59
Ferric Oxide	Fe_2O_3	4.72	0.34	12.75	1.99
Magnesia	MgO	2.16	4.68	6.56	0.38
Sulphuric Anhydride	SO_3	2.32	trace	trace	-
Potassium Oxide	K_2O	0.55	0.47	0.60	-
Sodium Oxide	Na_2O	0.17	0.24	2.40	0.92
Carbonic	CO_2	-	-	0.24	-
Loss on Ignition		1.17	-	-	10.88
Insoluble Residue		0.50	-	-	-
Combined Water		-	-	0.40	-
Total Carbon		-	-	0.07	-
Total Sulphur		-	1.73	trace	-

Table 3.2 CHEMICAL COMPOSITION OF CONSTITUENTS

The sand used was calcareous quartz from Tilcon Ltd; Dock Acres Quarry, Carnforth. The sand ranges from coarse silt to fine gravel with medium and coarse fractions predominating. The majority of the grains were subangular to angular with occasional rounded and subrounded grains. Many of the larger grains had freshly fractured surfaces. Surface textures were predominantly granular though some smooth and crystalline surface occurred.

The 3/4 inch and 3/8 inch Whinstone aggregates which are crushed quartz dolerite (Basalt) came from Hargreaves Quarries Ltd;, High Force Quary, Middleton-in-Teeside, Co. Durham. The chemical analysis and the properties of the aggregates are also shown in Table 3.2. Figure 3.1 shows the grading curves for the aggregates, together with the standard curves for the aggregate from British Standard BS 882 (1973).

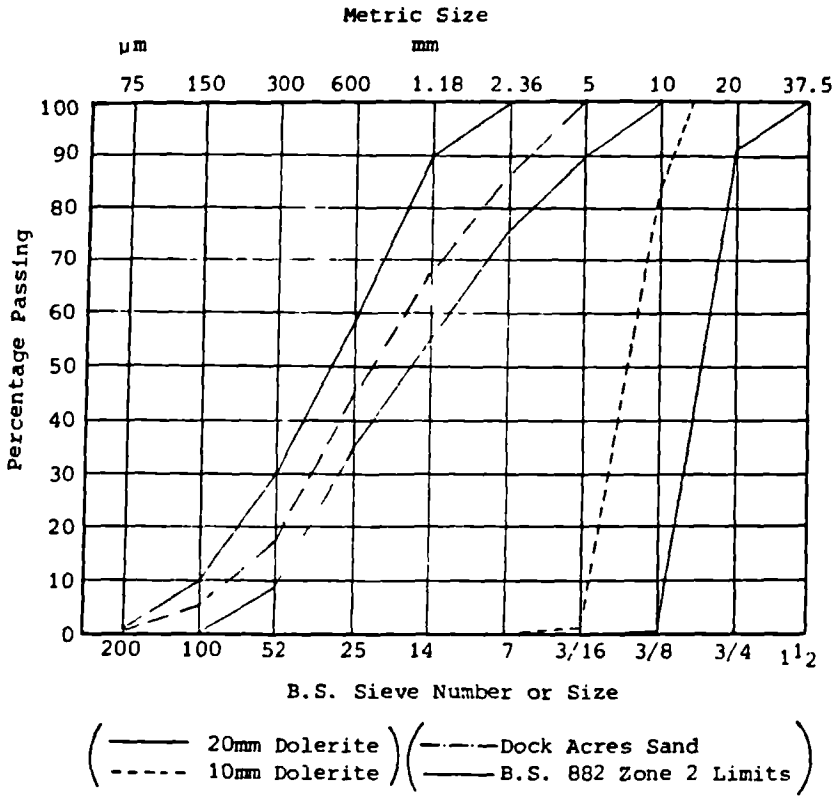

Figure 3.1: Grading curves for the aggregates.

The concrete for both "LTS" and "RTS" were mixed in a "Liner Cumflow" mixer in separate batches, each weighing 100 kg.

All the aggregates were stored in separate sealed bins and the moisture content of each aggregate was checked before it was used by drying a sample in an oven at 105 ^{o}C. The moisture content was less than 0.5% by weight for each batch.

Nine, 4 inch cubes and three, 12 inch cylinders were also cast from each batch. The details of casting and curing for the cubes and cylinders is given in Section 3.3.6 and Section 3.4.5 for each batch.

Table 3.3a gives the mean compressive strength of concrete used for the experiments, and Table 3.3b lists the specific gravity values (supplied with the materials used in the concrete mix).

DAYS AFTER CASTING CONCRETE	DAYS AFTER CASTING 7	28	90
Compressive Strength N/mm^2	36-37	52-53	62-63

Table 3.3a: Mean compressive strength of concrete.

	AGGREGATE	SAND	CEMENT	CEMSAVE
Specific Gravity	2.95	2.62	3.12	2.93

Table 3.3b: Specific gravity values of the materials used.

3.3 "LINER TEST SERIES" ("LTS")

3.3.1 INTRODUCTION

The experimental set up was designed to study in a simulated way, the effects of rapid heating applied to the steel liner of a Fast Reactor Containment Vessel. The existence and influence of pore pressures in the concrete, adjacent to and behind the liner caused by heat transmission through the liner were monitored. The deflection of the liner under the combined effects of pore pressure and temperature were recorded. The concrete temperatures and pore pressures were measured at various positions along the length of the specimen. Heating was supplied by molten lead pre heated to the required temperature inside the furnace, by a submersible spiral heater inside the lead and a rope heater wrapped around the external surface of the mild steel top ring holding molten lead. After testing, the concrete samples were extracted from the specimen and moisture distribution was determined.

3.3.2 DESIGN AND DESCRIPTION OF EQUIPMENT

The detailed design, description and the dimensions of components used in "LTS" are given in Appendix I. However, a brief account of the set up is described in this section and Figure 3.2 shows a test cell for the "LTS".

The concrete cast inside the cell represented a section of a concrete wall behind the liner of the Fast Reactor Containment Vessel. A stainless steel diaphragm (simulated steel liner) was used to contain and seal the concrete in the cylindrical cell at the top end, and a rectangular mild steel base plate at the bottom end. The stainless steel diaphragm was bolted between the mild steel top ring and the mild steel cylindrical cell. The mild steel top ring was designed to hold the molten lead, lead pouring assembly and heaters at the time of testing.

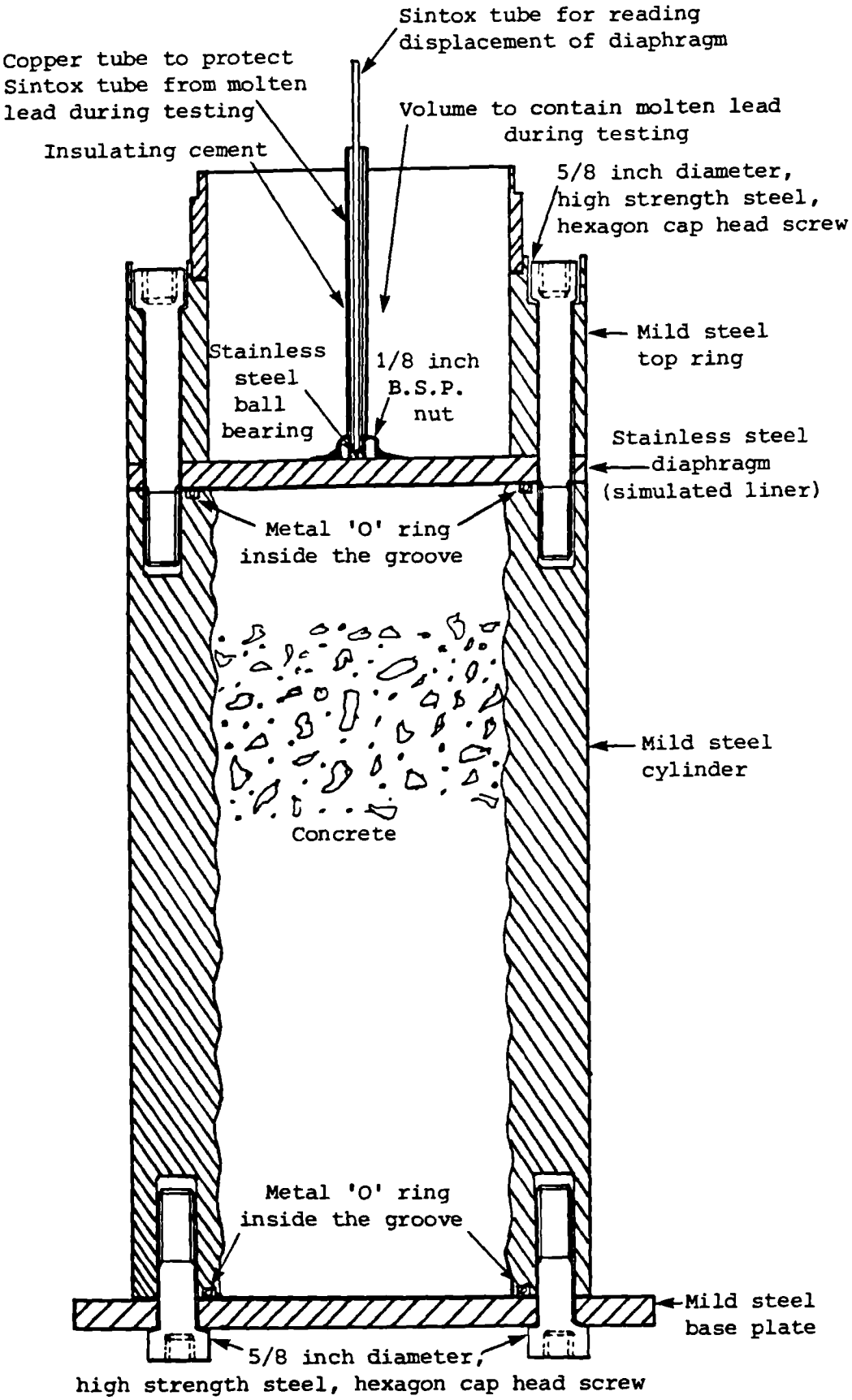

Figure 3 2.

Cross-sectional view of a typical "Liner Test Series" cell, without instrumentation.

To prevent any leakage between the stainless steel diaphragm and the mild steel cylinder, a gas filled, metal "O" ring seal was used inside a circular groove in the mild steel cylinder, as described in Appendix I, Section I.7.

Two types of base plates were used at the bottom end of the steel cylinder.

1. For sealed and partially sealed specimens, a solid rectangular plate was bolted to the bottom end of the steel cylinder. Once again a metal "O" ring provided the pressure seal for the sealed specimen and a high temperature asbestos gasket was used for sealing the partially sealed specimen between the base plate and the steel cylinder, as described in Appendix I, Section I.7.

2. To allow the pore pressure of heated concrete to escape from the unheated end, a circular hole was drilled in the centre of the steel base plate of one-end sealed specimen. No pressure seal was used between the base plate and the steel cylinder in this case.

The instrumentation was introduced through the steel cylinder walls diametrically opposite each other. Nickel/Chromium, Nickel/Aluminium thermocouples (Chapter 4, Section 4.4) measured the temperature inside the concrete, along the outside of the steel cylinder and inside the molten lead. The pore pressure of the heated concrete was recorded by casting a sintered bronze porous plate inside the concrete (Chapter 4, Section 4.2.3.2). A small bore copper tube (connected between the porous plate and the pressure measuring instruments on the instrumentation board) filled with liquid, transmitted the pore pressure of the heated concrete to the pressure accessory and the transducer. A back pressure system was incorporated on the instrumentation board, to maintain a constant volume of the liquid in the pressure measuring system, and to achieve a "no volume change" pore pressure measurement (Chapter 4, Section 4.2.6).

To keep the water in the small bore copper tube in liquid form, to prevent the increase of liquid temperature, and to avoid condensation inside the copper tube during testing, a cooling system (Chapter 4, Section 4.2.4) was designed. Cold tap water was circulated through the cooler and cooled the copper tubes passing through the cooler, when the specimen was heated during the experiment.

The central deflection of the diaphragm was measured using a transducer assembly (Chapter 4, Section 4.3), mounted on top of the Sintox tubes and steel balls. The temperatures for the inside and the outside Sintox tubes were recorded at 5 positions along the length of each tube. Then by applying a temperature correction to the experimentally measured deflection, the pressure deflection of the stainless steel diaphragm was separated from the Sintox tube expansions, as explained in Appendix IV.

The lead pouring assembly (Appendix I, Section I.9) was attached to the mild steel top ring. Three thermocouples were incorporated in this assembly, to record the temperature of the stainless steel diaphragm at the lead-diaphragm interface and inside the molten lead away from the diaphragm, and to control the thermostat of the internal submersible spiral heater.

The specimens were heated by three independent heating systems:

i. A rope heater was wrapped around the outside of the mild steel top ring.

ii. The molten lead was pre-heated to the required temperature inside the furnace and was poured on top of the stainless steel diaphragm, as described in Section 3.3.8 later.

iii. A spiral submersible heater was used inside the molten lead in the mild steel top ring

The whole assembly was thermally insulated by Kaowool glass fibre (high temperature) insulation paper (Section 3.3.3).

The testing of the test cells was carried out by clamping the handles of the steel cylinder on the test rig (Appendix I, Section I.10).

3.3.3 HEATING DESIGN AND INSULATION

As a test requirement:

- the concrete in the steel cylinder adjacent to the stainless steel diaphragm was subjected to a thermal shock, thus

establishing a thermal gradient through the length of the concrete.

- the instrumentation was introduced through the heating medium to measure the central deflection of the stainless steel diaphragm.

To fulfil the above requirements two heating methods were considered during the initial stages of the design.

a. A spiral heating element placed inside the grooves of a circular fire clay housing (Plate 3.1) was considered. It was rejected on the basis that, due to the limited space available for heating the diaphragm, the heating element had to be over rated to produce the required heating rate, and thus the heating element would normally burn out after 5 to 10 minutes of sustained heating. The high rate of heat loss to the metal assembly was a major factor in the failure of the heating element.

b. After considering the above factors it was decided to use a combination of heating techniques, as any one heating method did not provide sufficient heat in the limited space available. The final heating design chosen for the experimental programme of "LTS" consisted of the following three modes of heating.

1. Molten lead pre-heated to 650 ^{o}C in the furnace was poured into the mild steel top ring through the lead pouring assembly (Appendix I, Section I.9). After comparing the properties of lead with other metals (e.g. tin and sodium) which could be used as a heating medium, lead was selected for good thermal properties, higher density, lower cost and easier availability, as explained below:

i. Although sodium and tin have higher heat contents than lead, as shown in Figure 3.3 (Metals Handbook, 1948), tin was ruled out due to the cost and non availability of the metal, and sodium was too volatile and dangerous to be considered for these tests.

ii. However, the actual weight of the molten metal required was estimated and the total heat capacity for each metal was calculated (Chemical Engineer's Hand Book, 1973). The results (Figure 3.4 and Table 3.4) showed that the total heat capacity

of molten lead was higher than sodium and only slightly lower than tin. This was because the total weight of lead required for these experiments was higher than the other metals, due to its higher density. Table 3.5 lists the material properties of lead.

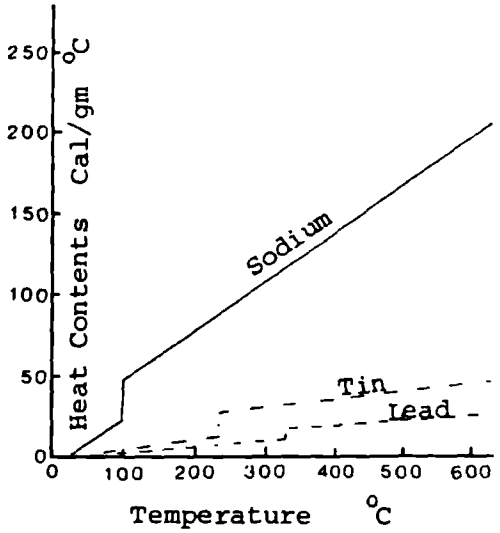

Figure 3.3:
Heat contents against temperature for Lead, Tin and Sodium.

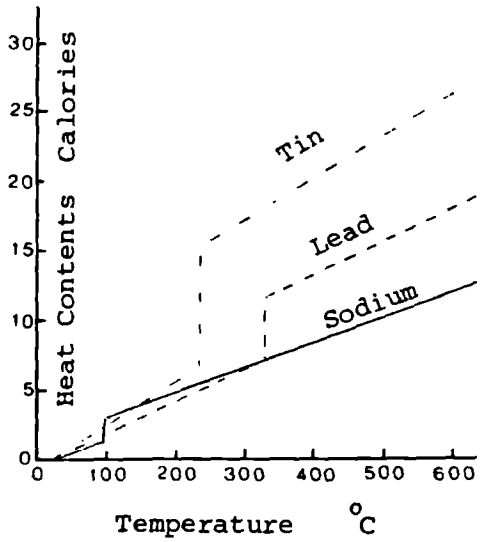

Figure 3.4
Total heat contents against temperature for Lead, Tin, Sodium.

Temperature °C	Heat Contents Cal/gm		
	Lead	Tin	Sodium
200	5.5 (s)	10.1 (s)	82.2 (l)
300	8.8 (s)	30.8 (l)	106.5 (l)
400	18.0 (l)	36.9 (l)	-------
500	21.3 (l)	43.1 (l)	-------
600	24.6 (l)	49.2 (l)	195.5 (l)
Notations in brackets are		s = solid	l = liquid

Table 3.4: Heat contents of lead, tin and sodium.

Density g/cc	Melting Point °C	Boiling Point °C	Sp. Heat at 20 °C cal/g/°C	Latent Heat of Fusion cal/g	Vapour Pressure at 815 °C Atmosphere
11.34	327.4	1740	0.031	6.26	0.0001

Table 3.5: Some of the properties of lead.

2. To keep the lead in its molten state and to increase the concrete temperature, a submersible spiral electrical heater shown in Plate-3.2 (rated at 1000 watts and 5 Amps) was selected. The electric current was controlled by a variable transformer and passed through a control box (Plate 3.5). The control box

contained an on-off switch, 2 fuses, a thermostat to control the temperature, a red indicator light, a voltmeter and an ammeter. The internal heater was screwed to the mild steel top ring and rested above the lead pouring assembly (Plate 3.7 & 3.8). Plate 3.5 shows the variable transformer, control box and the spiral heater connected to the steel top ring, without the lead pouring assembly. The variable transformer used with the heater had the capability of increasing the mains supply to 275-300 volts.

3. To compensate for heat losses through the metal surfaces, a rope heater (Plate 3.4) was clamped around the steel top ring under jubilee clips shown in Plate 3.8. The rope heater operated with a high current (45 amps) and a low voltage (55 volts). A welding machine used with 13 amp power supply provided the voltage to this heater. To monitor the current input from the mains supply to the welding machine, an ammeter was installed in the circuit between the welding machine and the mains (13 amp) plug. Before starting the test the output voltage of the welding machine was set at its lowest value. After switching the welding machine on its output voltage was increased to 55 volts. The corresponding current drawn from the mains supply was 12-12.5 amps registered by the ammeter, thus making sure that the input current to the welding machine did not exceed the limit of the mains power supply. It was established on trials that the rope heater worked satisfactorily with the procedure as described above.

The test assembly was thermally insulated by 2 layers of 1/8 inch thick Kaowool fibre glass insulation paper, wrapped around the steel cylinder and around the rope heater, which was clamped to the outside of the steel top ring. Plates 3.9 & 3.10 show the insulation paper around the test cell. The top end of the steel top ring was insulated with metal plates coated with insulating high temperature cement, as explained in Appendix I, Section I.9, and shown in Plate 3.10.

3.3.4 TESTING AND CALIBRATION OF EQUIPMENT

Each individual item of the experimental set up was tested for safety and performance. After assembling the test cell and introducing the instrumentation, the subsidiary tests were carried out to check the pressure seals and the safety of the cell. The calibration tests were

carried out for Pressure/Deflection and Temperature/Deflection of the stainless steel diaphragm, as explained in Appendix III and Appendix IV respectively.

3.3.5 FINAL PREPARATIONS FOR CASTING CONCRETE

Once the calibrations and preliminary checks had been carried out, on the cells of the "Liner Test Series" the following pre-casting preparations were performed.

1. Cells were cleaned and weighed.

2. To prevent the blockage of the small bore copper tube during concrete casting, a small diameter flexible wire was introduced inside the copper tube, and the end of the tube was temporarily sealed with the Plasticine (Plate 3.6).

3. To prevent scratching of the polished groove for the 'O' ring seal, molten wax was poured in the groove (Plate 3.6).

4. To protect the threads of the bolts from concrete during casting, polystyrene plugs were inserted in the threaded holes at the bottom end of the mild steel cylinder (Plate 3.6).

5. Cells were weighed once again after carrying out (2) to (4), as described above. In this way knowing the weight of the test cell before and after casting concrete, the actual weight of concrete was determined.

6. To monitor the strength of concrete at various ages, three cylinders (4 inch diameter x 12 inch long) and nine, 4 inch cube moulds were also prepared to cast concrete. After the final preparations the test cells were ready to cast concrete.

3.3.6 CONCRETE CASTING AND CURING

The concrete was cast in the cells in one batch for the "LTS" as explained below (casting procedure and post-casting procedure):

3.3.6.1 CASTING PROCEDURE

1. The test cells were clamped on the vibrating table upside down, as shown in Plate 3.6.

2. Great care was taken to protect the instrumentation while pouring concrete in the mild steel cylinder and only a small quantity of concrete was poured in the mild steel cylinder at a time.

3. A "Liner Cumflow" mixer was used for mixing all the concrete used for the experimental work.

4. To compact the concrete properly and to exclude air from the mix, a "Kango" was used to vibrate each test cell individually.
   Note: Although the cells were clamped on the vibrating table, a "Kango" was used for vibrations, because the table was not working.

5. The top surface of each specimen was levelled and the cells were cleaned of any loose material after vibration and casting. Table 3.6 shows the details of concrete casting.

Type of Test Series	No. of Cells	No. of Cubes	No. of Cylinders	Weight of Batch
LTS	7	9	3	100 kg

Table 3.6: Details of the casting of concrete for the "LTS".

6. The test cells were removed from the vibrating table, weighed and after covering the exposed surface of concrete, the cells were left to cure overnight.

7. Nine, 4 inch cubes and three, 12 inch cylinders were also cast from the same mix and these were vibrated in the same way as the test cells.

8. The cubes and cylinders were left to cure overnight in their moulds with the top surface covered.

3.3.6.2 POST-CASTING PROCEDURE

The following procedures were carried out 24 hours after casting.

1. Loose material was removed from the test cells which were then weighed to determine the weight of concrete in each cell.

2. The test cell was clamped on the test rig as described in Appendix I, Section I.10.

3. Wax was cleaned from the circular groove and the polystyrene plugs were removed from the threaded holes in the bottom end of the mild steel cylinder.

4. The corresponding mild steel base plates were bolted to the bottom end of each mild steel cylinder, with the respective pressure seals between the cylinder and the base plate, as expained in Appendix I, Section I.7.

5. The central hole in the mild steel base plate of the one-end sealed specimen was sealed by sticking a metal disc to the base plate, to prevent moisture loss from the concrete surface.

6. All the specimens were reweighed to provide a reference value for future weighings. Table 3.7 gives the detail of the weights of test cells and concrete, before and after casting of concrete.

Classification of cell	Weight of cell before casting 'A' kg	Weight of cell after casting 'B' kg	Weight of concrete 'B' - 'A' kg
LTS-1	51.640	58.040	6.400
LTS-2	51.740	58.223	6.483
LTS-3	51.170	57.840	6.670
LTS-4	51.540	58.107	6.567
LTS-5	51.110	57.790	6.680
LTS-6	51.230	57.850	6.620

Table 3.7: Details of the weighing of concrete.

7. The sealed specimens were then cured in the curing room.

8. After demoulding, the cubes and cylinders were weighed and placed under water for curing.

3.3.7 SET UP OF SPECIMEN FOR TESTING

The test cell was taken out of the curing room three to four days prior to testing. It was weighed to measure any moisture loss during the curing period. The recorded weight loss was not more than 0.6 grams for any specimen, which repesents less than 1 % of the concrete total water content. This showed the adequate sealing of the specimens. The following procedure was carried out for the preparation of a specimen before testing and Plates 3.7 to 3.10 show the set-up of a specimen.

1. The test cell was secured on the test rig, as explained in Appendix I, Section I.10.

2. The Plasticine and the flexible wire (used for temporarily blocking the small bore copper tubes before casting concrete, Section 3.3.5) were removed from the copper tubes.

3. To fill the small bore copper tube and porous plate with liquid (water), a thin flexible tube was used with a hypodermic syringe. The flexible tube was attached to the needle, by slipping a sleeve onto the end of the needle and the flexible tube. The bond between the sleeve, needle and the flexible tube was provided by silicone rubber. The thin flexible tube was introduced inside the bore of the small bore copper tube pushing it right against the porous plate cast inside the concrete. The length of the copper tube between the cooler and the cone fitting at the end of the copper tube, was bent upward forming a smooth corner "L" shape. The cone fitting at the end of the copper tube after bending faced upward.

4. The lead pouring assembly without thermocouples was placed in position and was screwed at the top end of the mild steel top ring, as described in Appendix I, Section I.10.

5. The submersible spiral heater (Section 3.3.3) was introduced inside the mild steel top ring, and it was screwed to the outside of the top ring.

6. The external rope heater was secured around the outside diameter

of the top ring using two Jubilee clamps (Plates 3.7 & 3.8).

7. A thermocouple was placed underneath the external rope heater and three thermocouples were attached to the outside of the mild steel cylinder, one each at the top and the bottom end of the cylinder and the third halfway between the other two. Once again Jubilee clamps were used to clamp the thermocouples to the steel cylinder.

8. The plate carrying three thermocouples as an integral part of the lead pouring assembly, to measure the lead temperature and the temperature of the stainless steel diaphragm (Appendix I, Section I.9), was screwed to the lead pouring assembly.

9. The copper tube protecting the central Sintox tube from the molten lead (Appendix I, Section I.8), was screwed into the brass nut cemented to the middle of the stainless steel diaphragm. The outer surface of the brass nut and the copper tube was also completely covered with high temperature insulating cement, as shown in Plate 3.8.

10. The hypodermic was filled with distilled de-aerated water and by connecting it to the needle attached to the flexible tube, water was continously forced into the small bore copper tube, expelling the air out of the system (Plate 3.9). Once the water started to flow out of the copper tube free of air, the flexible tube was pulled out very slowly while still pushing the water into the copper tube. In this way the copper tube was completely filled with water and the porous plate was partially filled with water.

11. The extension copper tubes used for connecting the pressure fittings of the test cell to the pressure instrumentation board, were screwed to the fittings of the ball valve provided for connecting the instrumentation board and the specimen (Chapter 4, Section 4.2.6). Distilled and de-aerated water was allowed to flow through the copper tubes under a hydraulic head, by keeping the end of the tube under water in a beaker and by opening the appropriate valves (Chapter 4, Section 4.2.7). Each copper tube was then screwed to the corresponding pressure fitting on the specimen, while water was still flowing through the tube. After the removal of air each fitting was tightened individually for

every pressure point. The valves on the instrumentation board were shut and the mercury level in the Perspex blocks was adjusted and marked. Finally before the testing of the specimen the valve nearest to the specimen was opened and the whole set up was ready to measure the pore pressure.

12. All the thermocouples and pressure transducers were connected to the data logger and the chart recorder (Chapter 4, Section 4.4.2).

13. A 1/4 inch diameter high strength nylon tube was attached to the cold water tap and the bottom fitting of the cooler. One end of another similar nylon tube was connected to the top fitting of the cooler, while the other end of this nylon tube was placed and secured in the sink for the discharge of the circulated water from the cooler, as described in Chapter 4, Section 4.2.7.1.

14. The deflection measuring assembly (Chapter 4, Section 4.3) was set up and connected to the data logger and the chart recorder.

15. The top open end of the lead pouring assembly was covered by placing two steel plates coated with high temperature insulating cement. These coated plates also protected the instrumentation from the splashing of the molten lead, while pouring the lead at the start of the test.

16. The lead used for heating was weighed in the crucible and was placed inside the furnace for heating. The weight of the lead used for each test cell is shown in Table 3.8.

	LTS-1	LTS-2	LTS-3	LTS-4	LTS-5	LTS-6
Weight of Lead (kg)	8.009	8.008	7.995	8.015	8.006	8.012

Table 3.8: Weight of lead used for each test of the "LTS".

17. To heat the lead, the temperature of the furnace was set to 675 ^{o}C, and a Nickel/Chromium Nickel/Aluminium thermocouple was used to record the lead temperature inside the furnace.

18. The test cell, as shown in Plate 3.10 was then ready for testing.

3.3.8 TEST PROCEDURE

The actual testing was normally performed the day after setting up the test cell, as described in the previous section, and the following test procedure was carried out.

1. To heat and melt the lead, the furnace was switched on 2-3 hours before pouring the molten lead into the mild steel top ring and the lead temperature was continously monitored inside the furnace.

2. The external rope heater and the internal submersible spiral heater were plugged into their respective electrical circuits (Section 3.3.3), without switching them on.

3. All the instrumentation and the electrical connections were finally checked. The pressure and the deflection measuring devices were zeroed and were ready to be used.

4. The tap water was turned on to circulate cold water through the cooler to cool the small bore copper tubes passing through it (Chapter 4, Section 4.2.7.1), just before switching the external heater on.

5. Once the temperature of the lead inside the furnace had stabilised, the external rope heater, data logger, chart recorder, and a stop watch were simultaneously switched on.

6. The voltage of the welding machine was adjusted while monitoring the current on an ammeter in the circuit (Section 3.3.3).

7. Approximately 9 minutes after putting the external heater on, the internal submersible spiral heater was switched on. The voltage and current for the internal heater is shown in Table 3.9.

	LTS-1	LTS-2	LTS-3	LTS-4	LTS-5	LTS-6
VOLTAGE V	258	240	249	255	252	259
CURRENT A	4.7	4.4	4.5	4.6	4.5	4.7

Table 3.9: Voltage and current used for each test of the "LTS".

8. The furnace was switched off and the crucible containing molten lead was pulled out of the furnace onto a platform erected outside the furnace. The top layer (of froth) from the surface of the molten lead was removed, and then using a carrying rod with a hook, the crucible was carried to the test rig. The crucible was tilted by slipping a pipe over one of the legs of the crucible (Figure 3.5), and lead was poured into the funnel of the lead pouring assembly (Appendix-I, Section I.9). The whole procedure was performed swiftly wasting minimum time. The time taken (approximately) to take the lead out of the furnace until pouring and time for pouring can be seen in Table 3.10.

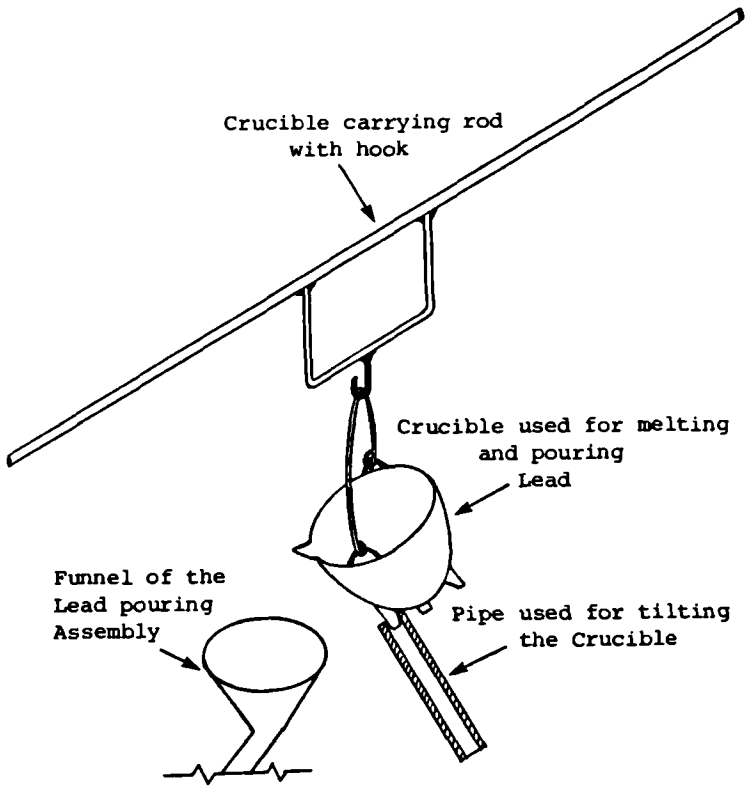

Figure 3.5: Crucible and carrying set-up used for pouring molten lead into the funnel of the lead pouring assembly.

TIME FOR	LTS-1 sec	LTS-2 sec	LTS-3 sec	LTS-4 sec	LTS-5 sec	LTS-6 sec
Taking Lead out	59	54	57	58	54	55
Pouring Lead	24	21	25	24	23	22

Table 3.10: Times for taking lead out and pouring lead.

9. The lead pouring procedure was carried out by three persons, while the fourth person recorded the times. I was therefore free to concentrate on the movement of moisture in or out of the porous plate by monitoring and adjusting the mercury level in the Perspex "U" tube on the pressure instrumentation board (Chapter 4, Section 4.2.6). As soon as the mercury level changed in any "U" tube, a back pressure was applied to level the mercury in the "U" tube (Chapter 4, Section 4.2.7), thus making sure no water movement into or out of the porous plate had taken place.

10. To keep the mercury level unchanged in the Perspex "U" tubes in the early stages of the test, back pressure was applied frequently.

    Plate 3.10 shows a test in progress.

11. After reaching the required objectives of the tests (Chapter 5, Section 5.1), heaters were switched off and were disconnected from their supplies.

12. The deflection measuring assembly and the Sintox tubes were removed from the test cell and all the ball valves were closed on the instrumentation board.

13. The copper tube protecting the central Sintox tube from the molten lead (Section 3.3.7 (9) & Appendix I, Section I.8), was pulled out of the lead by breaking the bond between the brass nut and the stainless steel diaphragm. To prevent the molten lead entering into the copper tube through the submerged end of the tube, the top end of the tube was blocked.

14. The internal submersible spiral heater and the lead pouring assembly was unscrewed and removed from the test cell, leaving

the specimen to cool overnight for dismantling.

15. Once the specimen had cooled down, the tap water was shut off and the nylon tubes were disconnected from the water tap and the cooler. The water from the cooler was discharged into a container placed under the cooler.

16. The extension copper tubes connected between the instrumentation board and the fittings at the end of the small bore copper tubes were disconnected from the fittings of the small bore copper tubes, and the fittings at the end of the copper tubes were sealed by screwing a blank nipple and union nut to the fitting.

17. After disconnecting the thermocouples from the data logger and the chart recorder, the fibre glass insulation paper, external rope heater and thermocouples clamped to the outside of the steel cylinder were removed.

18. The (1/8 inch B.S.P.) fittings screwed to the mild steel cylinder for passing the small bore copper tube and used for pressure sealing, were unscrewed and the cooler along with the copper tubes was removed from the specimen. The threaded holes in the steel cylinder (after unscrewing the fittings) were temporarily blocked by sticking masking tape over the holes.

19. To remove the mild steel top ring and the stainless steel diaphragm from the steel cylinder, the twelve 5/8 inch high strength steel hexagon cap head screws holding them together were unscrewed, and the concrete surface was exposed at the top end of the specimen. The exposed concrete surface was covered and sealed temporarily with masking tape.

20. Similarly the twelve 5/8 inch high strength steel hexagon cap head screws, holding the mild steel base plate to the mild steel cylinder were unscrewed and the base plate was removed from the cylinder. The concrete surface exposed at the bottom end of the specimen was also temporarily sealed with masking tape to prevent moisture loss during the extraction of the concrete, as explained in the next section.

21. The specimen was removed from the test rig and the only

instrumentation still attached to the mild steel cylinder was the thermocouples (used for measuring the concrete temperature). These thermocouples could not be taken out while the specimen was still on the test rig, due to lack of working space between the test cell and the rig (Plate 3.7). The thermocouples introduced inside the steel cylinder through the pressure glands screwed to the outside of the cylinder (Appendix-I, Section I.2), were removed from the cylinder by unscrewing the pressure glands. The threaded holes left vacant by the removal of the thermocouple fittings were temporarily blocked by covering the holes with masking tape.

The steel cylinder was machined to extract the concrete samples to determine the evaporable and the non-evaporable water contents, as described below.

3.3.9 CONCRETE EXTRACTION FROM STEEL CYLINDER, AND MEASUREMENT OF FINAL WATER DISTRIBUTION

Once the specimen was cooled down and all the instrumentation was removed from the steel cylinder, the cylinder was prepared for the extraction of the concrete samples.

To accommodate the steel cylinder on the cutting machine, the handles welded to the outside of the cylinder (Appendix I, Section I.2) were cut and the cylinder was clamped to the machine ("Miller"), as shown in Plates 3.11 & 3.12. Two 1/4 inch slots were machined opposite each other and to avoid heating of the metal, a cooling liquid was used to cool the metal during machining. The cutting speed and the depth of each cut were kept to a minimum . After each cut, metal was also allowed to cool before starting a second cut.

As soon as the cutter touched the concrete inside the steel cylinder, cutting was stopped and the cylinder was removed from the "Miller". The remaining portion of the steel cylinder wall was then split by pushing metal wedges in both the machined slots.

After splitting the steel cylinder the concrete was extracted from the cylinder in three modes, as explained below.

a. Firstly, one half of the cylinder was separated from the concrete

(Plate 3.13) while the concrete remained stuck to the other half, as shown in Plate 3.14. Then the concrete left in the other half of the steel cylinder, was removed by tapping with a hammer. Plate 3.15 shows the concrete sample extracted in this way.

b. Secondly, the complete concrete cylinder seen in Plate 3.16, stuck to the half segment (as (a) above) of the steel cylinder could not be removed by hammering and it was left in the split tube segment. Concrete samples were taken from this concrete cylinder, as described later in this section.

c. Thirdly, during the splitting of the steel cylinder the concrete split down the middle (Plate 3.17), with half the concrete stuck in each segment (Plate 3.18). It was not possible to remove the concrete from either segment; therefore it was left stuck to the steel cylinder and samples were extracted, as explained later in this section.

The concrete extracted from the cylinder was quickly sealed by cling film, aluminium foil and rubber sealant to avoid moisture loss from the concrete surface. The concrete samples were obtained from the concrete extracted out of the steel cylinder (discussed above), using the following procedures.

1. The concrete cylinder (Plate 3.15) which was extracted from the steel cylinder in the first instant (as (a) above), was cut with a diamond bladed masonary saw using a petroleum fraction as a coolant. The petroleum fraction used did not react with the concrete or change the water contents of the samples. The sizes and the locations of the cut slices were recorded and are presented later in this section (Table 3.11). Plate 3.19 shows typical slices cut from a concrete cylinder.

2. One and a half inch cores, as shown in Plates 3.20 & 3.21 were taken from the concrete left as a cylinder (in (b) above) and from the concrete split through its length (in (c) above), as shown in Plate 3.22. These samples were cored with a diamond edge coring drill by using the same petroleum fraction (as discussed in (1) above). Plates 3.20 to 3.22 also show the position of cores taken out from the specimen and Table 3.11 lists the mode of extraction and the types of samples obtained

for each test.

(i) Concrete cylinder, (ii) Concrete cylinder left in one segment (iii) Half of the concrete cylinder left in each segment

	LTS-1	LTS-2	LTS-3	LTS-4	LTS-5	LTS-6
Means of Extraction	(i)	(ii)	none	(iii)	(iii)	(iii)
Type of Samples	discs	cores	none	cores	cores	cores

Table 3.11: Modes of extraction and types of samples obtained from each test of the "LTS".

To prevent redistribution of water due to cooling, the time spent between the end of the test and the removal of the concrete sample was kept to a minimum.

3.4 "RELEASE TEST SERIES" ("RTS")

3.4.1 INTRODUCTION

Tests were carried out to monitor the pore pressure, temperature and weight loss, in uniformly heated concrete by breaking the seal of the specimen periodically. In order to investigate the relationship between pore pressure of concrete and loss of weight at constant temperature, similar type of tests were carried out by Sharp(1971) and Chapman(1976) on 4 inch diameter and 4 inch long specimens as previously described in Chapter 2.

The maximum test temperature used by Chapman (1976) for heating his specimens was 175 ^{o}C. The maximum test temperatures for the "RTS" specimens here was 350 ^{o}C, and the pore pressures generated inside the heated concrete at this temperature were approximately 3500 psi (24-25 N/mm^2). Therefore, to reduce the total force on the bolts and the end plates of the test cell, and to design the test cell for a safety factor greater 1.5, the specimens used for these experiments were 3 inch (76.2mm) diameter x 4 inch (101.6mm) long.

To test the behaviour of the instrumentation, the individual components of the test cells at high temperature and pressure, and the integrity of the complete test cell, two pilot tests were carried out.

It was from these tests that the sealing conditions and pressure release procedure described in this chapter were checked. The specimens were heated in the furnace.

3.4.2 DESIGN AND DETAILS OF EQUIPMENT

Appendix II describes the detailed design of the "Release Test Series", however, a brief description of the set up (Figure 3.6) is also given in this section.

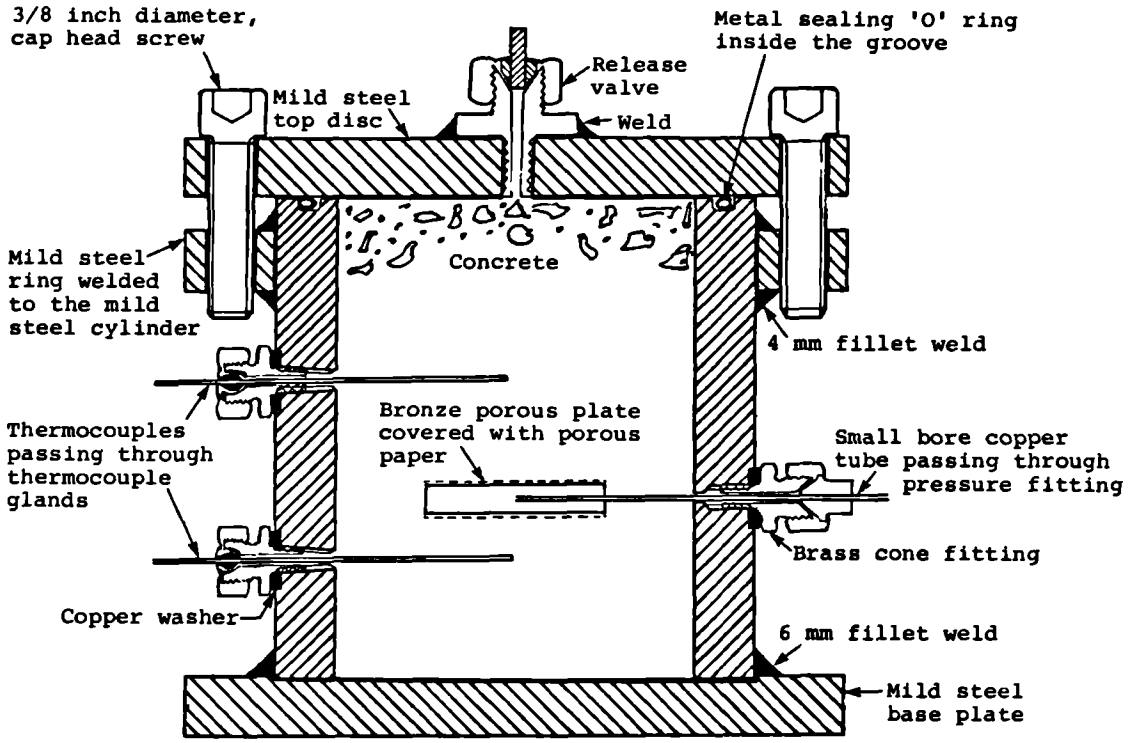

Figure 3.6: Cross-sectional view of a typical "Release Test Series" specimen, with instrumentation.

A mild steel cylinder with a mild steel disc welded on to its bottom end (Appendix II, Section II.2) was designed to test the concrete specimen. A mild steel ring was welded to the outside of the steel cylinder. The assembly was completed by a mild steel disc at the top end, bolted to the steel circular ring, using twelve 3/8 inch diameter high strength steel hexagon cap head screws. A metal "O" ring (gas filled), as shown inside a circular groove in Figure 3.6 and explained in Appendix II, Section II.4, was used to seal the joint between the top disc and the steel cylinder.

A release valve was welded to the centre of the top disc, to release the moisture (Appendix II, Section II.3). The instrumentation was introduced through the walls of the steel cylinder, diametrically opposite each other, to measure the temperature and the pore pressure of the concrete. The temperature inside the concrete was measured with two Nickel/Chromium Nickel/Aluminium thermocouples (Chapter 4, Section 4.4), inserted through the pressure glands (Appendix II, Section II.2).

A circular bronze porous plate connected to a small bore copper tube was cast inside the concrete to measure the pore pressure of the heated concrete (Chapter 4, Section 4.2.3.1). These copper tubes were passed through a cooler to prevent the temperature of the water rising inside the copper tubes (Chapter 4, Section 4.2.4.1). The porous plate was covered with a porous paper to prevent clogging of the pores of the porous plate during the casting of the concrete. The porous plates and the copper tubes were connected to the pressure measuring instruments (Chapter 4, Section 4.2.7), with the help of extension copper tubes.

The test cell was secured to a test rig (Appendix II, Section II.7), which was used to hold the cell during testing. The use of a test rig reduced the danger of damaging the instrumentation (e.g. copper tube or thermocouples).

3.4.3 HEATING DESIGN

A muffle furnace was used to heat the specimens of the "RTS". The original door of the furnace was removed and a new door constructed in two parts (Plate 3.27) was used with the furnace. The door was constructed with Tri-Mor (a high strength material capable of withstanding temperature up to 1100 ^{o}C).

The upper half of the door was screwed to the existing fittings of the original door on the furnace and the lower half of the door rested on the platform in front of the door opening of the furnace, as shown in Plate 3.28. The new door worked as an excellent barrier to shield the instrumentation from the radiant heat of the furnace.

3.4.4 EQUIPMENT TESTING AND PREPARATION BEFORE CASTING CONCRETE

All the cells of the "RTS" were hydraulically proof tested to an internal pressure of 3800 psi (26-27 N/mm^2) at room temperature. Any fitting showing signs of leakage was replaced with a new fitting and re-checked. The weld around the bottom plate was also tested for pressure leaks. After eliminating the leakage through seals and fittings, the cells were ready for final preparation before casting concrete and the following procedure was carried out.

1. The cells of the "RTS" were cleaned and weighed.

2. A small diameter flexible wire was inserted inside the small bore copper tube up to the bronze porous plate, and the pressure fitting at the end of the copper tube was sealed by Plasticine to prevent bleeding of mix water during casting and loss of moisture while curing (same as (2) in Section 3.3.5).

3. To protect the ground surface of the groove at the top of the steel cylinder while casting concrete, the groove was filled with molten wax. Plate 3.22 shows the groove filled with the wax.

4. Each cell was finally cleaned and weighed after addition of (2) and (3) described above.

5. Three cylinders and nine cube moulds were prepared in the same way as (6) in Section 3.3.5.

3.4.5 CONCRETE CASTING, SEALING AND CURING OF SPECIMEN

The "RTS" specimens were cast in one batch using the mix design, as described in Section 3.2. The casting and post-casting procedure described below was similar to that for the "LTS". Table 3.12 lists casting programme and details.

Type of Test	No. of Cells	No. of Cubes	No. of Cylinders	Weight of Batch
"RTS"	15	9	3	100 kg

Table 3.12: Details of concrete casting for the "RTS" specimens.

3.4.5.1 CASTING PROCEDURE

1. The unfilled test cells were clamped to the vibrating table, as shown in Plate 3.23.

2. Great care was taken to protect the instrumentation while pouring the concrete in the cylinder, and only a small quantity of concrete was poured at a time to achieve good compaction.

3. A "Liner Cumflow" mixer was used for mixing concrete, as described in (3) of Section 3.3.6.

4. A Kango hammer was used for vibration, as explained previously in (4) of Section 3.3.6.

5. The top surface of the concrete in each test cell was levelled (Plate 3.24).

6. The test cells were removed from the vibrating table and the exposed surface of concrete was then temporarily covered and the cells were left for curing overnight.

7. Nine cubes and three cylinders were cast, vibrated and cured the same way, as explained in (7 & 8) of Section 3.3.6.1.

3.4.5.2 POST-CASTING PROCEDURE

One day after casting, the following post casting exercise was carried out.

1. The test cells were cleaned, and each cell was weighed to determine the weight of concrete in the cell, as given in Table 3.13.

Classification of cell	Weight of cell before Casting 'A' gm	Weight of cell after casting 'B' gm	Weight of Concrete 'B' - 'A' gm
RTS-01	5642.1	6806.5	1164.4
RTS-02	5576.6	6736.1	1158.5
RTS-03	5548.6	6695.6	1147.0
RTS-04	5693.2	6858.5	1165.3
RTS-05	5451.2	6597.7	1146.5
RTS-06	5718.5	6865.5	1167.0
RTS-07	5701.7	6866.6	1164.9
PT-01	5645.8	6798.0	1152.2
PT-02	5645.6	6802.9	1157.3
CT-01	5576.7	6750.2	1173.5
CT-02	5574.8	6732.5	1157.7

Table 3.13: Weight measurements for the "RTS" specimens.

2. The base plate welded to the mild steel cylinder was temporarily screwed to a wooden table whilst bolting the top plate to the steel cylinder.

3. The wax used for protecting the polished surface of the groove (Section 3.4.4 (3)) was removed from the groove.

4. Then the metal "O" ring was placed inside the groove and it was bolted between the steel disc at the top end and the steel cylinder (Appendix II, Section II.4). The maximum recommended torque of 40 ft-lbs was applied to each bolt using a torque wrench and going up in four steps (10, 20, 30, 40 ft-lbs).

5. The specimens were re-weighed to provide the reference values for future weighings.

6. All the specimens were kept in the curing room in sealed conditions.

7. The cubes and the cylinders cast with this batch were demoulded, weighed and placed under water for curing.

3.4.6 PREPARATION OF SPECIMENS BEFORE TESTING

To prepare a specimen for testing, the test cell was taken out of the curing room two days before the start of the test, and the following procedure was carried out for its preparations.

1. The specimen was weighed to see if any moisture had been lost during the curing time. There was no weight loss of any

significance to report.

2. The specimen was mounted on the test rig (Appendix II, Section II.7) designed to hold the test cell, and the thermocouples were secured to the rig, as shown in Plate 3.25. The Plasticine covering the fitting at the end of the small bore copper tube of the the specimen and the flexible wire inserts (Section 3.4.4 (2)) were removed from the copper tube.

3. The copper tube of the specimen was filled with water, as described in Section 3.3.7.

4. The copper tubes and the ball valve between the specimen and the pressure measuring instruments on the instrumentation board were filled with water as below:

a. An extension copper tube used between the valve and the small bore copper tube of the specimen (Figure 3.7) was connected to the bottom end of the valve.

b. The other end of the extension copper tube was placed under water in a beaker.

c. The top end of the valve was connected to the instrumentation board (Chapter 4, Section 4.2.7.2).

d. Water was made to flow through the system until the air was expelled from all the components (Chapter 4, Section 4.2.7.2).

e. The end of the copper tube was removed from the water and it was connected to the fitting at the end of the copper tube of the specimen (Figure 3.7), while water was still flowing through the system.

f. After making sure that all air was removed from the system, the fitting (mentioned above) was tightened and the valve was closed.

g. The fitting at the top end of the valve (Figure 3.7) was unscrewed and the specimen was disconnected from the instrumentation board.

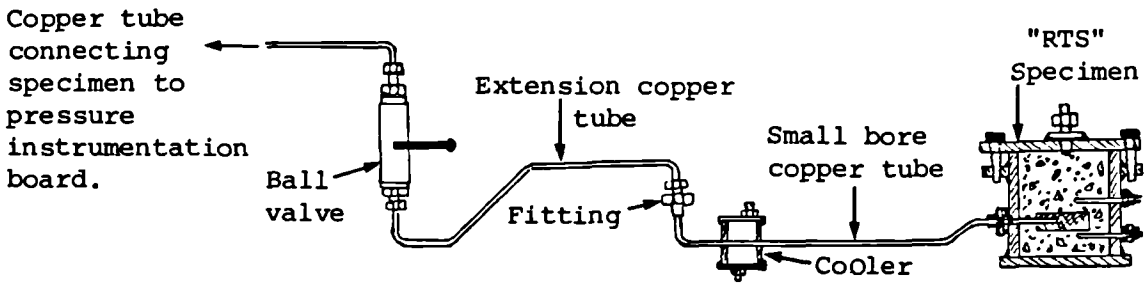

Figure 3.7: Pressure measuring system attached to a "RTS" cell.

5. The cooler used for cooling the copper tube (Chapter 4, Section 4.2.4.1) required the circulation of cold water, by connecting it to the cold water tap during testing. However, it was also necessary to disconnect the water supply for weighing the specimen. Therefore, to prevent introducing errors in weight measurements, a reliable and robust system was incorporated on the test rig (Appendix II, Section II.7). Two ball valves were provided in this system. One valve was placed between the water supply and one end of the cooler, and a similar valve was positioned between the sink and the other end of the cooler. Finally, flexible nylon tubes were used to connect the bottom fitting of each valve to the appropriate fitting of the cooler (Plate 3.25), whilst similar nylon tubes were used to connect the remaining fitting of each valve to the cold water tap or the sink.

6. To monitor the temperature of the copper tube, just outside the furnace door and close to the cooler, a thermocouple was clamped to the cooler under the Jubilee clamp.

7. The test rig with the test cell clamped to the rig was placed inside the furnace for final preparations before testing.

8. To measure the pore pressure of concrete during testing, the specimen was once again connected to the pressure instrumentation board, as described in (4) above and the appropriate ball valves were opened (Chapter 4, Section 4.2.7.2).

9. The nylon tubes between the water tap and the valve, and the sink and the valve, as explained in (5) above, were attached to the valves. The cold water tap was then opened and the water was allowed to flow through the cooling system. Plate 3.28 shows a

"RTS" specimen placed inside the furnace and connected to all the instrumentations.

10. For taking the intial weight of the specimen before switching the furnace on, the valves protecting the cooler were shut, the cold water tap was closed and the nylon tubes were disconnected from the valves.

11. After closing the ball valve (on the test rig), the fitting of the extension copper tube used for connecting the ball valve (on the test rig) to the instrumentation board was disconnected and a blank nipple was screwed to the top fitting of the valve instead.

12. All the thermocouple leads and wires were folded and resting them on the test rig, the specimen was weighed on the balance (Plate 3.26). This was the initial weight of the specimen and the specimen was weighed for recording the weight before and after each release process, as described in Section 3.4.7; hence knowing all the weights the weight loss due to release of moisture was determined.

13. The specimen was replaced in the furnace after weighing. All the thermocouples were plugged in the appropriate channels of the data logger and the chart recorder.

14. To connect the instrumentation board and the cold water tap to the specimen, procedure (8) and (9) described earlier in this section were repeated.

15. Finally the furnace door was closed and the specimen was ready for testing, as seen in Plate 3.29.

3.4.7 TEST PROCEDURE

Before switching the furnace on for the start of the test, all the fittings, joints and connections were checked and the pressure transducer was zeroed. Although the furnace door was adequate to thermally insulate (from heat) the instruments and the components of the "RTS" specimen outside the furnace (Section 3.4.3), an additional thermal insulation (in the form of Kaowool glass fibre mat) was placed between the furnace door and the test cell during testing.

The data logger and the chart recorder were switched on for a short time, to monitor the temperature and the pore pressure of the specimen before the start of the test. After taking the measurements the data logger and the chart recorder were switched off. The specimen was then ready for the start of the test and the following test procedure was carried out.

1. The furnace, data logger and chart recorder were switched on to start the test.

2. The readings of temperature, pore pressure and back pressure and time were recorded at predetermined intervals on the data logger using a time subroutine incorporated in the computer program. However, the pore pressure, the back pressure and the temperature with time were additionally recorded on the chart recorder continously.

3. As soon as the mercury level changed in the Perspex "U" tube, a back pressure was applied to the porous plate (Chapter 4, Section 4.2.7.2).

4. On reaching the test temperature, the ball valve on the test rig used to connect the specimen and the pressure measuring instruments on the instrumentation board (Section 3.4.6 (4)) was shut.

5. The pressure measuring system, the back pressure system and the extension copper tube connecting the valve (described in (4) above) to the instrumentation board were de-pressurised, and the valves number 1, 2 and 3 on the instrumentation board (Chapter 4, Section 4.2.6) were shut.

6. The specimen was disconnected from the instrumentation board, as described in Section 3.4.6 (11).

7. The thermocouple leads were disconnected from the recording instruments and were placed on the test rig.

8. The valves between the cooler and the water supply on the test rig were closed, the cold water tap was shut and the nylon tubes

connected to the top end of the valves were disconnected, as explained in Section 3.4.6 (10).

9. The specimen was removed from the furnace and weighed (Plate 3.26). It was then replaced back in the furnace and the furnace door was closed. The specimen was weighed to check if any weight loss had occurred during the heat-up period to the test temperature.

10. The specimen was connected to all the components by repeating the procedures (8), (9) and (13) as decribed in Section 3.4.6.

11. The time taken to take the specimen out of furnace until replacing it back in the furnace was recorded and generally the whole procedure did not take longer than 2 minutes.

12. The same procedure of recording all the test parameters and the application of the back pressure, as (2) and (3) above was repeated.

13. On reaching the steady-state conditions (constant readings of pressure with time), the release valve (Appendix II, Section II.3) was opened inside the furnace, and a small amount of moisture was allowed to escape, before closing the release valve. The time taken for the release of the moisture was recorded.

14. To disconnect and remove the specimen for measuring the weight loss due to the release of moisture, procedures (4) to (9) described above were repeated.

15. The specimen was replaced in the furnace after weighing and procedures (10) to (13) described above were repeated for further testing.

16. The test procedures discussed earlier in this section were repeated until no more moisture could be lost by using the same moisture release techniques.

17. In the early part of the tests, the release valve was left open for a few seconds to allow the fluid to escape. But in the later

stages of the experiments, the release valve was left opened for a much longer period to measure any loss of weight from the specimen (because most of the moisture had been lost from the concrete by reaching this stage).

18. Near the end of the experiment when the pore pressure in the concrete was just above atmospheric pressure, it was necessary to leave the release valve open for more than 30 minutes to attain a weight loss of one gram.

19. The test temperature of the specimen was cycled by $\pm 10\ ^{o}C$, when the recorded pore pressure of concrete was below the saturated vapour pressure of water for the corresponding temperature.

20. The test was considered complete once no weight loss was recorded after leaving the release valve open for more than an hour.

21. The furnace was switched off and the valve in the pressure measuring system was shut. However, the cold water was left circulating through the cooler and the specimen was left inside the furnace to cool.

22. Finally, the test cell was prepared to remove the concrete for further test, as described in the next section.

3.4.8 CONCRETE EXTRACTION FROM THE TEST CELL FOR FURTHER TESTING

Once the specimen had cooled down, the water supply to the cooler was shut off and the valves letting the water in and out of the cooler were closed. All the attachments were disconnected from the test cell and the cell was removed from the test rig. The small bore copper tube was broken close to the mild steel cylinder, the copper tube fitting on the cylinder was unscrewed and the threaded hole was temporarily sealed with masking tape. The two thermocouples were left intact with the specimen. The steel disc at the top end was removed from the mild steel cylinder and the exposed concrete surface was also temporarily sealed by covering it with masking tape.

The specimen was transported to the workshop for cutting the mild steel cylinder and the following procedure was applied for the removal of concrete.

1. The weld between the base plate and the steel cylinder was machined off on the lathe, thus removing the base plate from the cylinder. Once again the exposed concrete surface was sealed temporarily, with masking tape.

2. The cylinder was secured to an angle plate and after clamping it to the "Miller" (Plate-3.30), the cylinder was cut in three places (Plate 3.31). One cut was made either side of the thermocouples on the cylinder and the third cut was made through the cylinder diametrically opposite the thermocouples.

3. After machining, the cylinder was split to extract the concrete (Plate 3.32).

4. The concrete sample was extracted complete with the two embedded thermocouples still screwed to the cut strip of the steel cylinder (Plate 3.33).

The concrete sample was weighed immediately after its removal from the test cell and it was then placed in the furnace for further heating at the test temperature. The thermocouples were connected to the data logger for recording the temperature. The concrete sample was removed periodically to measure the weight loss. Heating was stopped when no more weight loss was measured and the experiment was concluded. The test results and the result of the weight loss at test temperature are described in Chapter 6, Section 6.3.2.

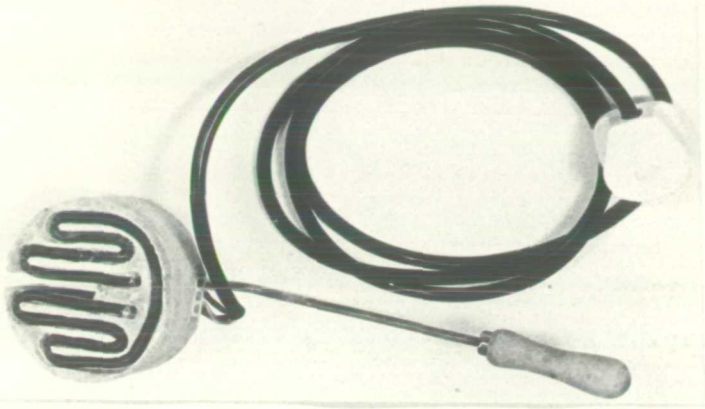

PLATE 3.1: HEATING ELEMENT IN CLAY HOUSING

PLATE 3.2: ELECTRICAL, SPIRAL HEATER

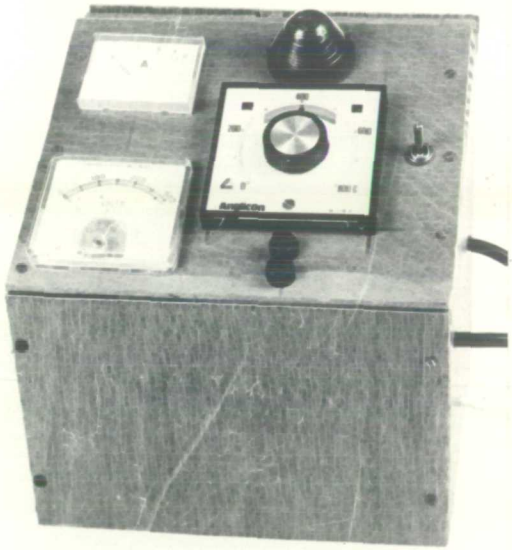

PLATE 3.3: CONTROL BOX FOR SUBMERSIBLE SPIRAL HEATER

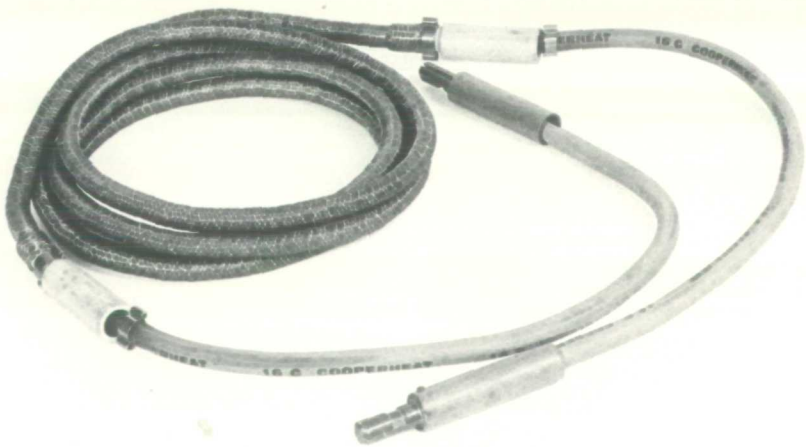

PLATE 3.4: ROPE HEATER

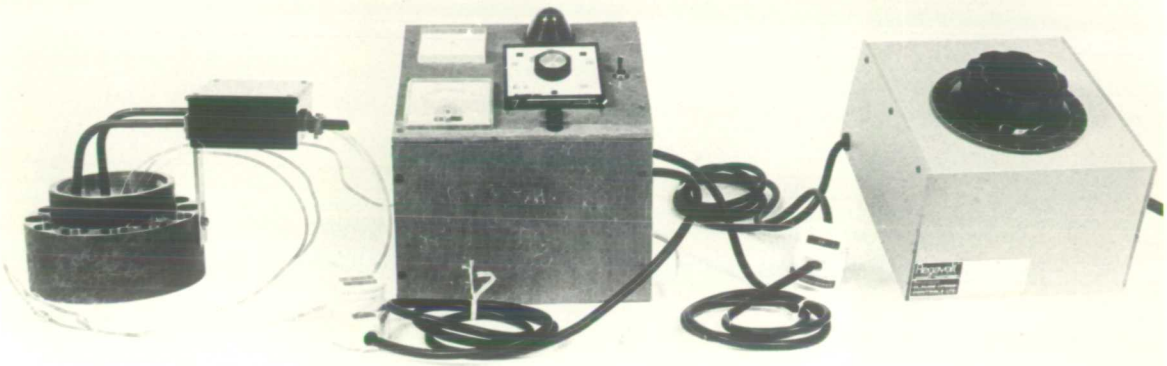

PLATE 3.5: VARIABLE TRANSFORMER, CONTROL BOX AND SPIRAL HEATER CONNECTED TO THE MILD STEEL TOP RING

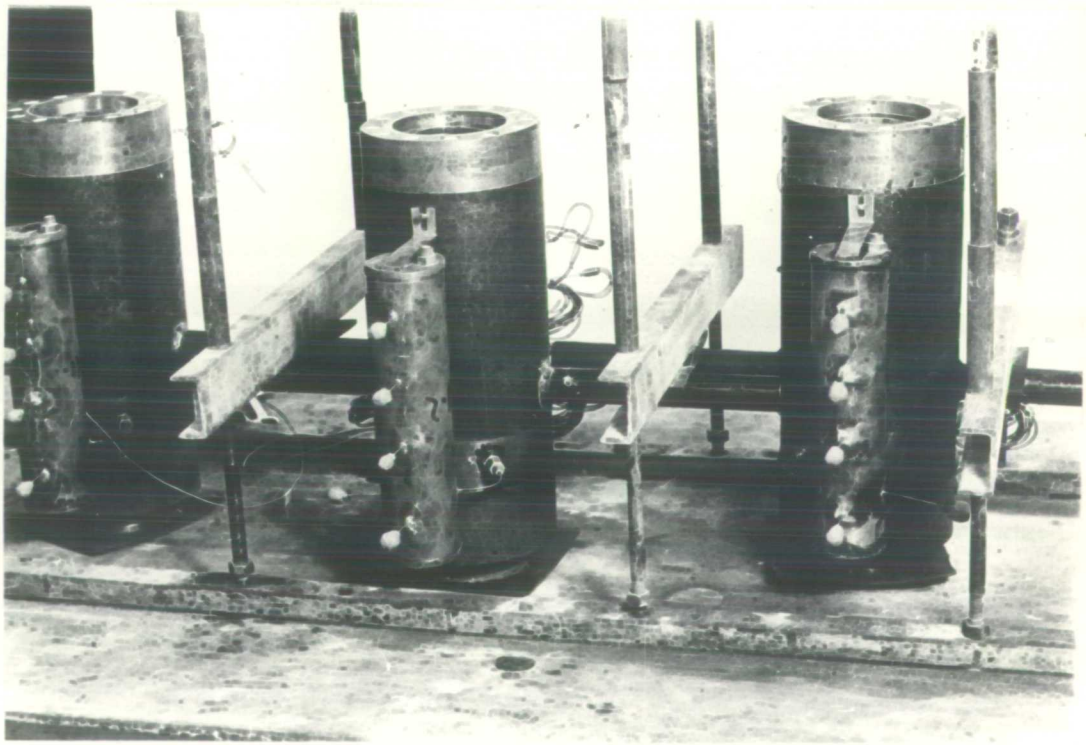

PLATE 3.6: "LTS" CELL CLAMPED ON VIBRATING TABLE FOR CASTING CONCRETE

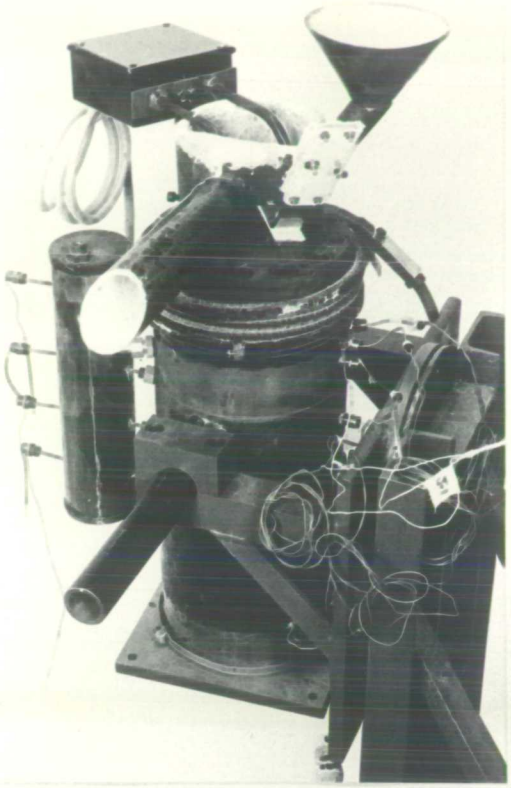

PLATE 3.7: FOR TITLE SEE BELOW

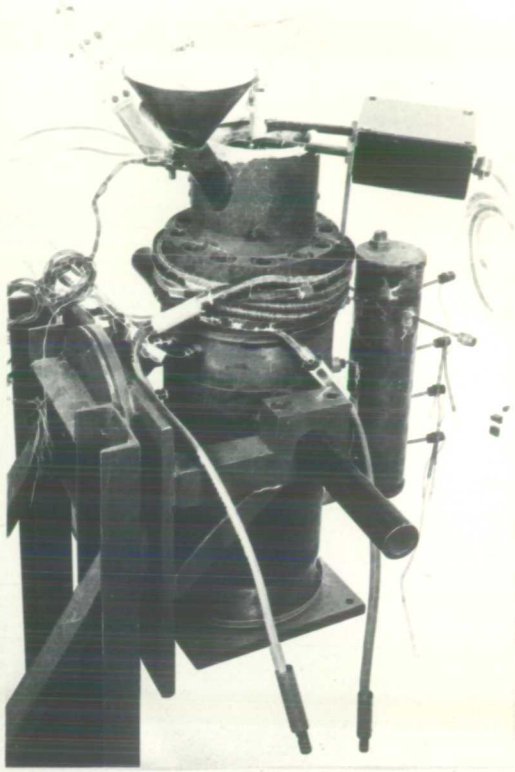

PLATE 3.8: FOR TITLE SEE BELOW

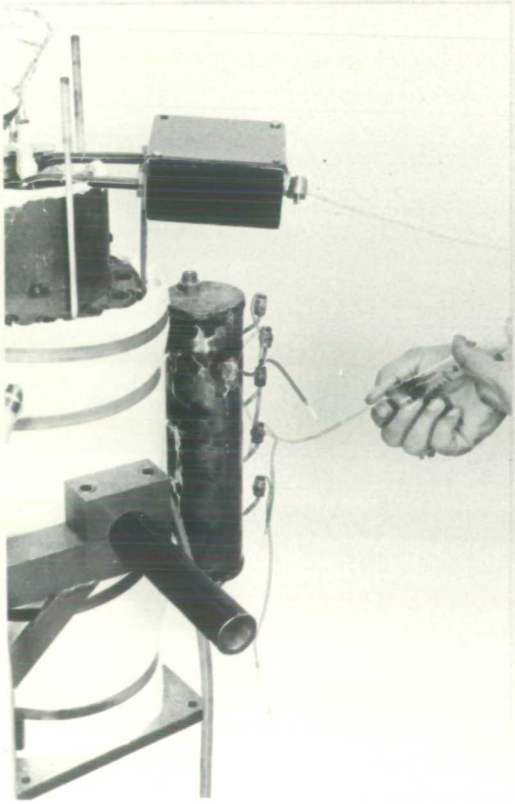

PLATE 3.9: FOR TITLE SEE BELOW

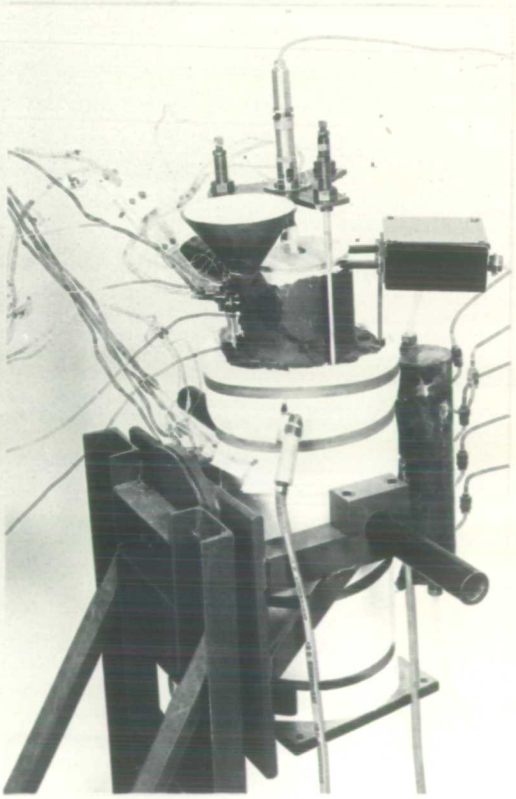

PLATE 3.10: FOR TITLE SEE BELOW

PLATE 3.7, 3.8, 3.9 & 3.10: "LTS" SPECIMENS, CLAMPED IN THE TEST RIG, DURING PREPERATION AND TESTING

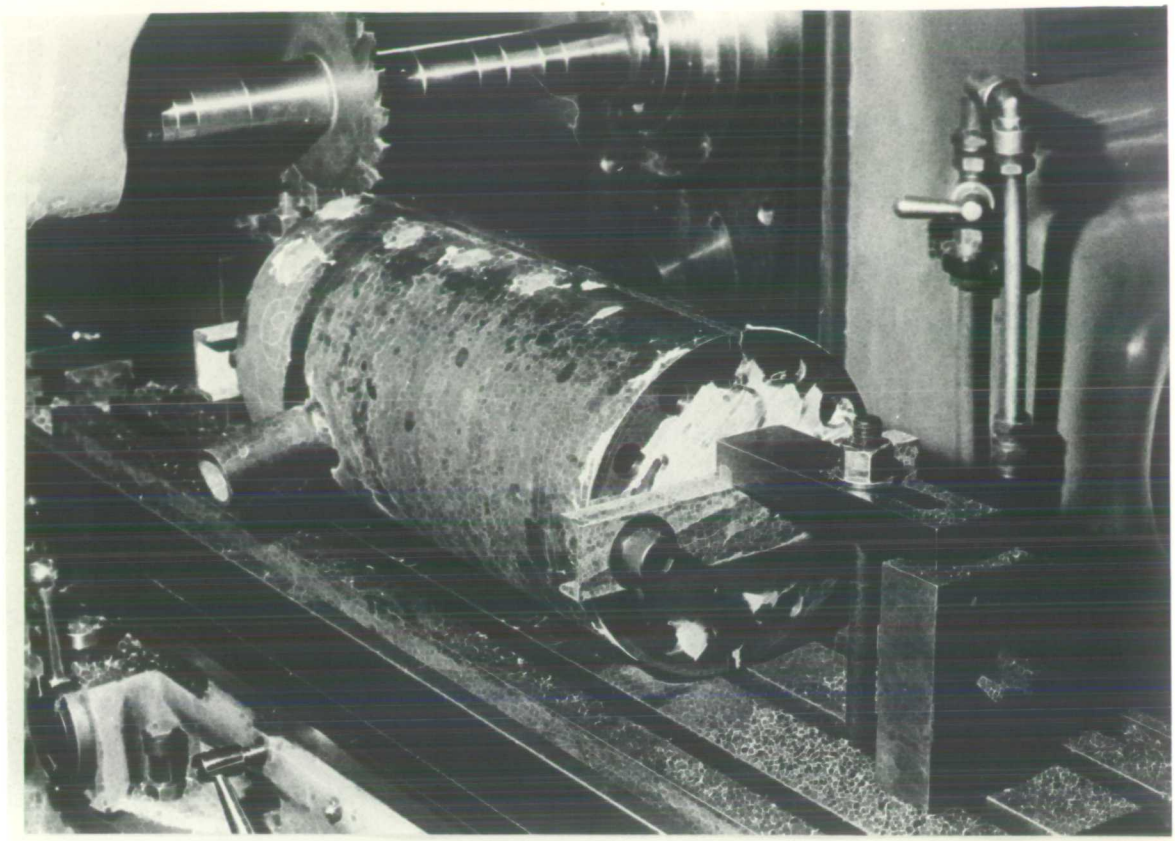

PLATE 3.11: FOR TITLE SEE BELOW

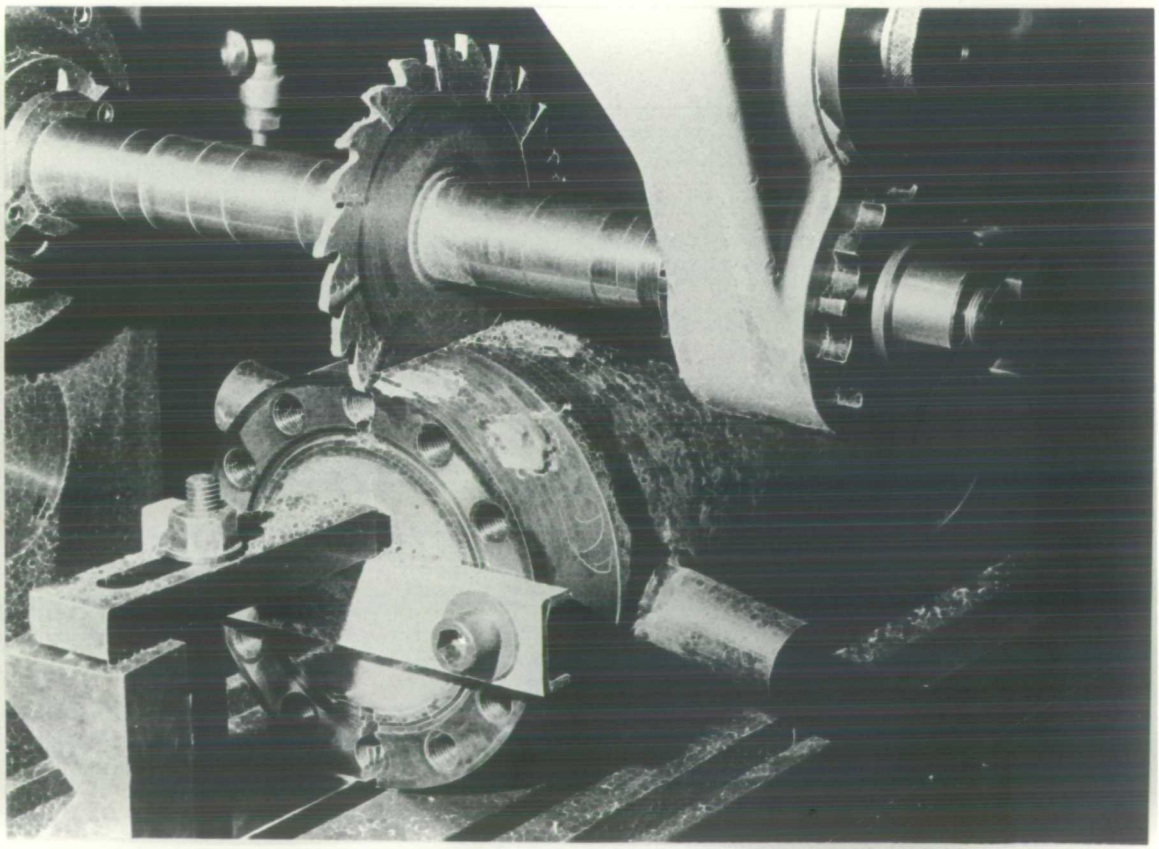

PLATE 3.12: FOR TITLE SEE BELOW

PLATE 3.11 & 3.12: MILD STEEL CYLINDER OF "LTS" SPECIMEN BEING MACHINED FOR THE REMOVAL OF CONCRETE

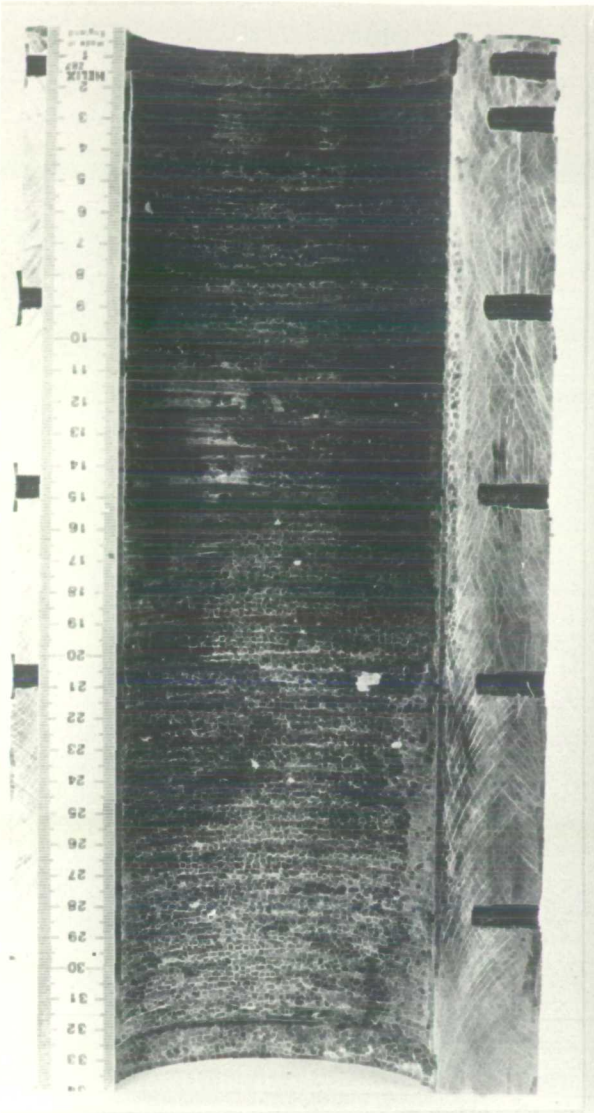

PLATE 3.13
HALF SEGMENT OF MILD STEEL CYLINDER AFTER MACHINING

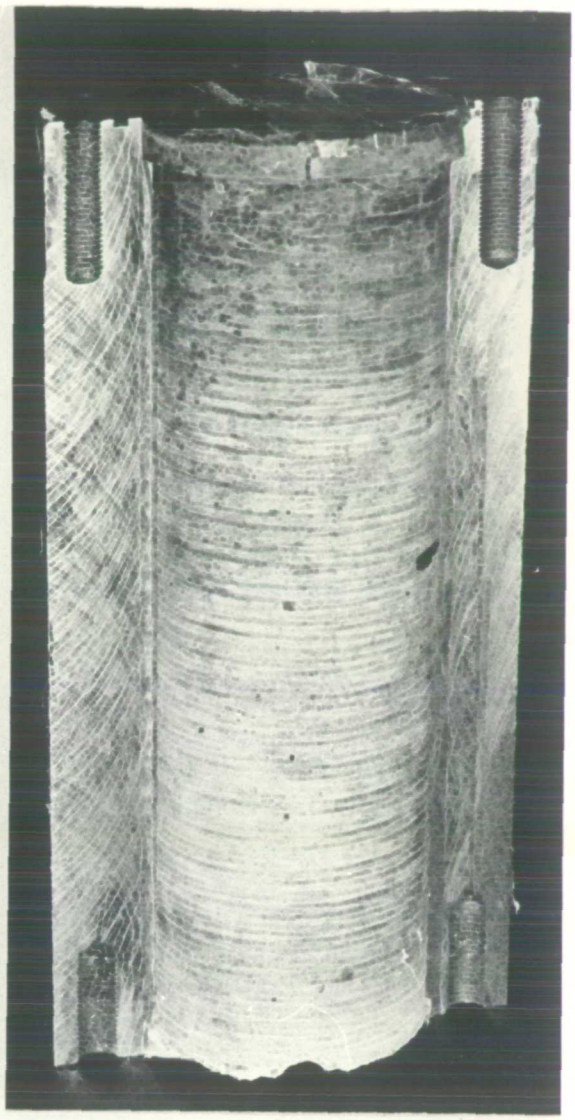

PLATE 3.14
OTHER, HALF SEGMENT OF MILD STEEL CYLINDER WITH CONCRETE

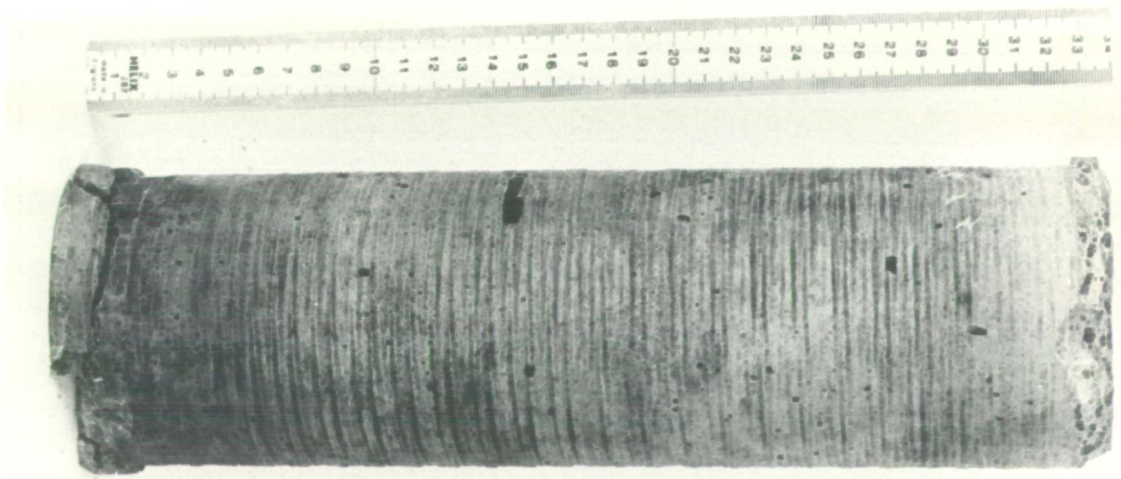

PLATE 3.15: CYLINDRICAL CONCRETE SAMPLE, REMOVED FROM MILD STEEL CYLINDER, AFTER MACHINING, AS SEEN IN PLATE 3.14

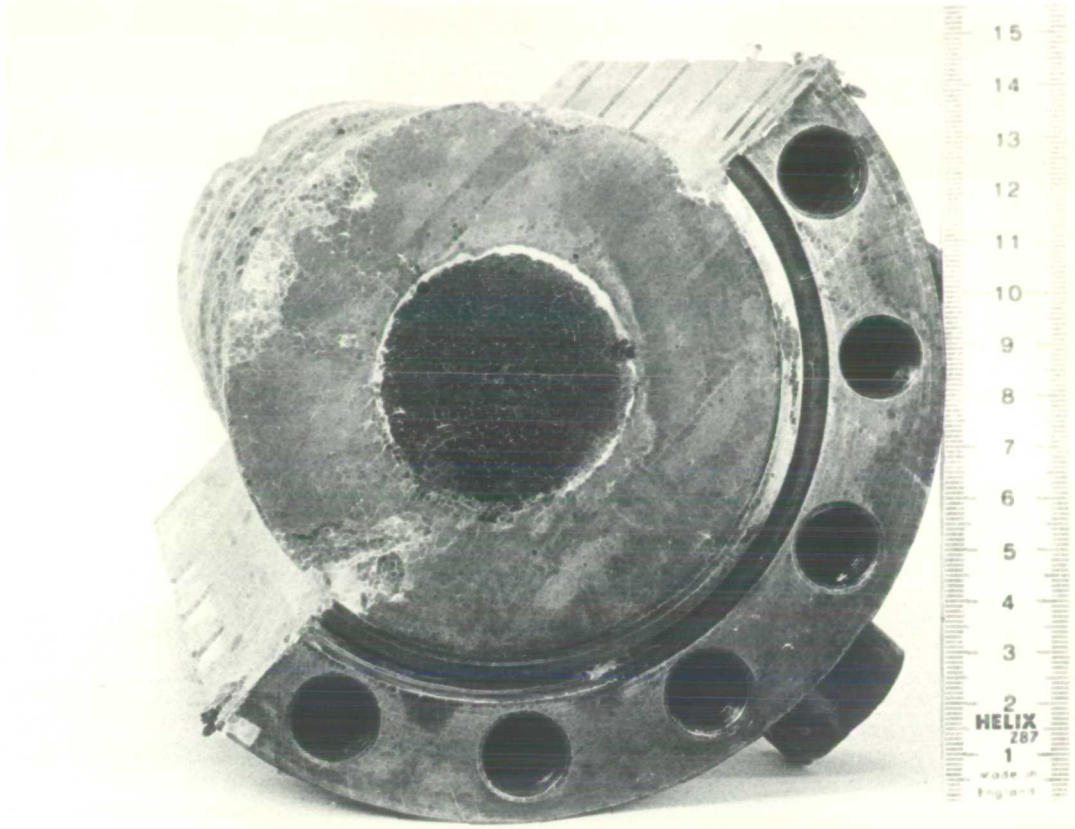

PLATE 3.16: CYLINDRICAL CONCRETE LEFT PERMANENTLY STUCK, TO EACH HALF SEGMENT OF MILD STEEL CYLINDER

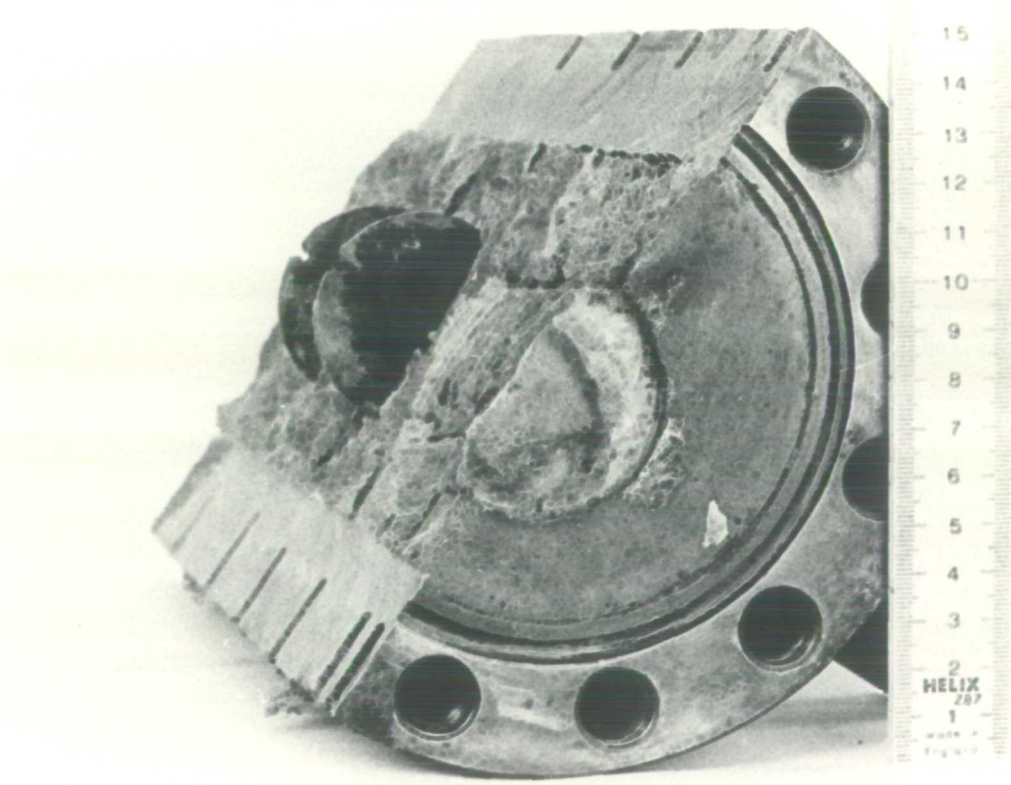

PLATE 3.17: SPLIT, CONCRETE CYLINDER, LEFT PERMANENTLY STUCK TO HALF SEGMENT OF MILD STEEL CYLINDER

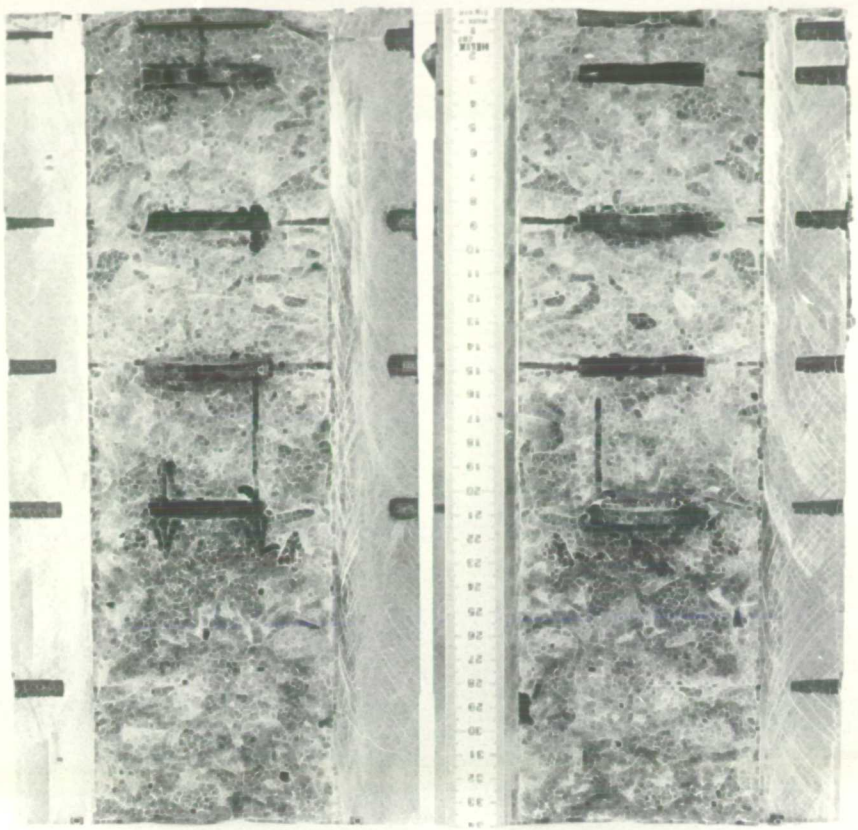

PLATE 3.18: SPLIT, CONCRETE CYLINDER, PERMANENTLY STUCK TO EACH HALF SEGMENT OF MILD STEEL CYLINDER

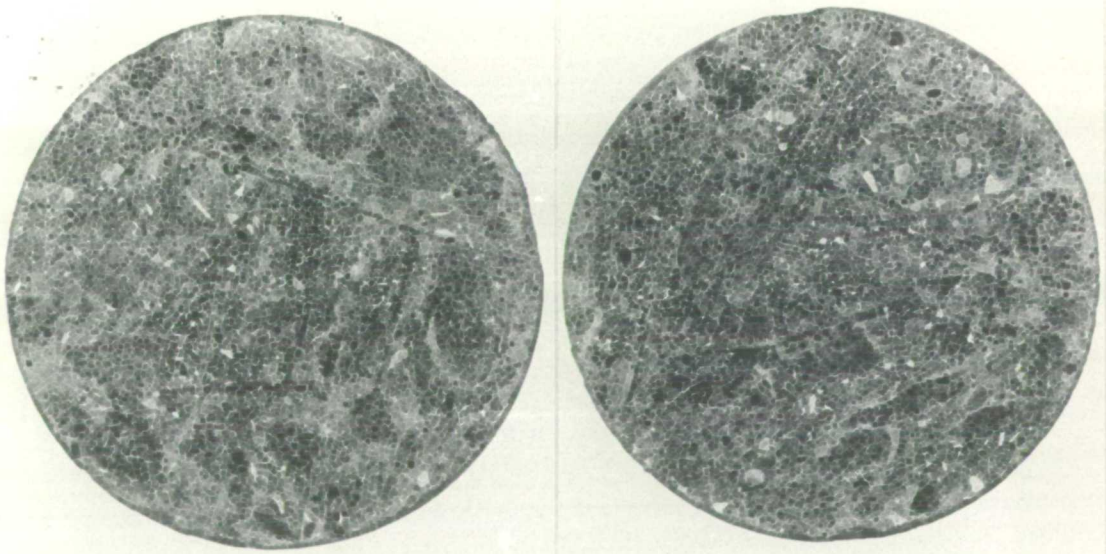

PLATE 3.19: SLICES CUT FROM CYLINDRICAL CONCRETE SAMPLE (PLATE 3.15)

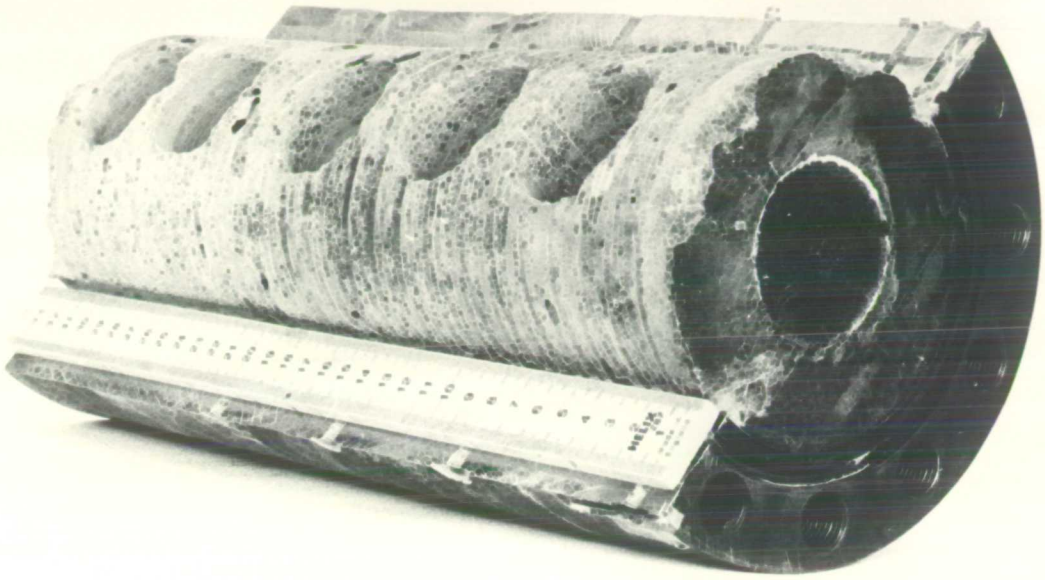

PLATE 3.20: FOR TITLE SEE BELOW

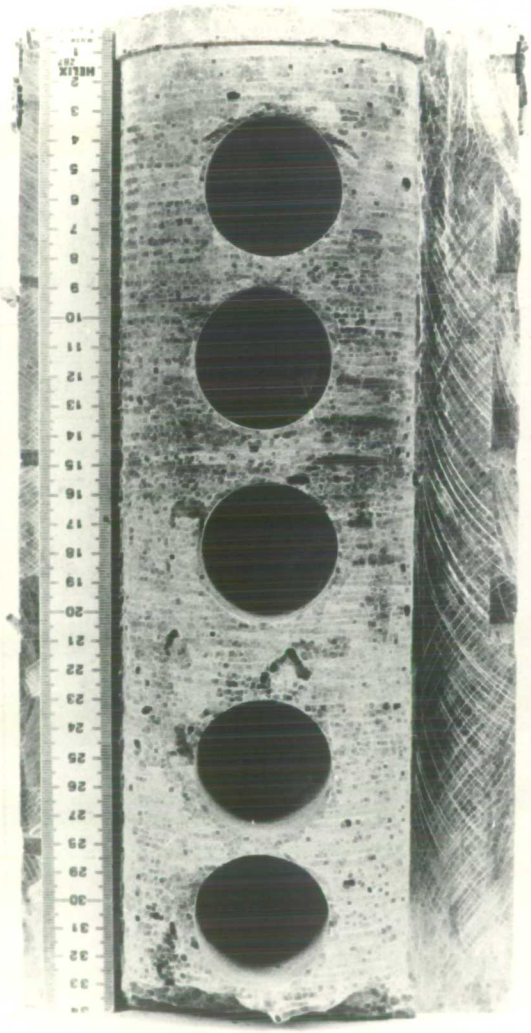

PLATE 3.21: FOR TITLE SEE BELOW

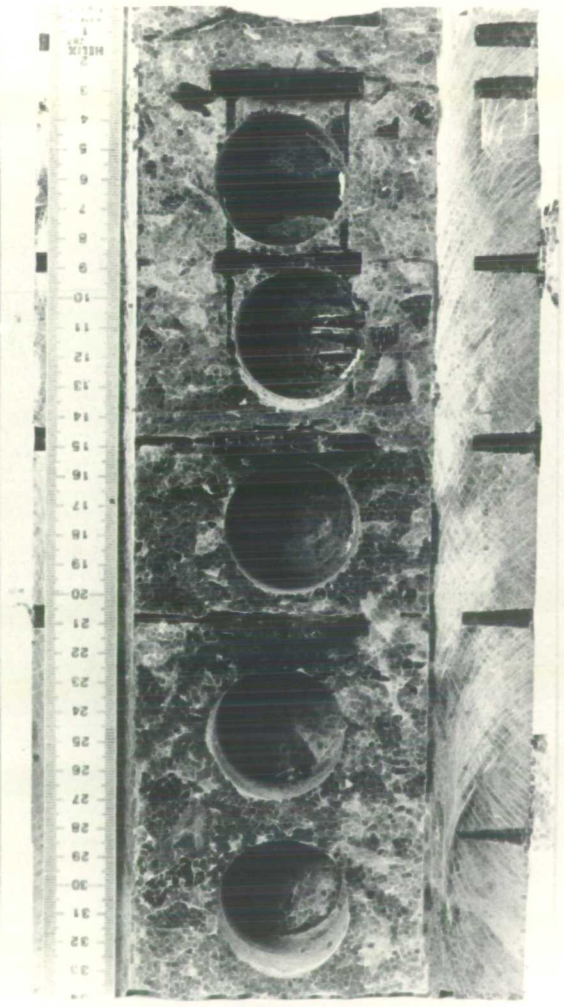

PLATE 3.22: FOR TITLE SEE BELOW

PLATE 3.20, 3.21 & 3.22: 1.5 INCH CORES EXTRACTED FROM VARIOUS CONCRETE SPECIMENS OF "LTS"

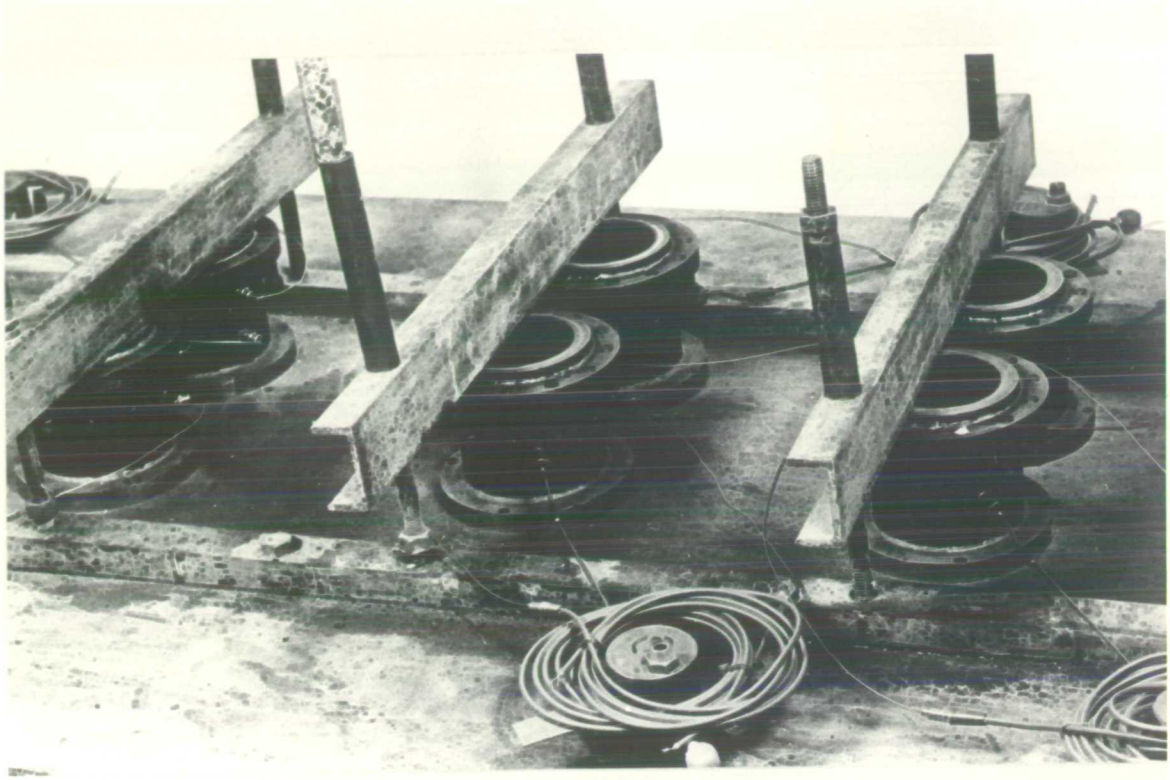

PLATE 3.23
"RTS" CELLS CLAMPED ON VIBRATING TABLE FOR CASTING CONCRETE

PLATE 3.24
"RTS" SPECIMEN JUST AFTER CASTING CONCRETE

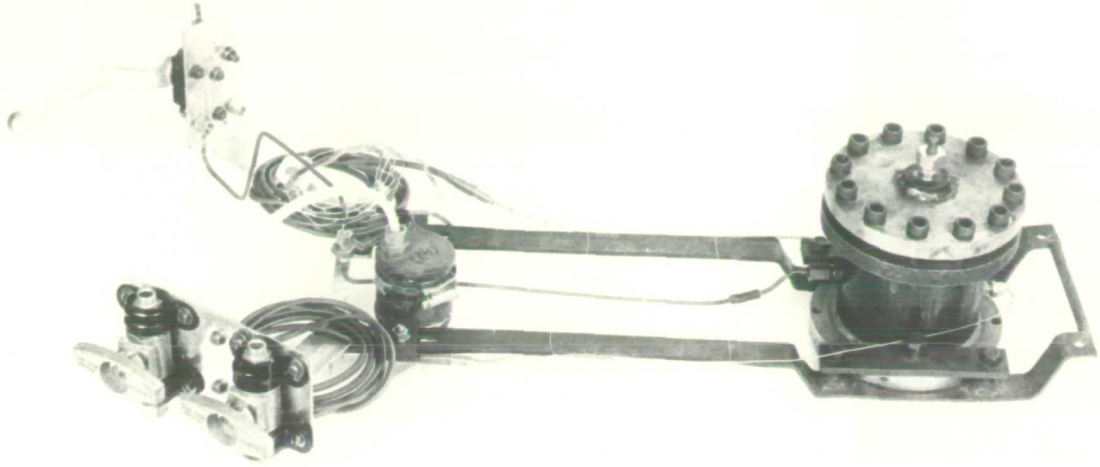

PLATE 3.25: "RTS" SPECIMEN SECURED TO THE TEST RIG

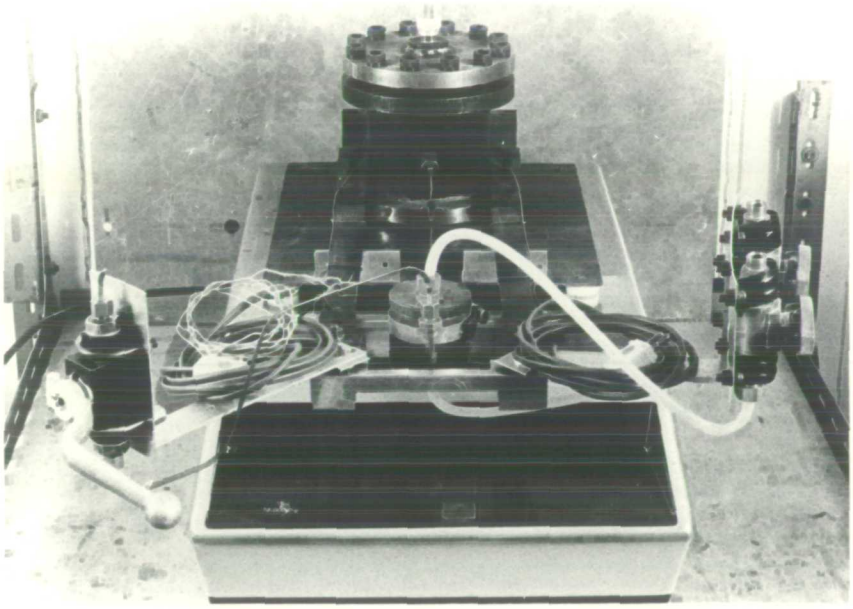

PLATE 3.26: "RTS" SPECIMEN BEING WEIGHED ON THE BALANCE

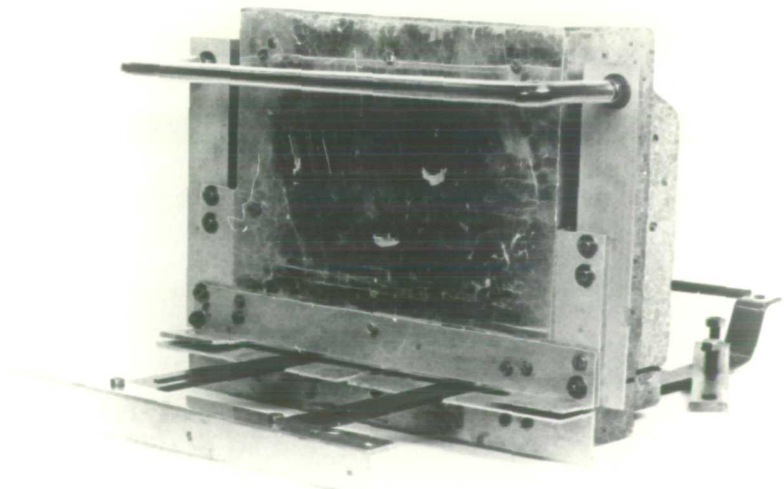

PLATE 3.27: FURNACE DOOR CAST IN TWO PARTS

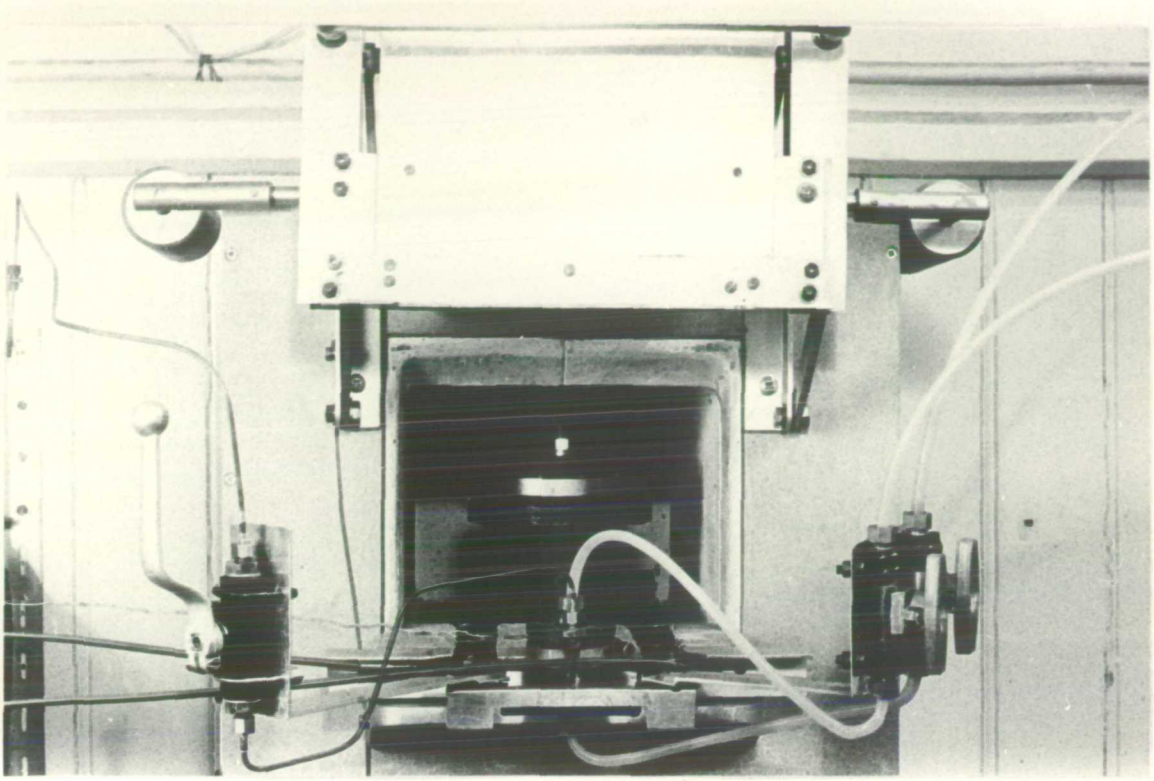

PLATE 3.28: "RTS" SPECIMEN INSIDE THE FURNACE

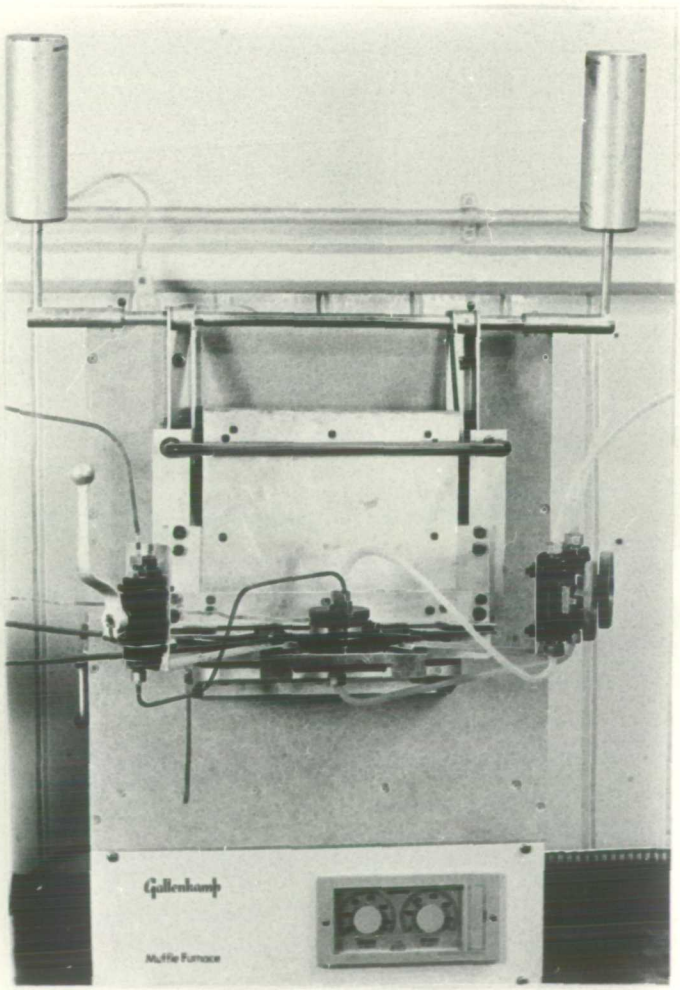

PLATE 3.29: "RTS" IN THE FURNACE READY FOR TESTING

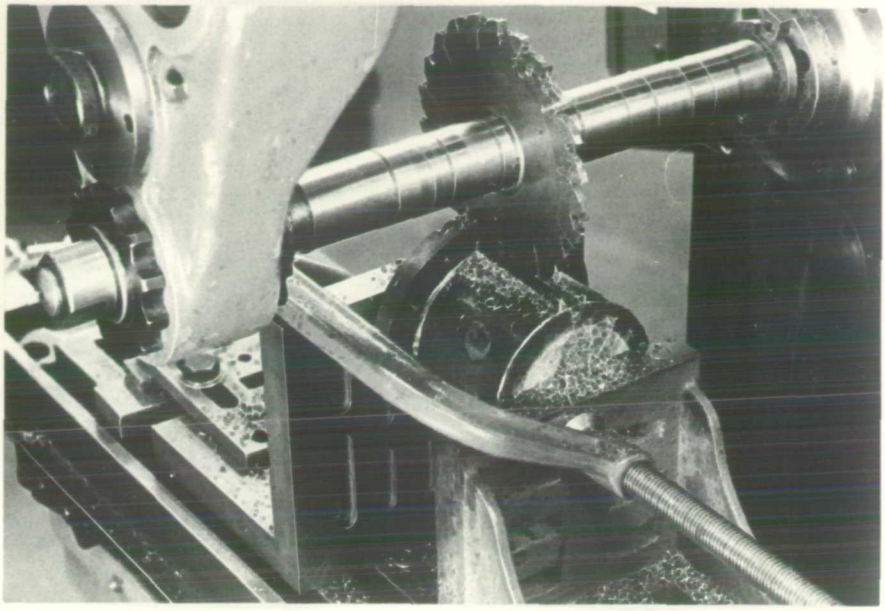

PLATE 3.30: "RTS" CELL BEING MACHINED

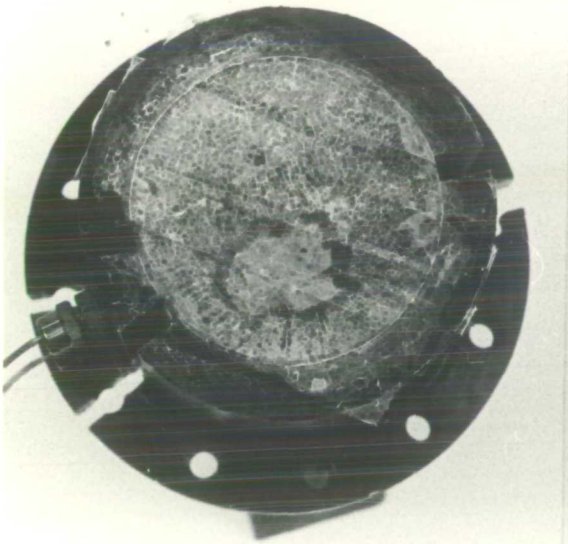

PLATE 3.31
"RTS" CELL AFTER MACHINING

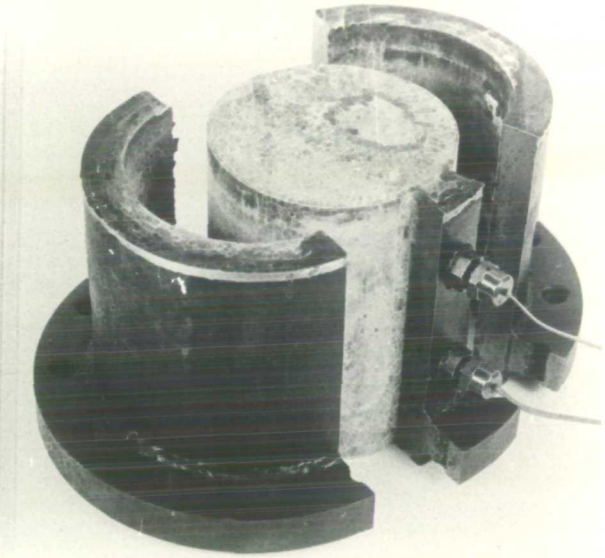

PLATE 3.32
"RTS" CELL AFTER SPLITTING

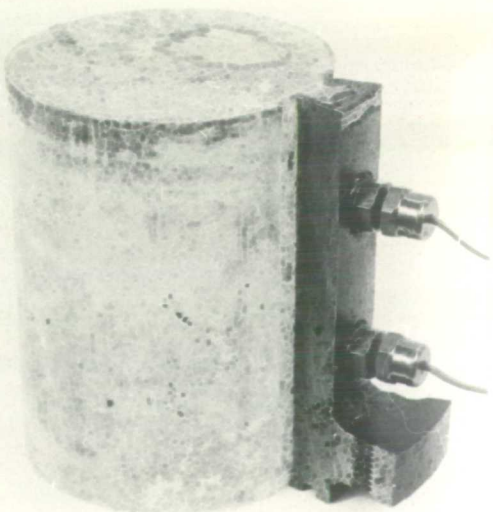

PLATE 3.33
CYLINDRICAL CONCRETE SAMPLE,
EXTRACTED FROM "RTS" CELL

CHAPTER 4

INSTRUMENTATION

4.1 INTRODUCTION TO EXPERIMENTAL PROGRAMME

The experimental programme was designed to monitor pore pressure, temperature, weight loss, evaporable and non-evaporable water content of heated concrete and the central deflection of a stainless steel diaphragm (simulated liner). The major factors for the design of the experiments were: the size of the specimen, sealing techniques and the methods of introducing the instrumentation into the specimen. The durability of the test assembly under thermal shock was of paramount importance. The requirements of instrumentation design considered before selecting the instrumentation are given below.

1. Reproduceable measuring techniques with no zero drift.

2. Robustness of instrumentation against temperature and pressure.

3. Measurement of pore pressure at no volume change (i.e. the fluid used for the measurement of pressure should not enter or escape the specimen).

4. The cost and availability of the instrumentation.

4.2 PORE PRESSURE MEASUREMENT IN CONCRETE

4.2.1 INTRODUCTION

The pore pressure measuring techniques in undrained triaxial test samples of soils were developed many years ago (Bishop and Henkel, 1962). The pore pressures in soil are hydraulic and the pore pressures in heated concrete are mainly due to gas, vapour and expansion of liquid.

Bremer (1967) recorded the pore pressures in concrete by casting a porous material inside concrete and connecting it to a Bourdon type pressure gauge. He showed that if a porous component is embedded inside concrete and provided the volume of the inclusion is small compared with the surrounding concrete, the pressure in the pore of the porous component will be equal to the pressure of the surrounding concrete. Therefore it is possible to measure the pressure of concrete by measuring the pressure of the component.

The internal volume of a Bourdon type pressure gauge changes with the application of pressure and fluid could flow from the porous inclusion into the gauge. This could produce an error in the recorded pressure. Hence, the method used by Bremer (1967) was not suitable for the measurement of pressure reported in this thesis.

Sharp (1971) developed a technique for measuring pore pressure in heated concrete by casting-in a sintered bronze porous plate in concrete and measuring the pressure by connecting it to the Bourdon pressure gauge through a Perspex "U" tube filled with mercury (Figure 4.1). He introduced a screw operated ram into the circuit between the Bourdon pressure gauge and the "U" tube, to provide the back pressure, and maintain the mercury level in the "U" tube to its original level. By applying the back pressure and maintaining the mercury level, the fluid in the porous plate was kept at its original volume. Therefore the pressure recorded by the Bourdon gauge was the true pressure of the fluid.

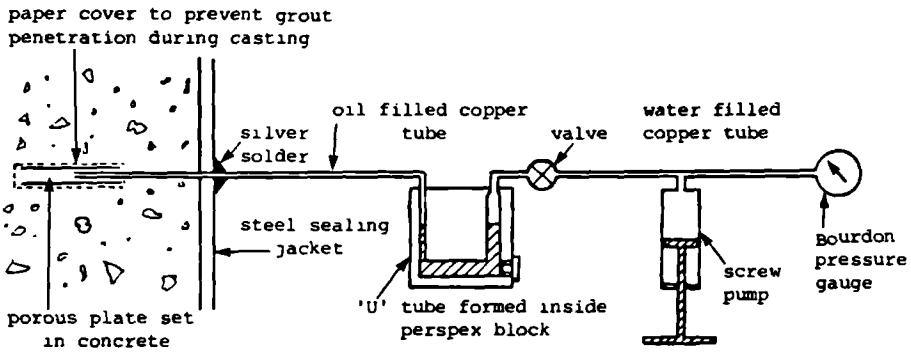

Figure 4.1: Pore pressure measuring system used by Sharp (1971).

To control the volume of fluid in the porous plate as accurately as possible, the arm of "U" tube nearest to the porous plate was made as narrow as possible so that a small change in the volume produced a large movement in mercury level. This system worked satisfactorily when the concrete was in saturated state or the pressures were changing slowly. However, extreme care was needed when the concrete was in un-saturated state or the pressures were changing rapidly, because the movement of the liquid into the Bourdon gauge would result in the volume changing so rapidly that it could be possible for the mercury to be forced into one limb, resulting in fluid or vapour loss from the porous plate.

Chapman (1976) modified the pore pressure measuring techniques developed by Sharp (1971). He also used a sintered bronze porous plate cast into the concrete specimen and connected it to a small bore copper tube which was bent to form a "U" outside the seal. The end of this tube was soldered to a fitting which was screwed to a Klinger valve. The pressure attachments were moved from one pressure point to another. He introduced a Model UC3 Universal Transducing Cell, into the pressure measuring system, instead of a Bourdon gauge as previously used by Sharp (1971). He did not use the Perspex "U" tube filled with mercury for monitoring the movement of fluid into or out of the porous plate as used by Sharp.

To ensure no volume change occurred when pressure measurements were made, Chapman also used a screw ram to provide back pressure in the attachment (Figure 4.2). After connecting the attachment to the Klinger valve nearest to the specimen, he recorded the pressure of the specimen by applying the back pressure to the attachment, and the transducer. His applied back pressure was equal to the previously recorded pressure at that pressure point. The difference between the back pressure applied and the transducer read out recorded, was also taken. Any difference between these two meant that the measurement was not true "no volume change" measurement. Consequently if the pressure on the read out was lower than the back pressure applied, the back pressure was adjusted to a value halfway between the initial back pressure and that recorded. The Klinger valve was then opened quickly and the new pressure was recorded. Using this method he adjusted the back pressure until it was equal to the pressure in the porous plate. Chapman used the same attachment with each pressure point by connecting the attachment to each position in turn; this overcame the need for a separate instrument at each of the large number of measuring points.

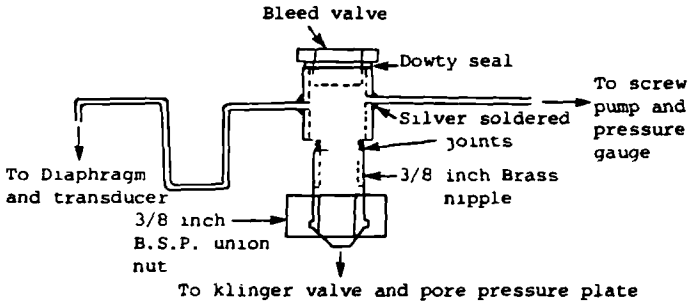

Figure 4.2: Pore pressure measuring system used by Chapman (1976).

This method was considered for use in the experimental programme, but it was rejected on three counts.

i. The pore pressures developed during heating were changing rapidly with time and the procedure for back pressure adjustment used by Chapman (1976) could not be applied satisfactorily.

ii. Pore pressure was monitored only at five locations; therefore an independent system for measuring pressure could be used for each pressure point.

iii. There was no visual check on the movement of fluid either into or out of the porous plate.

The pressure measuring system was modified and improved, and this system (Section 4.2.2) incorporated a design, where:

a. A Universal Transducing Cell was used with pressure attachments, for accurate measurements.

b. The movement and control of fluid from the porous plate was monitored by a mercury filled "U" tube, constructed in a Perspex block, and by applying back pressure by either a screw operated ram or a hydraulic pump depending on the pressure.

4.2.2 TRANSDUCER AND ACCESSORIES DETAILS AND DESIGN

The pore pressure of concrete was recorded by a flexible modular measuring system, developed by Statham Instruments Inc. of California. The modular system consists of the "Universal Transducing Cell" (UTC),

accessory heads and electronics (or measuring devices), as shown in Figure 4.3.

Figure 4.3: A typical "Universal Transducing Cell" with accessory head and electronics.

The transducer (Plate 4.1) is a zero-length unbonded strain gauge. A little force or displacement is required to actuate the unbonded strain-sensitive filaments and owing to the zero-length design, the filaments can not be broken by overtravel. The specifications of the transducer are given in Table 4.1.

Resolution	Natural Frequency Without Accessory	Full Scale Output	Rated Excitation	Bridge Resistance
Infinitesimal	~ 300 Hz	12 mv/v	5v (dc/ac)	350 Ohms

Table 4.1: Specifications of a Universal Transducing Cell.

The UTC is an extremely sensitive device capable of making precise measurements of force and displacement. When the UTC is combined with the appropriate transducing module (accessory heads) it is also capable of measuring a variety of parameters such as pressure, strain, hardness, surface tension and displacement etc. The accessories are available for substantial reduction or extension of the UTC measurement range for force or displacement. The accessory head used with the transducer for pore pressure measurement, was a pressure accessory with interchangeable diaphragms, Model UGP4 (Plate 4.1). Table 4.2 gives the specifications of the pressure accessory.

Non-Linearity & Hysteresis	Temperature ^{o}C	Pressure Media	Thermal Zero Shift
< 0.25 % Fs	-54 To +121	Fluid & Gases	0.01 % FS/^{o}F

Table 4.2: Specifications of the pressure accessory.

By changing the diaphragms, it was possible to measure pressure from 0 to 5000 psig (0-350 Kg/cm^2), 5000 psig being full scale output. Two ranges of diaphragm 0-2000 psig and 0-5000 psig were used for the

pressure measurement throughout the experimental programme. The diaphragm ranges available to be used with the system are given in Table 4.3.

The diaphragm ranges are in psig. from 0 to the following values											
1	2	5	10	20	50	100	200	500	1000	2000	5000

Table 4.3: Diaphragm ranges available for use with the system.

The filament of a UTC is designed in such a way that it can not be broken by overtravel. However, an overload protection device in the form of a clip was placed over the sensing tip of the transducer to protect it from any damage and also provide an overtravel or load limit of 150% on the transducer, by using this clip (i.e. for 0 to 2000 psig diaphragm load limit was 3000 psig). The set up for the accessory and the UTC is described in Section 4.3.

The UTC had been tested previously by Chapman (1976) for a period of one year for zero drift. He also continously used these transducers in his experimental work for over a year and reported no problems of zero drift with any transducer. The typical calibration results for a transducer (reproduced from his thesis in Figure 4.4), show no variations in the transducer output. The tests (described here) were not run for longer than two weeks and the problem of zero drift was not encountered. However, all the transducers used were tested for zero drift and worked satisfactorily.

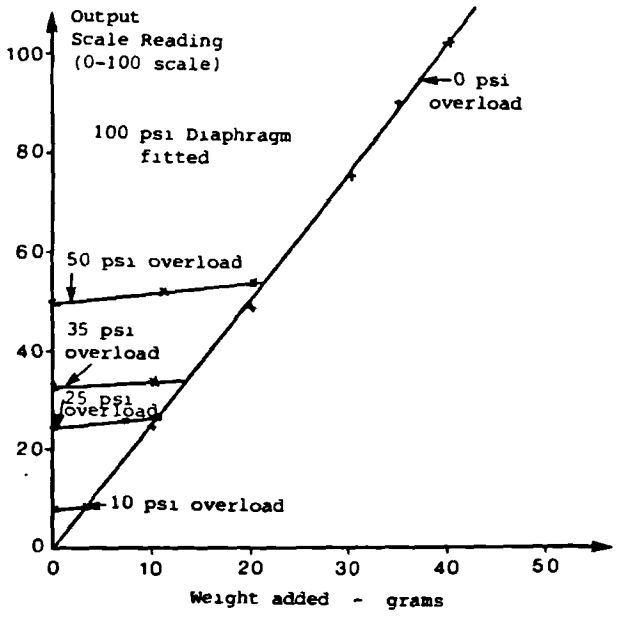

Figure 4.4:

Typical results of a Universal Transducing Cell tested for zero drift by Chapman (1976).

The other subsidiary tests carried out on the transducers are described below.

i. By keeping the input voltage constant and maintaining a given pressure the output voltage was recorded against time. The results showed that all the transducers output voltage remained constant with time at the given pressure and constant input voltage.

ii. The output was also recorded against the pressure for different input voltages to the transducer. It was observed that the output voltage was related to the input voltage and Figure 4.5 shows the result for a typical transducer with 5000 psig diaphragm.

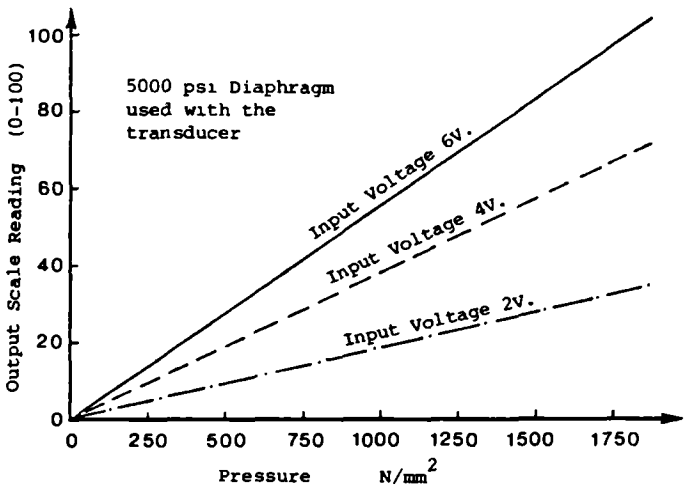

Figure 4.5: Pressure against output voltage at different input voltages for a typical transducer.

The subsidiary tests showed that output was related to input, and therefore, it was important to use the same input voltage for a specific transducer during calibration and main experimental programme.

The input voltage for two of the transducers using 0-5000 psig diaphragms was supplied by an independent Farnell laboratory transformer for each transducer. The transformer supplied 6 volts d.c. for each transducer.

The remaining four transducers using 0-2000 psig diaphragms were energised by the internal energisation of the data logger and this

energisation remained constant throughout the experimental programme. The output from the transducer was recorded on a data logger and the chart recorder.

All the transducers used with the pressure accessories were individually calibrated against Bourdon pressure gauges for constant input voltage, which remained unchanged throughout the testing and the calibration factor was evaluated. The calibration factor of each transducer was incorporated into a computer program used with the data logger for the measurement of pressure. Similarly the output scale of the chart recorder was adjusted for the calibrated pressure. The calibration of all the transducers were checked after every test to make sure that the transducers were not malfunctioning.

4.2.3 POROUS PLATES

The sintered bronze porous plates with a porosity of 39%, 1/4 inch thick and of a different size for each experimental series were embedded inside concrete to measure pore pressure. The size of the porous plates used for the "RTS" and the "LTS" was selected in such a way as to keep the volume of the porous components cast inside concrete small as compared with the surrounding concrete. The porous plate was prepared for each experiment, as described below.

4.2.3.1 "RELEASE TEST SERIES" POROUS PLATE

The pore pressure in the "RTS" was only measured at one point and the procedure for the preparation of the porous plate is given below:

1. A 1.5 inch diameter porous plate was cut and machined.

2. To accommodate the small bore copper tube (Section 4.2.5.1), a 3/32 inch diameter hole was drilled to a depth of 3/4 inch through the side of the porous plate.

3. To prevent the pores of the porous plate getting filled with cement grout during the casting of concrete, the porous plates were covered with high temperature porous paper. This paper was capable of withstanding 600 ^{o}C without destruction.

4. The porous paper was stuck to the porous plate with Heamatite

high temperature sealing compound around the edges.

5. To precisely locate the porous plate in the concrete during casting, two 8 B.A. studs were used as spacers between the base plate and the porous plate (Figure 4.6). Two clearance holes for 8 B.A. studs were drilled through the porous plate with the porous paper stuck on it and the 8 B.A. studding was secured to the porous plate using 8 B.A. nuts. Plate 4.2 shows a porous plate after machining and another one with porous paper and studding in position. The method of connecting the porous plate to the small bore copper tube is described in Section 4.2.5.1.

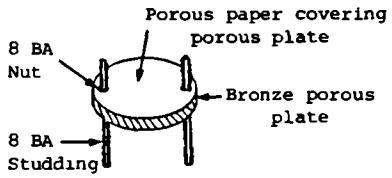

Figure 4.6:
Bronze porous plate used to measure the pore pressure of concrete in the "RTS".

4.2.3.2 "LINER TEST SERIES" POROUS PLATE

1. The pore pressure of concrete was measured at five different positions (Chapter 3, Section 3.3.2). Therefore 5 circular porous plates of 2 inches diameter were cut and machined for every test.

2. To accomodate the small bore copper tube a hole 3/32 inches diameter and 1 inch deep was drilled through the side of the porous plates.

3. All the porous plates were covered with high temperature porous paper, as described in Section 4.2.3.1 (3).

4. The high temperature porous paper was stuck to the porous plates with Heamatite high temperature sealing compound around the edges (Section 4.2.3.1 (4)). Plate 4.3 shows porous plates with and without the porous paper.

5. To prevent movement and dislocation of the porous plate during casting of concrete, all the plates were spaced to the required distance using 8 B.A. studding. Three clearance holes for 8 B.A. studding were drilled through the porous paper and the porous plate (Plate 4.3). The studding was secured to all the five

porous plates with 8 B.A. nuts (Figure 4.7). The method of connecting the porous plates to the small bore copper tube is explained in Section 4.2.5.2.

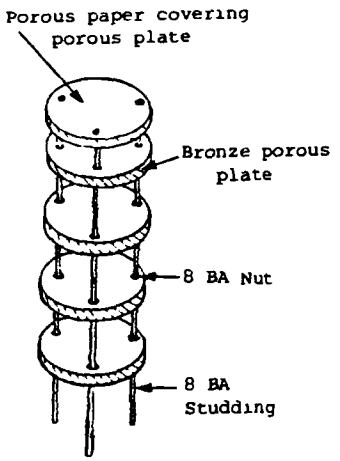

Figure 4.7:

Bronze porous plates used to monitor the pore pressure of concrete in the "LTS", assembled together with 8 B.A. studding.

4.2.4 COOLER OR HEAT EXCHANGER DESIGN

To cool the vapour or heated liquid in the small bore copper tube, transmitting the pore pressure of concrete to the pressure measuring instrumentation board (Section 4.2.6), a cooler was designed for the circulation of cold water during testing. The copper tubes passed through the cooler and cold water was used for cooling these tubes by circulating tap water through the cooler. The design and construction of the cooler for each test series is described below.

4.2.4.1 "RELEASE TEST SERIES" COOLER

1. The cooler was constructed from a copper tube (2 inch i.d. by 2 inch long).

2. Two holes (3/32 inch diameter each) were drilled through the wall of the cooler diametrically opposite each other to pass the small bore copper tube.

3. An end cap of the same wall thickness as the copper tube of the cooler was designed for either end.

4. To connect the cooler to the tap water and the drain with the help of nylon tubes (for circulating the cold water), a 1/4 inch B.S.P. stud coupling was silver soldered to each end cap.

5. To secure the cooler to the test cell a brass strip was also silver soldered to the end cap used at the bottom end (Plate 4.4).

6. The cooler was put together by first passing the copper tube through the two 3/32 inch diameter holes (as in (2) above). The copper tube was then silver soldered to the wall of the cooler and an end cap was soft soldered to each end of 2 inch copper tube. Plate 4.4 shows the cooler complete with fittings.

4.2.4.2 "LINER TEST SERIES" COOLER

1. The copper tube used as a cooler for the "LTS" was similar in diameter to the "RTS" cooler (Section 4.2.4.1 (1)). The length of the tube for the cooler in this case was 12 inches.

2. To pass five small bore copper tubes through the cooler, five sets of two holes (3/32 inch diameter) were drilled diametrically opposite each other through the wall of the cooler.

3. Same as Section 4.2.4.1 (3).

4. Same as Section 4.2.4.1 (4).

5. A brass strip soldered to the end cap used at the bottom end was screwed to the outside of the mild steel cylinder (Plate 4.7).

6. The cooler was put together once again by passing each copper tube through the holes drilled opposite each other in the wall of the cooler. The tubes were silver soldered to the wall of the cooler, and an end cap was soft soldered to each end of 2 inch copper tube, as explained previously in Section 4.2.4.1 (4). Plate 4.7 shows the completed cooler attached to the steel cylinder.

4.2.5 PORE PRESSURE ATTACHMENTS

The pore pressure of concrete was transmitted by connecting a small bore copper tube to a porous plate at one end and a brass parallel stud coupling at the other end. The copper tube passed through the cooler (Section 4.2.4) and then through the wall of the mild steel

cylinder. To prevent the pressure leaking through the wall of the cylinder, the copper tube passed through a fittings (Appendix I, Section I.2 and Appendix I, Section II.2). The detail and procedures for putting the pressure attachments on the mild steel cylinder are described below for each test series.

4.2.5.1 "RELEASE TEST SERIES" PRESSURE ATTACHMENTS

1. The copper tube was cut to the required length and a brass parallel stud coupling (1/8 inch B.S.P.) was silver soldered to one end.

2. After passing the copper tube through the cooler it was silver soldered to the cooler (Section 4.2.4.1).

3. To seal the pressure between the coupling (screwed to the mild steel cylinder, as described in Appendix II, Section II.2) and the copper tube:

i. A 3/32 inch clearance hole was drilled in a copper blank, the copper tube was positioned in the hole and it was silver soldered to the blank.

ii. An olive was positioned on the copper blank and using a stainless steel fitting provided for crimping the olive on to the blank, the olive was crimped on the blank.

iii. The copper tube was introduced through the coupling (screwed to the steel cylinder) and pressure seal was completed by tightening the olive under the nut to this coupling.

4. The end of the copper tube was pushed into the hole drilled in the porous plate and the tube was cemented to the plate using Heamatite high temperature sealing compound (Section 4.2.3.1). Plate 4.5 shows the pore pressure attachment (without passing through the steel cylinder wall) and Plate 4.6 shows the steel cylinder with complete pressure attachment.

4.2.5.2 "LINER TEST SERIES" PRESSURE ATTACHMENTS

1. Pore pressure was monitored at five positions inside the concrete samples in the "LTS".

2. Five small bore copper tubes were cut and a nipple was silver soldered to one end of each tube. The nipple was used under a union nut for sealing the pressure between the copper tube and the coupling screwed to the steel cylinder, as described in Section 4.2.5 above.

3. The copper tubes were passed through the cooler and were silver soldered to the cooler, as explained in Section 4.2.4.2.

4. A brass parallel stud coupling (1/8 inch B.S.P.) was silver soldered to the end of each copper tube nearest to the cooler.

5. All the copper tubes were introduced into the steel cylinder through the couplings on the cylinder and then the end of each tube inside the cylinder was pushed into the hole of the respective porous plate (Section 4.2.3.2).

6. The copper tube and porous plates were stuck together with Heamatite high temperature sealing compound.

7. The nipples were tightened into the couplings under the union nuts. Plate 4.7 shows the copper tube with all the couplings and cooler attached to the mild steel cylinder and Plate 4.8 shows the positioning of the porous plates with the rest of the assembly.

4.2.6 PRESSURE INSTRUMENTATION BOARD

To record the pore pressure of heated concrete, the transducers with pressure accessories, valves, Perspex blocks with "U" tube constructed inside the blocks, back pressure system and other fittings were mounted on a wooden board, as shown in Plate 4.9.

As the pore pressure was monitored at five positions inside the "LTS" specimens, a transducer with the pressure accessory was used with each Perspex 'U' tube filled with mercury. Only one common system for

providing the back pressure to all the pressure measuring positions was used.

A transducer with the pressure accessory was incorporated in the back pressure system for recording the back pressure independently. The ball valves, with no volume change principle and capable of working safely under a pressure of 6000 psi (41-42 N/mm^2), were introduced into the system to protect the components. A parallel stud coupling (1/4 x 1/4 inch or 1/4 x 1/8 inch B.S.P.) was screwed to either end of the valve to connect them to the copper tubes, and Dowty seals provided the pressure seals between the couplings and the valve.

The pressure instrumentation board description is separated here into two sections for explaining the pressure measuring and the back pressure system, as described below.

4.2.6.1 PRESSURE RECORDING SYSTEM

The pressure recording system is further divided into three catagories.

(a) PRESSURE MEASURING DEVICES AND THEIR SET UP
(b) PRESSURE POSITIONS P_2- P_5
(c) PRESSURE POSITION P_1

(a) PRESSURE MEASURING DEVICES AND THEIR SET UP

The procedure for connecting the transducer to the pressure accessory is outlined below.

1. The respective pressure measuring diaphragm (Section 4.2.2) was attached to the pressure accessory for each pressure position.

2. A protection clip was placed over the tip of the Universal Transducing Cell for each transducer and the transducer was screwed to the pressure accessory.

3. To secure the transducer and the accessory to the instrumentation board, an 'L' shaped bracket was screwed between the transducer and the pressure accessory and the bracket was then screwed to the board, as shown in Plate 4.9.

The pressure diaphragm used at each pressure position is shown in Table 4.4 and these values were marked on the board (Plate 4.9).

Pressure Position	P_1	P_2	P_3	P_4	P_5
Diaphragm used (psi)	5000	2000	2000	2000	2000

Table 4.4: Pressure diaphragm used at each position.

(b) PRESSURE POSITIONS P_2-P_5

The pressure measuring positions P_2-P_5 (Plate 4.9) were slightly different from position P_1. Hence, the connections and set up for positions P_2-P_5 (Figure 4.8) are summarised below, while the pressure position P_1 will be described later in part (c).

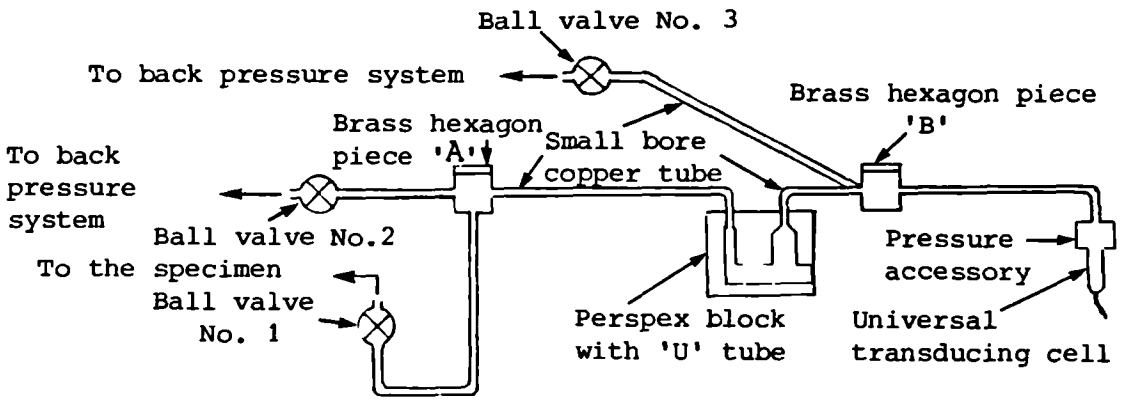

Figure 4.8: Transducer and pressure set up for pressure position P_2-P_5.

1. To enable precise control of the quantity of liquid moving into or out of the porous plate, the diameter of one limb of the 'U' tube constructed in the Perspex block (Plate 4.10), was smaller than the other (Figure 4.9). A brass parallel stud coupling (1/8 inch x 1/4 inch B.S.P.) was screwed to each vertical limb of the 'U' tube, while a stainless steel nut was screwed into the horizontal limb of 'U' tube. Dowty seals provided sealing for all the connections.

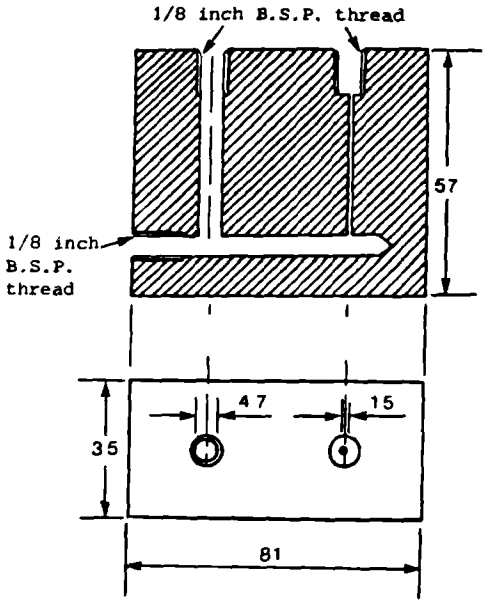

Figure 4.9:

'U' tube constructed in a Perspex block for checking and adjusting the movement of liquid.

2. The smaller diameter limb of the 'U' tube was connected to the ball valve nearest to the concrete specimen through an air bleed valve. The bleed valve was made of a brass hexagonal piece shown as 'A' in Figure 4.8.

3. A heaxagonal brass bar was machined for 1/8 inch B.S.P. threads and three holes were drilled to accommodate three copper tubes.

4. The copper tubes were silver soldered to the hexagonal piece after inserting the tubes in the drilled holes. A brass nipple was silver soldered to the other end of each copper tube with a union nut surrounding it.

5. A 1/8 inch B.S.P. screw was used as an air bleed valve with the Dowty seal providing the pressure sealing. The method for connecting the hexagonal piece 'A' and the other fittings (Figures 4.8 & 4.10) together is explained below:

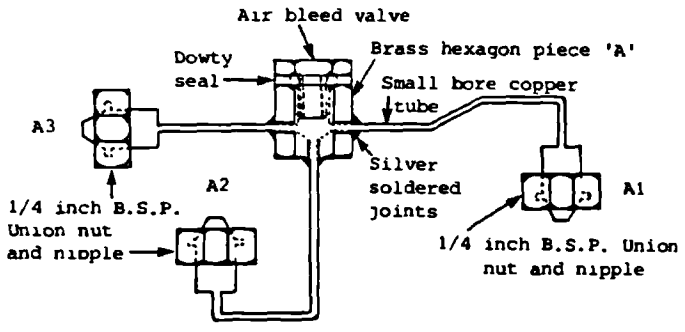

Figure 4.10:

A brass hexagonal piece 'A' used as air bleed valve.

i. Union nut A1 was screwed to the coupling on the smaller limb of the 'U' tube.

ii. Union nut A2 was screwed to the bottom coupling of the ball valve number 1 (Figure 4.8) between the concrete specimen and the 'U' tube.

iii. Union nut A3 was connected to ball valve number 2. This valve was used, to fill the system with water and to protect the pressure measuring system from the back pressure, as described later in Section 4.2.6.2.

6. Another brass hexagonal piece 'B' (Figures 4.8 & 4.11) was constructed in the same way as piece 'A' described above. However, in this hexagonal piece all the copper tubes were introduced through its sides and then silver soldered together, as explained in (4) above.

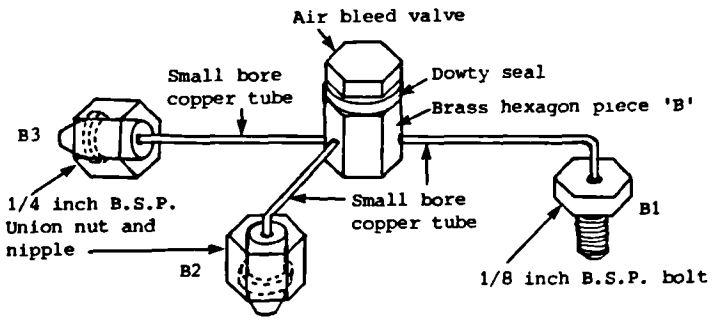

Figure 4.11:

A brass hexagonal piece 'B' used as air bleed valve.

7. A bolt (1/8 inch B.S.P.) was drilled and soldered to one end of one of the copper tubes. A brass nipple was soldered to the end of each of the remaining two copper tubes with union nut surrounding it, in the same way as for the brass hexagonal piece 'A'. The three fittings soldered to the hexagonal piece 'B' (Figures 4.8 & 4.11) were connected to the rest of the fittings as described below:

i. The bolt B1 was screwed to the top end of the pressure measuring accessory used with the transducer.

ii. The union nut B2 was screwed to the fitting of the bigger limb of the 'U' tube.

iii. The union nut B3 was connected to the ball valve number 3. This

valve was incorporated in the back pressure system, to apply the back pressure to the porous plate through the Perspex 'U' tube, as described later in Section 4.2.6.2.

iv. A Dowty seal provided pressure seal between fitting B1 and the pressure accessory.

8. The strength of the Perspex blocks was unpredictable, and therefore the Perspex block was strengthend by reinforcing it with two mild steel strips. One of the strips was placed at the bottom end of the block while the other strip was resting on the couplings at the top end, as shown in Plate 4.9 and Figure 4.12. The bolt near the screw at the bottom end of the Perspex 'U' tube was tightly pressed against this screw to provid resistance against lateral movement.

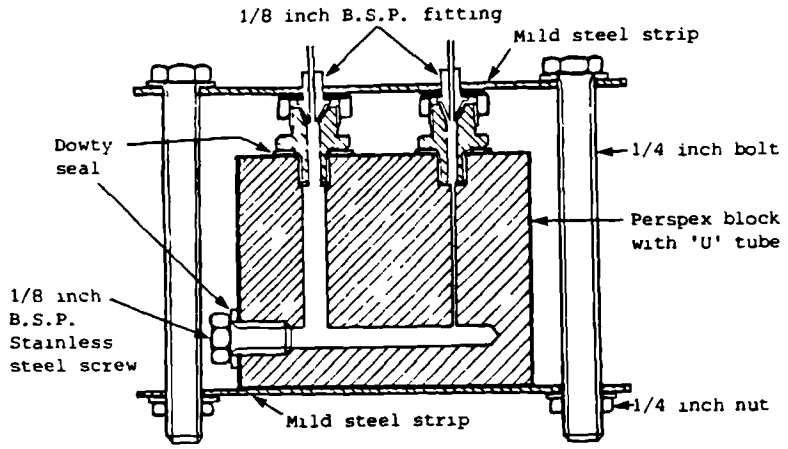

Figure 4.12: Perspex block reinforced with mild steel strips.

9. Both the plates used with the Perspex block were pre-stressed to take the forces produced by the application of pressure to the liquid in the limbs of the 'U' tube.

10. All the Perspex 'U' tubes were tested to a pressure of 2500 psi (17-18 N/mm^2) five times or more without any problems. The estimated pore pressures for positions P_1 to P_5 (used for the "LTS") were not expected to be greater than 2000 psi (13-14 N/mm^2), and no problems were encountered in using these pressure positions.

The pore pressure for the "RTS" was only measured at one position, and

it was expected to be in excess of 14 N/mm^2 for temperatures greater than 300 ^oC. It was therefore decided to modify pressure position P_1 for the measurement of these pressures.

(c) PRESSURE POSITION P_1

The construction of the pressure measuring system for position P_1 was identical in most respects to that for positions P_2 to P_5, as described in (b) above. However, to protect the Perspex block from pore pressure exceeding 14 N/mm^2, three extra valves (numbered 4-6) were provided in the pressure circuit at location P_1 (Figure 4.13). The Perspex 'U' tube was by-passed, by closing the valve number 5 & 6 either side of the 'U' tube, and opening the valve number 4 positioned above the 'U' tube (Figure 4.13).

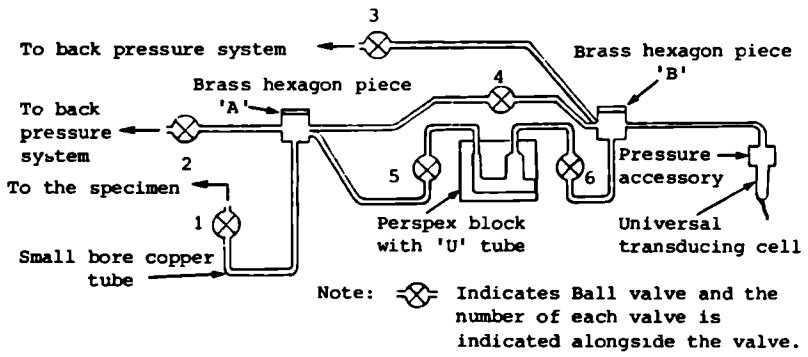

Figure 4.13: Transducer and pressure set up for pressure measuring position P_1.

To construct and operate the pressure position P_1, the following steps were taken.

1. An additional small bore copper tube with a fitting soldered to its end, was silver soldered to each brass hexagonal piece 'A' and 'B', as described above and shown in Figure 4.13.

2. The ball valve number 4 was screwed between these copper tubes.

3. The ball valve number 5 was screwed to the copper tubes between the hexagonal piece 'A' and the fitting on the narrow limb of the 'U' tube (Figure 4.13, Plate 4.9).

4. The ball valve number 6 was connected between the hexagonal piece 'B' and the fitting on the wider limb of the 'U', as shown in Figure 4.13 and Plate 4.9.

5. The valve number 5 and 6 were open and valve number 4 was shut during the testing, for pressure below 14 N/mm^2. However, valves number 5 and 6 were closed and valve number 4 was opened if the pressure exceeded 14 N/mm^2, as explained earlier in this section.

The pressure recording system was thus completed in this way and the procedure to fill this system with water is discussed in Section 4.2.6.3.

4.2.6.2 BACK PRESSURE SYSTEM

It was not possible to provide a separate system for applying back pressure to each pressure measuring point independently. A system was designed to apply the back pressure to each pressure position by opening the appropriate valve and keeping the remaining valves closed, hence, protecting other pressure positions. Figure 4.14 shows the back pressure system diagramatically and the following procedure was carried out to put the back pressure system together.

1. The fittings of the ball valves number 2 and 3 (Figures 4.8 and 4.13) not connected to the fittings of the pressure system were connected to a common reservoir (Plate 4.9). Small bore copper tubes with fittings silver soldered to each end of the copper tubes were used to connect the valves and the reservoir.

2. The reservoir made from a brass tube had eleven holes drilled and threaded for 1/8 B.S.P. threads.

3. The surface around the threaded holes was spot faced and (1/4 inch x 1/4 inch B.S.P.) parallel stud couplings were screwed to the reservoir. A Dowty seal provided the pressure seal between the couplings and the reservoir.

4. Ten of the couplings (numbered 1 to 10 in Figure 4.14) were connected to the ten ball valves, which were placed between the pressure recording system and the back pressure system. The

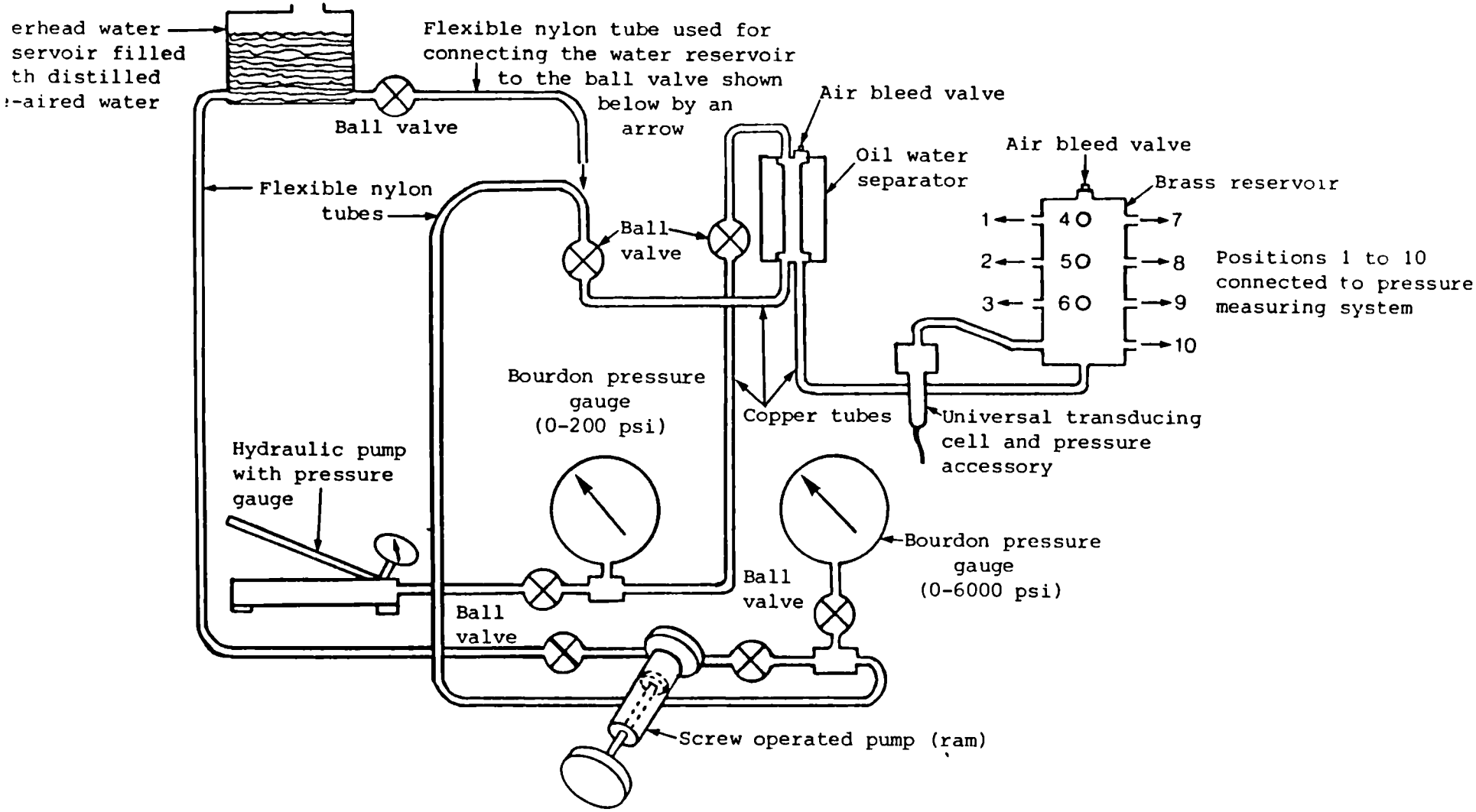

Figure 4.14: Back pressure system used for the application of back pressure.

eleventh fitting was connected to the pressure accessory of the transducer via a copper tube and parallel stud coupling (Plate 4.9 & Figure 4.14), to record the back pressure.

5. The ends of the brass tube of the reservoir were externally threaded and end caps were screwed to the top and bottom ends. A Dowty seal underneath each end cap provided the pressure seal at each end of the brass tube.

6. To bleed the air from the brass reservoir, a parallel stud coupling (1/8 inch x 1/4 inch B.S.P.) was screwed in the middle of the top end cap. A Dowty seal was used between the coupling and the end cap for sealing. A blank nipple was screwed under a union nut at the top end of the coupling.

7. To connect the brass reservoir to the oil-water separator, as described in (8) below, a parallel stud coupling (1/4 inch x 1/4 inch B.S.P.) was screwed in the centre of the bottom end cap. Once again a Dowty seal was used for providing the pressure sealing between the cap and the coupling.

8. A Perspex block called an oil-water separator, was designed to visually monitor the mixing of water and hydraulic oil. To achieve this 1/2 inch diameter hole was drilled in a Perspex block (2 inch x 2 inch x 6 inch long) and each end of the hole in the Perspex block was threaded for 1/2 inch B.S.P. threads, as seen in Figure 4.15.

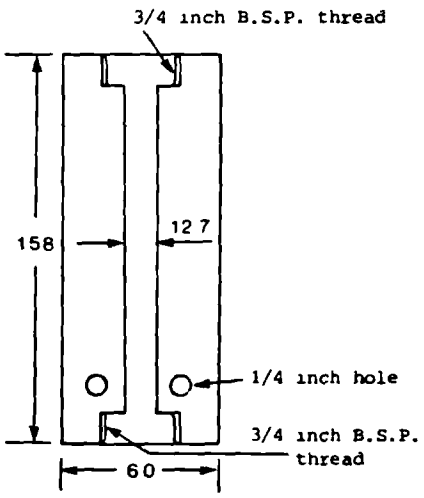

Figure 4.15:

Oil-water separator constructed from Perspex, after machining.

9. Two identical fittings (Figure 4.16) were constructed from a

brass rod, and two 1/8 inch B.S.P. stud couplings were screwed to each of the fittings (Figure 4.16). Dowty seals were used between the couplings and the fittings to seal for pressure, as shown in Figure 4.16.

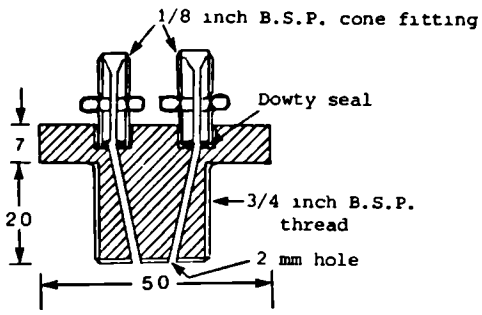

Figure 4.16:

Brass fitting used at the end of the oil-water separator.

10. One of these fittings was screwed to the threads on either ends of the oil-water separator with a Dowty seal between the two providing the pressure seal, as shown in Plate 4.9.

11. To reinforce and protect the Perspex block (Section 4.2.6.1), once again a mild steel plate was used at the top and another one at the bottom end of the fitting, as seen in Plate 4.9. These reinforcing plates were connected with four, 1/4 inch diameter bolts using a nut at each end of the bolt.

12. One of the 1/8 inch B.S.P. couplings at the bottom end of the oil-water separator was connected to the coupling at the bottom end of the reservoir (Figure 4.14 & Plate 4.9). A copper tube with nipples soldered to each end of the copper tube was used to connect the reservoir to the oil-water separator.

13. The second B.S.P. coupling at the bottom end of the oil-water separator was connected to a ball valve using a similar copper tube and fitting (Figure 4.14 & Plate 4.9), as described above.

14. The other end of the valve was designed to be connected to a screw operated ram and a (0-200 psi) Bourdon pressure gauge (Figure 4.14). This end could alternatively be connected to an overhead reservoir holding distilled de-aerated water, to fill the system with water under hydraulic head, as shown in Figure 4.14.

15. One of the two couplings at the top end of the oil-water

separator was used as an air bleed valve by screwing a blank nipple under a union nut in the coupling, whereas the second coupling was connected to a ball valve.

16. The opposite end of this valve was permanently attached to a (0-6000 psi) Bourdon pressure gauge and a hydraulic pump, as shown in Plate 4.9 & Figure 4.14.

All the ball valves were screwed to the wooden board using 'U' bolts and nuts. The Perspex block with the 'U' tube, brass reservoir, Perspex oil-water separater, Bourdon pressure gauges and the brackets holding the transducers and the pressure accessories were bolted to the board using the appropriate length of bolts and nuts. The pressure instrumentation board was used for the measurement of the pore pressure for both the "LTS" and the "RTS" by connecting it to the specimen with extension of small bore copper tubes discussed later in Section 4.2.7.

4.2.6.3 PROCEDURE FOR FILLING THE SYSTEM WITH LIQUID

To fill the pressure recording system and back pressure system installed on the instrumentation board, the following procedure was carried out.

1. An overhead reservoir filled with distilled de-aerated water, was connected to the ball valve designed to be used between the oil-water separator and the screw ram, as described previously in Section 4.2.6.2.

2. All the valves number 2 and 3 (Plate 4.9, Figure 4.8 & 4.13) connecting the back pressure to the pressure measuring side on the instrumentation board were closed.

3. The couplings connecting copper tubes to the oil-water separator, the brass reservoir, the ball valves and the pressure accessory with the transducer in back pressure system were connected and tightened.

4. The air bleed valve on top of the brass reservoir was also closed to prevent water entering the reservoir before filling the oil-water separator and bleeding air from the separator.

5. The ball valve between the overhead water reservoir and oil-water separator was opened and water was allowed to flow into the separator. This was done by opening the air bleed valve and the coupling connecting copper tube to the ball valve between the hydraulic pump and the separator incorporated at the top end of the separator (Figure 4.14).

6. Once all the air was expelled from the couplings, ball valves, copper tubes and the oil-water separator, then the air bleed valve was shut.

7. To expel air from the copper tube, the ball valve, and the hydraulic hose connected to the Bourdon pressure gauge and the hydraulic pump, the hydraulic pump was slightly pressurised, the ball valve between the pump and the oil-water separator was opened and hydraulic oil was allowed to flow from the end of the copper tube loosely screwed to the top coupling of the separator. The nut was tightened while still applying pressure with the pump, thus making sure all the air was expelled from the system.

8. After bleeding all the air from the back pressure system up to the oil-water separator, the air bleed valve on top of the brass reservoir was opened and water was allowed to flow into the reservoir while drawing the air out through the bleed valve. The bleed valve was then closed, with water still flowing under the hydraulic head of water from the overhead reservoir.

9. The union nut screwed to the coupling at the top of the pressure accessory of the transducer (Section 4.2.6.2 (4)) used to record the back pressure was unscrewed. Keeping this end of the copper tube under water in a beaker, the air was driven out from the copper tube connecting the pressure accessory to the brass reservoir.

10. The end of the copper tube was removed from the water and the nut was tightened to the coupling at the top of pressure accessory while water was still flowing through it. The pressure accessory was previously filled with de-aerated water.

11. The union nuts at the end of the copper tubes screwed to the

couplings of the ball valves (numbers 1 to 10 between the back pressure system and the pressure measuring system Section 4.2.6.2 (4)), were disconnected from the valves. The end of each copper tube was kept in water and air was expelled from the tubes one by one. The nuts were then screwed and tightened to the couplings of the valves, while water was still flowing through them. The whole back pressure system was completely filled with de-aerated water in this way.

12. To fill the pressure measuring system with water, the fittings soldered to the end of the copper tubes (Section 4.2.6.1) were tightened to the stud couplings of the appropriate ball valves.

13. The pressure accessories were filled with distilled de-aerated water making sure no air was entrapped in the accessories.

14. The 1/8 inch B.S.P. brass bolt used to connect the rest of the system to the pressure accessory (Section 4.2.6.1) was kept under water in a beaker.

15. The nipples and the union nuts at the end of the copper tubes (used to connect the copper tubes and the Perspex 'U' tube (Section 4.2.6.1)), were unscrewed from the couplings on the 'U' tube and these were also placed under water in a beaker.

16. The valves between the back pressure and pressure measuring system were opened one at a time with the back pressure system previously filled with water and still connected to the overhead water reservoir (Section 4.2.6.2). Air was expelled from the valves, the copper tubes and all the fittings by allowing the water to flow through these components.

17. The end of the copper tube with the brass bolt soldered to the end was removed from the water in the beaker (as (14) above) and it was screwed to the top of the pressure accessory while water was flowing through the copper tube.

18. The valve between the specimen and the pressure measuring system was opened (Section 4.2.6.1) and water was allowed to flow through it under a hydraulic head. After making sure all the air was removed from the valve, the fittings and the copper tube,

the valve was closed.

19. The Perspex 'U' tube was filled with water removing all the air. The required amount of mercury was then carefully introduced in the 'U' tube and the mercury level was marked on the Perspex.

20. The end of the copper tubes used to connect the Perspex 'U' tube (as explained in (15) above) were removed from the beaker and each nipple was simultaneously screwed slowly to the couplings of the Perspex 'U' tube, while water was still flowing through the copper tubes. The fittings were then tightened to prevent any pressure leak.

21. The bolts screwed into the brass hexagonal pieces 'A' and 'B' (Section 4.2.6.1) were loosened and any remaining air was expelled from the whole system, by the flow of water from the overhead reservoir through the back pressure and pressure measuring systems.

22. All the valves on the instrumentation board were closed and the transducers were screwed into the pressure accessories, as described in (Section 4.2.6.1 (a)).

25. Finally the mild steel reinforcing plates were positioned at the top and bottom end of the Perspex 'U' tube and the Perspex oil-water separator. These plates were then bolted together, as described ealier in Section 4.2.6.1 and 4.2.6.2 respectively. The instrumentation board was ready for connection to the specimen and to record the pore pressure of heated concrete during testing.

4.2.7 PROCEDURE FOR PORE PRESSURE MEASUREMENT

The procedure for recording the pore pressures of the heated concrete was identical for both test series. However, the pressure was monitored at five positions in the "Liner Test Series" and only at one location for the "Release Test Series", as described in Section 4.2.5. The following procedure was carried out for the connection of the specimen to the instrumentation board.

1. After removing the Plasticine from the fittings of the copper

tubes connected to the porous plate of the specimen, the copper tubes were filled with liquid using a hypodermic syringe described in Chapter 3, Section 3.3.7.

2. To connect the pressure measuring system to the specimen, an extension copper tube was used with a nipple silver soldered to each end and union nuts around the nipples (Figure 4.17). The length of each extension copper tube used depended upon the distance between the coupling at the end of the small bore copper tube of the specimen ("LTS") and the appropriate valve on the instrumentation board. For the "RTS" specimen the extension copper tube was connected between the pressure instrumentation board and the valve protecting the pressure system (Appendix II, Section II.7, Chapter 3 Section 3.4.6 and Section 4.2.7.2)

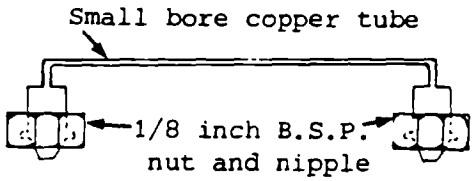

Figure 4.17:
Extension copper tube with the fittings.

3. The fitting at one end of the extension copper tube was tightly screwed to the coupling of the ball valve number 1 (Section 4.2.6.1). To make sure that all the air had been removed from the copper tube, the other end of the tube was left under water in a beaker.

4. The valve between the oil-water separator and the overhead reservoir was opened.

5. The valve number 2 (Section 4.2.6.1) was also opened. This valve was designed:

i. To fill the water in the extension copper tubes before the start of the experiment, because it was not possible to use the valve number 3 to fill the copper tube with water, due to the presence of mercury in the Perspex 'U' tube.

ii. To protect the pressure measuring side of the instrumentation board during the application of the back pressure.

iii. To adjust the mercury level in the Perspex 'U' tube before the start of the test (by opening the valve number 2 and valve number 3 for every 'U' tube independently).

6. The valve number 1 was opened and air was expelled from the copper tube by the flow of water through the copper tube described in (3) above.

7. The end of the extension copper tube was removed from the beaker. The fitting at the end of the copper tube was screwed to the coupling at the end of the small bore copper tube for the "LTS" and to the coupling of the ball valve for the "RTS" (as described in (2) above). This was done while water was still flowing through the extension copper tube.

8. After tightly screwing the fittings of the extension copper tube, the valve number 3 was also opened and the mercury level inside the Perspex 'U' tube was adjusted and marked.

9. The valve between the water reservoir and the back pressure system was shut. The water reservoir connection at the top end of the valve was unscrewed and the screw operated ram with Bourdon pressure gauge (0-200 psi) was connected to the top coupling of the valve (Section 4.2.6.2). This valve was designed to be used, either with the water reservoir to fill the system with water, or with the screw operated ram for the application of the back pressure at pressures up to 200 psi, as described in Section 4.2.6.2.

10. All the valves were closed and the instruments on the instrumentation board connected to the specimen were ready to be used during the experiments. The following procedure was carried out to record the pressure and the application of the back pressure for the "LTS" and the "RTS" tests.

4.2.7.1 "LINER TEST SERIES" PORE PRESSURE MEASUREMENT

i. The valve number 1 was opened, connecting the instrumentation board to the specimen.

ii. To provide the back pressure with the screw pump up to 200 psi,

the valve between the screw operated ram and the back pressure system was opened.

iii. Before starting the experiment, the transducers were energised and were connected to the recording instruments (i.e. data logger and chart recorder). The pressure measuring devices were zeroed.

iv. The experiment was switched on (Chapter 3, Section 3.3.8).

v. The back pressure and the pore pressure of the concrete was continously recorded on the chart recorder for the first pressure position. However, all the pressures were also recorded on the data logger.

vi. After the start of the test there was no significant development of pore pressure inside the concrete for about 10 minutes, because during this period only the internal spiral heater and the external rope heater were heating the steel top ring (Chapter 3, Section 3.3.3). The concrete temperature at the concrete-diaphragm interface did not increase above 40 ^{o}C on average. No back pressure was applied at any of the pressure measuring points.

vii. A thermal shock was applied to the stainless steel diaphragm by pouring the molten lead into the steel top ring, consequently establishing a thermal gradient inside the concrete. The concrete temperature was therefore increased sharply, creating a pore pressure and the mercury level dropped inside the limb of the Perspex 'U' tube nearest to the specimen.

viii. To compensate the drop of mercury level in the Perspex 'U' tube, the pressure inside the back pressure system was increased to the same level as the pore pressure of concrete, for the pressure position where the adjustment of the mercury level was required .

ix. The ball valve number 3 described in Section 4.2.6.1 was opened and applying the back pressure, the mercury level inside the Perspex 'U' tube was corrected.

x. Knowing the pore pressure of the concrete from the recorded values (as explained in (v) above), the back pressure

was applied very precisely to each pressure point whenever there was need to apply the back pressure.

xi. As soon as the mercury level in the 'U' tube was adjusted, the valve number 3 was closed.

xii. This procedure of the application of the back pressure (described in (viii)-(xi) above) was repeated, as soon as the level of mercury was seen changing in any of the 'U' tubes.

xiii. The back pressure was generally applied more often during the early part of the testing, for the pressures up to 150-200 psi. However the need for application of the back pressure was less frequent with time and increase of pore pressure, as the pressure measuring system stabilized and the system became self-adjusting.

xiv. To apply a back pressure greater than 200 psi (Section 4.2.6.2), a hydraulic pump was used. The valve connecting the screw ram to the back pressure system was closed and the valve connecting the hydraulic pump to the back pressure system was opened.

xv. The back pressure was precisely applied at each pressure point and the mercury level in the smaller limb of the 'U' tube never dropped more than 3-4mm during any experiment.

4.2.7.2 <u>"RELEASE TEST SERIES" PORE PRESSURE MEASUREMENT</u>

i. After connecting the test cell to the instrumentation board the valve number 1 (Section 4.2.6.1 and Section 4.2.7) and the valve protecting the pressure measuring system of the "RTS", as described in Chapter 3, Section 3.4.6 & Section 4.2.7, were opened.

ii. Same as (ii) of the "Liner Test Series" in Section 4.2.7.1 above.

iii. Same as (iii) of Section 4.2.7.1.

iv. The experiment was switched on (Chapter 3, Section 3.4.6).

v. The pore pressure of the concrete was only monitored at one position in the "RTS". Therefore the pore pressure of the

concrete and the back pressure were recorded continously on the chart recorder as well as on the data logger.

vi. The concrete temperature increased slowly with time, as the specimen was being heated uniformly inside a furnace. Hence, the pore pressures inside the concrete also developed smoothly and the mercury level in the smaller diameter limb of the 'U' tube dropped with the increase of the pore pressure.

vii. To adjust the mercury level in the 'U' tube the back pressure was applied in a similar way as described for the "LTS" procedures ((viii) through to (xiv) discussed in Section 4.2.7.1).

viii. The application of the back pressure was only required at one position for the "RTS" experiments and it was found by experience that hardly any back pressure adjustment was required for pressure greater than 1000 psi, as the system became self-adjusting at higher pressures.

ix. The Perspex 'U' tube was protected with three extra ball valves, as described in Section 4.2.6.1 (c) for the measurement of pressure over 14 N/mm^2. Therefore the pore pressure for test temperatures of 325 ^oC, 342 ^oC and 350 ^oC was recorded without monitoring the mercury level in the Perspex 'U' tube above $14N/mm^2$.

x. As described earlier in (vii) above, no back pressure was required for higher pressures and it was confidently assumed that no water was moving into or out of the porous plate inside the concrete.

xi. To check the above assumption that water was not moving either way, the back pressure equal to the recorded pore pressure was applied to the back pressure system, and by quickly opening the valve number 3, both the back pressure and the concrete pore pressure were recorded before closing the valve.

xii. On comparing the values of the back pressure and the pore pressure of the concrete it was established that the difference between the two values was not greater than 0.01 N/mm^2. This minimal difference of readings proved that there was no need to

apply the back pressure after the Perspex 'U' tube was not in use.

xiii. Once the release procedure (Chapter 3, Section 3.4.7) was carried out and the pore pressures of concrete were less than 14 N/mm^2, the back pressure was again supplied through the Perspex 'U' tube.

4.3 DEFLECTION MEASUREMENT

The central deflection of the stainless steel diaphragm was measured for the "LTS" to investigate the relationship between the pore pressure of concrete and the deflection of the steel liner of a Fast Breeder Reactor.

To record the deflection of the stainless steel diaphragm a transducer with the displacement magnifying accessory was mounted in a displacement measuring assembly, which was supported on three Sintox tubes. Each Sintox tube was positioned on top of a stainless steel ball resting on the stainless steel diaphragm. The central deflection of the diaphragm was transferred to the transducer by a fourth Sintox tube, placed between the magnifying accessory and the stainless steel diaphragm, on top of the steel ball. Plate 4.11 shows the transducer assembly with all the components.

The Sintox tubes were used for protecting the transducer and its accessories from the direct application of temperature and to protect the central Sintox tube from molten lead. A copper tube was screwed to a brass nut which was cemented to the stainless steel diaphragm (Appendix I, Section I.8). The details for setting-up the displacement measuring devices and their calibrations are described below.

4.3.1 TRANSDUCER AND ACCESSORIES DETAILS AND CALIBRATIONS

A Universal Transducing Cell similar to the one used for measuring the pore pressure of concrete (Section 4.2.2) was used to measure the deflection of the diaphragm. The transducer itself could measure the maximum displacement of 0.005 inch (0.12mm) with infinitesimal resolution. However, as explained in Section 4.2.2 the displacement accessories can be used with the transducer to magnify the

displacements without losing the accuracy of the transducer. Therefore, a linear displacement accessory, model UD3, with 0.1 inch maximum displacement was used with the transducer. Plate 4.12 shows the transducer, displacement accessory, Sintox tube and steel ball.

The transducer was screwed into the displacement accessory and it was energised by a Farnel power supply unit.

The deflection was recorded on the data logger and the chart recorder simultaneously by connecting the output from the transducer to both the measuring devices.

The transducer with the displacement accessory was calibrated against a micrometer (Plate 4.13). The calibration set up consists of a micrometer clamped between two metal blocks, which were then screwed to a mild steel plate. A transducer holding bracket supplied with the transducer was screwed to the steel plate. The transducer with the displacement accessory was secured to this bracket, using a lock nut on the accessory, ensuring that the central point on the micrometer tip and the measuring tip on the displacement accessory were in a straight horizontal line. The transducer was energised and the calibration was carried out as follows.

To record the transducer output the chart recorder and the data logger were switched on. The chart recorder module recording the deflection was zeroed. A known displacement was applied to the transducer by turning the micrometer. The output scale of the chart recorder was adjusted, using the facility provided on the module of the chart recorder for the selected input values.

The calibration coefficient was determined by recording the output voltage on the data logger at a given input voltage, and the equivalent micrometer reading. The output voltage of the transducer varies with input voltage for a given parameter (Section 4.2.2). Figure 4.18 shows the transducer output plotted against the displacement for various input voltages. It was therefore necessary to use the same input voltage for all the tests and to maintain it during the testing.

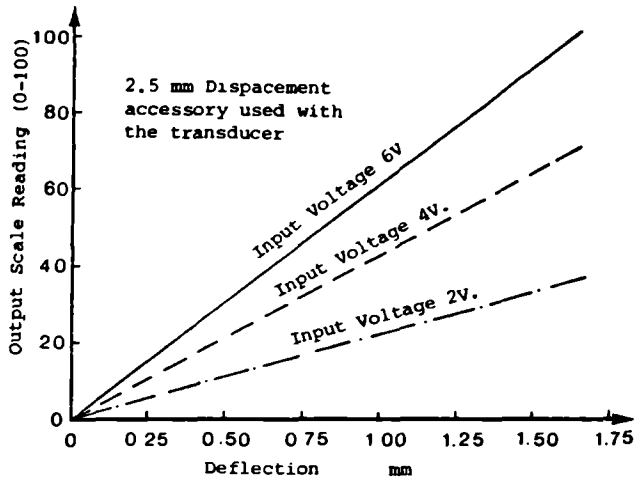

Figure 4.18:

Output voltage against displacement for various input voltages.

The calibration coefficient obtained was incorporated in the computer program used for logging the experimental values, thus converting the recorded voltages into inches.

4.3.2 TRANSDUCER ASSEMBLY DESIGN AND DETAILS

The central deflection of the stainless steel diaphragm was measured by mounting the transducer and the displacement accessory into the transducer holding assembly (Plate 4.11). The design, construction and the use of the assembly is described below.

1. A triangular piece was cut from 1/8 inch thick steel plate. A hole (1/2 inch diameter) was drilled in the centre of the triangular plate and a hole was also drilled and tapped for 1/2 inch B.S.F. threads in each corner of the triangular plate, as shown in Figure 4.19.

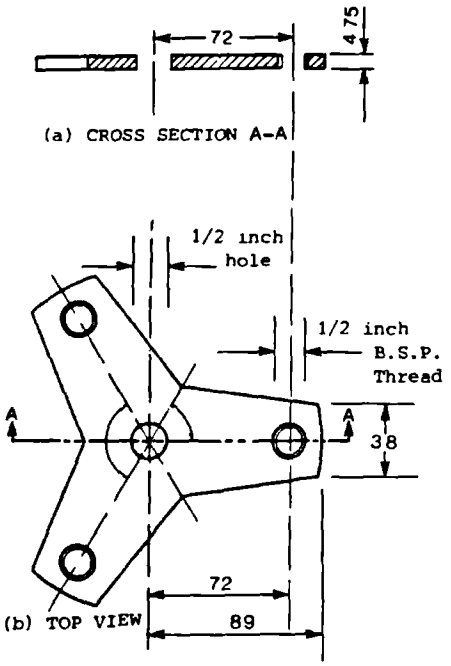

Figure 4.19:

Triangular mild steel plate used as transducer accessory.

Note: All the dimensions are in mm unless specified otherwise.

2. The transducer and the displacement accessory were screwed to an invar fitting, which was secured to the triangular plate through the central hole with the help of a nut.

3. To make this fitting, a 20 mm diameter rod was cut to size and a hole was drilled through the centre of the rod (Figure 4.20). The top end of the drilled hole was threaded to accommodate the displacement accessory and the transducer. The external diameter at the bottom end of the rod was machined and threaded for 1/2 inch B.S.F. threads. A groove was machined through the wall of the fitting on one side for visually inspecting the contact between the central Sintox tube and the tip of the displacement accessory. Three 8 B.A. threads were tapped through the wall of the fitting and using a 8 B.A. screw (with a lock nut) in each thread, the central Sintox tube was located under the tip of the displacement accessory (Plate 4.11). A hole was also drilled through the side of the fitting to introduce the thermocouple to measure the temperature of the Sintox tube at the junction of the Sintox tube and the displacement accessory.

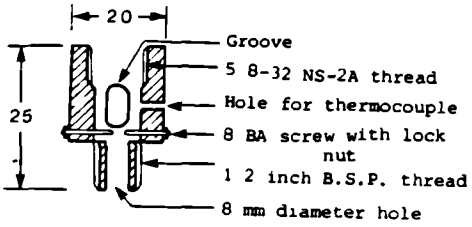

Figure 4.20:

Central Invar fitting used for holding a transducer.

4. The whole assembly rested on top of three Sintox tubes with the help of three adjustable fittings screwed to the ends of the triangular plate (Plate 4.11). One of the adjustable fittings was 3 inches long (Figure 4.21(a)), while the remaining two fittings were only 2 inches long, as shown in Figure 4.21(b).

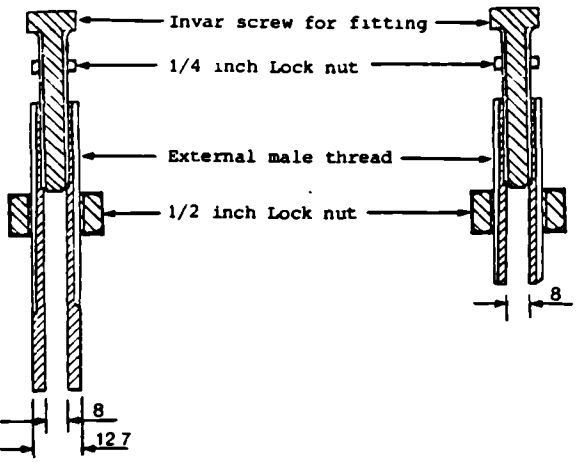

(a) 3 inch long Invar adjustable fitting. (b) 2 inch long Invar fitting

Figure 4.21: Adjustable Invar fittings.

5. All the adjustable fittings were made from a 1/2 inch diameter Invar rod. The required length of the fitting was cut and a hole was drilled through the centre of each fitting. The top portion of the hole was internally threaded to accommodate 1/4 inch B.S.F. screws. These screws were used to adjust the height and the level of the assembly over three Sintox tubes with respect to the central Sintox tube. The screws used for all the three fittings were of the same design. These were machined from a 1/2 inch diameter Invar rod and were externally threaded for 1/2 inch B.S.F. threads, as seen in Figure 4.21(a).

6. The 2 inch long adjustable fittings were externally threaded for the whole length, while the 3 inch long fitting was only threaded to a length of 2 inchs.

7. To locate a thermocouple for measuring the temperature at the top of the external Sintox tube, a slot was machined in the 2 inch long Invar fitting.

8. The fittings were screwed to the triangular plate and a 1/2 inch B.S.F. nut was used to lock each fitting in position (Plate 4.11 & Figure 4.22). Invar was used for the good thermal properties of the material (e.g. low thermal expansion etc.).

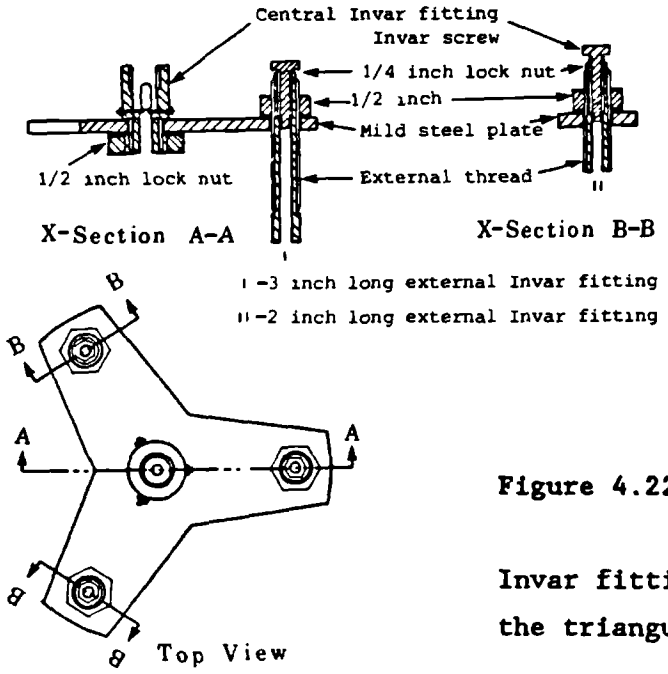

Figure 4.22:

Invar fittings attached to the triangular plate.

4.3.3 SINTOX TUBE AND STEEL BALL DETAILS

The deflection measuring system designed for the "LTS" had to absorb a thermal shock and resist deformation during pouring of the molten lead used to heat the stainless steel diaphragm (Chapter 3, Section 3.3.3). Many materials were considered to transmit the central deflection of the stainless steel diaphragm to the transducer. Finally Sintox tube made of ceramic material (6.35mm o.d. x 3.17mm i.d. x 255mm long) was selected for its good thermal properties. The Sintox tube could withstand a thermal shock and would not deform up to a temperature of 1450 ^{o}C. Three Sintox tubes were also used to carry the transducer assembly (Section 4.3.2).

Each Sintox tube rested on a stainless steel ball 1/16 inch in diameter, as seen in Plate 4.11. The steel balls were used to

locate the tubes in position.

4.3.4 DEFLECTION MEASUREMENT DETAILS AND PROCEDURES

The deflection measuring assembly (Plate 4.11) was used to measure the central deflection of the diaphragm. The set up before starting the experiment and the deflection measuring procedure is described below.

1. Three stainless steel balls were introduced into the holes drilled in the mild steel top ring, as described in Appendix I, Section I.4. The fourth steel ball was placed in the central indentation machined on the stainless steel diaphragm (Appendix I, Section I.3).

2. The Sintox tubes were positioned on top of the steel balls.

3. Thermocouples were attached to one of the three outside Sintox tubes to measure the temperature of the tube during testing, as explained in Appendix IV, Section IV.2. Each thermocouple was attached to the tube by placing and screwing a thermocouple under a brass fitting (Figure 4.23).

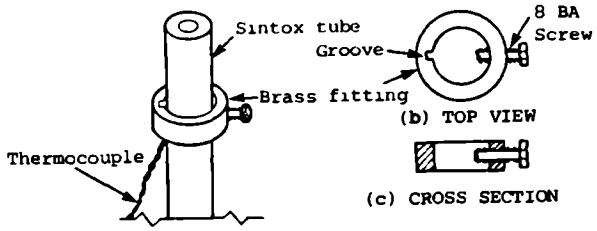

Figure 4.23:

Brass fitting used for connecting the thermocouple to the Sintox tube.

4. The temperature at the top of the external tube was recorded by introducing a thermocouple through the adjustable fitting explained in (7) below and Section 4.3.2 previously.

5. The temperature of the central Sintox tube was measured at four places by thermocouples inserted through the holes drilled in the copper tube protecting the Sintox tube from the molten lead (Appendix I, Section I.8). The temperature at the top end of the central tube was measured by a thermocouple introduced inside the invar fitting holding the deflection accessory (Section 4.3.2)

and explained in (7) below.

6. The transducer assembly was placed on top of the external Sintox tubes and the central Sintox tube was positioned under the tip of the deflection accessory by adjusting the three 8 B.A. screws (Section 4.3.2).

7. Thermocouples were finally introduced into the external and the internal Invar fittings through the positions provided for the thermocouples explained in (4), (5) above and in Section 4.3.2 previously.

8. The transducer was connected to the data logger and the chart recorder. The transducer assembly was levelled by using the three adjustable fittings (section 4.3.2). A circular spirit level was used on top of the assembly to monitor the adjustment of the assembly.

The deflection measuring assembly mounted on the test rig (Plate 3.10 Chapter 3) was ready for the measurement of the central deflection of the stainless steel diaphragm.

4.4 TEMPERATURE MEASUREMENT

4.4.1 THERMOCOUPLE DESIGN AND CALIBRATION

The main criteria for the design of the thermocouples were the temperature range, sensitivity, robustness and means of pressure sealing between the thermocouple and the steel cylinder through which these thermocouple were passing. Nickel/Chrome, Nickel/Aluminium (Type K) thermocouples were selected to measure all the temperatures in the experimental work described in this thesis. The thermocouples used inside the concrete and the molten lead were mineral insulated. Stainless steel was used as sheathing material and all thermocouples were factory manufactured. The flexible wire for the thermocouples of the "RTS" was also screened.

To seal between the thermocouples and the steel cylinder a pressure gland recommended by the manufacturers for use with these particular thermocouples was used. Plate 4.14 shows the two types of sheathed

thermocouples and the exploded view of the pressure gland.

The male 1/8 inch B.S.P. tapered fittings were screwed into tapped holes in the steel cylinders of the "LTS" and the "RTS" (Appendix I, Section I.2 and Appendix II, Section II.2). A copper washer was used between the flange of the fitting and the cylinder to give an additional pressure sealing. The position where the copper washer was used was spot faced (Appendix I, Section I.2 and Appendix II, Section II.2).

The seal between the thermocouple sheath and the fitting was provided by positioning an olive over the thermocouple sheath (Plate 4.15) and screwing the nut on to the fitting. The olive was set on the sheath and as it screwed into the cone under the nut, it provided efficient sealing between the thermocouple and the pressure glands. Plate 4.15 shows the thermocouple passing through the pressure gland without being screwed to the steel cylinder. Plates 4.16 and 4.17 show the pressure glands and the thermocouple screwed to the steel cylinder for both the "LTS"" and the "RTS" respectively.

For temperature measurements outside the concrete where pressure sealing was not required and no moisture was present, flexible wire, Nickel/Chrome, Nickel/Aluminium thermocouples with fibre glass sheathing were used.

Extension lead corresponding to type K thermocouple was used where the original thermocouple lead was not long enough to reach the recording instrument. The extension lead was connected to the thermocouple lead using a socket and plug (designed and recommended by the manufacturer for connecting both the leads together). The extended thermocouples were checked for performance against the thermocouples without the extension leads and showed that there was no interference or change in the temperatures measured by the extended thermocouples.

All the thermocouples were calibrated in ice and hot water tub (0 to 100 ^{o}C) against a mercury thermometer, and the difference in temperature was not greater than 0.1 ^{o}C over full scale.

4.4.2 TEMPERATURE MEASURING PROCEDURE

The temperatures were measured by connecting the flexible wires of the thermocouples into the satelite cabinet of the data logger. The cabinet of the data logger had a cold reference junction for the thermocouples, and temperature was directly recorded in degrees celsius using an appropriate computer program in the data logger.

The temperature of the lead-diaphragm interface inside the molten lead, and the concrete-diaphragm interface inside the concrete of the "LTS" was additionally recored on the chart recorder. Each thermocouple measuring these temperatures was extended with a pair of extension cables and the connector plug (as described in the previous section). One of the extension cables for each thermocouple was connected to the data logger and the second extension cable of the same thermocouple was connected to the chart recorder. In this way the temperature was monitored continously for the lead-diaphragm and the concrete-diaphragm interface in addition to recording these temperatures on the data logger. The temperatures of the "RTS" were also recorded on both the recording instruments, as explained above.

The flat bed chart recorder had a capability to house modules for different types of thermocouples. These modules had a cold end reference junction incorporated for the particular thermocouple.

4.5 WEIGHT MEASUREMENT

The weight of specimens was measured by electronic balances of two types.

(a) A top loading Sartorius balance up to 16 kg.
(b) A top loading Metler balance for weights over 16 kg.

The weight of "LTS" cells was more than 16 kg, hence the weight was recorded by the Metler balance, whereas the Sartorius balance was used to monitor all the rest of the weights throughout the experimental programme. The sensitivity of balance (a) was 0.1 gm over the full range and the sensitivity of balance (b) was 1 gm over the full range.

To protect the Sartorius balance (Plate 4.18) from heat while measuring the weight of the heated samples, and the specimen of "RTS",

an insulated platform was used between the specimen and the top loading surface of the balance.

The rectangular platform shown resting on the balance in Plate 4.18 was made of 1/8 inch thick mild steel plate, and to insulate the balance from the platform a (1/2 inch diameter) P.T.F.E. foot was screwed to each corner of the platform.

Plate 3.26 of Chapter 3 shows a "RTS" cell being weighed during testing.

4.6 VARIOUS TYPES OF WATER MEASUREMENT IN "LINER TEST SERIES" AT THE END OF TESTING

To determine the values of non-evaporable water (W_n) and evaporable water (W_e) content of concrete for a "LTS" specimen, samples were removed from the specimen (Chapter 3, Section 3.3.9) and the following procedure was carried out to obtain the variables for calculations.

1. Each sample was weighed after removal from the specimen (W_w).

2. The sample was dried to a constant weight at 105 ^{o}C inside an oven (W_{105}).

3. It was then placed in a dessicator and air was evacuated from the sample.

4. On maintaining a vacuum of 1 atmosphere, water was allowed to flow into the dessicator under vacuum, and further evacuation performed.

5. After completely de-airing the sample, vacuum was removed and the sample was left submerged under water for 24 hours.

6. The submerged weight of the sample (W_{sub}) was measured, as shown in Figure 4.24. The temperature of the water the sample was submerged in was also monitored.

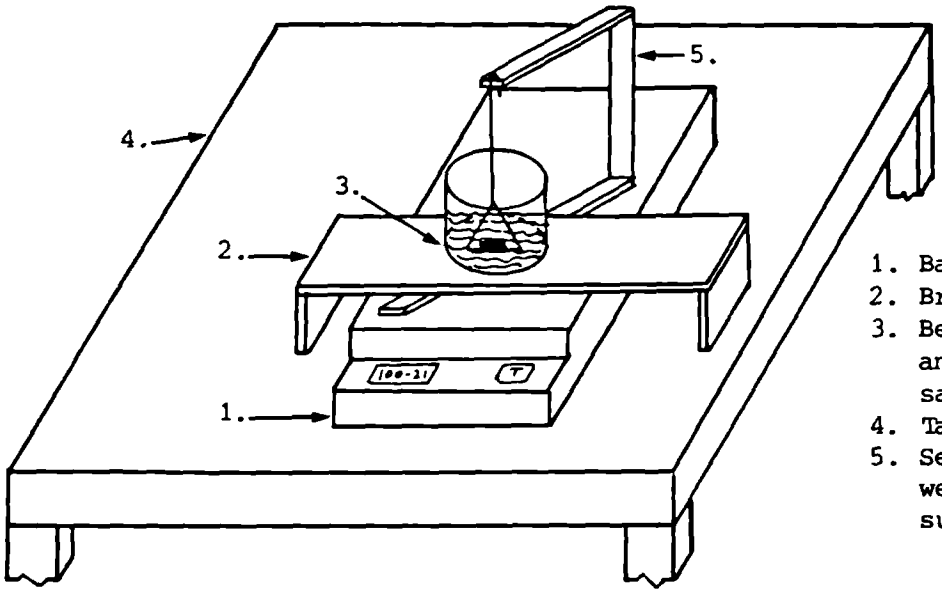

KEY

1. Balance
2. Bridge
3. Beaker with water and submerged sample
4. Table
5. Set up for weighing the submerged sample

Figure 4.24: Set up for measuring the submerged weight of the sample.

The theory and concept for the calculations of the weight of non-evaporable and evaporable water are discussed in the following sections for two cases.

4.6.1 DETERMINATION OF NON-EVAPORABLE AND EVAPORABLE WATER CONTENT

CASE 1

The equations used for evaluating non-evaporable and evaporable water content are developed. The method used by Greathead (1986) for the application of concrete density correction due to the settlement of aggregates (Section 4.6.1.1) is incorporated into these equations.

By definition, the Archimedes Principle states that the apparent loss in weight of a body immersed in liquid divided by the density of liquid equals the volume of liquid displaced. Therefore:

$$\frac{W_{105} - W_{sub}}{p_w} = V_a + V_c + V_n \qquad 4.1$$

where:

V_a = Volume of aggregate

V_c = Volume of Cementitious materials

V_n = Effective specific volume of non-evaporable water. The assumption is made that $V_c + V_n$ equals volume of hydrated products plus volume of unreacted cementitious materials.

p_w = Density of liquid used for submerged weighing at corresponding liquid temperature.

V_n is further related (Greathead, 1986) as:

$$V_n = (1\text{-BETA}).\ V_n$$

Where "Volume Factor", BETA, is defined as a dimensionless constant determining the relationship between the volume of hydration products and the amount of non-evaporable water in the cement. The maximum value of BETA of 0.345 was experimentally evaluated by him for a Cemsave/SRPC blend. It was the same material which has been used in the experiments here. However, BETA equals 0.254 for ordinary Portland cement, again evaluated by him. The value of BETA therefore lies between 0.254 to 0.345.

Now subsituting value of V_n in equation 4.1 we have:

$$\frac{W_{105} - W_{sub}}{p_w} = V_a + V_c + (1 - BETA).\ V_n \qquad 4.2$$

The effective density of non-evaporable water (p_n) by definition is:

$$p_n = W_n/V_n = p_w/(1\text{-BETA})$$

because p_w, the density of water in the bulk state is related to p_n, as above (Greathead, 1986).

Equation 4.2 for the volume of solid (V_s) can be written as:

$$V_s = V_a + V_c + W_n/p_n \qquad 4.3$$

Now if p_a, W_a and p_c, W_c are the densities and the weights of aggregate and cementitious materials respectively, the corresponding aggregate/cement (r) and water/cement (s) ratios are:

$$r = W_a/W_c \quad \text{and} \quad s = W_t/W_c$$

where: W_t is the original weight of mix water in the specimen.

By subsitution the equation 4.3 becomes:

$$V_s = W_c\ .\ (r/p_a + 1/p_c + s/p_n\ .\ (W_n/W_t)) \qquad 4.4$$

Now assuming that dry concrete consists of aggregates, cement and non-evaporable water and considering the fact that part of the cement is combined with the non-evaporable water chemically, to form various compounds (products of hydration) and taking into account the aggregate/cement ratio (r) and water/cement ratio (s), we get:

$$W_{105} = W_a + W_c + W_n$$

$$W_{105} = W_c \, (r + 1 + s(W_n/W_t)) \qquad 4.5$$

To obtain W_{105}/V_s, equation 4.5 is divided by equation 4.4

$$\frac{W_{105}}{V_s} = z = \frac{W_{105} \cdot p_w}{W_{105} - W_{sub}} = \frac{(r + 1 + s\,(W_n/W_t))}{r/p_a + 1/p_c + (W_n/W_t) \cdot s/p_n} \qquad 4.6$$

The basic equation for non-evaporable water (W_n) as a fraction of the original mix water (W_t) in a specimen can be represented by rearranging the above equation, as:

$$\frac{W_n}{W_t} = \frac{(r + 1)/z - r/p_a - 1/p_c}{s(1/p_n - 1/z)} \qquad 4.7$$

Note: The mix design used for this thesis was identical to the mix design used by Greathead (1986), therefore the values of p_a, p_c, p_n and s for this work are identical to his values determined by him experimentally.

$$p_a = 2.902 \text{ g/cm}^3, \quad p_c = 3.03 \text{ g/cm}^3, \quad s = 0.39, \quad p_n = 1.47$$

The value of r (aggregate/cement) is obtained as described later in Section 4.6.1.1.

The weight of evaporable water (W_e) by definition is the amount of water lost at 105 ^{o}C by heating concrete to a constant weight loss.

$$W_e = W_w - W_{105}$$

where:

W_w is the weight of the concrete sample (after extraction, as discussed in Chapter 3, Section 3.3.9) before drying.

The weight of evaporable water per unit weight of dry concrete is:

$$\frac{W_e}{W_{105}} = \frac{W_w - W_{105}}{W_{105}}$$

On rearranging the equation for the amount of evaporable water (W_e) in a specimen as a fraction of the original mix water (W_t) and substituting the value of W_{105} from eqution 4.5, the equation for evaporable water per unit weight of mix water is:

$$\frac{W_e}{W_t} = \frac{W_w - W_{105}}{W_{105}} \cdot \frac{1 + r}{s + W_n/W_t} \qquad 4.8$$

In order to solve equation 4.7 and 4.8, the value of r for the samples extracted from various positions of the "LTS" specimen are obtained, as discussed in the following section.

4.6.1.1 CORRECTION FOR AGGREGATE/CEMENT RATIO DUE TO SETTLEMENT OF AGGREGATES

The concrete samples removed from the "LTS" specimens (Plate 5.4) clearly show that the ratio of aggregate to paste varies throughout the depth of concrete. The concrete poured first has greater amount of aggregates than the concrete placed at subsequent levels. In Plate 5.4 slice numbered as 2 represents the sample of concrete poured in before slice number 5, 9, and 12 into the test cell. It is therefore evident that slice 12 has less aggregates than the remaining samples. Greathead (1986) studied the effect of aggregate settlement and correlated between the original concrete density and aggregate/cement ratio. He showed that if the density varies then the value of aggregate/cement ratio (r) varies as:

$$r = r + 18.83D_{po} \qquad 4.9$$

where:

D_{po} is the change in density with relation to the position of sample removed from the specimen.

The variation of D_{po} is plotted against relative position of concrete in the "LTS" specimen in Figure 4.25. The axis marked as top represents the concrete poured in first while casting the specimens, as it is worth recalling that concrete was cast in the "LTS" cells by clamping these upside down (Plate 3.6), as explained in Chapter 3, Section 3.3.6.1.

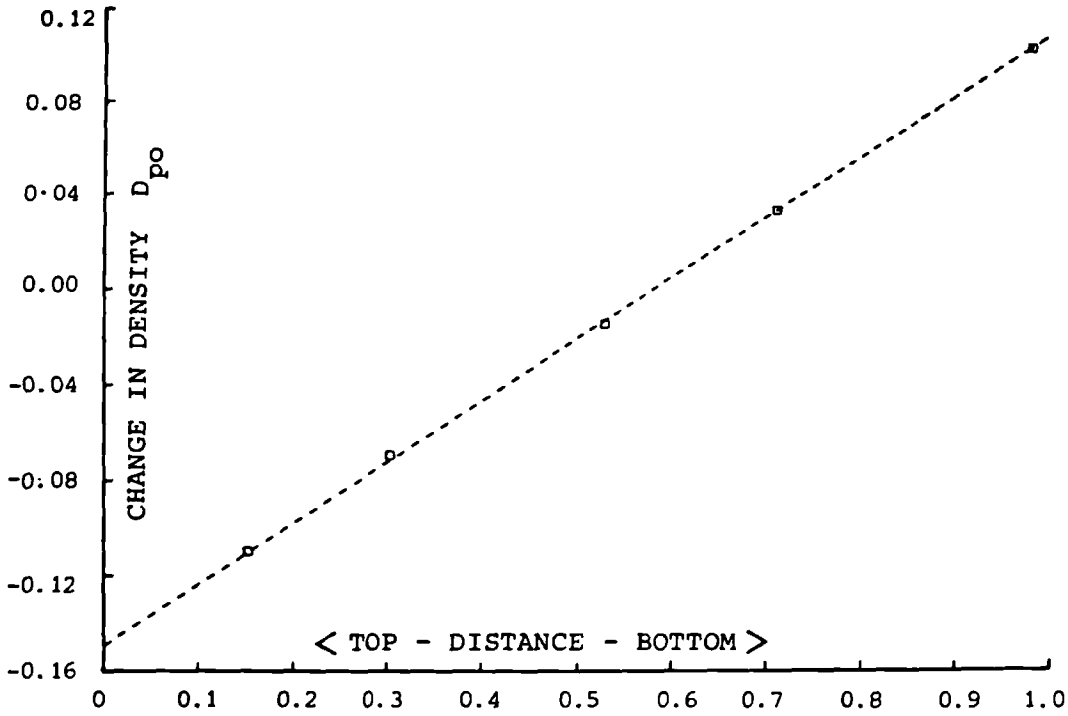

Figure 4.25: Change in density against relative position of concrete for the "LTS" specimen.

The value of D_{po} was read from Figure 4.25 for corresponding distance of the extracted sample. Subsituting D_{po} in equation 4.9 the value of r was computed for obtaining W_n/W_t and W_e/W_t. The results for W_n/W_t and W_e/W_t are discussed in Chapter 5, Section 5.3.5.

4.6.2 DETERMINATION OF EVAPORABLE AND NON-EVAPORABLE WATER CONTENT CASE 2

The method used by Chapman (1976) for working out the various quantities of water was modified for the mix design used in this work and these equations are postulated in the following sections. The way measurements were performed and the notations used in Section 4.6 and 4.6.1 are repeated here.

4.6.2.1 EVAPORABLE WATER CONTENT

As before the weight of evaporable water (W_e) per unit weight of dried concrete (W_{105}) is given by:

$$\frac{W_e}{W_{105}} = \frac{W_w - W_{105}}{W_{105}}$$

To assess the amount of water lost during the "LTS" tests, the evaporable water (W_e) is expressed in terms of the total mixing water (W_t). It is assumed that dry concrete is a mixture of aggregate, cement and non-evaporable water, which is not strictly true as part of the cement combines with the non-evaporable water in a chemical bond to form various compounds (products of hydration). Therefore:

$$W_{105} = W_c + W_a + W_n$$

$$= W_t \frac{(1 + W_a/W_c)}{W_t/W_c} + W_n/W_t$$

Note: As previously, for this work $W_a/W_c = 3.969$ and $W_t/W_c = 0.39$

Therefore:

$$\frac{W_e}{W_t} = \frac{W_e - W_{105}}{W_{105}} (12.741 + W_n/W_t) \qquad 4.10$$

4.6.2.2 NON-EVAPORABLE WATER CONTENT

Once again the procedure for drying and weight measurements, as discussed in Section 4.6 and 4.6.1 are used for working out the equations here. By applying Archimedes principle as previously for equation 4.1, we have:

$$\frac{W_{105} - W_{sub}}{p_w} = V_a + V_c + V_n$$

Therefore:

$$\frac{W_{105} - W_{sub}}{p_w} = W_c (W_a/W_c \cdot 1/P_a + 1/P_c + W_n/W_t \cdot W_t/W_c \cdot 1/p_n) \qquad 4.11$$

Now as before:

$$W_{105} = W_a + W_c + W_n = W_c (W_a/W_c + 1 + W_t/W_c \cdot W_n/W_t) \qquad 4.12$$

Dividing equation 4.12 by equation 4.11:

$$\frac{W_{105}\, p_w}{W_{105} - W_{sub}} = \frac{W_a/W_c + 1 + (W_t/W_c \cdot W_n/w_t)}{W_a/W_c \cdot 1/p_a + 1/p_c + W_t/W_c \cdot W_n/W_t \cdot 1/p_n} \qquad 4.13$$

Note: The values of p_a, p_c, p_n and W_t/W_c (s) as in Section 4.6.1 and

W_a/W_c (r) = 3.969 same as given earlier in Section 4.6.2.1.

Now after subsituting the above values (all metric units) in equation 4.13 and after re-arranging the modified equation is:

$$\frac{W_n}{W_t} = \frac{4.969 \cdot \frac{W_{105} - W_{sub}}{W_{105}\, P_w} - 1.698}{0.26531 - 0.39 \cdot \frac{W_{105} - W_{sub}}{W_{105}\, P_w}} \qquad 4.14$$

4.6.3 ASSESSMENT FOR THE WATER REMAINING IN THE SPECIMEN

The water lost or gained from various positions of a specimen can be found:

- by subtracting the evaporable and non-evaporable water from the total mixing water

- by plotting the total water content per unit weight of mix water against the distance below the diaphragm for each sample, and then measuring the areas of water loss and water gain (Figure 4.26), by using a planimeter or counting squares.

Now to obtain the water remaining in the specimen, the difference between weight of water lost and weight of water gained is subtracted from the weight of total mix water. The weight of total mix water is known from the weight of concrete in the specimen at the time of casting and mix design. Figure 4.26 reproduced from the results of the "LTS" discussed in Chapter 5, shows these values ploted.

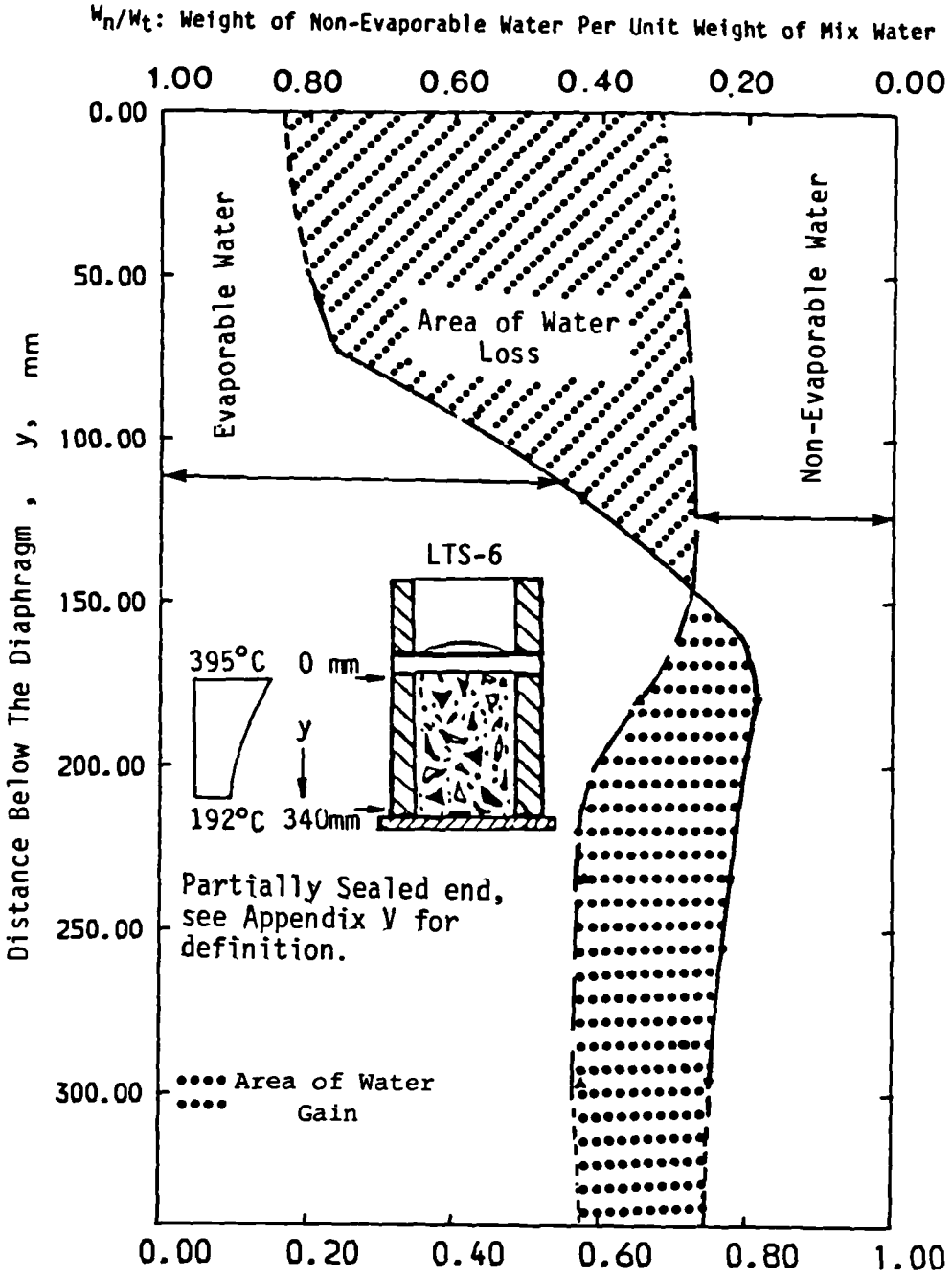

Note: Time from start of heating 270 minutes.

Figure 4.26 :

Phase Diagram for Water obtained by Gravimetric Measurements Specimen No: LTS-6

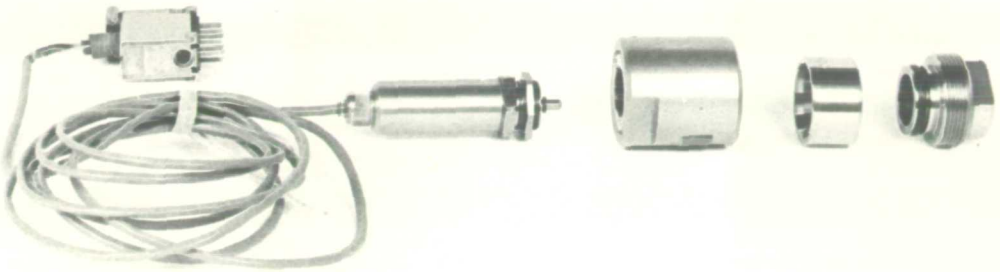

PLATE 4.1: "THE UNIVERSAL TRANSDUCING CELL" AND EXPLODED VIEW OF A PRESSURE ACCESSORY

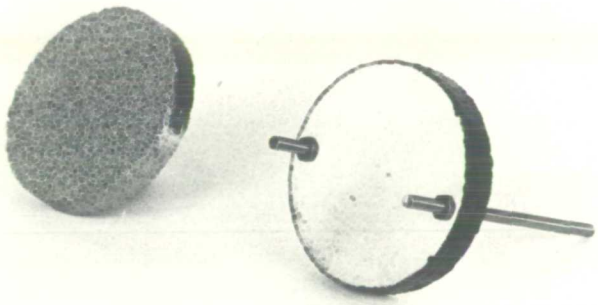

PLATE 4.2: POROUS PLATE USED FOR "RTS"

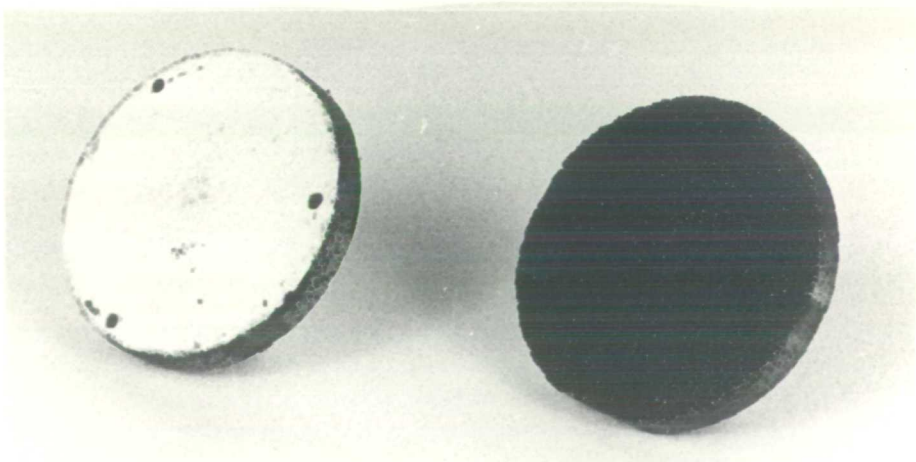

PLATE 4.3: POROUS PLATE USED FOR "LTS"

PLATE 4.4: COOLER ASSEMBLY USED FOR "RTS"

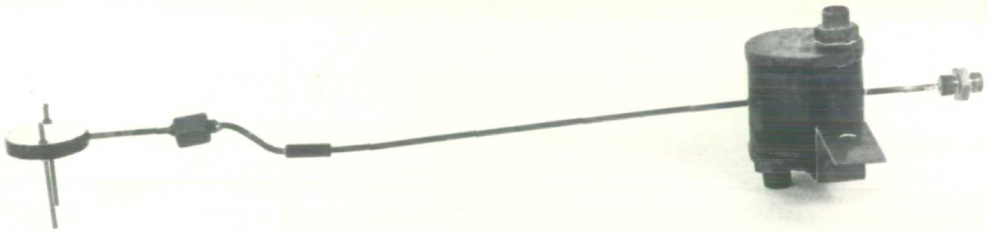

PLATE 4.5: PRESSURE MEASURING SYSTEM USED FOR "RTS"

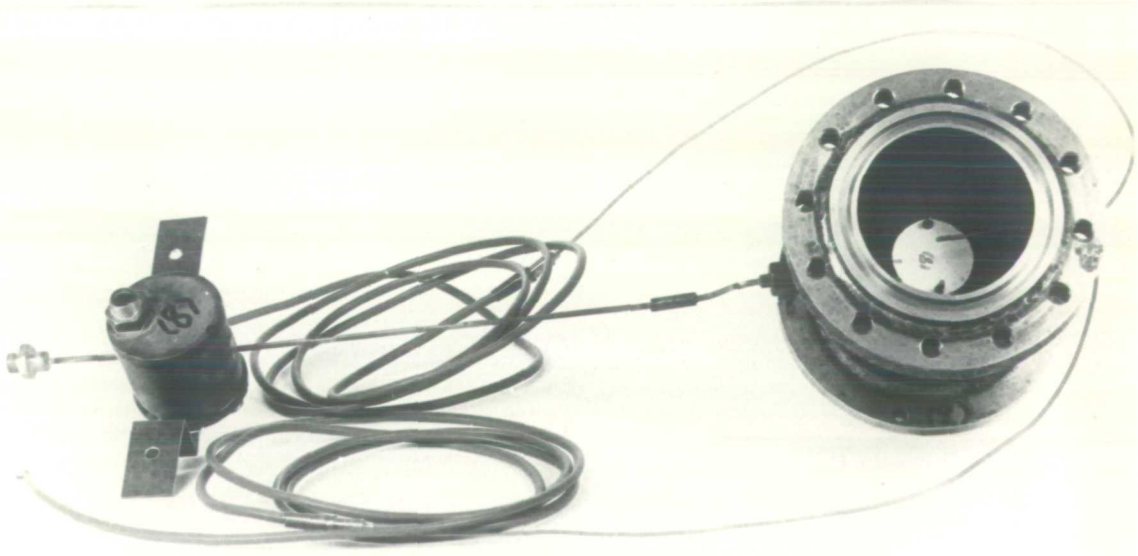

PLATE 4.6: PRESSURE MEASURING SYSTEM INTRODUCED INTO "RTS" SPECIMEN

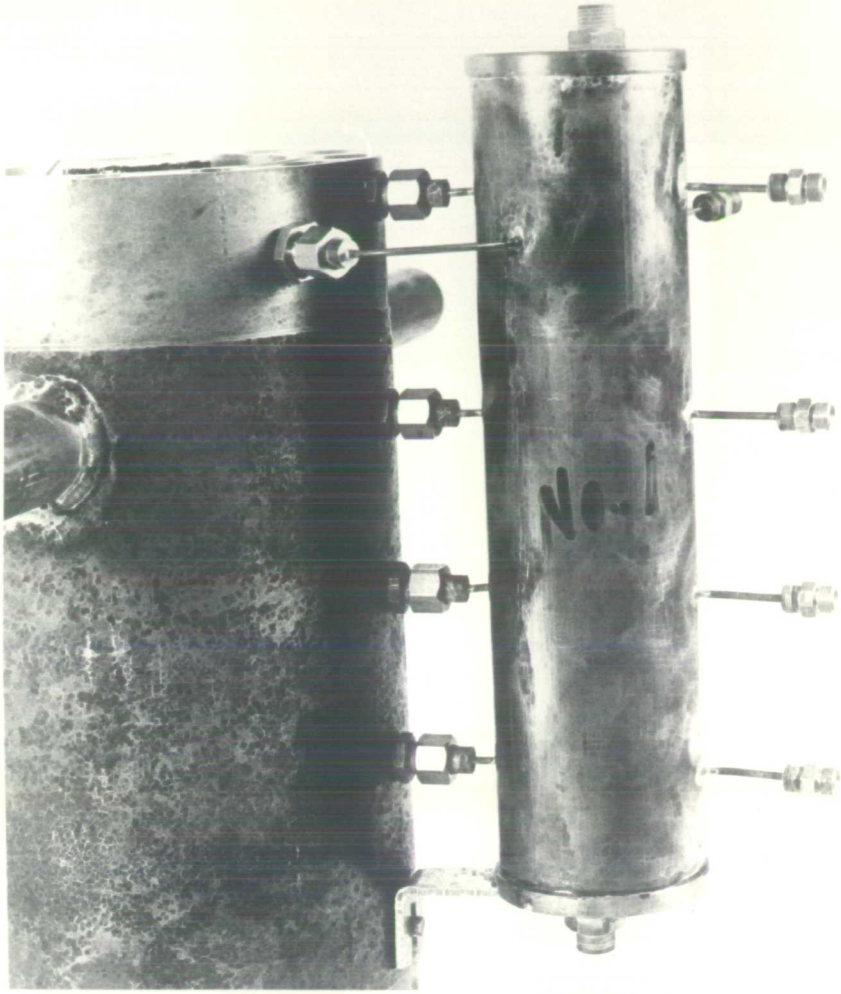

PLATE 4.7: "LTS" COOLER ASSEMBLY ATTACHED TO A CELL

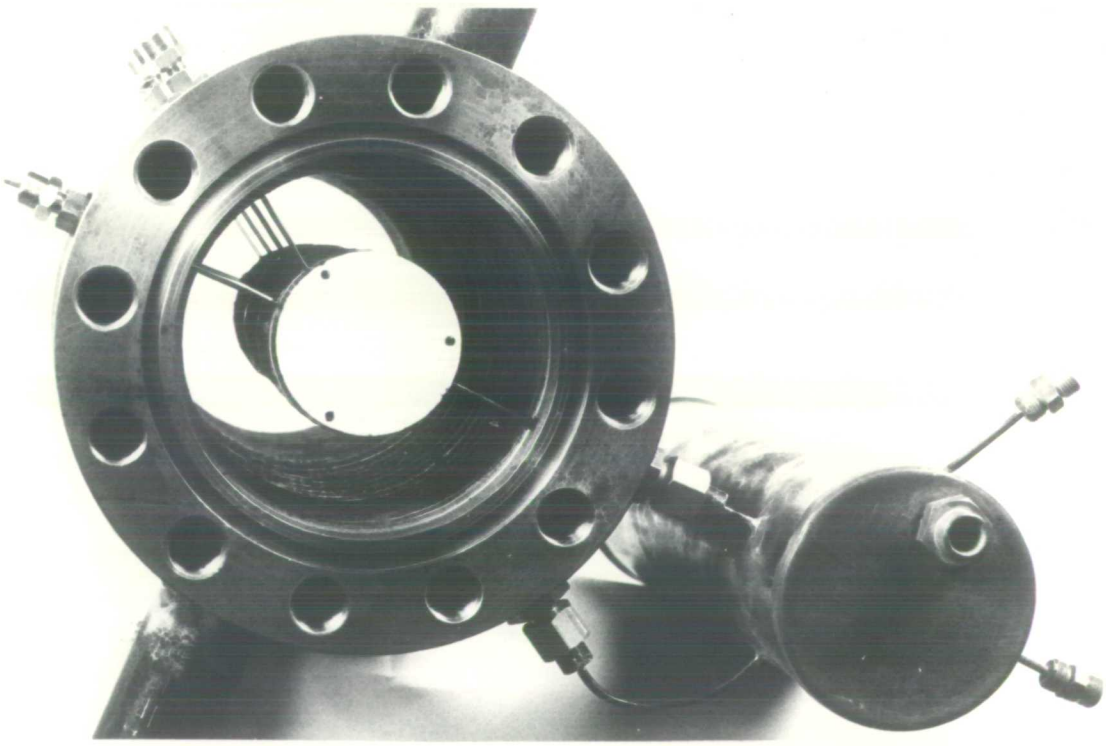

PLATE 4.8: PORE PRESSURE MEASURING SYSTEM INTRODUCED INTO "LTS" CELL, SHOWING INSTRUMENTATION POSITIONS

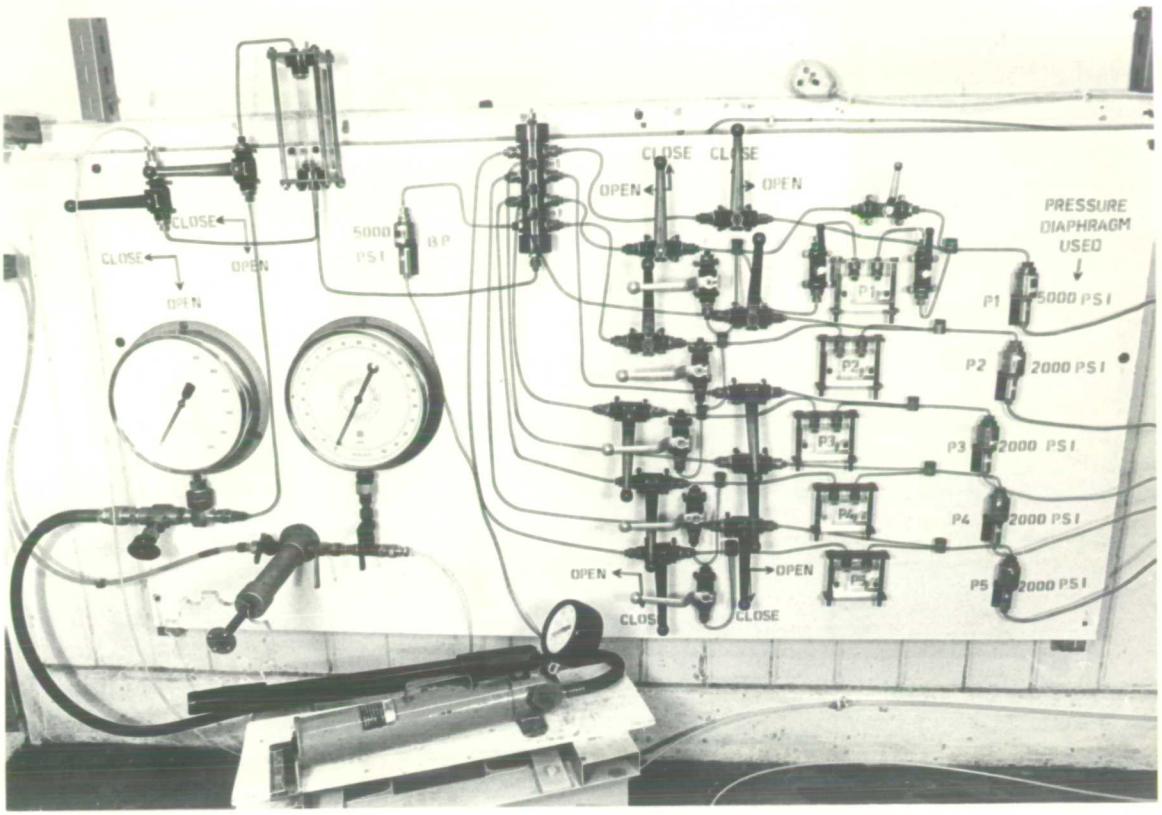

PLATE 4.9: PRESSURE RECORDING INSTRUMENTATION BOARD

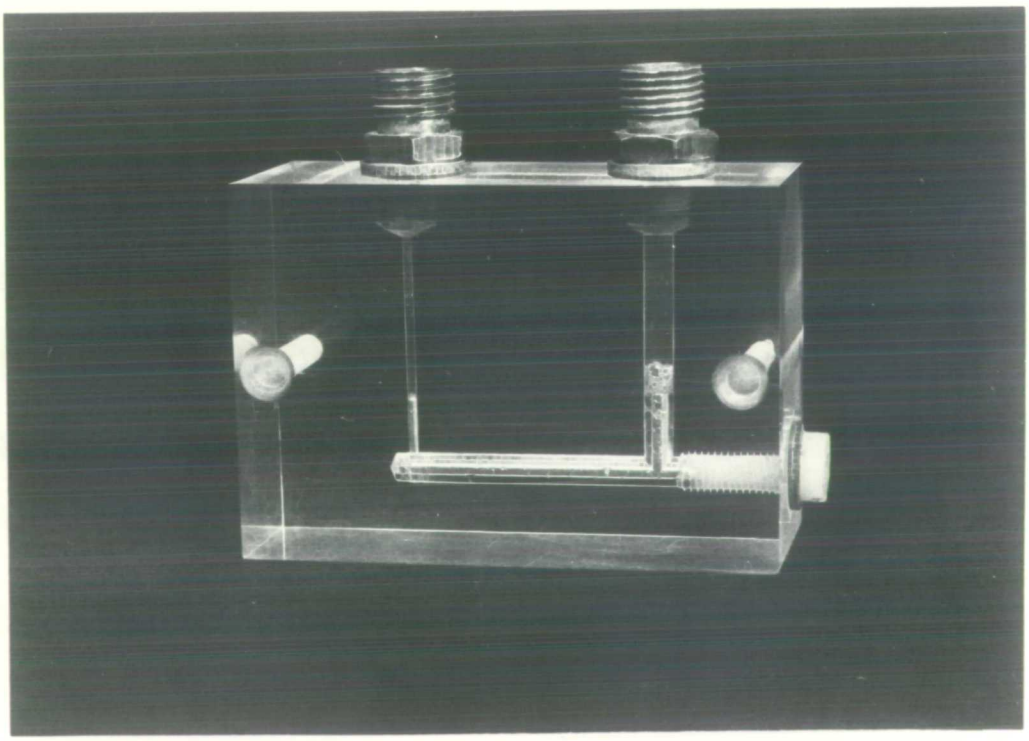

PLATE 4.10: PERSPEX BLOCK WITH 'U' TUBE CONSTRUCTED INSIDE

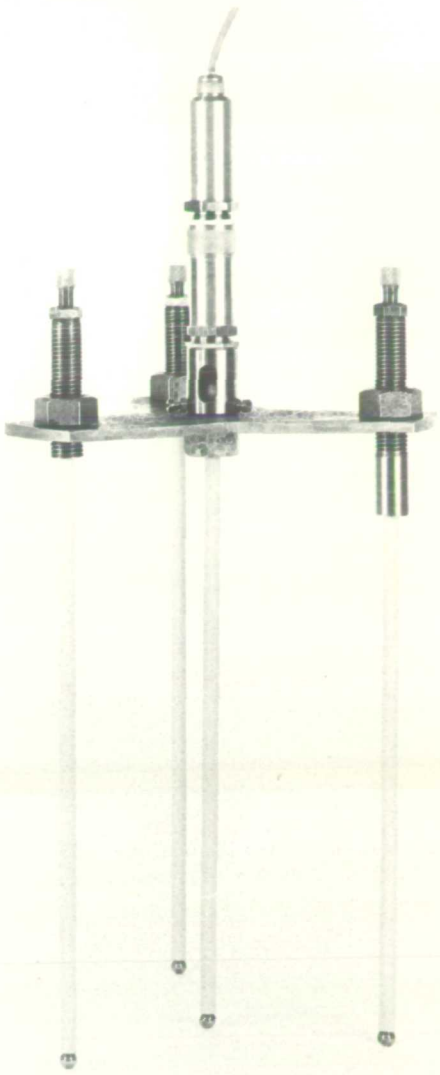

PLATE 4.11
DEFLECTION MEASURING SET UP

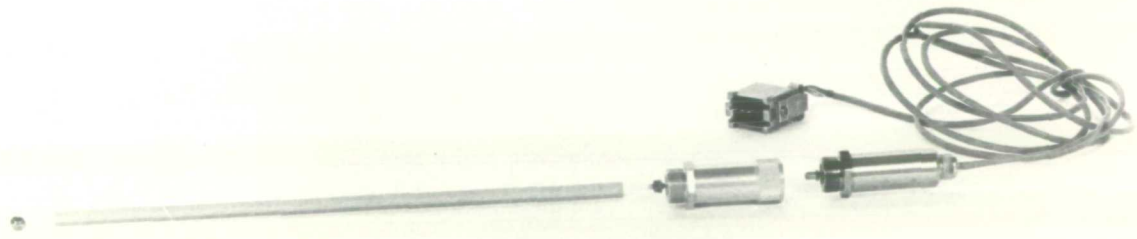

PLATE 4.12: TRANSDUCER, DISPLACEMENT ACCESSORY, SINTOX TUBE, AND STEEL BALL

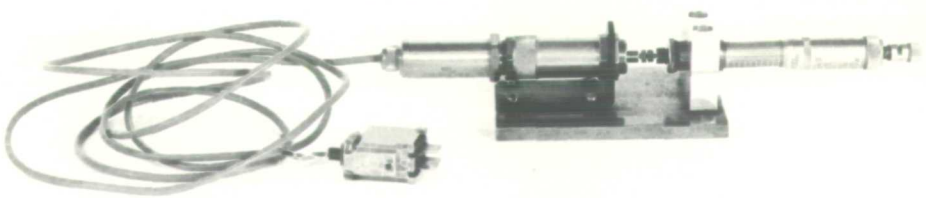

PLATE 4.13: DEFLECTION CALIBRATION OF THE TRANSDUCER

PLATE 4.14: TWO TYPES OF THERMOCOUPLES AND EXPLODED VIEW OF PRESSURE GLAND

PLATE 4.15: THERMOCOUPLE WITH PRESSURE GLAND

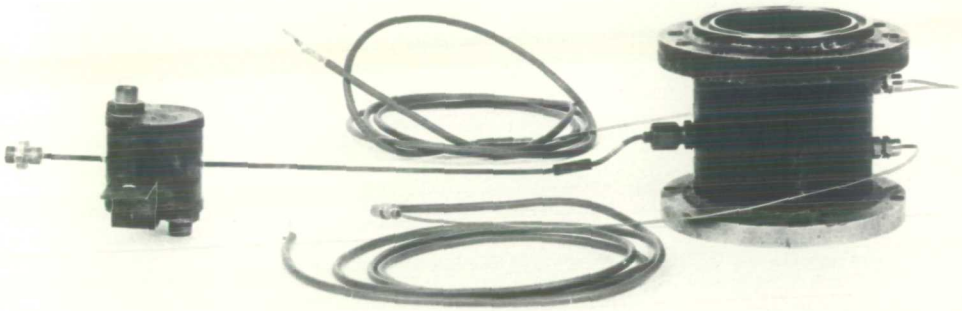

PLATE 4.16: THERMOCOUPLES CONNECTED TO "RTS" CELL

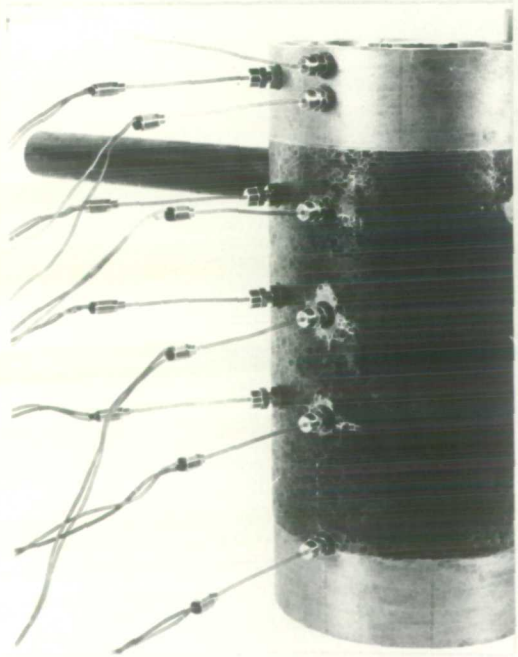

PLATE 4.17
THERMOCOUPLES CONNECTED TO "LTS" CELL

PLATE 4.18
BALANCE USED FOR WEIGHING

CHAPTER 5

SIMULATED PRESSURE VESSEL LINER TESTS OR "LINER TEST SERIES"

Note: Figures are appended at the end of this chapter.

5.1 INTRODUCTION AND OBJECTIVES

The experimental programme carried out was to study the magnitude of pore pressure and moisture migration in concrete subjected to rapid heating and therefore to a time-varying temperature gradient. The deflection of a stainless steel diaphragm in contact with the heated concrete widens this investigation (Figures 5.61 to 5.72).

The objective was to simulate a loss of cooling accident in a Fast Breeder Reactor (FBR), modelling a scenario in which liquid sodium comes into contact with the steel liner, thus causing sudden heating of the adjacent concrete. A pressure gradient and moisture gradient would be established in the concrete after the heating accident. Pore pressures behind the steel liner would produce stresses and deflections in the liner. Possible damage to the liner and its fixing would depend upon the magnitude of these pressures.

The tests performed to study the development of pore pressures in concrete at elevated temperatures and various sealing conditions are listed in Table 5.1.

SPECIMEN NO.	BOTTOM END SEALING CONDITIONS	CONCRETE-DIAPHRAGM INTERFACE TEMP. °C	LEAD-DIAPHRAGM INTERFACE TEMP. °C	TEST AGE days
PT-01				
LTS-1	Unsealed	390	406	772
LTS-2	Unsealed	385	402	1178
LTS-3	Sealed	387	406	563
LTS-4	Sealed	388	405	1175
LTS-5	Partially Sealed	397	406	871
LTS-6	Partially Sealed	395	405	895

Sealed: Completely sealed all around
Unsealed: Sealed at heated end and along the sides only
Partially Sealed: Sealed at heated end and along the side but partially sealed at the end away from heat

Table 5.1: Specimen coding and detail of the "Liner Test Series" tests

5.1.1 PILOT TESTS

Specimen PT-01 was used for checking, developing and finalising the instrumentation and the integrity of the experimental equipment.

5.1.2 "LINER TEST SERIES" EXPERIMENTS

Specimen LTS-1 to LTS-6 formed the main experiments of liner test programme and the detailed information for the "Liner Test Series" ("LTS") is available in:

- Chapter 3 for experimental design and techniques
- Appendix I for methods of construction of individual items and
- Chapter 4 for instrumentation design and methods of recording test parameters.

A brief description of the test procedures and test parameters is given below:

5.1.2.1 TEST PROCEDURES

All the tests of the "LTS" were performed close to 400 ^{o}C, using a combination of heating arrangements (Chapter 3, Section 3.3.3) given below:

a. Molten lead, pre-heated to a temperature of 650-675 ^{o}C was used for rapid heating.

b. A spiral heater placed inside the molten lead supplied continuous heat throughout the test.

c. A rope heater wrapped around the steel ring, used as a pot for holding molten lead, was used to reduce the heat loss.

Heat loss was further reduced by insulating the test cell, with a high temperature fibreglass paper.

Testing procedures are briefly described as follows (see; Chapter 3, Section 3.3.8 for detailed test procedures):

1. Water was circulated for cooling the small bore copper tubes

(transmitting pore pressure of concrete).

2. Data recording instruments, external rope heater and internal submersible spiral heater were switched on.

3. Molten lead was poured on top of the stainless steel diaphragm at a temperature of approximately 650 ^{o}C.

4. Test parameters (described in Section 5.1.2.2) were recorded.

5. Back pressure was applied for maintaining mercury level in "U" tubes (used in pressure recording as described in Chapter 4, Section 4.2.7), for recording the pore pressure of concrete with no volume change.

6. Heaters were switched off, after reaching the required temperature and the specified time.

7. Appropriate fittings and instruments were removed from the test cell and after cooling, the specimen was dismantled for extraction of concrete samples for final water distribution measurements (Chapter 3, Section 3.3.9).

5.1.2.2 TEST PARAMETERS

With reference to the figures at the end of the chapter, the following parameters were recorded:

1. Variation with time of temperature and pore pressure inside concrete at positions: T_1 - T_7 and P_1 - P_5 (Figures 5.1 to 5.30).

2. Diaphragm temperatures (see Figures 5.37 to 5.42).

3. Central diaphragm deflection (see Figures 5.49 to 5.59, odd number figures only).

4. Temperature of the molten lead in the middle of the lead pool away from metal surfaces.

5. Temperature at positions denoted by, 0, 1, 2, 3, 4 and 5 in

Figure IV.3 on the Sintox tubes (Appendix IV), for thermal expansion corrections as discussed in Section 5.1.3.

6. Evaporable and non-evaporable water contents at the end of each test. Concrete samples were removed for weight and weight change measurements to be made on further drying, to quantify the final moisture distribution (Figures 5.98 to 5.103 and 5.106 to 5.117).

5.1.3 CONTROL AND CALIBRATION TESTS

To separate the diaphragm deflection from the temperature effects and the thermal expansion of any other components, the following control and calibration tests, as discussed in detail in Appendix III and IV were performed.

1. Each diaphragm was calibrated under hydraulic pressure at room temperature, to give pressure/deflection characteristics (Appendix III).

2. Temperature deflections (with no pressure present) of the diaphragm were investigated (Appendix IV). The temperatures of these investigations were similar to those for the experiments involving pore pressures. It was also decided to carry out further calibration tests:

a. To determine the coefficient of thermal expansion for the Sintox tubes (Appendix IV, Section IV.2).

b. To establish an empirical relationship for the separation of diaphragm deflection from deflection due to thermal effects, as described in Appendix IV, Section IV.3.

c. Then using this empirical relationship the deflection due to pressure alone was separated from the temperature deflection effects (Appendix IV, Section IV.4).

5.2 PRESENTATION OF TEST RESULTS

The results of "LTS" specimens are presented as follows:

1. **"EXPERIMENTAL" RESULTS:** Raw data, as obtained from the experiments are classified and plotted as **"experimental"** results.

2. **"EXPERIMENTALLY DEDUCED" RESULTS:** The experimental data were processed using the calibration factors from Appendix III or Appendix IV and results are presented as **"experimentally deduced"** results.

3. **"THEORETICAL" RESULTS:** The experimental values were used to calculate results and the data plotted as **"theoretical"** results.

4. **"INTERPOLATED" RESULTS:** To compare the results obtained for "LTS" tests against the results of the control or calibrated tests (Appendix III or Appendix IV), one of the "LTS" test parameters (i.e. pore pressure) was used and interpolation was carried out for the other factor (i.e. central deflection of the stainless steel diaphragm) from the pressure/deflection calibration tests of Appendix III for the corresponding diaphragm. These results are presented as **"interpolated"** results.

5.2.1 "EXPERIMENTAL" RESULTS

The "experimental" results for the "LTS" tests are presented as follows:

1. Spatial temperature distributions and their variations with time (Figures 5.1 to 5.6). In these figures the following notations have been adopted:

   - curve No.1: Temperature at start of the test
   - curve No.2: Temperature immediately prior to pouring molten lead (Chapter 3, Section 3.3.8)
   - curve No.3: First temperature recorded after pouring molten lead on to the diaphragm
   - curve No.4 to last: Time-variation of temperatures as recorded while lead pool was maintained at approx. 400 ^{o}C

Figures 5.1 and 5.2 correspond to the unsealed experiments and temperature was recorded on the concrete surface at the unsealed end; i.e. 340mm from the diaphragm. However, for the sealed and partially sealed tests (Figures 5.3 to 5.6) temperature records were made to a

depth of 279.5mm only.

2. Localised pore pressure distributions and their variations with time; Figures 5.7 to 5.12.

3. Localised pressure variations with time; Figures 5.13 to 5.18.

4. Localised pore pressure variations with temperature; Figures 5.19 to 5.24.

   Note: The records of pore pressures and temperatures in concrete were made at corresponding distance below the diaphragm (i.e. T_1-P_1, T_2-P_2 etc.).

5. Comparison of pore pressure variations with temperature for all specimens at interface of diaphragm with concrete; Figure 5.24a.

6. The overlaying tranparencies on Figures 5.19 to 5.24a represent the saturation vapour pressure (svp) of water for corresponding temperatures.

7. Localised temperature variations with time at selected distances from diaphragm for all specimens; Figures 5.25 to 5.30.

8. Collective results for each specimen; Figures 5.31 to 5.36 are:

   - variations of pore pressure with time,
   - variations of pore pressure with temperature,
   - variations of temperature with time.

9. Variations of diaphragm temperature with time from start of heating; Figures 5.37 to 5.42.

10. Variations of central diaphragm deflection with time from start of heating; Figures 5.49 to 5.59 (odd numbers only).

5.2.2 "EXPERIMENTALLY DEDUCED" RESULTS

The "experimentally deduced" results are:

1. Variations of average temperature rise with time, for Sintox

tubes of diaphragm deflection measuring apparatus (seen in Plate 4.11 of Chapter 4); Figures 5.43 to 5.48.

Note: Average temperature for central and outside Sintox tube was calculated as described in Appendix IV, Section IV.2.2, and these data formed the basis of temperature deflection corrections to be applied to the recorded diaphragm deflections (as seen in Appendix IV, Section IV.3.3 and Section IV.4).

2. Central diaphragm deflection caused by pore pressures of concrete, ploted against time; Figures 5.62 - 5.72 (even numbers only), and Figures 5.73 - 5.83 (odd numbers only).

3. Variations of central diaphragm deflections with interface pressure only; Figures 5.85 to 5.95 (odd numbers only).

4. Results of water distribution in unheated concrete are shown in:

- Figure 5.97 for phase diagram
- Figure 5.104 for evaporable water distribution
- Figure 5.105 for total water content distribution.

Note: These results formed the basis for analysing test results for final water distribution in concrete (Section 5.3.5).

5. Phase diagrams for water in concrete at the end of "LTS" tests; Figures 5.98 to 5.103.

6. Evaporable water distribution at the end of tests; Figures 5.106 to 5.116 (even numbers only).

7. Total water contents distribution at the end of tests; Figures 5.107 to 5.117 (odd numbers only).

5.2.3 "THEORETICAL" RESULTS

Temperature correction to central diaphragm deflection from measured temperatures of Sintox tubes forming part of deflection measuring apparatus (see; Plate 4.11); Figures 5.50 - 5.60 (even numbers only).

5.2.4 "INTERPOLATED" RESULTS

The "interpolated" results are given below:

1. Variation of central diaphragm deflection against time, where the diaphragm deflection is predicted from the knowledge of the concrete-diaphragm interface pressures via the hydraulic pressure/deflection calibration curves of Figure III.4 in Appendix III; Figures 5.74 to 5.84 (even numbers only).

   Note: These results are plotted alongside the corresponding "experimentally deduced" results (i.e. temperature expansion corrected) for comparison and checking of the correction procedures.

   The variation of central diaphragm deflection is plotted against the concrete-diaphragm interface pressure, obtained from the calibration curve of hydraulic pressure against deflection (Figure III.4); Figures 5.86 to 5.96 (even numbers only).

5.3 DISCUSSION AND EXAMINATION OF EXPERIMENTAL RESULTS

The "experimental" results are discussed and examined as follows:

1. Thermal effects of rapid heating on the stainless steel diaphragm (simulated liner), and the establishment of temperature gradient inside the concrete behind the diaphragm (Section 5.3.1).

2. Development and migration of pore pressures in heated concrete (Section 5.3.2).

3. Central deflection of the diaphragm (Section 5.3.3).

4. Prediction of pore pressures behind the diaphragm (once the diaphragm deflection is known) in Section 5.3.4.

5. Moisture migration and final water distribution(Section 5.3.5).

6. Overall effects of the "experimental" results particularly in relation to the steel liner and concrete behind the liner of a

reactor vessel (Section 5.3.6).

5.3.1 THERMAL EFFECTS RESULTS

The results of thermal effects on the diaphragm are discussed below:

1. After pouring molten lead (heated to ~650-675 ^{o}C) on top of the stainless steel diaphragm (Section 5.1.2.1) the following observations (as seen in Figures 5.37 to 5.42) were made:

   - temperature at the lead-diaphragm interface quickly reached ~450 ^{o}C.
   - lead-diaphragm interface temperature fell below 300 ^{o}C within a matter of seconds after reaching the above temperature.

2. The lead temperature further away from the diaphragm remained above 350 ^{o}C at all times indicating that a small layer of lead close to the diaphragm solidifies (as the lead temperature falls below melting point).

3. The lead and lead-diaphragm interface temperature increased as heat was supplied by submersible spiral heater and the rope heater.

4. On reaching 400 ^{o}C the submersible heater was thermostatically controlled and the lead-diaphragm interface temperature was maintained approximately between 400-405 ^{o}C, for the remaining part of the test.

5. Transmission of heat through the diaphragm increased the concrete-diaphragm interface temperature (Figure 5.37 to 5.42) and the influencing factors for temperature rise in concrete were:

   - thickness and coefficient of thermal conductivity of diaphragm
   - temperature loss through metal surfaces surrounding concrete
   - thermal conductivity and thermal diffusivity of concrete.

The reasons for 1., 2. and 3. above are that:

a. As molten lead came into contact with cold metal surfaces energy

was exchanged.

b. Diaphragm temperature increased and lead temperature dropped.

c. The submersible spiral heater then supplied the heat resulting in the increase of lead temperature.

The temperature excursion on concrete on the other hand was due to the heat transfer through the diaphragm.

Concrete-diaphragm interface temperature closely followed the trend of temperature rise of the lead-diaphragm interface, without the fall in temperature as seen in lead-diaphragm interface temperature (which was due to the splash of molten lead on the diaphragm).

The concrete-diaphragm and lead-diaphragm temperature continued to rise although the rate of increase slowed down after the initial sharp rise, as the lead temperature was controlled at ~400 ^{o}C.

The concrete-diaphragm interface temperature lagged behind the lead-diaphragm interface temperature for all the tests of "LTS". The difference between the two temperatures decreased with time (as seen in Figures 5.38 and 5.41), and could be attributed to:

- magnitude and rate of temperature rise.
- heat diffusion into the concrete.
- length of time of heating concrete, and
- final temperature distribution in concrete.

5.3.1.1 THERMAL GRADIENT RESULTS FOR CONCRETE

Results of temperature gradient measurements in concrete are discussed below:

1. As the concrete-diaphragm interface temperature increases, the temperature in the concrete mass is increased.

2. The slope and shape of the curve between T_1 and T_7 (Figures 5.1 to 5.6) depended upon:

- rate and duration of heating (Figures 5.25 to 5.30)

- concrete conductivity and the way water was distributed in concrete (as discussed in 3. below).

3. As the hot end temperature (at concrete-diaphragm interface) increased a pressure gradient (Section 5.3.2) was established inside the concrete resulting in the movement of moisture away from the heated end. Thermal conductivity of concrete decreased in drier areas and the rate of increase of temperature slowed down. The moisture moved into the cooler regions and the rate of temperature rise in these regions increased, due to the increase in concrete conductivity (Zangle, Sadouki and Wittmann, 1989).

4. The temperature variations in concrete (Figure 5.25 to 5.30) did not depend upon the sealing conditions.

However, the sealing conditions of concrete did affect the pore pressure and moisture migration inside concrete, as discussed in the following section.

5.3.2 PORE PRESSURE RESULTS

A pore pressure gradient was established in the concrete behind the diaphragm, as temperature gradient was set up in concrete, on the application of rapid heating. The results are discussed as follows:

1. The pore pressure at position P_1 increased rapidly (see Figures 5.13 to 5.18) and followed the pattern of temperature rise at corresponding position T_1 (Figures 5.25 to 5.30).

2. Pore pressures at position P_2 to P_5 (at this stage of testing) were unchanged or close to atmospheric values (zero gauge pressure), as shown in Figures 5.7 to 5.12.

3. Pore pressures started to rise at each pressure position P_1 to P_5, as the concrete temperature increased with time.

4. The behaviour of pore pressure results at P_1 with temperature at T_1 for all the specimens were identical for the initial pressure rise (Figure 5.24a), showing the consistency and the reproducibility of test procedures and results.

5. After the initial sharp increase in pore pressure (at P_1), the rate of increase of pore pressure at this position slowed down.

6. Pore Pressures values at P_2 to P_5 continued to rise and the rate of generation of pressure increased.

The factors responsible for the above results are:

a. Pore pressure generation in concrete with the application of temperature is from liquid water, and/or water vapour and air inside the pores of concrete, as described in Chapter 6, Section 6.6.

b. As the temperature increases at T_1, pore pressure increases at P_1 correspondingly.

c. Temperature and pore pressures at other positions inside concrete are still lower at this stage.

d. A pressure difference exists between P_1 and the rest of the mass of concrete in cooler regions.

e. On further heating a pressure gradient similar to a temperature gradient is established inside concrete.

f. Pore pressures migrate from higher pressure positions into the regions with lower pressures and pore pressure migration depends upon:

- magnitude of temperature and pore pressures
- porosity and permeability of concrete.

g. As the concrete temperature continues to increase, the pore pressures at all pressure measuring positions (P_1 to P_5) keep on rising.

h. Rate of pressure increase at P_2 to P_5 is greater than P_1, as the pores at these positions become saturated, due to the movement of moisture from hotter zones to the cooler regions (see Section 5.3.5).

The "experimental" results for the above criteria can be summarised as follows:

i. On inspecting Figure 5.24a, it is seen that the pore pressures around 0.8 N/mm^2 and ~160 ^oC started to drop due to the movement of moisture and pressure away from P_1.

ii. Correspondingly P_2 at the time of T_1-P_1 reaching 170 ^oC had only reached 60-70 ^oC (Figures 5.19 to 5.24).

iii. With the passage of time P_1 increased slowly. However, P_2 to P_5 increased faster and a point was reached at P_2 where moisture moved away from this position and the rate of increase of pressure at P_2 slowed down.

iv. Now superimposing the overlay representing svp on Figures 5.19 to 5.24 for corresponding temperatures, it is shown that T_1-P_1 and T_2-P_2 moved into un-saturated drier region and T_3-P_3 to T_5-P_5 moved into saturated zone (as seen in Plates 5.1 to 5.4 by lighter regions representing un-saturated zone and darker regions representing saturated zone in concrete and discussed later in Section 5.3.5), where pressure was higher than svp for the corresponding temperature.

v. A point was reached where the pressure values at all pressure measuring positions are nearly equal (Figures 5.13 to 5.18). Similar affects were noticed by Sharp (1971) in his experimental results.

vi. The reason (for v. above) could be that the pores in concrete acted as continuously connected channels whilst the porosity of concrete and the length of specimen were major additional factors affecting the point of equal pressures.

The overall pore pressure values depended upon the sealing condition of concrete as explained below.

5.3.2.1 UNSEALED OR ONE-END SEALED SPECIMEN RESULTS

If concrete is sealed at the hotter end and along the sides, pressure is released at the cooler end and as the pressure front progresses through concrete to the unsealed end, pressure values start to fall.

Results of unsealed specimen (LTS-1 and LTS-2) are discussed below:

1. On continued heating of LTS-1, although temperature increased, pore pressure values carried on dropping after reaching maximum values, as shown in Figures 5.13 and 5.19.

   Note: LTS-1 was heated until such time as pore pressure values reached atmospheric conditions (as discussed in Section 5.3.5, for analysing water distribution in concrete at the end of the test).

2. For LTS-2, heating was stopped when the pressure just started to fall (Figures 5.14 and 5.20) after reaching a maximum. This was done to enable the corresponding moisture distribution to be determined at the end as discussed later in Section 5.3.5.

One of the interesting features encountered in LTS-1 was the increase of pore pressure at all pressure measuring positions on the downward pressure curve (Figures 5.13 and 5.19) around 0.60 N/mm^2, after ~180 minutes of heating from the start of the test, before falling back again on reaching a pressure of 0.80 N/mm^2. The reasons for this phenomenon could be attributed to:

i. Clogging of pores in the cooler region as water accumulated into this zone after migration from hotter regions, temporarily sealing the path of moisture loss, by effectively reducing the permeability of concrete in this region. Similar behaviour was encountered by Greathead (1986) while studying the permeability of concrete using identical mix design.

ii. Chemical reactions responsible for breaking the hydrate structure and debris filling the pores (as reported by Greathead from electron micrograph analysis).

iii. Enhancement of hydration of unhydrated cementitious materials (Cement + Cemsave) in the presence of increased water and temperature.

The increase of pressure was not sustained for long. It followed the downward trend suggesting temporary clogging of the pore structure in the cooler regions.

In specimen LTS-1, water dripped out of the concrete from the cooler unsealed end of the specimen, showing that the pore pressure gradient was certainly responsible for forcing the water out of the concrete. The rate of water loss would, therefore depend upon:

- concrete permeability
- properties of permeating fluid
- pore structure of concrete
- state and quantity of water held in concrete
- rate of temperature rise
- rate and magnitude of of pore pressure generation.

The pore pressure values for LTS-1 and LTS-2 (Figure 5.19 and 5.20 respectively) compared with the svp of pure water (from corresponding graph on transparency for superimposing on Figure 5.19 and 5.20) showed that:

a. Pore pressures were higher for all the recorded values before migration of moisture.

b. Pore pressure at P_1 and P_2 started to fall below svp when moisture and pressure migrated from these regions.

c. Pore pressures at P_3, P_4 and P_5 remained higher than svp on ascending curves (in Figures 5.19 and 5.20), as moisture moved into these regions.

d. Pore pressures were higher than svp where concrete pores were saturated with liquid water (and/or water vapours) and air was present in concrete pores.

5.3.2.2 SEALED AND PARTIALLY SEALED SPECIMEN RESULTS

The increase in pore pressures in the initial stages of the test (Figure 5.24a) for sealed (LTS-3 and LTS-4) and partially sealed specimens (LTS-5 and LTS-6) were similar to the results of unsealed specimens (LTS-1 and LTS-2 discussed in the previous section).

As the initial rise in the rate of pore pressure dropped for P_1, and once all the values of P_1 to P_5 were equal (as described in Section 5.3.2), pore pressure continued to rise with increasing temperature and time inside the sealed specimens of LTS-3 and LTS-4 (Figures 5.15, 5.16, 5.21 and 5.22).

The pressure values at P_3, P_4 and P_5 for LTS-3 and LTS-4 were above svp at all times during testing but the pore pressures of P_1 and P_2 dropped below svp at a temperature of 170-175 ^{o}C.

For LTS-3, heating was stopped before reaching the peak pore pressure (Figures 5.15 & 5.21).

The LTS-4 test was concluded on detection of a slight leak from one of the fittings, to avoid further moisture loss from the concrete (Figures 5.16 & 5.22).

The pore pressure results of partially sealed specimens (LTS-5 and LTS-6) fell between the results of one-end sealed and sealed specimens. The pressure rising trends were similar to the sealed specimens, although restricted pressure loss could take place and pressures would start to drop at that stage (Figures 5.17, 5.18, 5.23 and 5.24).

For test LTS-5, heating was stopped when the pore pressure was dropping, whereas for test LTS-6, it was concluded on reaching the maximum pressure value when pore pressure had just started to drop. This was done to quantify the distribution of water in concrete at various times for partially sealed concrete (Section 5.3.5).

Once again pore pressure behaviour for LTS-5 and LTS-6 compared with svp (see Figures 5.23 & 5.24 along with the overlays respectively) was similar to that described earlier in this section for LTS-3 and LTS-4.

5.3.3 DIAPHRAGM DEFLECTION RESULTS

Central diaphragm deflection was recorded in the tests of "LTS" under pressure and thermal effects and "experimental" results consist of:

a. Deflection due to pore pressures,

b. Deflection due to temperature effects.

To understand the mechanism of diaphragm deflection and to separate pressure deflection from deflection due to temperature, the calibration tests described in Section 5.1.3 were performed.

The calibration tests showed that the additional apparent deflection in the "LTS" experiments was the result of differential thermal expansion of the 4 Sintox tubes.

Results of central deflection of the diaphragm are:

1. Deflection due to pressure (Figures 5.62 to 5.72, even numbers only) can be attributed to pore pressure of concrete at concrete-diaphragm interface (P_1).

2. Deflection corresponds to rise and fall of pore pressure at P_1.

3. To check the relationship between pore pressure (P_1) at concrete-diaphragm interface and diaphragm deflection (Figures 5.85 to 5.95, odd numbers only), the results are compared with interpolated deflections for P_1 (Figures 5.86 to 5.96, even numbers only) for the same diaphragm as explained in Section 5.2.4 for "Interpolated" results.

4. Figure 5.86 ("interpolated" results) compared to Figure 5.85 ("experimentally deduced" results) of LTS-1 shows excellent agreement and likewise the agreement is excellent for the results of the rest of the tests of "LTS".

The results show that pore pressures in concrete can significantly contribute to the deflection of the diaphragm (simulated liner) and if

the pore pressures do not dissipate into the concrete, the deflection due to these pressures could harm the steel liner of a Fast Breeder Reactor, as described later in Section 5.3.6.

5.3.4 ESTIMATION OF PORE PRESSURE AT CONCRETE-DIAPHRAGM INTERFACE WITH DIAPHRAGM DEFLECTION KNOWN

Calculations can be performed to evaluate pore pressure behind the diaphragm provided diaphragm deflection along with other parameters involved to solve the equation are known. The practical use for this is to evaluate the magnitude of pore pressure behind the liners of Fast Breeder Reactors which would indicate the states of water in the concrete shield.

To proceed with the estimation, records should be made of:

- deflection of the liner
- temperature of the liner and the instruments measuring deflection
- thickness of the liner and its properties
- the edge fixity of the liner
- separation of pore pressure deflection from any other deflection due to thermal effects.

Considering a circular plate with fixed edges the following equation can be used for evaluating pore presures. However, using an appropriate equation and edge fixity, any shape of plate can be considered.

Note: The equation is rearranged from Timoshenko (1940) and the thermal expansion of the plate is not taken into account for the plate deflection.

$$P = 5.33 \delta_{max} E h^3 / r^4 (1 - v^2)$$

where:

- P = uniform pressure behind the plate
- δ_{max} = maxium deflection in the centre of the plate
- E = modulus of elasticity
- h = plate thickness
- r = plate radius
- v = Poisson's ratio

As an example, considering a fixed edge stainless steel (316) circular

plate with the following data, the value of pressure P is evaluated:

$P = ?$ (Unknown)

$\delta_{max} = 0.15$ mm

$E = 19.3\ 10^4$ N/mm^2

$v = 0.29$

$r = 50$ mm

$h = 10$ mm

$$P = 5.33 \delta_{max} E h^3 / r^4 (1 - v^2)$$

$$P = \frac{5.33 * 0.15 * 19.3\ 10^4 * (10)^3}{(50)^4 * (1 - (0.29)^2)}$$

$$P = 26.955 \text{ N/mm}^2$$

5.3.5 MOISTURE MIGRATION AND FINAL WATER DISTRIBUTION RESULTS

Concrete samples were removed from the "LTS" specimens at the end of each experiment (Chapter 3, Section 3.3.9) and used to measure the final water distribution of the heated concrete as described in Chapter 4, Section 4.6.

Additionally a specimen, identically cast and cured as the "LTS" specimens was used as an unheated sample for obtaining final water distribution in unheated concrete (described in Section 5.2.2) and these results serve as reference points for analysis of the "LTS" results.

5.3.5.1 UNSEALED OR ONE-END SEALED RESULTS

LTS-1 and LTS-2 were sealed at the heated end only and examination of the results of these tests showed:

1. Water was lost from all regions of the heated concrete of LTS-1 (Figures 5.98 & 5.107).

2. The overall result for LTS-1 was an appreciable amount of water loss from concrete compared with the total weight of mix water.

3. For LTS-1, water loss from concrete closer to the heated and sealed end was greater than the water loss from the open end away from heat.

4. Water was lost from concrete from a section ~0-160mm below the

diaphragm and water was gained in the remaining section of concrete for LTS-2 (Figures 5.99).

5. The overall result for LTS-2 was slight loss of water from concrete compared with the total weight of mix water.

The tests conditions for LTS-1 and LTS-2 were as follows:

a. LTS-1 was heated until the pore pressures in concrete were $-0.41\ N/mm^2$ (see Figures 5.13 & 5.19 and Section 5.3.2.1).

b. LTS-2 heating was stopped when pore pressures in the concrete started to drop after reaching the maximum values (see Figures 5.14 & 5.20 and Section 5.3.2.1).

The results obtained for both these tests showed that:

i. Evaporable water loss occurred throughout the length of concrete for LTS-1.

ii. Evaporable water was lost from the top 160mm and accumulated in the lower section of concrete for LTS-2.

iii. Non-evaporable water values stayed almost constant throughout the length of concrete for both LTS-1 and LTS-2, although a small amount of non-evaporable water was lost from the concrete near the heated end.

iv. As the concrete was only sealed at one end, evaporation took place from the open end and a drying front moved into the concrete towards the heated end.

5.3.5.2 SEALED SPECIMEN RESULTS

Heating was stopped for test LTS-4 when a slight leakage was detected from one of the fittings.

The results for this test are explained as follows:

1. Moisture migrated away from the hot end towards the cooler the

regions of concrete.

2. Water accumulated in the lower half section of concrete.

3. Quatitities of both evaporable and non-evaporable water were lost from the heated end.

4. The quantity of evaporable as well as non-evaporable water increased in water-gain areas and the total water contents were greater than unity.

5. At the end of the test the lower half of the concrete was saturated with water driven from the heated end (Figure 5.100).

6. No water was lost from the specimen but water simply moved from the water-loss region into the water-gain region (Figure 5.100).

7. Comparison between Plate 5.1 and Figure 5.100 from LTS-4 shows that water migrated from the top 110mm of concrete below the diaphragm into the lower section of concrete after heating.

Note: Lighter regions in Plate 5.1 represent areas of water-loss and darker regions represent areas of water-gain.

5.3.5.3 PARTIALLY SEALED SPECIMEN RESULTS

Specimens LTS-5 and LTS-6 were partially sealed at the end away from the heated end and heating was stopped for each test as described in Section 5.3.2.2 earlier.

The results showed that:

1. Moisture migrated from the hotter region into the cooler region (Figures 5.101 & 5.103 for LTS-5 and LTS-6 respectively).

2. For both LTS-5 and LTS-6, water was lost to the atmosphere as a result of partial sealing.

3. In LTS-5, water accumulated in the concrete nearer the cooler end as shown by Figure 5.101 and Plate 5.2.

4. The overall effect for LTS-5 was a greater loss of water from the heated half and moisture movement into cooler regions from where a considerable amount was lost.

5. In LTS-6, water migrated from the hotter to the cooler region as seen in Figure 5.103 and Plate 5.3.

5.3.5.4 COMPARISON OF RESULTS OBTAINED BY DIFFERENT METHODS

A comparison is made of the various quantities of water in the concrete at the end of the tests, as calculated by different methods described in Chapter 4, Section 4.6. The results from LTS-5 were used for the calculations in both the methods.

a. **Ist Method:**
The provision for different densities of concrete in different areas as described in Chapter 4, Section 4.6 and Figures 5.101, 5.112 and 5.113 show the results calculated by using this method.

b. **2nd Method:**
The equations derived from Chapman (1976) for the concrete used in this thesis did not consider the variation of concrete density through the length of concrete specimen and the results obtained using this method are shown in Figures 5.102, 5.114 and 5.115 for LTS-5.

Both these methods are compared as follows:

1. Figures for LTS-4 to LTS-6 in conjunction with Plate 5.1 to 5.3 for these tests show good agreement of the results as all the figures were drawn from the calculations performed by the first method.

2. Concrete removed from the specimens for gravimetric measurements (seen in Plate 5.4) showed the way in which aggregate and hydrate products exist at various positions in the concrete:

i. Discs numbered 2, 5, 9 and 12 for LTS-1 represent various positions in concrete from top to the bottom (recalling the fact

that the concrete in the mild steel cylinder was cast upside down as described in Chapter 3, Section 3.3).

ii. Disc number 2 represents the concrete poured before disc number 5, 9 and 12 (where disc number 12 was poured in last of all).

iii. Disc number 2 had a greater quantity of aggregate than disc 12 and disc 5 & 9 fall between the two discs.

5.3.5.5 GENERAL DISCUSSION OF FINAL WATER DISTRIBUTION RESULTS

The results of these tests are summarised as follows:

1. Loss of moisture from concrete was dependent upon:

   - permeability of concrete
   - length of concrete specimen
   - sealing condition
   - duration of heating
   - magnitude of temperature and pore pressure
   - temperature and pore pressure gradient

   where: pore pressure gradient is dependent upon temperature magnitude and intensity of heating.

2. Variation of evaporable water was greater than the variation of non-evaporable water which remained uniform.

3. Accumulation of water in the moisture gain areas of concrete enhanced the hydration of unhydrated cementitious materials, and increased temperature accelerated this phenomenon.

4. The quantity of non-evaporable water increased in water gain regions as a result of increased hydration and that was the reason the maximum value of weight of non-evaporable water per unit weight of mix water (W_n/W_t) was found in water-gain regions where the total water contents (W_t) were greater than unity.

5. The quantity of non-evaporable water was slightly reduced in water loss regions with continued heating as dehydration takes place and chemisorbed water was lost from the hydrate structure, thus reducing W_n/W_t values from this area.

6. The quantity of evaporable water was greater in water-gain areas and the weight of evaporable water per unit weight of mix water (W_e/W_t) was increased.

7. The quantity of evaporable water decreased in water-loss regions resulting in lowering of W_e/W_t values.

8. Minimum values of W_e/W_t and W_n/W_t were encountered in water-loss region.

9. Water is lost from the open end due to evaporation, and the evaporation front moved into concrete from the open end depending upon:

- duration of testing and
- concrete temperature at the open end.

10. Water was seen physically dripping out from the open end away from heated zone, emphasizing the presence and significance of pore pressures inside the concrete as a major factor responsible for the migration of moisture.

11. Moisture released from concrete consists of liquid water, water vapour, steam and air. The overall effect of moisture loss from concrete is a drop of pore pressures in concrete in the region of moisture loss.

12. Pore pressures increase in the regions where water accumulates and pore pressures are greater than svp of pure water in water gain regions at corresponding temperature due to the saturation of water in this region.

13. However, the pore pressures are lower than svp for corresponding temperature in un-saturated water loss regions as moisture migrates away from these regions.

14. In sealed concrete moisture migrates away from the heated end and accumulates in the cooler region, where the total amount of water (W_t) would be greater than unity.

15. Water is evenly distributed in water accumulation areas, as concrete can only maintain a certain amount of water in its pores and all the water cannot be squeezed into the regions of concrete furthest away from heated zone.

16. For partially sealed concrete (when partial sealing is provided at the end away from heat source) it is much more difficult to forecast the way in which water would be distributed in different regions of concrete during testing.

17. The effectiveness of cold end sealing would play a major role for the release of moisture in addition to the other factors.

5.3.6 OVERALL EFFECTS OF THE RESULTS PARTICULARLY WITH RELATION TO A REACTOR VESSEL

The results of the liner test are analysed for cooling accidents in Fast Breeder Reactors, considering a scenario in which liquid sodium comes into contact with the steel liner and rapid heating is applied to concrete behind the liner .

Complete analysis of the concrete used behind the liner or effects of pore pressures are beyond the scope of research carried out for this work. However, the experimental results discussed previously are applied to the concrete and the liner of FBR and the effects of these results on the concrete and the steel liner are highlighted.

The following criteria are examined before the dicussion of the results:

a. The purpose of using concrete behind the steel liner is to provide:

   - structural strength and stability
   - nuclear and thermal shielding.

b. Rapid heating of concrete would alter the properties of concrete resulting in upsetting the moisture equilibrium of concrete (Kamp et al, 1987), which is primarily responsible for maintaining the nuclear shielding.

c. It is essential to maintain a sufficient amount of water evenly distributed through the mass of concrete.

d. Movement of moisture from one region to another would create zones of dry and wet concrete under the effects of thermal and pressure gradients, resulting in hydrothermal reactions in concrete (Lankard et al, 1970).

Some remarks in the light of the experimental results are outlined in the following paragraphs:

1. Application of high temperature on the steel liner would transmit heat to the mass concrete behind the liner setting up a thermal gradient in the concrete.

2. A pressure gradient is produced due to the application of a thermal gradient causing moisture to migrate from hotter zones with high pore pressures to the cooler regions with lower pore pressures.

3. Permeability increases in hotter regions near the heated end and pressure rapidly dissipates away from this zone (Schneider et al, 1985, 1987, 1989). The regions of increased permeability could be attributed to:

   - hydrothermal reactions, or drying, or thermal damage and
   - increase of pore volume, or
   - a combination of these factors.

4. The migrated moisture accumulates in the cooler regions forming a barrier to moisture migration and hence lowering the concrete permeability in this zone.

5. As pore filling increases, the pores become saturated and the continuous presence and increase of temperature would increase the pore pressure in excess of saturation vapour pressure (svp) for the corresponding temperatures.

6. The continued heating would result in migration of moisture from accumulated zones to the outer cooler regions and a subsequent loss of moisture from concrete.

7. An evaporation drying front opposite to the migration front would progress into the central regions of concrete if the concrete is not sealed at the outer surface (Kordina et al, 1979 and Takeda et al, 1987).

8. If the external surface of the concrete wall is either completely sealed or partially sealed then the moisture loss may be avoided at the expense of the accumulation of moisture in the outer zones.

9. Overall effects of the pressure front advancing away from the hot surface of the liner would be that:

- the pressure on the hot side would be relatively uniform and below svp,
- the pressure would rise sharply in the regions of moisture barrier or moisture accumulated zones above svp.

10. If the concrete is completely sealed from all sides and heating continues for a long time, the pore pressures throughout the length of concrete wall would reach a uniform value. This could be due to the formation of continuous channels inside the concrete.

11. Another practical factor resulting in the creation of a moisture barrier is the reduced permeability in central regions of mass concrete due to the first application of temperature (due to heat of hydration) during curing (Greathead, 1986).

12. Moisture migration, changing amounts of water in pores or the varying degrees of pore filling in combination with elevated temperatures in concrete can alter the chemistry and pore structure of concrete (Chapman, 1976 and Schneider et al, 1985).

13. As temperature rises in concrete, the average size of pores increases while the water content decreases (Kordina et al, 1979).

14. Consequently, the average thermal diffusivity of concrete decreases significantly with increasing temperature (Cheung, Baker and Bingle, 1976).

15. One of the phenomena involved in heating concrete would be a process of dehydration taking place in concrete near the heated surface where drying occurs, resulting in the release of moisture from the hydrate (Schneider et al, 1989).

16. Rate of dehydration would depend on the rate of heat diffusion into the interior of the heated concrete (Cheung et al, 1976).

17. Dehydration proceeds rather rapidly and it could be considered to occur almost simultaneously with temperature rise in concrete.

18. On the other hand the hydration of unhydrated cement continues in the region with excess moisture due to the presence of temperature coupled with hydrothermal reactions, and some of the moisture is taken up by the hydration process. However, hydration would proceed rather more slowly than the dehydration process.

19. Generation of excess hydrostatic pressures due to the imposition of a thermal gradient could affect the stability of the steel liner if these pressures are not allowed to dissipate and may also damage concrete by hydraulic fracture.

20. Loss of moisture (on a large scale) from concrete under thermal and pressure gradients would reduce the effectiveness of concrete for shielding purposes.

21. Construction joints, reinforcement bars and prestressing ducts and tendons would provide a path for release of moisture and pore water pressures.

22. Therefore in designing the concrete for the reactor vessels, in order to avoid hydraulic fracture of concrete and deformation of the steel liner due to these pressures, a balance has to be maintained for having sufficient amount of water in concrete for nuclear shielding purposes and still avoid the generation of excess pore pressures and the migration of moisture.

23. Generation of zones of high pore pressures should be avoided to minimise moisture migration, as one of the major factors

responsible for the movement of moisture in the heated concrete in the reactor wall would be a pore pressure gradient (generated due to thermal gradient).

5.4 SUMMARY OF EXPERIMENTS AND CONCLUSIONS

5.4.1 SUMMARY OF EXPERIMENTS

The cylindrical concrete specimens were heated non-uniformly to a temperature of 400 ^{o}C, by rapid heating through a stainless steel diaphragm. The heated end and sides of each specimen were sealed, to prevent the loss of moisture and pressure, whereas the end away from heating was either sealed, partially sealed or unsealed.

All the specimens were cured in a sealed atmosphere, avoiding evaporation drying during the curing period.

In the "Liner Test Series" experiments, records were made with time for:

- temperature and pore pressures in concrete,
- central deflection of the stainless steel diaphragm, and
- moisture movement and pore pressure migration through the length of concrete for different sealing conditions.

Concrete samples were extracted from the specimen at the end of the tests and by applying gravimetric measuring techniques the states and quantities of water were analysed and the mode and extent of moisture movement through concrete studied.

The thermal and the pressure gradient effects on the types of water were discussed with reference to concrete properties.

The implications of the experimental results for the behaviour of the steel liner and adjacent concrete of a Fast Breeder Reactor were studied for a cooling accident in a scenario in which sodium liquid came into contact with the liner.

5.4.2 CONCLUSIONS

1. For each test, sudden heating of a diaphragm to 400 ^{o}C created a thermal gradient in the adjacent concrete. A typical value was ~0.4 ^{o}C/mm within 3 minutes of heating.

2. The highest pressure, recorded 260 minutes after commencement of heating, was 9.5 N/mm^2 (for LTS-5).

3. The high temperatures created a pressure gradient behind the diaphragm, for which a typical value after 3 minutes of heating was ~(0.001 N/mm^2)/mm.

4. Pressure predictions based on recorded temperatures (at concrete/diaphragm interface after ~20 minutes of heating) were seen to be a factor of 1.5 to 2.5 too high at a temperature of 200 ^{o}C. The pressure of 9.5 N/mm^2 at 395 ^{o}C (at concrete/diaphragm interface after 275 minutes of heating) was a factor of 3 to 4 below the value predicted based upon the saturation vapour pressure of water at 395 ^{o}C. This is because of the rapid movement of moisture from the hottest zones.

5. Pressures in the unsaturated zone i.e. within 25mm of the diaphragm were slightly above saturation vapour pressure, but only for a period of less than 3 minutes after commencement of rapid heating, while temperatures were below 150 ^{o}C. Beyond these times and temperatures, pressures fell below saturation vapour pressure.

6. The total pore pressure at a specified temperature in concrete remote from the diaphragm (~25mm or more), containing free water but not physically saturated, is more than 50% greater than the saturated vapour pressure of pure water at that temperature (after ~35 minutes of heating).

7. In these tests the sealing condition at the 'cold' boundary (which was 340mm away from the diaphragm) became influential only after 65 minutes of heating.

8. In these experiments which simulate a loss of coolant accident,

the generation of higher temperatures and pressures, cause drying in the concrete close to the diaphragm (<25mm away) within 3 minutes of commencement of heating. Under normal operating conditions drying in this region would not occur for many years. This highlights the importance of understanding the migration of moisture in concrete under elevated temperature conditions.

9. The availability of excess water in the saturated zones coupled with elevated temperature results in enhanced hydration (detected by an increase in the amount of non-evaporable water e.g. Figure 5.100).

10. In the hottest zones, drying causes degradation to the hydration products resulting in reduced non-evaporable water content after a sustained period of heating for 10-12 hours.

11. The possibility of attaining ~10 N/mm^2 of pressure behind the steel liner of a Fast Breeder Reactor is a reality in an accident, and should therefore be considered at the design stage.

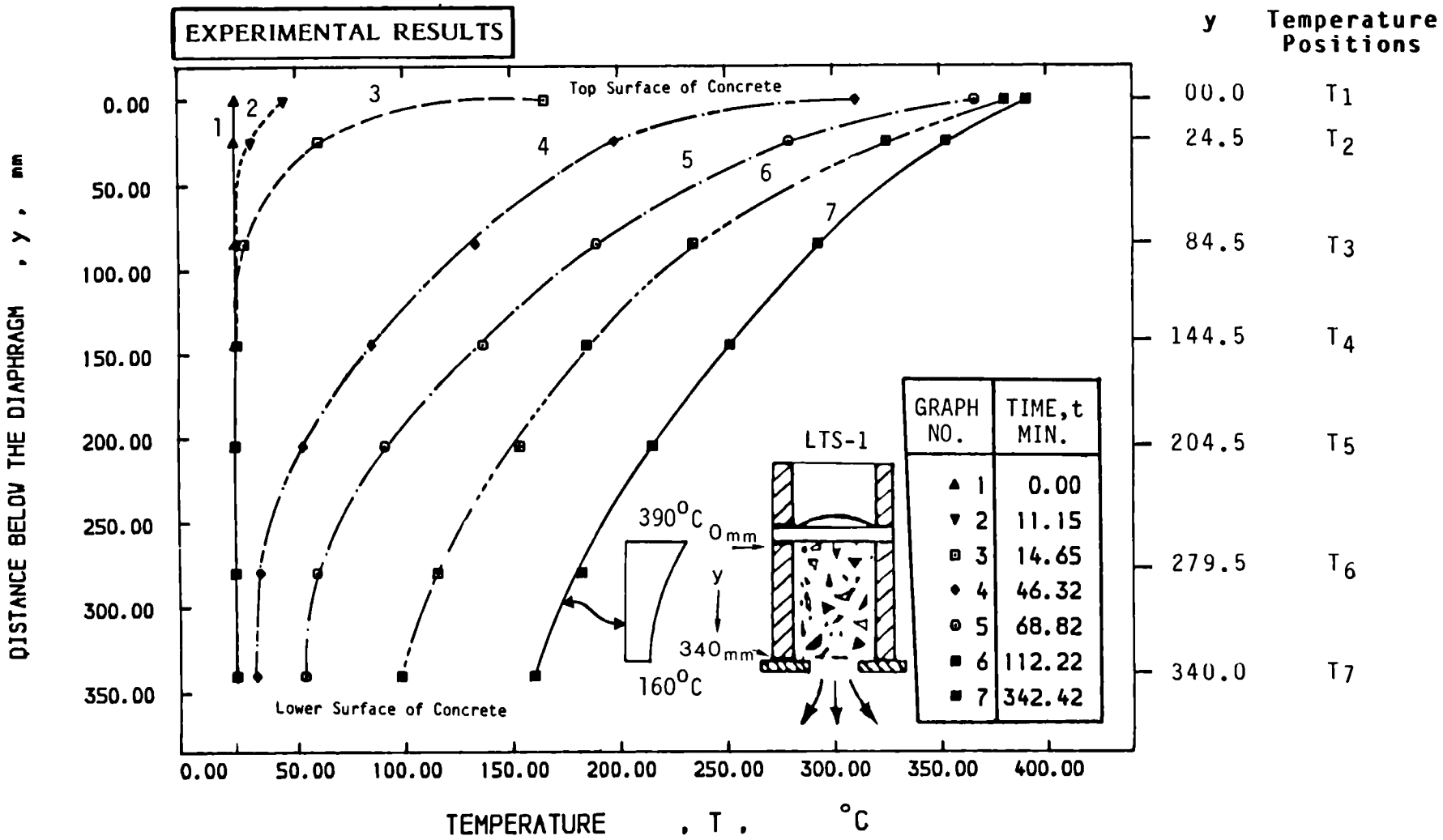

Figure 5.1 : Temperature Distributions in Concrete at selected Times from Start of Heating Specimen No: LTS-1

Note: ↝ For final temperature distribution (390 & 160 °C); see Fig. 5.25

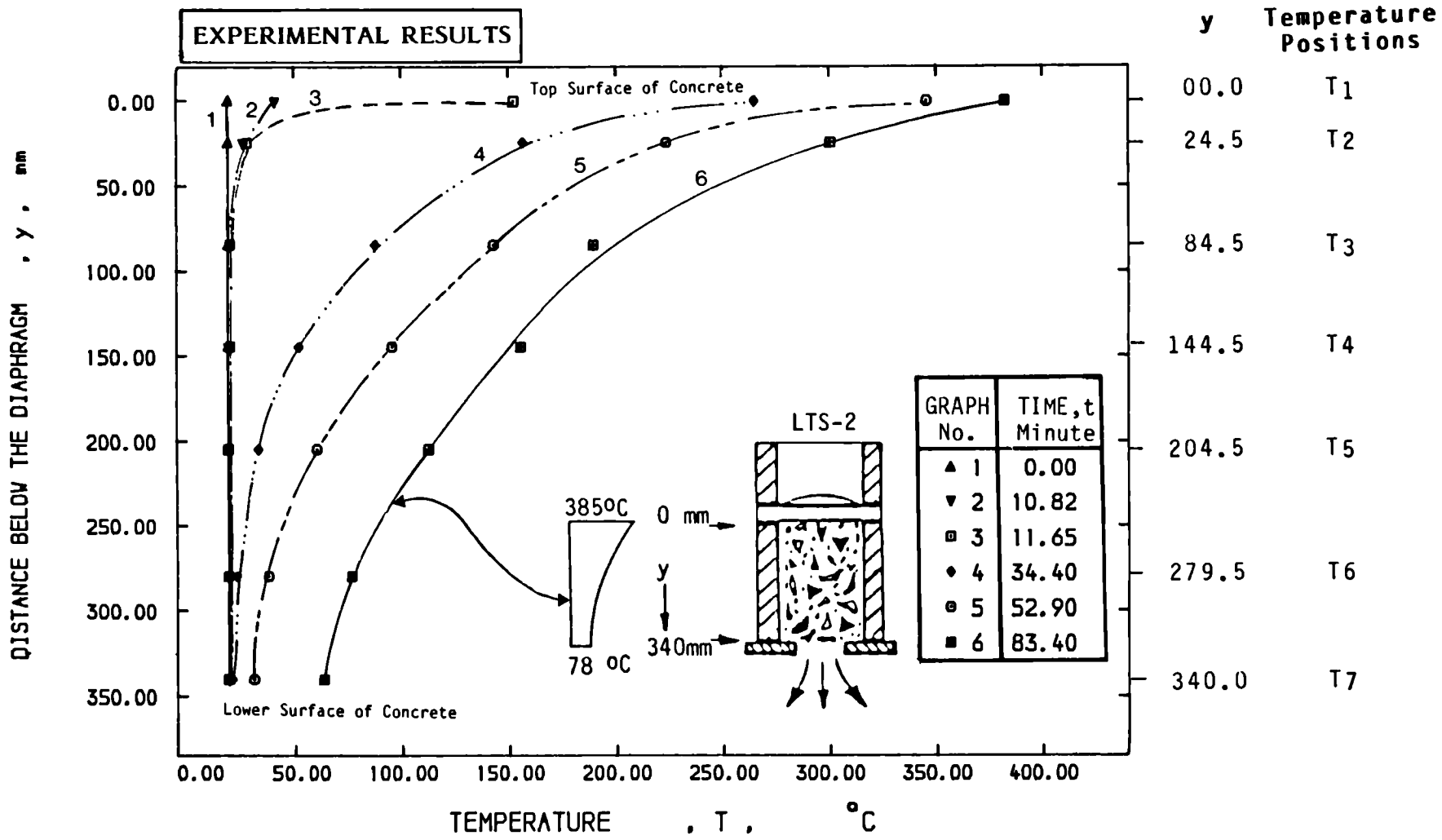

Figure 5.2 : Temperature Distributions in Concrete at selected Times from Start of Heating Specimen No: LTS-2

Note: ↷ For final temperature distribution (385 & 78 °C); see Fig. 5.26

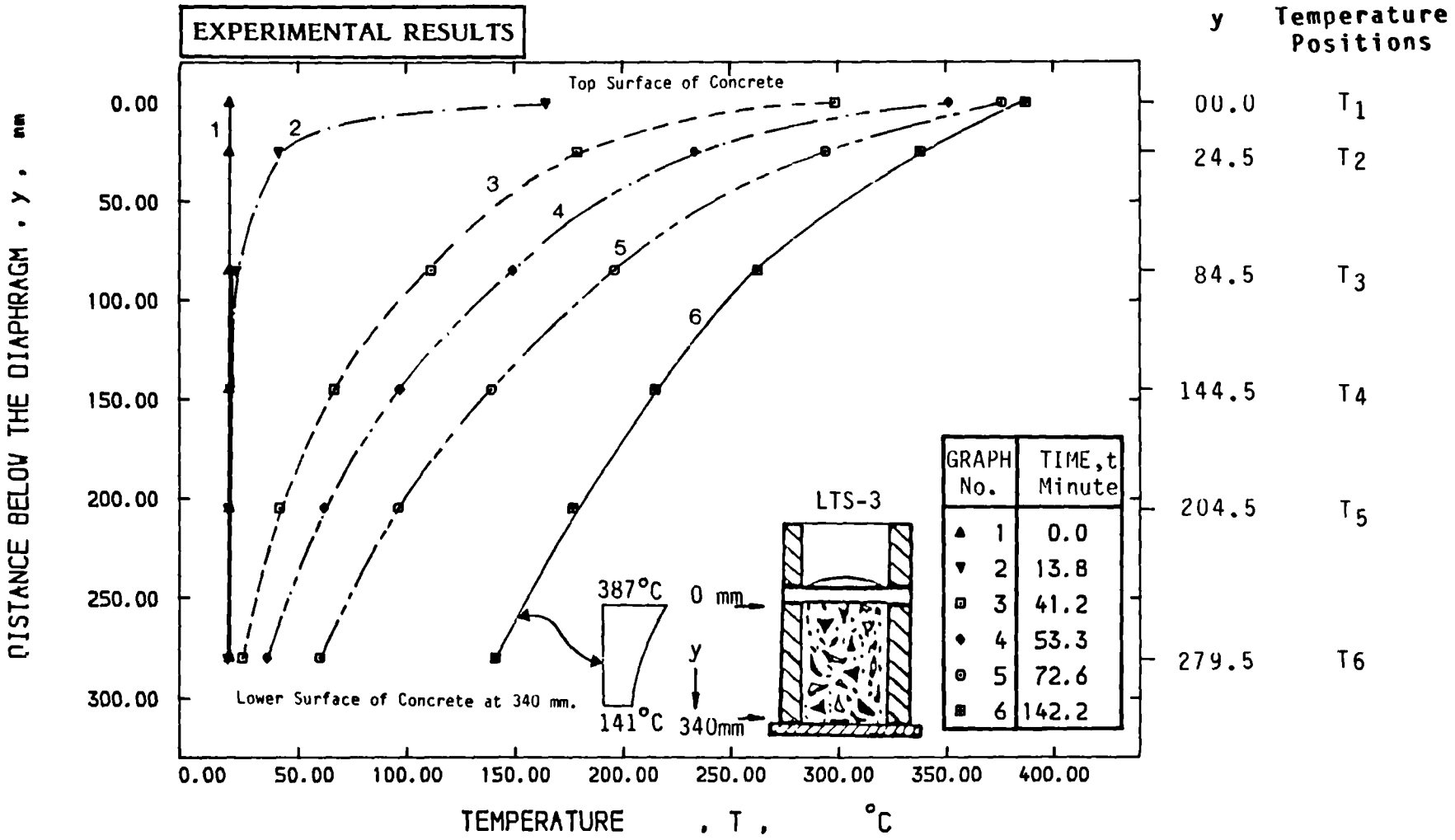

Figure 5.3 : Temperature Distributions in Concrete at selected Times from Start of Heating Specimen No: LTS-3

Note: ↔ For final temperature distribution (387 & 141 °C); see Fig. 5.27

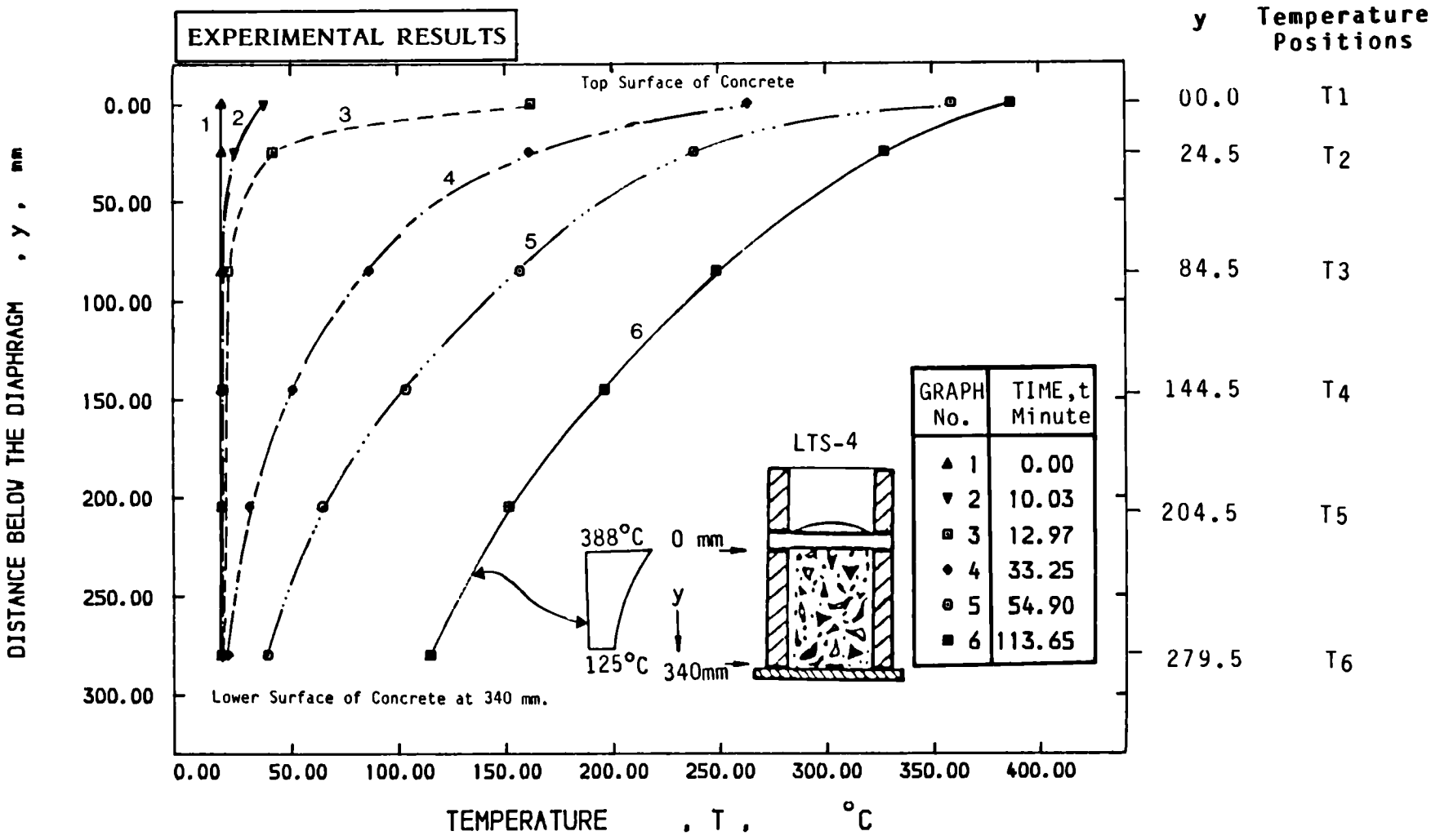

Figure 5.4 : Temperature Distributions in Concrete at selected Times from Start of Heating Specimen No: LTS-4

Note: ↝ For final temperature distribution (388 & 125 °C); see Fig. 5.28

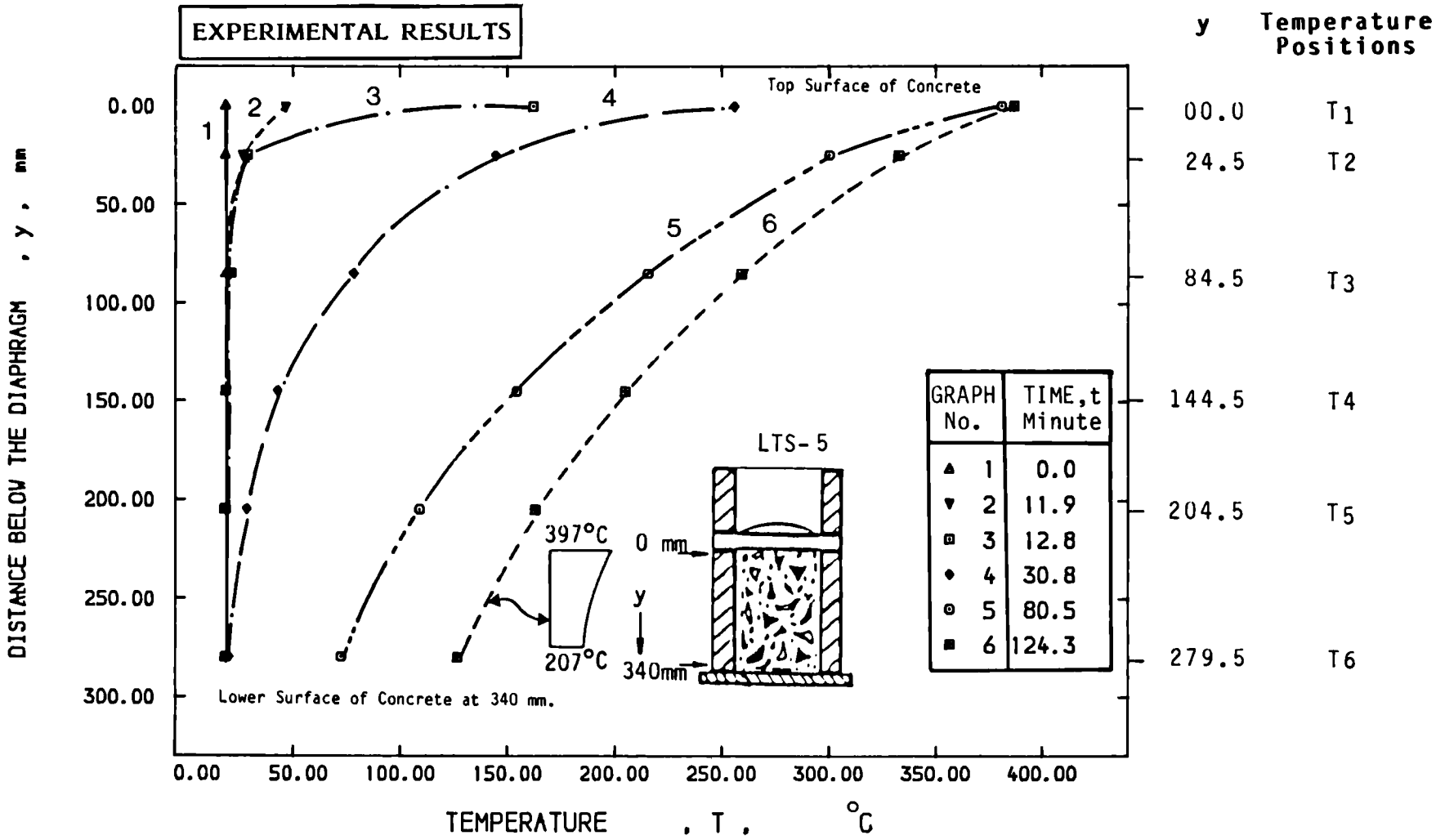

Figure 5.5 : Temperature Distributions in Concrete at selected Times from Start of Heating Specimen No: LTS-5

Note: ↖↘ For final temperature distribution (397 & 207 °C); see Fig. 5.29

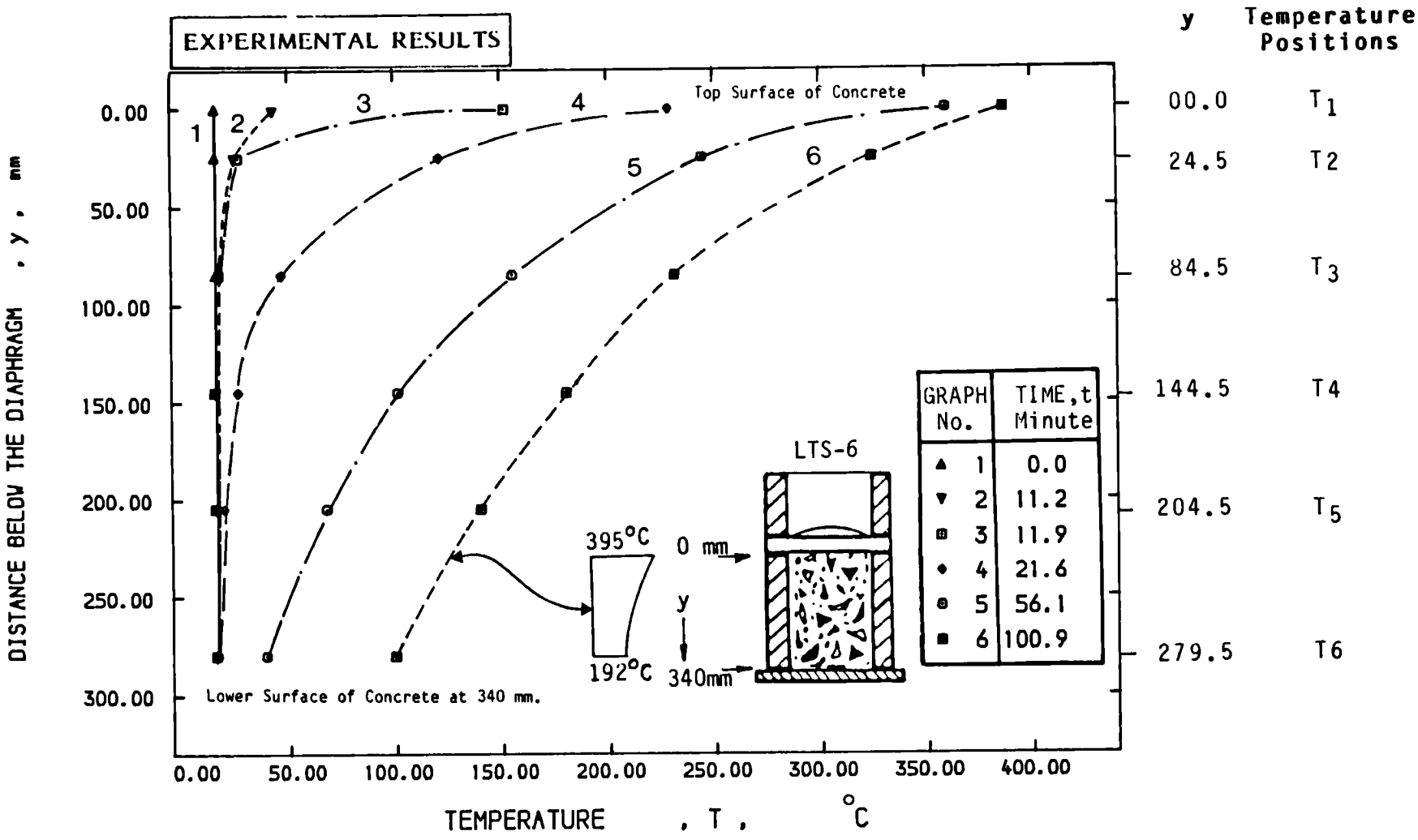

Figure 5.6 : Temperature Distributions in Concrete at selected Times from Start of Heating Specimen No: LTS-6

Note: ↔ For final temperature distribution (395 & 192 °C); see Fig. 5.30

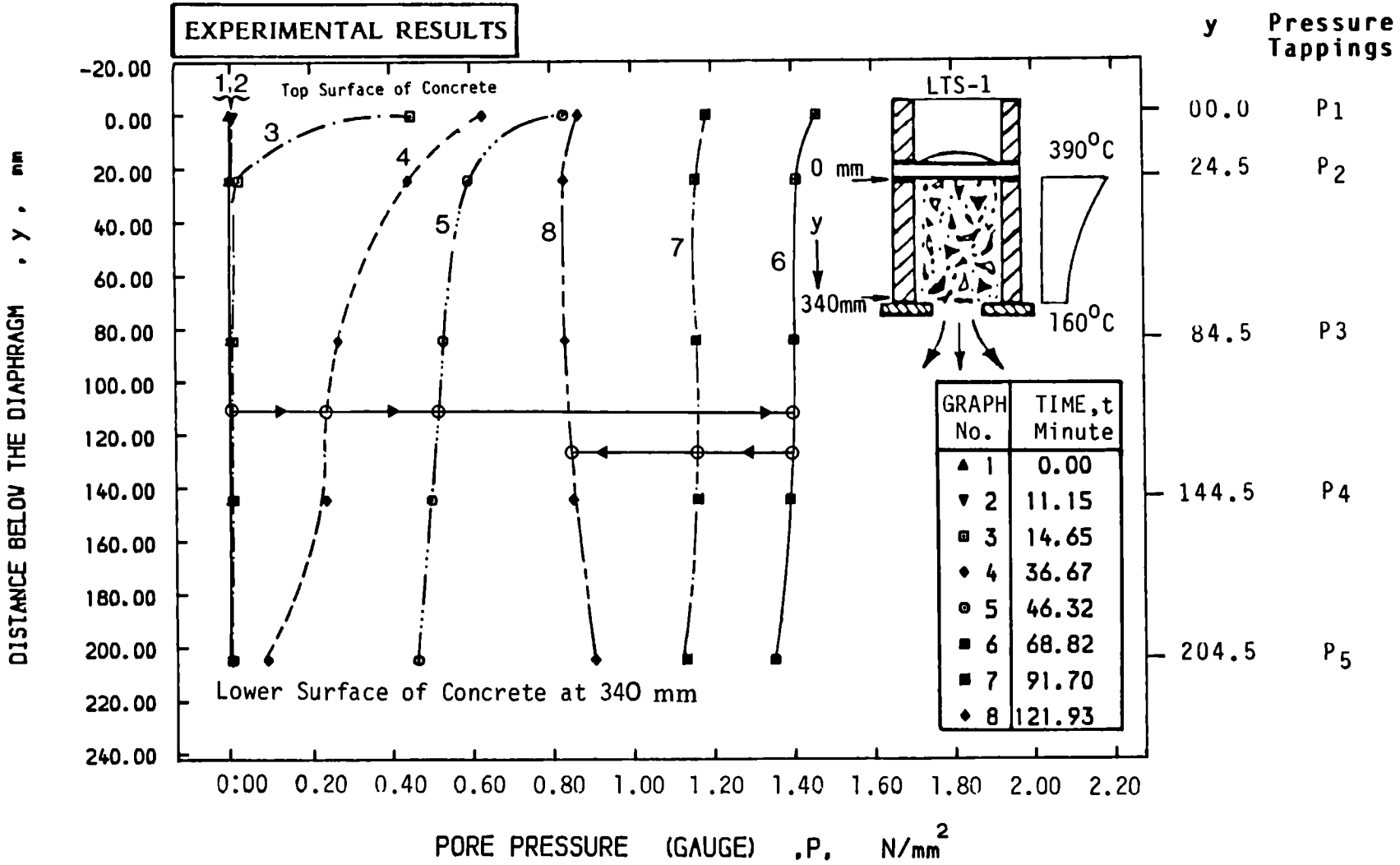

Figure 5.7 : Pore Pressure Distributions in Concrete at selected Times from Start of Heating Specimen No: LTS-1

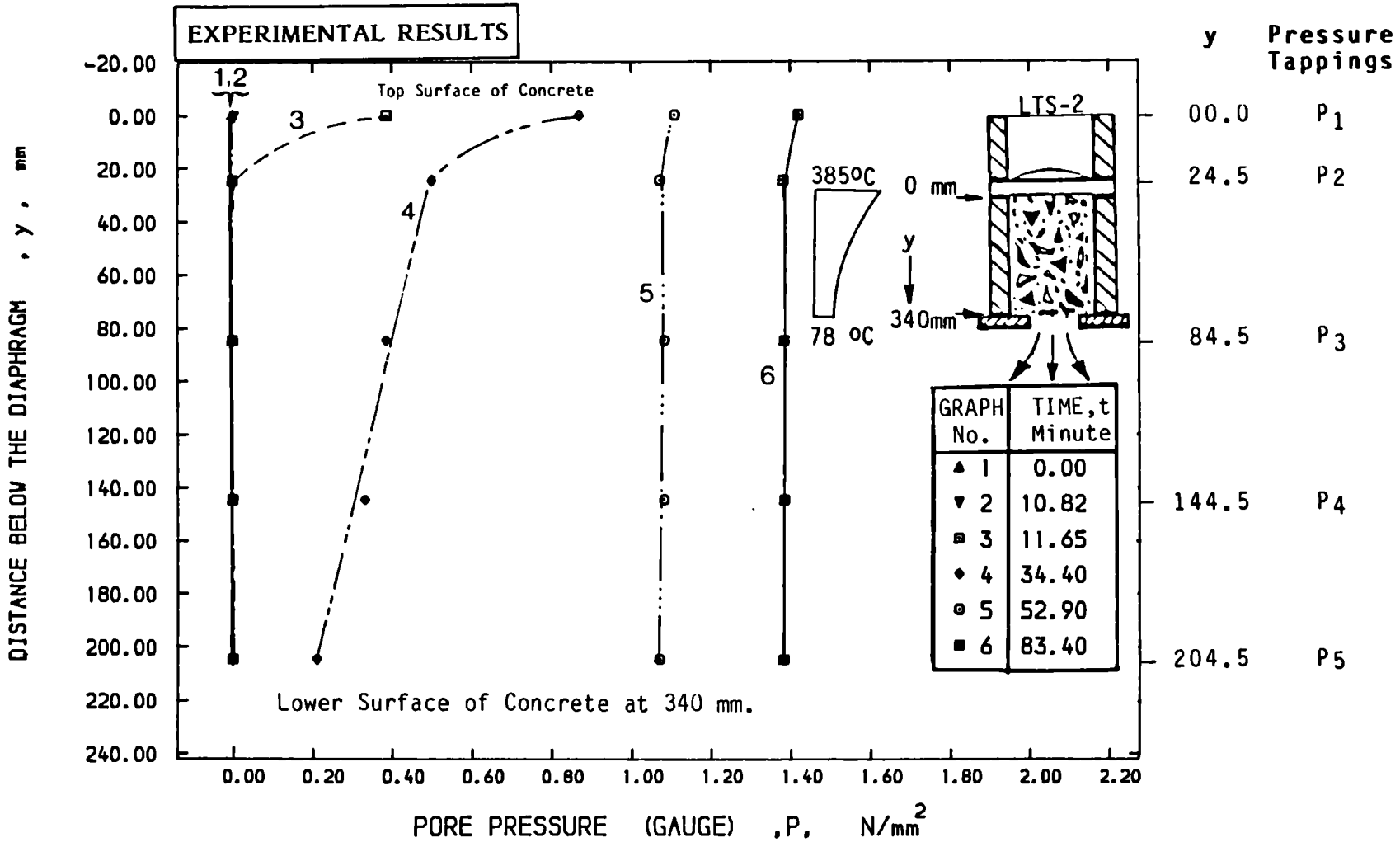

Figure 5.8 : Pore Pressure Distributions in Concrete at selected Times from Start of Heating Specimen No: LTS-2

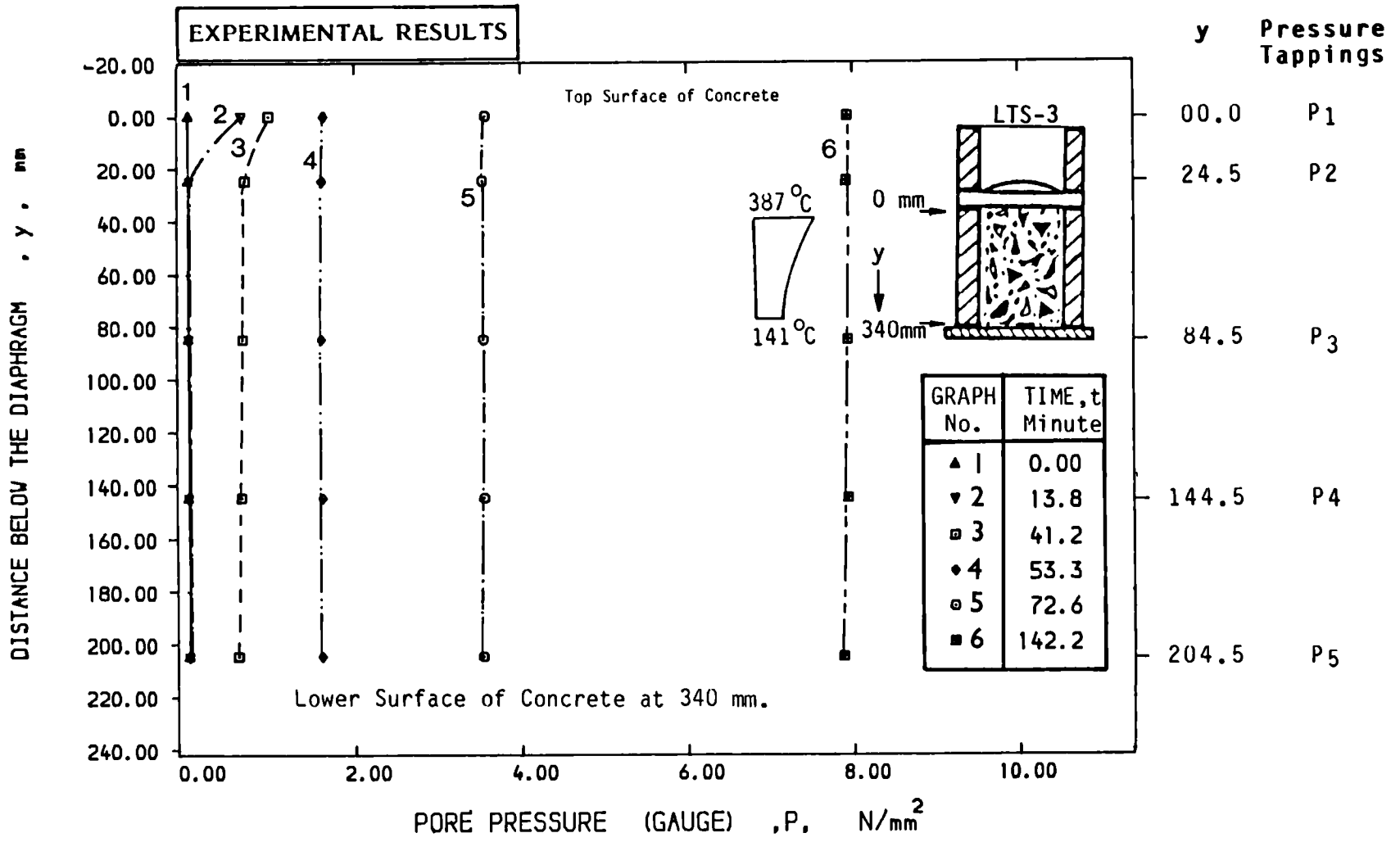

Figure 5.9 : Pore Pressure Distributions in Concrete at selected Times from Start of Heating Specimen No: LTS-3

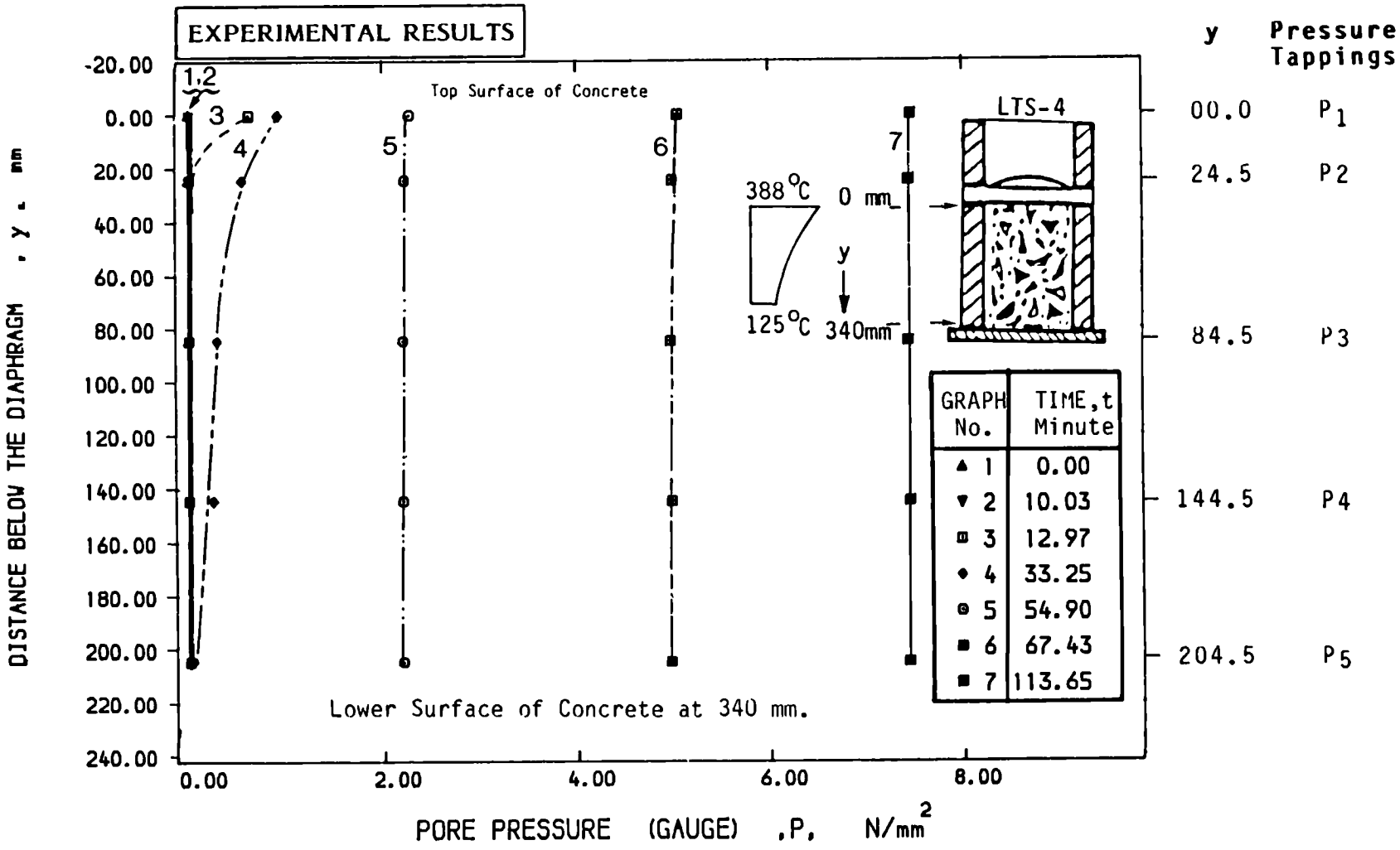

Figure 5.10 : Pore Pressure Distributions in Concrete at selected Times from Start of Heating Specimen No: LTS-4

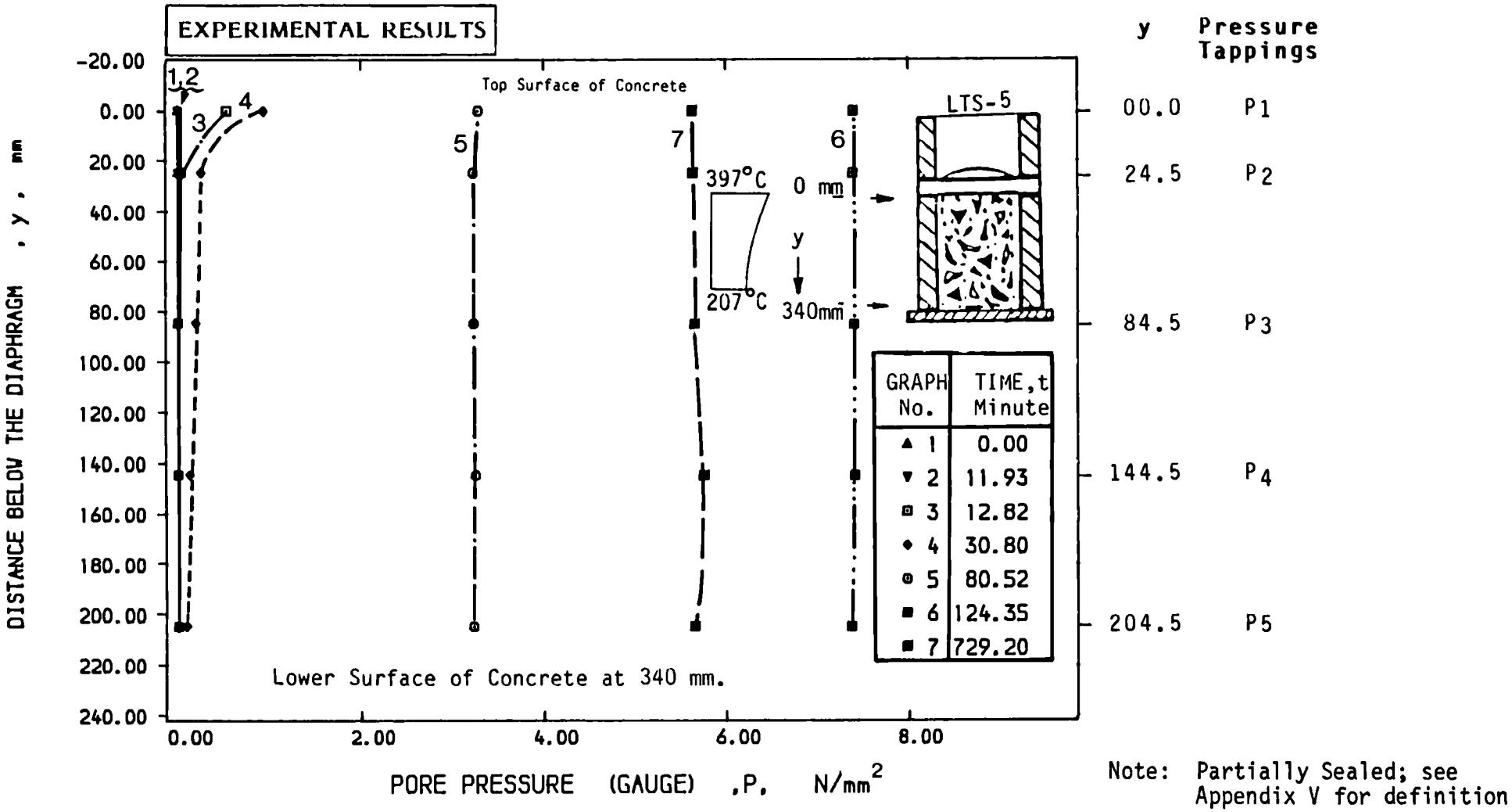

Figure 5.11 : Pore Pressure Distributions in Concrete at selected Times from Start of Heating Specimen No: LTS-5

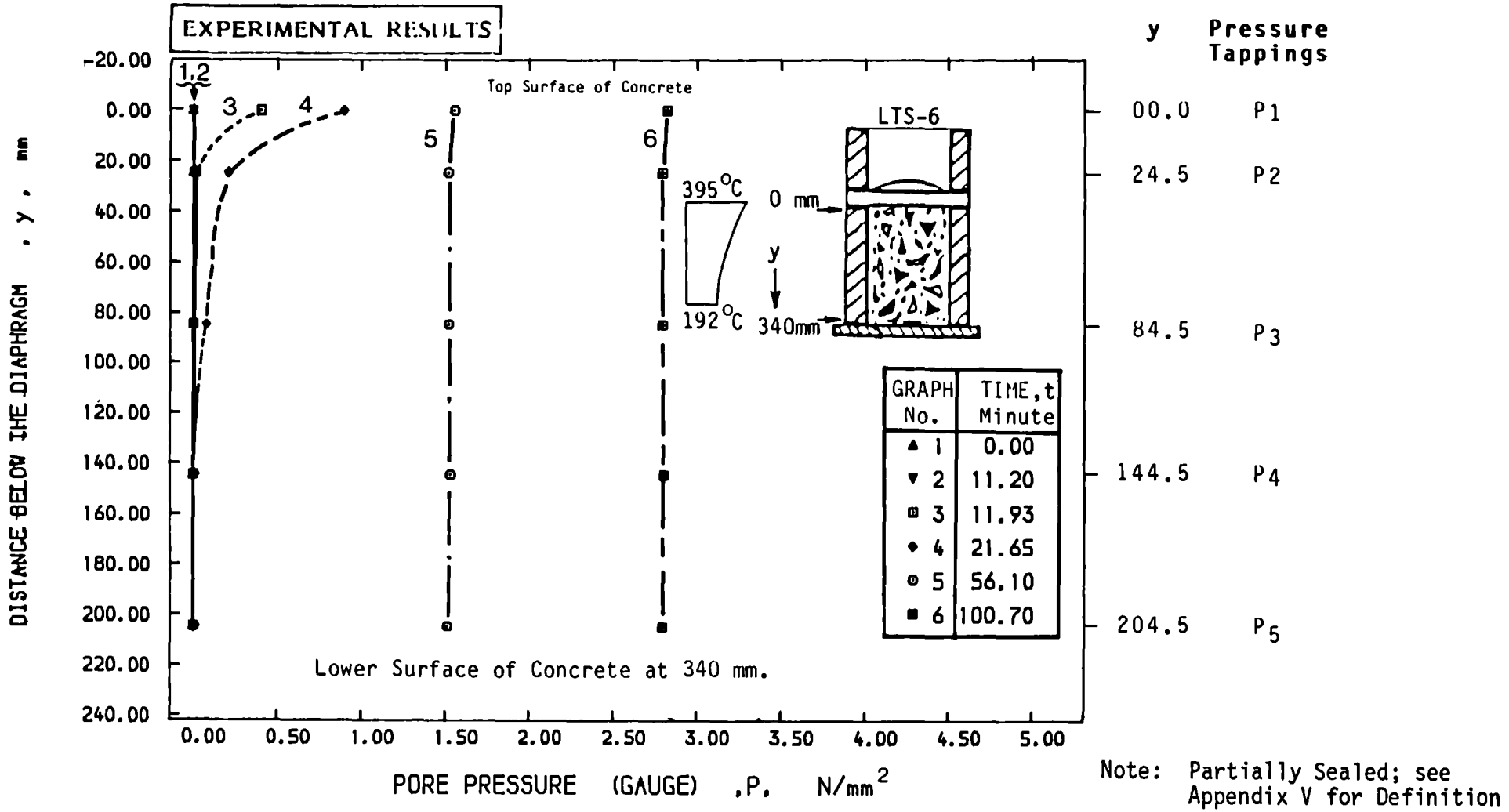

Figure 5.12 : Pore Pressure Distributions in Concrete at selected Times from Start of Heating
Specimen No: LTS-6

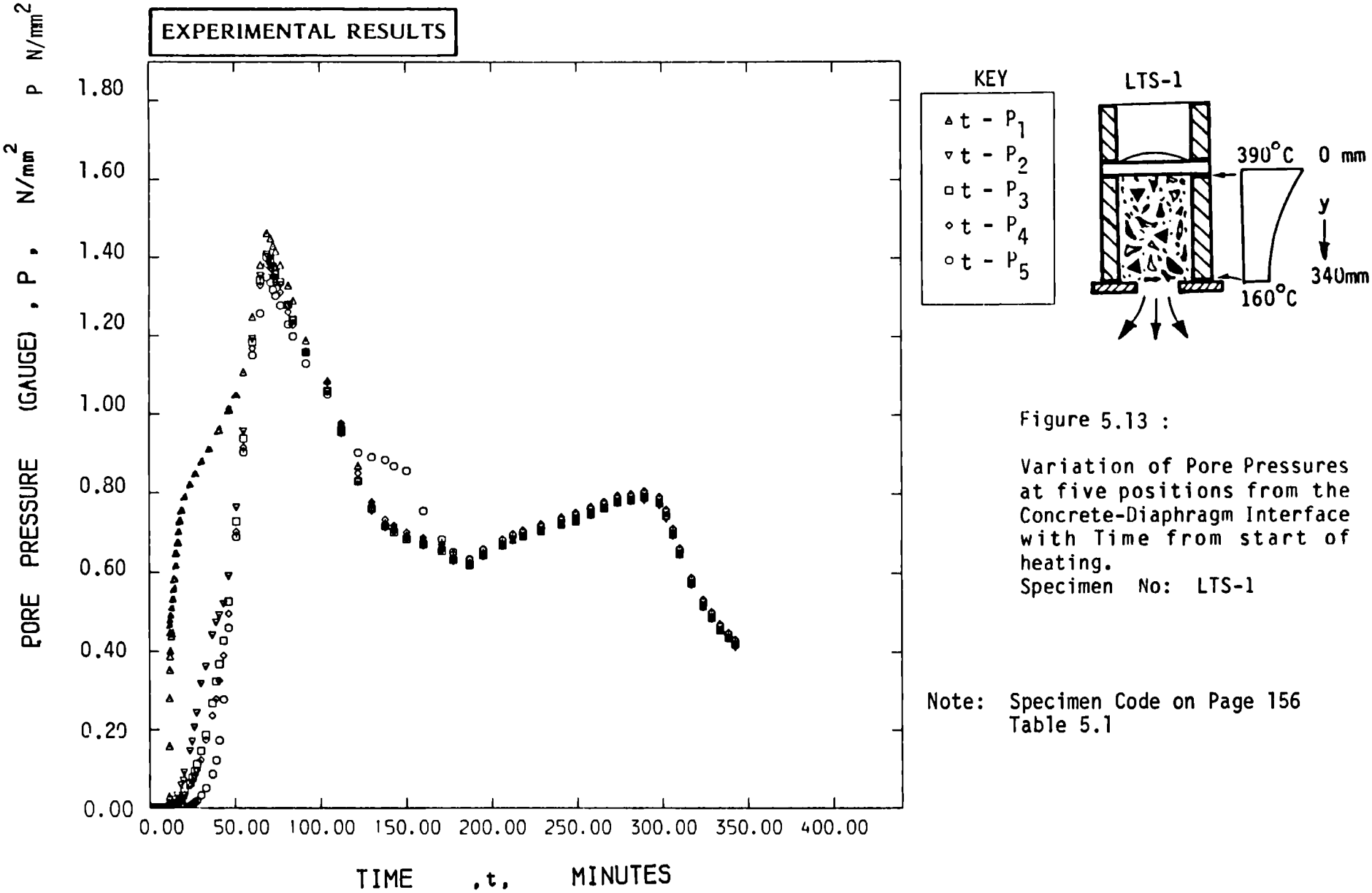

Figure 5.13 :

Variation of Pore Pressures at five positions from the Concrete-Diaphragm Interface with Time from start of heating.
Specimen No: LTS-1

Note: Specimen Code on Page 156 Table 5.1

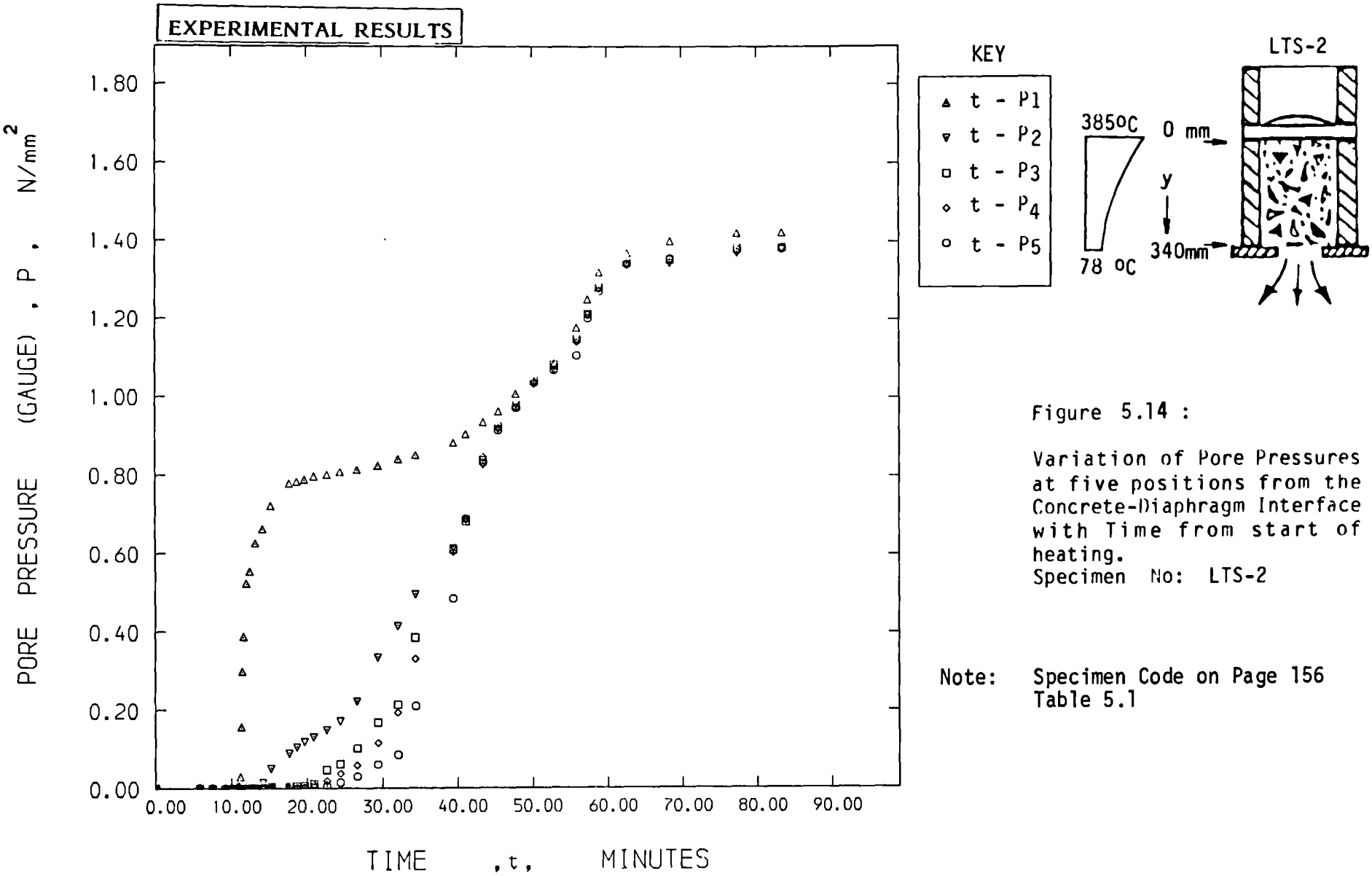

Figure 5.14 :

Variation of Pore Pressures at five positions from the Concrete-Diaphragm Interface with Time from start of heating.
Specimen No: LTS-2

Note: Specimen Code on Page 156 Table 5.1

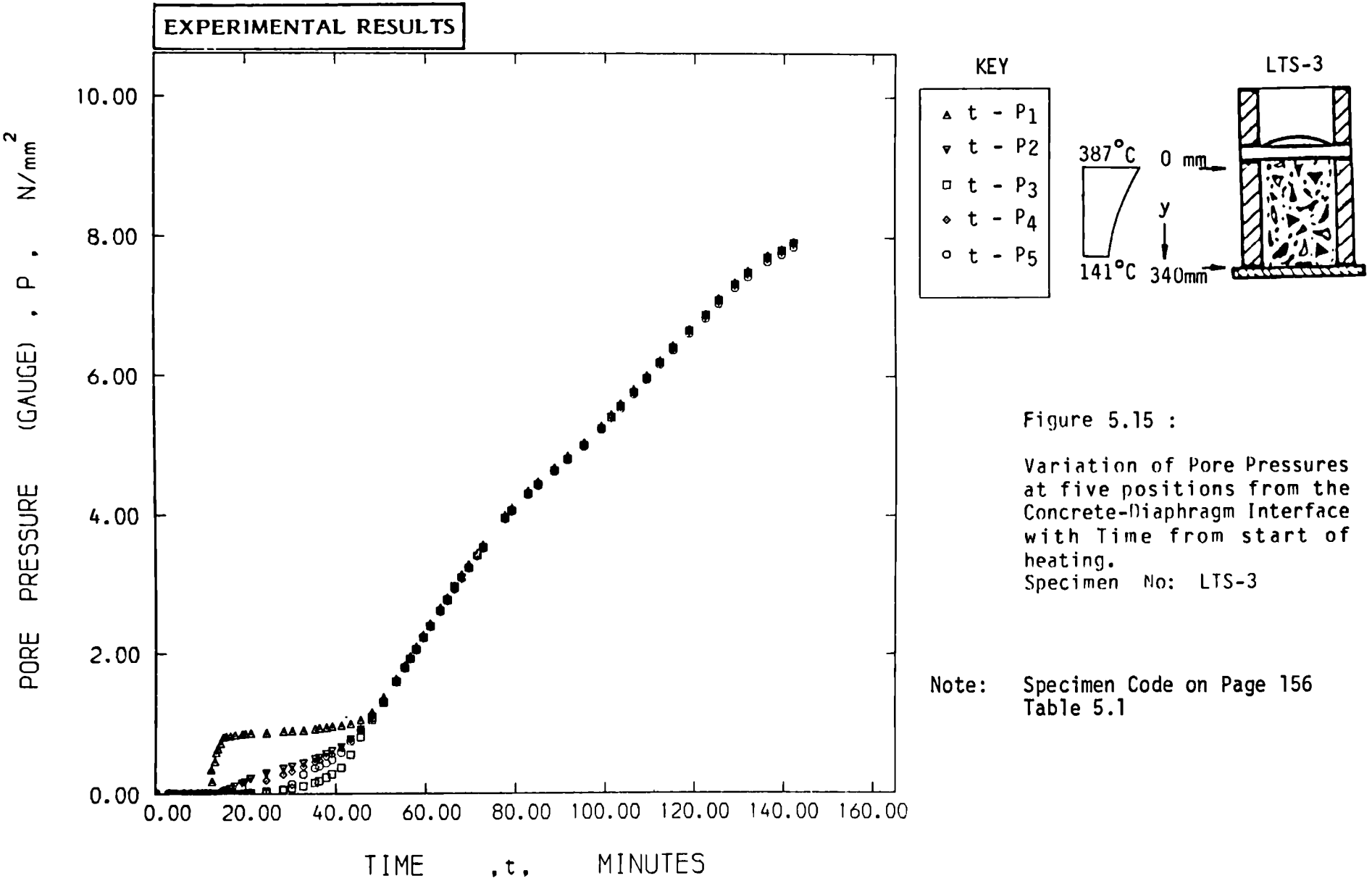

Figure 5.15 :

Variation of Pore Pressures at five positions from the Concrete-Diaphragm Interface with Time from start of heating.
Specimen No: LTS-3

Note: Specimen Code on Page 156 Table 5.1

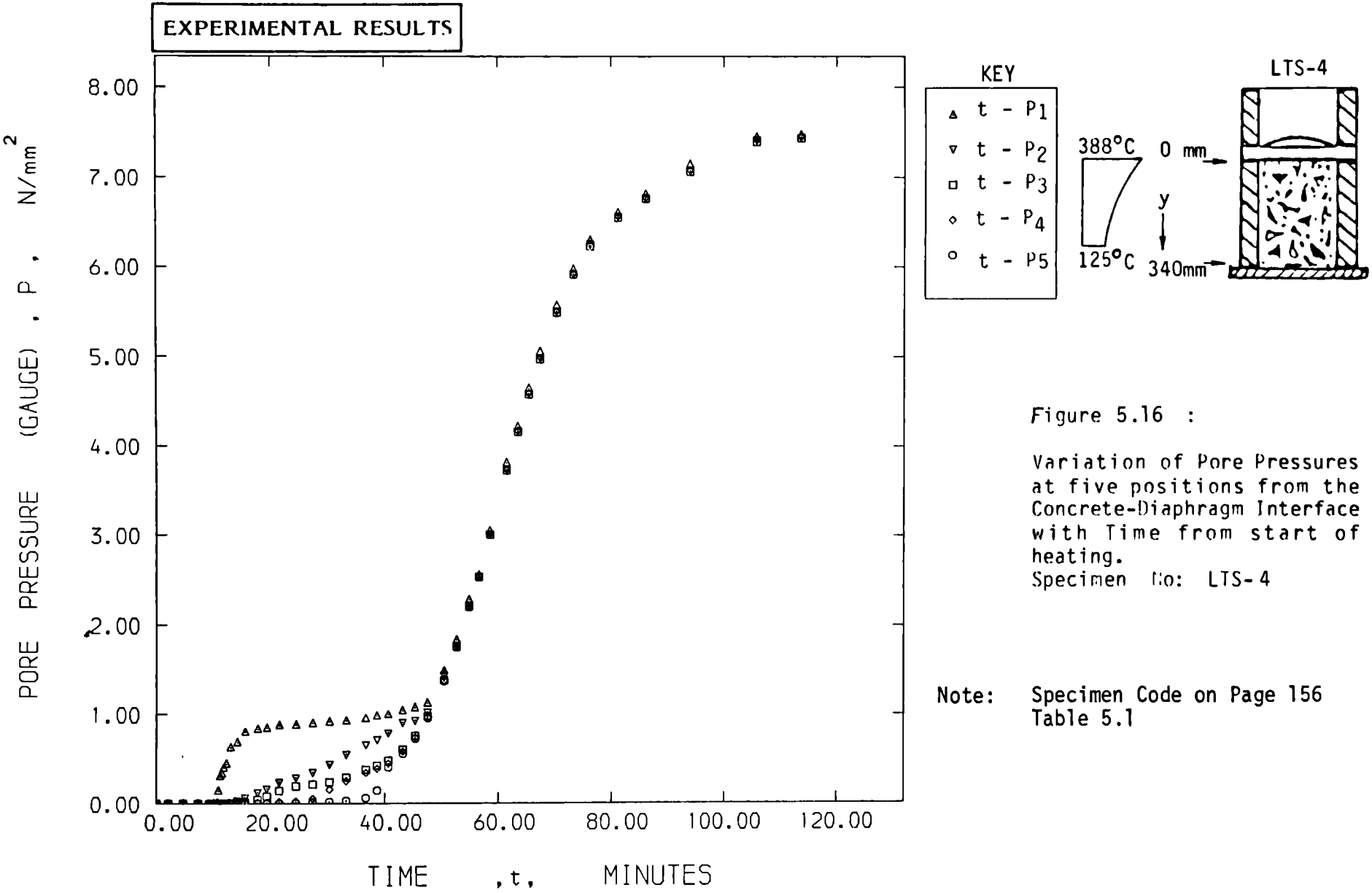

Figure 5.16 :

Variation of Pore Pressures at five positions from the Concrete-Diaphragm Interface with Time from start of heating.
Specimen No: LTS-4

Note: Specimen Code on Page 156 Table 5.1

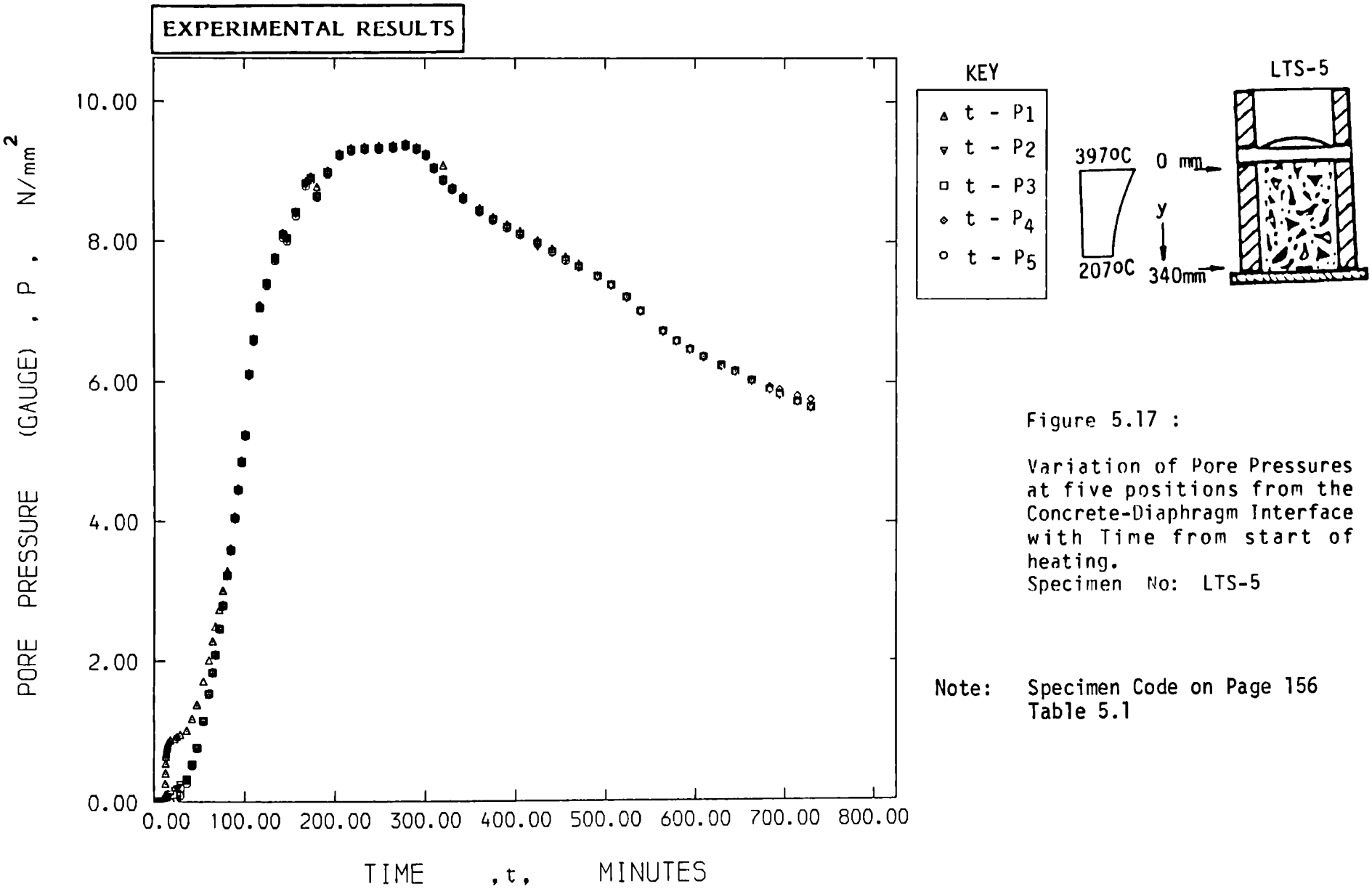

Figure 5.17 :

Variation of Pore Pressures at five positions from the Concrete-Diaphragm Interface with Time from start of heating.
Specimen No: LTS-5

Note: Specimen Code on Page 156 Table 5.1

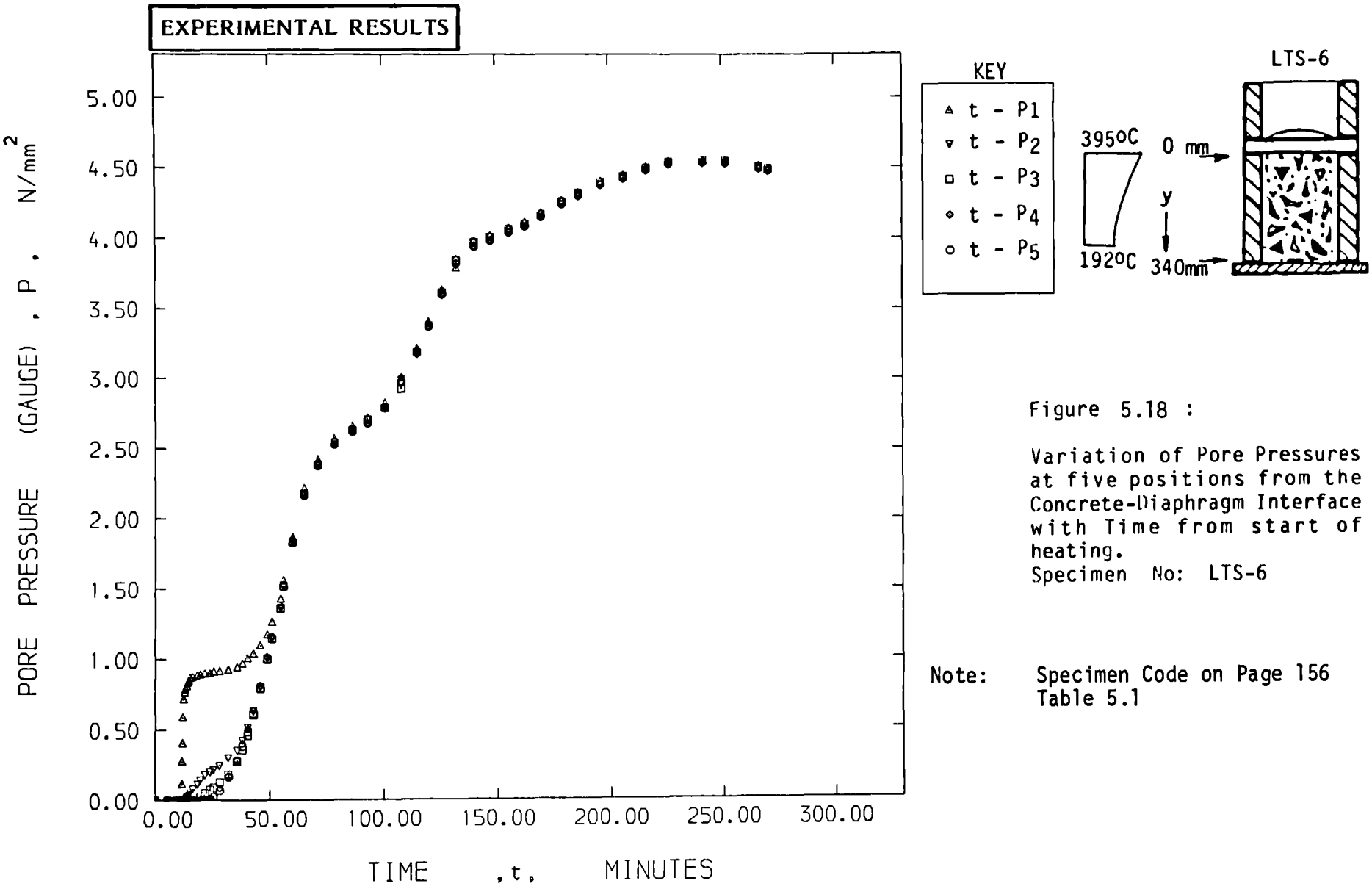

Figure 5.18 :

Variation of Pore Pressures at five positions from the Concrete-Diaphragm Interface with Time from start of heating.
Specimen No: LTS-6

Note: Specimen Code on Page 156 Table 5.1

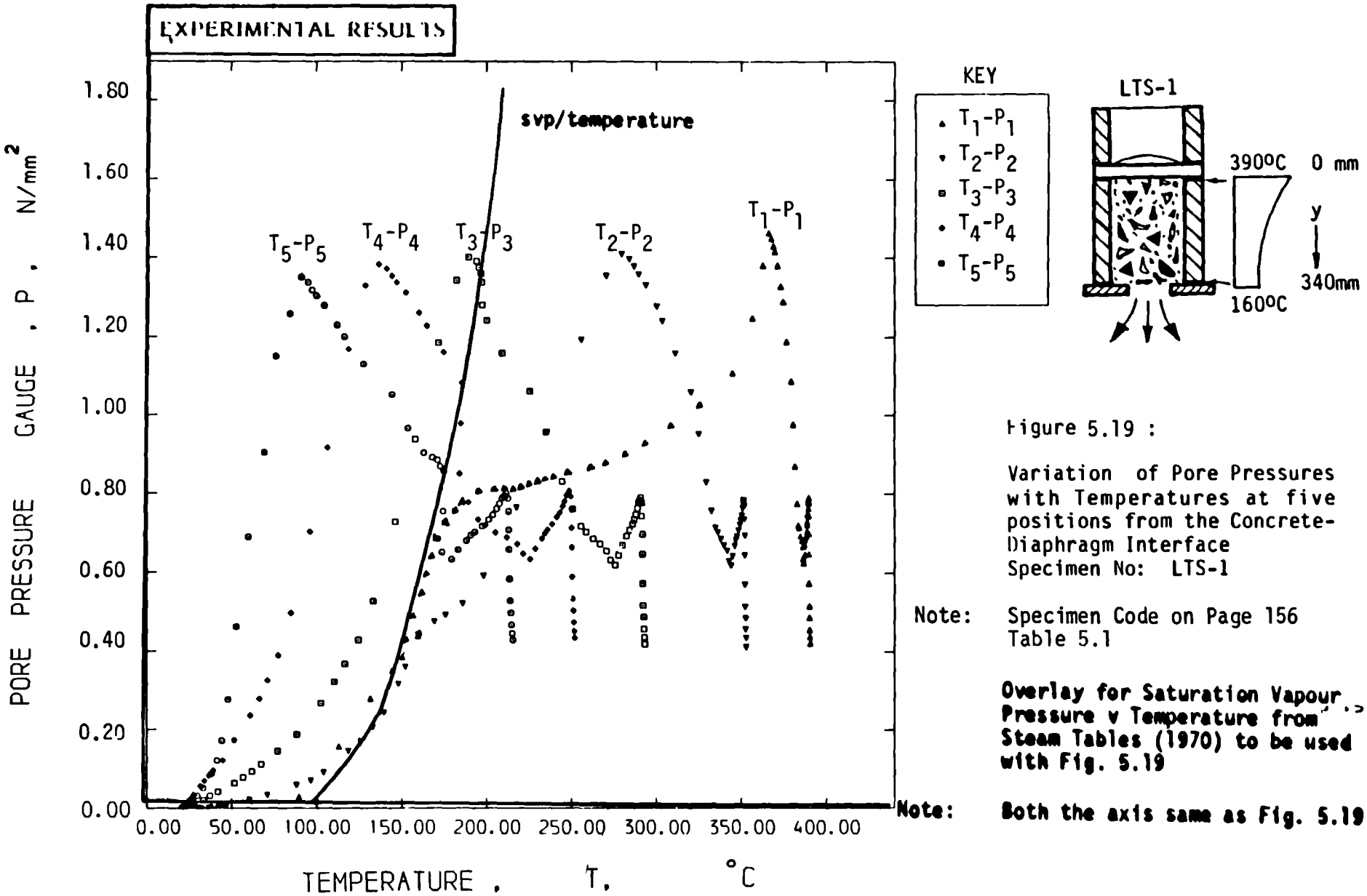

Figure 5.19 :

Variation of Pore Pressures with Temperatures at five positions from the Concrete-Diaphragm Interface
Specimen No: LTS-1

Note: Specimen Code on Page 156 Table 5.1

Overlay for Saturation Vapour Pressure v Temperature from Steam Tables (1970) to be used with Fig. 5.19

Note: Both the axis same as Fig. 5.19

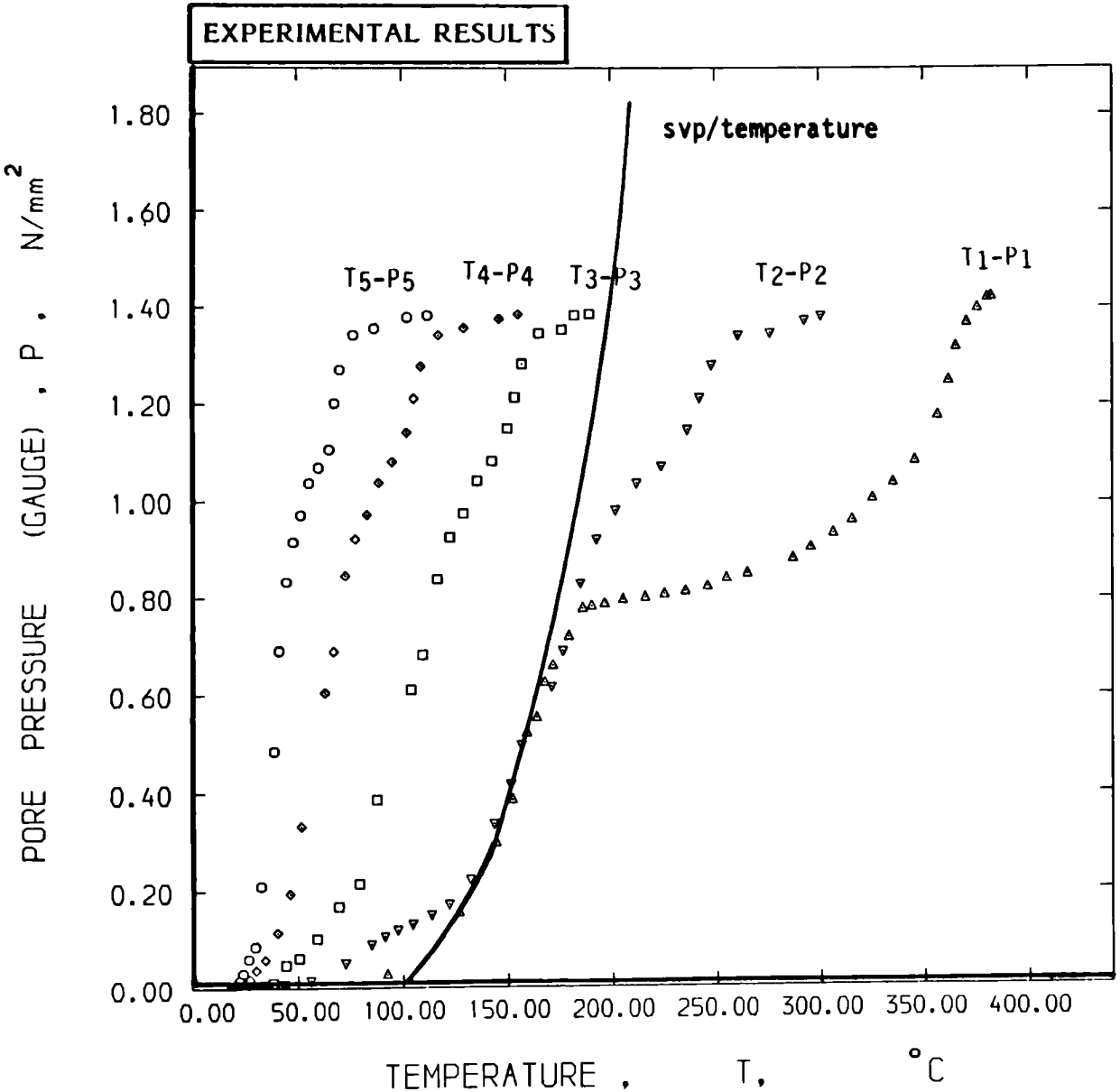

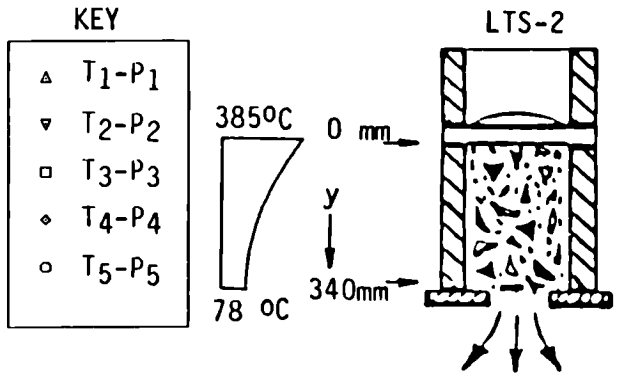

Figure 5.20 :

Variation of Pore Pressures with Temperatures at five positions from the Concrete-Diaphragm Interface
Specimen No: LTS-2

Note: Specimen code on Page 156 Table 5.1

Overlay for Saturation Vapour Pressure v Temperature from Steam Tables (1970) for use with Fig. 5.20

Note: Both the axis same as Fig. 5.20

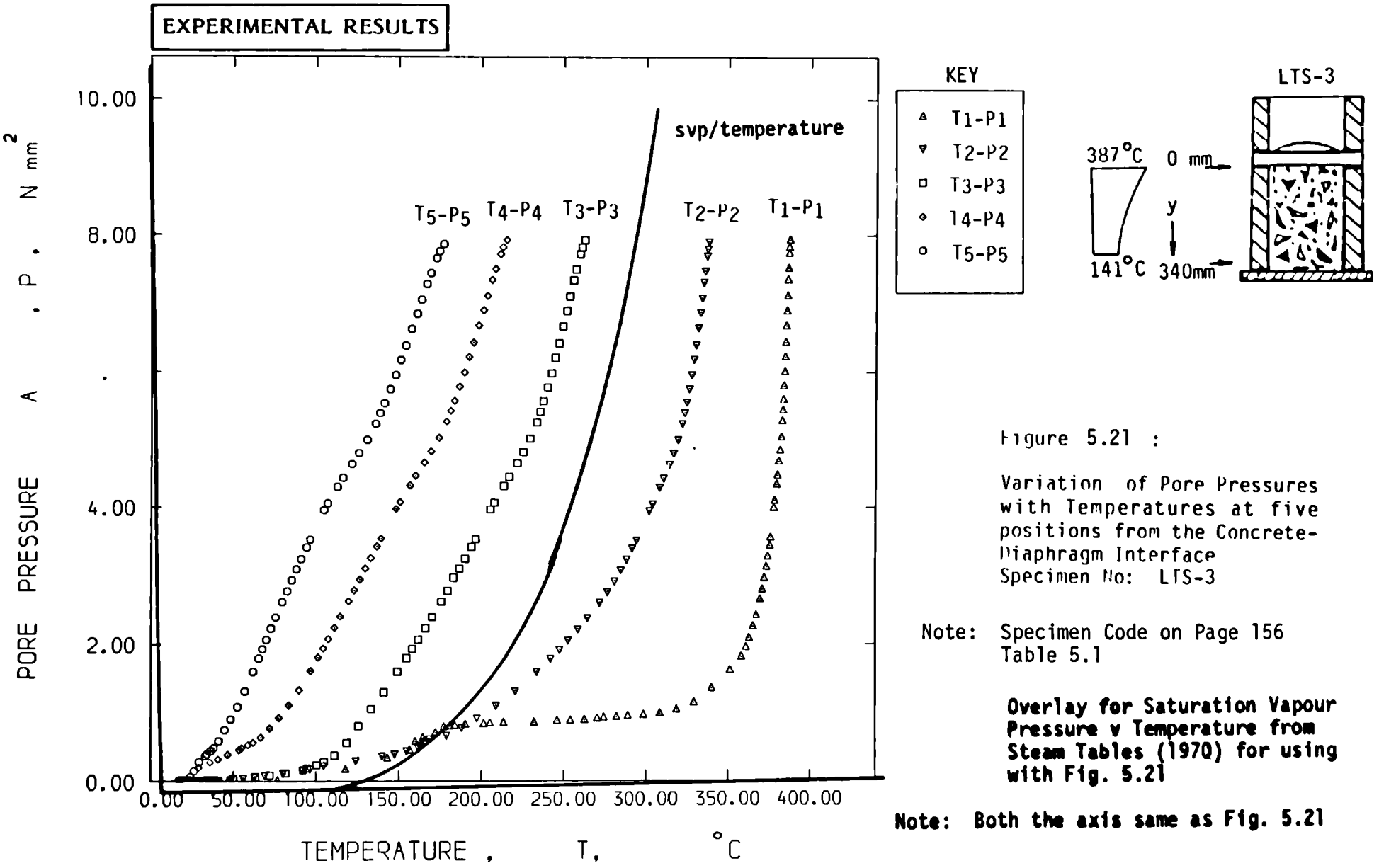

Figure 5.21 :

Variation of Pore Pressures with Temperatures at five positions from the Concrete-Diaphragm Interface
Specimen No: LTS-3

Note: Specimen Code on Page 156 Table 5.1

Overlay for Saturation Vapour Pressure v Temperature from Steam Tables (1970) for using with Fig. 5.21

Note: Both the axis same as Fig. 5.21

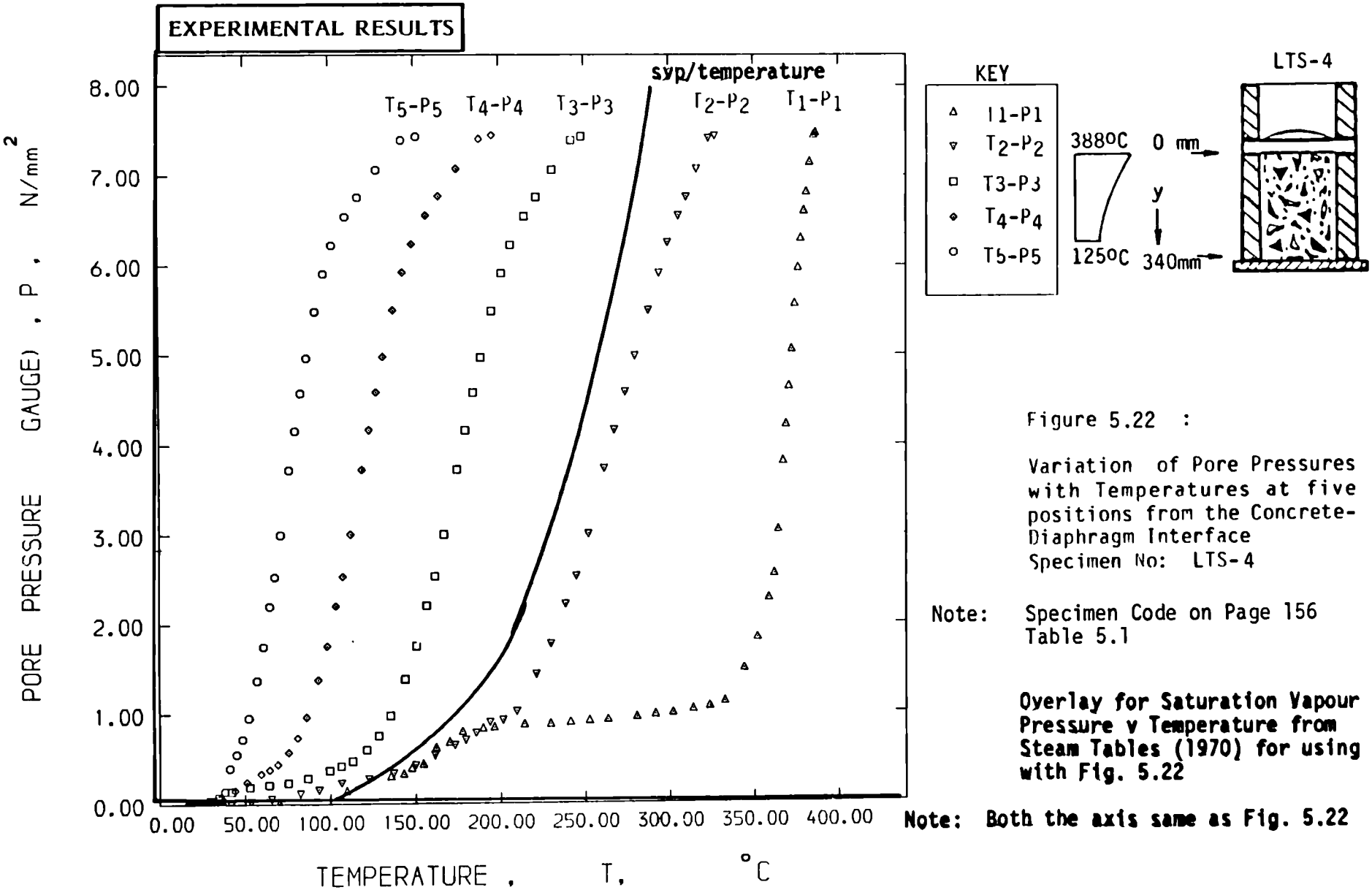

Figure 5.22 :

Variation of Pore Pressures with Temperatures at five positions from the Concrete-Diaphragm Interface
Specimen No: LTS-4

Note: Specimen Code on Page 156 Table 5.1

Overlay for Saturation Vapour Pressure v Temperature from Steam Tables (1970) for using with Fig. 5.22

Note: Both the axis same as Fig. 5.22

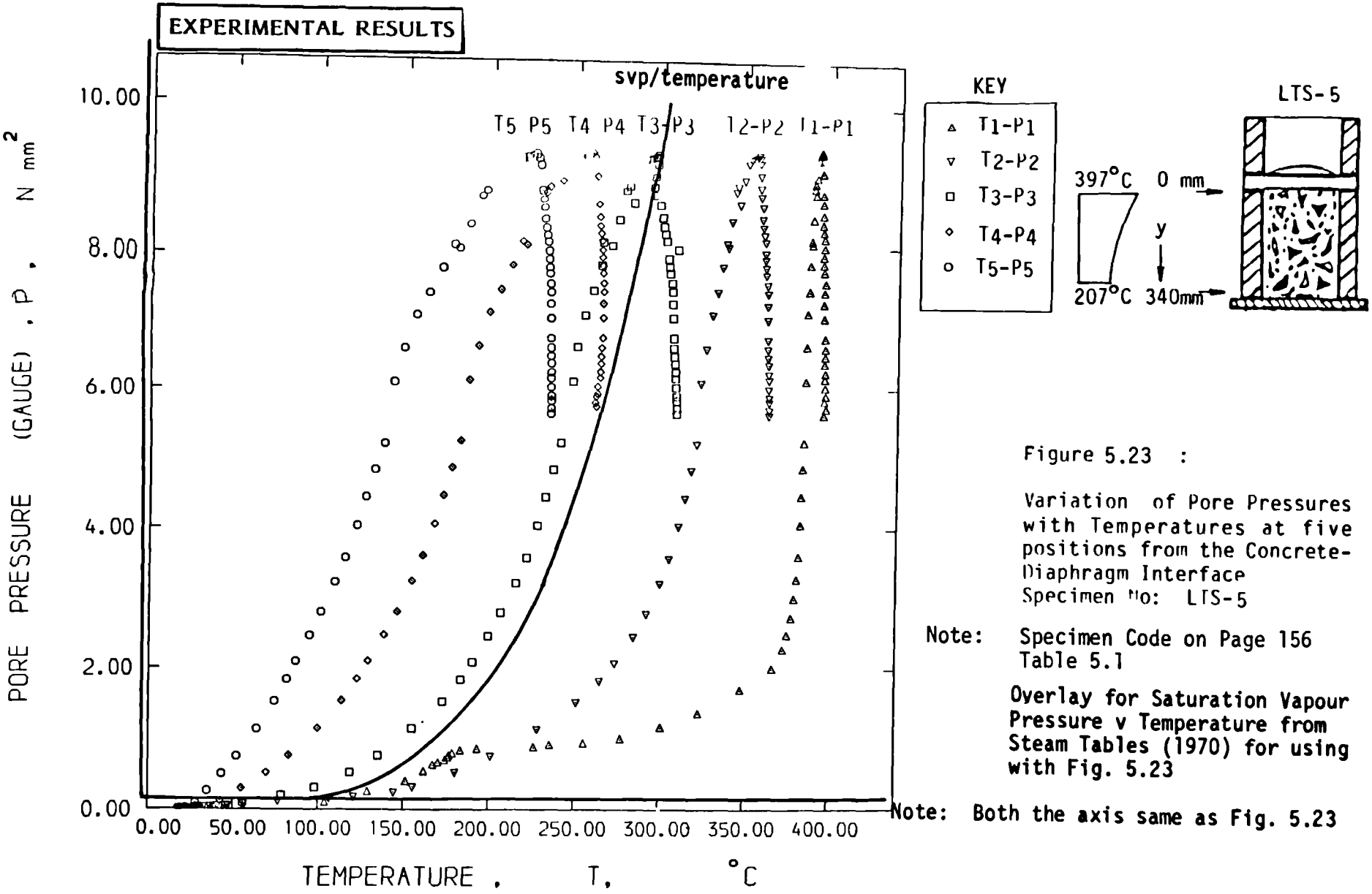

Figure 5.23 :

Variation of Pore Pressures with Temperatures at five positions from the Concrete-Diaphragm Interface
Specimen No: LTS-5

Note: Specimen Code on Page 156 Table 5.1

Overlay for Saturation Vapour Pressure v Temperature from Steam Tables (1970) for using with Fig. 5.23

Note: Both the axis same as Fig. 5.23

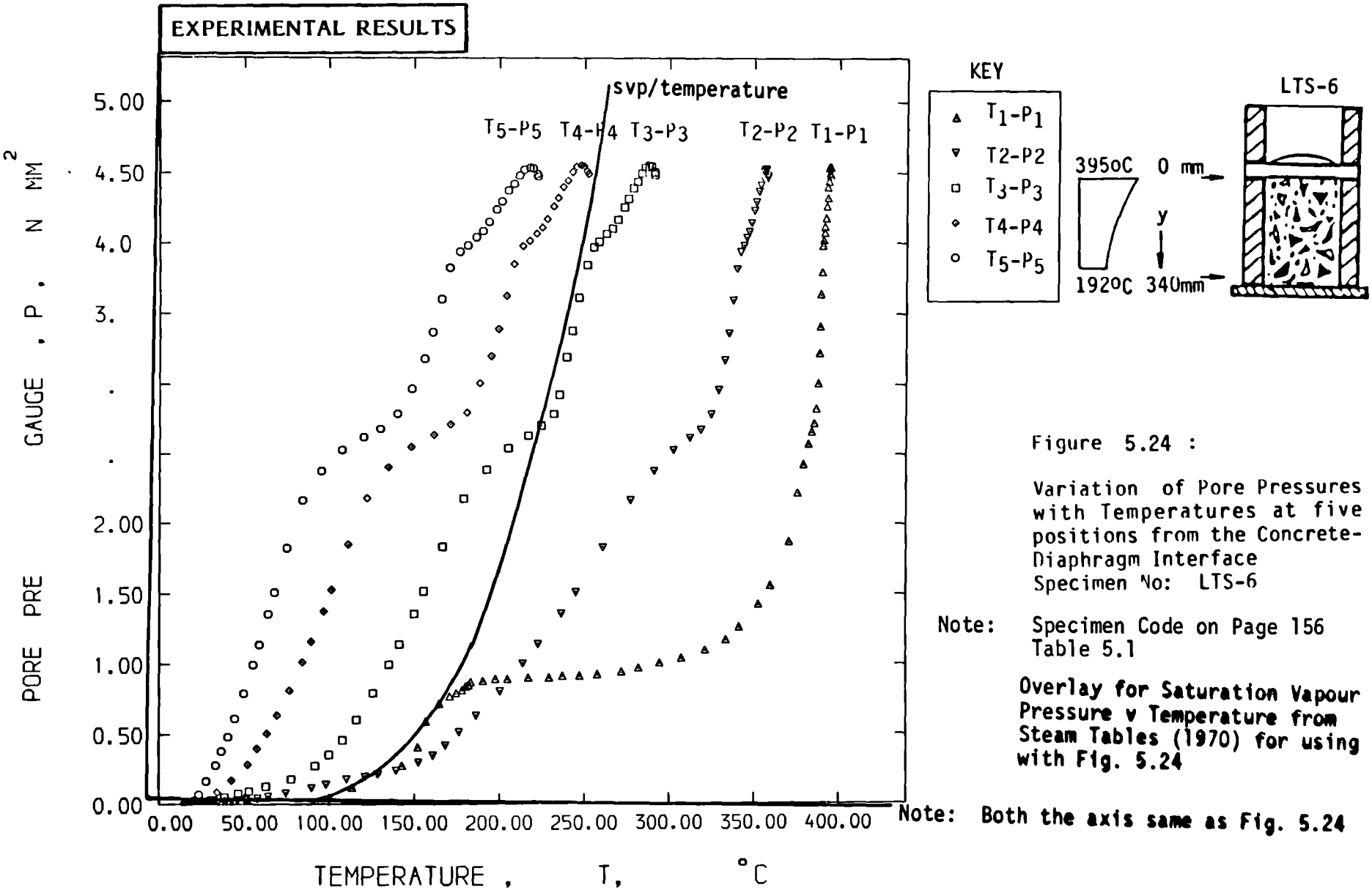

Figure 5.24 :

Variation of Pore Pressures with Temperatures at five positions from the Concrete-Diaphragm Interface
Specimen No: LTS-6

Note: Specimen Code on Page 156 Table 5.1

Overlay for Saturation Vapour Pressure v Temperature from Steam Tables (1970) for using with Fig. 5.24

Note: **Both the axis same as Fig. 5.24**

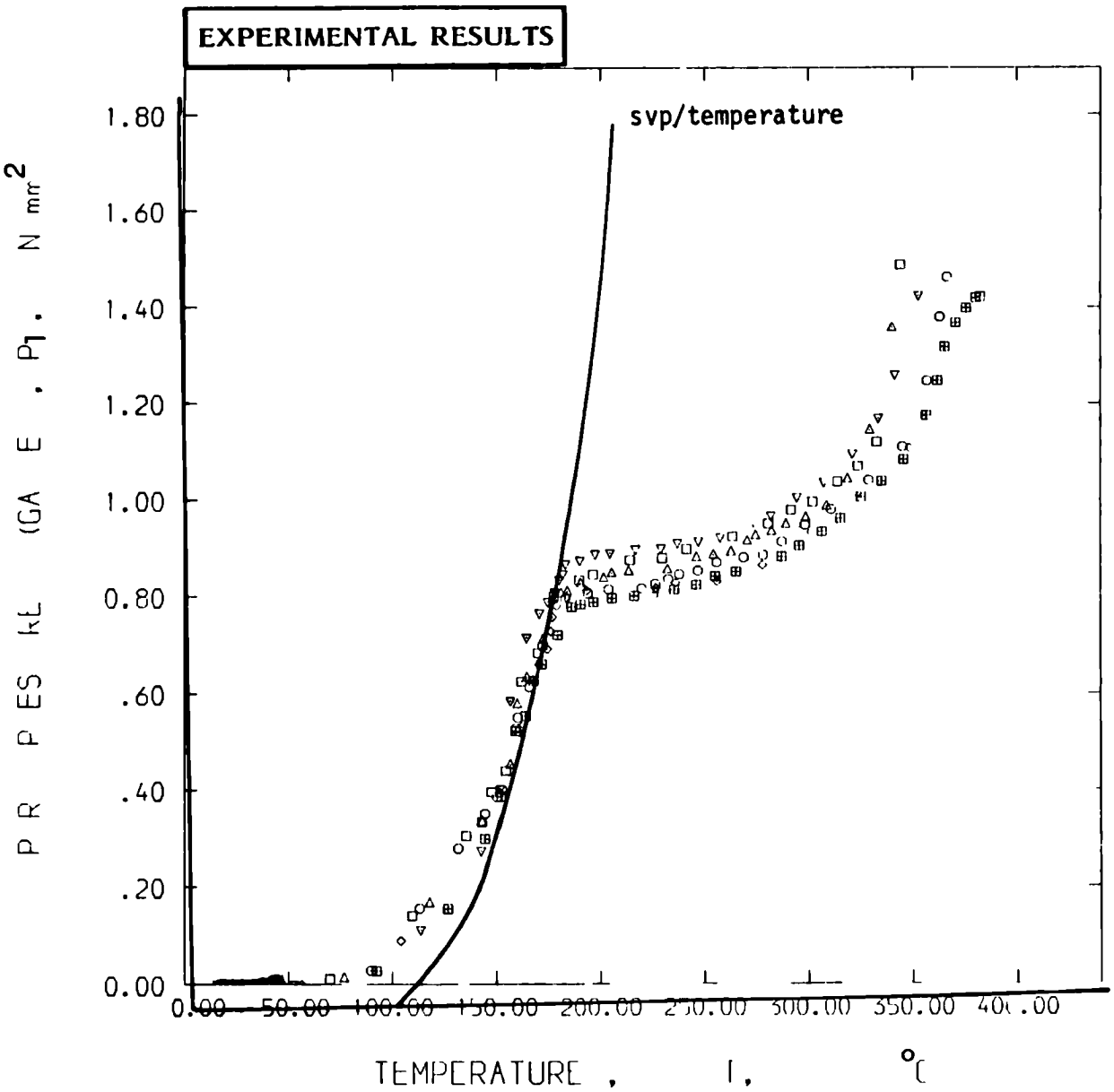

Figure 5.24a :

Variation of Pore Pressures (P_1) with Temperatures (T_1) for the initial stages of heating for all "LTS" Specimens

Note: Specimen Code on Page 156
Table 5.1 for Saturation Vapour Pressure v Temperature from Steam Tables (1970) for using with Fig. 5.24a

Note: Both the axis same as Fig. 5.24a

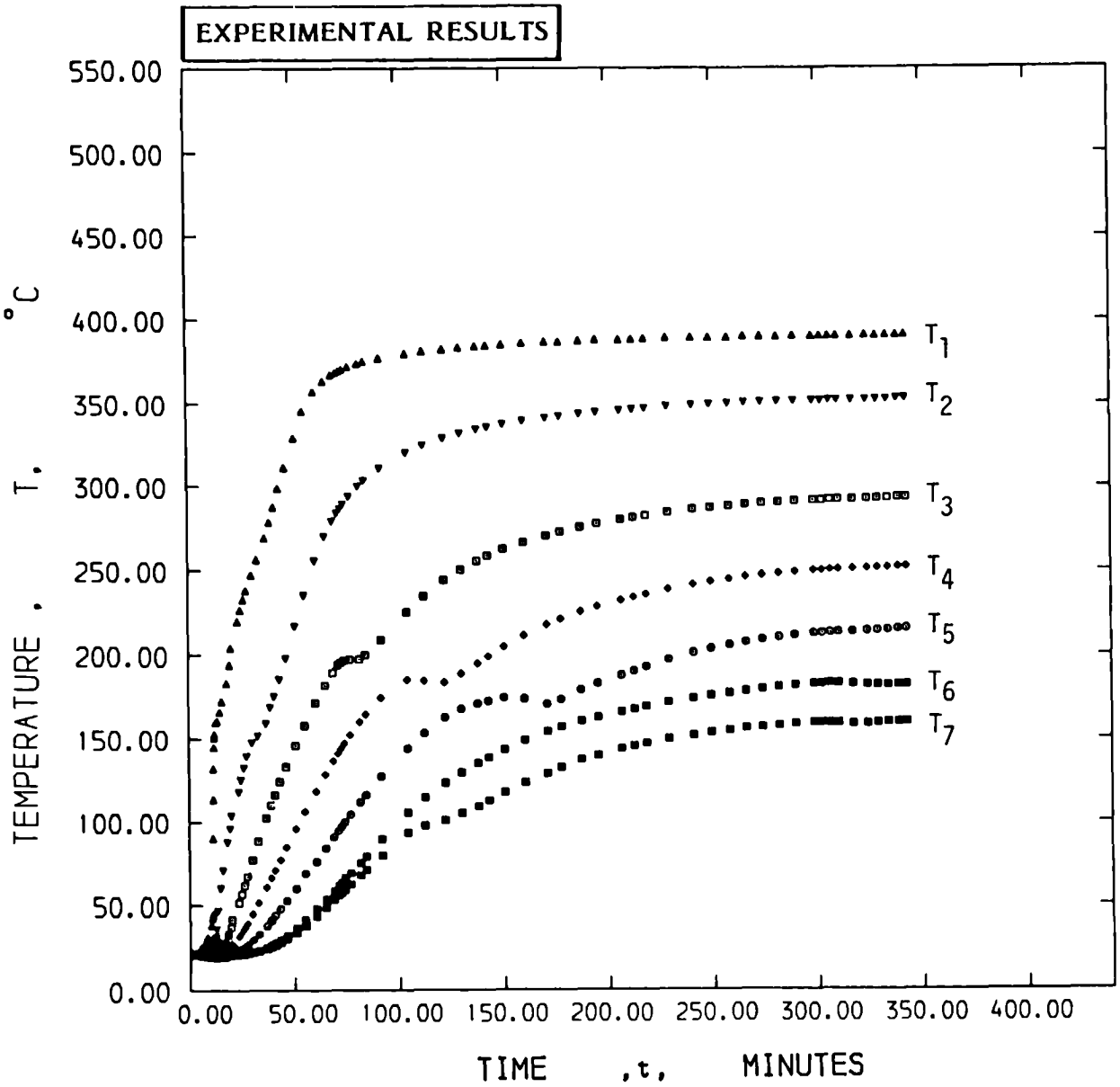

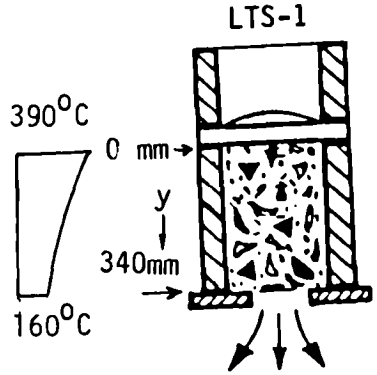

Figure 5.25:

Variation of Temperatures at seven positions from the Concrete-Diaphragm Interface with Time from start of heating.
Specimen No: LTS-1

Note : Specimen Code on Page 156 Table 5.1

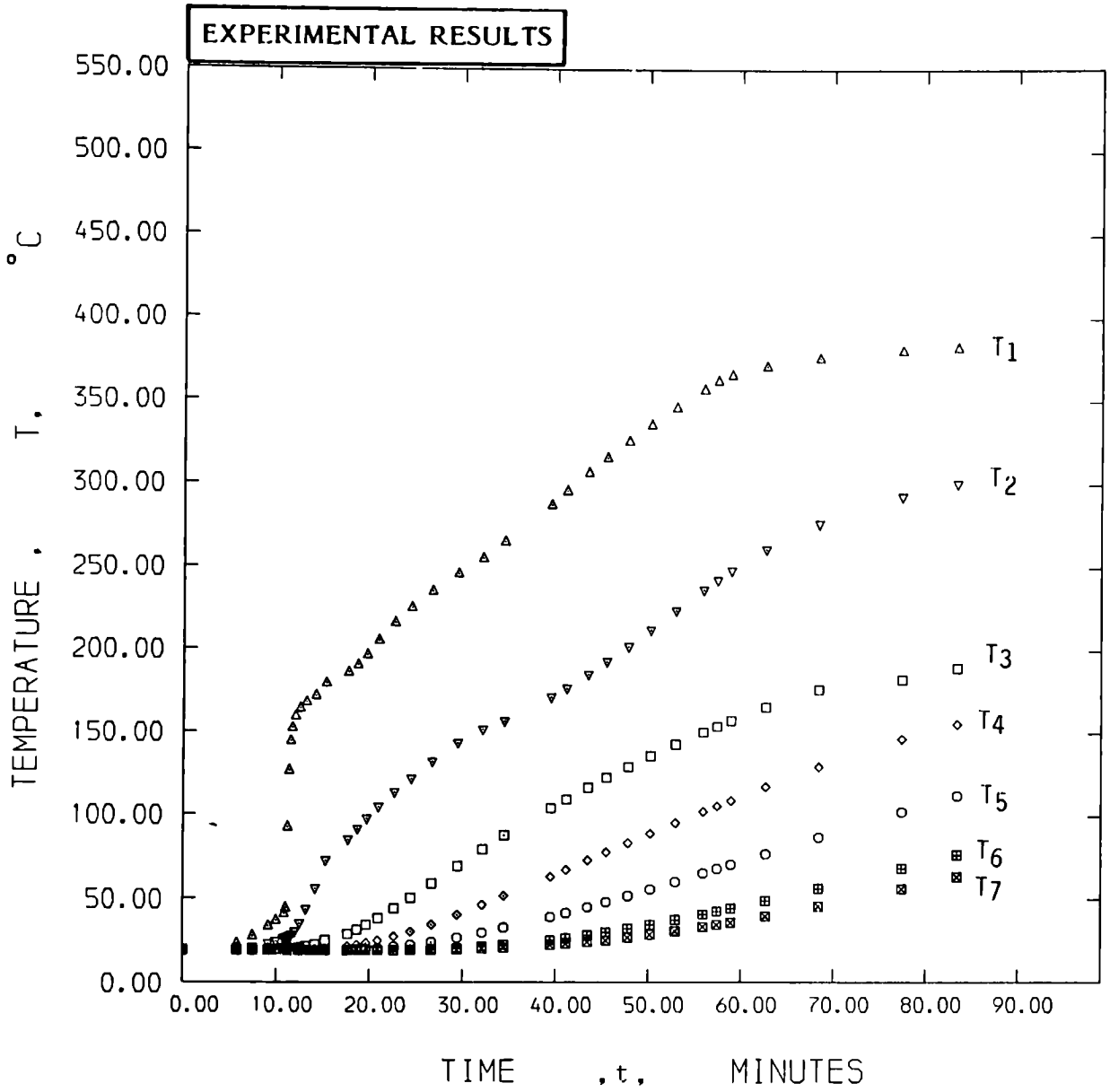

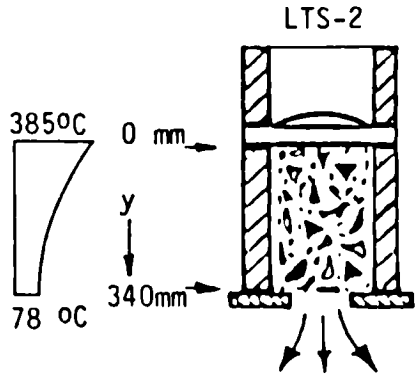

Figure 5.26:

Variation of Temperatures at seven positions from the Concrete-Diaphragm Interface with Time from start of heating.
Specimen No: LTS-2

Note: Specimen Code on Page 156 Table 5.1

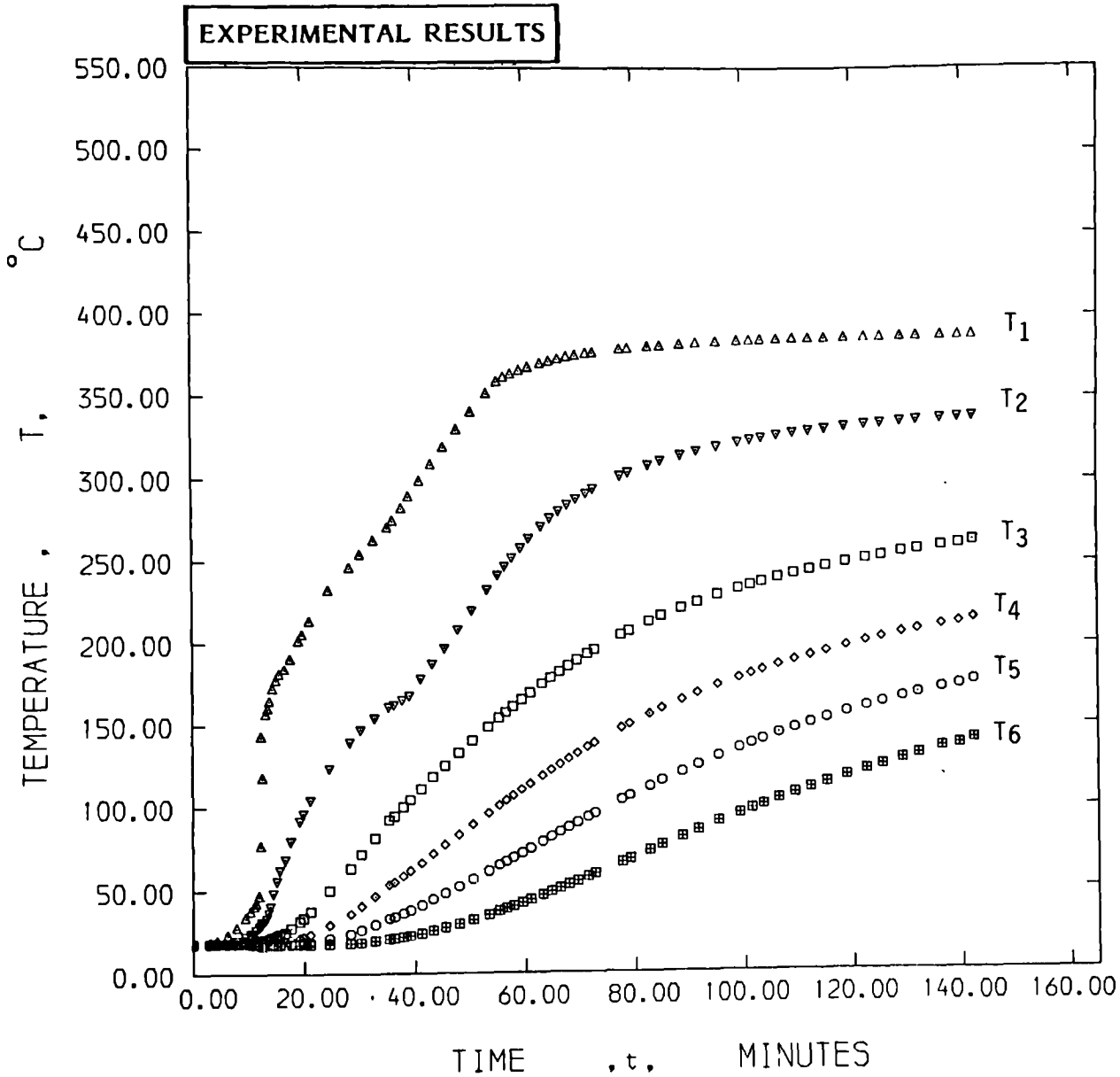

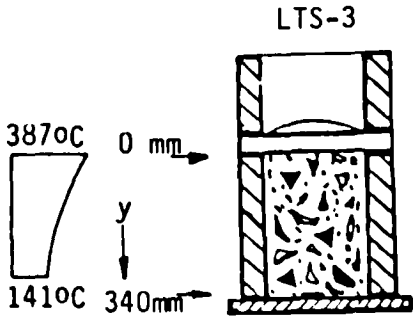

Figure 5.27:

Variation of Temperatures at seven positions from the Concrete-Diaphragm Interface with Time from start of heating.
Specimen No: LTS-3

Note: Specimen Code on Page 156 Table 5.1

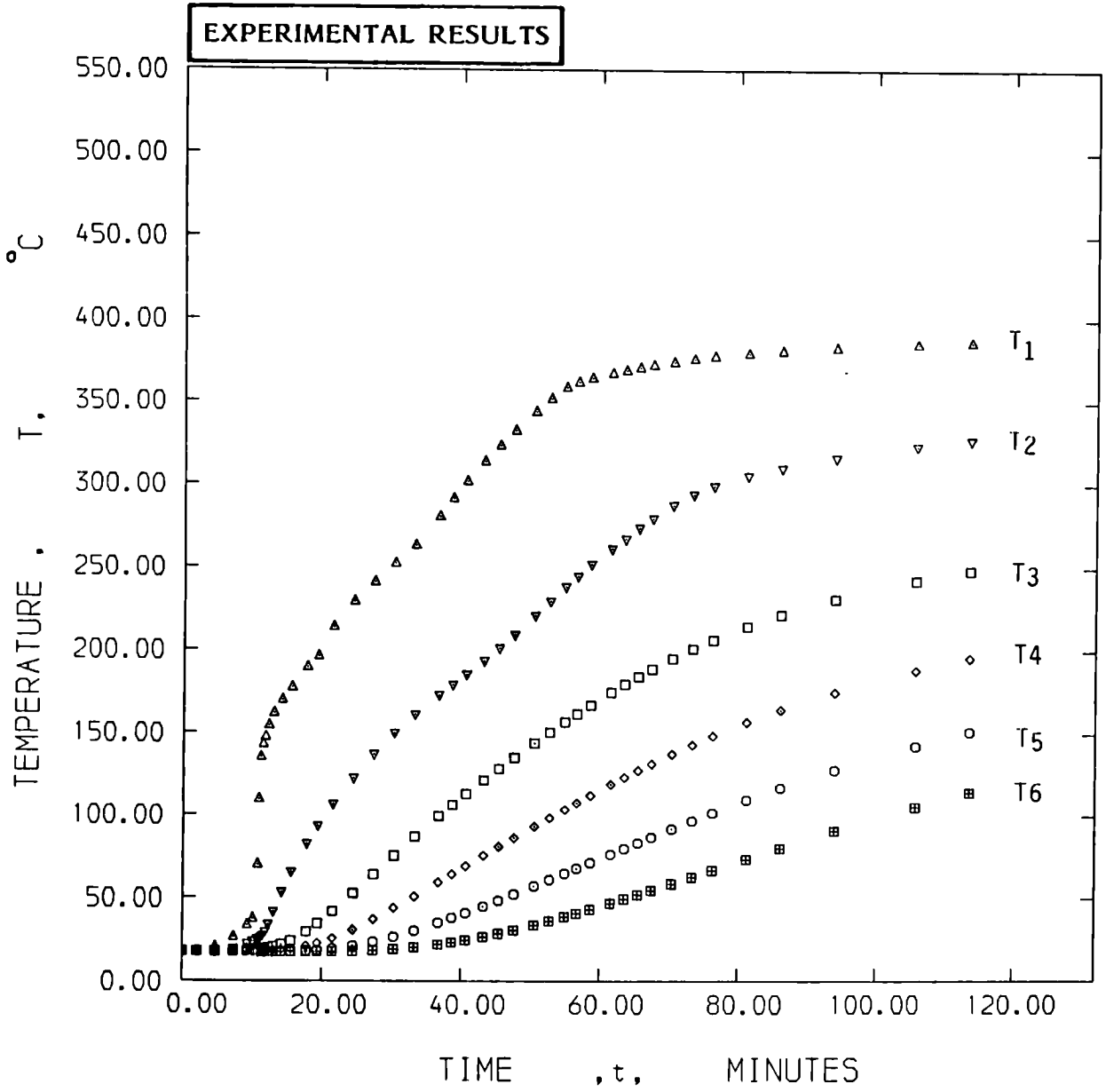

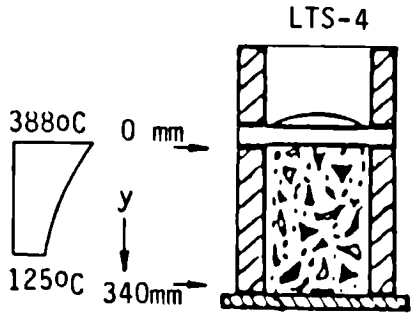

Figure 5.28:

Variation of Temperatures at seven positions from the Concrete-Diaphragm Interface with time from start of heating.
Specimen No: LTS-4

Note: Specimen Code on Page 156 Table 5.1

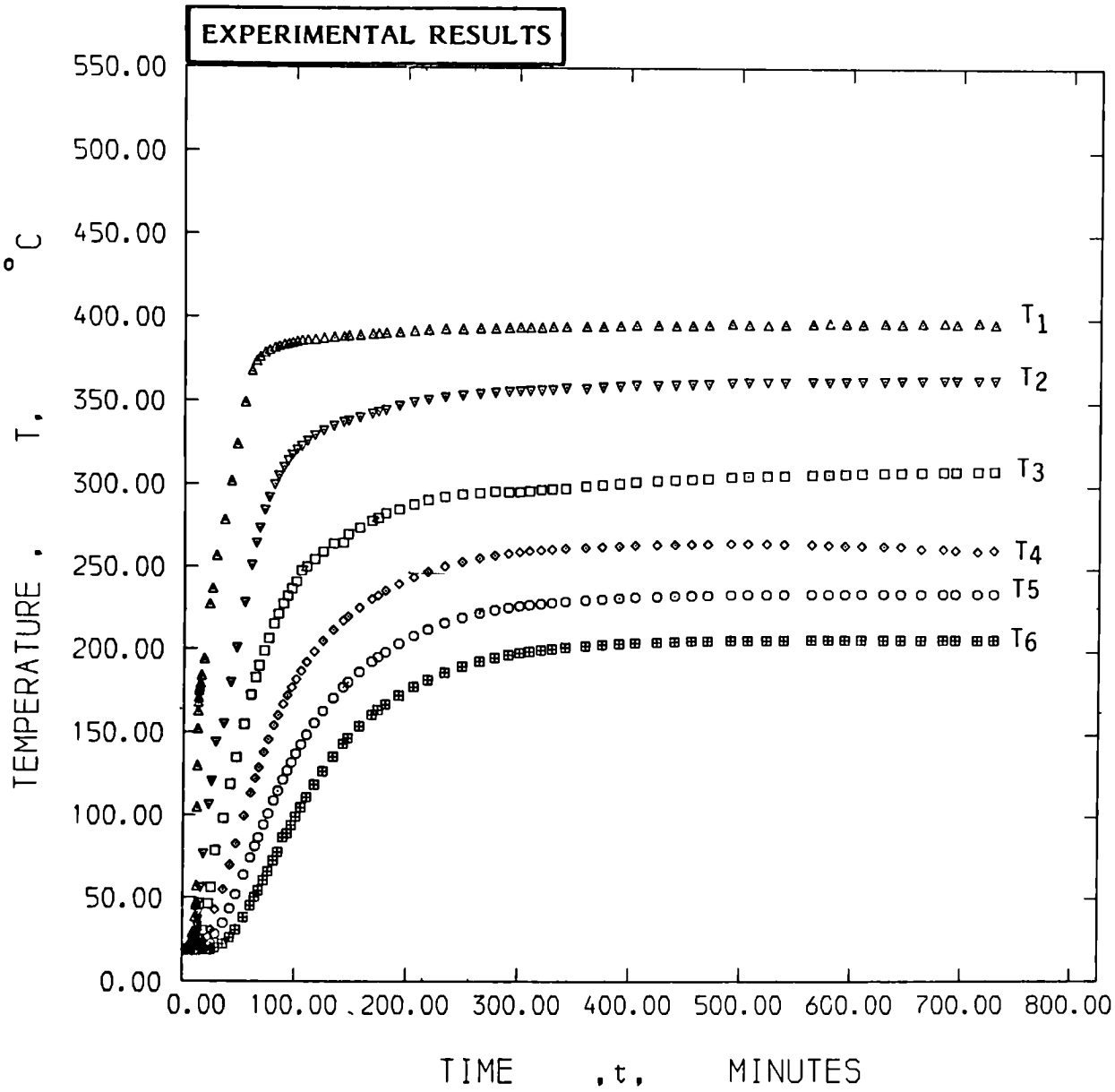

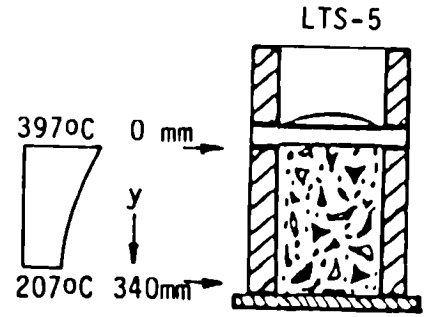

Figure 5.29:

Variation of Temperatures at seven positions from the Concrete-Diaphragm Interface with Time from start of heating.
Specimen No: LTS-5

Note: Specimen Code on Page 156 Table 5.1

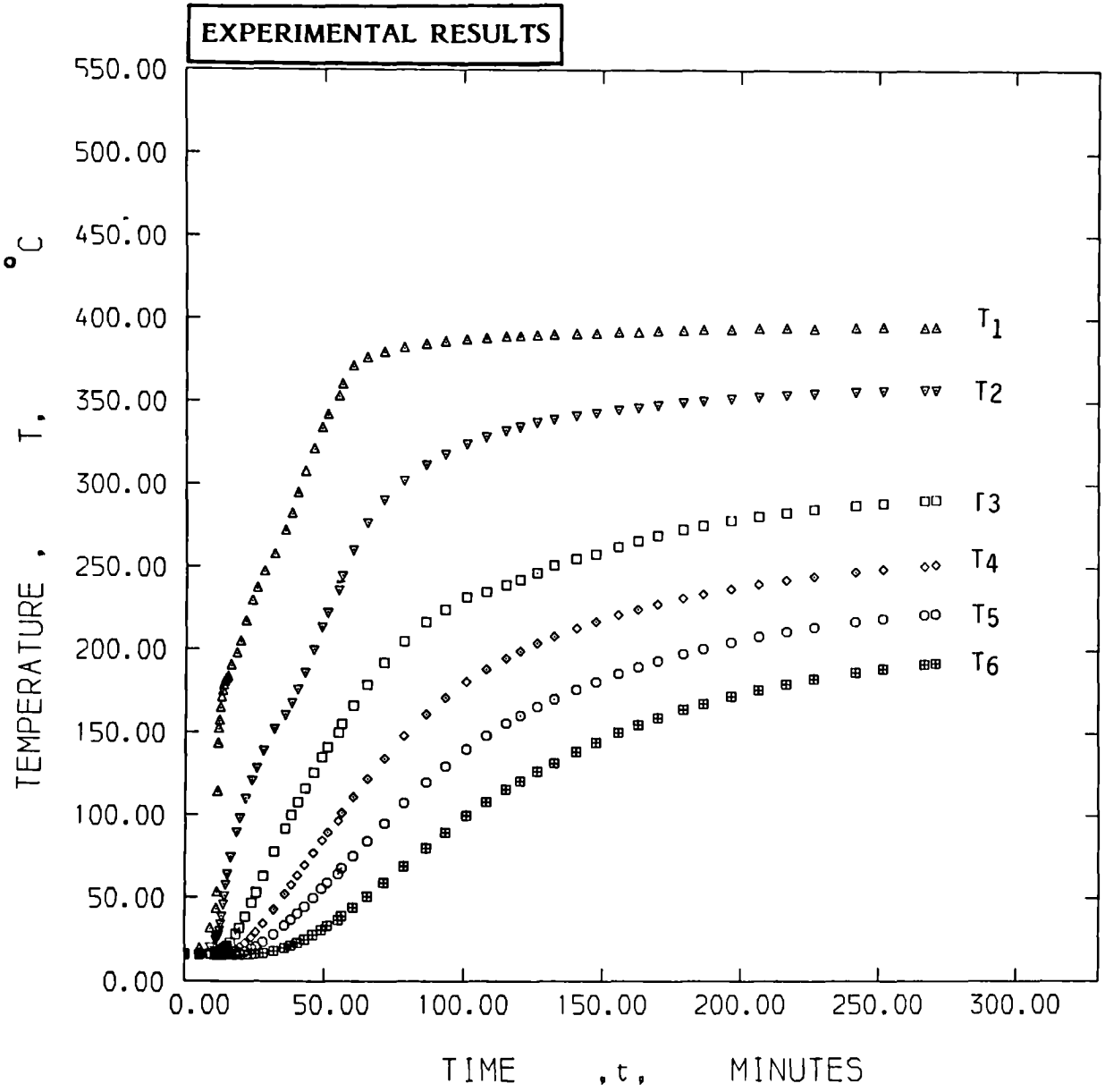

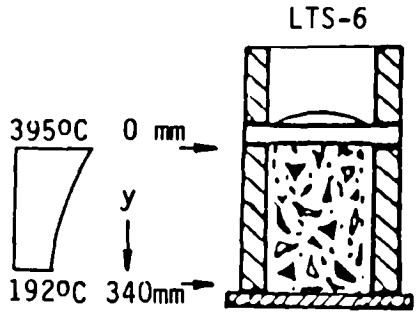

Figure 5.30:

Variation of Temperatures at seven positions from the Concrete-Diaphragm Interface with Time from start of heating.
Specimen No: LTS-6

Note: Specimen Code on Page 156 Table 5.1

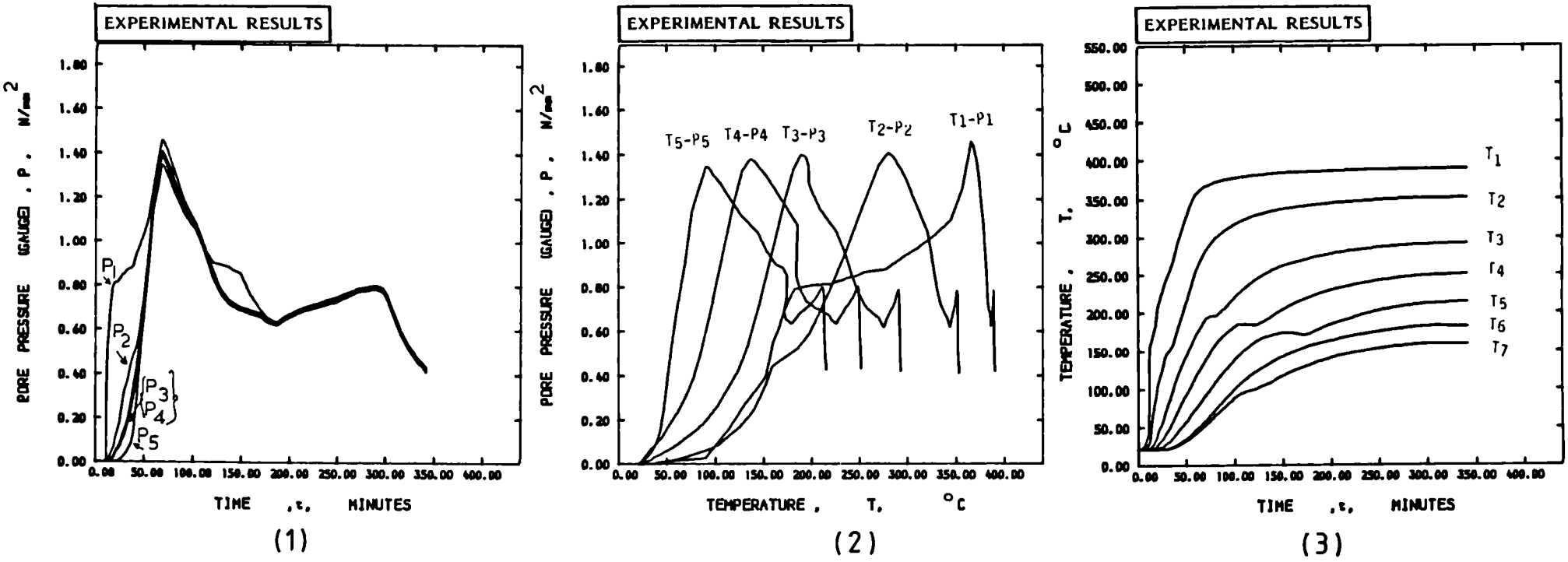

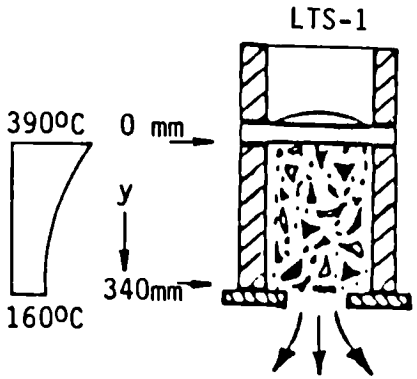

Figure 5.31: (1) Variation of Pore Pressures with Time from Start of Heating

(2) Variation of Pore pressures with Temperatures

(3) Variation of Temperatures with Time from Start of Heating

Note : (1), (2), (3) Plotted for Comparison from Fig. 5.13 , Fig. 5.19 Fig. 5.25 Specimen No: LTS-1

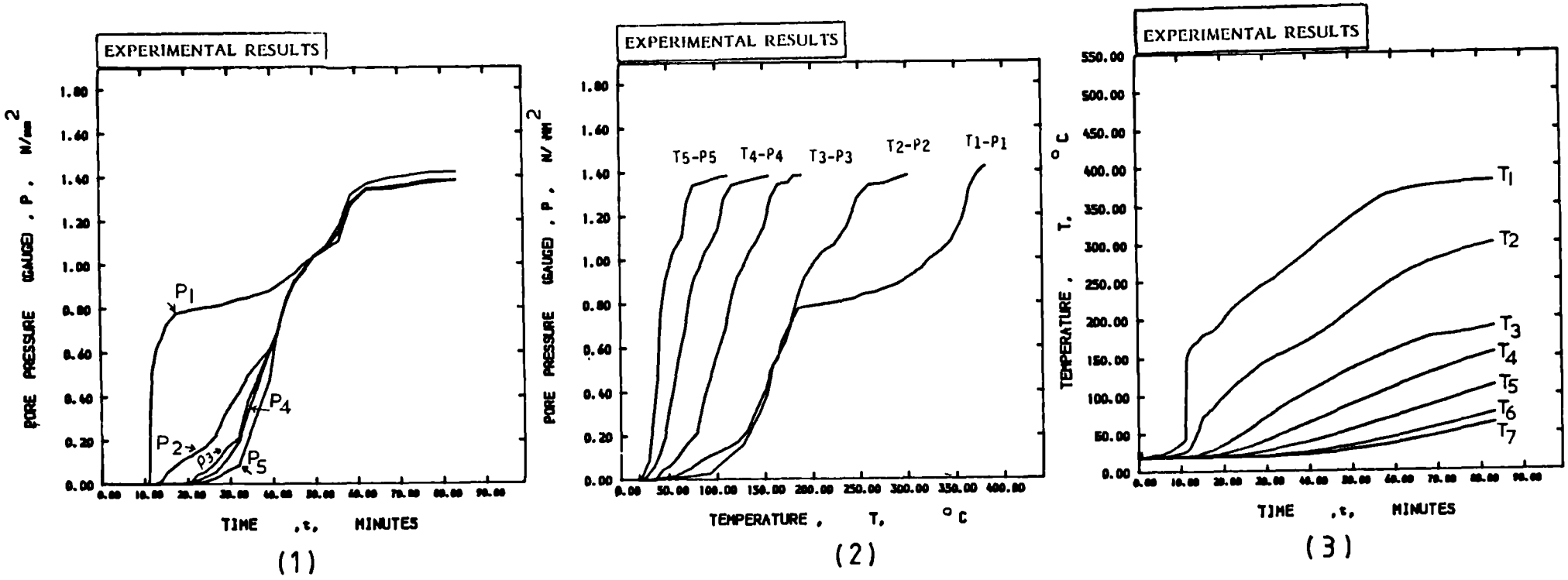

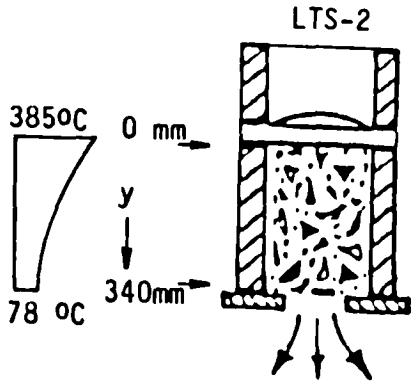

Figure 5.32: (1) Variation of Pore Pressures with Time from Start of Heating

(2) Variation of Pore pressures with Temperatures

(3) Variation of Temperatures with Time from Start of Heating

Note : (1), (2), (3) Plotted for Comparison from Fig. 5.14 , Fig.5.20
Fig. 5.26 Specimen No: LTS-2

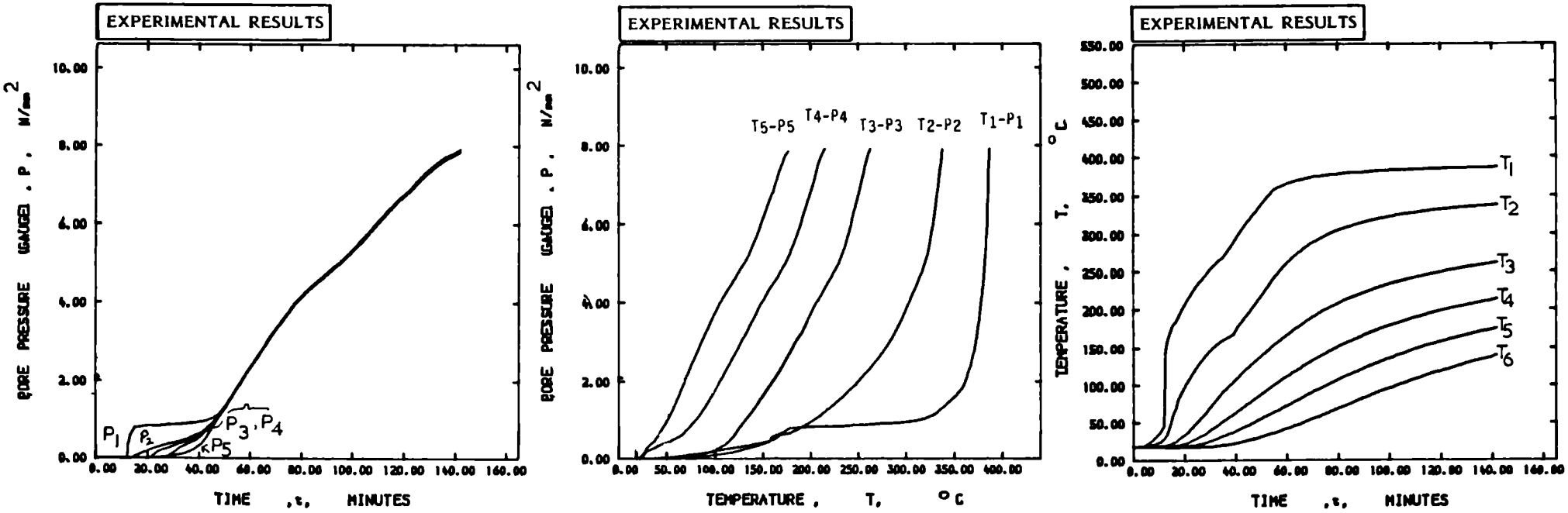

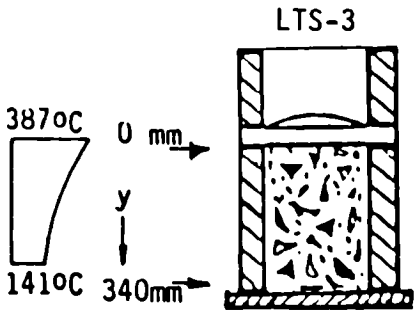

Figure 5.33: (1) Variation of Pore Pressures with Time from Start of Heating

(2) Variation of Pore pressures with Temperatures

(3) Variation of Temperatures with Time from Start of Heating

Note : (1), (2), (3) Plotted for Comparison from Fig. 5.15 , Fig. 5.21 Fig. 5.27 Specimen No: LTS-3

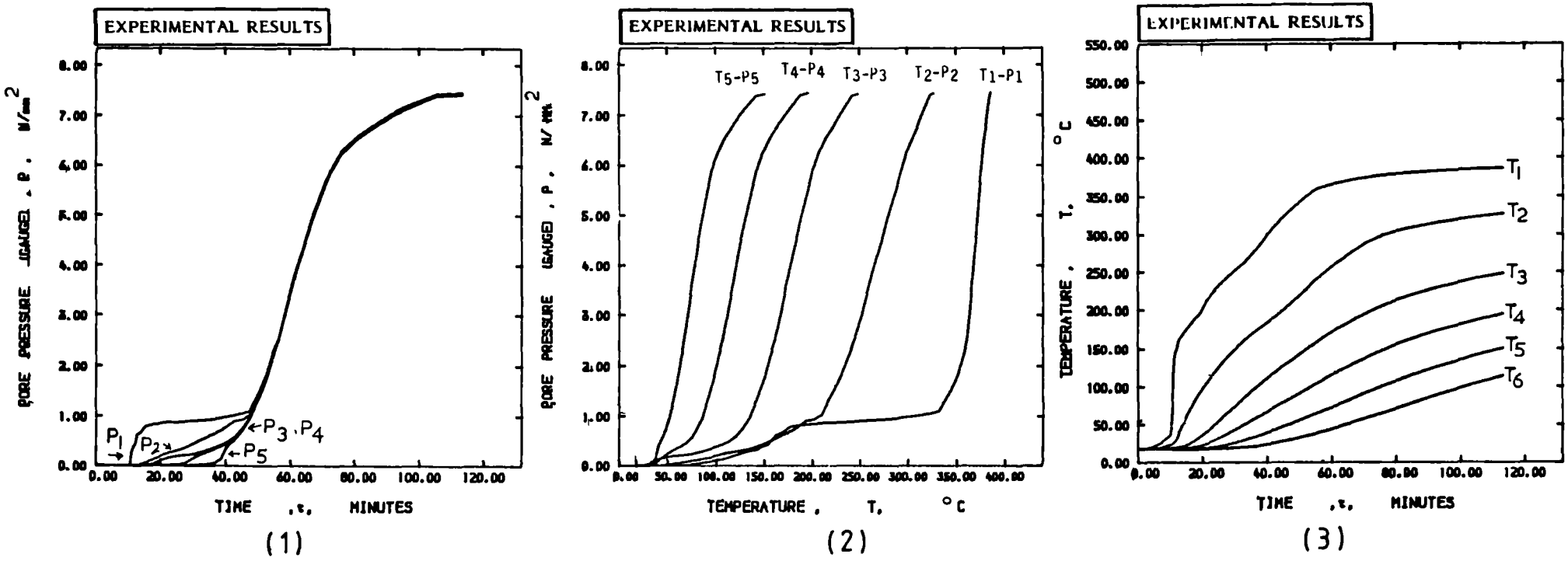

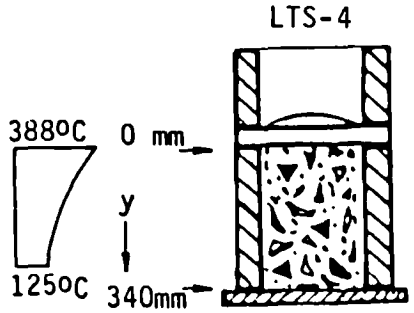

Figure 5.34: (1) Variation of Pore Pressures with Time from Start of Heating

(2) Variation of Pore pressures with Temperatures

(3) Variation of Temperatures with Time from Start of Heating

Note : (1), (2), (3) Plotted for Comparison from Fig. 5.16 , Fig. 5.22 Fig. 5.28 Specimen No: LTS-4

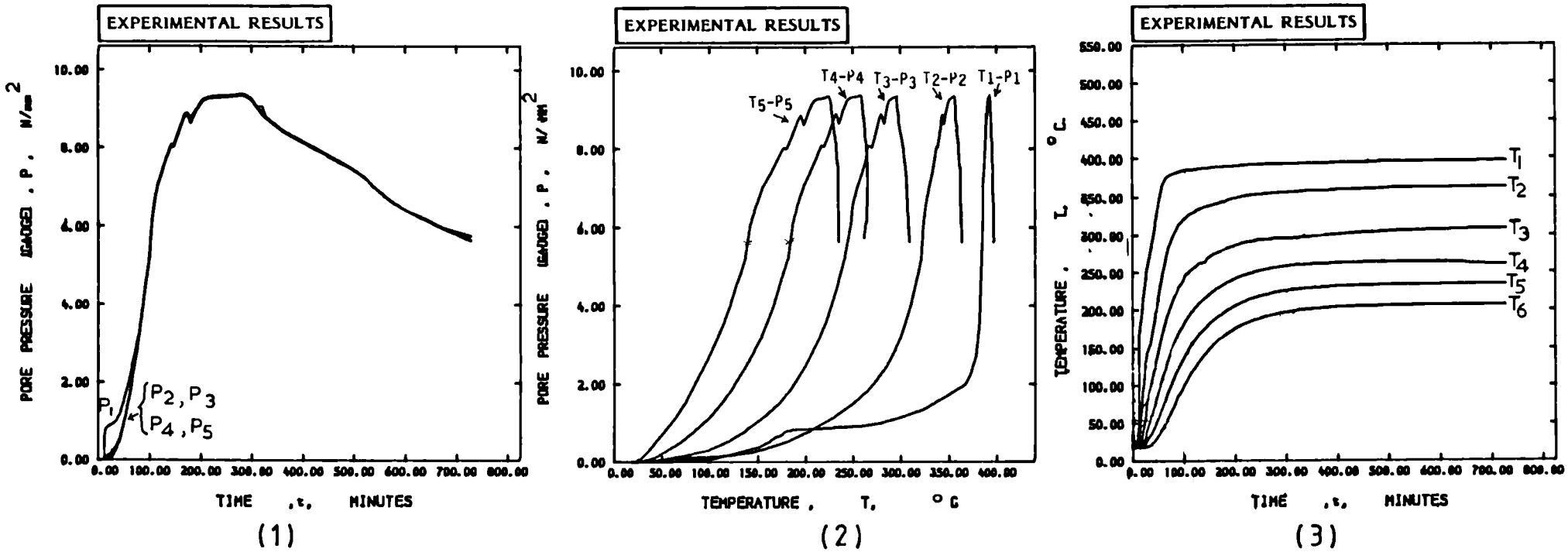

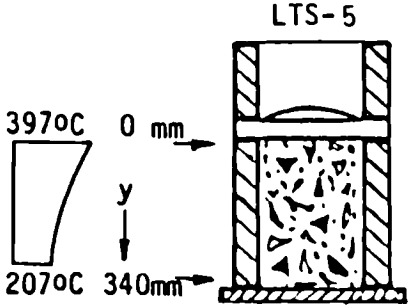

Figure 5.35: (1) Variation of Pore Pressures with Time from Start of Heating

(2) Variation of Pore pressures with Temperatures

(3)Variation of Temperatures with Time from Start of Heating

Note : (1), (2), (3) Plotted for Comparison from Fig.5.17 , Fig.5.23 Fig. 5.29 Specimen No: LTS- 5

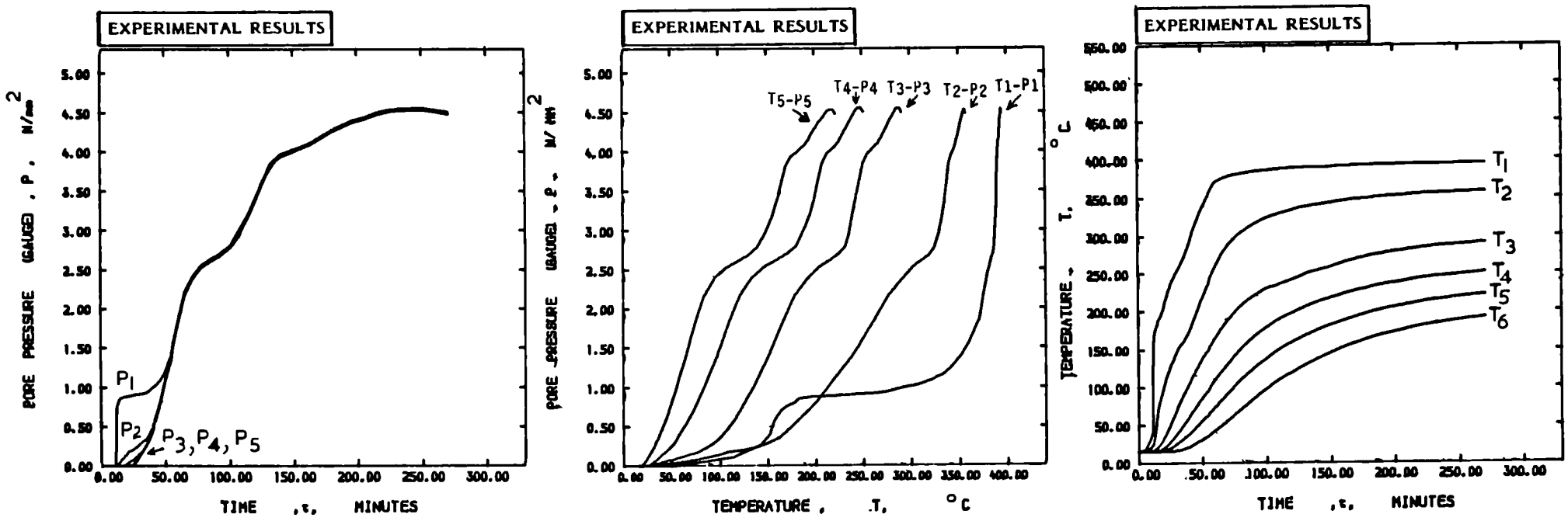

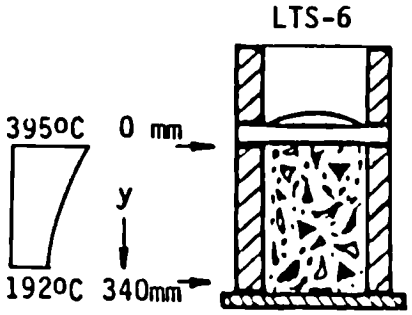

Figure 5.36: (1) Variation of Pore Pressures with Time from Start of Heating

(2) Variation of Pore pressures with Temperatures

(3)Variation of Temperatures with Time from Start of Heating

Note : (1), (2), (3) Plotted for Comparison from Fig. 5.18 , Fig. 5.24 Fig. 5.30 Specimen No: LTS-6

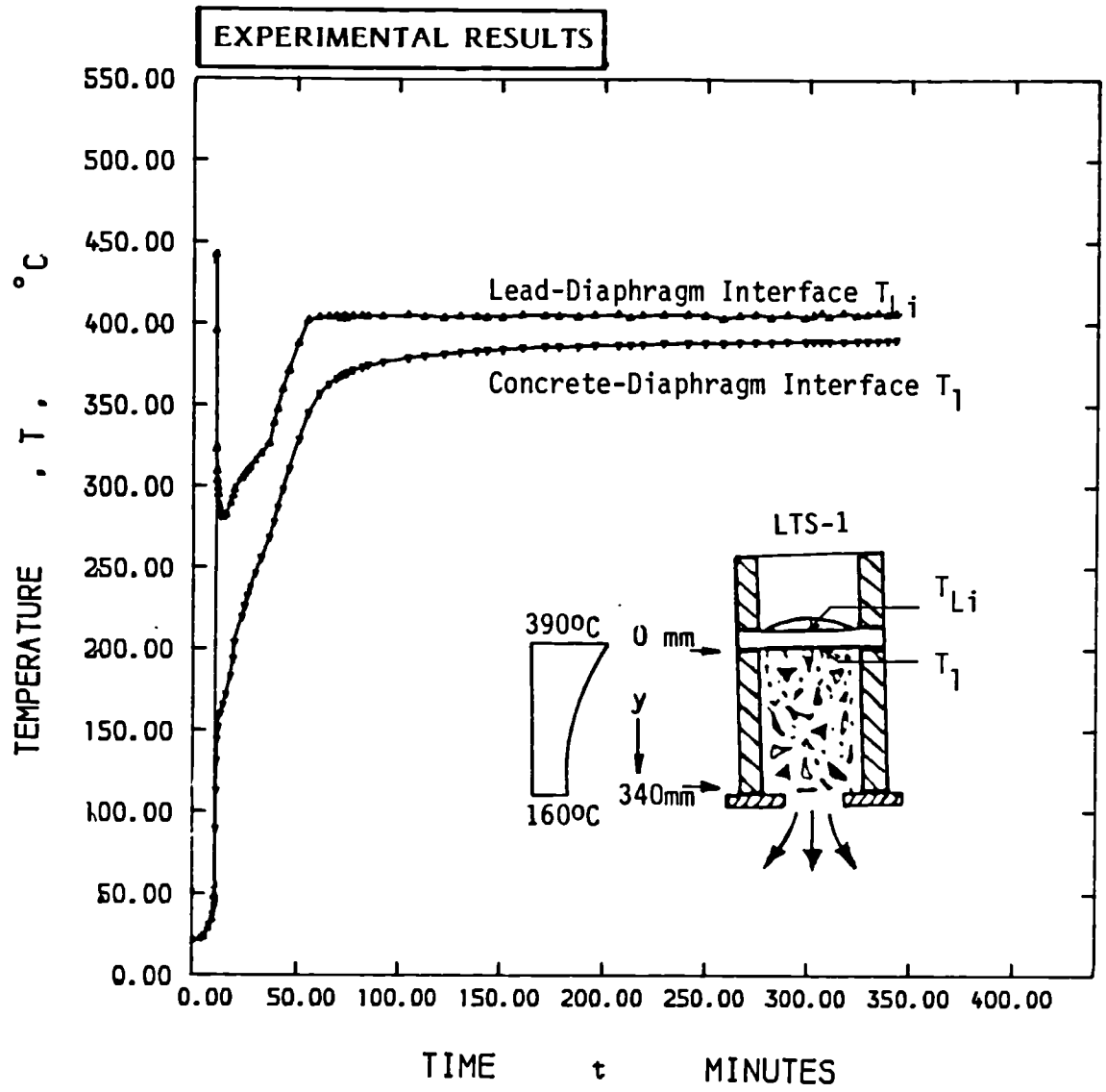

Figure 5.37: Variation of Diaphragm Temperatures, with Time from Start of Heating Specimen No: LTS-1

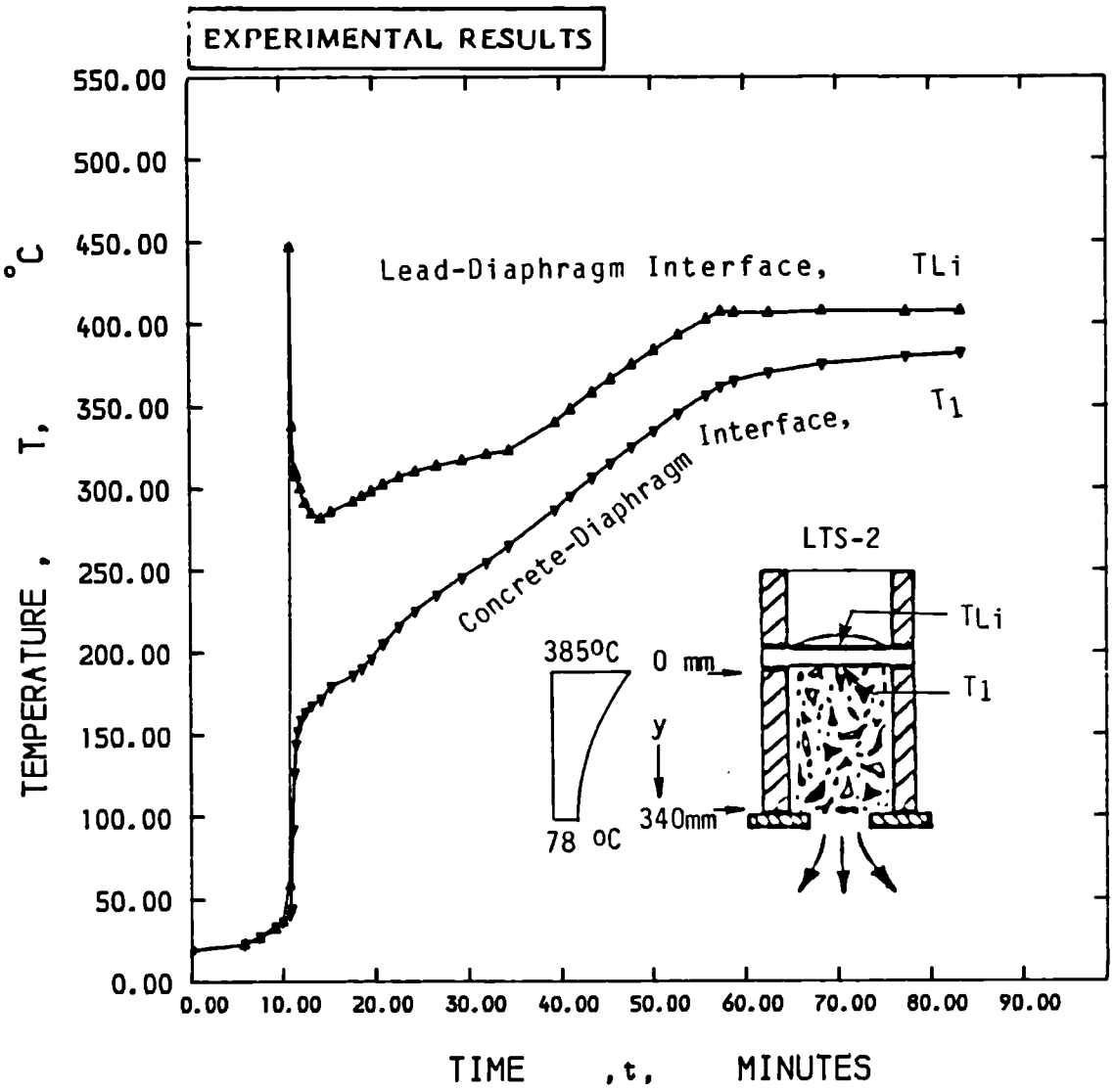

Figure 5.38: Variation of Diaphragm Temperatures, with Time from Start of Heating Specimen No: LTS-2

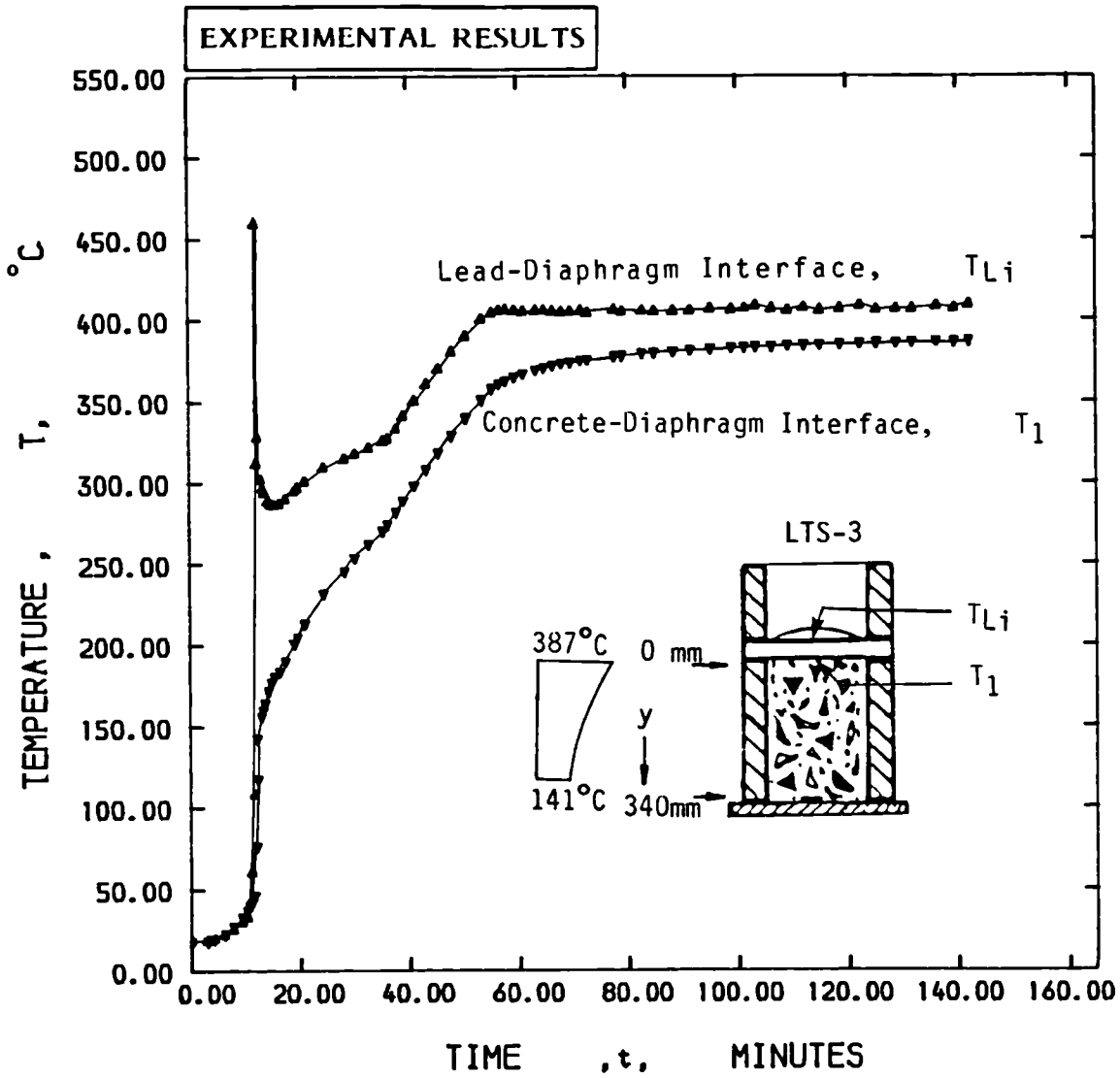

Figure 5.39: Variation of Diaphragm Temperatures, with Time from Start of Heating Specimen No: LTS-3

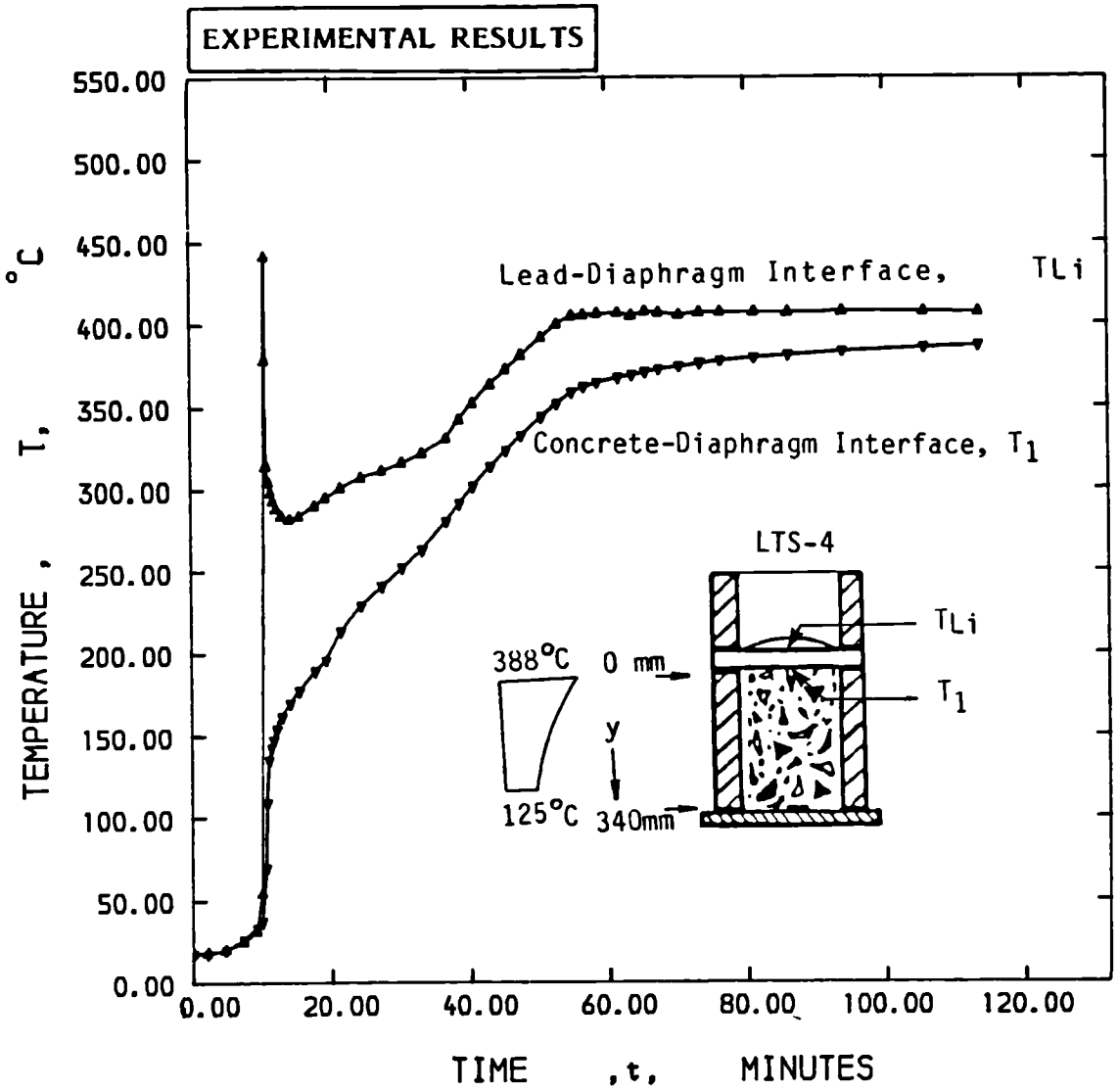

Figure 5.40: Variation of Diaphragm Temperatures, with Time from Start of Heating Specimen No: LTS-4

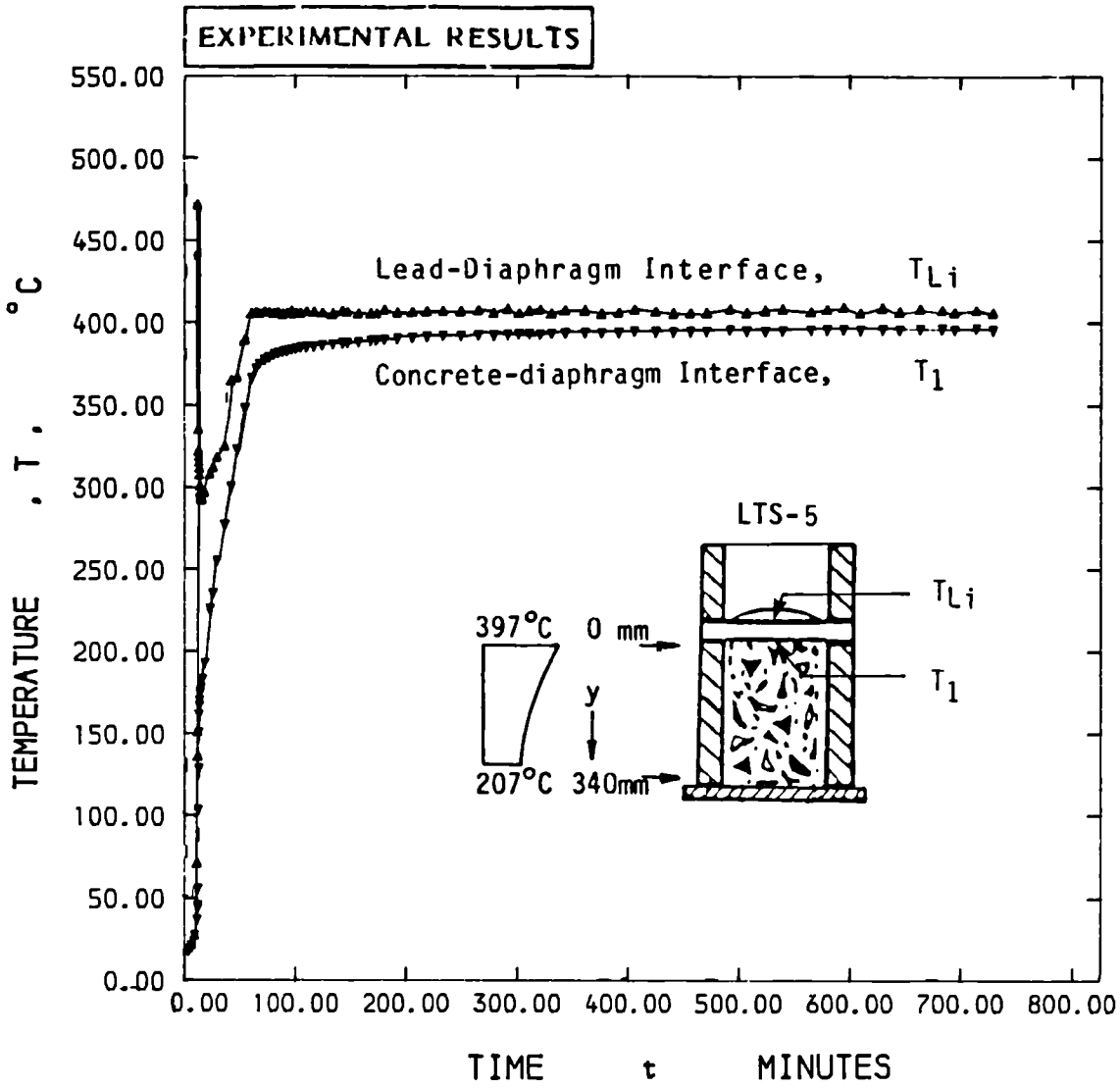

Figure 5.41: Variation of Diaphragm Temperatures, with Time from Start of Heating Specimen No: LTS-5

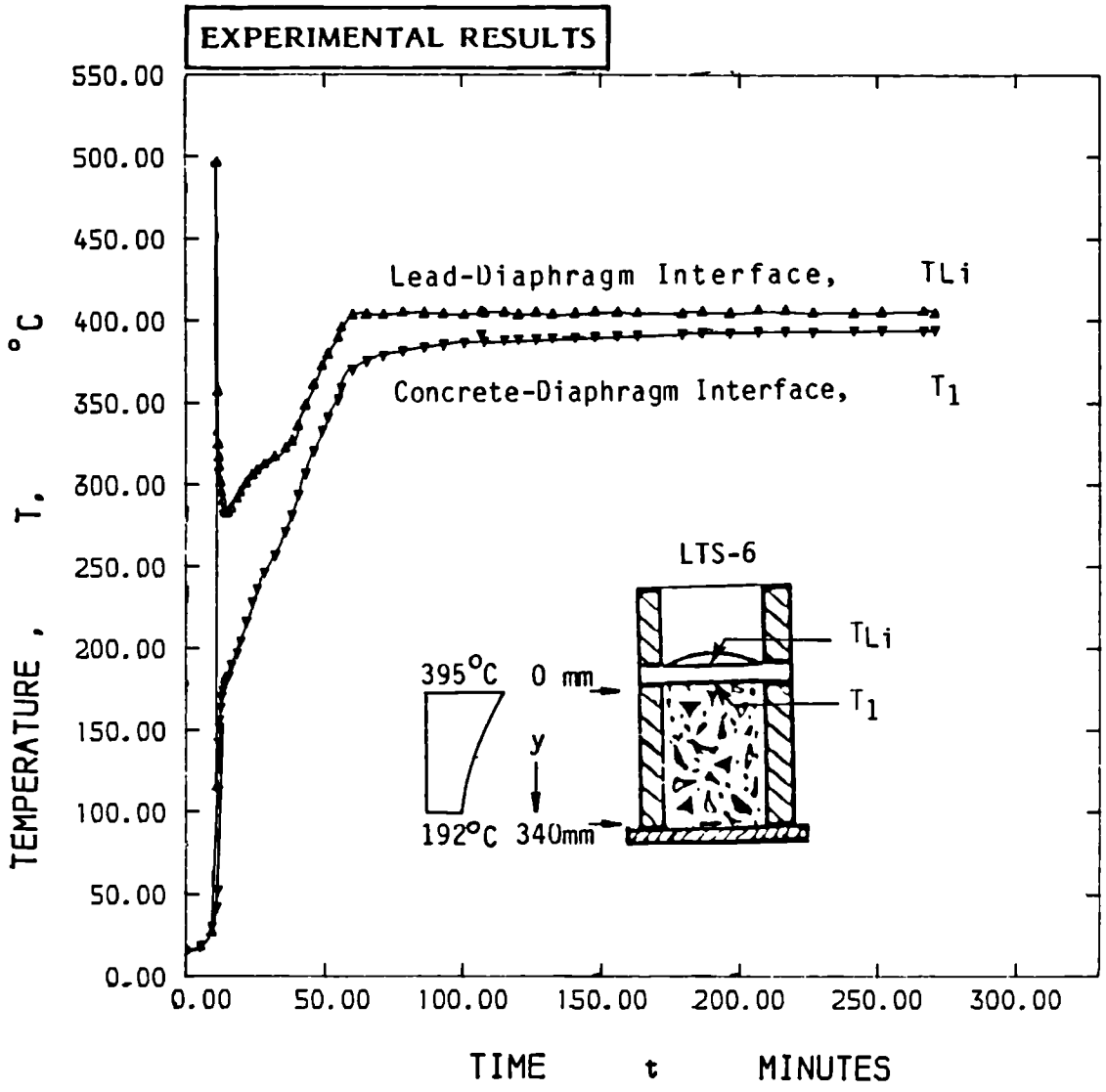

Figure 5.42: Variation of Diaphragm Temperatures, with Time from Start of Heating Specimen No: LTS-6

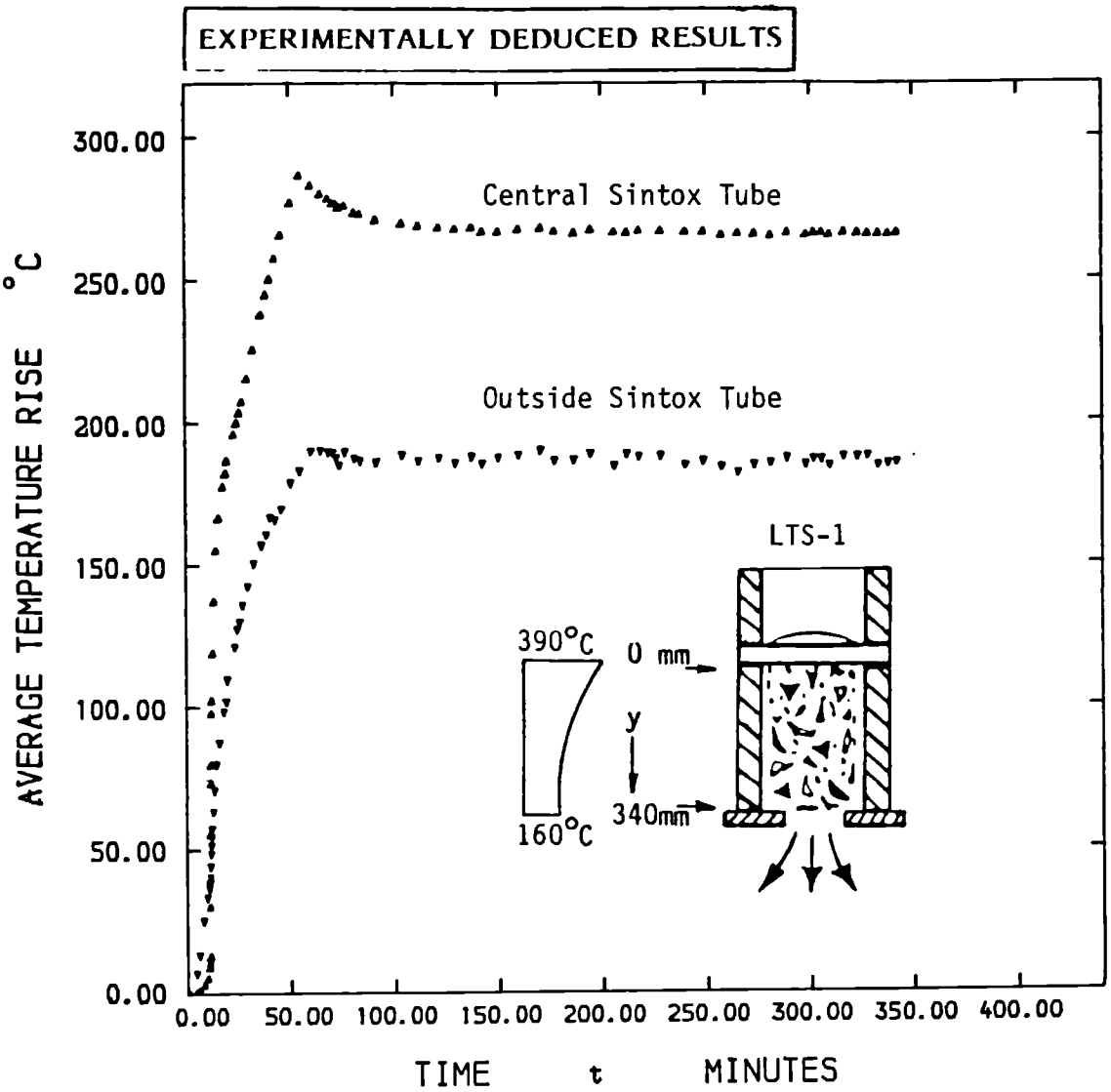

Figure 5.43: Variation of Average Temperature Rise, with Time from Start of Heating for 'central' & 'outside' Sintox Tubes Specimen No: LTS-1

Note: Average Temperature Defined in Appendix IV, See Fig. 3.2 & Plate 3.10 for location of Sintox Tubes.

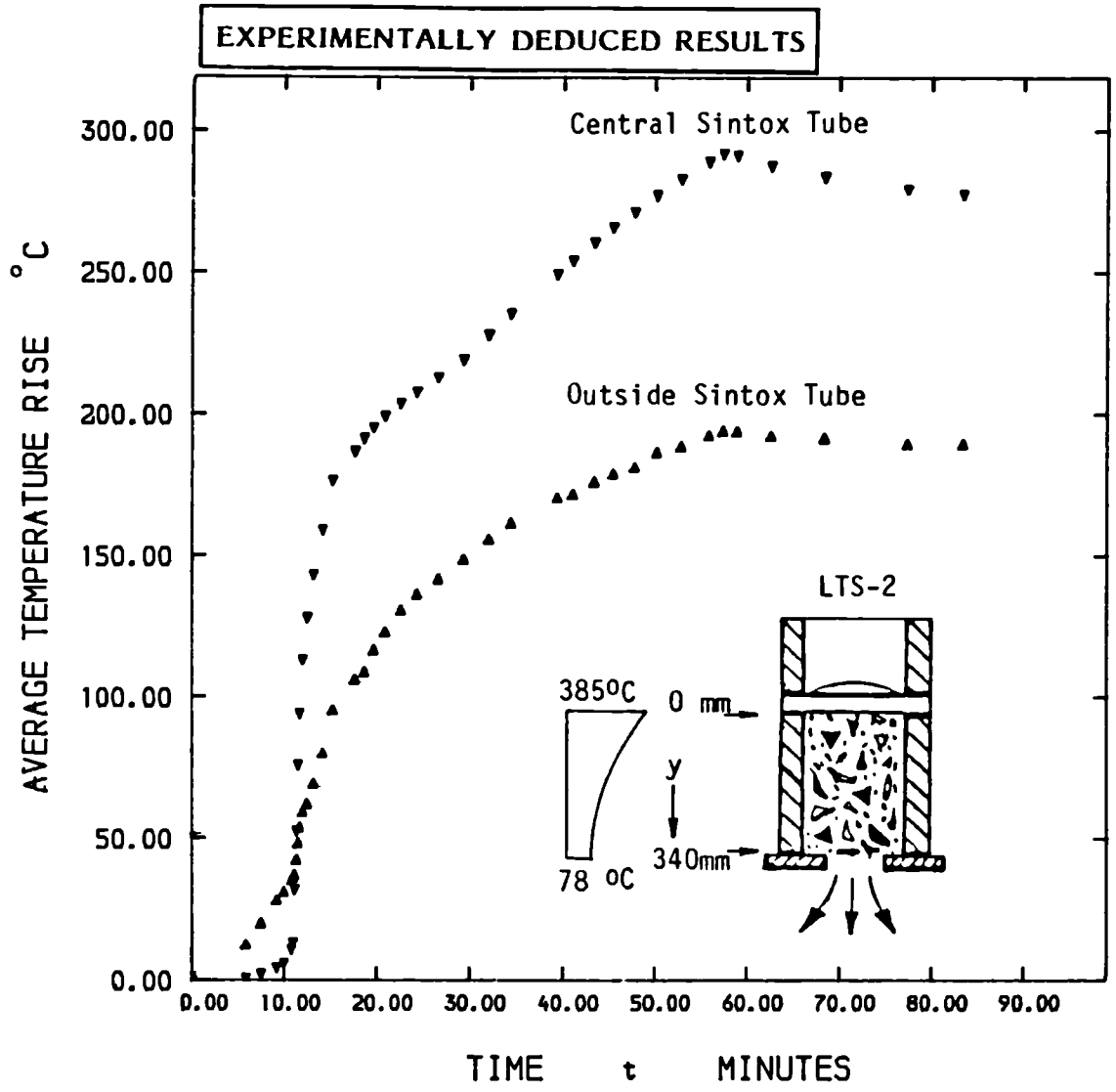

Figure 5.44: Variation of Average Temperature Rise, with Time from Start of Heating for 'central' & 'outside' Sintox Tubes Specimen No: LTS-2

Note: Average Temperature Defined in Appendix IV, See Fig. 3.2 & Plate 3.10 for location of Sintox Tubes.

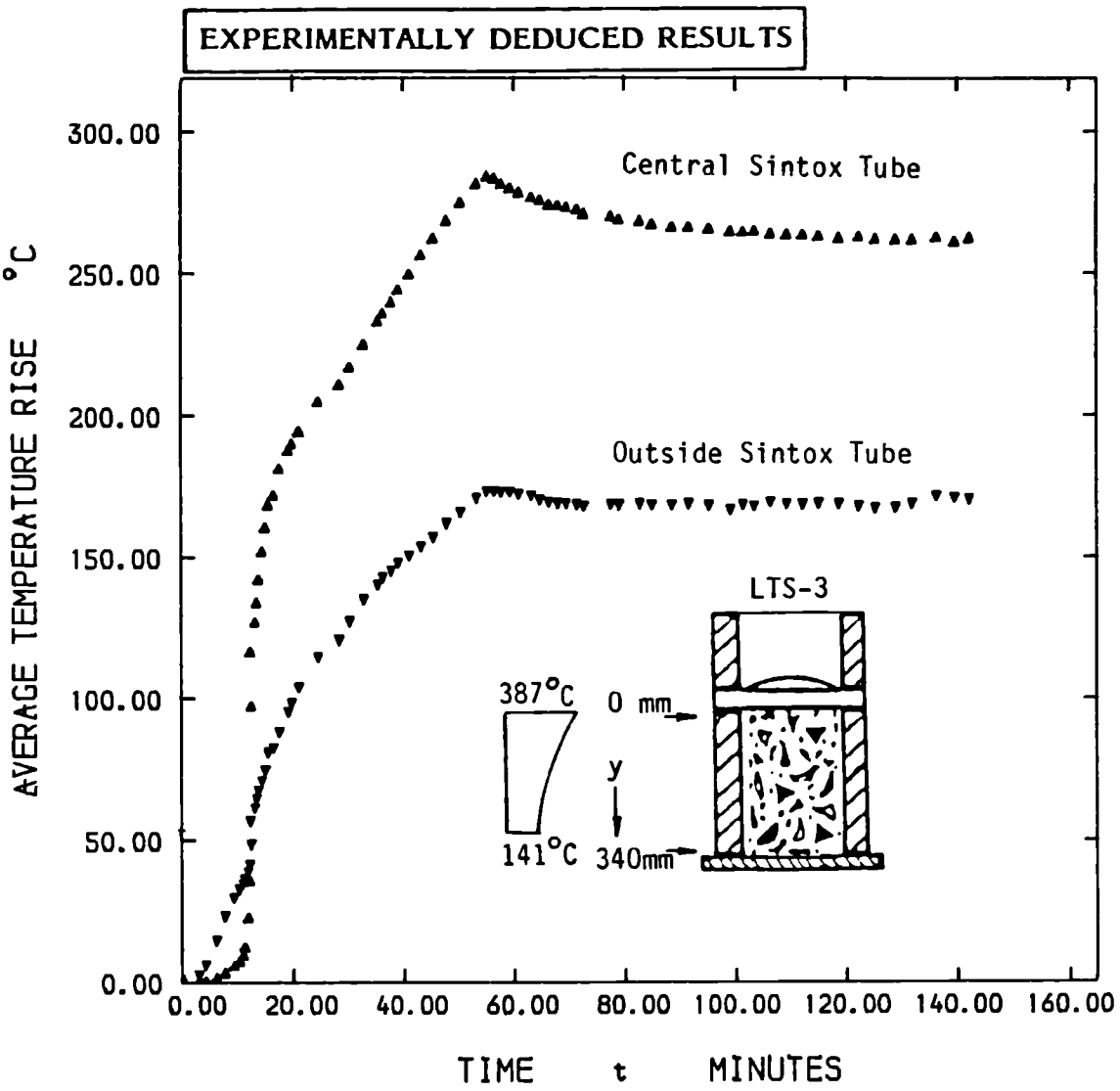

Figure 5.45: Variation of Average Temperature Rise, with Time from Start of Heating for 'central' & 'outside' Sintox Tubes Specimen No: LTS-3

Note: Average Temperature Defined in Appendix IV, See Fig. 3.2 & Plate 3.10 for location of Sintox Tubes.

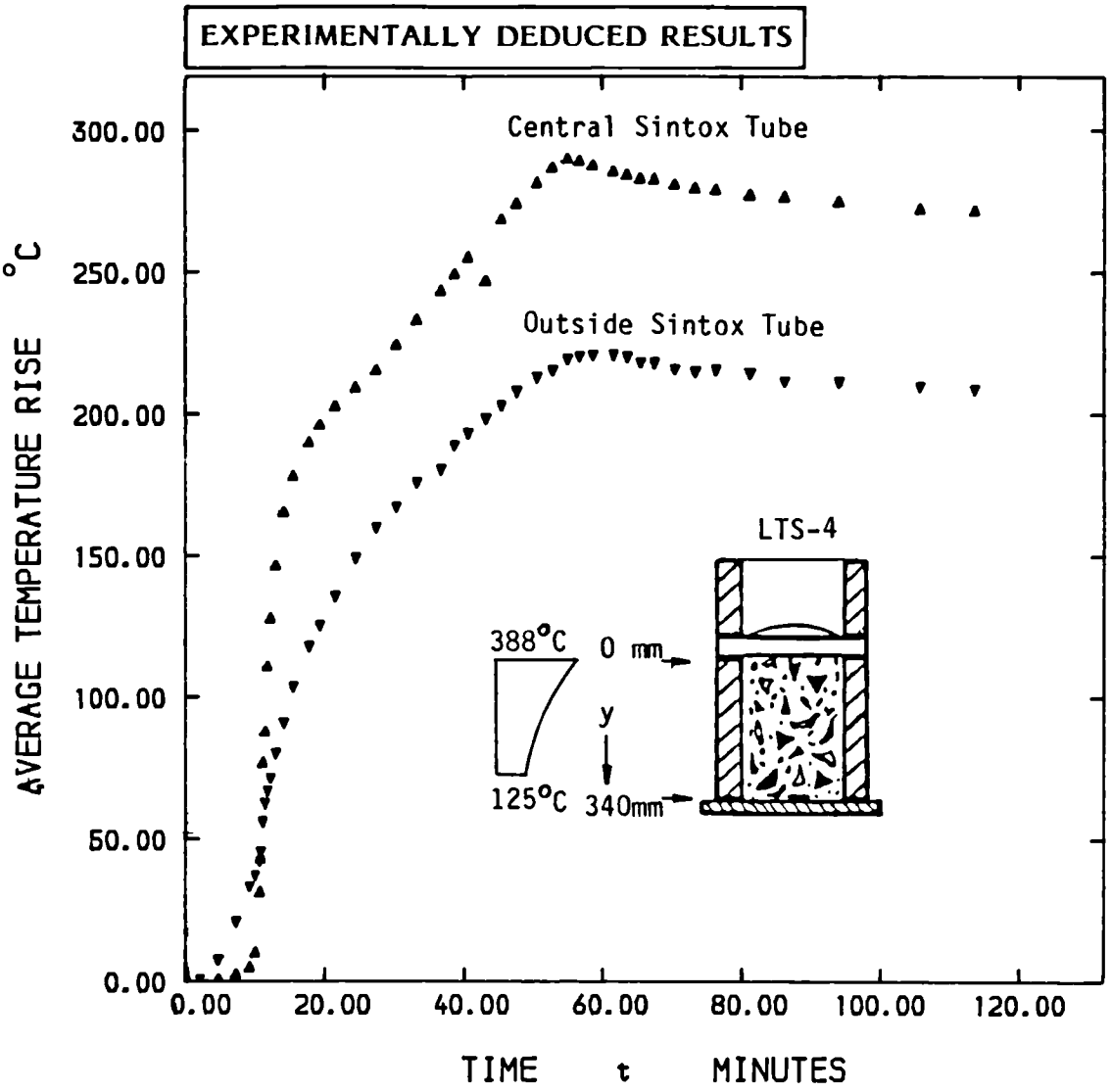

Figure 5.46: Variation of Average Temperature Rise, with Time from Start of Heating for 'central' & 'outside' Sintox Tubes Specimen No: LTS-4

Note: Average Temperature Defined in Appendix IV, See Fig. 3.2 & Plate 3.10 for location of Sintox Tubes.

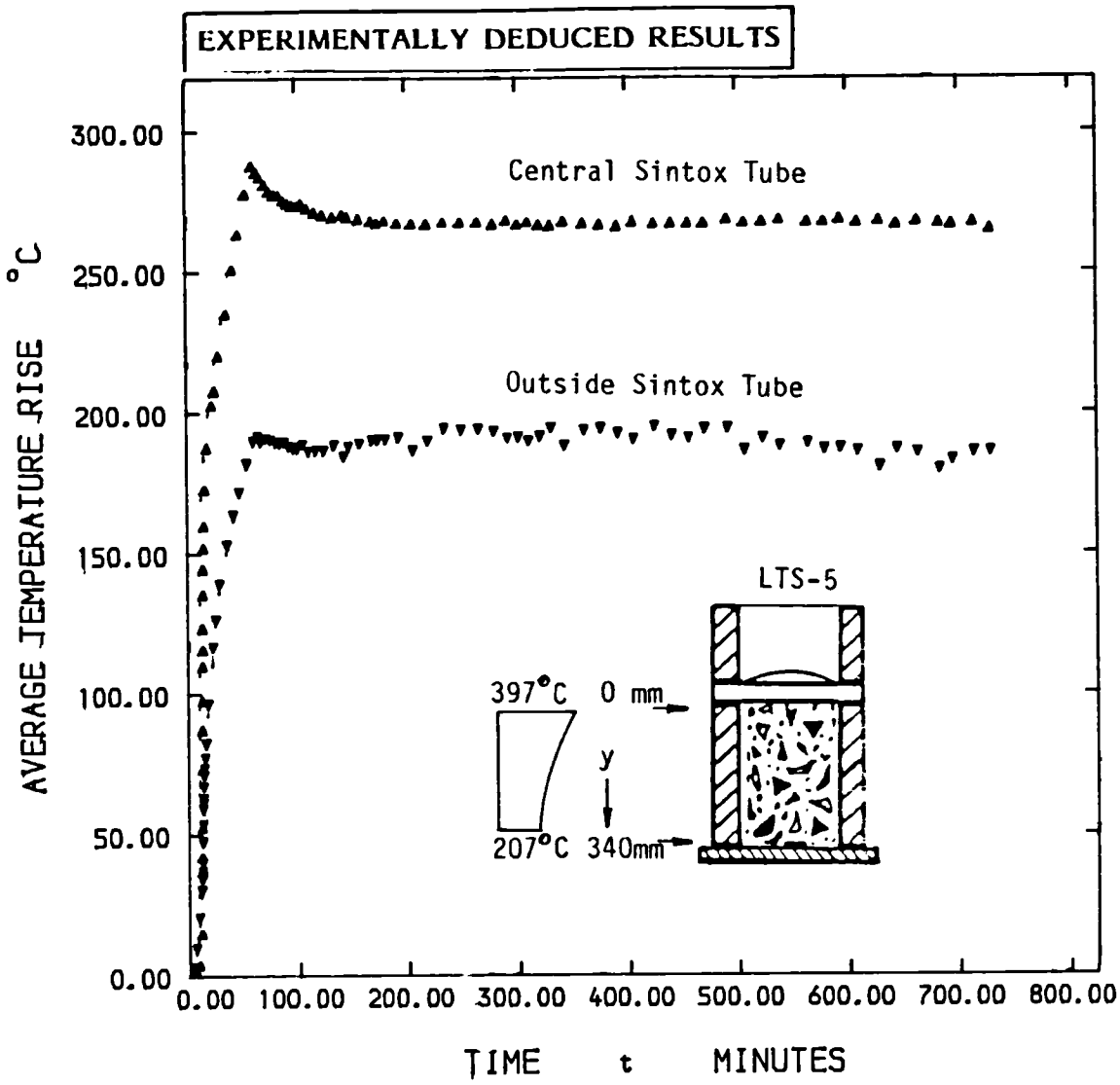

Figure 5.47 : Variation of Average Temperature Rise, with Time from Start of Heating for 'central' & 'outside' Sintox Tubes Specimen No: LTS-5

Note: Average Temperature Defined in Appendix IV, See Fig. 3.2 & Plate 3.10 for location of Sintox Tubes.

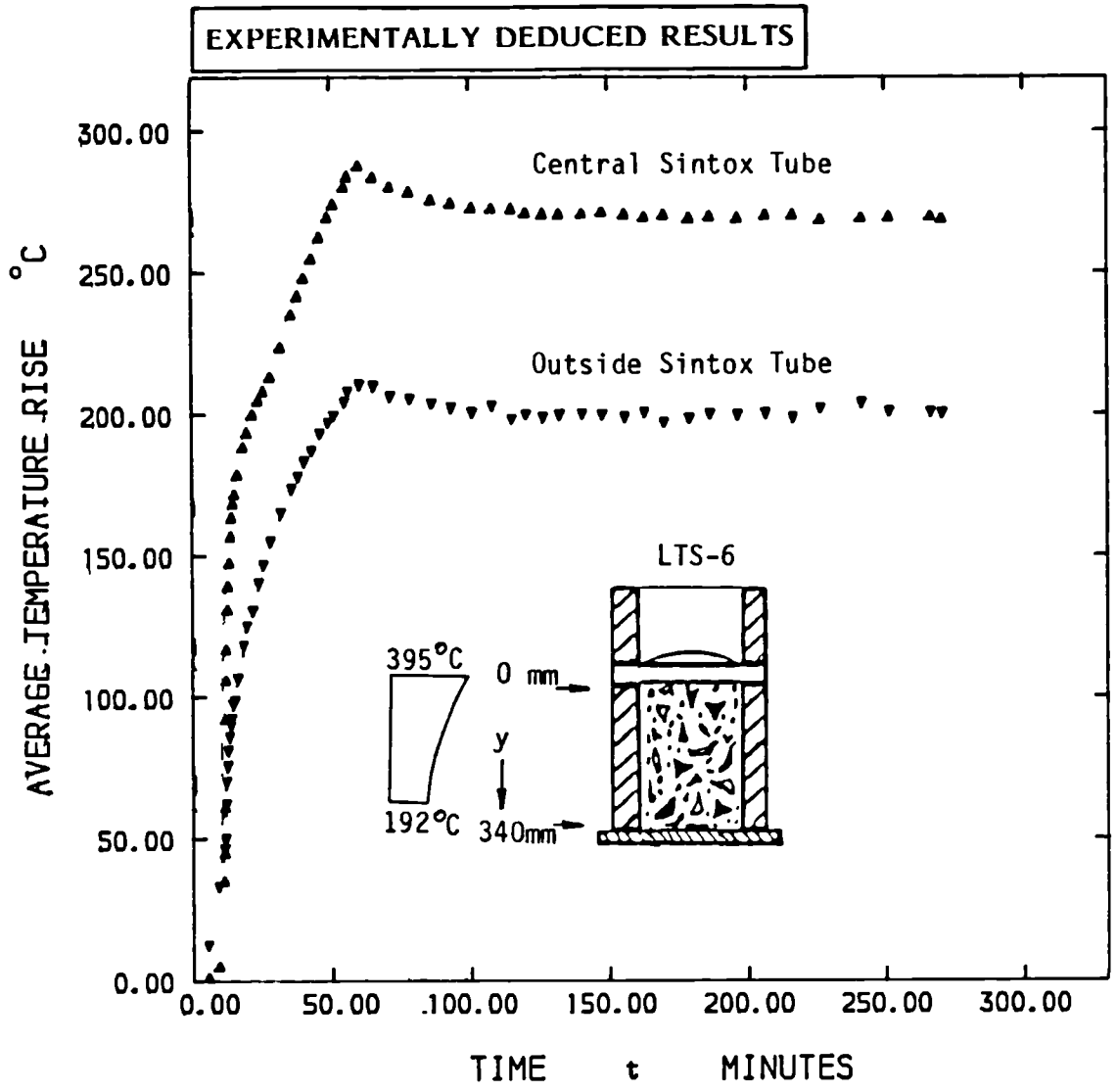

Figure 5.48 : Variation of Average Temperature Rise, with Time from Start of Heating for 'central' & 'outside' Sintox Tubes Specimen No: LTS-6

Note: Average Temperature Defined in Appendix IV, See Fig. 3.2 & Plate 3.10 for location of Sintox Tubes.

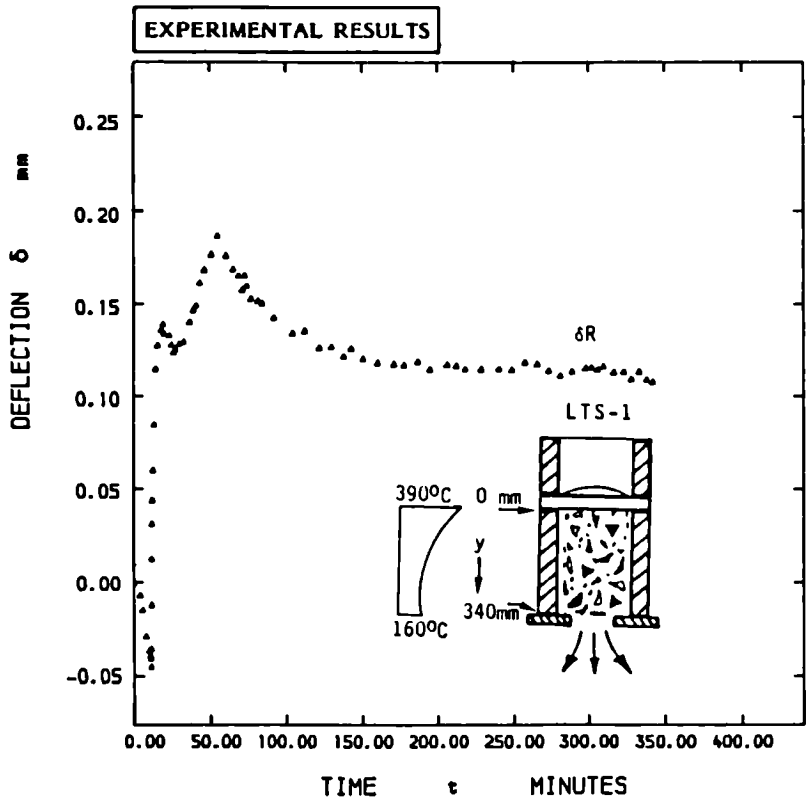

Figure 5.49:

Variation of Diaphragm Deflection with Time from Start of Heating Specimen No: LTS-1

Note : Values are Recorded and Uncorrected for Expansion of Sintox Tubes

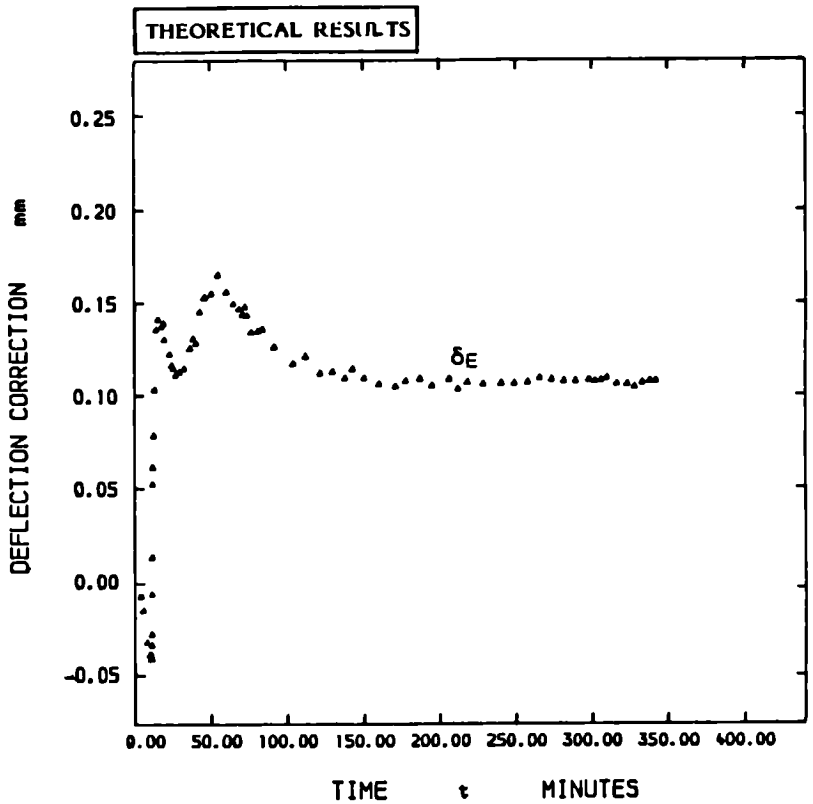

Figure 5.50:

Temperature Correction to Recorded Deflections of Diaphragm, due to Thermal Expansion of Sintox Tubes Specimen No: LTS-1

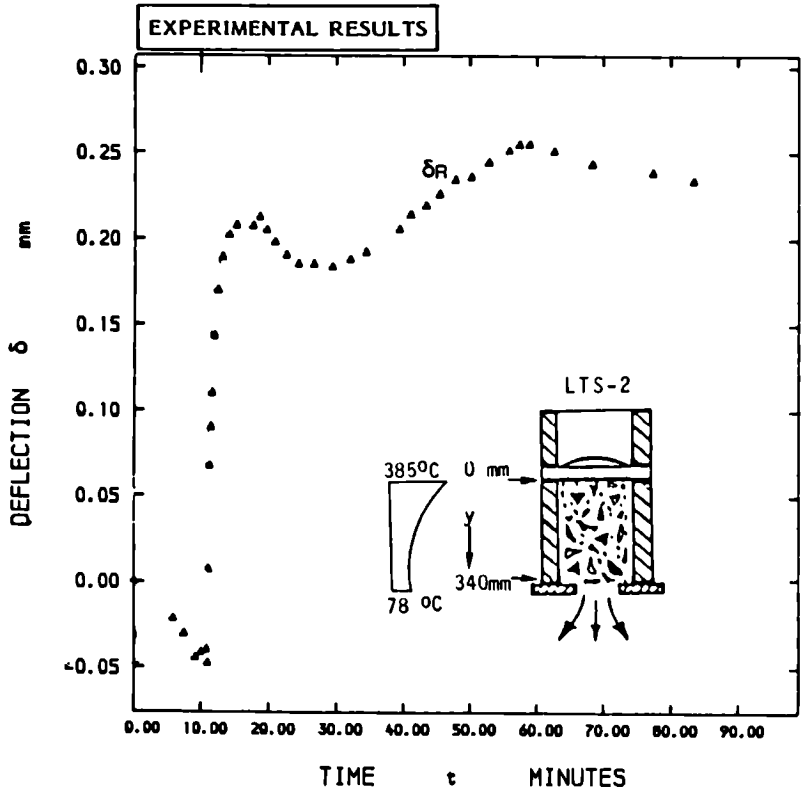

Figure 5.51

Variation of Diaphragm Deflection with Time from Start of Heating Specimen No: LTS-2

Note : Values are Recorded and Uncorrected for Expansion of Sintox Tubes

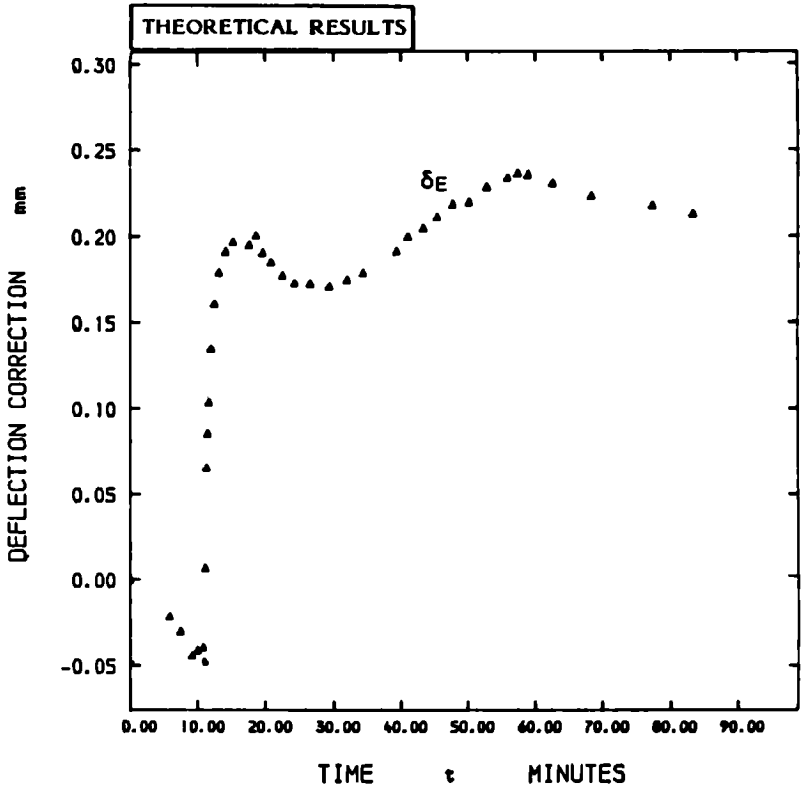

Figure 5.52

Temperature Correction to Recorded Deflections of Diaphragm, due to Thermal Expansion of Sintox Tubes Specimen No: LTS-2

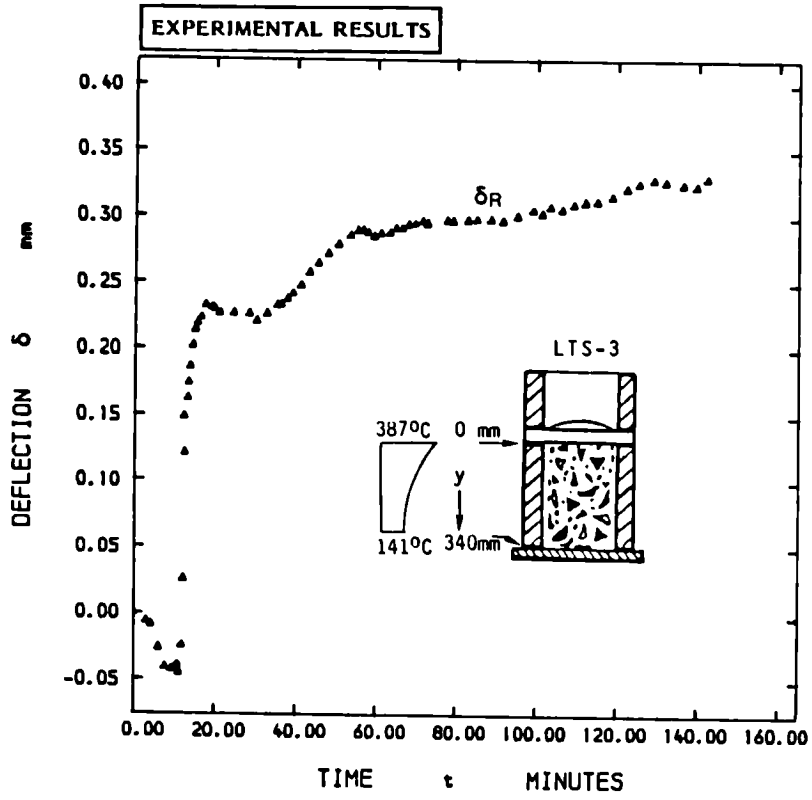

Figure 5.53:

Variation of Diaphragm Deflection with Time from Start of Heating Specimen No: LTS-3

Note : Values are Recorded and Uncorrected for Expansion of Sintox Tubes

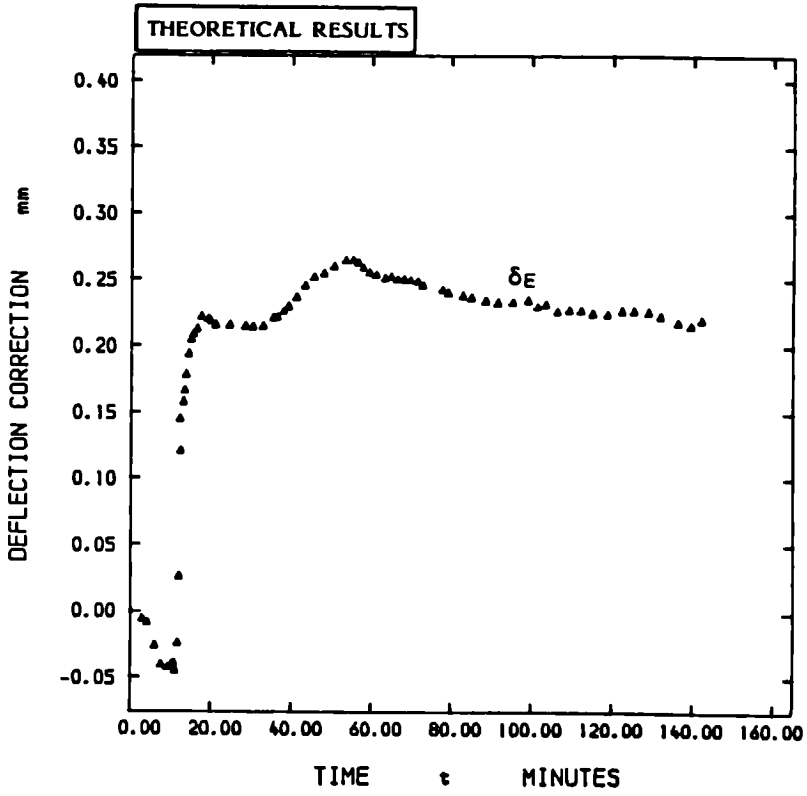

Figure 5.54:

Temperature Correction to Recorded Deflections of Diaphragm, due to Thermal Expansion of Sintox Tubes Specimen No: LTS-3

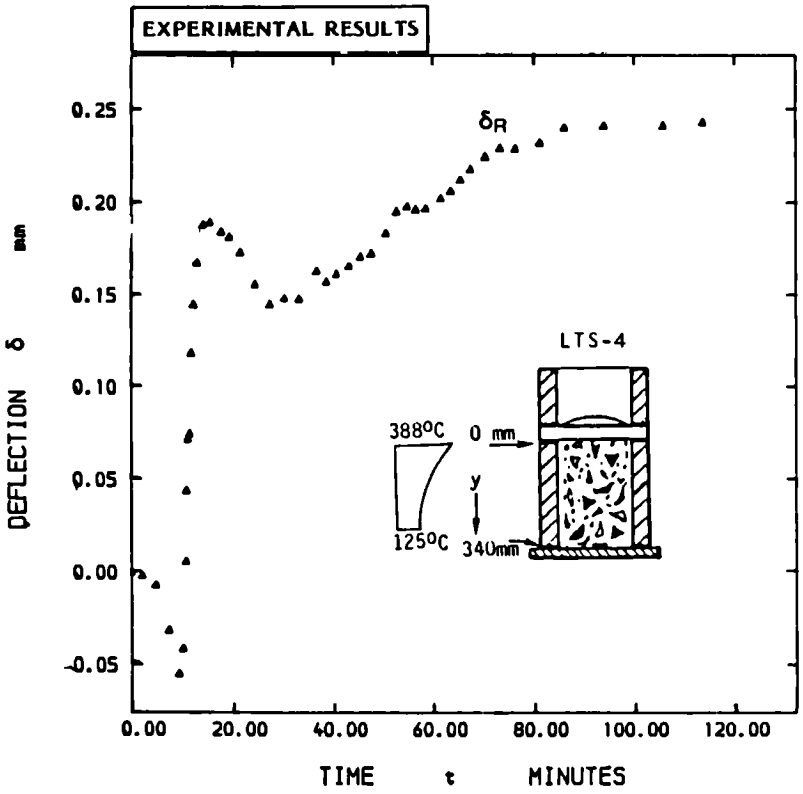

Figure 5.55:

Variation of Diaphragm Deflection with Time from Start of Heating Specimen No: LTS-4

Note : Values are Recorded and Uncorrected for Expansion of Sintox Tubes

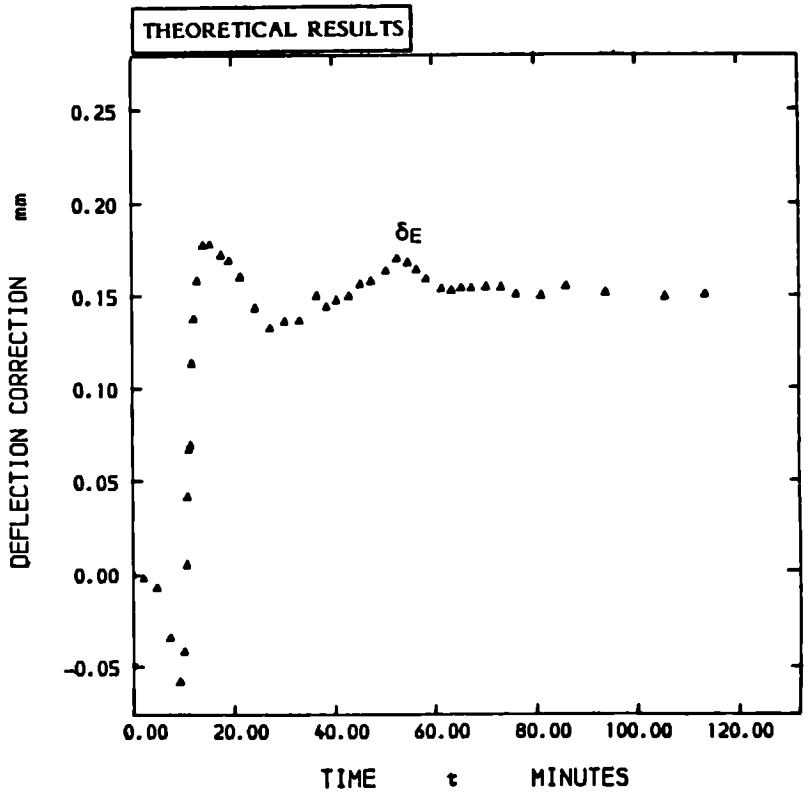

Figure 5.56:

Temperature Correction to Recorded Deflections of Diaphragm, due to Thermal Expansion of Sintox Tubes Specimen No: LTS-4

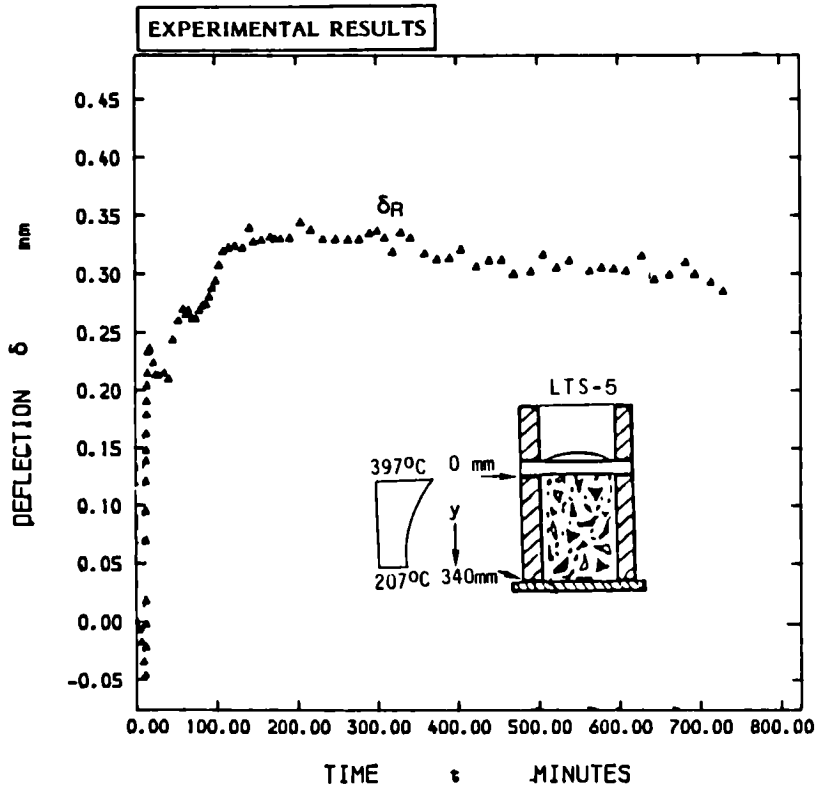

Figure 5.57:

Variation of Diaphragm Deflection with Time from Start of Heating Specimen No: LTS-5

Note : Values are Recorded and Uncorrected for Expansion of Sintox Tubes

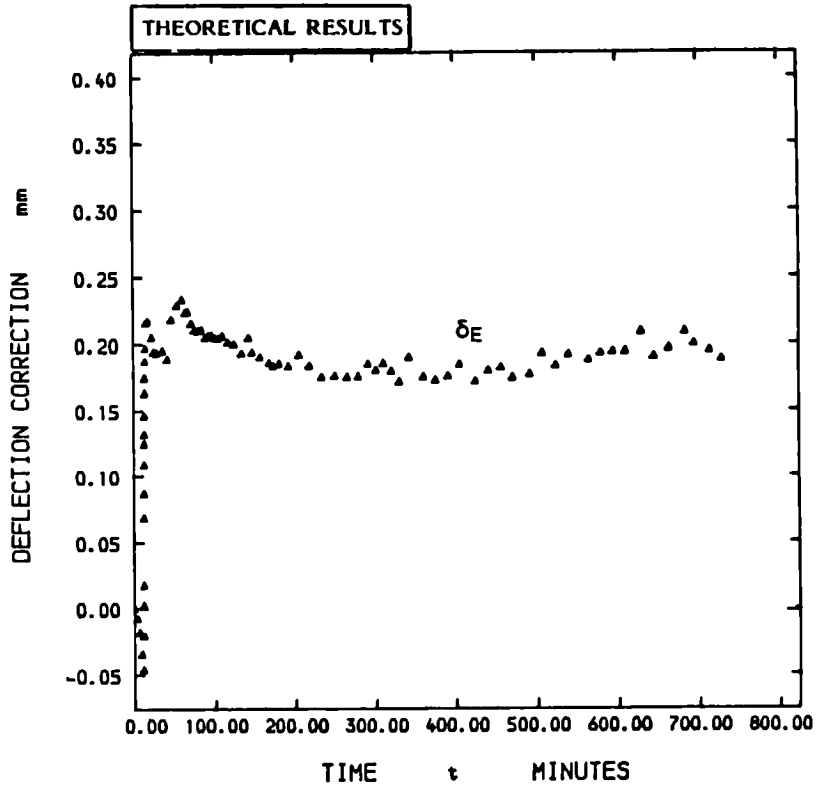

Figure 5.58:

Temperature Correction to Recorded Deflections of Diaphragm, due to Thermal Expansion of Sintox Tubes Specimen No: LTS-5

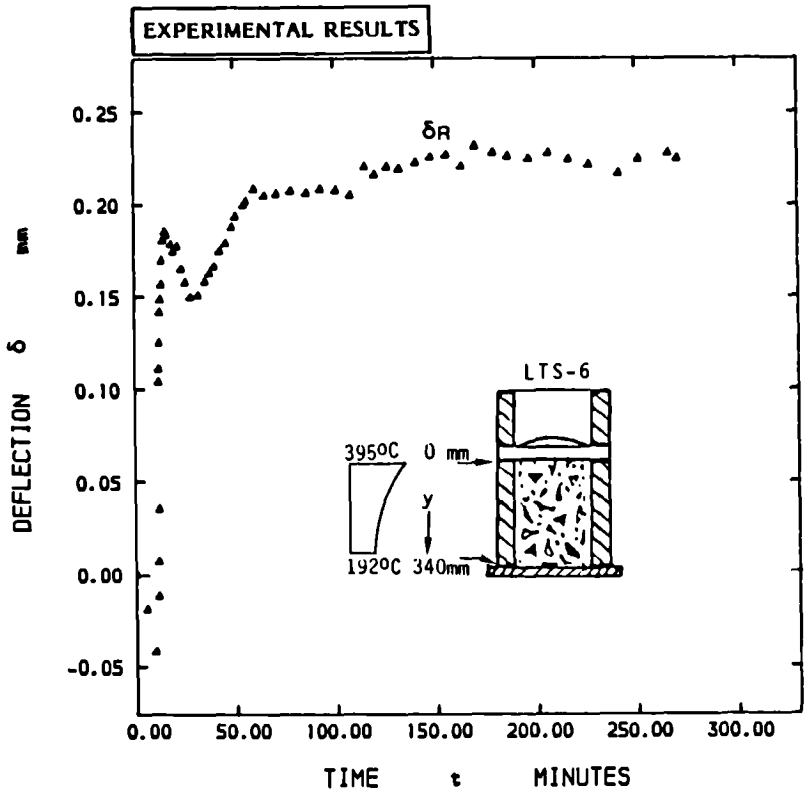

Figure 5.59:

Variation of Diaphragm Deflection with Time from Start of Heating Specimen No: LTS-6

Note : Values are Recorded and Uncorrected for Expansion of Sintox Tubes

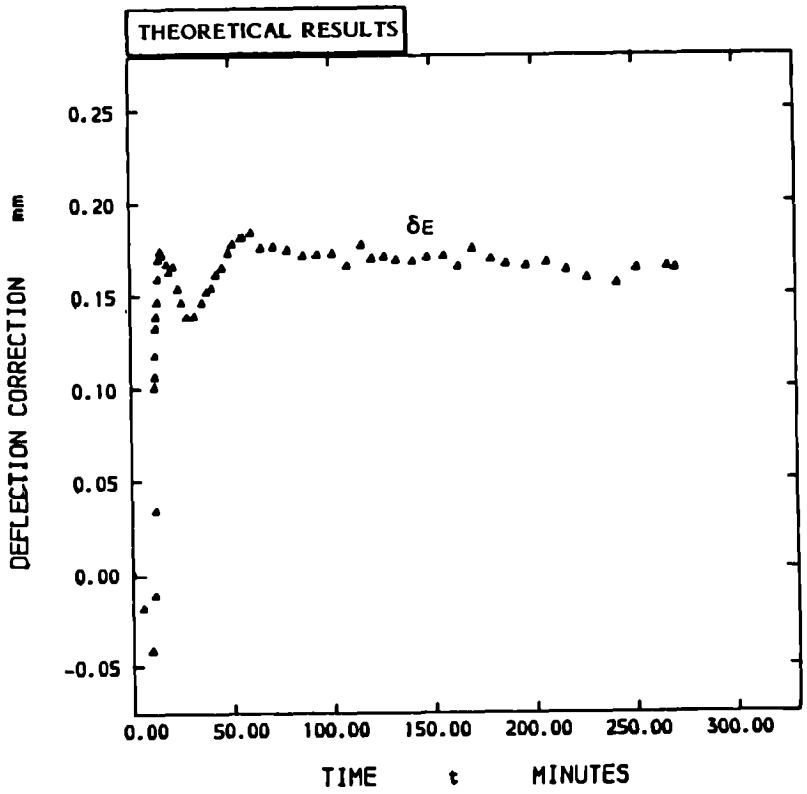

Figure 5.60:

Temperature Correction to Recorded Deflections of Diaphragm, due to Thermal Expansion of Sintox Tubes Specimen No: LTS-6

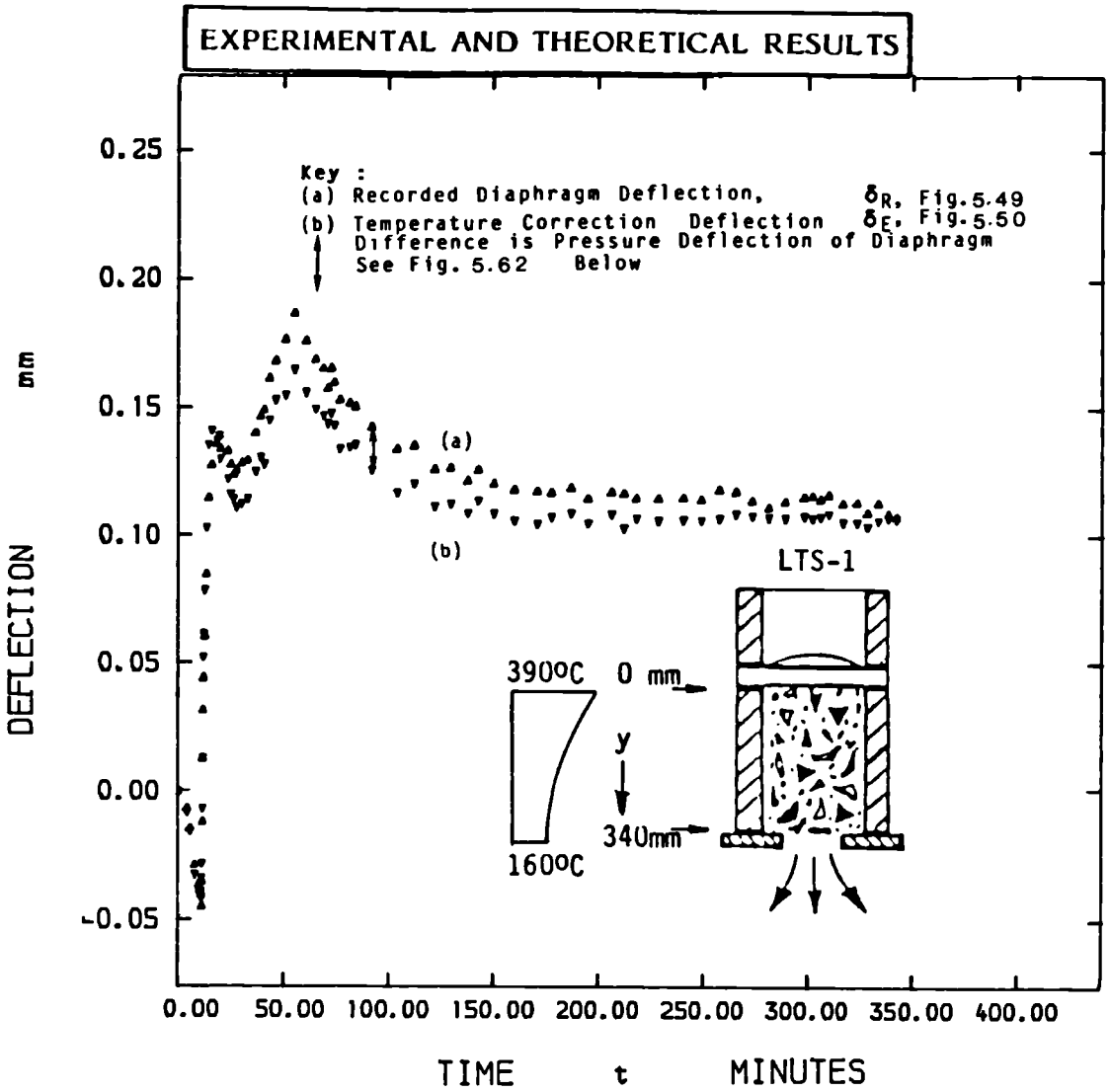

Figure 5.61:

Variation of Diaphragm Deflection, and Sintox Tubes Expansion, with Time from start of Heating Specimen No: LTS-1

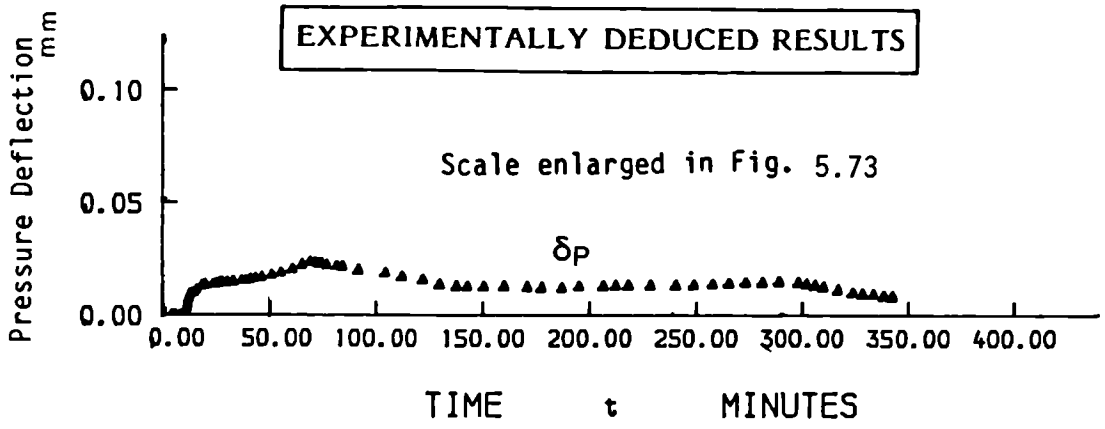

Figure 5.62:
Pressure only Deflection of Diaphragm with Time from Start of Heating Specimen No: LTS-1

Note : $\delta_P = \delta_R - \delta_E$
δ_R = Recorded Diaphragm Deflection, Fig. 5.49
δ_E = Temperature Correction Deflection due to Expansion of Sintox Tubes, Fig. 5.50

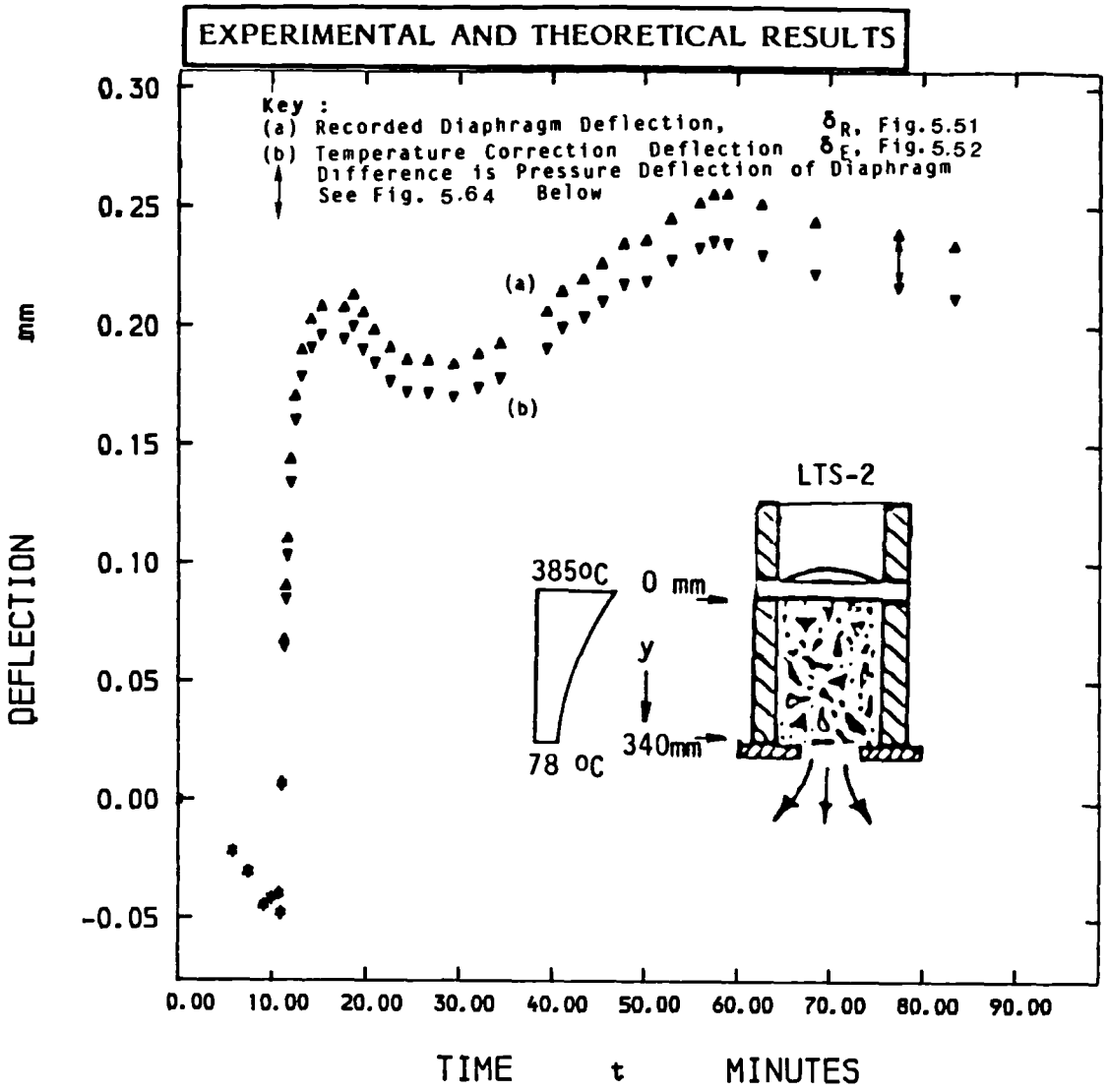

Figure 5.63:

Variation of Diaphragm Deflection, and Sintox Tubes Expansion, with Time from start of Heating Specimen No: LTS-2

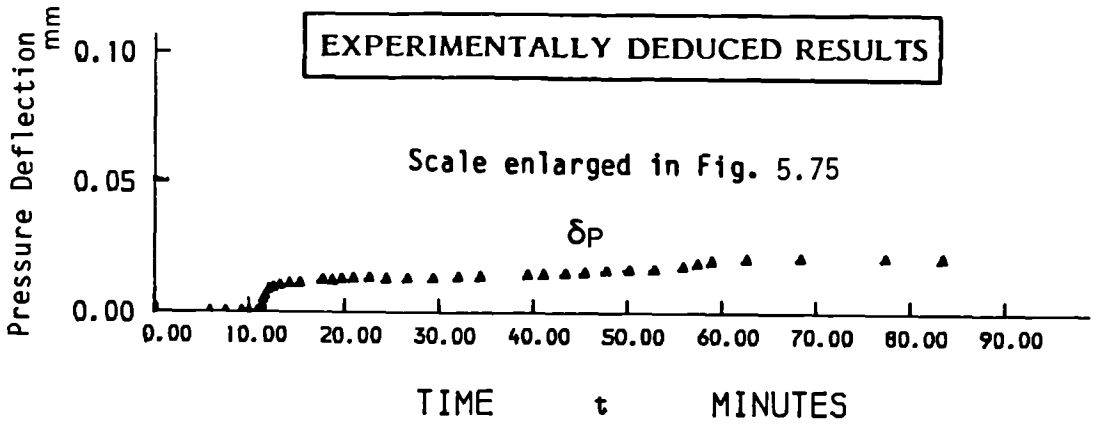

Figure 5.64:
Pressure only Deflection of Diaphragm with Time from Start of Heating Specimen No: LTS-2

Note : $\delta_P = \delta_R - \delta_E$
δ_R = Recorded Diaphragm Deflection, Fig. 5.51
δ_E = Temperature Correction Deflection due to Expansion of Sintox Tubes, Fig. 5.52

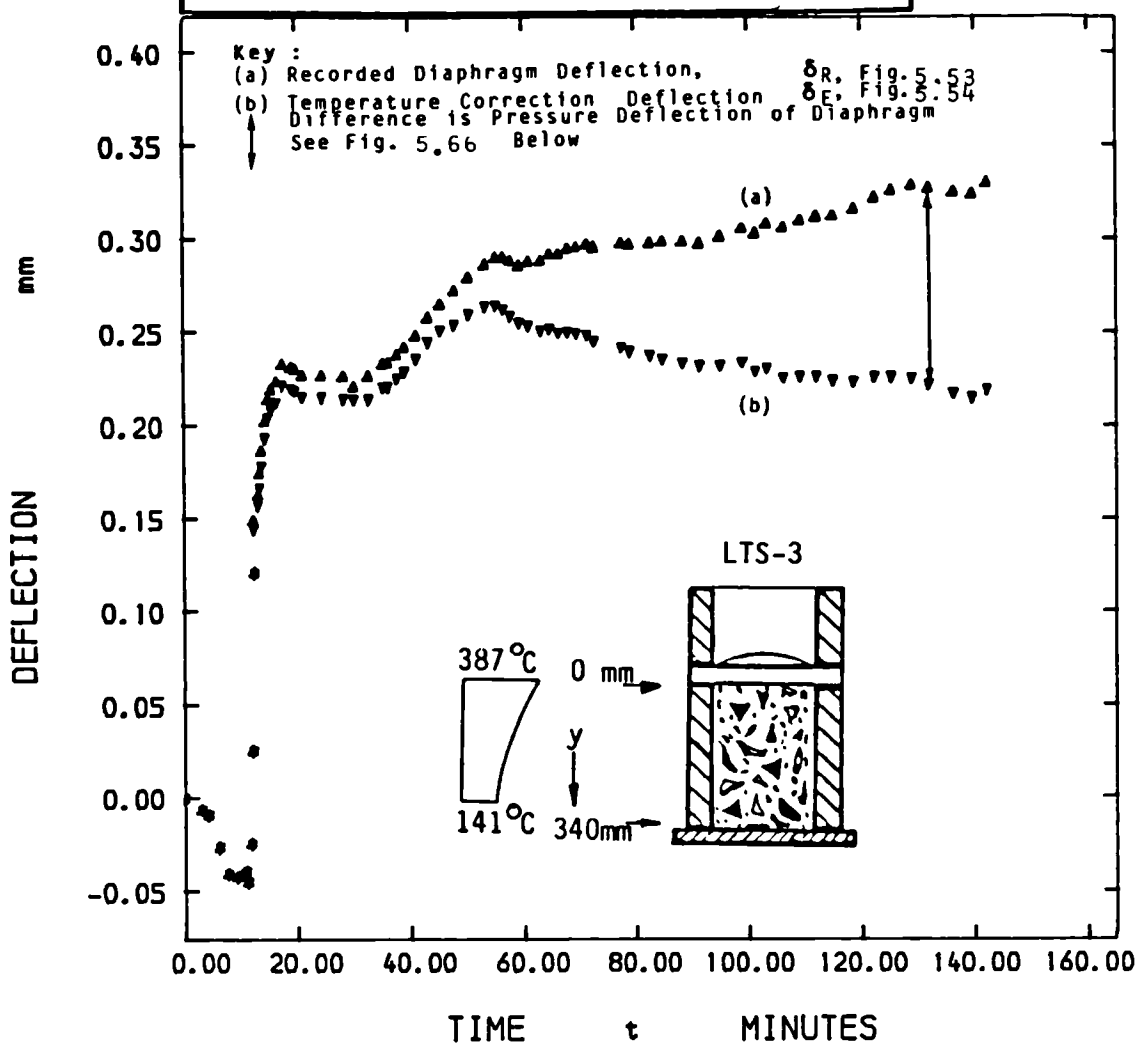

Figure 5.65:

Variation of Diaphragm Deflection, and Sintox Tubes Expansion, with Time from start of Heating Specimen No: LTS-3

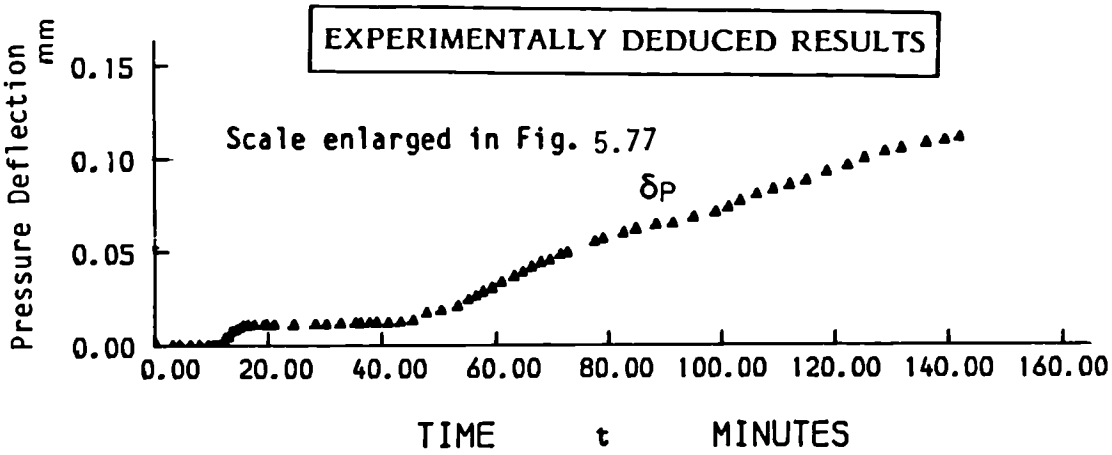

Figure 5.66:
Pressure only Deflection of Diaphragm with Time from Start of Heating Specimen No: LTS-3

Note : $\delta_P = \delta_R - \delta_E$
δ_R = Recorded Diaphragm Deflection, Fig. 5.53
δ_E = Temperature Correction Deflection due to Expansion of Sintox Tubes, Fig. 5.54

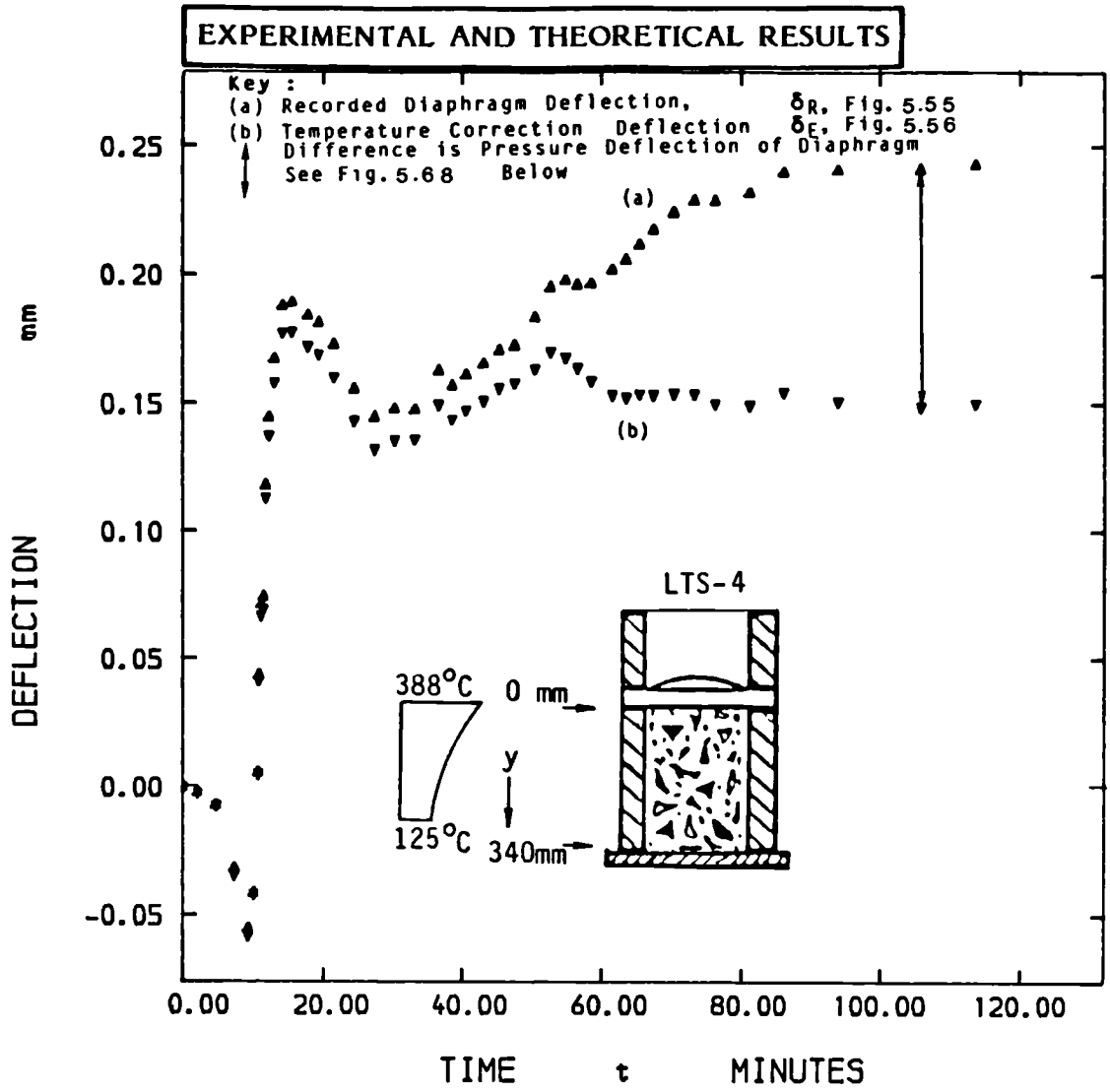

Figure 5.67:

Variation of Diaphragm Deflection, and Sintox Tubes Expansion, with Time from start of Heating Specimen No: LTS-4

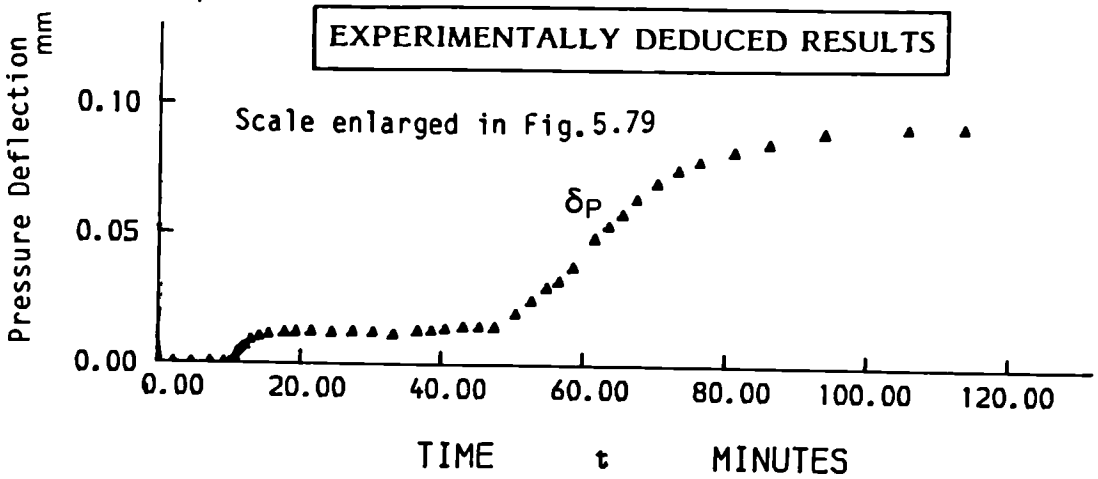

Figure 5.68:
Pressure only Deflection of Diaphragm with Time from Start of Heating Specimen No: LTS-4

Note : $\delta_P = \delta_R - \delta_E$
δ_R = Recorded Diaphragm Deflection, Fig. 5.55
δ_E = Temperature Correction Deflection due to Expansion of Sintox Tubes, Fig. 5.56

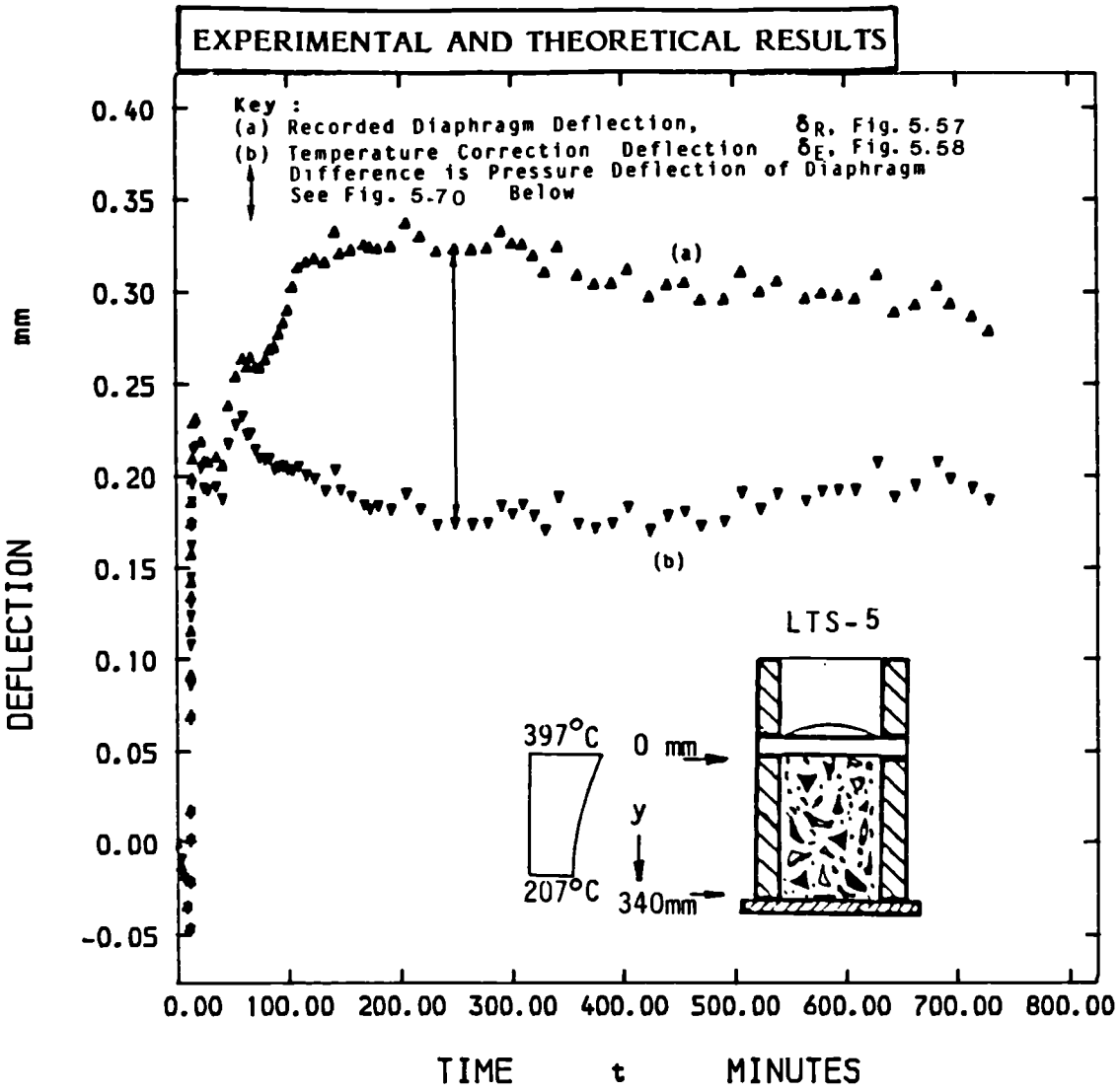

Figure 5.69:

Variation of Diaphragm Deflection, and Sintox Tubes Expansion, with Time from start of Heating Specimen No: LTS-5

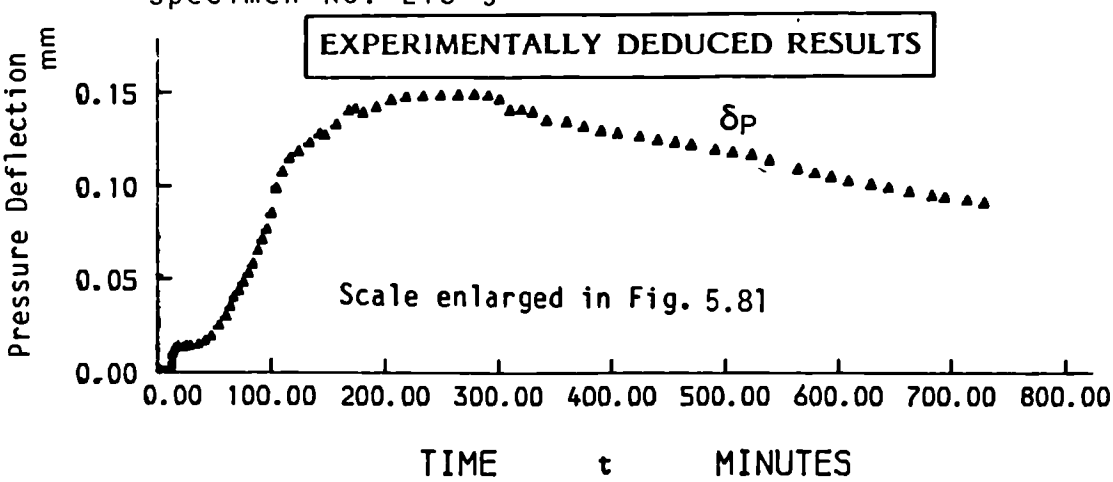

Figure 5.70:
Pressure only Deflection of Diaphragm with Time from Start of Heating Specimen No: LTS-5

Note : $\delta_P = \delta_R - \delta_E$
δ_R = Recorded Diaphragm Deflection, Fig. 5.57
δ_E = Temperature Correction Deflection due to Expansion of Sintox Tubes, Fig. 5.58

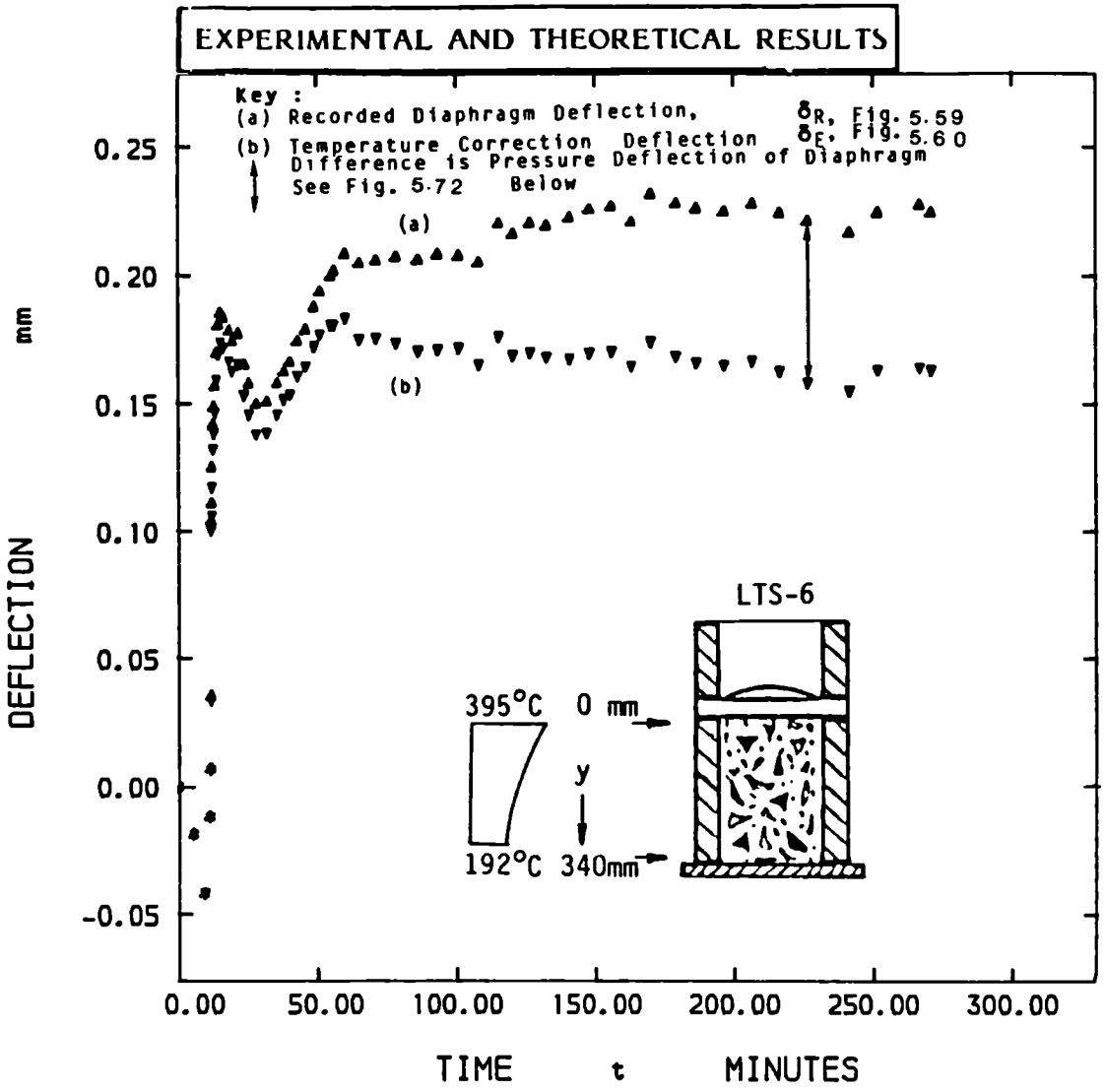

Figure 5.71:

Variation of Diaphragm Deflection, and Sintox Tubes Expansion, with Time from start of Heating Specimen No: LTS-6

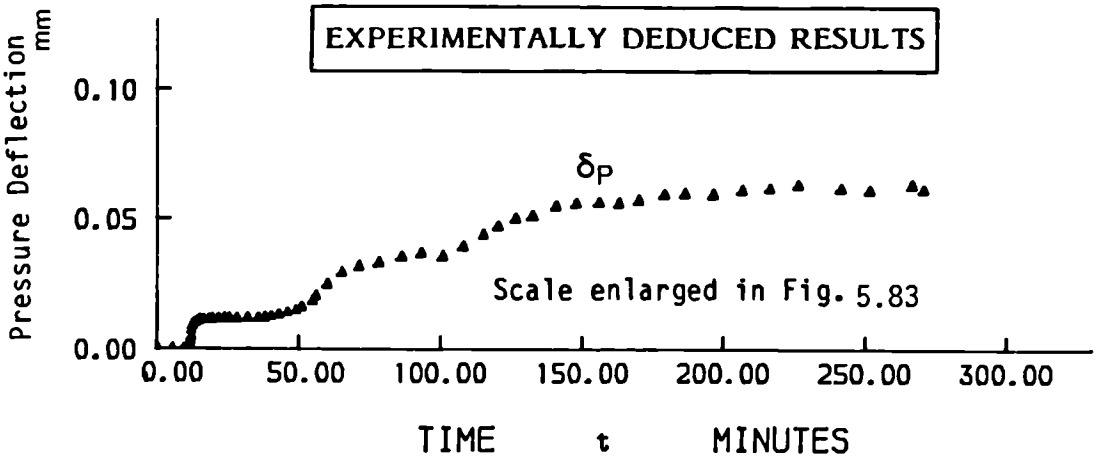

Figure 5.72:
Pressure only Deflection of Diaphragm with Time from Start of Heating Specimen No: LTS-6

Note : $\delta_P = \delta_R - \delta_E$
δ_R = Recorded Diaphragm Deflection, Fig.5.69
δ_E = Temperature Correction Deflection due to Expansion of Sintox Tubes, Fig.5.60

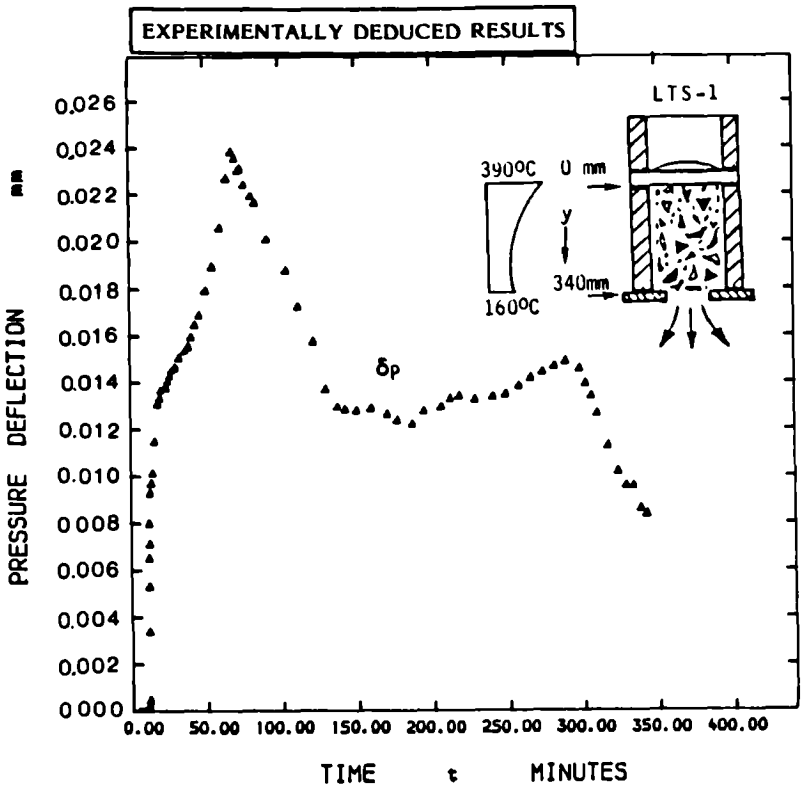

Figure 5.73:

Pressure only Deflection of Diaphragm with Time from Start of Heating Specimen No: LTS-1

Note : $\delta_P = \delta_R - \delta_E$
δ_R = Recorded Diaphragm Deflection, Fig. 5.49
δ_E = Temperature Correction Deflection due to Expansion of Sintox Tubes, Fig. 5.50

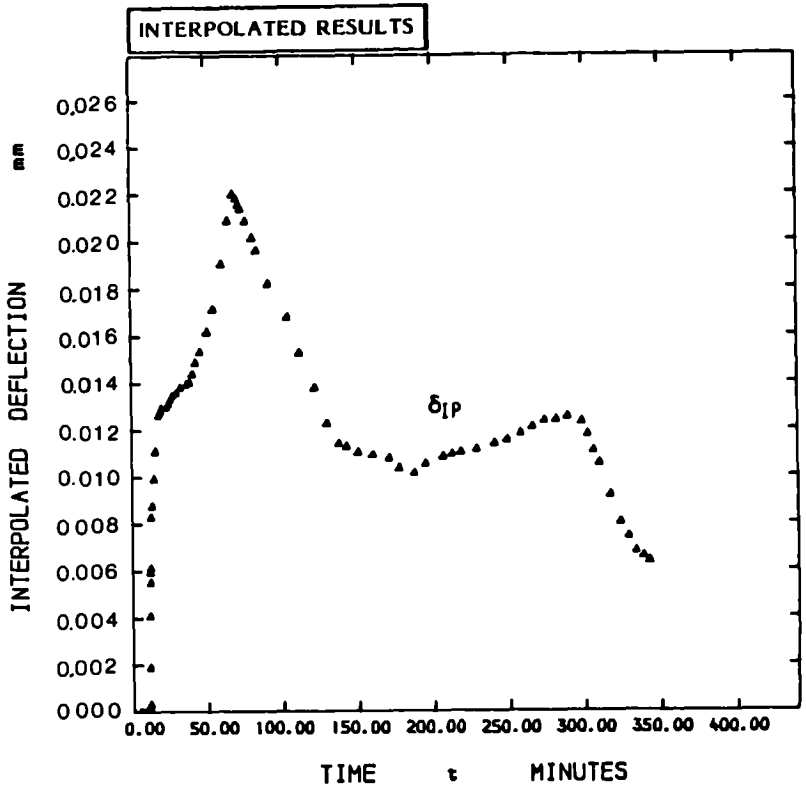

Figure 5.74:

Diaphragm Deflection with Time from Start of Heating Specimen No: LTS-1

Note : Diaphragm Deflection, δ_{IP}, Derived from Pore Pressures P_1 and Interpolation from Pressure / Diaphragm Deflection Calibration Test Figure III.4(a) of Appendix III

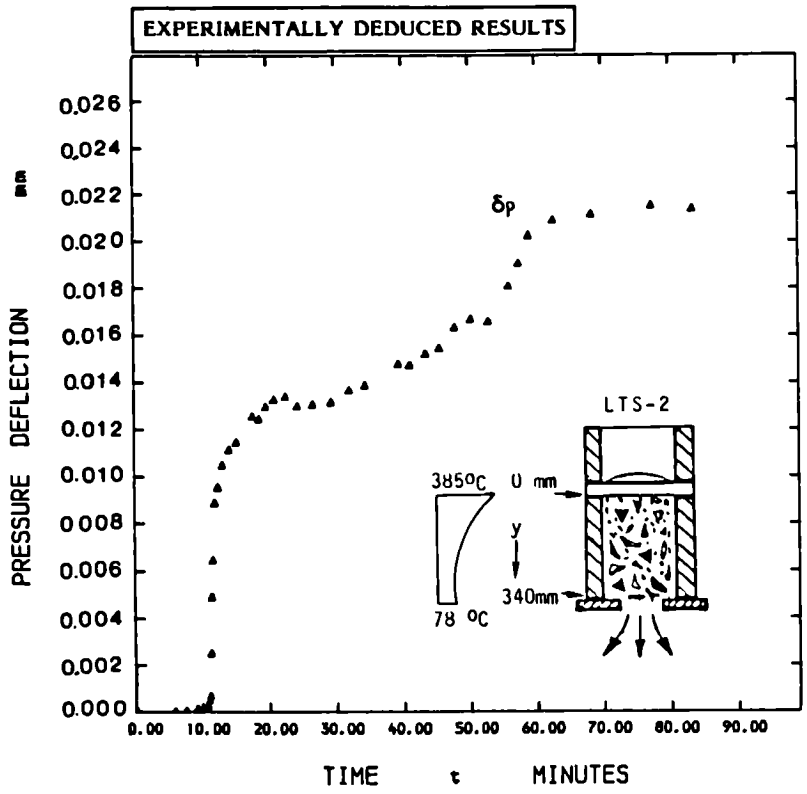

Figure 5.75:

Pressure only Deflection of Diaphragm with Time from Start of Heating Specimen No: LTS-2

Note : $\delta_P = \delta_R - \delta_E$
δ_R = Recorded Diaphragm Deflection, Fig. 5.51
δ_E = Temperature Correction Deflection due to Expansion of Sintox Tubes, Fig. 5.52

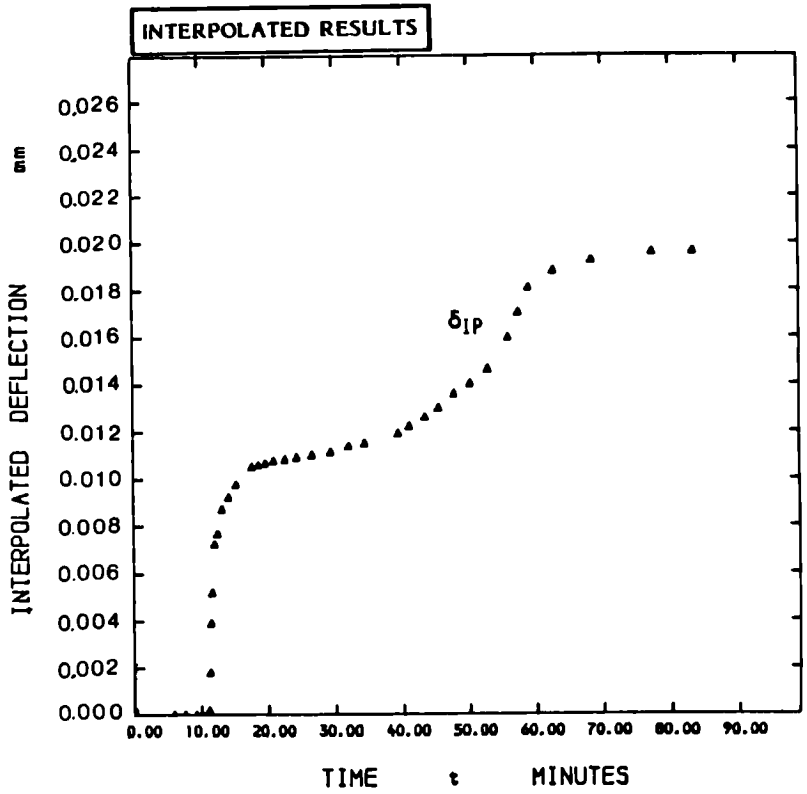

Figure 5.76:

Diaphragm Deflection with Time from Start of Heating Specimen No: LTS-2

Note : Diaphragm Deflection, δ_{IP}, Derived from Pore Pressures P_1 and Interpolation from Pressure / Diaphragm Deflection Calibration Test Figure III.4(b) of Appendix III

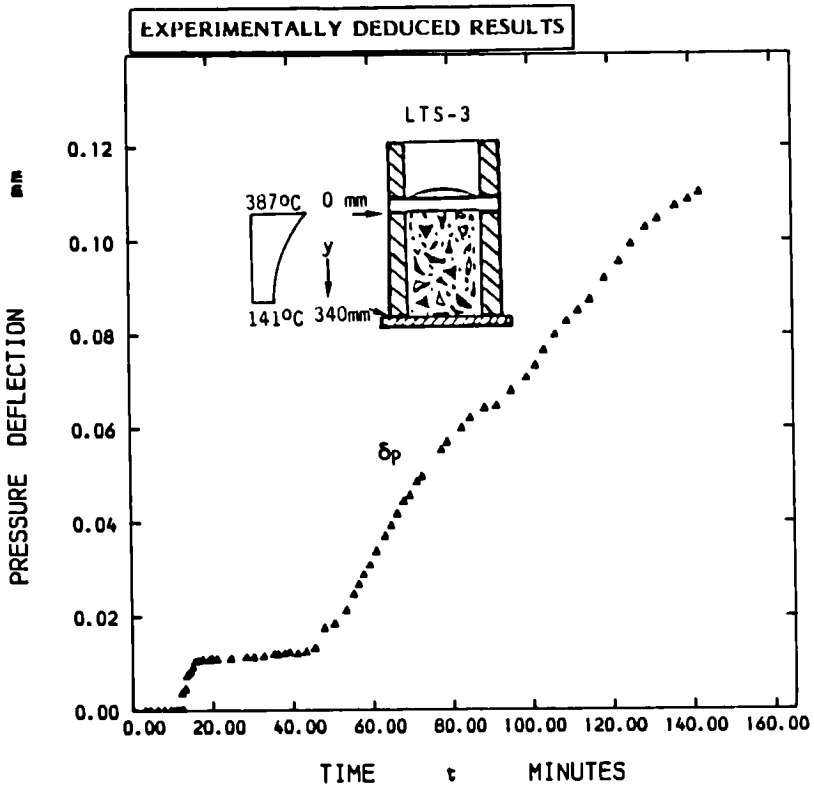

Figure 5.77:

Pressure only Deflection of Diaphragm with Time from Start of Heating Specimen No: LTS-3

Note : $\delta_P = \delta_R - \delta_E$
δ_R = Recorded Diaphragm Deflection, Fig. 5.53
δ_E = Temperature Correction Deflection due to Expansion of Sintox Tubes, Fig.5.54

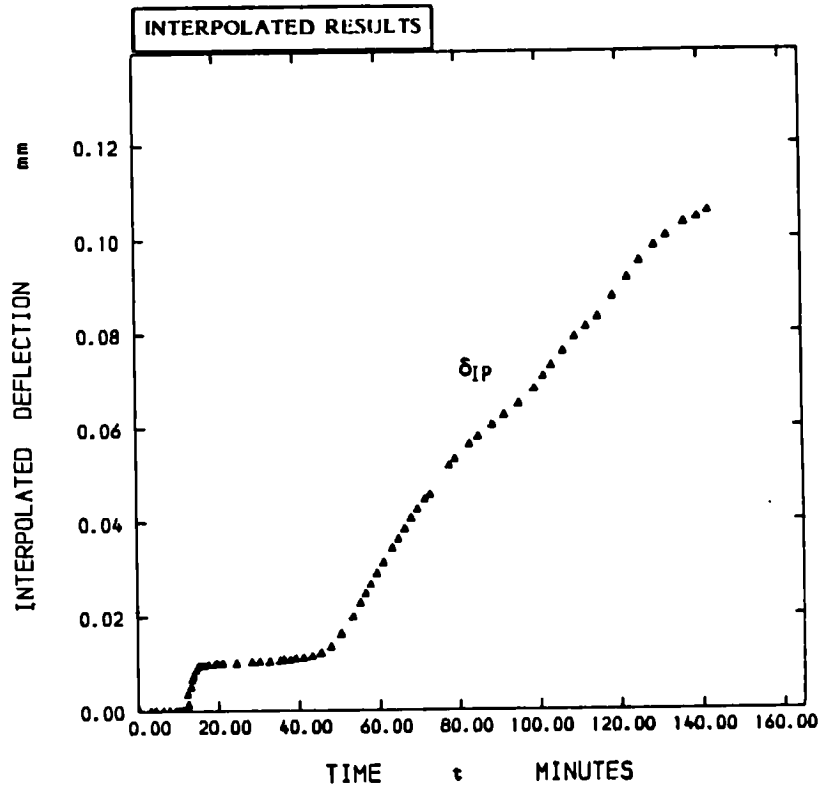

Figure 5.78:

Diaphragm Deflection with Time from Start of Heating Specimen No: LTS-3

Note : Diaphragm Deflection, δ_{IP}, Derived from Pore Pressures P1 and Interpolation from Pressure / Diaphragm Deflection Calibration Test Figure III.4(c) of Appendix III

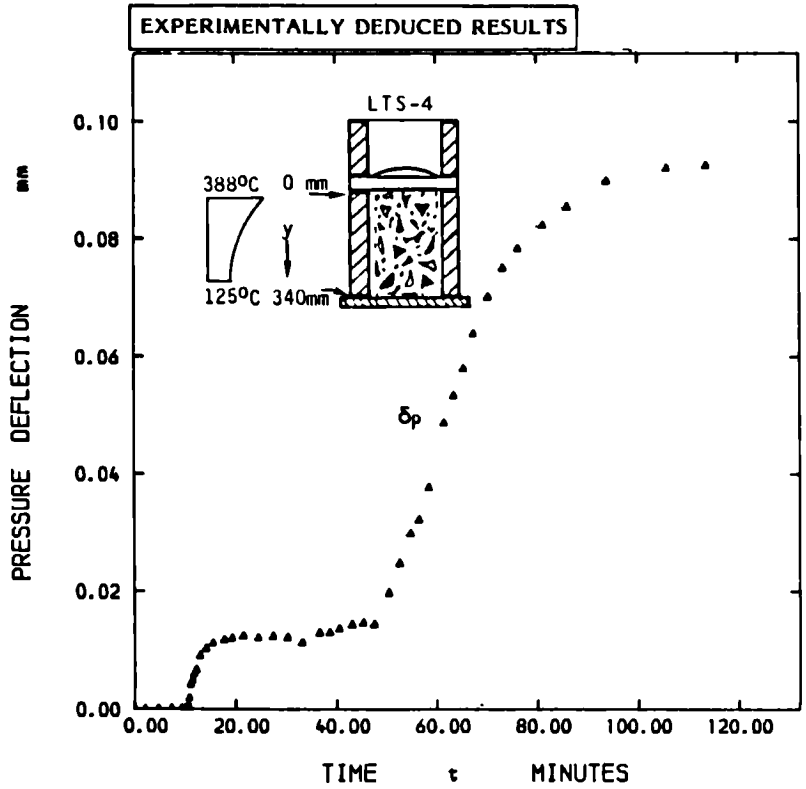

Figure 5.79:

Pressure only Deflection of Diaphragm with Time from Start of Heating Specimen No: LTS-4

Note : $\delta_P = \delta_R - \delta_E$
δ_R = Recorded Diaphragm Deflection, Fig. 5.55
δ_E = Temperature Correction Deflection due to Expansion of Sintox Tubes, Fig.5.56

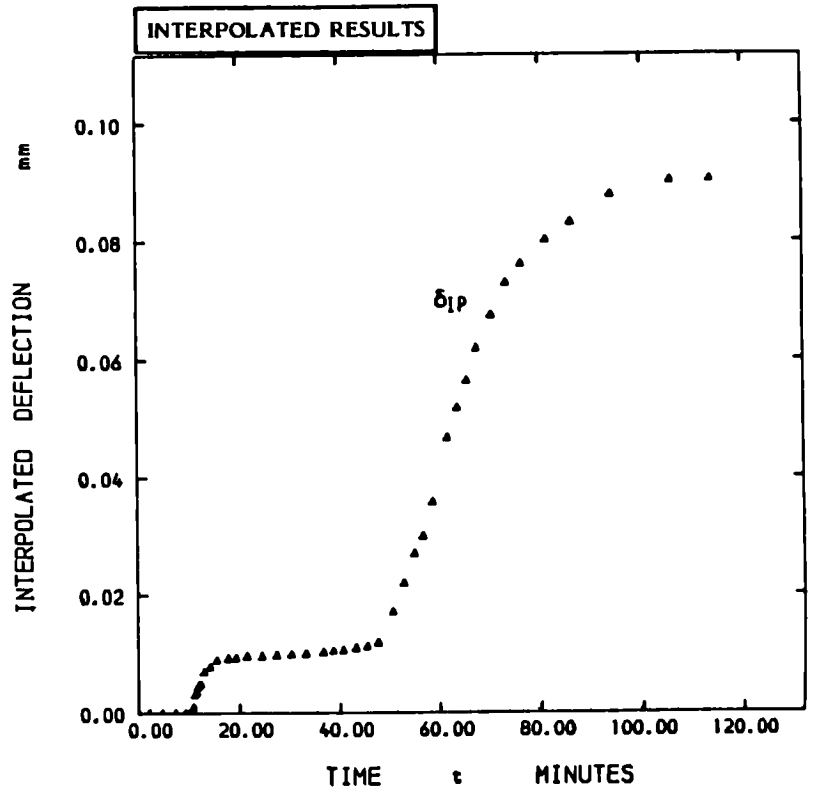

Figure 5.80:

Diaphragm Deflection with Time from Start of Heating Specimen No: LTS-4

Note : Diaphragm Deflection, δ_{IP}, Derived from Pore Pressures P_1 and Interpolation from Pressure / Diaphragm Deflection Calibration Test Figure III.4(d) of Appendix III

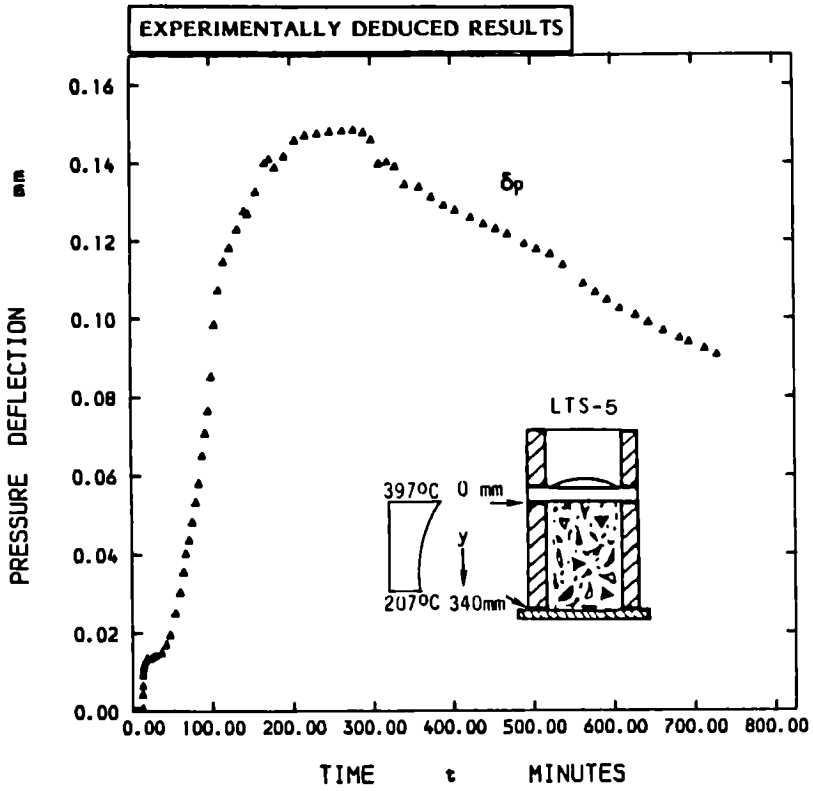

Figure 5.81:

Pressure only Deflection of Diaphragm with Time from Start of Heating Specimen No: LTS-5

Note : $\delta_P = \delta_R - \delta_E$
δ_R = Recorded Diaphragm Deflection, Fig. 5.57
δ_E = Temperature Correction Deflection due to Expansion of Sintox Tubes, Fig. 5.58

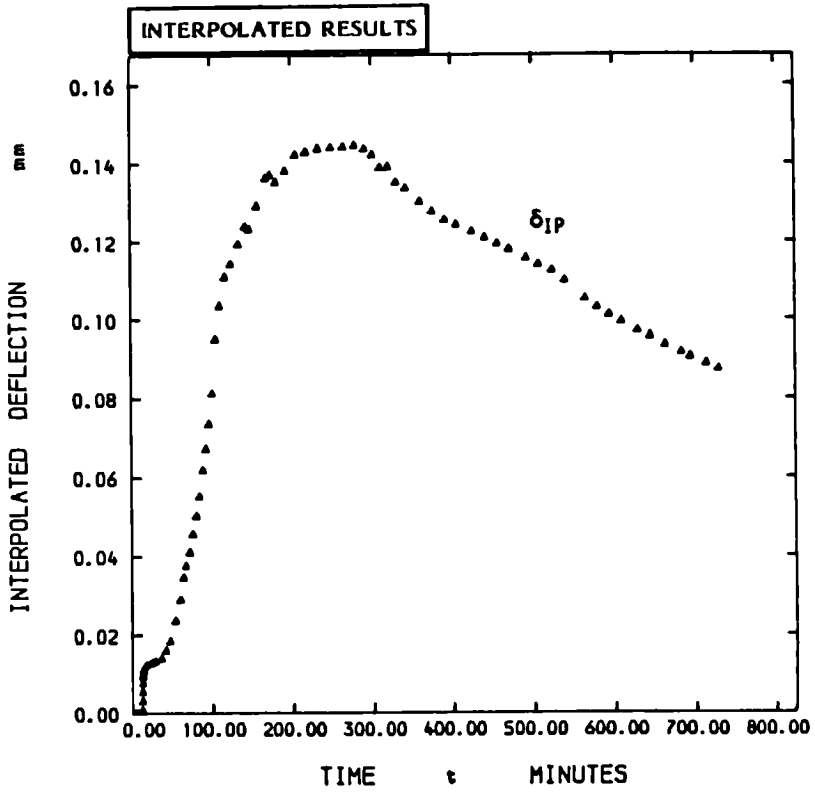

Figure 5.82:

Diaphragm Deflection with Time from Start of Heating Specimen No: LTS-5

Note : Diaphragm Deflection, δ_{IP}, Derived from Pore Pressures P_1 and Interpolation from Pressure / Diaphragm Deflection Calibration Test Figure III.4(e) of Appendix III

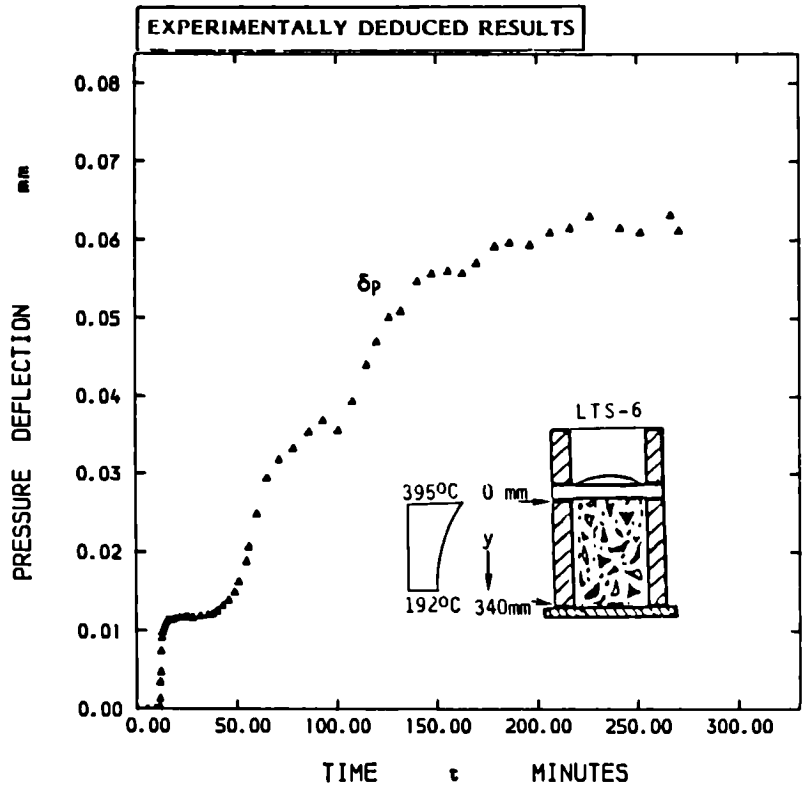

Figure 5.83:

Pressure only Deflection of Diaphragm with Time from Start of Heating Specimen No: LTS-6

Note : $\delta_P = \delta_R - \delta_E$
δ_R = Recorded Diaphragm Deflection, Fig. 5.59
δ_E = Temperature Correction Deflection due to Expansion of Sintox Tubes, Fig.5.60

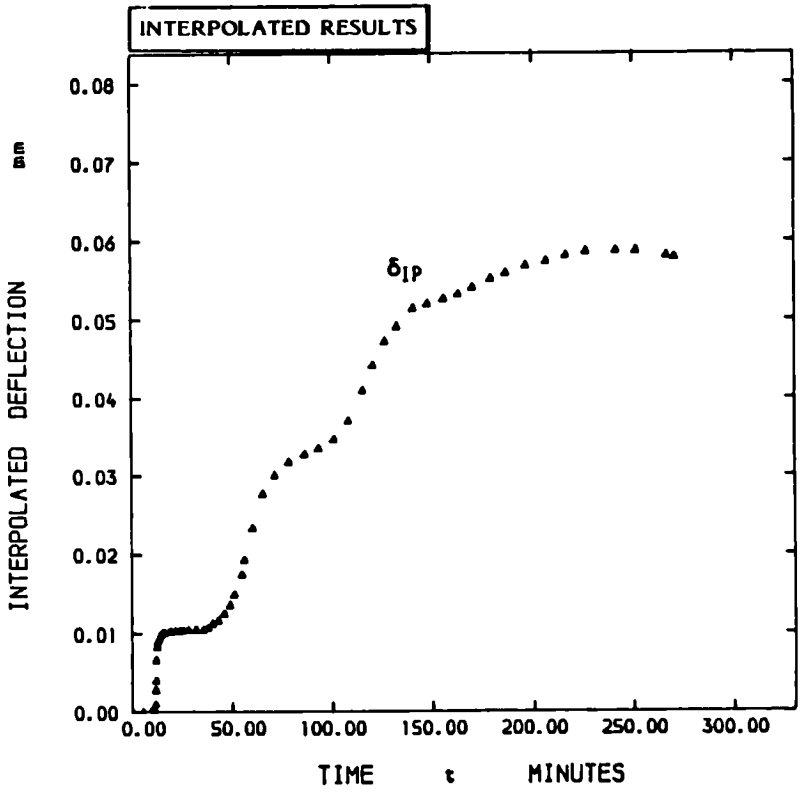

Figure 5.84:

Diaphragm Deflection with Time from Start of Heating Specimen No: LTS-6

Note : Diaphragm Deflection, δ_{IP}, Derived from Pore Pressures P_1 and Interpolation from Pressure / Diaphragm Deflection Calibration Test Figure III.4(f) of Appendix III

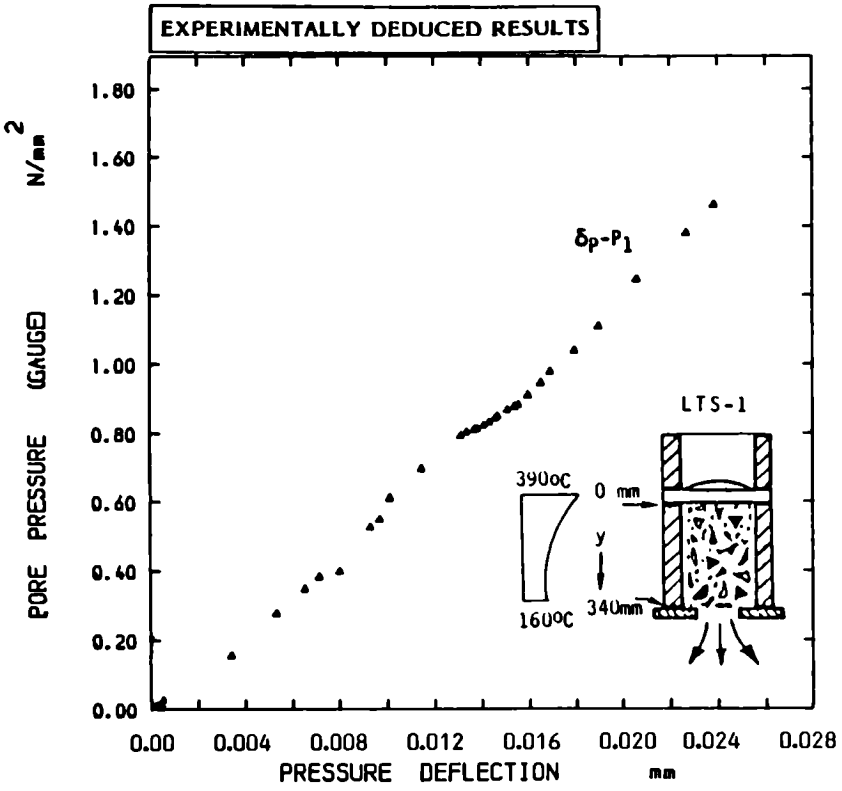

Figure 5.85:

Variation of Pore Pressures with Pressure only Deflection of Diaphragm Specimen No: LTS-1

Note : $\delta_P = \delta_R - \delta_t$
δ_R = Recorded Diaphragm Deflection, Fig. 5.49
δ_t = Temperature Correction Deflection due to Expansion of Sintox Tubes, Fig.5.50

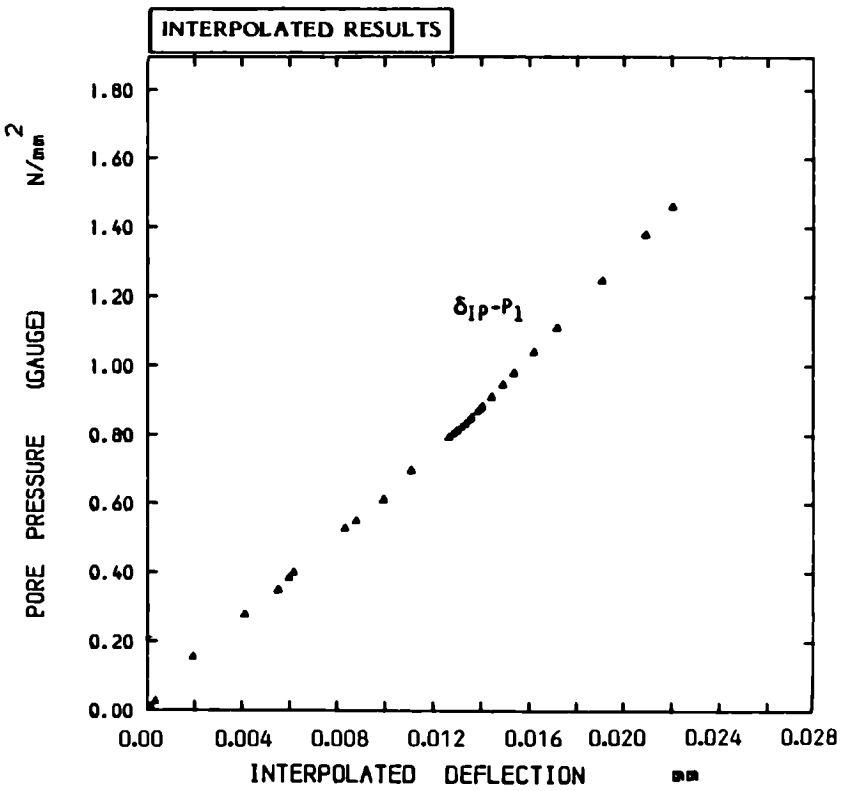

Figure 5.86:

Part of Pressure / Diaphragm Deflection Calibration Curve for Comparison with Experimental Results of Figure 5.85

Note : Diaphragm Deflection, δ_{IP}, Derived from Pore Pressures, P_1, and Interpolation from Pressure / Diaphragm Deflection Calibration Test Figure III.4(a) of Appendix III

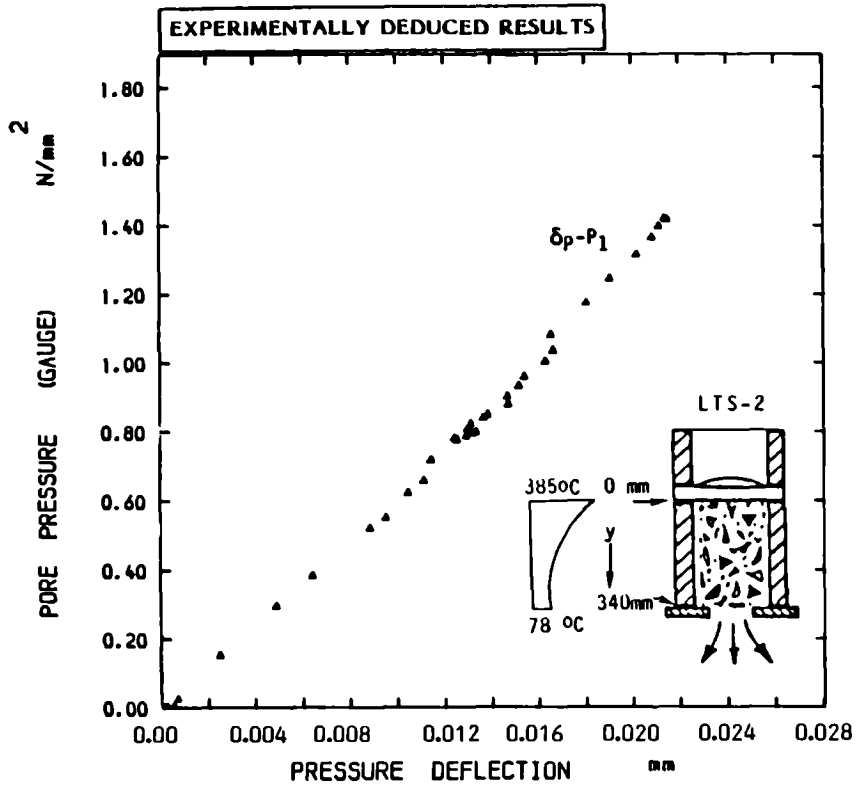

Figure 5.87:

Variation of Pore Pressures with Pressure only Deflection of Diaphragm Specimen No: LTS-2

Note : $\delta_P = \delta_R - \delta_E$
δ_R = Recorded Diaphragm Deflection, Fig. 5.51
δ_E = Temperature Correction Deflection due to Expansion of Sintox Tubes, Fig. 5.52

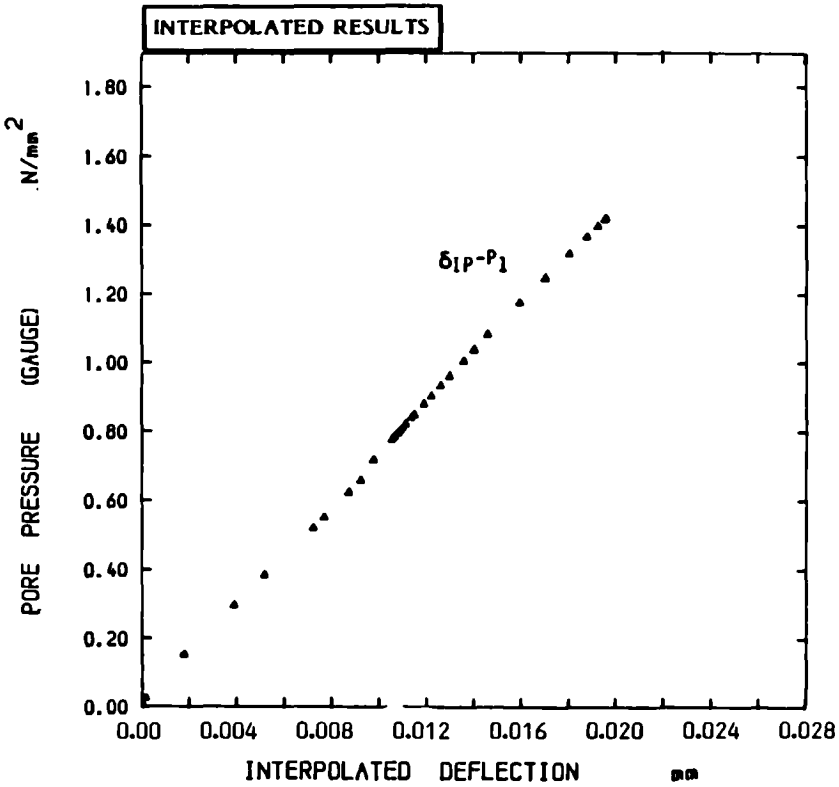

Figure 5.88:

Part of Pressure / Diaphragm Deflection Calibration Curve for Comparison with Experimental Results of Figure 5.87

Note : Diaphragm Deflection, δ_{IP}, Derived from Pore Pressures, P_1, and Interpolation from Pressure / Diaphragm Deflection Calibration Test Figure III.4(b) of Appendix III

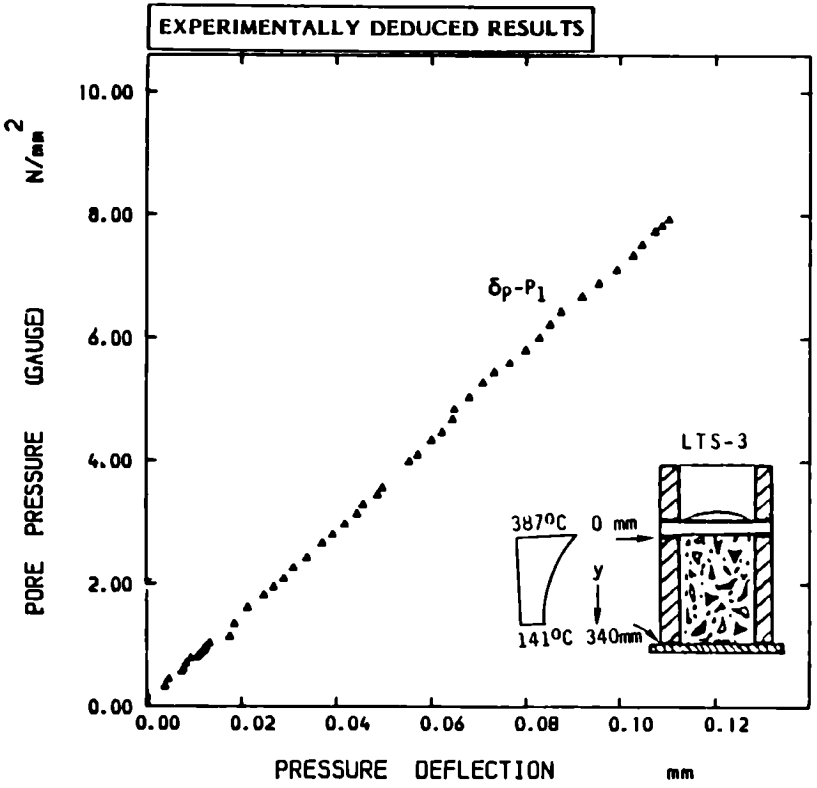

Figure 5.89:

Variation of Pore Pressures with Pressure only Deflection of Diaphragm Specimen No: LTS-3

Note : $\delta_P = \delta_R - \delta_E$
δ_R = Recorded Diaphragm Deflection, Fig. 5.53
δ_E = Temperature Correction Deflection due to Expansion of Sintox Tubes, Fig. 5.54

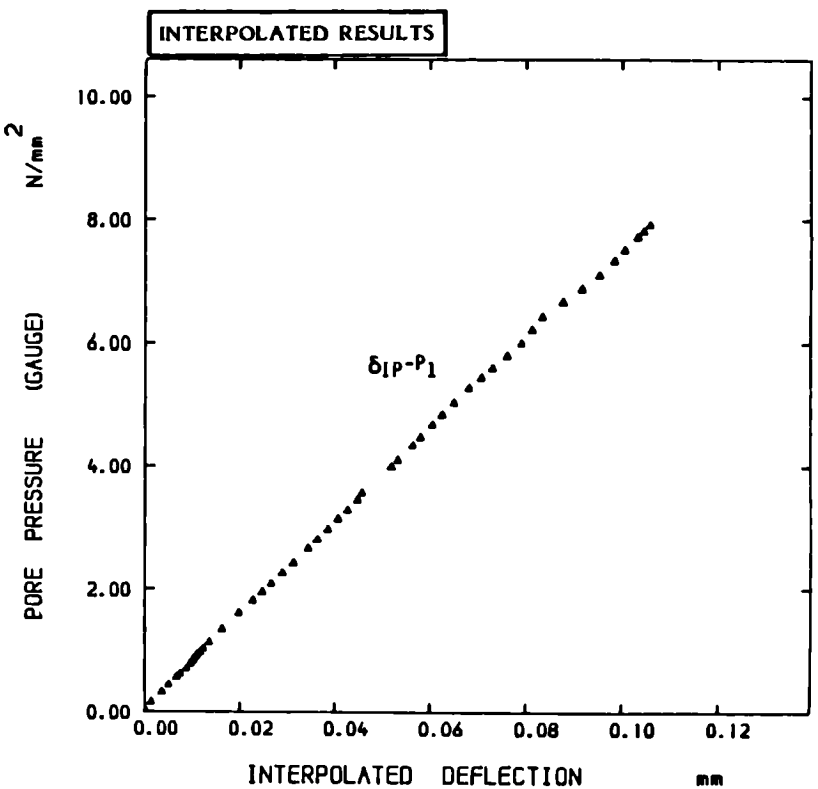

Figure 5.90:

Part of Pressure / Diaphragm Deflection Calibration Curve for Comparison with Experimental Results of Figure 5.89

Note : Diaphragm Deflection, δ_{IP}, Derived from Pore Pressures, P_1, and Interpolation from Pressure / Diaphragm Deflection Calibration Test Figure III.4(c) of Appendix III

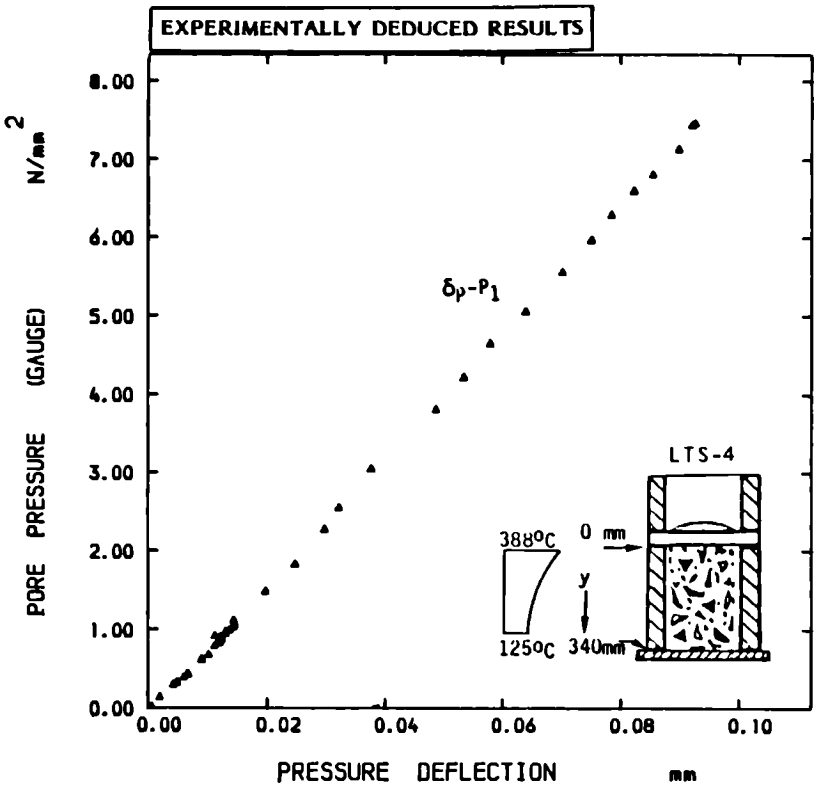

Figure 5.91:

Variation of Pore Pressures with Pressure only Deflection of Diaphragm Specimen No: LTS-4

Note : $\delta_P = \delta_R - \delta_E$
δ_R = Recorded Diaphragm Deflection, Fig. 5.55
δ_E = Temperature Correction Deflection due to Expansion of Sintox Tubes, Fig. 5.56

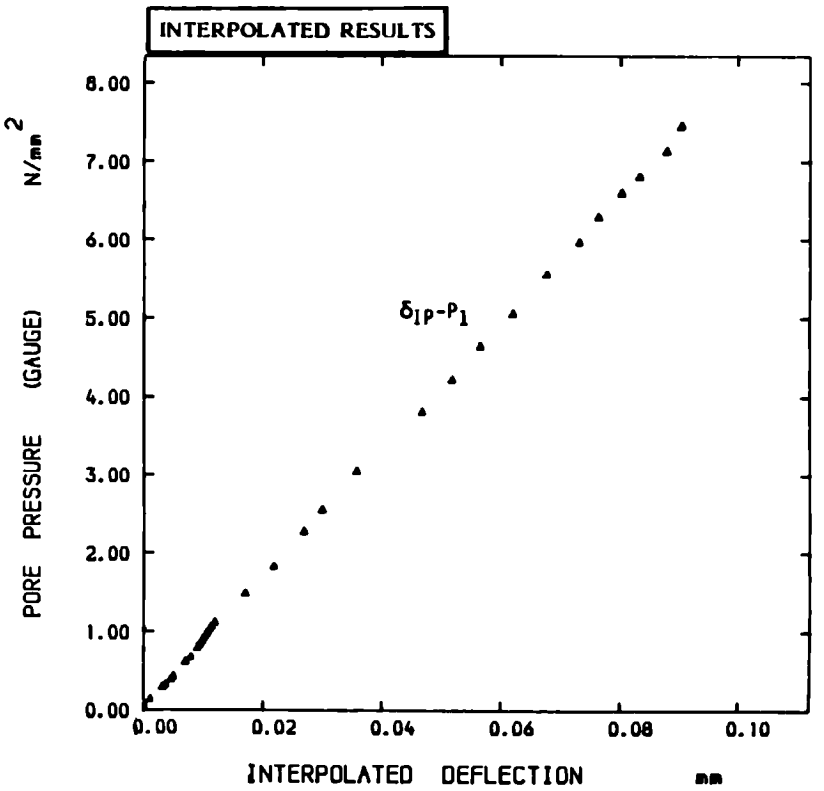

Figure 5.92:

Part of Pressure / Diaphragm Deflection Calibration Curve for Comparison with Experimental Results of Figure 5.91

Note : Diaphragm Deflection, δ_{IP}, Derived from Pore Pressures, P_1, and Interpolation from Pressure / Diaphragm Deflection Calibration Test Figure III.4(d) of Appendix III

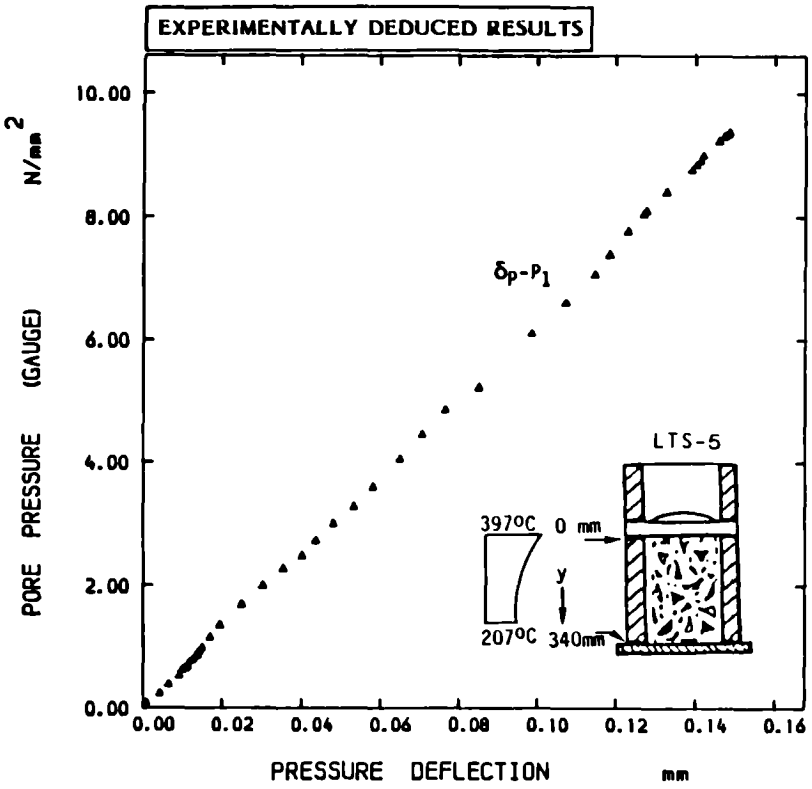

Figure 5.93:

Variation of Pore Pressures with Pressure only Deflection of Diaphragm Specimen No: LTS-5

Note : $\delta_P = \delta_R - \delta_E$
δ_R = Recorded Diaphragm Deflection, Fig. 5.57
δ_E = Temperature Correction Deflection due to Expansion of Sintox Tubes, Fig. 5.58

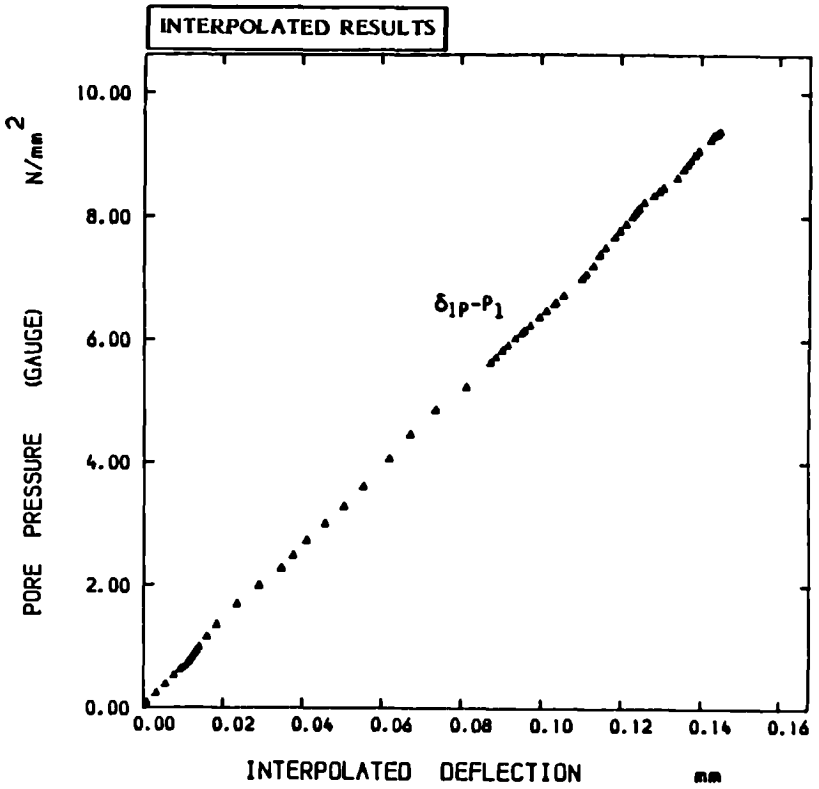

Figure 5.94:

Part of Pressure / Diaphragm Deflection Calibration Curve for Comparison with Experimental Results of Figure 5.93

Note : Diaphragm Deflection, δ_{IP}, Derived from Pore Pressures, P_1, and Interpolation from Pressure / Diaphragm Deflection Calibration Test Figure III.4(e) of Appendix III

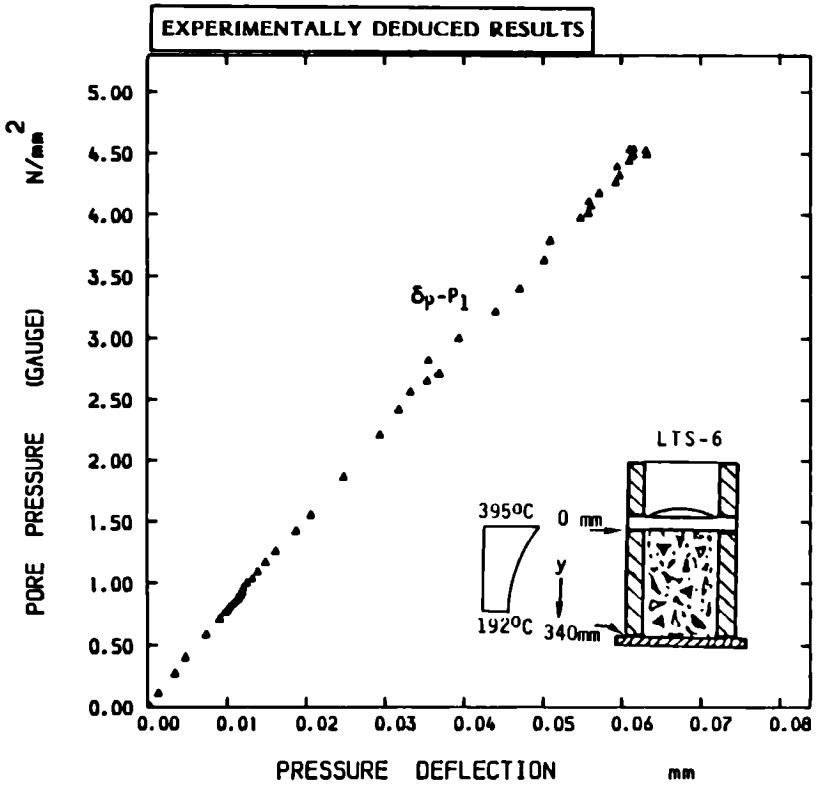

Figure 5.95:

Variation of Pore Pressures with Pressure only Deflection of Diaphragm Specimen No: LTS-6

Note : $\delta_P = \delta_R - \delta_E$
δ_R = Recorded Diaphragm Deflection, Fig.5.59
δ_E = Temperature Correction Deflection due to Expansion of Sintox Tubes, Fig. 5.60

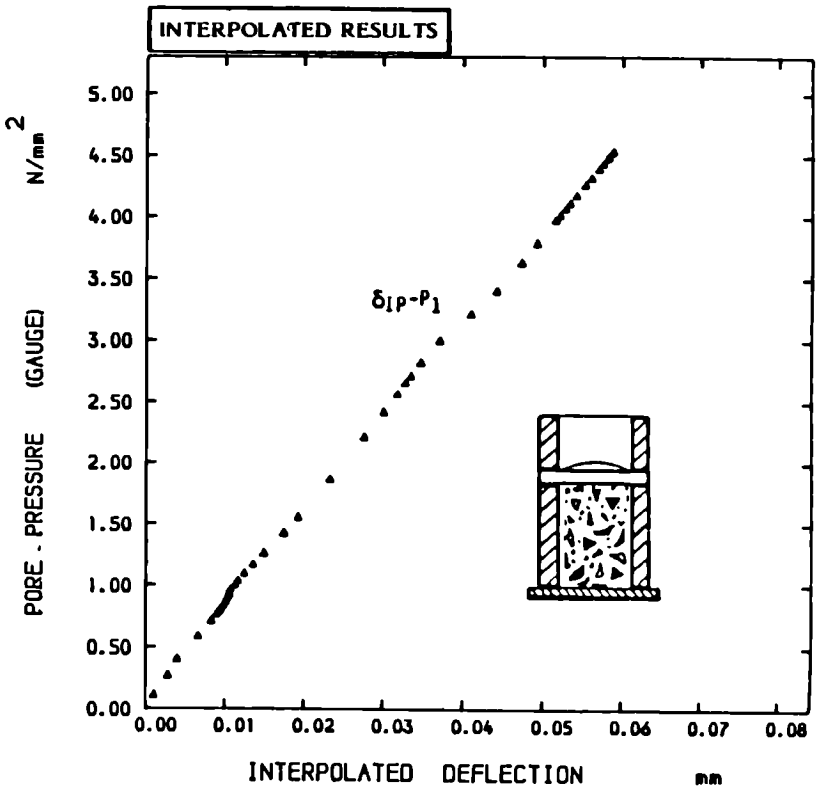

Figure 5.96:

Part of Pressure / Diaphragm Deflection Calibration Curve for Comparison with Experimental Results of Figure 5.95

Note : Diaphragm Deflection, δ_{IP}, Derived from Pore Pressures, P_1, and Interpolation from Pressure / Diaphragm Deflection Calibration Test Figure III.4(f) of Appendix III

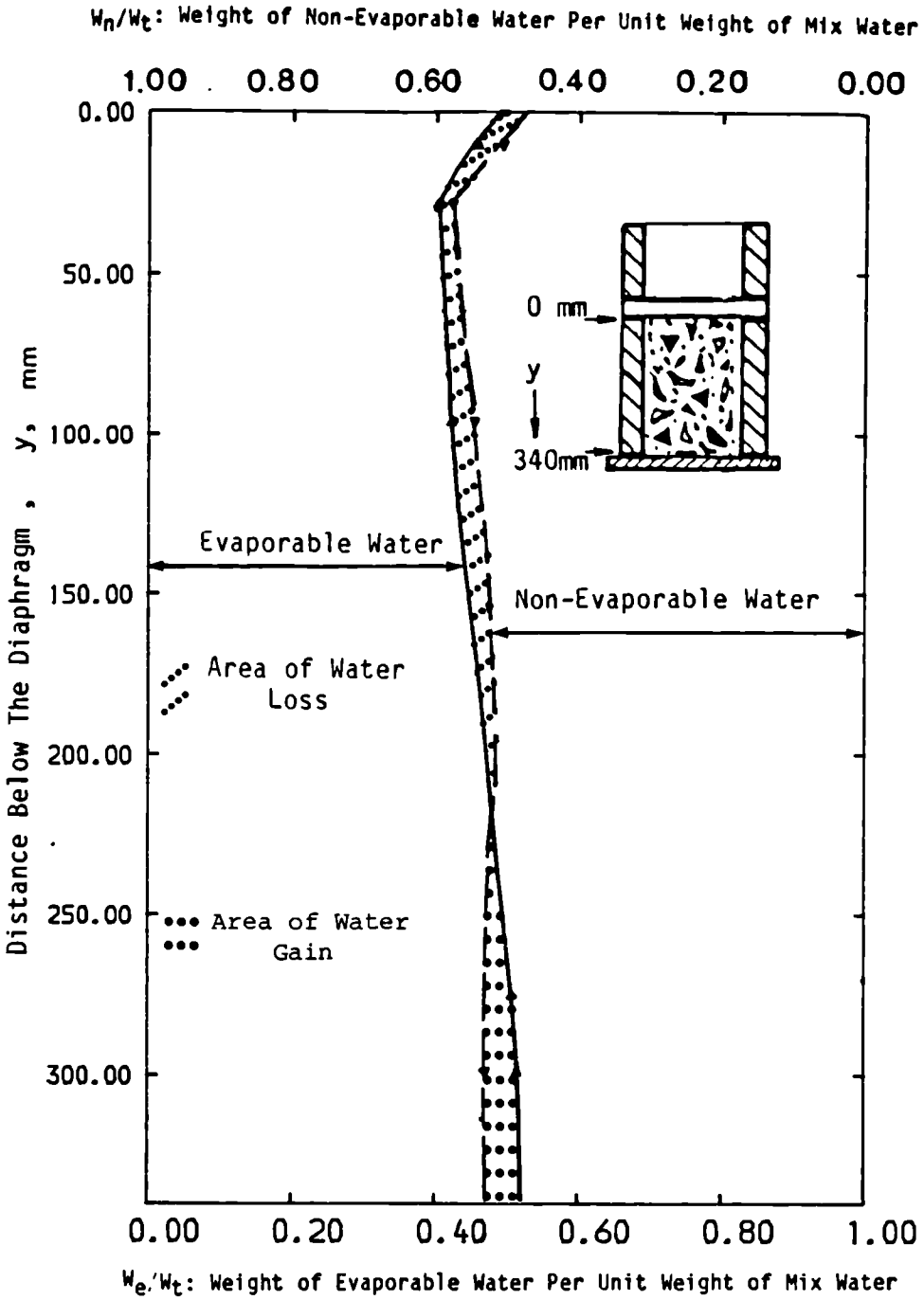

Figure 5.97:

Phase Diagram for Water obtained by Gravimetric Measurements Unheated Specimen

W_n/W_t: Weight of Non-Evaporable Water Per Unit Weight of Mix Water

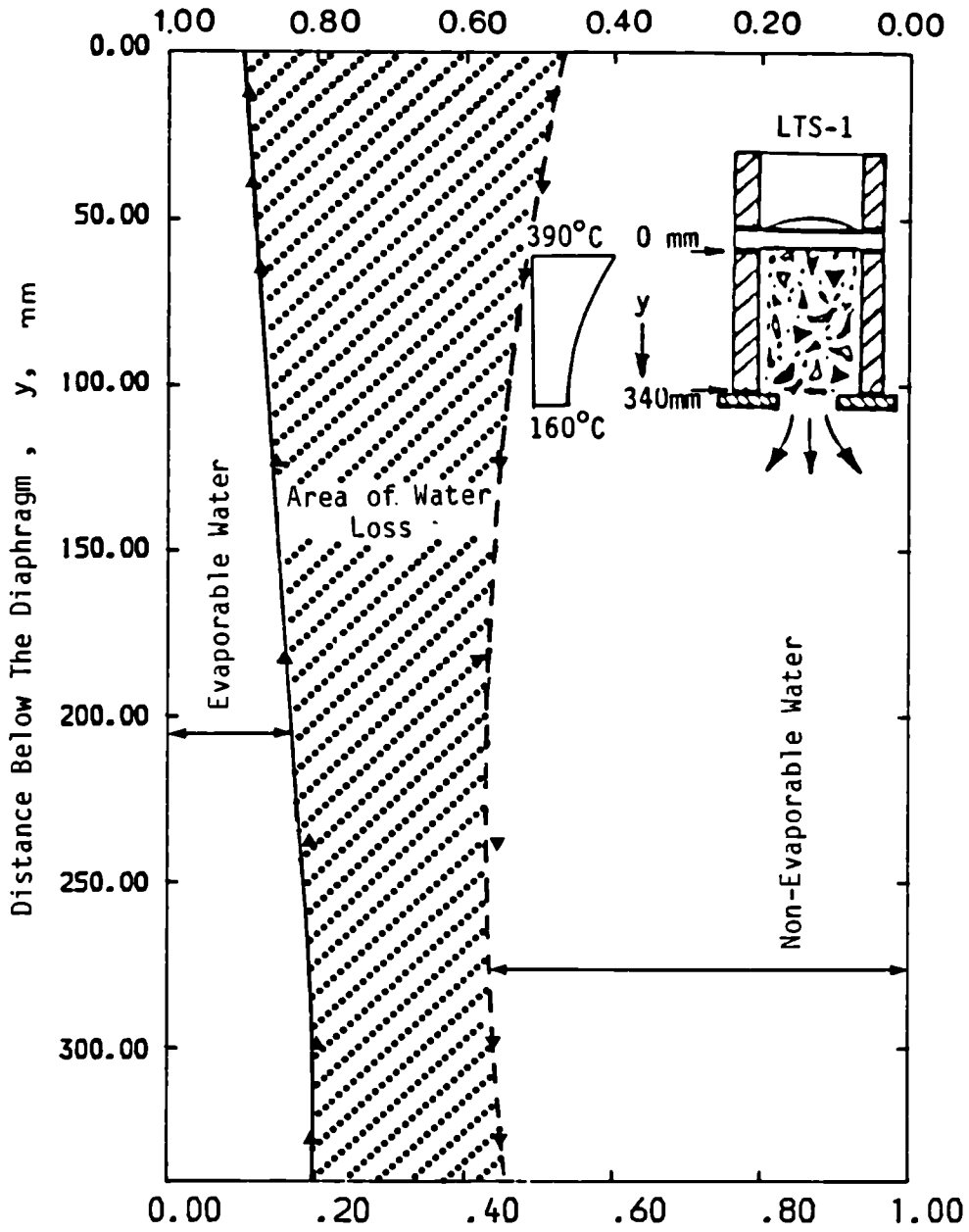

W_e/W_t: Weight of Evaporable Water Per Unit Weight of Mix Water

Note: Time from start of heating 342 minutes.

Figure 5.98:

Phase Diagram for Water obtained by Gravimetric Measurements Specimen No: LTS-1

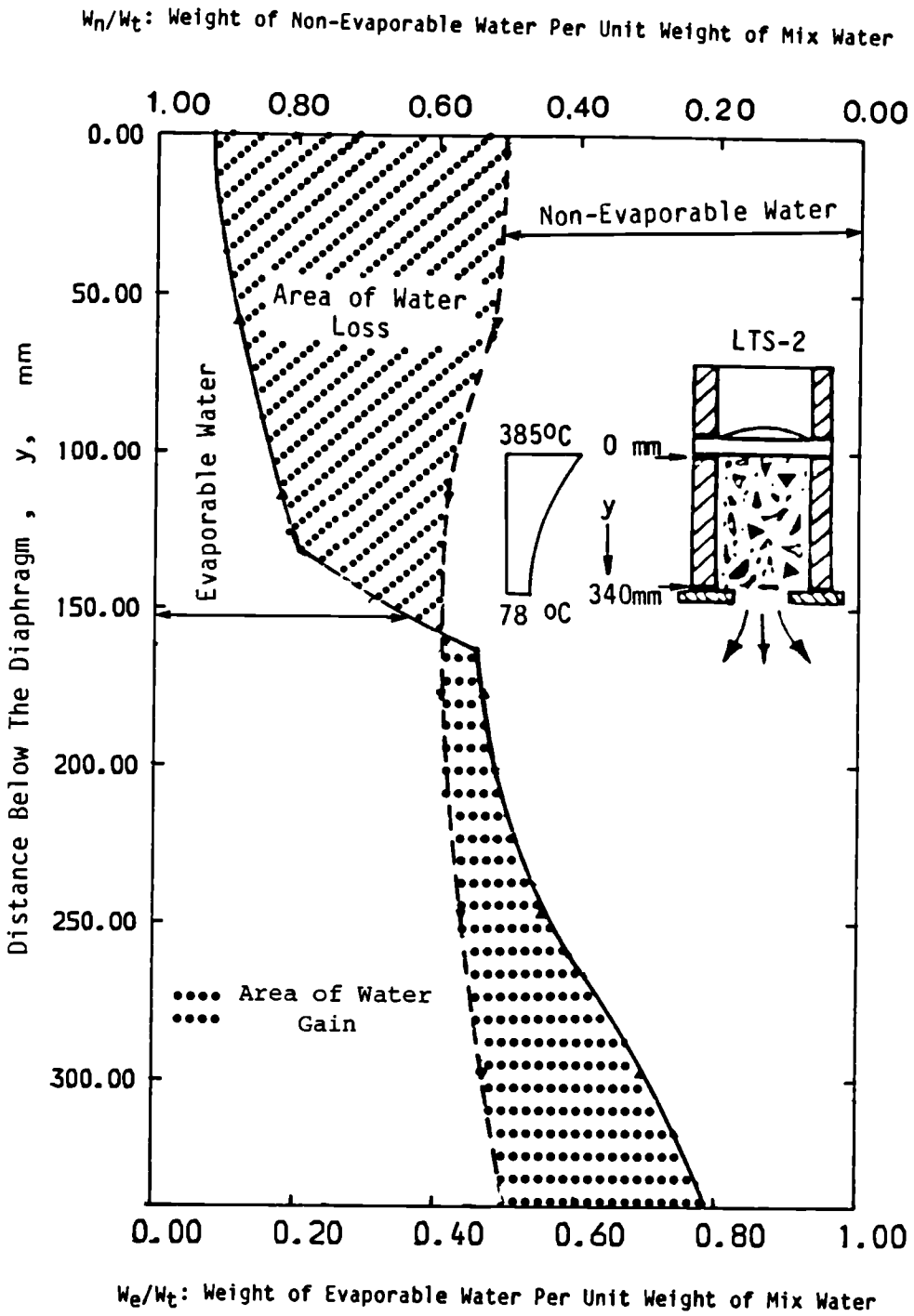

Note: Time from start of heating 87 minutes.

Figure 5.99:

Phase Diagram for Water obtained by Gravimetric Measurements Specimen No: LTS-2

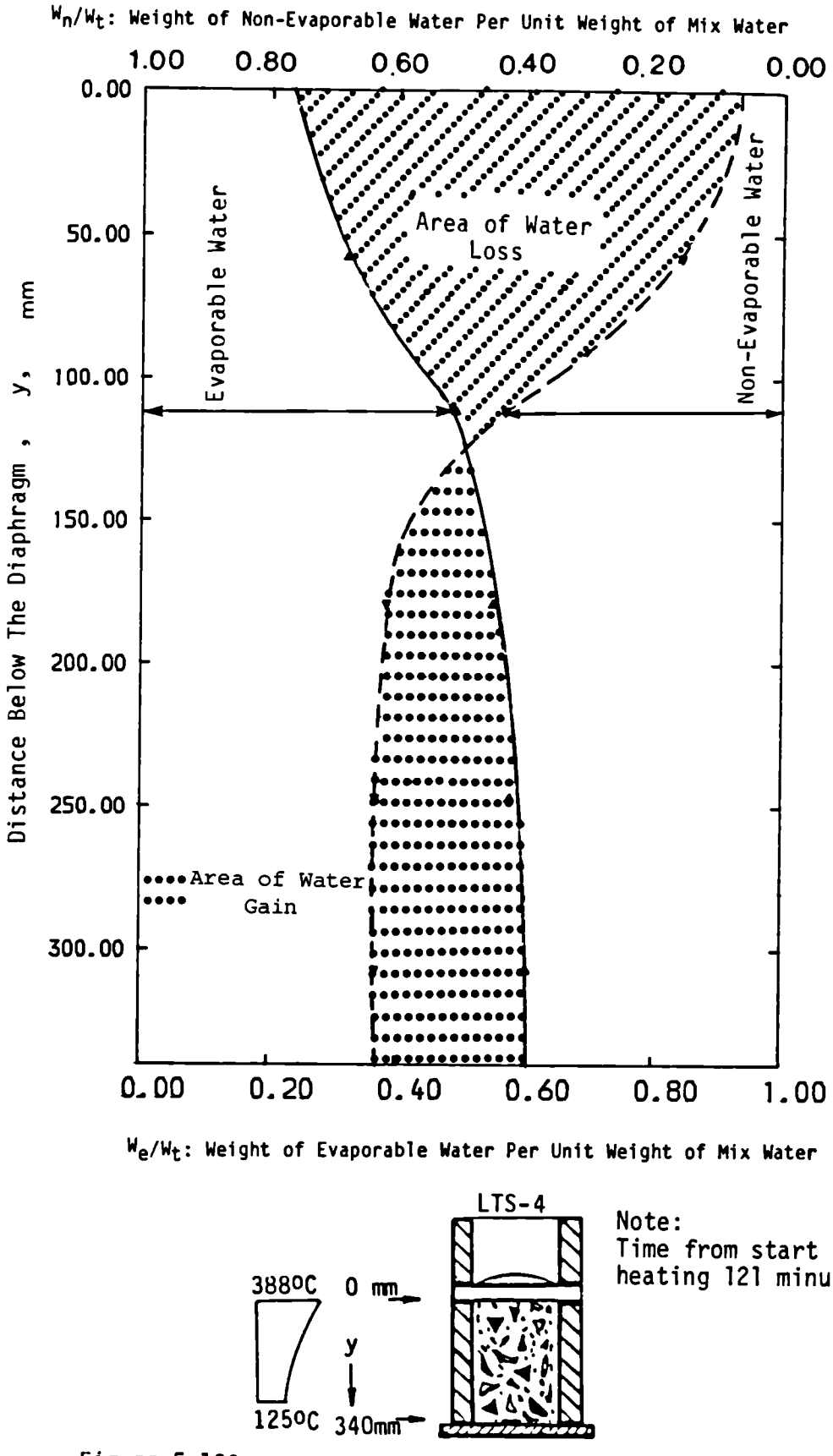

Figure 5.100:

Phase Diagram for Water obtained by Gravimetric Measurements Specimen No: LTS-4

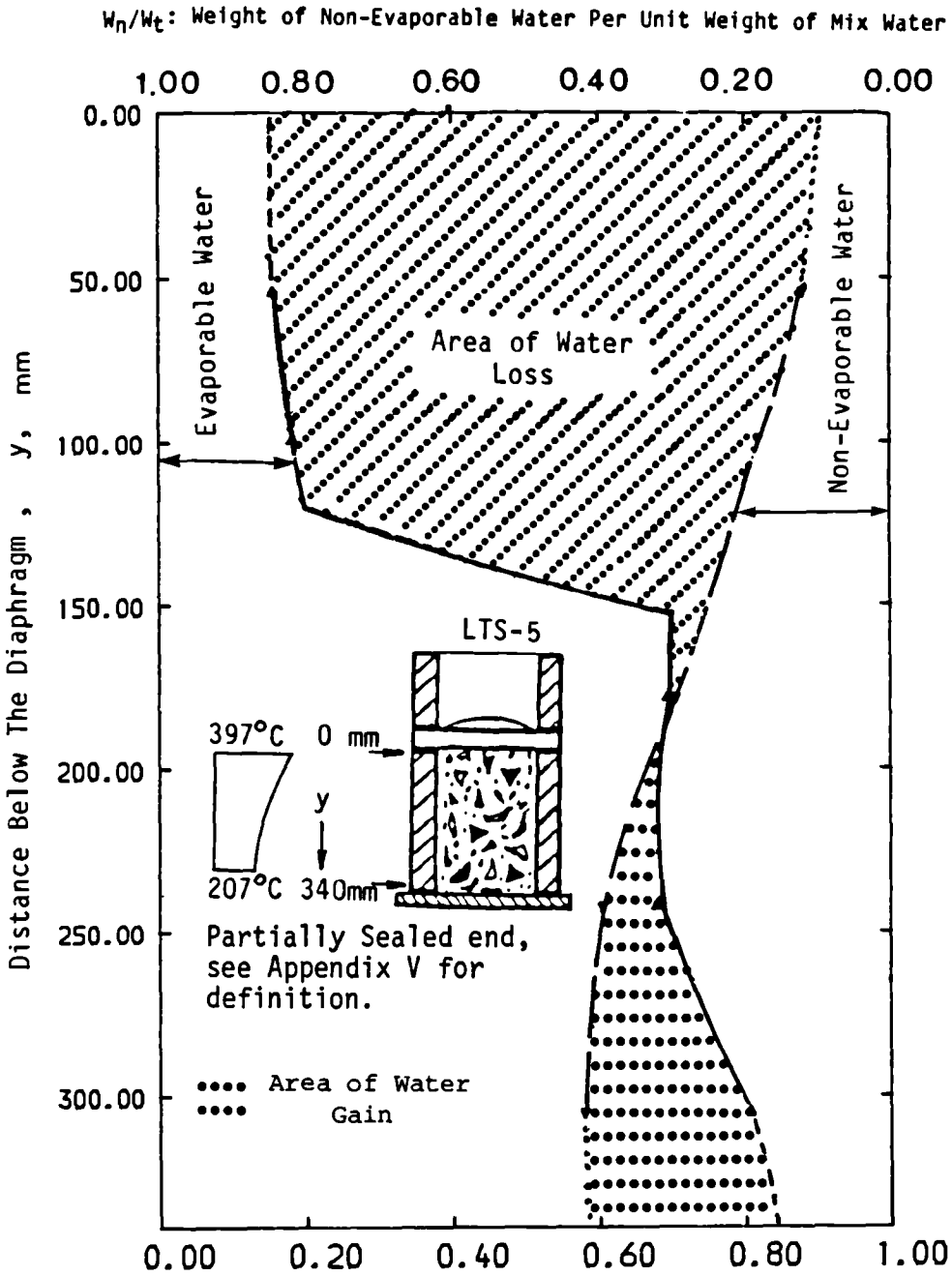

Note: Time from start of heating 729 minutes.

Figure 5.101:

Phase Diagram for Water obtained by Gravimetric Measurements Specimen No: LTS-5

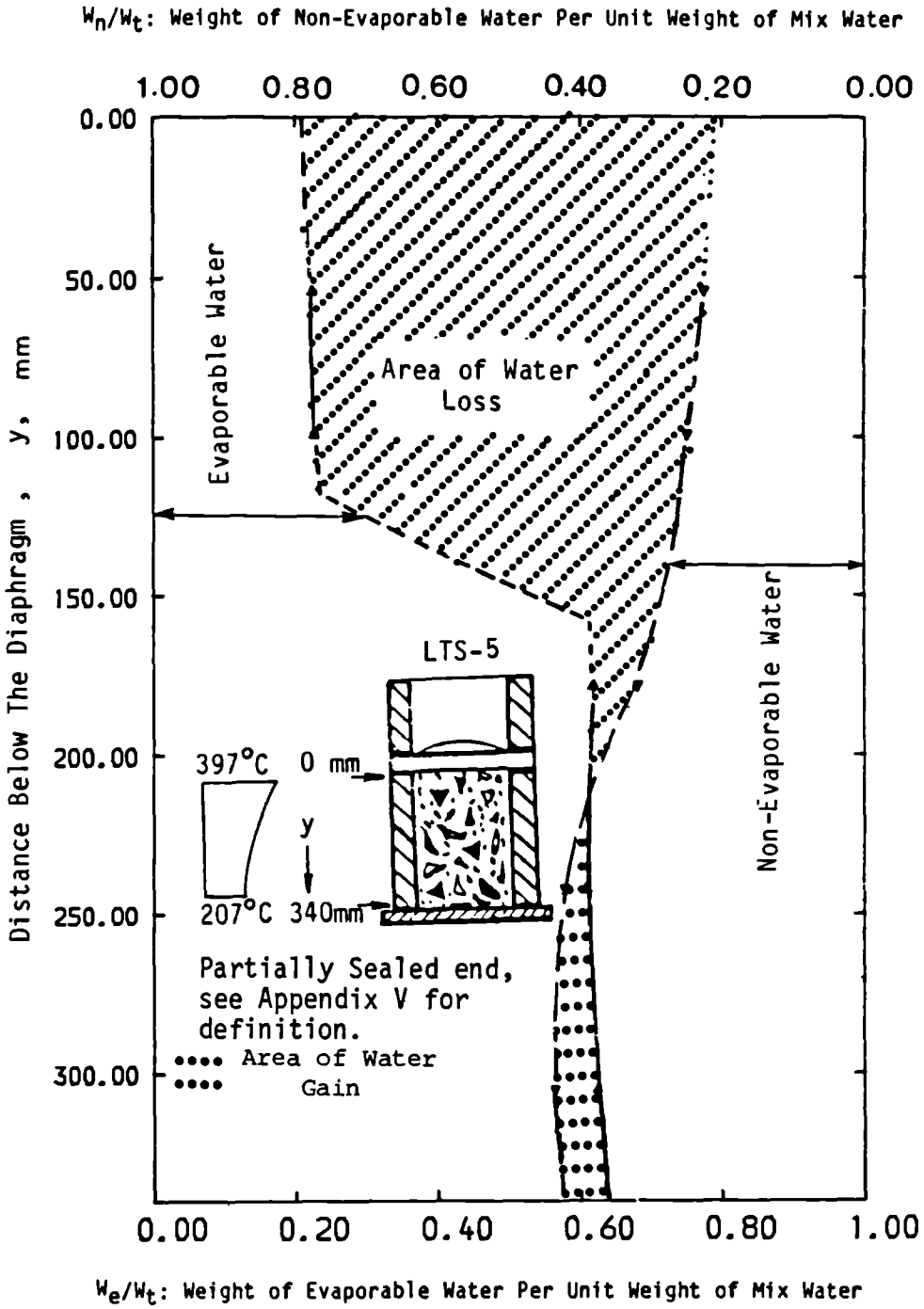

Note: Time from start of heating 729 minutes.

Figure 5.102:

Phase Diagram for Water obtained by Gravimetric Measurements Specimen No: LTS-5

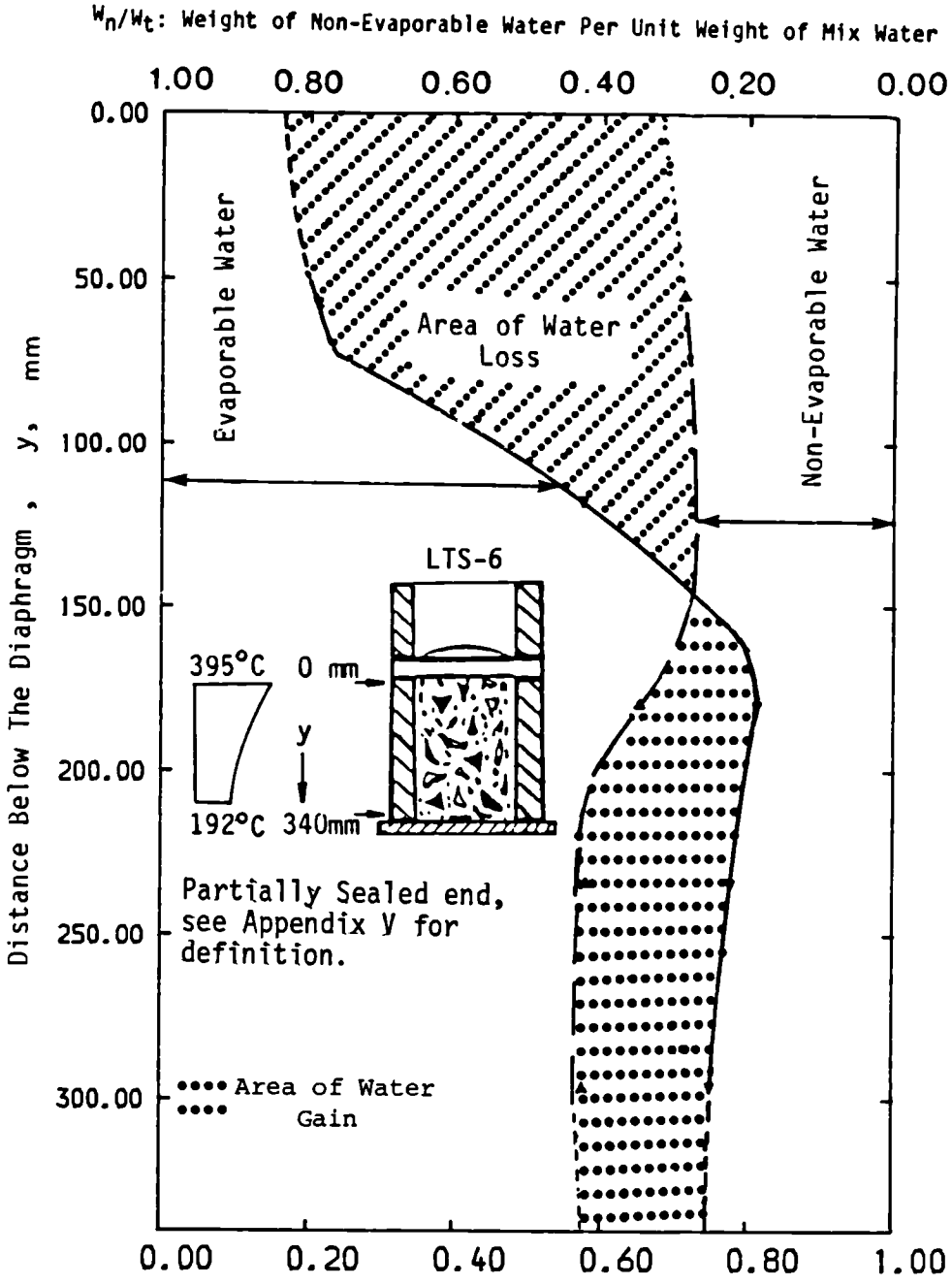

Note: Time from start of heating 270 minutes.

Figure 5.103:

Phase Diagram for Water obtained by Gravimetric Measurements Specimen No: LTS-6

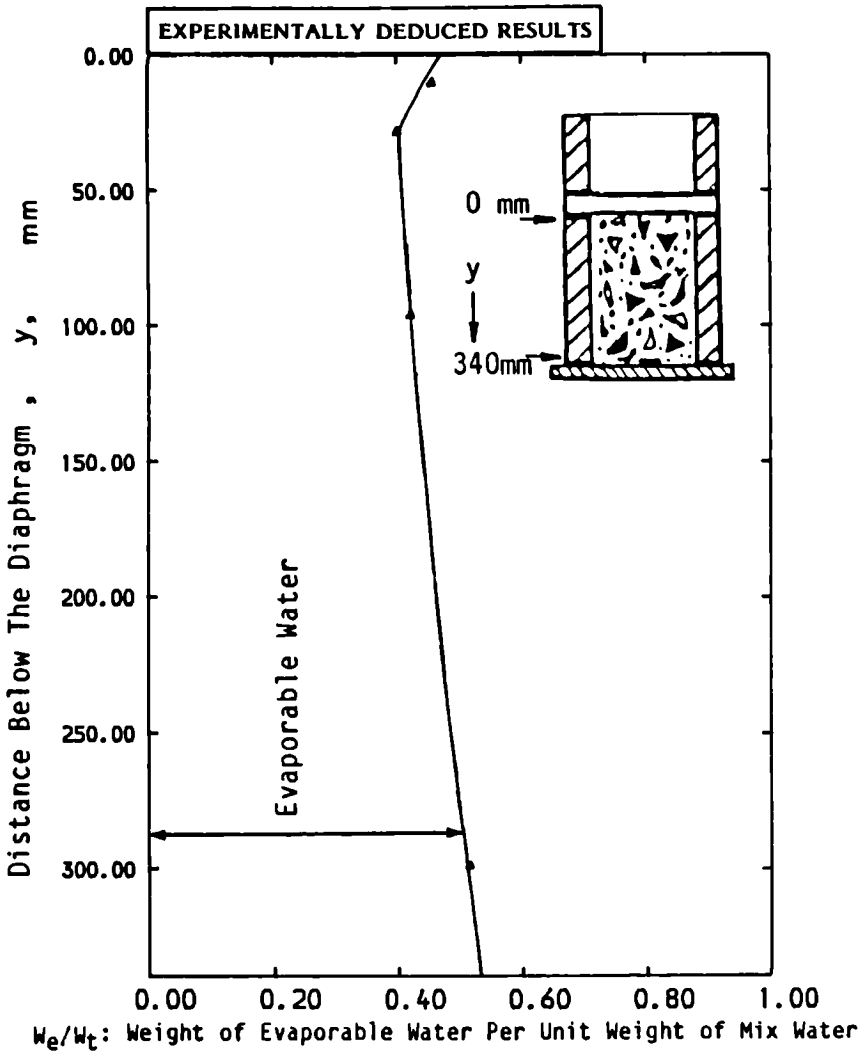

Figure 5.104:
Evaporable Water Distribution obtained by Gravimetric Measurements - Unheated Specimen

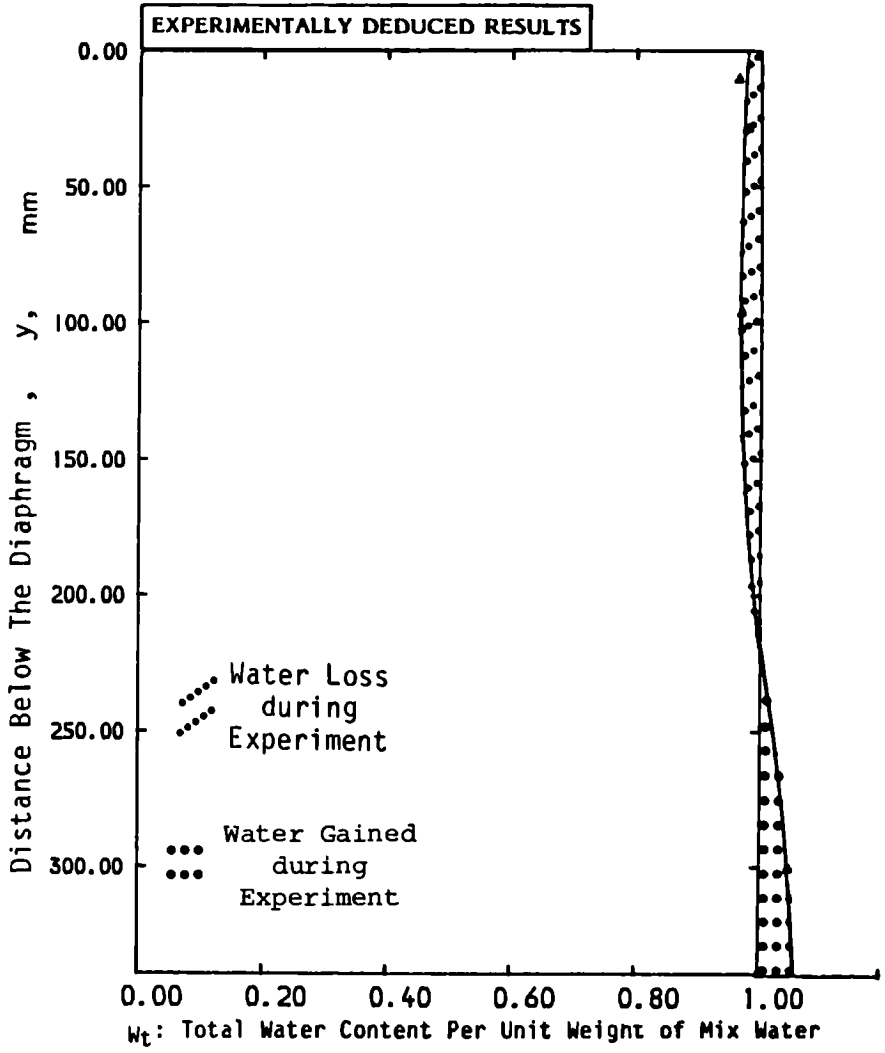

Figure 5.105:
Total Water Content Distribution obtained by Gravimetric Measurements - Unheated Specimen

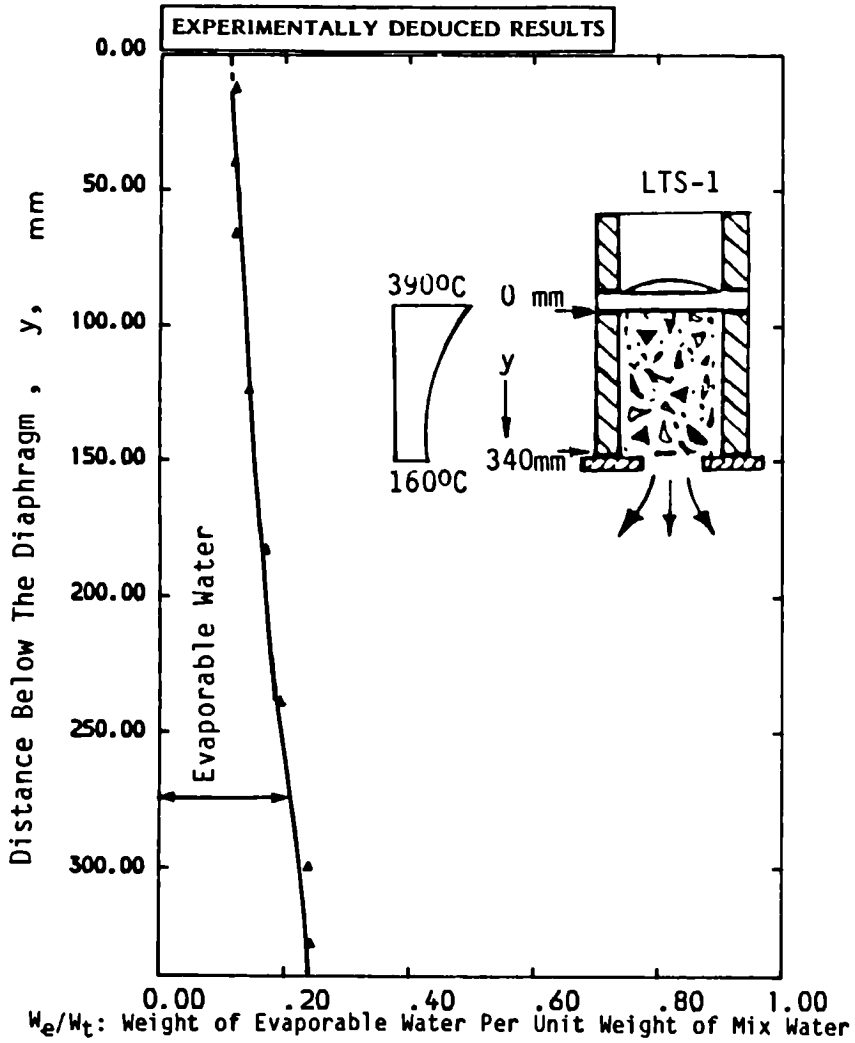

Figure 5.106:
Evaporable Water Distribution obtained by Gravimetric Measurements - Specimen No: LTS-1

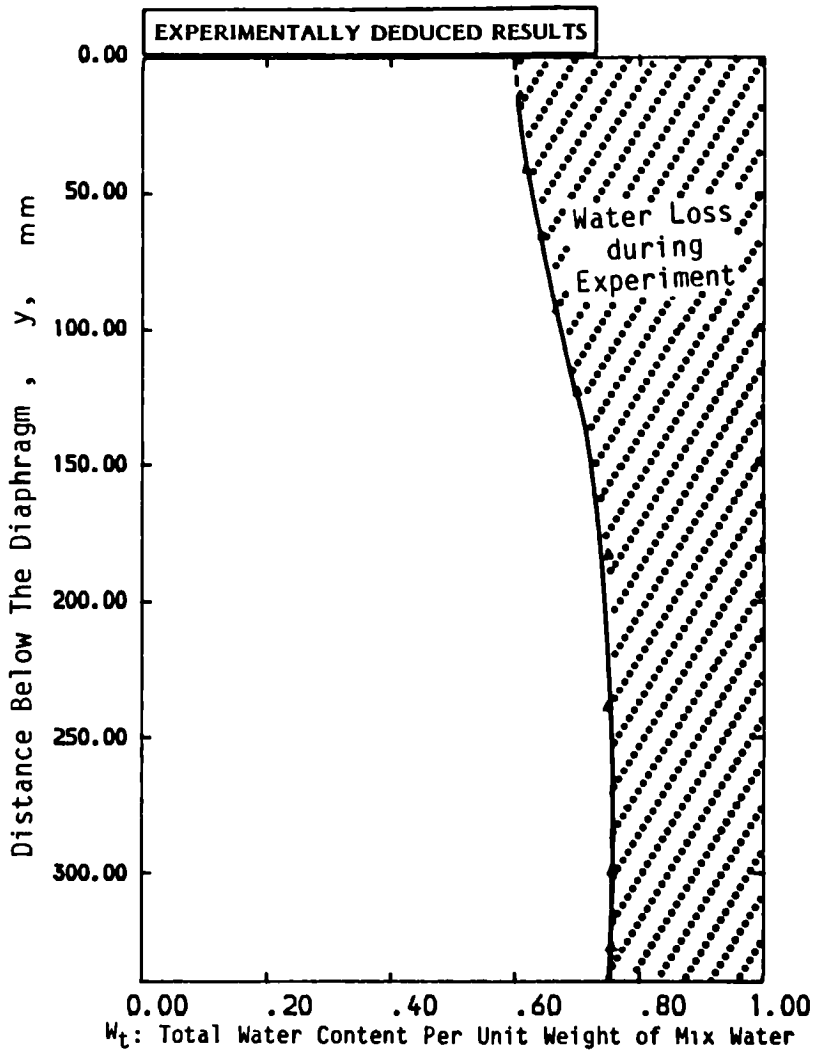

Figure 5.107:
Total Water Content Distribution obtained by Gravimetric Measurements - Specimen No: LTS-1

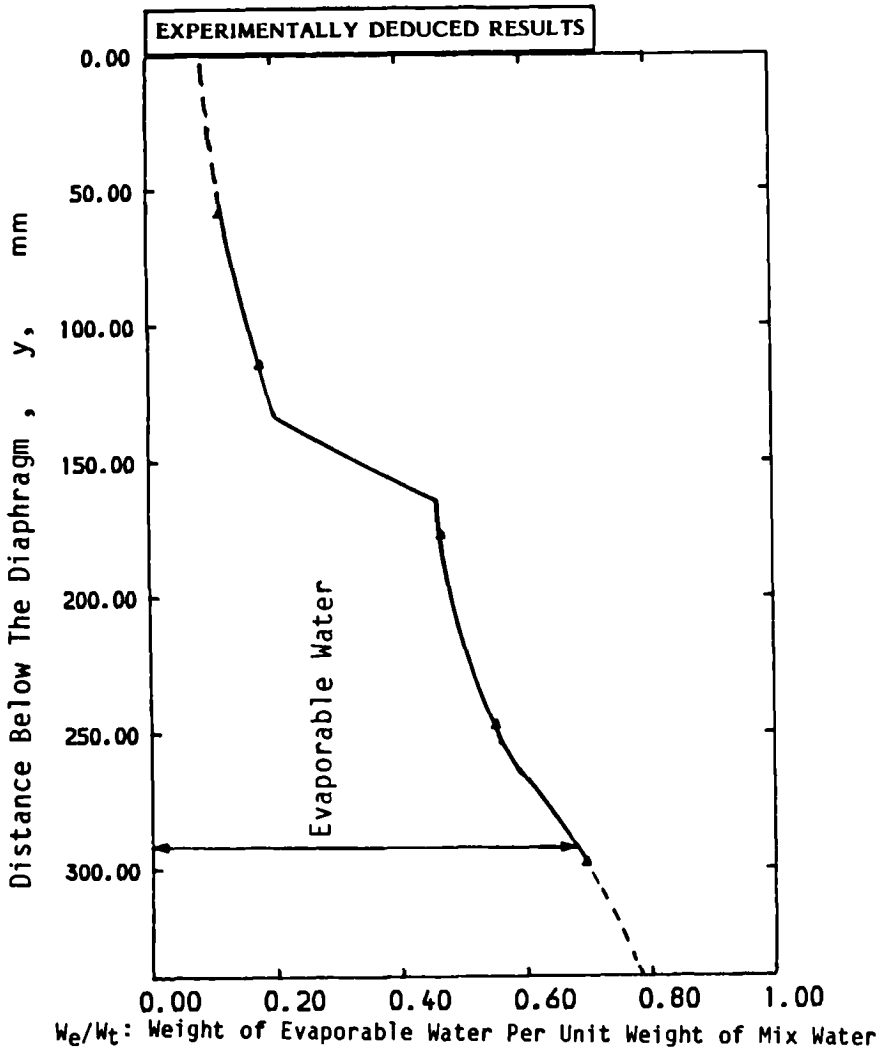

Figure 5.108:

Evaporable Water Distribution obtained by Gravimetric Measurements Specimen No: LTS-2

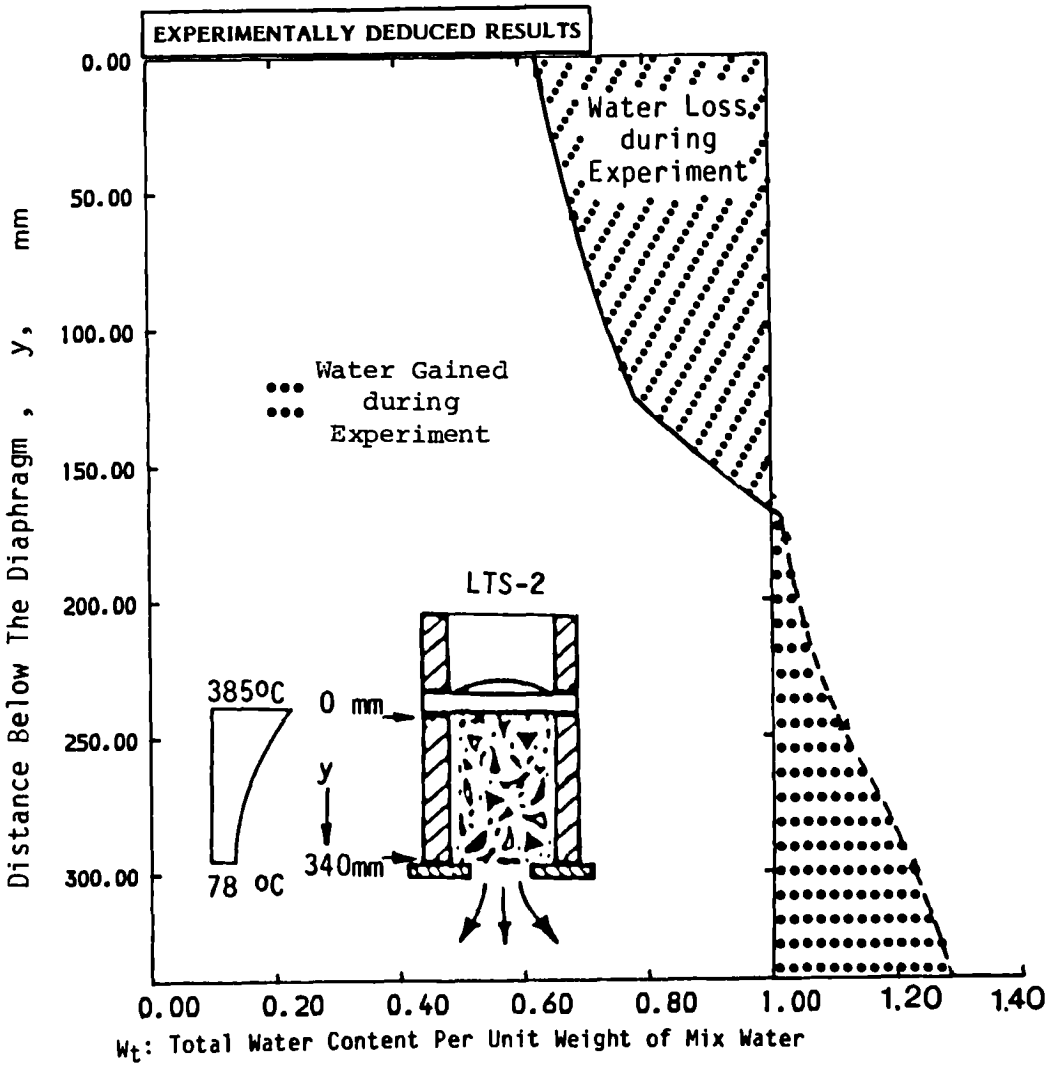

Figure 5.109:

Total Water Content Distribution obtained by Gravimetric Measurements Specimen No: LTS-2

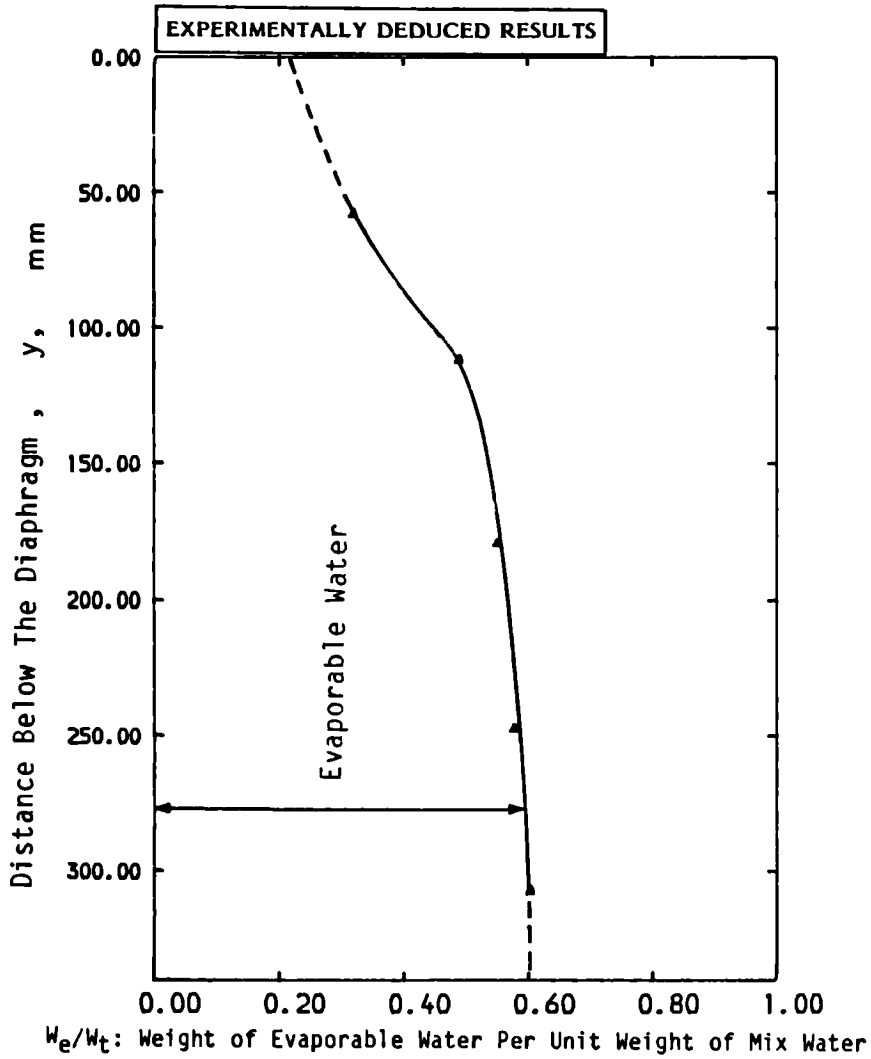

Figure 5.110:

Evaporable Water Distribution obtained by Gravimetric Measurements Specimen No: LTS-4

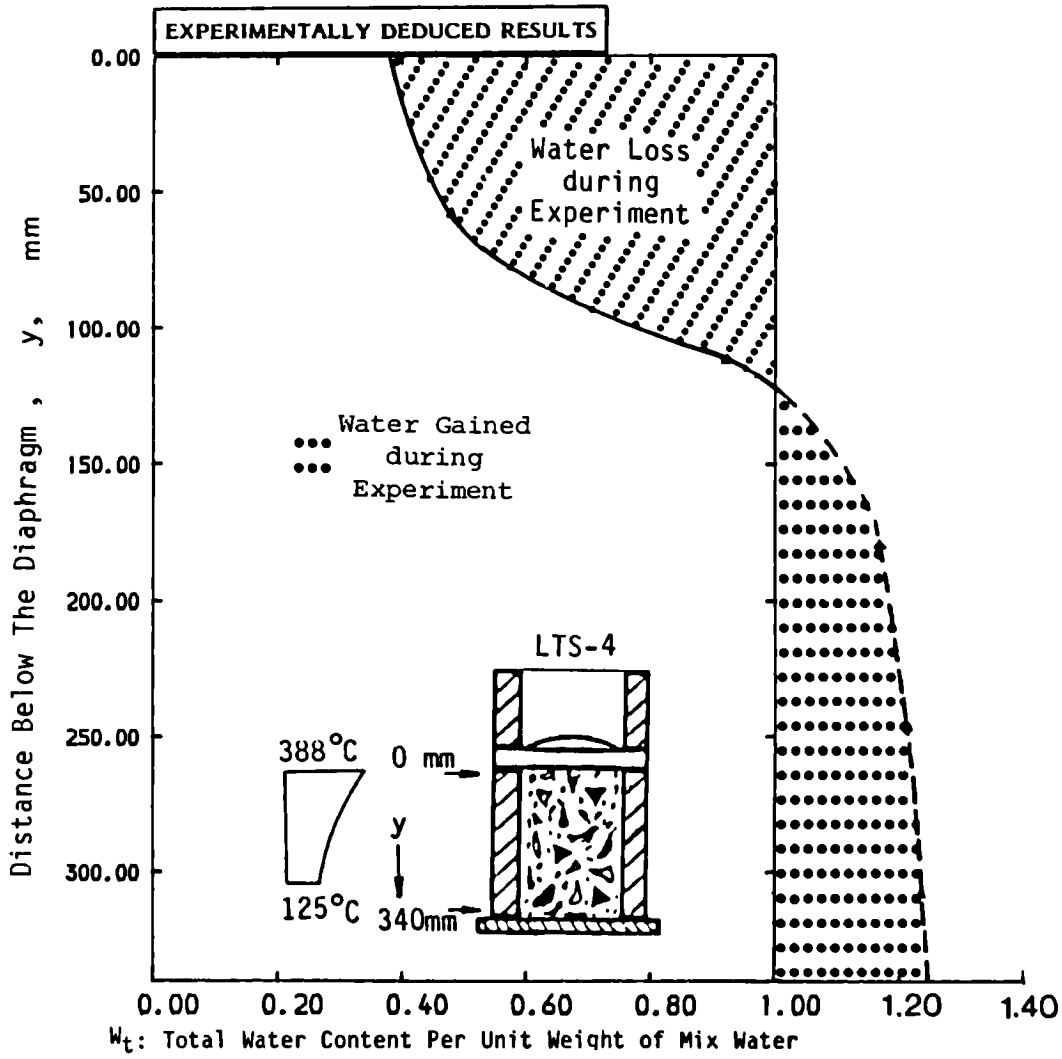

Figure 5.111:

Total Water Content Distribution obtained by Gravimetric Measurements Specimen No: LTS-4

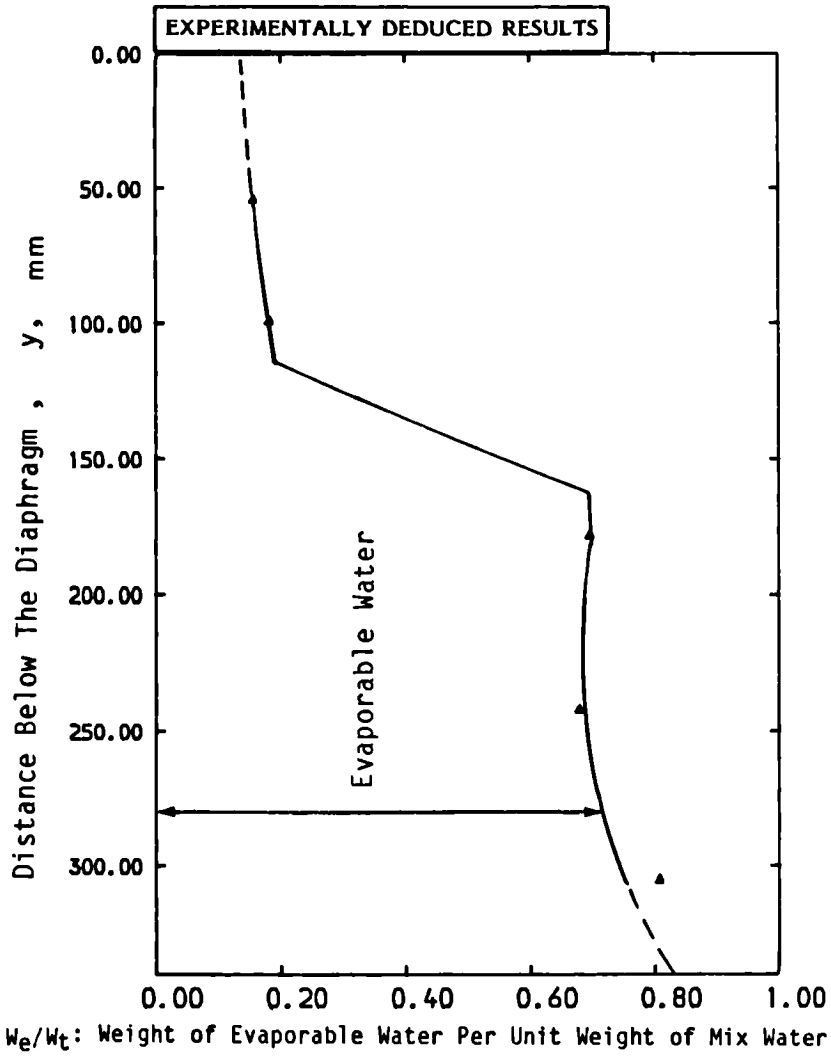

Figure 5.112:

Evaporable Water Distribution obtained by Gravimetric Measurements Specimen No: LTS-5

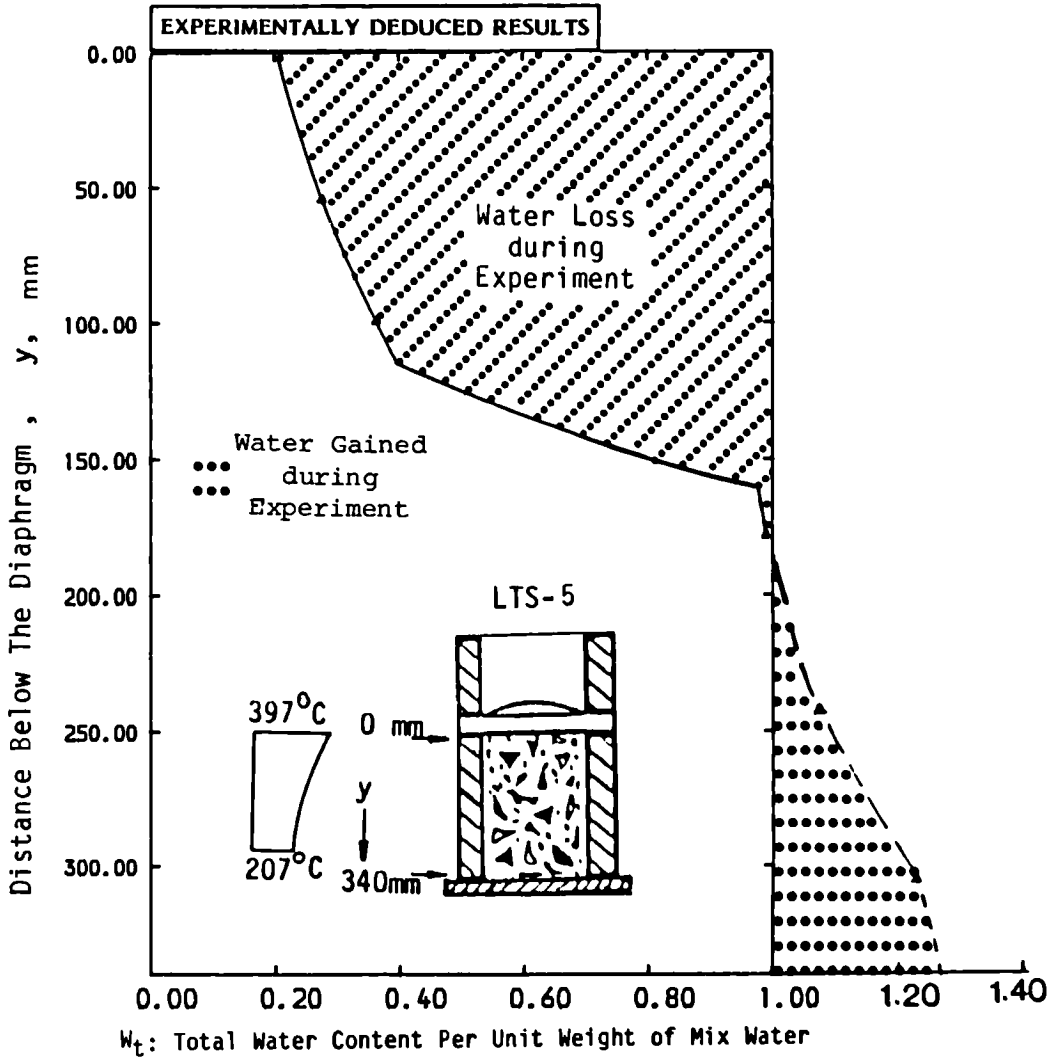

Figure 5.113:

Total Water Content Distribution obtained by Gravimetric Measurements Specimen No: LTS-5

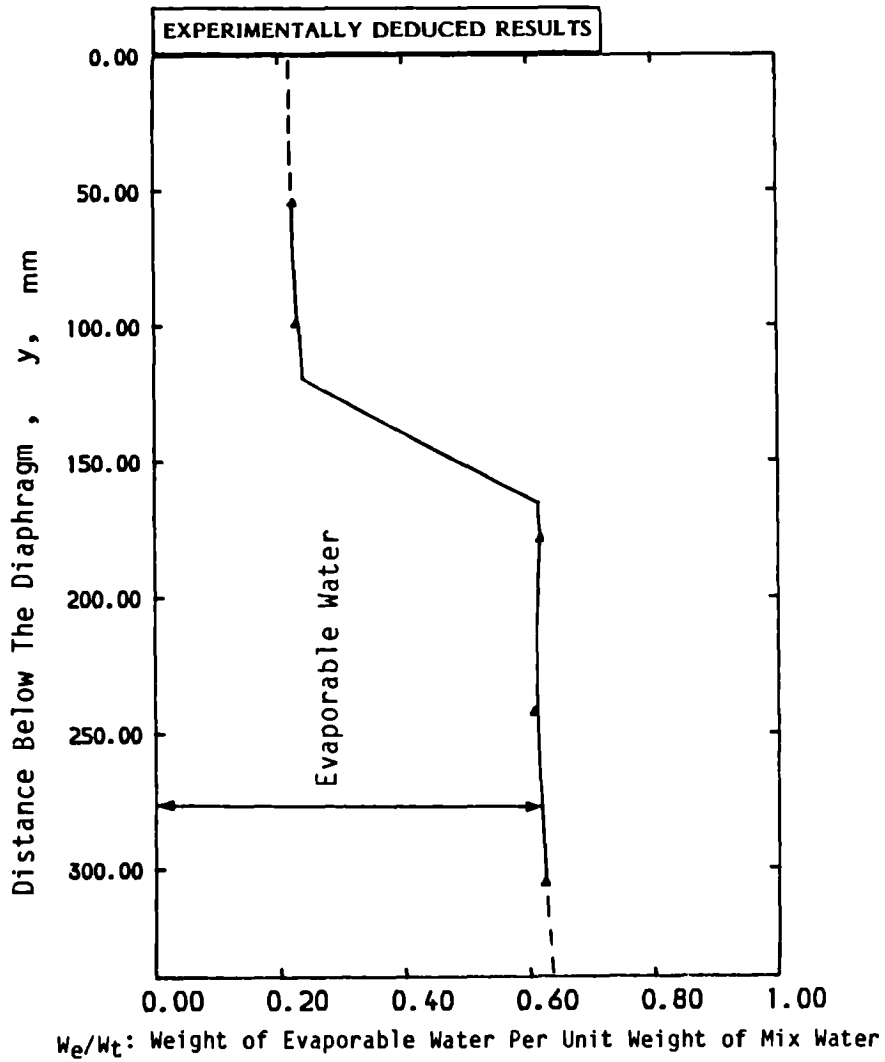

Figure 5.114:
Evaporable Water Distribution obtained by Gravimetric Measurements - Specimen No: LTS-5

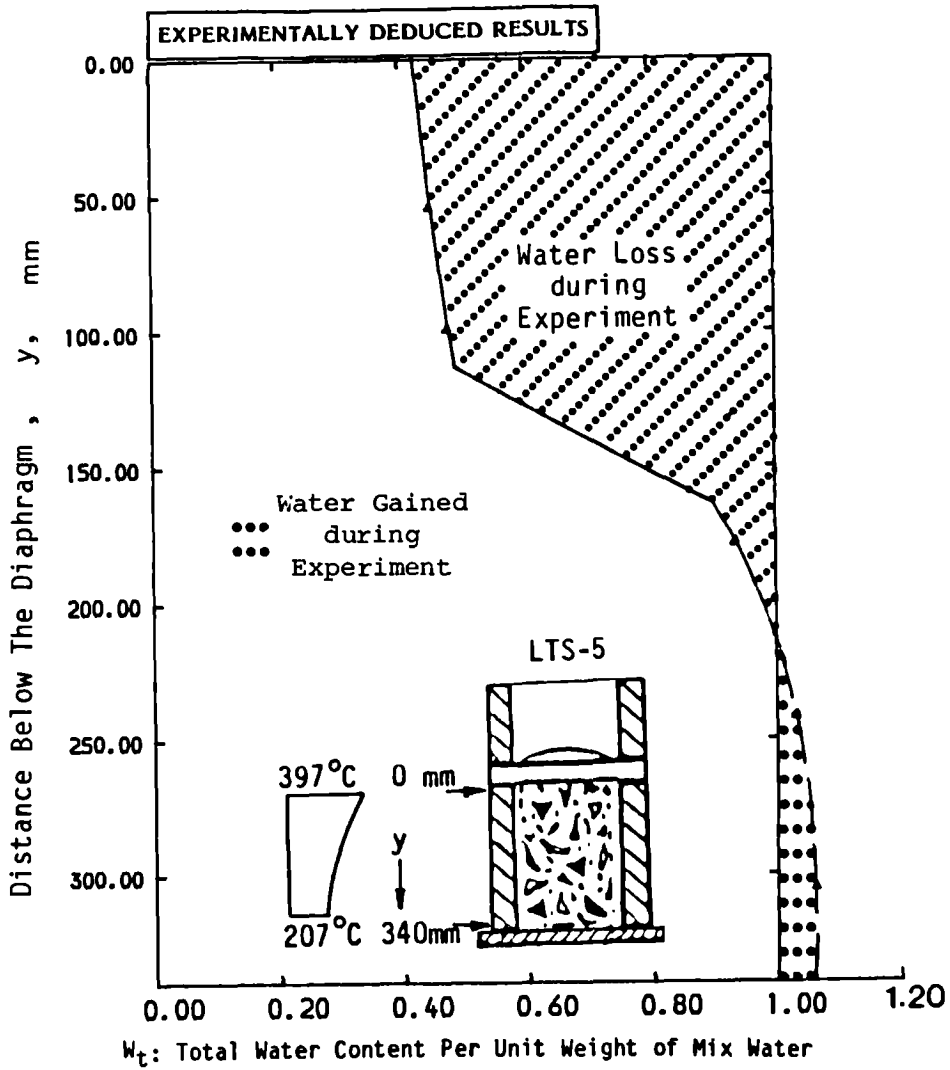

Figure 5.115:
Total Water Content Distribution obtained by Gravimetric Measurements - Specimen No: LTS-5

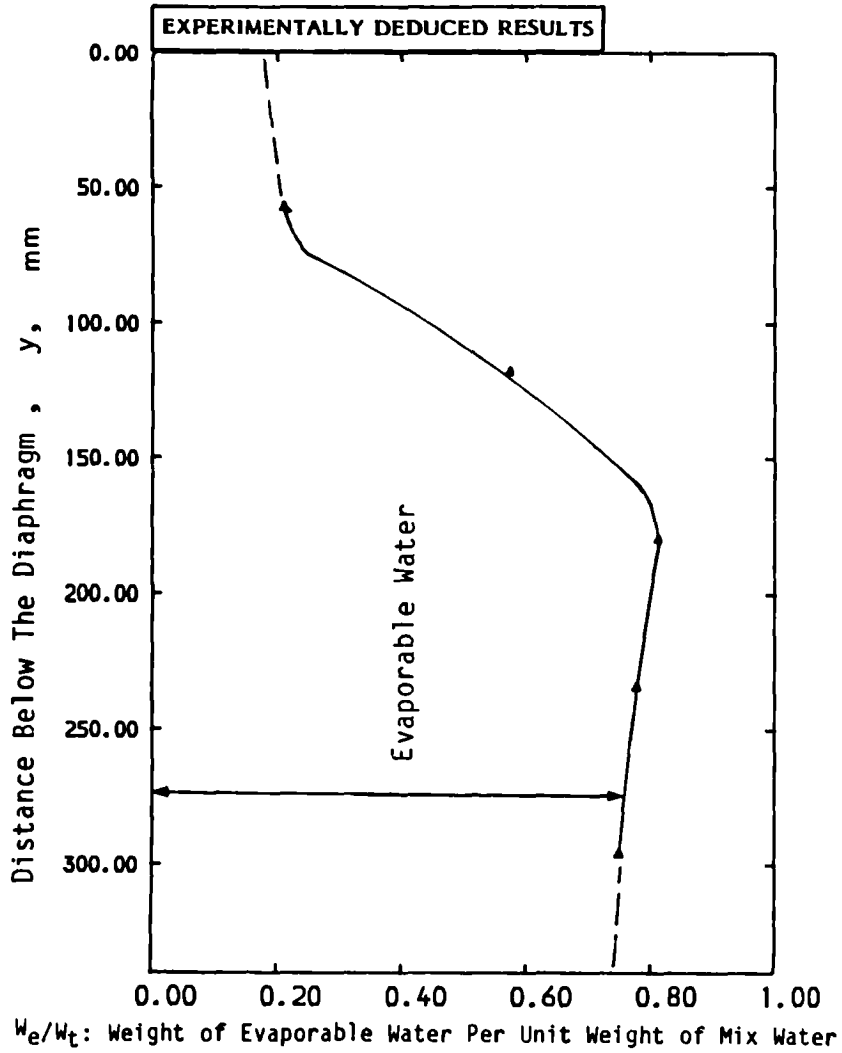

Figure 5.116:

Evaporable Water Distribution obtained by Gravimetric Measurements Specimen No: LTS-6

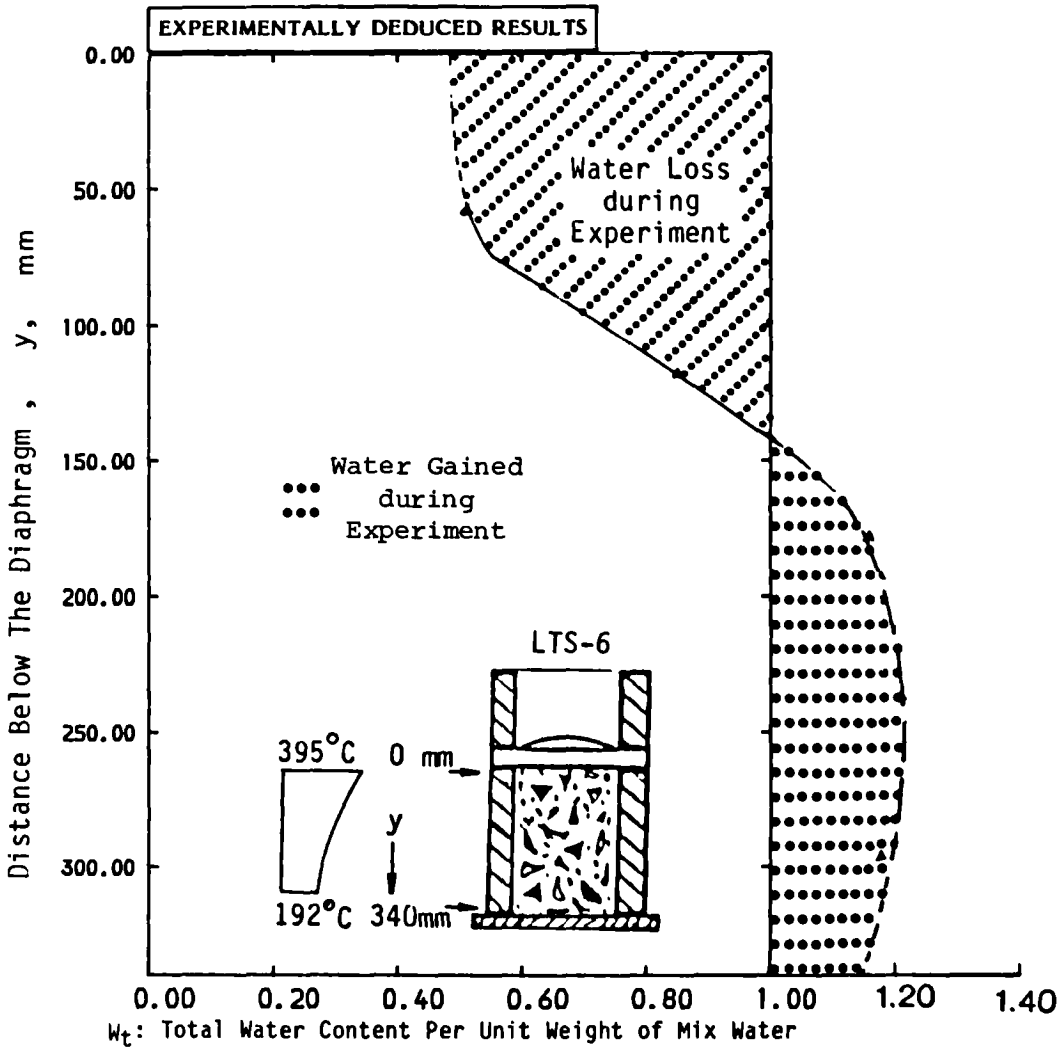

Figure 5.117:

Total Water Content Distribution obtained by Gravimetric Measurements Specimen No: LTS-6

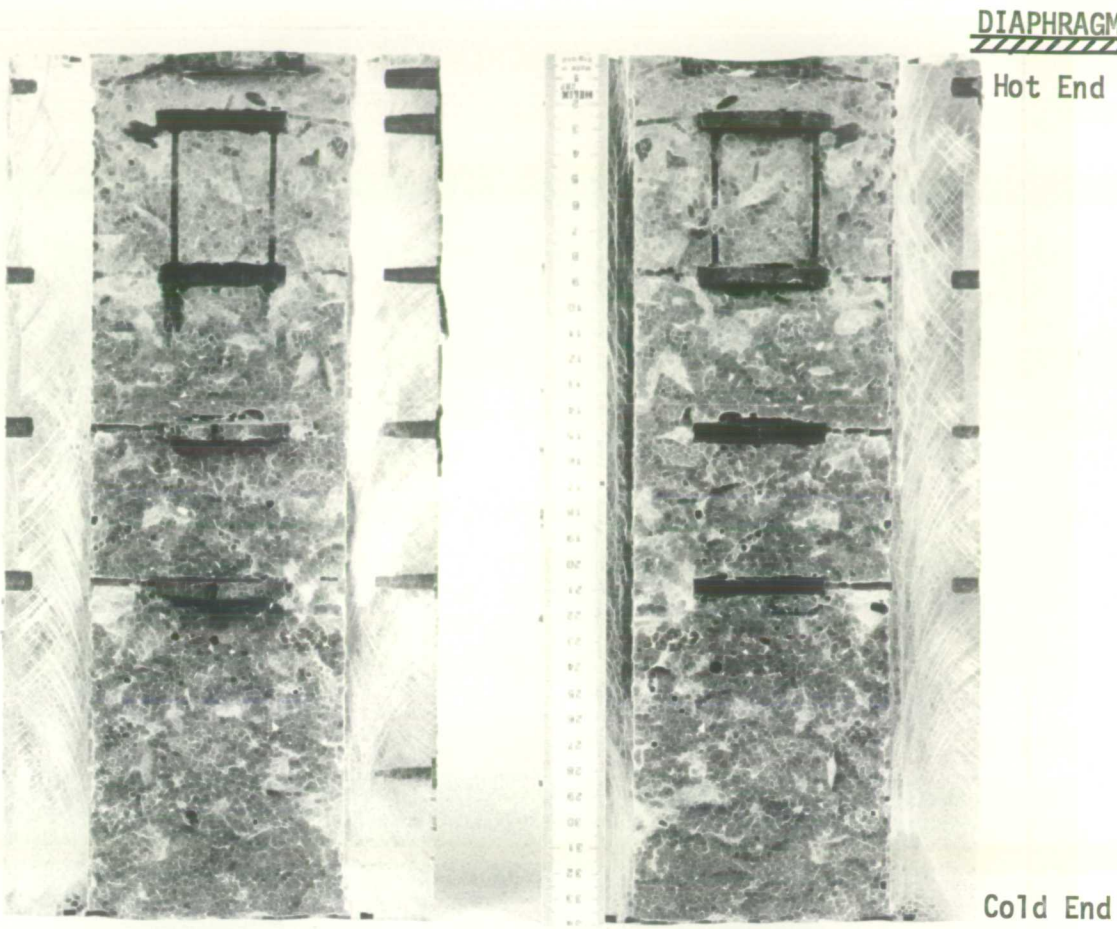

PLATE 5.1: LTS-4 SPECIMEN AFTER SPLITTING FOR GRAVIMETRIC MEASUREMENTS

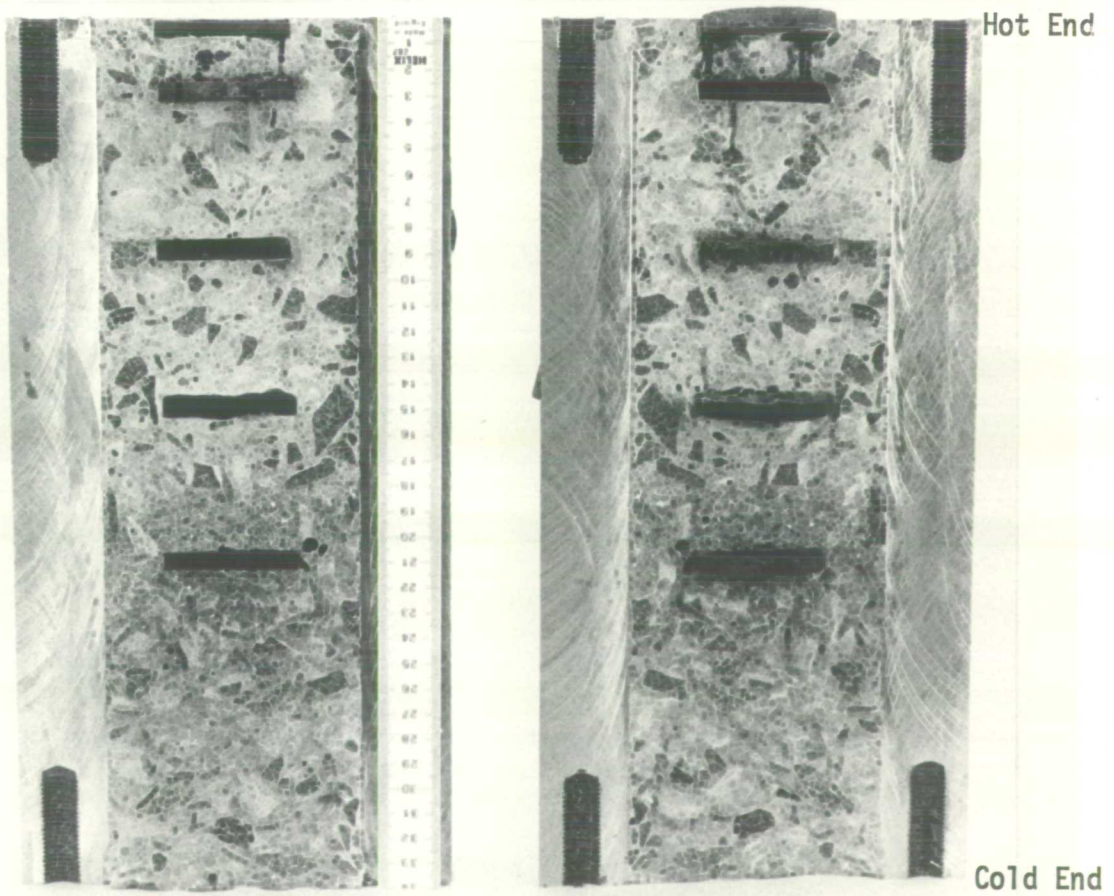

PLATE 5.2: LTS-5 SPECIMEN AFTER SPLITTING FOR GRAVIMETRIC MEASUREMENTS

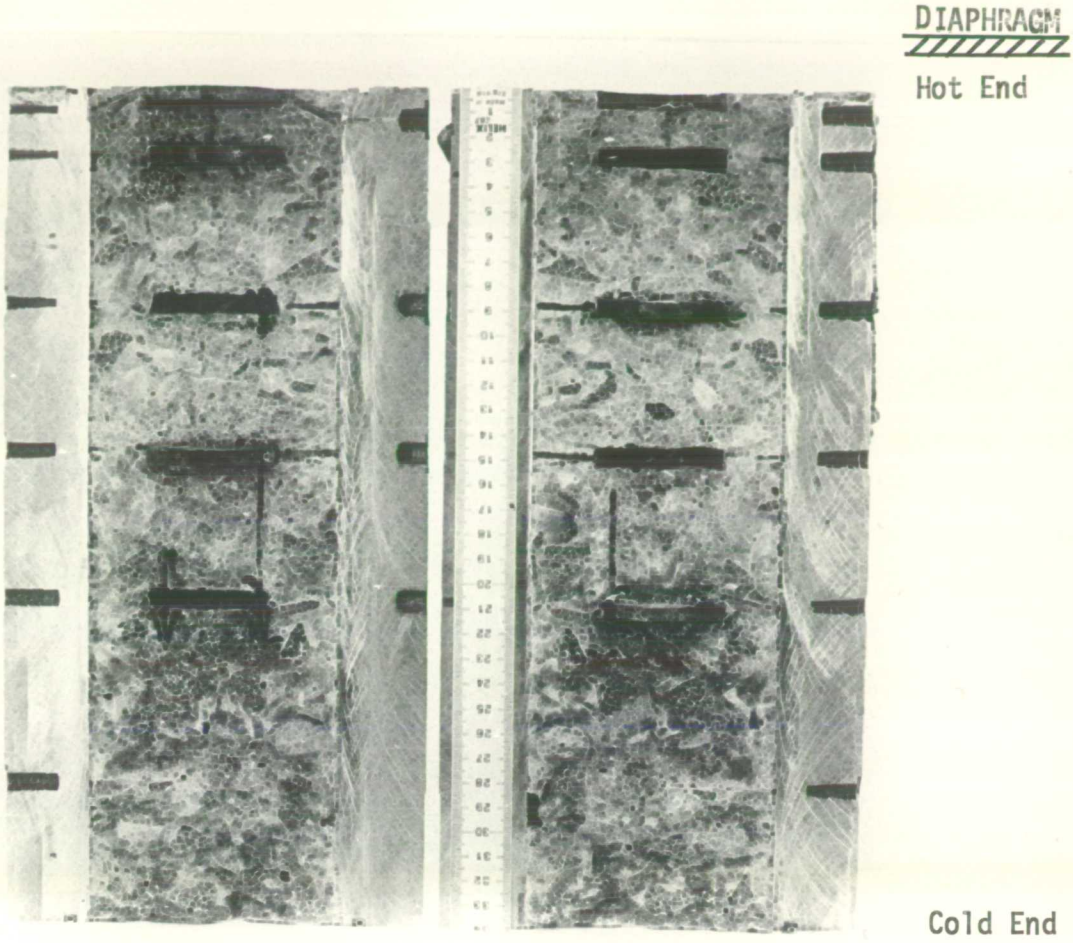

PLATE 5.3: LTS-6 SPECIMEN AFTER SPLITTING FOR GRAVIMETRIC MEASUREMENTS

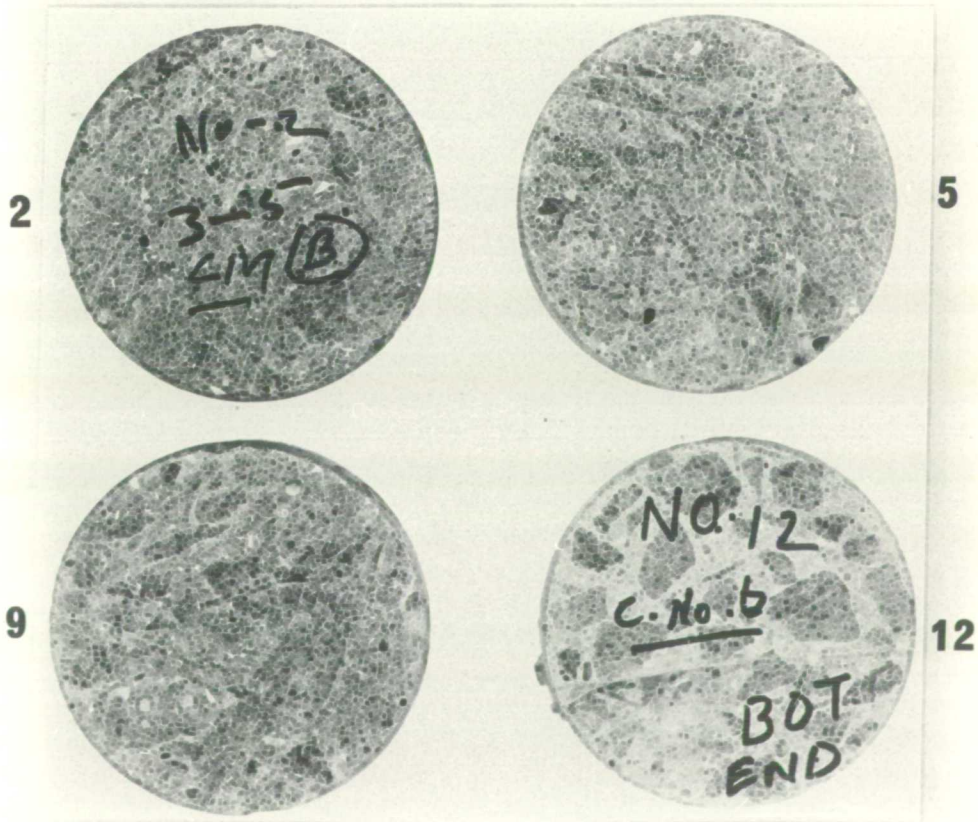

PLATE 5.4: SLICES CUT FROM LTS-1 CONCRETE SPECIMEN (PLATE 3.15)

CHAPTER 6

"RELEASE TEST SERIES"

Note: Figures for this chapter are appended at the end of the text.

6.1 INTRODUCTION AND OBJECTIVES

The "Release Test Series" ("RTS") was designed to monitor the pore pressure developed in sealed concrete heated to uniform temperatures. The seal of each sample was periodically broken and fluid was allowed to escape. The weight of the sample was recorded before and after performing each release operation. The test was concluded when no more weight could be lost at the test temperature. The main objectives of the test were:

1. To analyse the relationship between temperature and pore pressure of concrete heated to a constant temperature in 'as cast' condition;

2. To study the effects of moisture loss on the pore pressure/temperature relationship in concrete.

The design, construction, casting and testing procedures are discussed in detail in Chapter 3 and Appendix II. Chapter 4 describes the instrumentation. The concrete used for the "RTS" was identical to the concrete used for the "Liner Test Series" (see Chapter 3, Section 3.2 for mix details).

Table 6.1 lists the testing conditions and specimen coding used for this series.

SPECIMEN NO.	TEST TEMPERATURE ^{o}C	TEST AGE (days)	TEST DESCRIPTION
PT-1&2			Pilot Tests
CT-1	105,250,275,300,325	409	Control Test
CT-2	342,350,400	1182	Control Test
RTS-01	300	390	Actual Test
RTS-02	342	380	// //
RTS-03	250	1200	// //
RTS-04	275	1208	// //
RTS-05	300	1215	// //
RTS-06	325	1222	// //
RTS-07	350	1230	// //

Table 6.1: Specimen coding and detail of all the tests for "RTS".

The test categories listed in Table 6.1 are discussed below:

6.1.1 PILOT TESTS

Specimens PT-1 and PT-2 were used for checking, developing and finalising the integrity of the test cells and their instrumentation.

6.1.2 CONTROL TESTS

Specimens CT-1 and CT-2 were used as control tests for the determination of evaporable and non-evaporable water contents over a range of temperatures; see Section 6.3.1.

6.1.3 RELEASE TESTS

RTS-01 to RTS-07 formed the main release test programme at six temperatures (Table 6.1) and two average ages (393 and 1209 days).

The results are represented in Figures 6.1 to 6.14 for the influence of temperature and Figure 6.15 for the effect of age.

Similar experiments have been reported by other researchers, Sharp (1971) and Chapman (1976). The main features of their tests were:

a. Sharp (1971):
- his concrete contained flint aggregate
- the age of the concrete at testing was only 41 days
- the maximum test temperature was 150 ^{o}C.

b. Chapman (1976):
- the aggregate used by him was limestone
- the concrete was tested for average ages of 49 and 365 days
- the test temperatures were: 105, 125, 150 and 175 ^{o}C.

These studies have been reviewed in Chapter 2.

6.2 TEST PROCEDURE AND PURPOSE OF THE TESTS

The test procedure is described in Chapter 3, Section 3.4.7. However, a brief description of the procedure and the purpose of the tests are outlined below.

6.2.1 TEST PROCEDURE FOR RELEASE TESTS

1. The specimen was weighed after removing it from the curing room, to see if weight was lost during the curing period.

2. The specimen was prepared (Chapter 3, Section 3.4.6) and placed in the furnace and the furnace was switched on.

3. The variations of temperature and pore pressure with time were recorded.

4. To check if any weight was lost from the specimen during its heating period, the specimen was quickly removed from the furnace on reaching the test temperature. It was weighed and again quickly replaced in the furnace.

5. The test parameters described in (3) above were recorded again.

6. On attaining the steady-state conditions (when pressure was constant with time), the release valve was opened for a short time inside the furnace and moisture in the form of air and steam was allowed to escape.

7. The specimen was quickly removed again from the furnace, weighed and replaced in the furnace.

8. The records were made of the time taken to release moisture and the time taken for the weighing procedure.

9. The procedure described (in 3 to 8) above was repeated until it became difficult to obtain a weight loss at the test temperature, by leaving the release valve open for aproximately a minute. At this stage the test temperature was cycled by $\pm 10\ ^{o}C$ to obtain the pore pressures.

10. The test was considered to be complete when no weight was lost after leaving the release valve open for more than an hour.

11. The furnace was switched off and the test cell was left in the furnace to cool, before the extraction of the concrete sample for

further weight loss measurements at the test temperature (Chapter 3, Section 3.4.8).

6.2.2 PURPOSE OF RELEASE TESTS

The Release Tests allowed the following observation and records to be made for each selected test temperature:

1. The magnitude of pore pressure on heating, for comparison with the svp of water at the same temperature (for unsaturated concrete containing air and free water the observed pressure can exceed the svp).

2. The pressure/temperature characteristics of the concrete; for a small fluctuation of temperature ($\pm$ 10 ^{o}C) around the test temperature, at a range of different water contents after periodic controlled releases of water vapour and air.

3. The controlled moisture loss characteristics of concrete at constant temperature and the relationship between moisture loss and pore water pressure at constant temperature.

6.2.3 TEST PROCEDURE AND PURPOSE OF CONTROL TESTS

The purpose was twofold as described below along with the test procedure:

1. To determine the evaporable water content by drying to constant weight at a temperature of 105 ^{o}C. The concrete specimen was removed from its steel jacket to enable drying to take place inside an oven.

2. To determine the non-evaporable water content corresponding to each temperature (Table 6.1), by additional weight loss measurements at each of a range of successively increased temperatures (held constant until no further weight reduction occurred).

A description of the weight loss measurements and the water contents determined from these is given in Section 6.3.1.

6.3 RESULTS

The experimental results are presented under the following headings:

1. Control Test Results (Section 6.3.1), Figures 6.2 to 6.14 (even numbers only)

2. "Release Test Series" Results (Section 6.3.2), Figures 6.1 to 6.24

These results are then compared with theoretical predictions (Section 6.4) for the behaviour of water in an inert porous material (ipm) when subjected to specific temperature changes; Figure 6.29.

6.3.1 CONTROL TEST RESULTS

Table 6.2 lists the data for the control and release tests.

CONTROL TESTS DATA

TEST DESCRIPTION	TEST AGE (days)	WT. OF MIX WATER (W_t in gm)	WT. OF CEMENTITIOUS MATERIALS (W_c in gm)
CT-1	409	85.31	218.74
CT-2	1182	83.97	215.33

CONTROL TESTS AND "RTS" TESTS RESULTS DEDUCED FROM CONTROL TESTS

TEST TEMPERATURE	WT. OF WATER LOST gm		RATIO OF WT. OF H_2O LEFT TO W_c IN		RATIO OF WT. OF H_2O LEFT TO W_c IN "RTS"*	
^oC	CT-1	CT-2	CT-1	CT-2	CT-1	CT-2
105	51.3	49.5	0.155	0.160	---	---
250	15.9	15.1	0.083	0.089	---	0.081
275	1.2	1.4	0.077	0.083	---	0.080
300	2.7	2.0	0.065	0.069	0.062	0.073
325	1.8	2.2	0.057	0.062	---	0.063
342	1.2	1.0	0.051	0.059	0.050	---
350	0.5	0.6	0.049	0.056	---	0.051

Note: Cementitious Materials represent Cement + Cemsave

* "RTS" values obtained by removing the sealing jacket are deduced from the control tests (CT-1 and CT-2)

Table 6.2: Original data and results for control and release tests.

The control tests were used to formulate the following relationships for evaluating the "RTS" results (i.e. evaporable and non-evaporable water contents, gel and capillary water, theoretical amount of non-evaporable water for 100% hydration and degree of hydration (Section 6.3.2)):

1. By definition, the water lost from concrete at 105 ^{o}C when heated to a constant weight loss, is the evaporable water, and the amount of water retained in the concrete is termed as non-evaporable water.

2. All the "RTS" specimens were tested at temperatures greater than 105 ^{o}C. It was therefore obvious that a portion of non-evaporable water would also be lost from the test specimens along with the evaporable water.

3. One would expect the ratio of the water remaining to the weight of cement left in the control specimen to be the same as the value obtained when the "RTS" specimen was dried to constant weight at the test temperature (after extracting the concrete from the test cell).

4. Knowing the weight of mix water (W_t) and the weight of cementitious materials (W_c, where: W_c = Cement + Cemsave) in both the control specimen and the release test specimen (from the mix proportion), the parameters discussed at the start of this section were obtained by formulating the equations given below.

5. As the weight of mix water (W_t) and the weight of evaporable water (W_e: water given up at 105 ^{o}C) are known from the control tests, the weight of non-evaporable water lost (W_{nl}) in the concrete specimen can be calculated as:

$$W_{nl} = W_t - W_e - W_{nr} \qquad 6.1$$

where:

W_{nl} = weight of non-evaporable water lost at test temperature
W_t = weight of mix water
W_e = weight of water lost at 105 ^{o}C or evaporable water
W_{nr} = weight of non-evaporable water remaining in specimen

6. The total non-evaporable water (W_n) in the specimen is:

$$W_n = W_{nl} + W_{nr} \qquad 6.2$$

7. Weight of evaporable water (W_e) is therefore given as:

$$W_e = W_t - W_n \qquad 6.3$$

8. The ratio of weight of non-evaporable water lost to weight of cementitious materials, can be obtained by dividing equation 6.1 by W_c (Weight of Cementitious materials):

$$W_{nl}/W_c = W_t/W_c - W_e/W_c - W_{nr}/W_c \qquad 6.4$$

9. Now subsituting and re-arranging the above equation:

$$W_e/W_c = W_t/W_c - W_n/W_c \qquad 6.5$$

The ratios of weight of water left to weight of cementitious materials for control tests and release tests are shown in Table 6.2.

From the mix proportion, theoretical amount of non-evaporable water for 100% hydration, non-evaporable water and the degree of hydration for each specimen were estimated as follows:

a. The ratio $W_n/W_c = 0.23$ for 100% hydration (from Sharp, 1971 and Chapman, 1976); therefore:

$$W_n = 0.23\ h\ W_c \qquad 6.6$$

where:

W_n and W_c = same as defined previously
h = the fraction of hydrated cementitious materials.

b. Using this equation the theoretical amount of non-evaporable water can be calculated by subsituting the value of W_c for each test and assuming 100% hydration (h = 1).

c. The same equation can be used for evaluating the degree of hydration (h) when W_n and W_c are known.

The following equations can be used to calculate the quantities of gel and capillary water.

The volume of the solid products of hydration, V_{sol} is:

$$V_{sol} = (h\ W_c/p_c) + (W_n/p_n) \qquad 6.7$$

where:

p_n = apparent density of non-evaporable water

p_c = density of cementitious materials (p_c is taken as the average density of cement and Cemsave here)

Note: $p_c = 3.03p_w$ and $p_n = 1.47p_w$ (for the concrete used here)
These values were reported by Greathead (1986).

p_w = density of water

Subsituting these values and equation 6.6 in equation 6.7:

$$V_{sol} = 0.49\ h\ (W_c/p_w) \qquad 6.8$$

Assuming porosity of the gel to be 28% (Powers, 1947):

$$V_{gel}/(V_{gel} + V_{sol}) = 0.28 \qquad 6.9$$

where:

V_{gel} = volume of gel

Subsituting for V_{sol} from equation 6.8 the volume of gel (V_{gel}) is:

$$V_{gel} = 0.19\ h\ W_c/p_c \qquad 6.10$$

Now assuming the density of gel and capillary water approximately equal to that of free water, the weight of gel water (W_{gel}) is:

$$W_{gel} = 0.19\ h\ W_c = 0.83\ W_n \qquad 6.11$$

If no water escapes from the specimen, the weight of capillary water (W_{cap}) is given by:

$$W_{cap} = W_t - W_{gel} - W_n = (W_t/W_c - 0.42\ h)\ W_c \qquad 6.12$$

The quantities of gel (W_{gel}) and capillary water (W_{cap}) at room temperature were calculated from the above equations for the "RTS" specimens (see example below). These values are marked on Figures 6.2 to 6.14 (even number figures only) and relate to the start of the test i.e. before any release.

EXAMPLE FOR RTS-01:

W_t = 84.64gm or 100% of mix water (obtained from concrete casting information)

W_e = 50.87gm or 60.10% of mix water (deduced from control test)

Now:

$W_n = W_t - W_e = 84.64 - 50.87 = 33.77$gm or 39.89% of mix water

$W_{gel} = 0.83\ W_n = 0.83 \times 33.77 = 28.03$gm or 33.11% of mix water

$W_{cap} = W_t - W_{gel} - W_n = 84.64 - 28.03 - 33.77 = 22.84$gm or 26.98% of mix water

6.3.2 "RELEASE TEST SERIES" RESULTS

The results are presented as follows.

Figures 6.1 to 6.13 (odd numbers only) show:

1. The pore pressure of concrete against the concrete temperature (as shown by a circle and a dot).

2. The svp of steam against temperature (represented by a solid line), to compare the above results with svp of steam.

Figures 6.2 to 6.14 (even numbers only) show:

1. The pressure against the weight loss for each specimen.

2. The values of evaporable water, non-evaporable water, gel and capillary water, and non-evaporable water for 100% hydration.

3. The weight remaining after heating the sample to constant weight at the test temperature (after the removal of concrete specimen from steel jacket). These values are ploted as a percentage of the mix water.

4. The weight of mix water remaining in each specimen, and the weight of mix water per unit weight of cement (cement represents cementitious materials i.e. cement + Cemsave).

5. The time after heating (in hours as marked on each graph), to illustrate the time scale for testing. This time has no

significance on the results of the tests.

Figures 6.17 to 6.23 show pressure against temperature for cycling test temperature by ± 10 °C at various weight losses.

Figure 6.24 is reproduced from Figures 6.17 to 6.23.

Figure 6.24a is redrawn by connecting the centre points of each graph from Figure 6.24, and shows the pressure against the temperature for specified percent loss of mix water for all the "RTS" tests. The overlay represents the graphs reproduced from Steam Tables (1970).

Table 6.3 lists:

i. The ratios of the weight of evaporable and non-evaporable water to the weight of cementitious materials (W_e/W_c and W_n/W_c).

ii. The ratios of the weight of evaporable and non-evaporable water to the weight of total mix water (W_e/W_t and W_n/W_t).

iii. The calculated degree of hydration (where maximum value for 100% hydration = 1).

SPECIMEN NO.	TEST TEMPERATURE	W_e/W_c	W_n/W_c	W_e/W_t	W_n/W_t	DEGREE OF HYDRATION
RTS-01	300 °C	0.238	0.152	0.609	0.391	0.662
RTS-02	342 °C	0.236	0.154	0.604	0.396	0.670
RTS-03	250 °C	0.238	0.151	0.612	0.388	0.656
RTS-04	275 °C	0.233	0.157	0.598	0.402	0.683
RTS-05	300 °C	0.235	0.155	0.603	0.397	0.674
RTS-06	325 °C	0.232	0.158	0.594	0.406	0.687
RTS-07	350 °C	0.235	0.154	0.602	0.397	0.669

Table 6.3: Data for temperature, ratios of the weight of water to the weight of cementitious materials and degree of hydration.

6.4 THEORETICAL MODEL

In order to understand the phenomenon and the effects of moisture release from sealed concrete, heated to a constant temperature, an explanatory model of an inert porous material (ipm) has been analysed

with respect to the following (Chapman, 1976):

1. The interrelation of pore pressure and temperature; (Section 6.4.1)

2. The influence of moisture concentration on pore pressure, (Section 6.4.2)

3. The construction of the ipm model (Section 6.4.3)

4. Finally, the predictions from the ipm are compared with the experimental data from the concrete i.e. a non-inert material (Section 6.5)

The following assumtions are made for the properties of the model.

a. The pores of the inert body have a finite volume and are interconnected.

b. The pore volume remains unaffected by the change of temperature.

c. The pores contain water vapour and/or liquid water and air only.

d. No reactions take place between the materials mentioned in (a) and (c) above.

e. The pressure in the pores is the sum of the partial pressures of air and water vapour.

f. The porous material remains physically unaltered by any loss of fluid.

6.4.1 PREDICTION OF PORE PRESSURE CHANGES WITH TEMPERATURE IN A SEALED INERT POROUS MATERIAL

For an ipm containing liquid water and air voids the application of temperature rise will create pore pressures. These may be described as follows:

1. The liquid water expands thus reducing the pore volume available

to the air, increasing the air pressure.

2. The svp of water is increased. This increases the pore vapour pressure so long as liquid water is still present.

3. The temperature of the air is increased and this creates additional pore air pressures.

The increase in the pressure of air is very much dependent upon:

- the ratio of the volume of liquid water to air inside the pores at the start of heating $(V_l/V_g)_i$

- the increase in temperature of the pore solution (water and air).

The above relationships could theoretically be explained by considering that the pore volume remains constant. Then varying the percentages of water (by volume) and air present in the pore, the system was heated to 800 ^{o}C and variation of pore pressures against temperature were calculated (Greathead, 1986). The results are shown in Figures 6.25 and 6.26 and are discussed below:

i. The pressure generated due to the presence of air with different quantities of water is estimated by using the ideal gas equation and Henry's constant, by first fixing the percentage of water by volume (or the initial ratio of the volume of liquid water to the volume of air $(V_l/V_g)_i$ and then applying the temperature.

ii. As the percentage of water by volume increases, the total pressure increases considerably for the corresponding temperature (Figure 6.25).

iii. As $(V_l/V_g)_i$ increases, the pressure contributed by air is enhanced.

iv. As the liquid phase expands and reduces the available vapour space, the air component is a major factor towards the total pressure. This is illustrated by the case for 90% water by volume, where at 170 ^{o}C, the air component still generates 50% of the total pressure (Greathead, 1986).

v. The increase in pore air pressure further increases the pore water pressure and at equilibruim the total pressure would be greater than the svp for the corresponding temperature, although normally under atmospheric conditions the liquid water would vapourise.

6.4.2 EFFECTS OF MOISTURE RELEASE ON INERT POROUS MATERIAL

Now considering that the sealed ipm has reached steady-state at a constant temperature with the condition in its pores prevailing as outlined in the previous section, the following points are noted:

1. As the specimen seal is broken for a few seconds, moisture in the form of steam and air is allowed to escape.

2. The mass left in the porous body at constant temperature will now occupy a greater volume than it did previously and it has effectively expanded.

3. The fluid given off in theory should be air. However, in practice it is a mixture of air and steam (as water in the pores would turn into steam).

4. The pressure of air will be reduced due to the decrease of the mass of air, reducing the degree of compaction and the magnitude of pressure in liquid water, thus resulting in lowering of the total pressure, as explained in the previous section.

5. The svp of water still remains constant at this stage.

6. The liquid will then vapourise to saturate the vapour inside the porous material and will replace the steam lost in the release procedure. The pressure at this stage will be lower by the amount of pressure equivalent to the reduction in air pressure.

7. On repeating the release procedure and losing more fluid, the pressure values drop further.

8. Once all the air is lost from the material, the pores will be mainly filled with saturated water vapour and liquid water. At

this stage the pore pressure is equal to the svp at the test temperature.

9. The fluid release will now mainly be in the form of steam and as the steam escapes more liquid water vapourises to saturate the material. At this stage the overall pore pressure still remains constant and equal to the svp at the test temperature, as long as water remains in the pores.

10. On further releases a point is reached where all the water has vapourised to steam. The pores at this stage are filled with superheated steam.

11. The density of the superheated steam is reduced as further fluid is released and the total pressure starts to drop. It is expected that the drop of pressure follows the relationship between the density of superheated steam and its pressure at the test temperature for the ipm.

12. Figure 6.27 shows pressure v temperature at various densities of superheated steam (Steam Tables, 1970) and Figure 6.28 plots pressure v density of superheated steam at constant temperatures (Steam Tables, 1970) corresponding to the test temperatures for the "RTS". It is evident from both these figures that the relationship between the density and the pore pressure is temperature dependent and the slope for the graphs becomes steeper the higher the temperature. This relationship is discussed further, when comparing and discussing the test results with the ipm model (Section 6.5).

6.4.3 THE MODEL OF INERT POROUS MATERIAL

The changes in pore pressure inside the ipm when fluid is allowed to escape at constant temperatures is diagramatically shown in Figure 6.29 and the curves are explained by:

a. Defining points "A", "B", "C" and "D" (Section 6.4.3.1)

b. Discussing the slopes of the lines between these points (Section 6.4.3.2).

6.4.3.1 DEFINITIONS OF THE POINTS ON THE CURVE

The position and the variation of various points on the curves of Figure 6.29 are defined and discussed below:

1. Point "A" is the position for maximum values of pore pressures before losing any fluid from the ipm. The position of "A" on the vertical axis is dependent upon the test temperature and the initial volume of liquid water to volume of air $(V_l/V_g)_i$ in the pores of the ipm.

2. Point "B" is the point where all the air has been expelled from the pores of the material and all the pores at this stage are filled with liquid water and saturated water vapour. The position of "B" is dependent upon the rate of fluid release, the time for which seal is broken, and the permeability of the material to the escaping fluid.

3. Point "C" is the position at which the density of the superheated steam is such that the svp can just be maintained at the test temperature. This is a definite point in the specimen with large interconnected pores. However, point "C" is more difficult to define in specimens with small and partially connected pores.

4. Point "D" is the point at which no further fluid loss takes place at the test temperature. The pressure at this time is atmospheric.

6.4.3.2 THE SLOPE OF CURVES BETWEEN ADJACENT POINTS

The slopes of the graphs (Figure 6.29) between adjacent points, are analysed below:

1. The slope and shape of the line "A-B" depends upon:

   - rate of fluid release,
   - time for which seal is broken, and
   - permeability of the material.

i. It is expected that in a material with large interconnected

pores, the point "B" would be a definite point on the curve with an abrupt change of slope, as shown by solid line in Figure 6.29.

ii. This is not the case for material with small and partially connected pores; the shape of the curve for such a material would be more like the graph shown by dashed lines (Figure 6.29) and the point "B" is not a well defined point in this case.

iii. The position of point "B" relative to the vertical axis would be affected by the test temperature and this should correspond to the svp at the test temperature.

iv. The position of point "B" along the horizontal axis is much more difficult to define, for the following reasons:

a. The liquid in the pores is water and the porous material is inert, the test temperature would have no effect upon the permeability of the material. Therefore the factors affecting the position of point "B" would be the rate of fluid release due to the test temperature and the length of time for which the seal was broken.

b. The higher the temperature the faster the air will be expelled from the material for a particular period of release, thus resulting in a steeper slope of line "A-B".

c. In real life one would also expect a certain amount of steam to be released in this part of the test at higher temperatures, which would decrease (negatively) the slope of line "A-B" and move point "B" further to the right on the horizontal axis.

d. However, the point "B" may exist between the dashed lines shown in Figure 6.29, and as discussed later (Section 6.5) this point will become even more difficult to define for concrete.

2. The line "B-C" corresponds to svp at the test temperature where:

i. Point "B" is the starting position for svp values and point "C" is the position where svp cannot be sustained for any further loss of moisture.

ii. Both "B" and "C" are definite points for an inert material with large interconnected pores, giving rise to a definite straight line graph.

iii. Dashed lines show the corresponding curves for a specimen with small pores which are only partially interconnected.

iv. On increasing the temperature, point "C" moves to the left, as the saturated density of superheated steam increases at any given temperature to sustain svp with temperature (Figure 6.28). Once again it shows that it is harder to define the exact position of point "C" on the curve.

3. The line "C-D" represents the portion of the curve between the points:

- where the svp of steam can just be maintained ("C"), and
- where no more fluid is lost at the test temperature and pore pressure is atmospheric.

i. The slope of the line "C-D" would increase (negatively) as the test temperature increases.

ii. The point "D" should be approximately the same regardless of the test temperature for the ipm model, as described in the previous section.

iii. The dashed lines in Figure 6.29 illustrate what actually appears to happen in a non-inert material with small and partially interconnected pores e.g. concrete, where the position of point "D" is temperature dependent.

6.5 COMPARISON BETWEEN THE MODEL OF INERT POROUS MATERIAL AND CONCRETE

Considering the concrete specimen under similar conditions, as applied to the ipm, the effects of temperature on concrete (Chapman, 1976) would be:

1. The expansion of the sealed concrete specimens.

2. The increase in the volume of gel pores, as the cement gel expands on heating. However, the volume of capillary pores will decrease slightly during this process.

5. The overall effect of the increase in temperature of concrete will most certainly be the increase of total pore volume.

Complex and complicated phenomena are at work, when concrete is heated to a uniform temperature and moisture is allowed to escape in a controlled fashion. The properties of concrete are different from the properties of the ipm model and the assumptions made for the ipm mode are not valid (Section 6.4).

To compare the concrete with the inert porous material, the curves of Figure 6.29 are divided into the following categories:

- Comparison of the curve between point "A" and "C" (Section 6.5.1.)
- Comparison of the curve between point "C" and "D" (Section 6.5.1.)

6.5.1 COMPARISON OF THE CURVE BETWEEN POINTS "A" AND "C"

The comparisons is made between the ipm model and the concrete with reference to the following properties:

1. The pore structure of concrete and types of water in these pores (Section 6.5.1.1).

2. The effects of dissolved salts and gases on the svp of water in concrete (Section 6.5.1.2).

6.5.1.1 PORE STRUCTURE OF CONCRETE AND TYPES OF WATER IN THESE PORES

The pore volume of concrete can be considered as finite, although its formation and value varies with degree of hydration. The process of hydration and its products along with types of pores, their structure and states of water in the pores of concrete are discussed below:

1. Two types of pores exist in concrete: **capillary pores & gel pores**

2. Capillary pores on average are larger than gel pores (18-20Å) by

a factor of 10 to 1000.

3. Capillary pores in concrete can be interconnected and depend upon: the degree of hydration of cement, water cement ratio used for the mix design and the amount of campaction during casting.

4. The solid contents of the paste increase in a mature and well cured cement paste due to the enhancement of hydration with age.

5. The capillaries are replaced by the formation of gel resulting in the discontiniuity of the capillary pores and replacing these by gel pores.

6. The permeability of concrete to air and water vapour, which depends upon the continuity of pores would definitely be decreased as the capillary pore volume decreases.

7. The large interconnected pores of ipm when heated to a constant temperature and releasing moisture periodically (Section 6.4) produce definite points "B" and "C" (Figure 6.29). However, these points would not be well defined for concrete and the permeability of concrete would influence the shape of the curves between points "B" and "C" (Figure 6.29, where the curve would fall between the dashed lines).

8. The capillary and gel pores contain:

- liquid water and/or water vapour (where pores can be partially or completely full).
- a certain amount of air.

9. The basis for the generation of the initial pore pressures in concrete is the same as the ipm model and the influencing factor for the development of pore pressure (before release of moisture) when concrete is heated to a constant temperature would be $(V_l/V_g)_i$, as discussed in Section 6.4.1.

10. The situation in concrete is slightly more complex than the inert model, as gel and capillary water are held in varying states in concrete pores.

11. The pore pressure at the initial stages of the test is not affected by the volume of non-evaporable or gel water, but it is only affected by the relative volume of capillary water and entrapped air (Sharp, 1971).

12. Hence, for the prediction of pore pressures at the initial stage one would discount the expansion of the gel water inside the gel pores and only consider the expansion of the capillary water and air in concrete pores.

A relationship can be developed for the assesment of initial ratio of the volume of liquid to gas $(V_l/V_g)_i$ in a concrete specimen by:

a. Considering the volume of porous plate embedded in concrete for the measurement of pore pressures (Chapter 4, Section 4.2.3).

b. Calculating the volumes of capillary water and gas:

$$(V_l/V_g)_i = (V_{cap} + V_{wp})/(V_g + V_{gp}) \qquad 6.13$$

where:

V_{cap} = volume of capillary water
V_{wp} = volume of water in porous plate
V_g = volume of air or gas filled capillaries
V_{gp} = volume of air or gas in porous plate

$$V_{cap} = W_c/p_w\ (0.39 - 0.42\ h) \qquad 6.14$$

$$V_g = 0.058\ h\ W_c/p_w \qquad 6.15$$

Note: Definitions of all symbols are the same as described previously.

The ratios of $(V_l/V_g)_i$ for the "RTS" specimens were calculated (from the volume of porous plate derived from Chapter 4, Section 4.2.3) and are listed in Table 6.4. These values were assessed for each specimen for two cases:

- porous plate completely saturated with water
- porous plate completely dry.

The porous plate in release test experiments may only be partially saturated, and the ratios would lie somewhere between the two limiting values.

SPECIMEN NO.	$(V_l/V_g)_i$, CASE-1, $V_{pw} = 0$ DRY POROUS PLATE	$(V_l/V_g)_i$, CASE-2, $V_{pg} = 0$ SATURATED POROUS PLATE
RTS-01	2.475	3.094
RTS-02	2.375	2.972
RTS-03	2.546	3.192
RTS-04	2.222	2.777
RTS-05	2.324	2.914
RTS-06	2.174	2.716
RTS-07	2.390	2.987

Table 6.4: Ratios of $(V_l/V_g)_i$ for "RTS" specimens.

When discussing the model for the inert porous material it was assumed that the water in the pores was free liquid. However, the water held in concrete can arbitrarily be divided (Powers et al, 1947), as:

a. **Evaporable water:** Capillary water in concrete can be termed as evaporable water

b. **Non-evaporable water:** gel or chemically bound water is called non-evaporable water.

Figure 6.31 shows these types of water held in a continuous varying degree of firmness (e.g. tightly or chemically bound in the hydrate products to free liquid water in the capillary pores).

The chemically bound and gel water was further divided into three categories depending upon the forces holding them together by Powers et al (1947).

1. **Zeolitic water:** this is the water packed between layers of crystal or in the interstices of the structure. It may be removed without forming a new solid phase and produces a smooth isobar on dehydration.

2. **Lattice water:** this is water of crystallisation in a hydrate that should not be associated chemically with the principal constituents of the crystal lattice. This water represents the case between chemically bound and zeolitic water and the isobars and isotherms for this type of water are stepped.

3. **Adsorbed water:** this is the water held by physical forces (known as Van der Waal forces) to the outer surface of the hydrate. These forces get weaker, as one moves away from the surface of

the hydrate.

Adsorbed water may be considered as a case between zeolitic and capillary water. Depending on the specific surface of hydrate, the proportions of this water held in concrete can be large.

The amounts of zeolitic and adsorbed water depend upon the temperature and pressure of the water vapour surrounding the solid and these amounts vary with changes in either pressure or temperature.

6.5.1.2 EFFECTS OF DISSOLVED SALTS AND GAS ON SATURATION VAPOUR PRESSURE IN CONCRETE

Another difference between the ipm model and concrete is that the liquid water in concrete is not pure water but contains dissolved salts. The values of saturation vapour pressure are reduced in the presence of these salts (Powers et al, 1947). The sources of dissolved salts in pore water of concrete are:

- cementitious materials,
- aggregates, and
- the composition of mix water.

Most of the chemical species found in cementitious materials and aggregates are either insoluble, or the solubility is so low that the effects may not be significant.

The solubility of **Potassium Hydroxide** and **Sodium Hydroxide** is significant (Handbook of Physics and Chemistry, 1979) and these solubilities increase with temperature, as shown in Figure 6.30 (Chemical Engineers Handbook, 1973).

The quantities of the dissolved salts calculated from the chemical composition of the cementitious materials (Chapter 3, Section 3.2) are as follows:

1. K_2O = 0.51% and Na_2O = 0.205% by weight (taken as an average for cement and Cemsave used in this project)

2. For 0.39 water/cementitious materials ratio (as used in this work), the corresponding value for (KOH) and (NaOH) is 0.0020

gm/gm and 0.0008 gm/gm of cementitious materials, respectively.

3. Considering that all the cementitious materials are hydrated the total amount of soluble salts would be 0.0028 gm/gm of cementitious materials.

4. Relating these figures to the degree of hydration, the molar concentration of soluble salts in water is approximately 2.8 gm moles/litre of water.

5. The svp depression in pore water of concrete caused by the solubility of these salts can be estimated from Table 6.5, which lists the depression of svp of pure water at various concentrations of dissolved salts (Handbook of Physics and Chemistry, 1979).

Concentration	Depression of svp due to dissolved salts N/mm^2	
gm mol/l	Potassium Hydroxide	Sodium Hydroxide
2.0	0.0084	0.0064
4.0	0.0186	0.0143
6.0	0.0307	0.0238
8.0	0.0427	0.0336
10.0	0.0500	0.0433

Table 6.5: Depression of svp due to dissolved salts.

Whilst the contribution of soluble salts from the aggregate is very low, the quantity of dissolved salts increases with temperature.

Considering the composition of the mix water, even in the worst condition of using sea water for mixing concrete, the soluble salts (~1 mole/kg) would only depress the saturation vapour pressure by 2-3% at the most (Greathead, 1986). The mix water used for mixing concrete was tap water and chances of dissolved salts present is very low. Hence, the depression due to the dissolved salt in mix water can be discounted.

The overall effects of dissolved salts will be the depression of pore pressure values for the plateau between point "B" and "C" on "RTS" graphs compared to ipm model.

Introduction of a small amount of gas into a system containing liquid and saturated vapour at constant temperature increases vapour pressure

and total pressure (Sears, 1953).

The possibility of gas evolution (as discussed in Section 6.6.1.2) exists in concrete, which would increase the pore pressure for the plateau of the curve between point "B" and "C".

Finally, the shape of the graph from "B" to "C" for release test specimens would be between the depressed values due to the solubility of the salts in pore water and the elevated values due to the introduction of gas.

6.5.2 COMPARISON OF THE CURVE BETWEEN POINTS "C" AND "D"

Finally the curve from point "C" to point "D" (Figure 6.29) for both concrete specimen and the ipm model is discussed and the difference between the two materials is highlighted.

The line from "C" to "D" is almost vertical for the ipm model and point "D" seems to be a common point for all the temperatures. However, in the concrete specimen this is not the case and dashed lines from "C" (Figure 6.29) downward represent the trend.

The reasons for the above are as follows:

1. More fluid can be given off from concrete specimen for any given pressure drop in the "RTS" specimen than in the inert model.

2. The only source of fluid in the ipm was inside the pores, but in concrete water is also released from the hydrate structure.

3. Some of this water is released, filling the pores and giving rise to higher pressure, which in turn is lost on release, resulting in further weight loss.

4. The water at this stage has probably been released from the hydrate structure.

5. The amount of the water driven off from the hydrate structure is time, temperature and pressure dependent.

6. The hydrate products would shrink due to the loss of this water, while increasing the pore volume and decreasing the density of superheated steam, resulting in a drop of pore pressure.

It was very difficult to attain equilibrium in this part of the test. The temperature was cycled by $\pm 10\ ^{o}C$ around the "RTS" test temperatures and the pore pressure and the temperature was recorded (Figure 6.17 to 6.24).

Figures 6.27 & 6.28 show that, as the water concentration decreases the variation in pressure decreases with temperature. This would be the case of releasing moisture from the ipm model. In analysing the actual release test results, a similar behaviour was encountered, as shown in Figure 6.24, suggesting the similarity between the ipm (Figure 6.27) and concrete.

The variation in pore pressure was much greater in concrete specimens for any corresponding temperature change. The variation of pressure with temperature increased with test temperature, suggesting that this process is temperature dependent. The portion of the curve between points "C" and "D", and the mechanism responsible for the loss of water between these points is difficult to explain.

However, to explain this mechanism, a connection may be considered between the free energy of water (between "C" and "D") held by the hydrate and that of the superheated steam causing the pore pressure. Powers et al (1947) showed that:

i. The adsorbtion of water occurs when the free energy of the free water or free vapour is greater than the free energy of the adsorbed or capillary condensed water.

ii. Applying the converse of their findings to the situation here, free energy of water in this region (between "C" and "D") must be greater than the free energy of the superheated steam, if water is lost from the hydrate.

iii. The free energy must be provided by the input of heat to maintain the constant temperature. As the test temperature increases more water can be driven off between these points contributing

towards the increase of pore pressure.

Another experimental observation, as discussed in Section 6.6 was that when the steel jacket was removed and the concrete specimen was dried at atmospheric pressure and the same test temperature, more water could be driven off. This effect would be contrary to the findings for the ipm when all the water is released at point "D".

The loss of water from concrete after removal from sealing jacket may be attributed to various factors e.g. rate effect for moisture release and surface area available for the water to be driven off. This effect is further discussed in Section 6.6.

6.6 DISCUSSION AND EXAMINATION OF EXPERIMENTAL RESULTS

The experimental results are discussed in the following two categories:

6.6.1 DISCUSSION OF "RELEASE TEST SERIES" RESULTS

The results of the "RTS" specimens can be analysed as follows:

6.6.1.1 DEVELOPMENT OF PORE PRESSURE ON FIRST HEATING

1. The value of the maximum recorded pressure is higher than the saturation vapour pressure of water for each corresponding test temperature (Figure 6.1 to 6.13, odd numbers only).

2. This is mainly attributed to the amount of air and water in concrete pores and depends upon the ratio of initial volume of liquid to volume of air $(V_l/V_g)_i$ inside the pores (Section 6.4.1). The ratio is calculated by:

   - assuming porous plate to be completely dry ($V_{wp} = 0$)
   - assuming porous plate to be completely saturated ($V_{gp} = 0$)
   - assuming that volume of gas does not decrease and
   - Knowing $(V_l/V_g)_i$, total pressure is obtained by estimating percentage of water and air in the pores (Figure 6.25).

3. The experimental values of gauge pressure are normally higher than the calculated values.

4. The excess of pressure above calculated values (as discussed earlier in this section) leads to the suggestion that it is not only the capillary water which contributes to the generation of pore pressure (as the calculations of $(V_l/V_g)_i$ were based upon). A certain amount of bound water and gas is also released from the hydrate structure which influences the gauge pressure.

5. The experimental results and analysis are consistent with the observations made by Sharp (1971), Chapman (1976) and Greathead (1986).

6. The excess in pressure is temperature dependent.

7. The age of concrete does not seem to influence the value of total pressure for mature concrete (in the range 1 to 3.5 years, Figure 6.15).

8. The concrete of younger age compared with mature concrete shows the age dependence for the generation of pressure, because the young concrete is chemically less stable and water held in concrete could vary for the following reasons:

i. Varying degree of hydration of cementitious materials

ii. Production of different volume and surface areas of the products of hydration, resulting in different "water adsorption".

iii. Introducing different surface forces (i.e. Van der Waal forces Section 6.5.1.3), which would be responsible for attraction or repulsion between the molecules, ions and groups of molecules etc.

The value of maximum pressure during the first heating cycle is closely related to point "A" shown on Figure 6.29 and discussed in Section 6.4.3.

6.6.1.2 RELEASE OF PRESSURE AND MOISTURE FROM CONCRETE

As discussed earlier in the construction of the ipm model (Section 6.4) and its comparison with the concrete (Section 6.5) it was observed that:

1. The release procedure results in loss of pore pressure and weight.

2. On subsequent heating to steady-state condition the maximum recorded pressure is lower than the previous value.

3. The loss of pressure and weight was attributed to the expulsion of air, although inevetably a certain amount of steam was also lost at the early stage of the test.

4. The slope of line "A-B" (Figure 6.29) depends upon temperature and pressure.

5. Points "B" and "C" were well defined for the ipm. However, these point could not be defined clearly for the "RTS" results (Section 6.5).

6. The slope of lines "A-B" and "B-C" for the release tests would be defined by joining the points "A", "B" and "C", and the resulting lines would fall between the dashed lines shown in Figure 6.29 (and outlined in Section 6.5).

7. Once all the air was lost from the specimen (at "B") the value of gauge pressure was constant with weight loss and at this stage the pore pressure was equal to the svp of water for the test temperature. Lines "B-C" represents this portion of the curve (Figure 6.29).

Figures 6.2 to 6.14 (even numbers only) have the svp values for the test temperature shown by dash dot lines. Comparing the experimental results with svp line it was seen that the svp line does not correspond exactly to release test results (where the pore pressure at this stage of the test should be equal to svp for the test temperature). The reasons for the divergence of the experimental

results from the svp could be attributed to:

- the effects of dissolved salts in water (Table 6.5),
- introduction of gas in the system, or
- combined effects of dissolved salts and the presence of gas.

The pressure values of plateau between "B" and "C" corresponding to the svp for release tests were mostly higher (~0.1 to 0.4 N/mm^2) than the svp of steam for the test temperature, suggesting the evolution of gas in concrete.

A quantitative proof of the evolution of gases (i.e. the collection and the analysis of the gases) is not available. However, when releasing the moisture from the "RTS" specimen a distinct smell accompanied the moisture loss. This experimental fact was also encountered in the "Liner Test Series" experiments, for the samples sealed at the heated end only (Chapter 5).

The introduction of gases could be atributed to:

a. Evolution of Carbon Dioxide (CO_2) and Hydrogen Sulphide (H_2S) from heated concrete containing cement and cemsave.

b. The break up of water reducing agent (Cormix P1).

c. Rey (1957), who studied the hydrated binders by Differential Thermal Analysis (DTA), showed the decomposition of hydrates and the thermal evolution of the hydrate consituents. He concluded that salts or other compounds in the hydrates start decomposing at a temperature of 70 ^{o}C.

The evolution of gases supports the point hypothesised by Sears (1953) as discussed in Section 6.5, highlighting the fact that a small amount of gas can have a greater influence on elevating the svp of steam at test temperature.

The elevations of pore vapour pressure would also be explained in thermodynamic terms by the dependence of vapour pressure on the total pressure, and applying the Gibb's Function G, a measure of the free energy of the system:

$$G = H - TS$$

where:

H = total enthalpy of the system

T = absolute temperature of the system

S = entropy of the system

The slope of the line beyond point "C" (the point where the svp cannot be sustained any longer at the test temperature and the density of superheated steam reduces) starts to increase and:

1. At this point the water evaporates and occupies greater volume, resulting in the drop of pore vapour pressure.

2. Point "C" (like point "B") cannot be defined precisely and depends on a number of factors discussed in Section 6.5.2.

3. The position of "C" is fairly static. However, it moves to the left with increasing test temperatures, indicating decrease in the density of superheated steam.

Line "C-D" is the falling portion of the curve from the point where the svp cannot be sustained any longer to the point where no more weight loss can be monitored by releasing the moisture at the test temperature using the same release techniques. For the ipm, line "C-D" ends at a definite point "D" (Section 6.4.3.1). For the "RTS" specimen the slope of line "C-D" is closer to the dashed lines shown in Figure 6.29 (Section 6.5.2) and it depends upon:

- the temperature
- the permeability of the material and
- the degree of inter-connection between the pores.

To obtain pore pressure and temperature variation at release points on line "C-D", the test temperature was cycled by $\pm 10\ ^{o}C$, as shown in Figure 6.24 (and discussed in Section 6.3.2).

To compare the release test results for pressure/temperature relationships (Figure 6.24 and 6.24a) with Steam Tables results (Figure 6.27), the results from Figure 6.27 are reproduced on a transparency as an overlay to Figure 6.24a. The results from these graphs are discussed and compared below:

1. The results from Steam Tables show a linear relationship.

2. The results from release tests also show a linear relationship between the experimental points for each test temperature (Figure 6.24).

3. The slope of the graphs for release test results are steeper than the slopes of graphs from Steam Tables for corresponding test temperatures and densities.

4. The pressure values for release tests were higher at the corresponding temperatures.

5. The weight losses for the release tests were greater at the corresponding temperatures.

6. A step relation (or missmatch) exists between the graphs of release tests for the different test temperatures (Figure 6.24).

The anomalies for the above facts can be summarised as:

a. Break up of hydrate structure of cementitious materials due to dehydration at elevated temperatures.

b. More water was made available due to dehydration.

c. The result is the generation of higher pore pressures and greater weight loss in concrete compared with the results from Steam Tables.

d. Different energy levels as input due to the different test temperatures, being responsible for releasing a different amount of water in concrete.

e. Longer time required by concrete to attain equilibrium at the corresponding test temperature.

f. Temperature rise increases the pore volume of concrete and releases chemisorbed or chemically combined water into concrete

pores.

g. The chemical reactions introduce gases in concrete.

h. The results of the above points give rise to higher pore pressures and greater weight loss on releasing the moisture.

The results from the release tests do not correspond to the results from Steam Tables and these experimental findings require further investigation.

6.6.2 DISCUSSION OF CONTROL TEST RESULTS

The control tests were performed by removing the concrete specimen from the sealing jacket and then by drying the concrete to a constant weight at 105 ^{o}C and at the test temperatures. The concrete for the control specimens was removed from the sealing jacket in the same way as the "RTS" specimens were removed from the sealing jacket for the constant weight loss measurements (as described in Section 6.3.2).

The control tests provide the comparison for the release tests. The points emerging from the control tests are given below:

1. The results were calculated as the ratios of water remaining in the specimen to the weight of cementitious materials, when dried to constant weight at the test temperature (Table 6.2).

2. Ratios of water remaining in the specimens to the weight of cementitious materials show a good agreement for both the control tests and the "RTS" test for the corresponding temperature (Table 6.2).

3. No age effect for mature concrete, as testing was performed when the concrete was over a year old for all the release tests.

4. Drying techniques do not affect the proportions of different types of water in concrete.

5. Degree of hydration is dependent upon the duration and the effectiveness of curing (e.g. cured in air, under water or

sealed).

6. The amount of non-evaporable water (chemically bound water) released from concrete specimens when heated to elevated temperatures is temperature dependent.

7. Techniques used for driving off this water influence the amount of water given off. No more water was lost from the "RTS" specimen after leaving the release valve open for a long time at the end of release tests. However, a certain loss of weight was still recorded when the sealing jacket was completely removed and the specimen was dried at the test temperature. The reasons for this are attributed to:

- the rate effect (i.e. the rate of moisture loss from concrete),
- the surface area available for the moisture release and
- the different drying mechanism at elevated temperatures.

8. The results from the control test specimens form a useful guide for calculating the various proportions of water in the "RTS" specimen, as discussed in Section 6.3.1 and Section 6.3.2.

6.7 SUMMARY OF EXPERIMENTS AND CONCLUSIONS

6.7.1 SUMMARY OF EXPERIMENTS

To determine the pressure-temperature relationship for a range of moisture contents, concrete containing Sulphate Resisting Portland Cement and Blastfurnace Slag (Cemsave) w s uniformly heated to various elevated temperatures. This was achieved by periodically releasing moisture from the specimens.

The studies were carried out to determine:

a. Variation of pore pressures with temperature and moisture contents.

b. Variation of pore pressures with temperature at a range of moisture and air contents in a model of inert porous material.

c. The difference between recorded pressures in the concrete

specimens and the predicted pressures from this model, as an aid to a better understanding of the behaviour of moisture in concrete.

6.7.2 CONCLUSIONS

1. Water in the pores of concrete expands when heated and decreases the volume available to the air contained, and thus increases the pore pressures.

2. The total pore pressure in sealed and heated concrete is higher than the saturation vapour pressure for the liquid alone. This is due to the presence of air.

3. On the performance of the release procedure, the pore pressure values reduce quickly to the saturation vapour pressure of water, because air and water vapours are expelled rapidly from the concrete.

4. At temperatures above 300 ^{o}C, no age effect was detected between concrete averaging 393 to 1209 days at start of test.

5. The amount of non-evaporable water driven off from concrete at elevated temperatures is temperature dependent.

6. The difference between pore pressures actually observed in unsaturated concrete and that expected theoretically, as based on Steam Tables and known original free water contents, demonstrates that concrete cannot be considered as an inert porous material, because of surface and hydration effects.

7. Finally, the results from the release tests do not correspond to the results from Steam Tables and these experimental findings require further investigation.

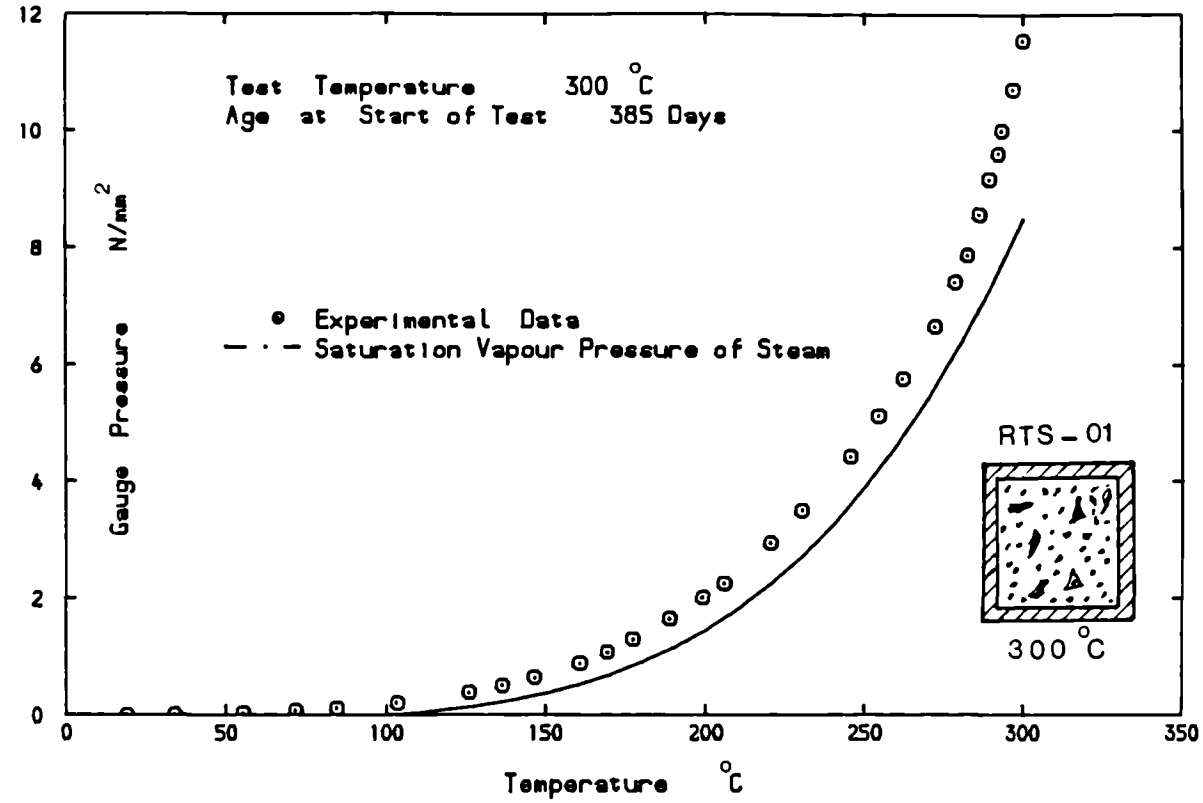

Figure 6.1: GAUGE PRESSURE AGAINST TEMPERATURE FOR SPECIMEN RTS-01

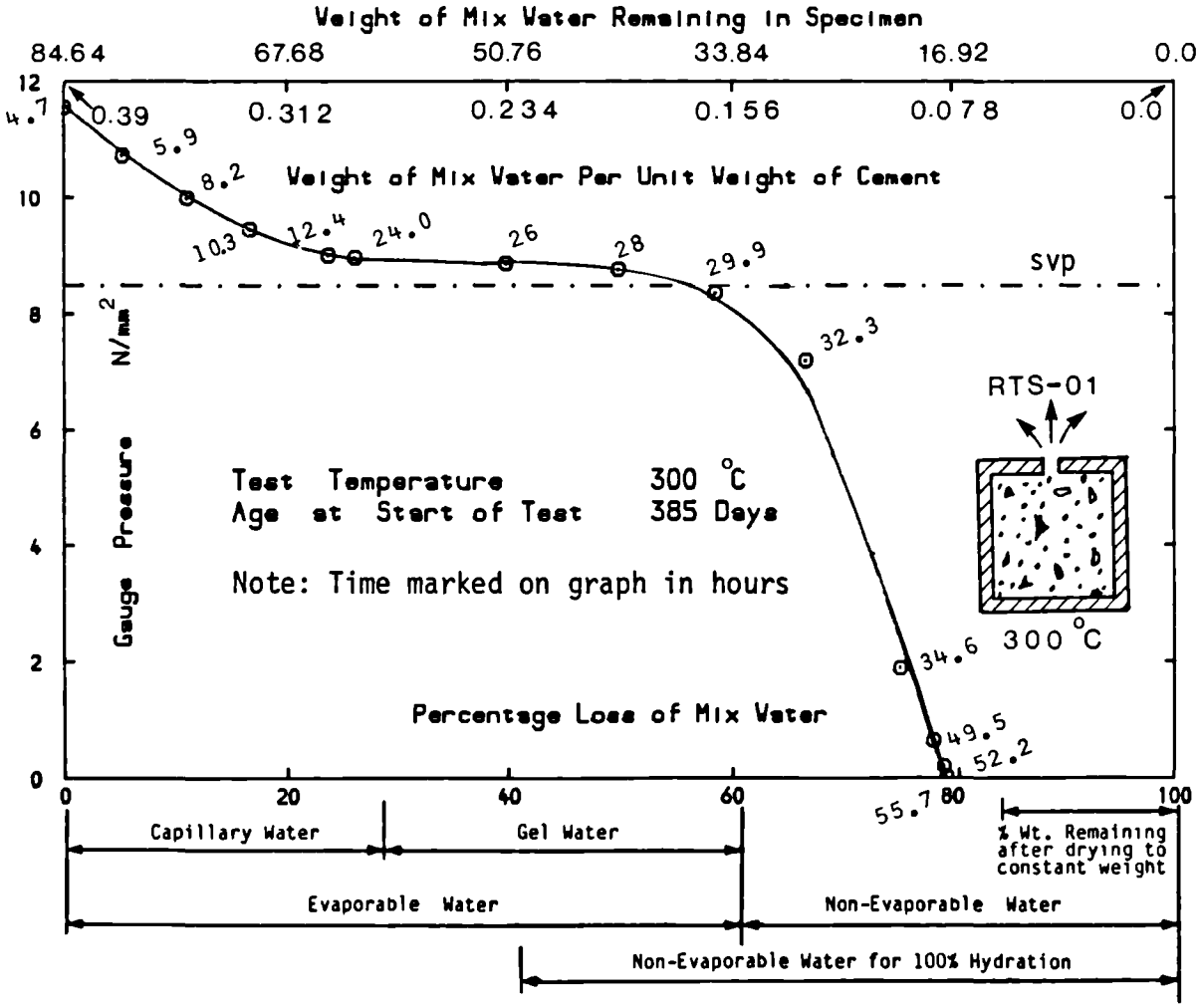

Figure 6.2: GAUGE PRESSURE AGAINST WEIGHT LOSS FOR SPECIMEN RTS-01

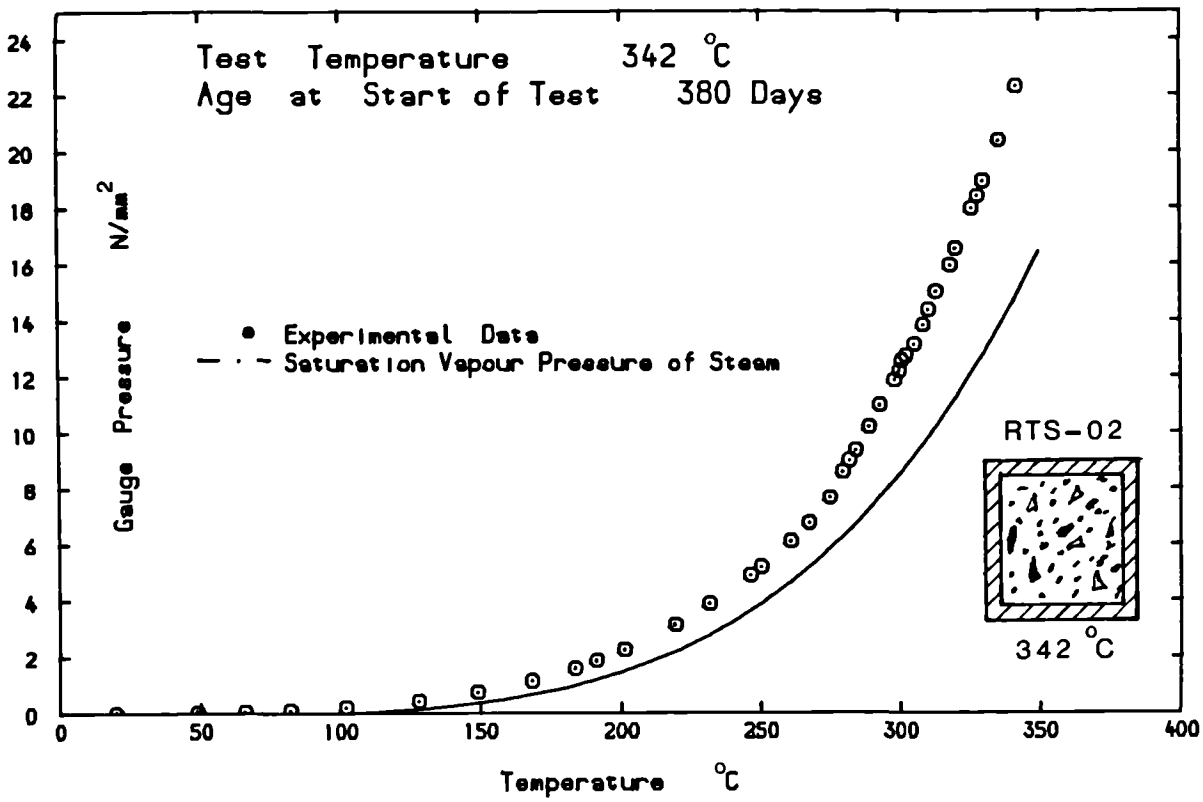

Figure 6.3: GAUGE PRESSURE AGAINST TEMPERATURE FOR SPECIMEN RTS-02

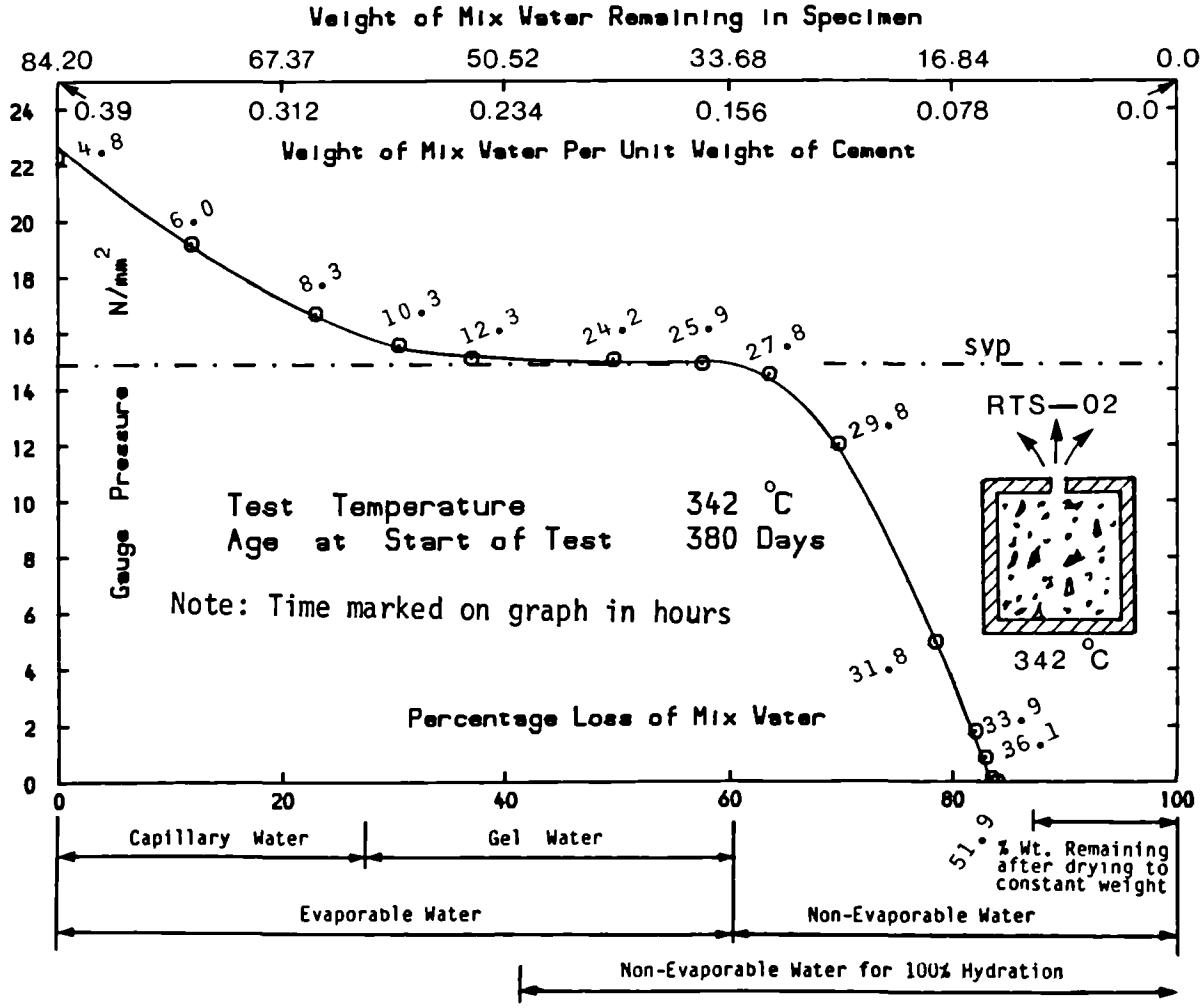

Figure 6.4: GAUGE PRESSURE AGAINST WEIGHT LOSS FOR SPECIMEN RTS-02

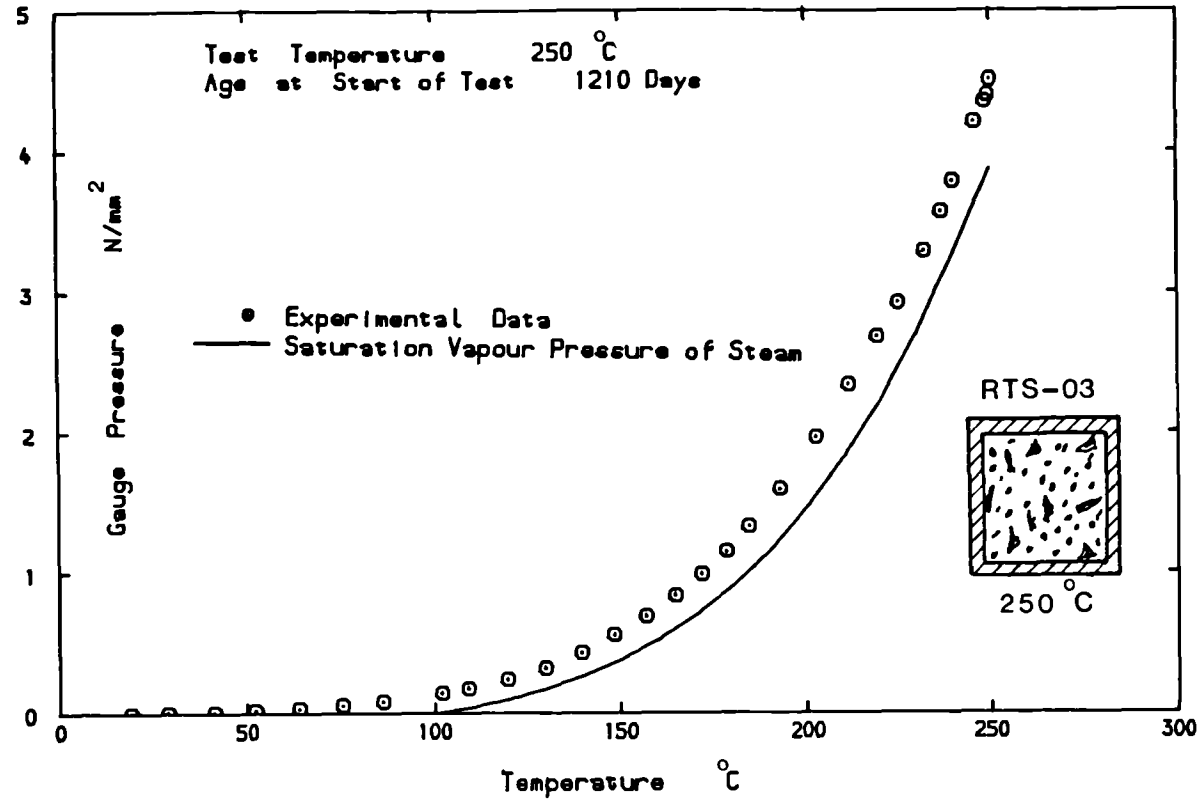

Figure 6.5: GAUGE PRESSURE AGAINST TEMPERATURE FOR SPECIMEN RTS-03

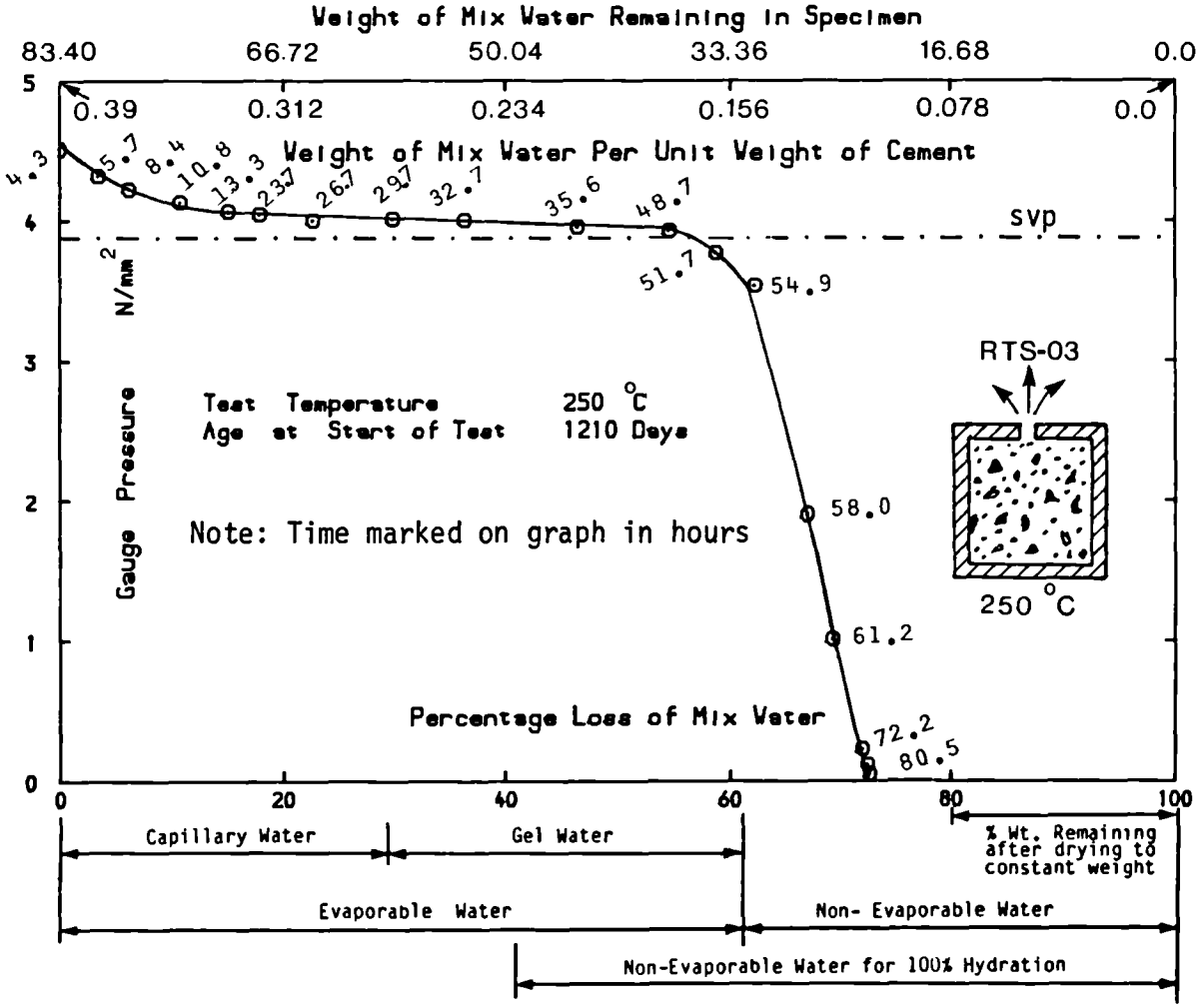

Figure 6.6: GAUGE PRESSURE AGAINST WEIGHT LOSS FOR SPECIMEN RTS-03

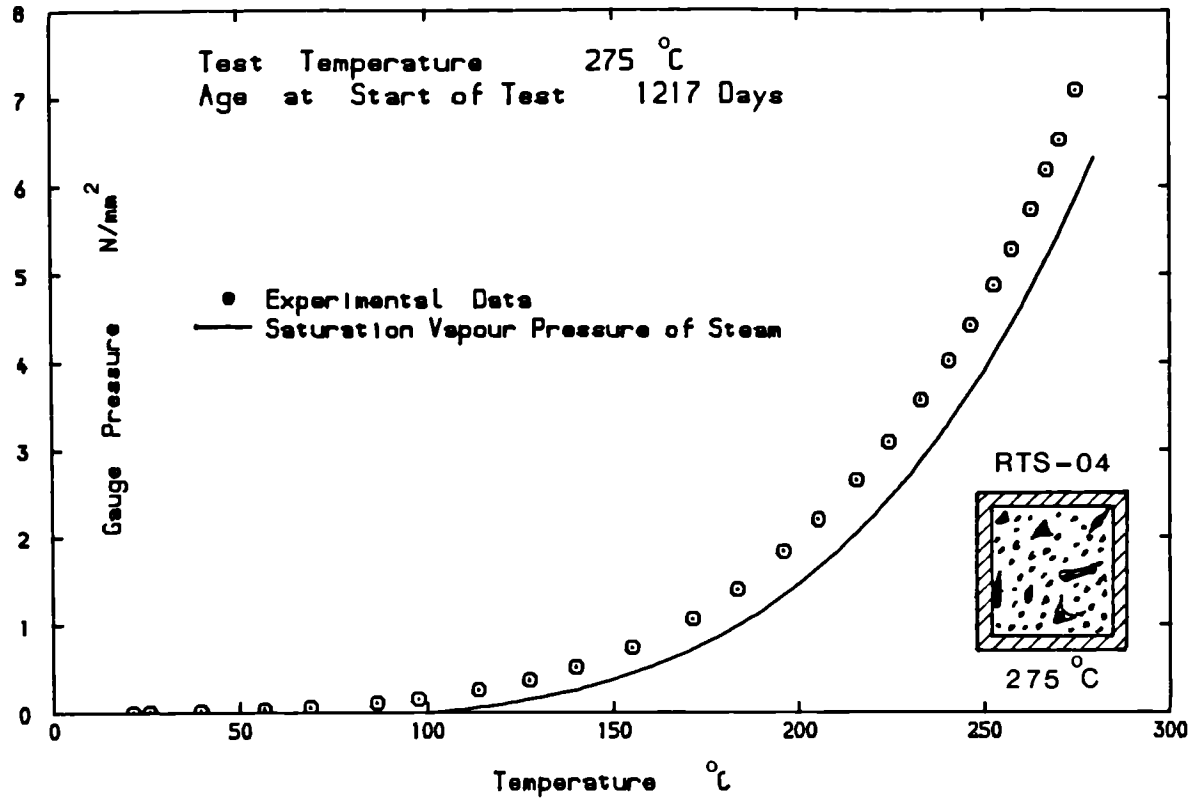

Figure 6.7: GAUGE PRESSURE AGAINST TEMPERATURE FOR SPECIMEN RTS-04

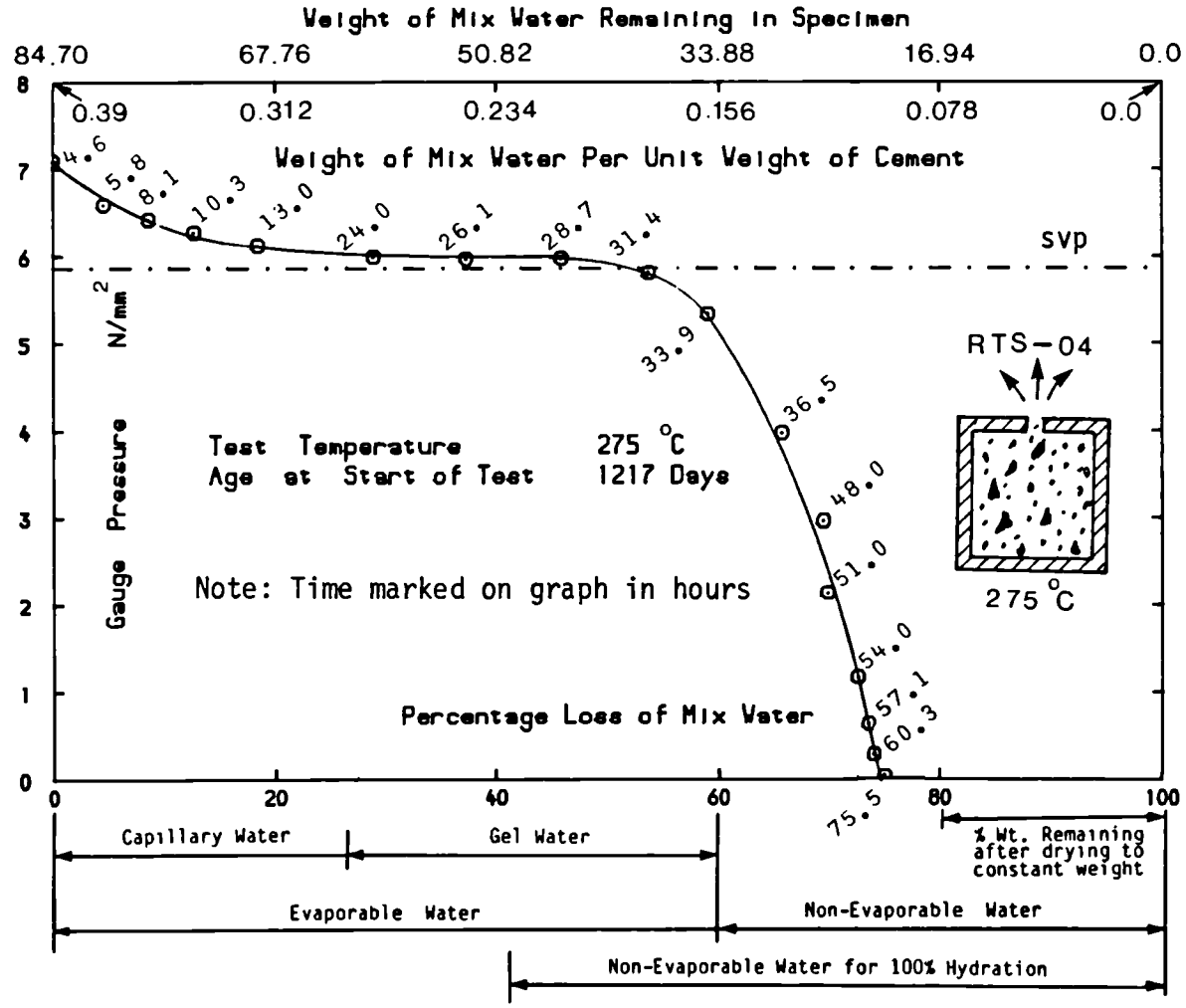

Figure 6.8: GAUGE PRESSURE AGAINST WEIGHT LOSS FOR SPECIMEN RTS-04

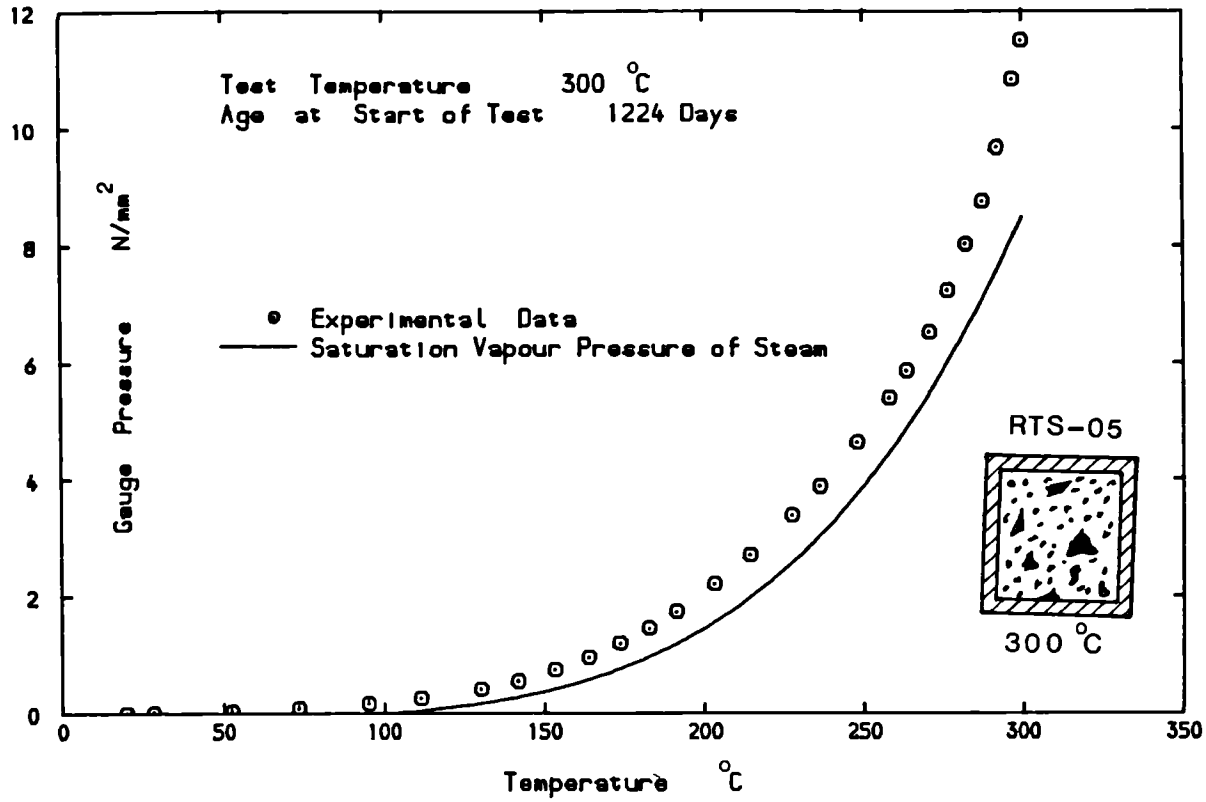

Figure 6.9: GAUGE PRESSURE AGAINST TEMPERATURE FOR SPECIMEN RTS-05

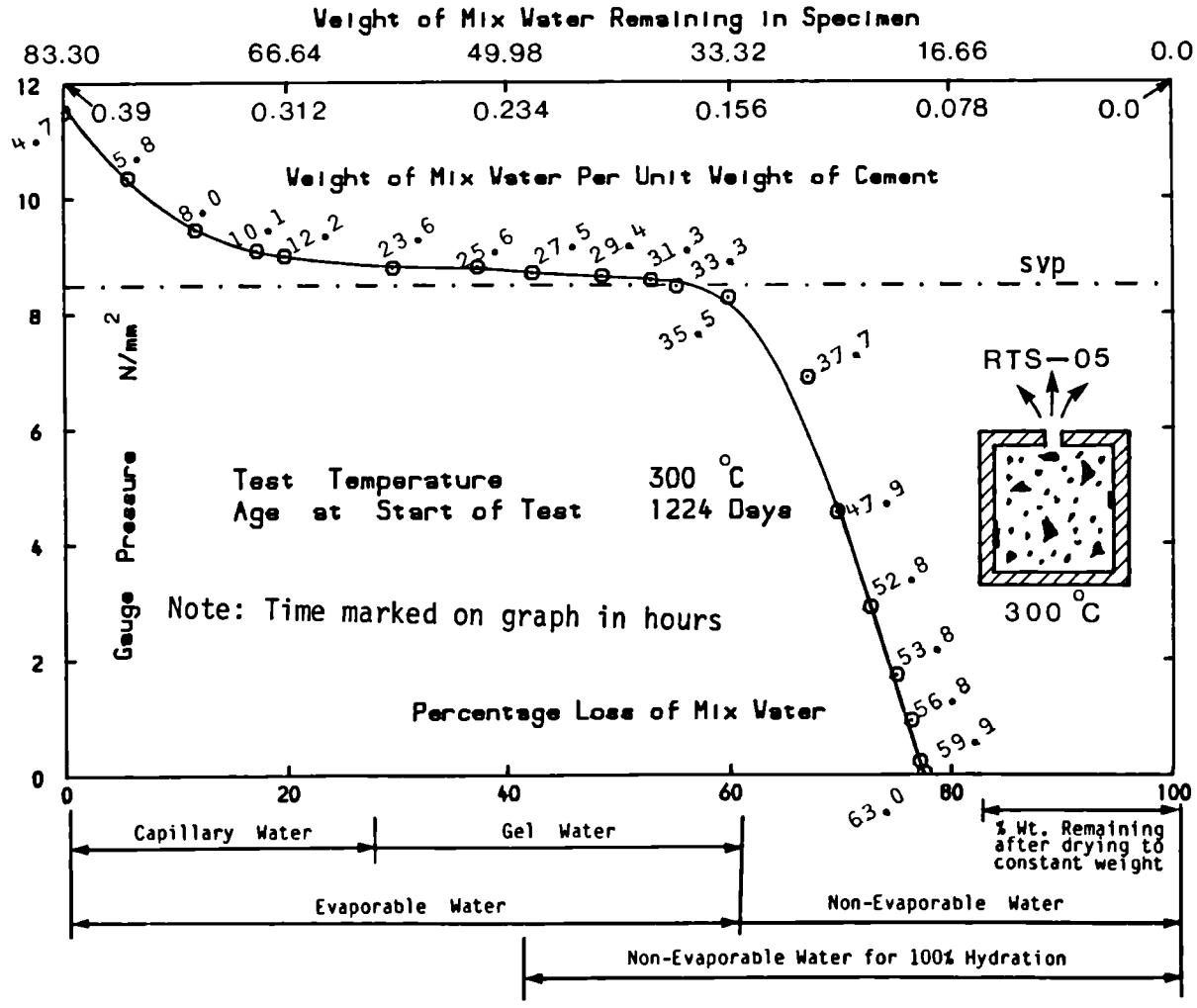

Figure 6.10: GAUGE PRESSURE AGAINST WEIGHT LOSS FOR SPECIMEN RTS-05

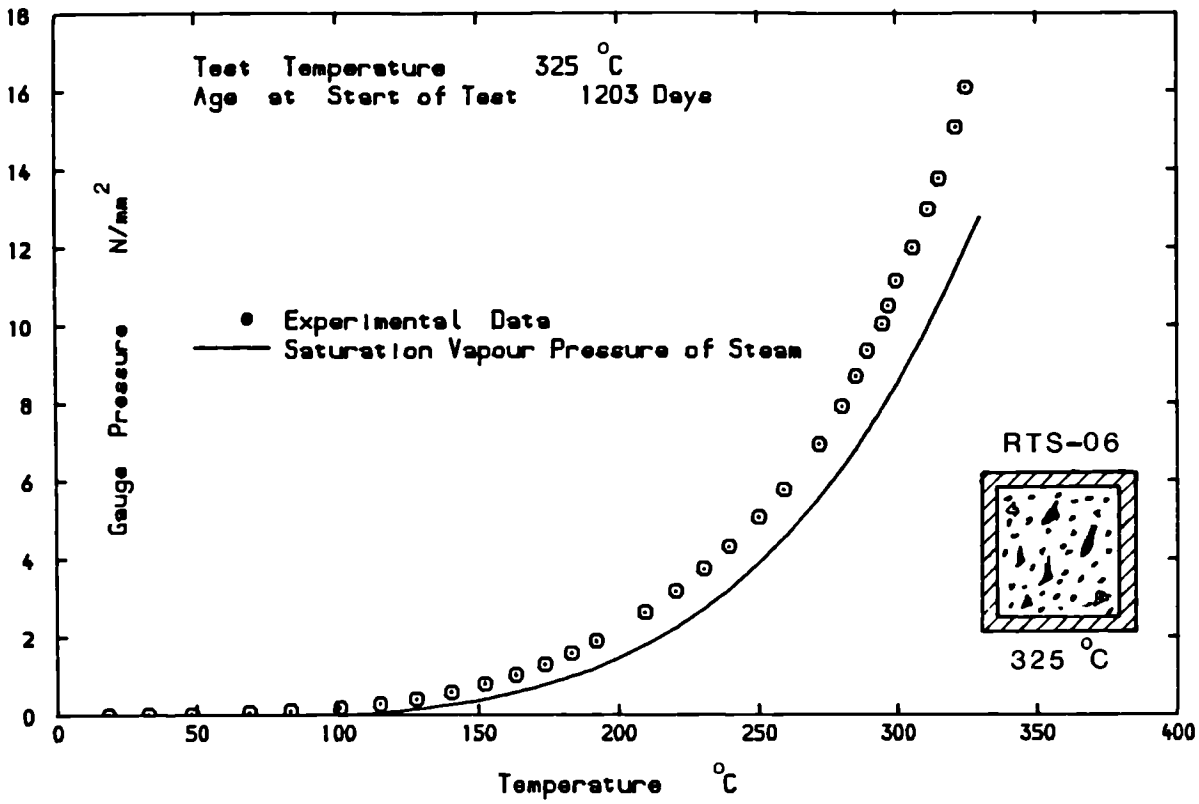

Figure 6.11: GAUGE PRESSURE AGAINST TEMPERATURE FOR SPECIMEN RTS-06

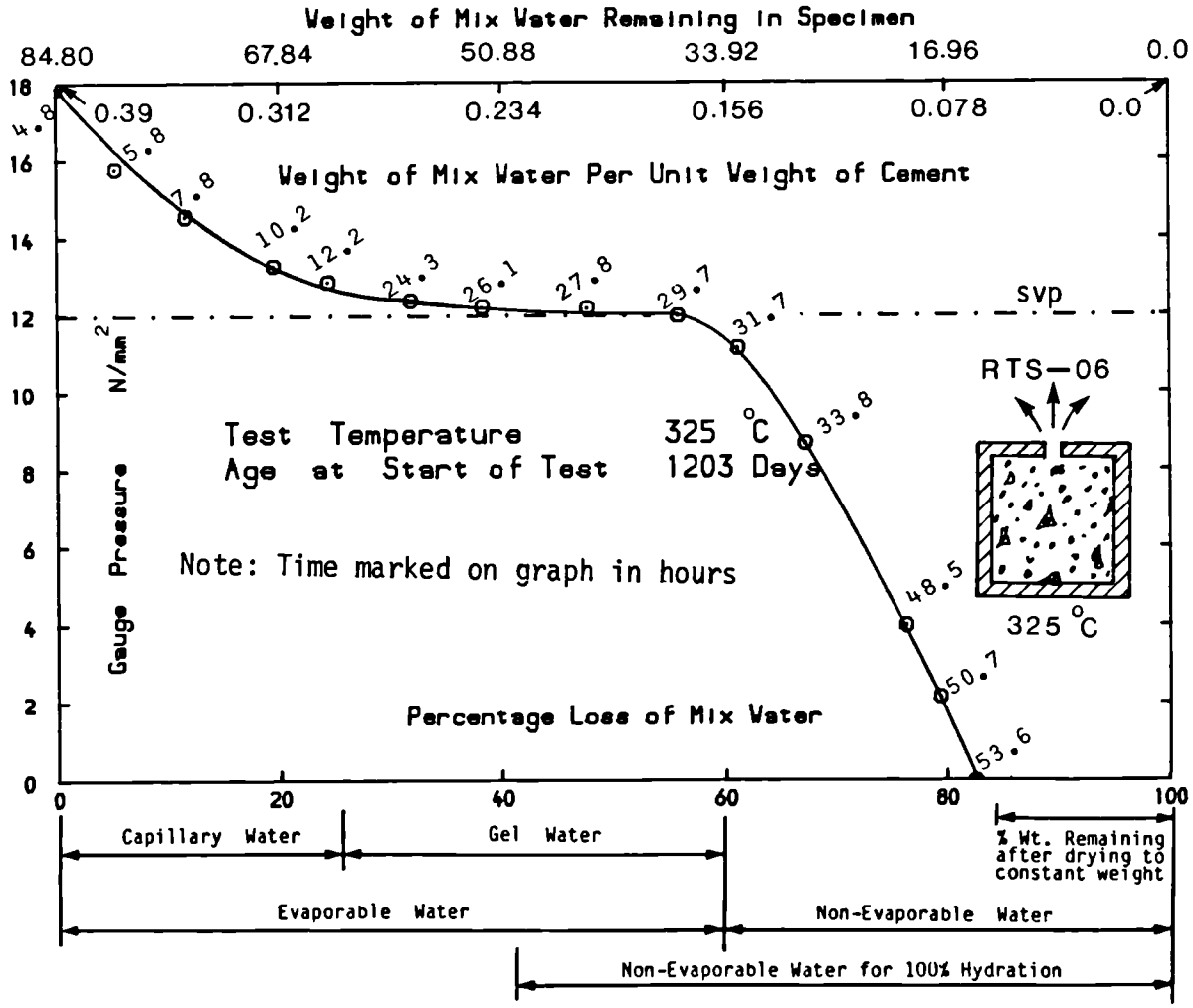

Figure 6.12: GAUGE PRESSURE AGAINST WEIGHT LOSS FOR SPECIMEN RTS-06

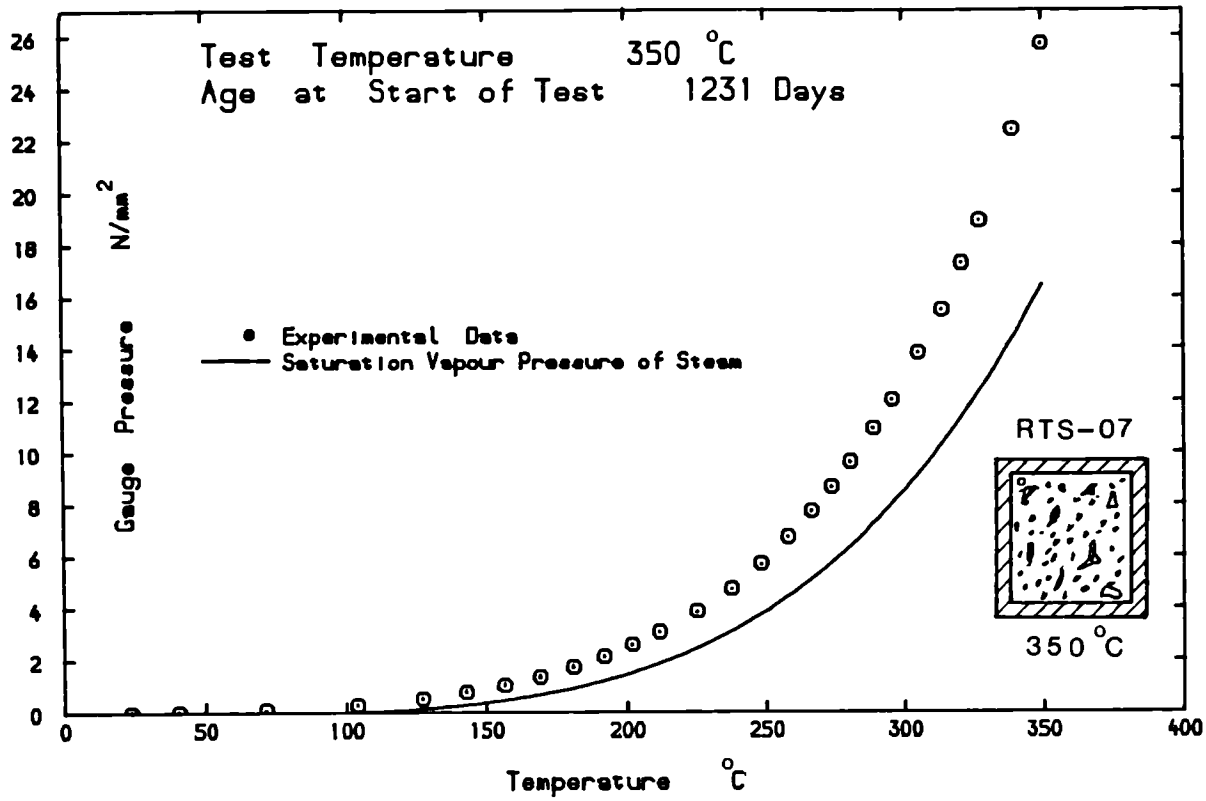

Figure 6.13: GAUGE PRESSURE AGAINST TEMPERATURE FOR SPECIMEN RTS-07

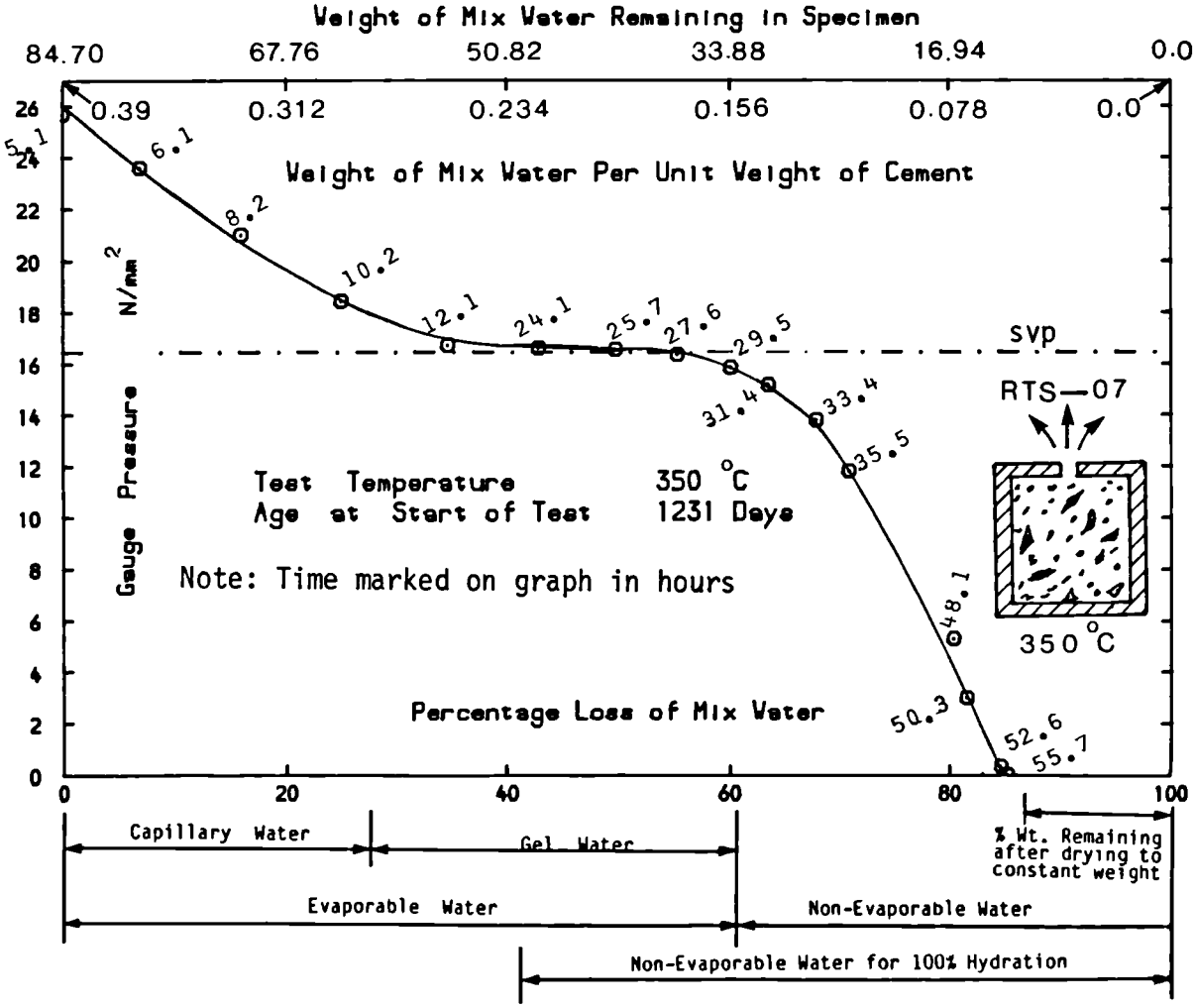

Figure 6.14: GAUGE PRESSURE AGAINST WEIGHT LOSS FOR SPECIMEN RTS-07

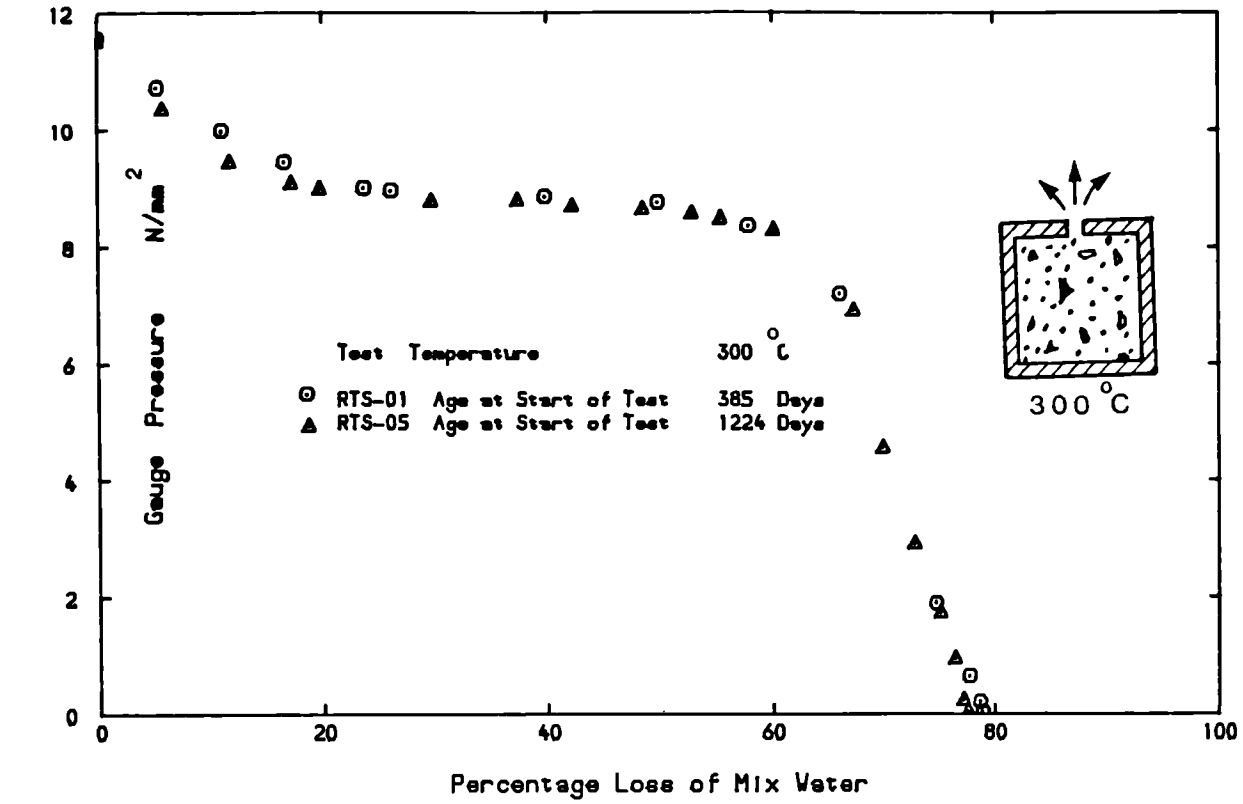

Figure 6.15: GAUGE PRESSURE AGAINST WEIGHT LOSS AT 300 °C FOR TWO AGES

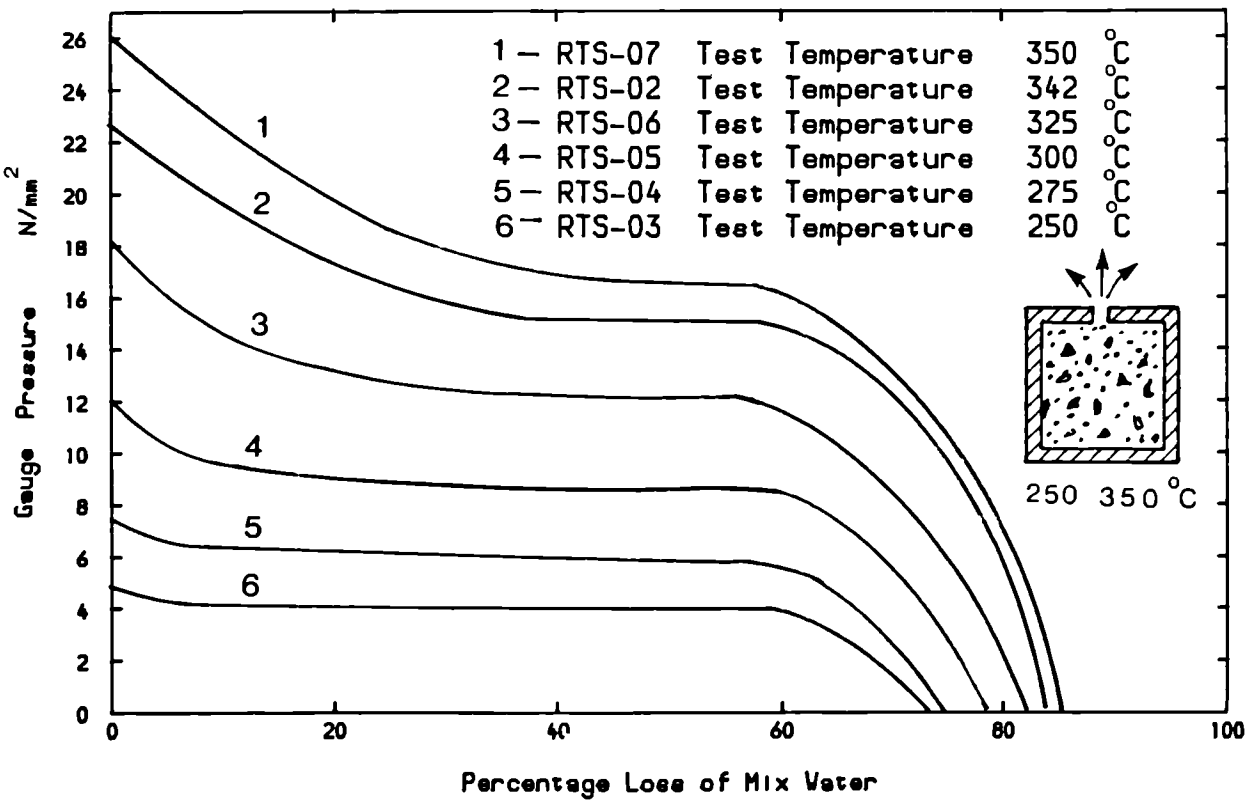

Figure 6.16: GAUGE PRESSURE AGAINST WEIGHT LOSS FOR COMPARISON

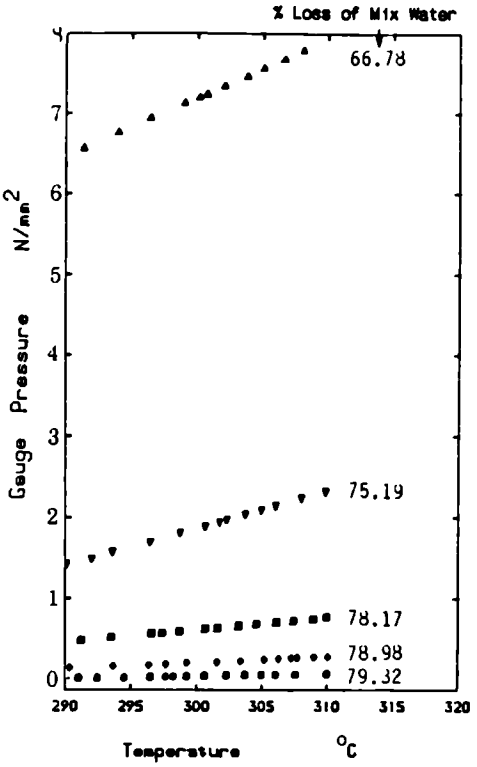

Figure 6.17:
GAUGE PRESSURE AGAINST TEMPERATURE AT VARIOUS WEIGHT LOSSES FOR RTS-01

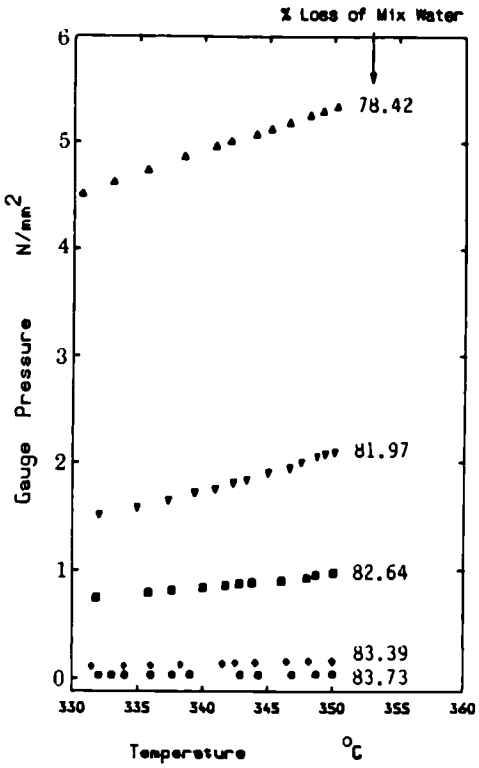

Figure 6.18:
GAUGE PRESSURE AGAINST TEMPERATURE AT VARIOUS WEIGHT LOSSES FOR RTS-02

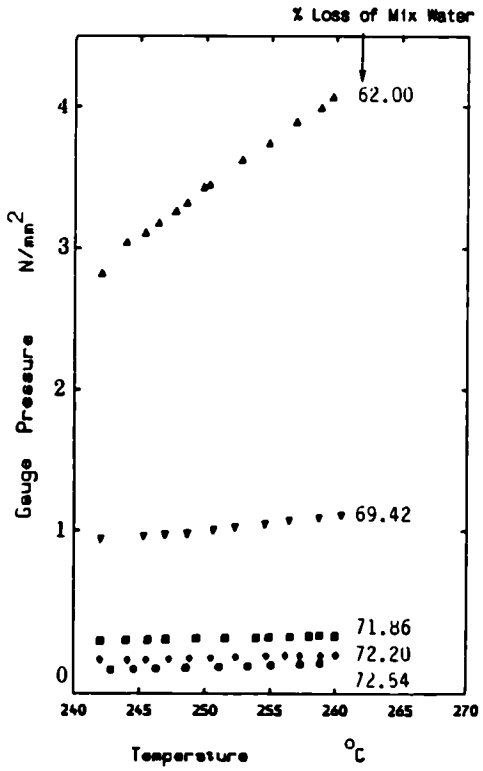

Figure 6.19:
GAUGE PRESSURE AGAINST TEMPERATURE AT VARIOUS WEIGHT LOSSES FOR RTS-03

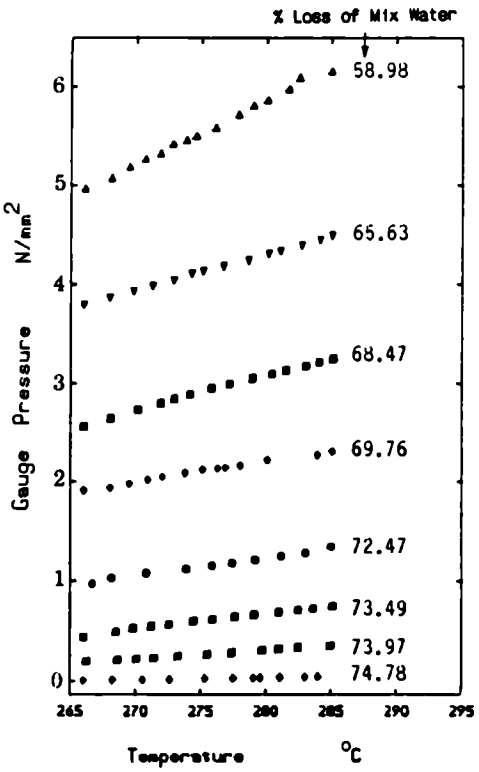

Figure 6.20:
GAUGE PRESSURE AGAINST TEMPERATURE AT VARIOUS WEIGHT LOSSES FOR RTS-04

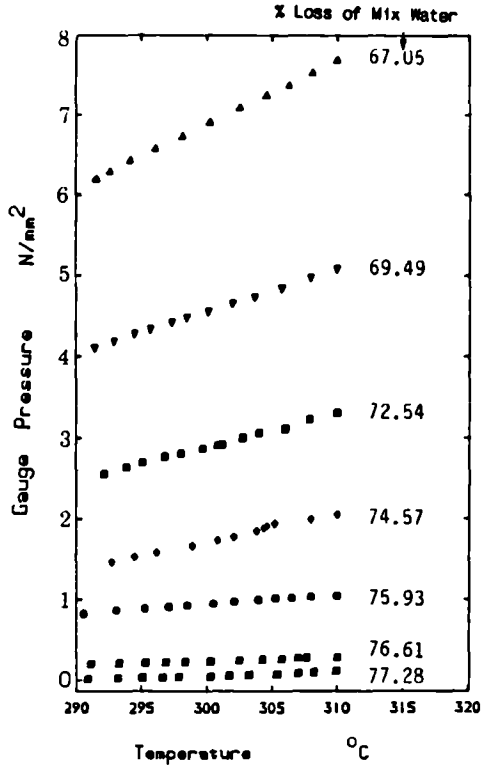

Figure 6.21:
GAUGE PRESSURE AGAINST TEMPERATURE AT VARIOUS WEIGHT LOSSES FOR RTS-05

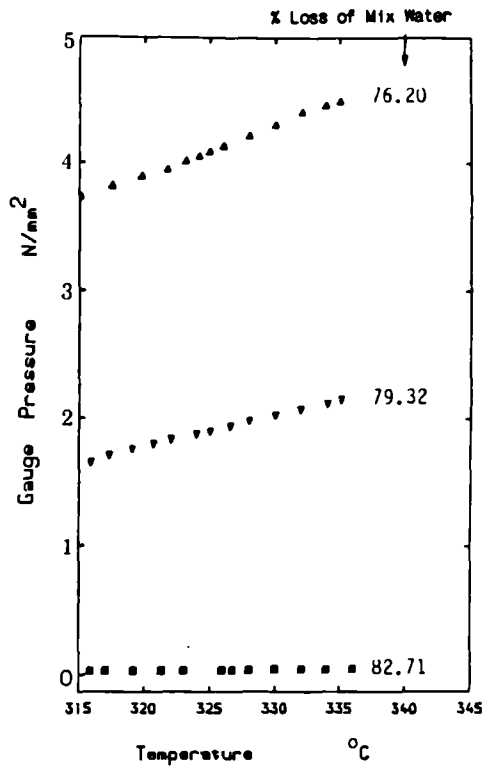

Figure 6.22:
GAUGE PRESSURE AGAINST TEMPERATURE AT VARIOUS WEIGHT LOSSES FOR RTS-06

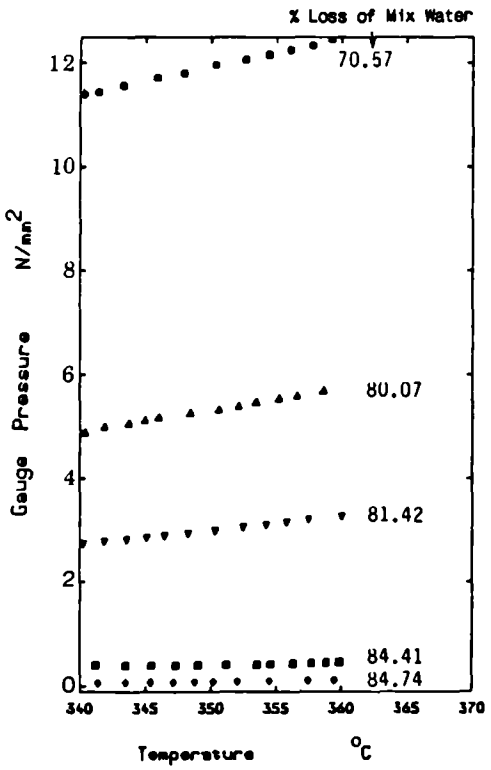

Figure 6.23:
GAUGE PRESSURE AGAINST TEMPERATURE AT VARIOUS WEIGHT LOSSES FOR RTS-07

Figure 6.24:
GAUGE PRESSURE AGAINST TEMPERATURE AT VARIOUS WEIGHT LOSSES FOR ALL RTS SPECIMEN

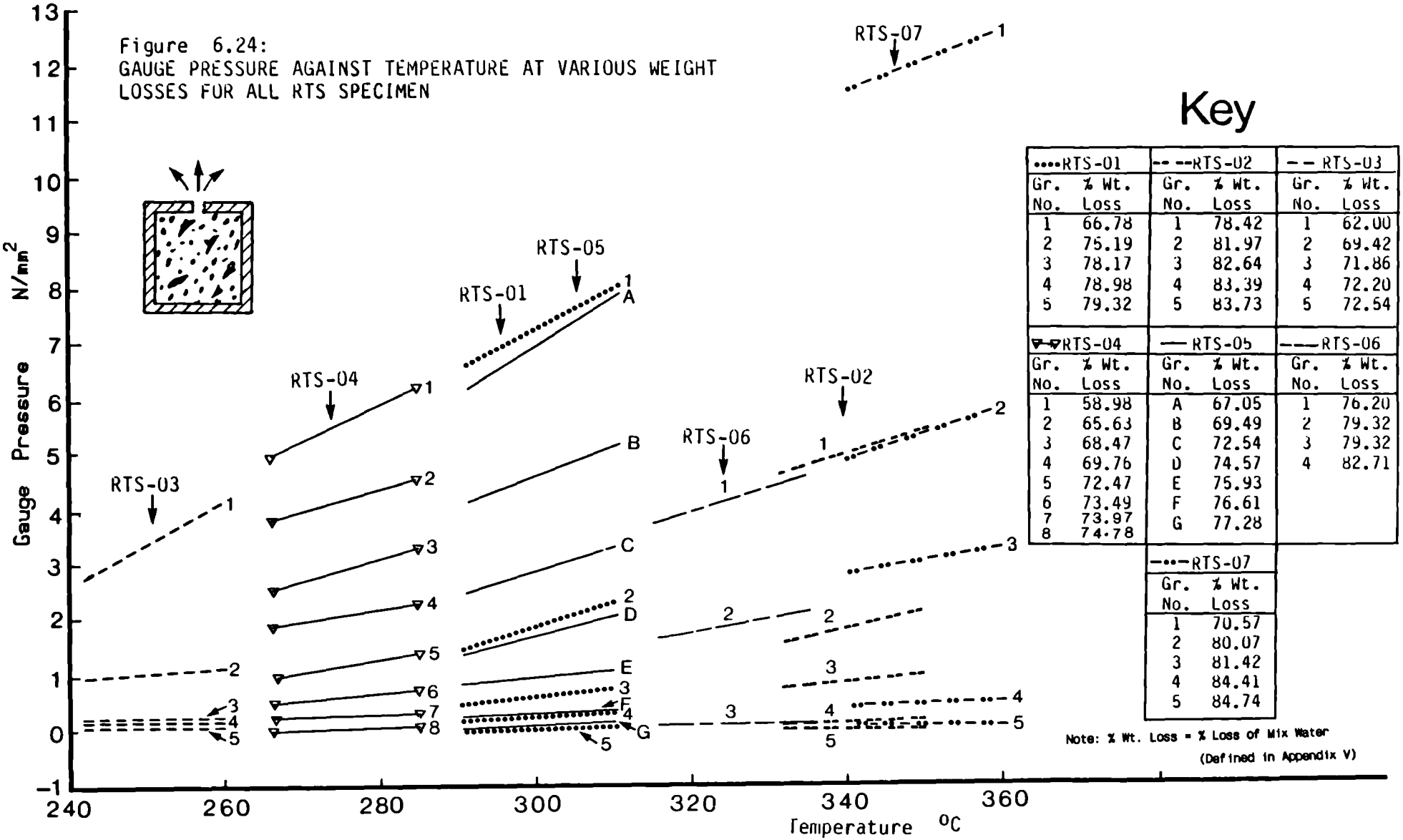

••••RTS-01	
Gr. No.	% Wt. Loss
1	66.78
2	75.19
3	78.17
4	78.98
5	79.32

-- --RTS-02	
Gr. No.	% Wt. Loss
1	78.42
2	81.97
3	82.64
4	83.39
5	83.73

-- RTS-03	
Gr. No.	% Wt. Loss
1	62.00
2	69.42
3	71.86
4	72.20
5	72.54

▽▽RTS-04	
Gr. No.	% Wt. Loss
1	58.98
2	65.63
3	68.47
4	69.76
5	72.47
6	73.49
7	73.97
8	74.78

— RTS-05	
Gr. No.	% Wt. Loss
A	67.05
B	69.49
C	72.54
D	74.57
E	75.93
F	76.61
G	77.28

——RTS-06	
Gr. No.	% Wt. Loss
1	76.20
2	79.32
3	79.32
4	82.71

-•--RTS-07	
Gr. No.	% Wt. Loss
1	70.57
2	80.07
3	81.42
4	84.41
5	84.74

Figure 6.24a:

GAUGE PRESSURE AGAINST TEMPERATURE AT VARIOUS WEIGHT LOSSES TAKEN AS MEAN VALUES FROM FIG. 6.24 FOR ALL RTS SPECIMEN

Note: % Wt. Loss = % Loss of Mix Water (Defined in Appendix V)

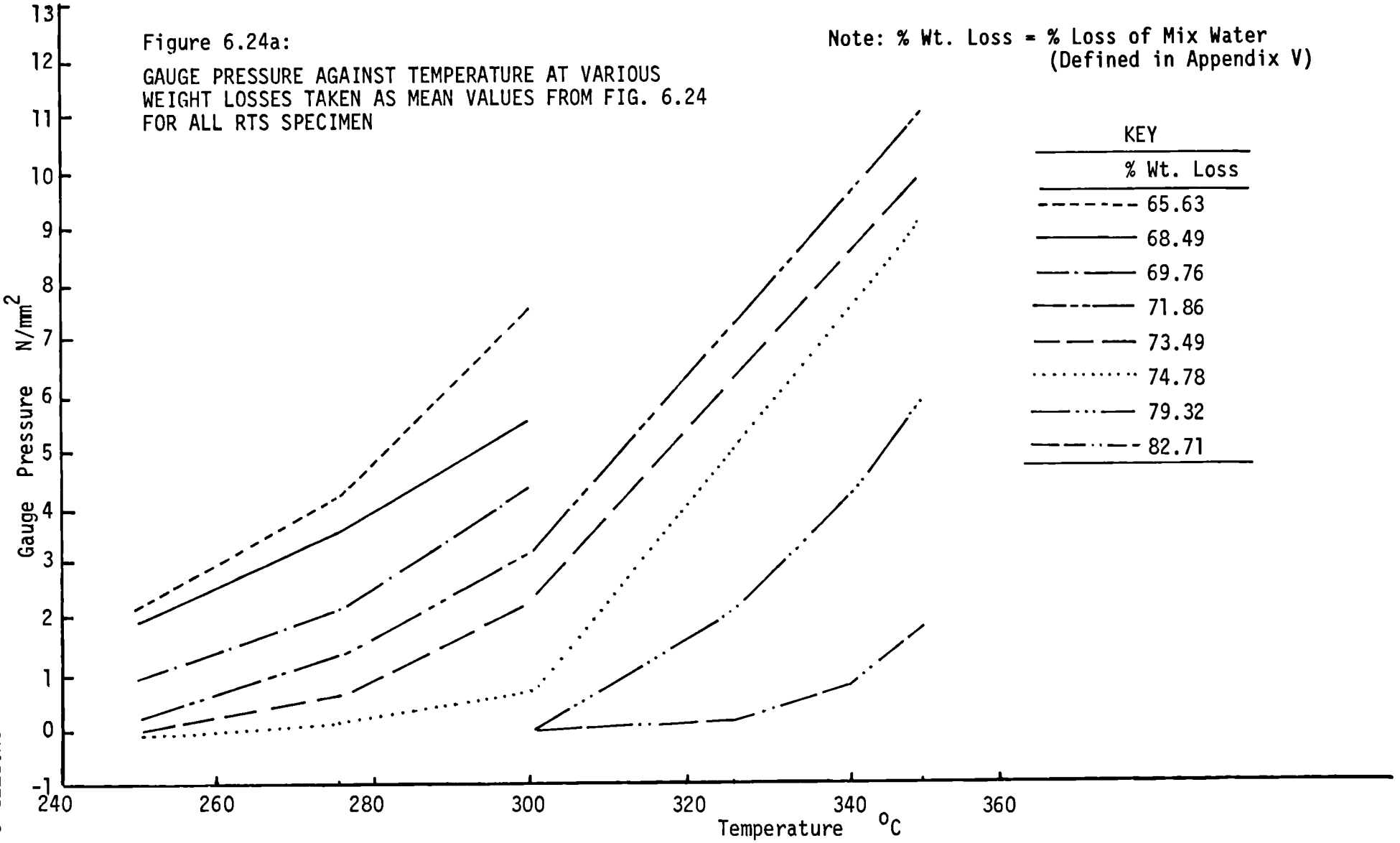

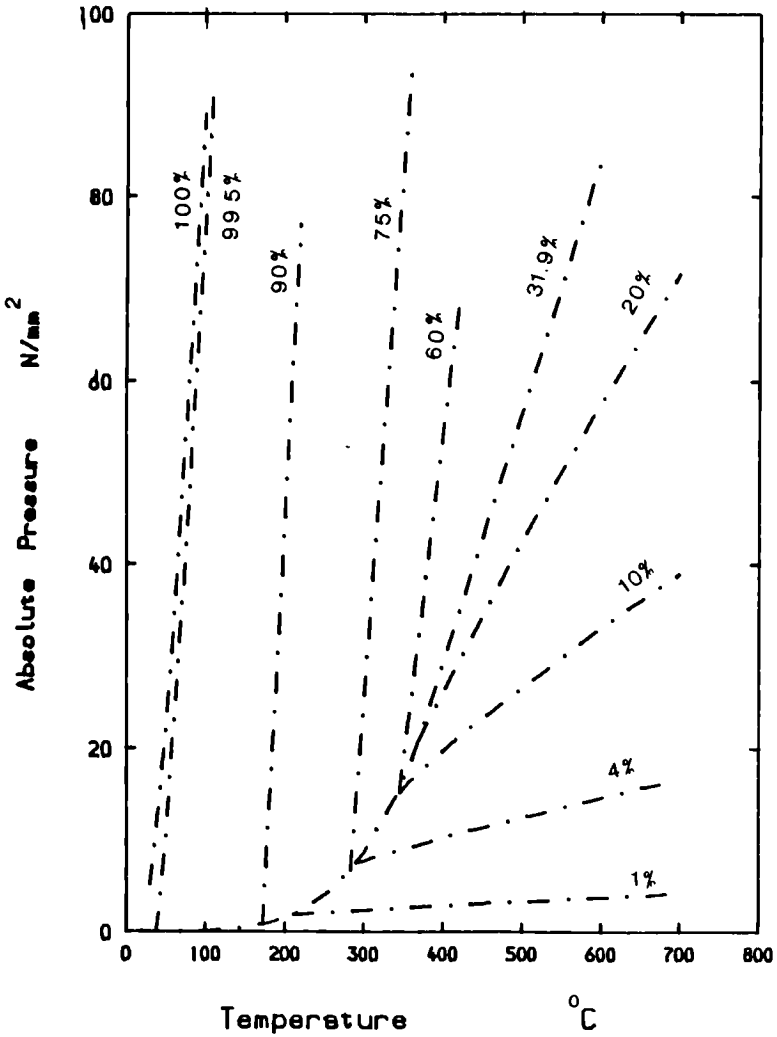

Figure 6.25: ABSOLUTE PRESSURE AGAINST TEMPERATURE OF PURE WATER IN % OF PORE VOLUME (GREATHEAD, 1986)

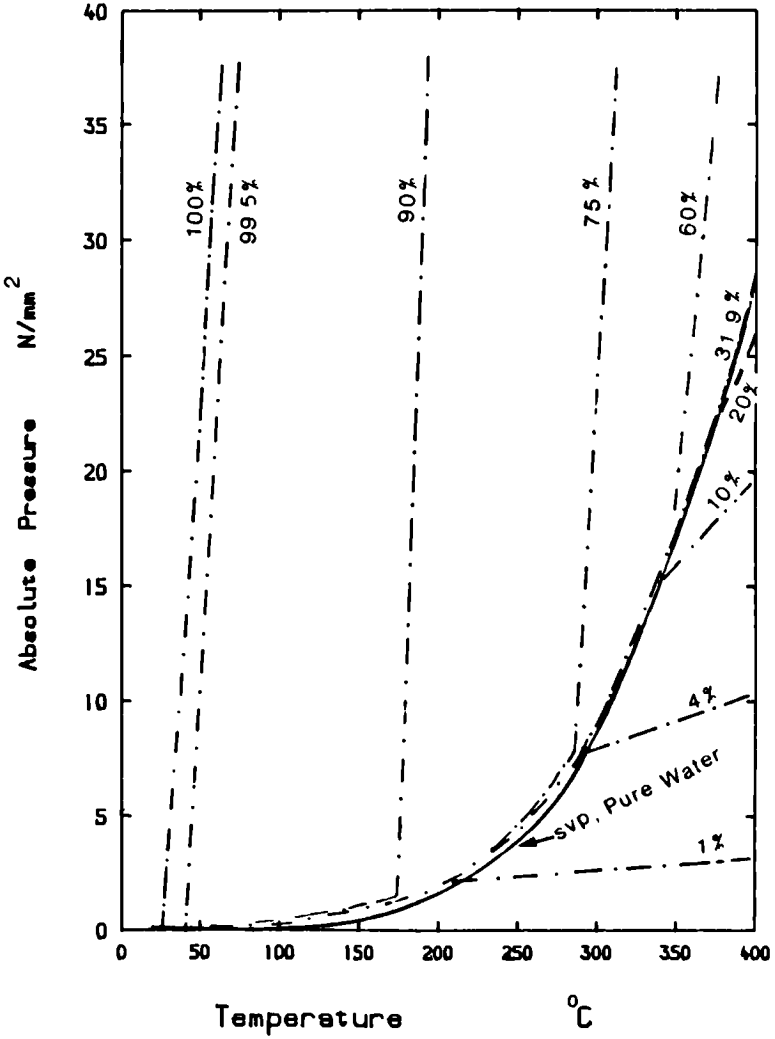

Figure 6.26: ABSOLUTE PRESSURE AGAINST TEMPERATURE FOR WATER IN % OF PORE VOLUME ON ENLARGED SCALE (GREATHEAD, 1986)

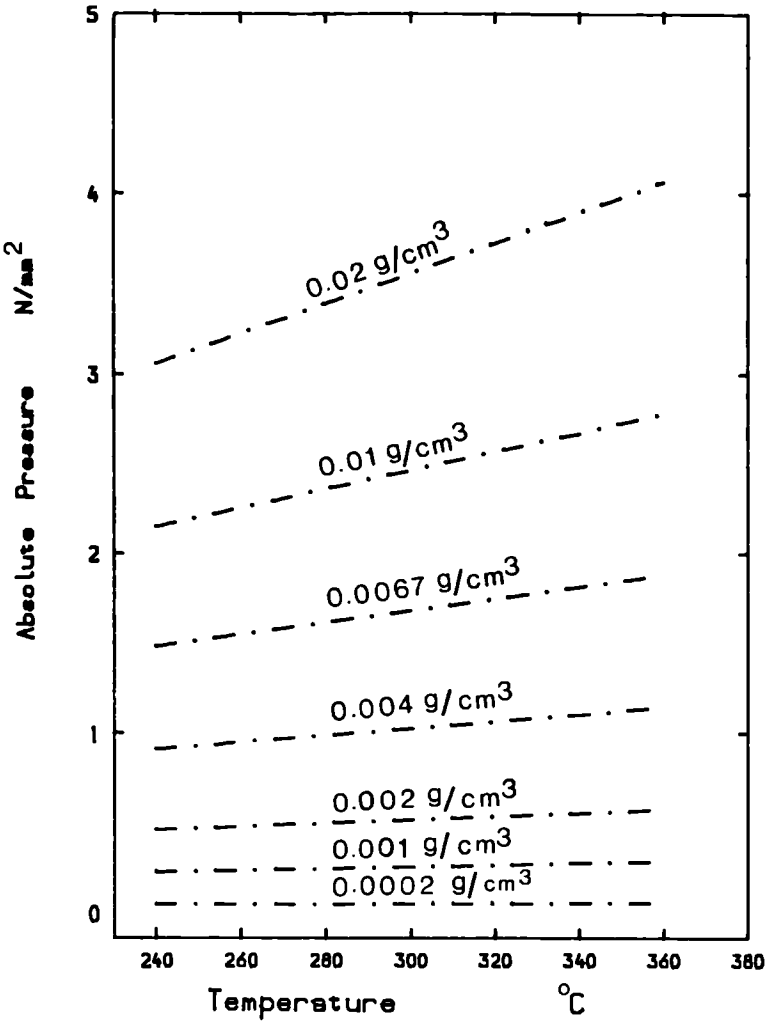

Figure 6.27: ABSOLUTE PRESSURE AGAINST TEMPERATURE AT VARIOUS DENSITIES OF SUPERHEATED STEAM (STEAM TABLES, 1970)

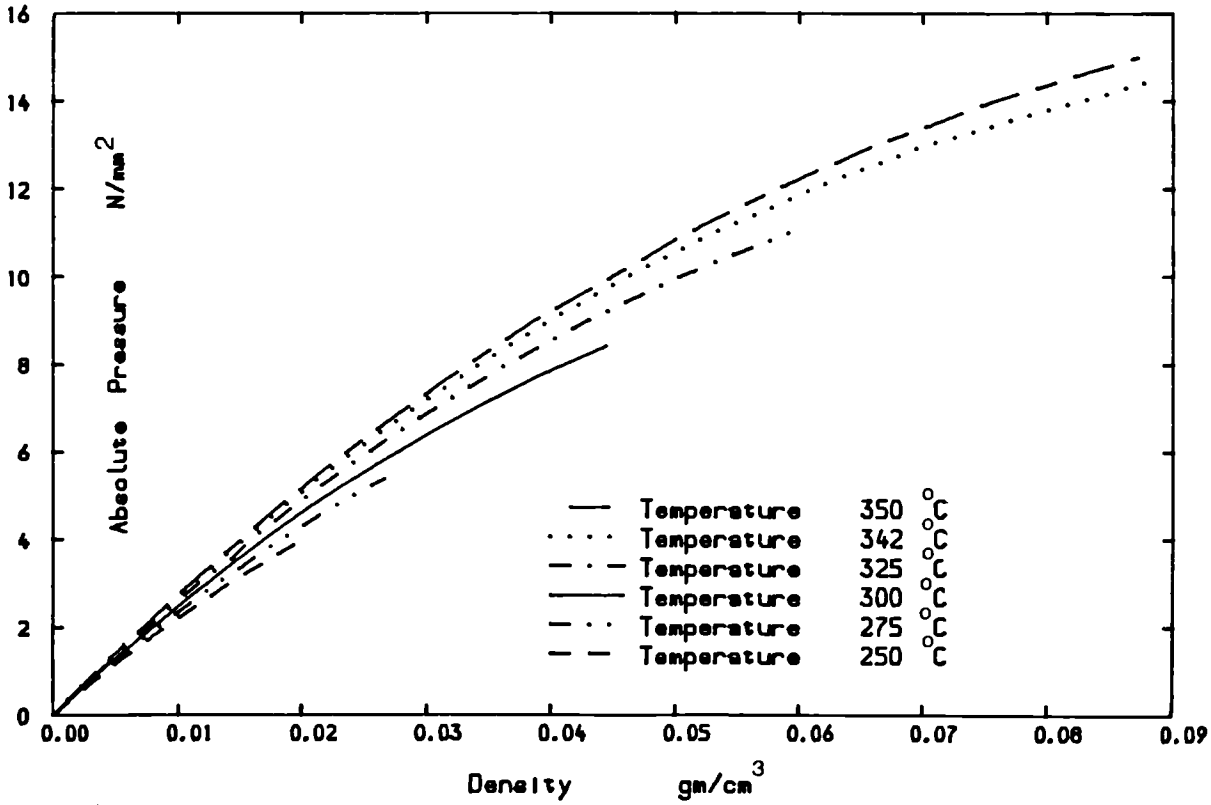

Figure 6.28: ABSOLUTE PRESSURE AGAINST DENSITY OF SUPERHEATED STEAM AT GIVEN CONSTANT TEMPERATURES (STEAM TABLES, 1970)

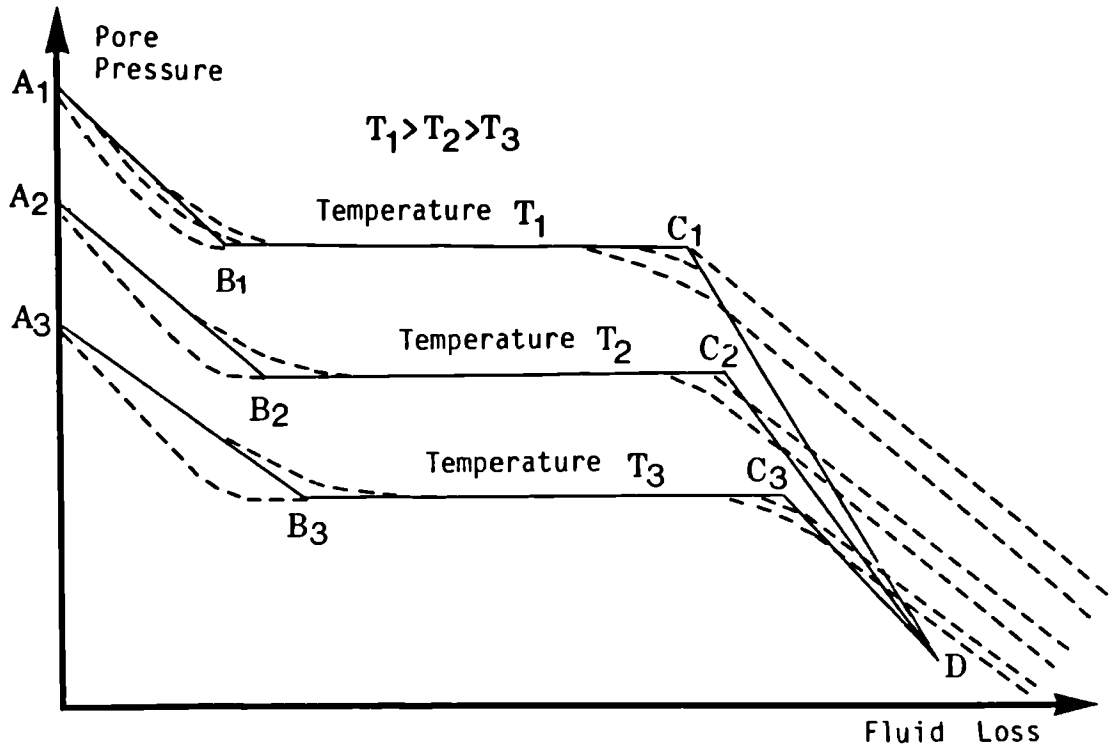

Figure 6.29: RELATIONSHIP BETWEEN PORE PRESSURE AND FLUID LOSS INSIDE AN IDEALISED MODEL AT VARIOUS TEMPERATURES

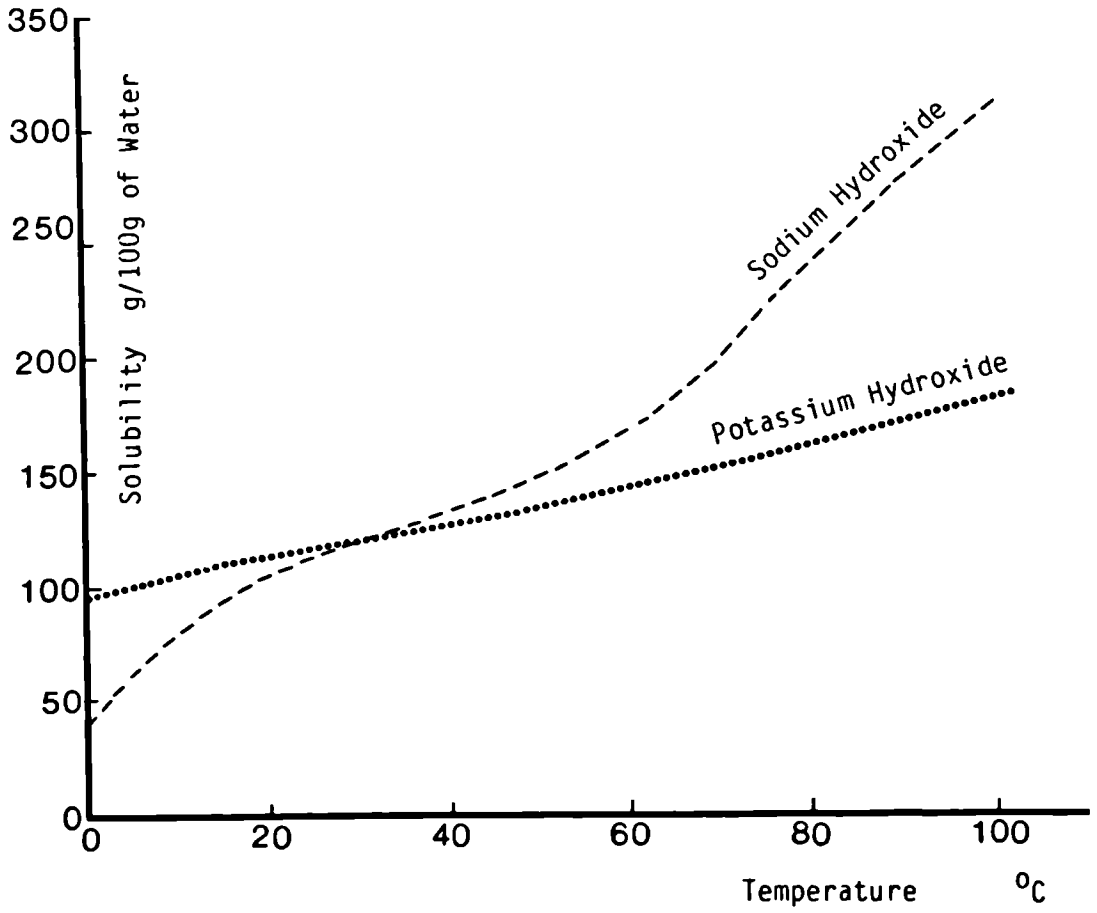

Figure 6.30: RELATIONSHIP BETWEEN THE SOLUBILITY OF POTASSIUM HYDROXIDE AND SODIUM HYDROXIDE WITH TEMPERATURE (HANDBOOK OF CHEMISTRY AND PHYSICS, 1979)

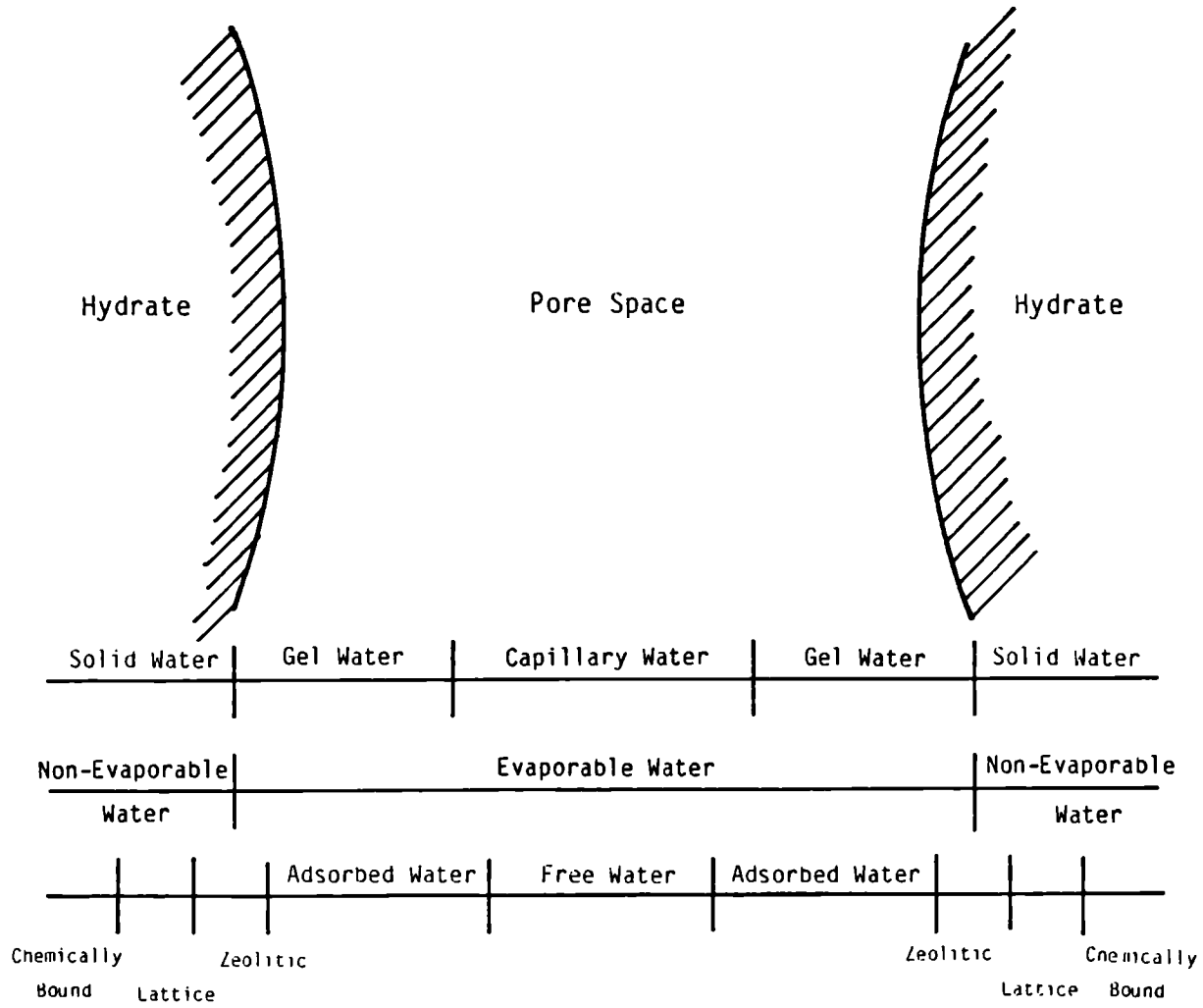

Figure 6.31: DIAGRAMATIC REPRESENTATION OF VARIOUS ARBITRARY STATES OF WATER IN CONCRETE

CHAPTER 7

CONCLUSIONS AND SUGGESTIONS FOR FUTURE WORK

7.1 CONCLUSIONS

Here general conclusions are drawn from non-uniformly heated concrete as employed in the simulated liner studies for a nuclear reactor and for uniformly heated concrete used to study the pore pressure behaviour at decreasing water content. The specific conclusions for each category of test are discussed at the ends of Chapters 5 and 6.

1. Pore pressures (~0.4 N/mm^2 at temperatures below 150 ^oC and within 3 minutes of commencement of rapid heating), exist in concrete behind the liner which are in excess of saturation vapour pressure of water.

2. As a result of these pressures, moisture migrates quickly away from hot zones (i.e. 20-40% of the original weight of mix water), and the first few minutes of heating are critical in terms of pore pressure and moisture migration adjacent to the liner.

3. The sealing conditions of concrete play a major role in the development of pore pressures in heated concrete, and typical values for:

   - uniformly heated sealed concrete where moisture migration does not take place were ~25 N/mm^2 at 350 ^oC

   - non-uniformly heated and sealed concrete, where moisture migrates away from hotter zones into cooler zones were ~8 N/mm^2 at 350 ^oC after ~60 minutes of heating

   - non-uniformly heated specimen with the cooler end open to the atmosphere, where moisture migration takes place were ~1.4 N/mm^2 at 350 ^oC after ~140 minutes of heating.

4. In simulated liner test for which transient conditions of temperature and pressure dominate, maximum concrete pore pressures behind the liner are not as high as in the constant temperature experiments (e.g. pressure in constant temperature

tests are ~3 times higher than the pressures in liner tests for the corresponding temperature).

5. The reinforcing bars, prestressing tendons, construction joints and prestressing ducts may provide routes for moisture movement and pressure loss during the process of heating concrete non-uniformly. These pathways could play a dominant role in eliminating high pore pressures.

6. Temperature and pore pressure gradients produce uneven moisture distribution in concrete (i.e. dry and wet zones). If heating is sustained for longer periods increasingly large regions of the concrete could dry out (with an associated loss in radiological protection capacity). For instance one-end sealed specimen of the "RTS" which was heated to 390 ^{o}C at the sealed end for ~342 minutes lost ~30% of the mix water (Figure 5.107). On the other hand accumulation of moisture driven from drying zones into increasingly wet zones could give rise to elevated pore pressures (especially if temperatures were still rising in the drying zones). This may result in high internal stresses and possibly hydraulic fracture of concrete.

7. Dry and wet zones can clearly be distinguished by visual inspection of cross-sections cut through the "Liner Test Series" specimens. Thus visual inspection would be a potentially useful post-accident diagnostic method.

8. The data obtained and analysed in this thesis show the significance of pore pressure and moisture migration in heated concrete. Therefore the engineers and the designers of concrete structures dealing with concrete subjected to temperatures above 250 ^{o}C should incorporate these parameters in design.

9. Possible means of avoiding high pore pressures behind the steel liner and reducing the associated risks include:

- introducing a thermal barrier in the form of fire bricks, or
- introducing a very porous layer of concrete adjacent to the liner.

10. Finally it is concluded that this work forms a useful data base for the analysis of moisture migration and pore pressures in concrete heated to high temperatures.

However, further experimental work and analysis should be carried out for all the important thermal properties of a range of concrete types. A databank should be compiled and should include information on the interactions of all materials and components used in design. The results should be made available to designers and engineers for predicting the long term behaviour of concrete (both as a material and as structural members) in the working environment to ensure good serviceability.

7.2 SUGGESTIONS FOR FUTURE WORK

Further experimental work should be carried out for monitoring moisture migration, pore pressures and other properties of concrete discussed below:

1. To study the decomposition and gas evolution from heated concrete, Differential Thermal Analysis (DTA), Thermal Gravimetric Analysis (TGA) and Evolved Gas Analysis (EGA) should be performed on heated and unheated concrete.

2. Pore size and pore size distribution should be analysed by mercury intrusion porosimeter for heated and un-heated concrete and cementitious materials. This would provide a clearer understanding of the phenomenon of dehydration in water loss regions and enhanced hydration in water gain regions.

3. Physico-chemical changes taking place in heated concrete should be investigated by using electron microscopy and x-ray diffraction. X-ray microprobe analysis could also be used for identifying the crystals of hydrates.

4. Variations in the porosity and permeability of concrete while being heated should be monitored to understand in greater depth moisture and pressure migration.

5. A less reactive and better understood porous material containing water, air and water vapours should be tested under similar condition as concrete to allow controlled comparative analysis (between the porous material and the concrete) of the effects of:

- surface forces

- hydrate chemistry and crystalline transitions of temperature

- pressure and moisture loss characteristics.

In summary for the effective study of the complicated problems of moisture migration and pore pressure in concrete under uniform and non-uniform temperatures, a multi-disciplinary team should work on a range of concretes, cements and admixtures, and compile a databank of the material properties. Mathematical and numerical models should also be developed to analyse the problems involved, and assist engineers, researchers and designers working in this field.

APPENDIX - I

DESIGN OF "LINER TEST SERIES"

I.1 INTRODUCTION

The "Liner Test Series" ("LTS") experiments were designed to monitor the pore pressures, moisture migration and temperature distribution inside a concrete cylinder under a thermal gradient. The combined effects of pore pressures and temperature on the liner of a Fast Breeder Reactor were simulated by a stainless steel diaphragm, and the central deflection of the diaphragm was measured. Plate I.1 & Figure I.1 show the exploded view, and Figure I.2 shows the cross-sectional view of a typical "LTS" cell without instrumentation. The design of the mild steel top ring was modified (Plate I.6) before assembling the components together. Plate I.1 does not show the modified steel top ring. The construction and description of each individual item of the "LTS" is outlined below.

I.2 MILD STEEL CYLINDER

To hold concrete a steel cylinder capable of sustaining pore pressures in excess of 17-18 N/mm^2 and temperatures up to 450 ^{o}C was designed. The following factors were considered to design this cylinder:

i. A factor of safety greater than 2 under the effects of temperature and pore pressure, to achieve structural integrity.

ii. An adequate surface to provide pressure sealing at each end of the cylinder.

iii. The availability of space to introduce the instrumentation into the concrete through the wall of the steel cylinder, and the provision of good pressure sealing for the fittings.

iv. The availability of space to accommodate the bolts in the wall of the cylinder at each end.

v. Considerations of casting and testing the concrete, and provision for the removal of concrete samples from the cylinder at the completion of the test (for final water distribution measurements).

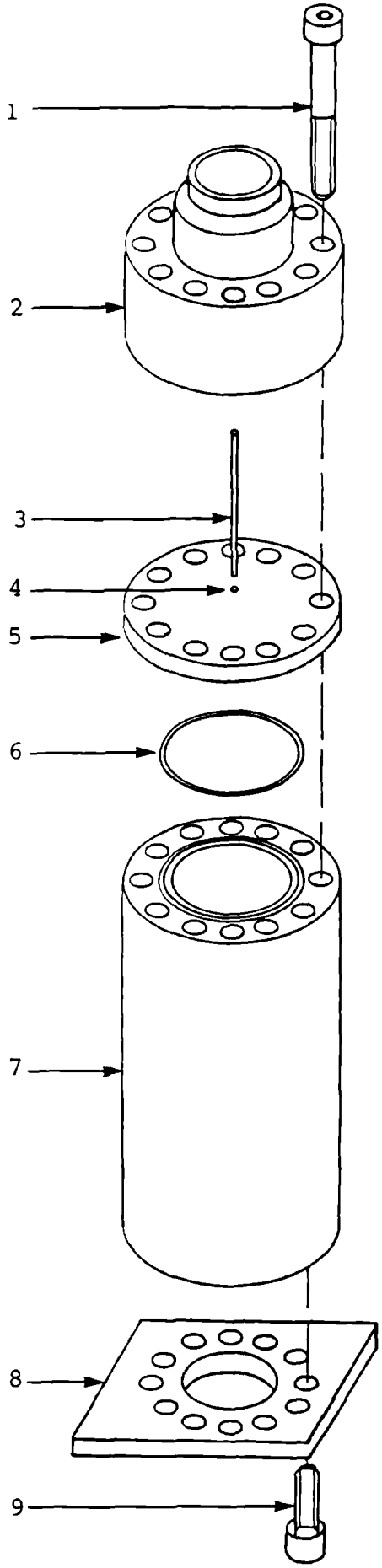

KEY

1. 5/8 inch diameter, high strength steel hexagon cap head screw
2. mild steel top ring
3. sintox tube
4. stainless steel ball bearing
5. stainless steel diaphragm
6. metal 'O' ring
7. mild steel cylinder
8. mild steel base plate for one end sealed specimen
9. 5/8 inch diameter, high strength steel hexagon cap head screw

Figure I.1:

Exploded, iso-metric view of "Liner Test Series" cell

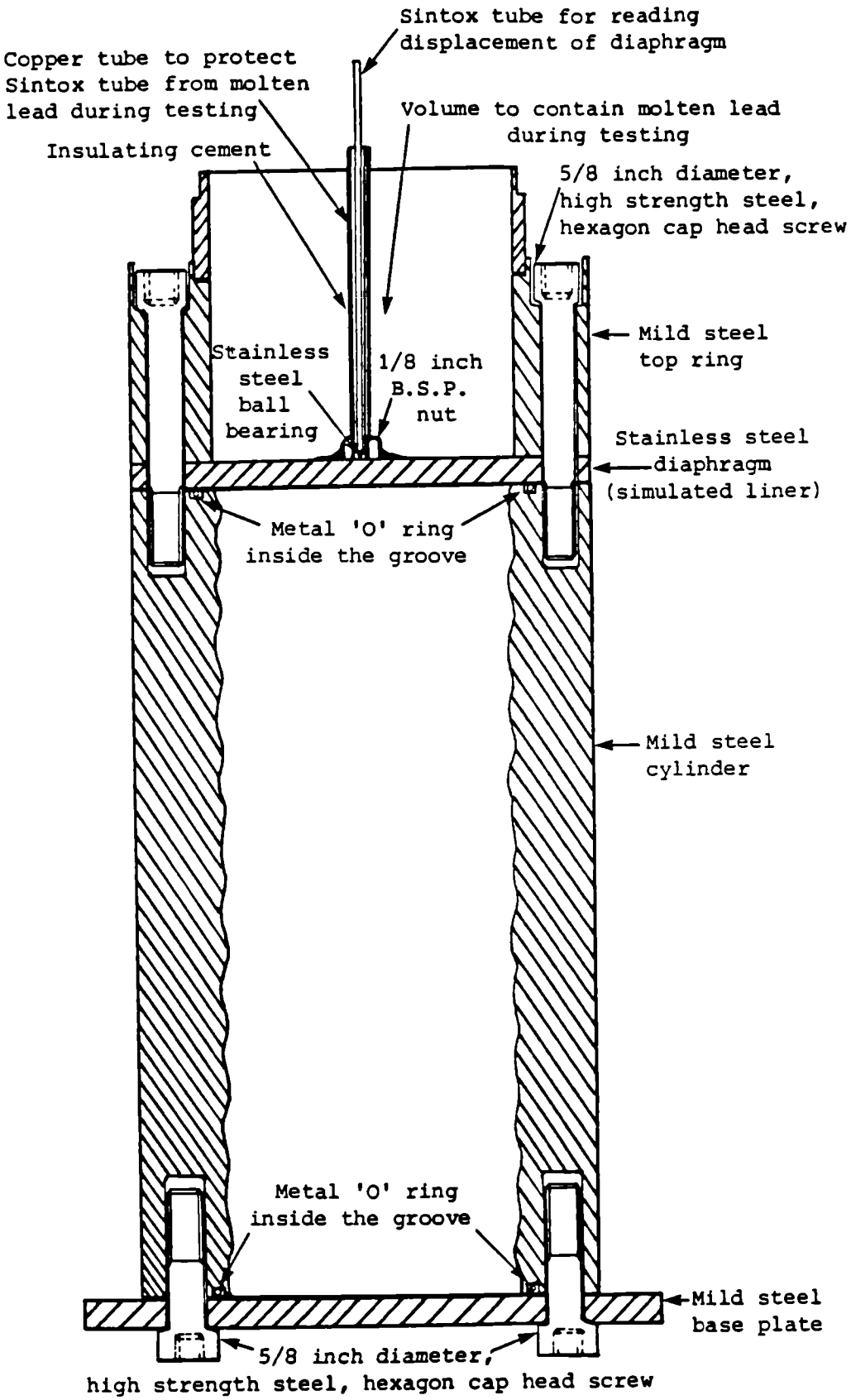

Figure I.2:

Cross-sectional view of a typical "Liner Test Series" cell, without instrumentation.

After reviewing many options, a thick wall mild steel seamless tube (Figure I.3) was selected, which satisfied the parameters described above (N.B. this tube is referred to as 'the mild steel cylinder' throughout the thesis).

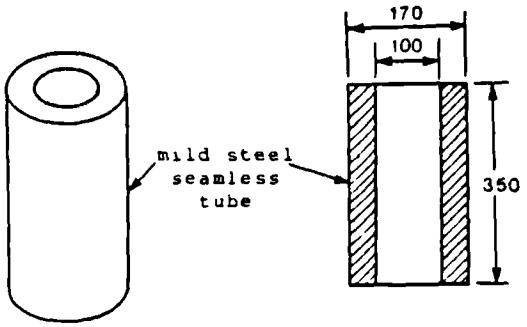

Figure I.3:

Mild steel cylinder before machining.

The following machining work was carried out on the steel cylinder (Figure I.4, Plate I.2).

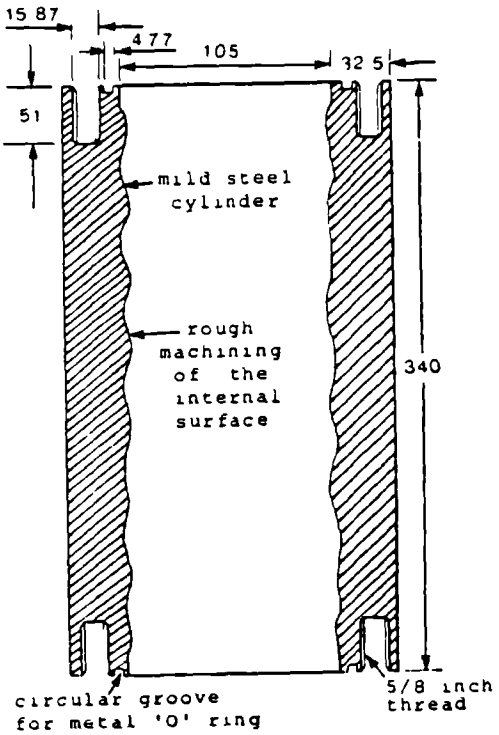

Figure I.4:

Mild steel cylinder after machining.

1. The internal suface of the cylinder was roughened, to achieve a good concrete to steel bond.

2. Twelve holes were drilled and tap ed for 5/8 inch diameter hexagon cap head screws at each end of the cylinder, to clamp the stainless steel diaphragm (at the top end) and the base plate (at the bottom end).

3. A circular groove was machined and polished at each end of the

cylinder for sealed specimen, to accommodate a metal 'O' ring for pressure sealing, as explained in Section I.7. However, for partially sealed and one-end sealed specimen, the groove was only machined and polished at the top end of the cylinder. Figure I.5 shows the enlarged cross-sectional view of a groove.

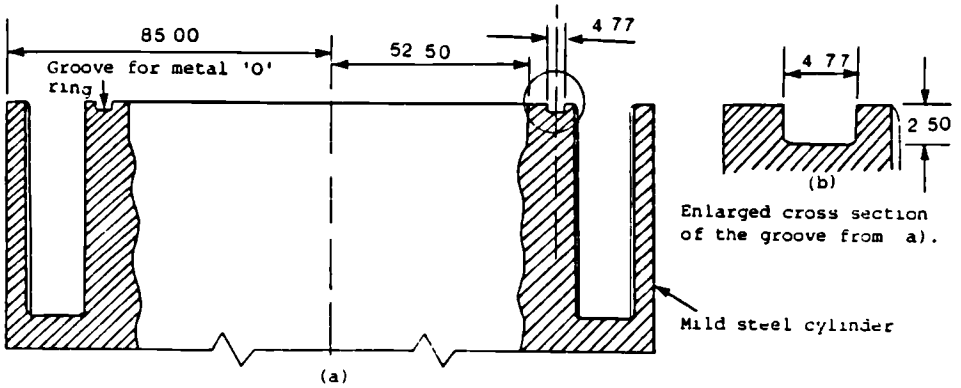

Figure I.5: Enlarged cross-sectional view of the groove.

4. To measure the pore pressure and the temperature of the concrete, the instumentation was introduced through the wall of the steel cylinder diametrically opposite each other (Figure I.6 and Plate 4.8 of Chapter 4), as described below:

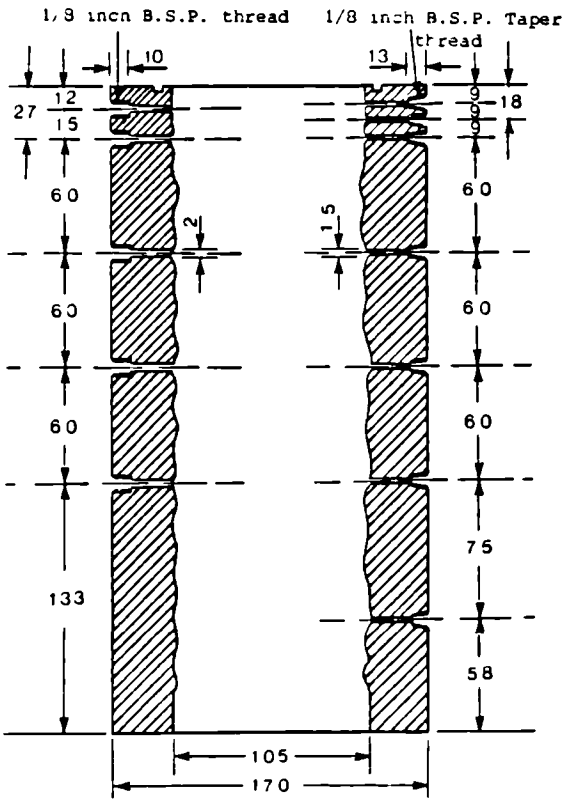

Figure I.6:

Cross-sectional view of the mild steel cylinder showing the instrumentation positions and dimensions.

PORE PRESSURE INSTRUMENTATION

- Five, 3/32 inch diameter holes were drilled through the wall of each cylinder.

- The external ends of these holes were drilled larger to a depth of 1/2 inch, and 1/8 inch B.S.P. parallel female threads were tapped in these holes to accommodate the pressure couplings. The surface around the threads on the outer surface of the cylinder was spot faced for a copper washer to provide pressure sealing between the couplings and the cylinder.

- The second instrumentation position (27mm from the top end of the cylinder) was staggered from the other four positions, to accommodate all the couplings in the limited space, as shown in Figure I.7a and Plate 4.7 of Chapter 4.

TEMPERATURE INSTRUMENTATION

- Seven 3/32 inch diameter holes were drilled through the wall of 4 cylinders, while ten holes (of the same diameter) were drilled for the remaining 2 cylinders diametrically opposite to the pressure couplings.

- The external ends of these holes were again drilled to a larger diameter, but 1/8 inch B.S.P. tapered threads were tapped in these holes.

- The surface around the threads on the outer surface of the steel cylinder was also spot faced for copper washer to provide additional pressure sealing between the fitting and the cylinder.

- The second instrumentation position (18mm from the top end of the cylinder) was again staggered from the remaining positions, to accommodate the thermocouple fittings in the limited space available (Figure I.7b and Plate 4.17 of Chapter 4).

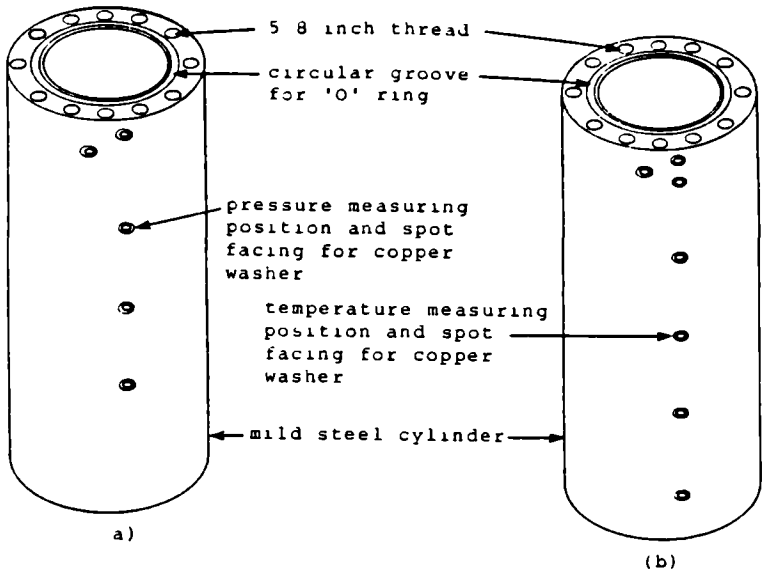

Figure I.7: Isometric view of the mild steel cylinder showing instrumentation positions.

5. Finally two mild steel pipes were welded to the outside of the steel cylinder opposite each other. These steel pipes were used as handles to lift and to secure the specimen to the test rig during testing (Section I.10).

I.3 STAINLESS STEEL DIAPHRAGM (SIMULATED LINER)

To simulate the steel liner of a FBR, a diaphragm was designed to transmit the heat to the concrete in the steel cylinder (Section I.2). The diaphragm was used as a sealed membrane providing the pressure sealing at the top end of the cylinder, by clamping a metal "O" ring inside the groove under the diaphragm. The main factors in the selection of the diaphragm were its material properties and the size. Type 316 stainless steel was preferred to the other materials for good thermal properties (e.g. thermal expansion and thermal shock etc.). The thickness of the diaphragm was calculated for a fixed edge plate (Timoshenko, 1940) and 9.5mm (3/8 inches) was adequate, safe and within the elastic limit for deformation.

Type 316 stainless steel discs (170mm o.d. and -9.75mm thick) were obtained, and twelve clearance holes (for 5/8 inch diameter hexagon cap head screws) were drilled in each diaphragm, as shown in Figure I.8 and Plate I.3 & I.4.

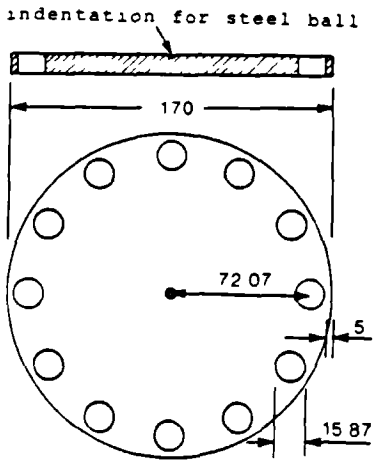

Figure I.8:

A stainless steel diaphragm (simulated liner).

An indentation was machined in the centre of the diaphragm at the top end (Figure I.8 and Plate I.4), to locate the steel ball (Section I.8) under the Sintox tube for measuring the deflection. The bottom surface of the diaphragm was machined and polished (to a finish of 32-16 microns, as shown in Plate I.3), to provide pressure sealing in conjunction with an "O" ring (Section I.7). The finished thickness of each diaphragm slightly varied after machining and polishing, and the thickness of each diaphragm was measured before assembling the test cells. Table I.1 gives the sizes of the diaphragms used for the tests of the "LTS".

	LTS-1	LTS-2	LTS-3	LTS-4	LTS-5	LTS-6
Size of Diaphragm (mm)	9.347	9.220	9.525	9.347	9.601	9.500

Table I.1: The thickness of each diaphragm for the "LTS".

I.4 MILD STEEL TOP RING

The heating design of the "LTS" (Chapter 3, Section 3.3.3) necessitated the use of a container to hold molten lead during testing and also to provide support for heaters, lead pouring assembly, deflection measuring set up and thermocouples at the top end. It was therefore decided to use a 76mm long (Figure I.9) top ring of the same material and similar inside and outside diameter, as the mild steel cylinder (Section I.2).

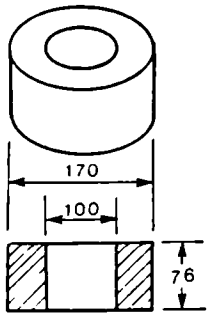

Figure I.9:

Mild steel top ring before machining.

The design of the top ring was developed in the following two stages:

FIRST STAGE

i. The top ring was machined (Figure I.10 and Plate I.5), and twelve clearance holes for 5/8 inch diameter screws were drilled at the same spacing as the holes for the stainless steel diaphragm (Figure I.2, Plate I.1). The top ends of these holes were drilled to a larger diameter for sinking the screw heads, as shown in Figure I.10 and Plate I.5.

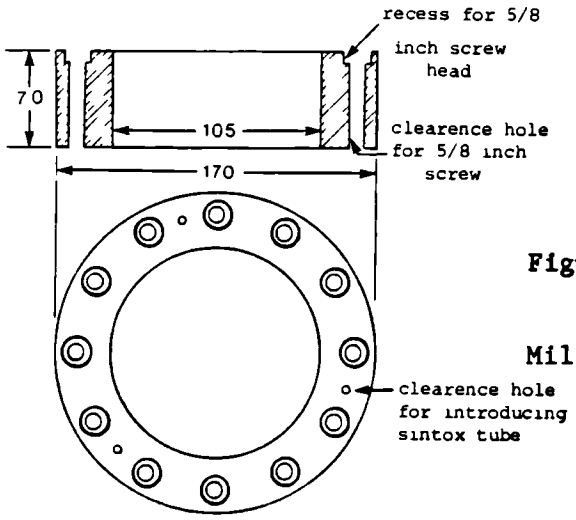

Figure I.10:

Mild steel top ring after machining.

ii. Three 1/4 inch diameter holes were also drilled through the wall of the top ring, to pass the Sintox tubes (Section I.8), as shown in Figure I.10 and Plate I.5.

SECOND STAGE

The size of the top ring constructed during the first stage was inadequate as a container, to hold the required amount of molten lead.

Therefore an extra length of mild steel tube was welded to the top ring, as described below.

i. The top and the bottom ends of the extension steel tubes were machined (Figure I.11 and Plate I.6).

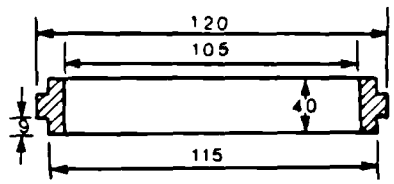

Figure I.11:
Extension mild steel tube after machining.

ii. To connect the extension steel tube to the steel top ring, the top ring was also machined from the top end, and both pieces were welded together (Figure I.12 and Plate I.7).

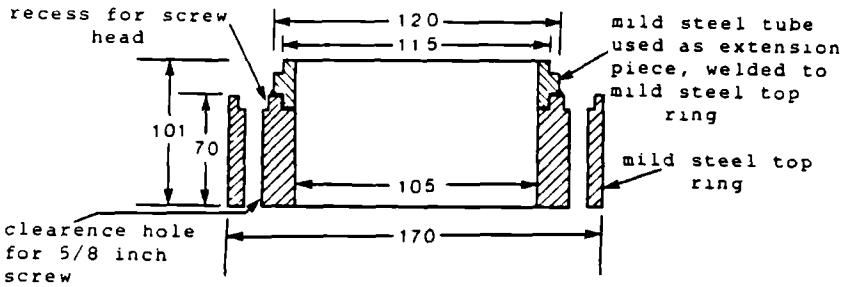

Figure I.12: Mild steel top ring after completion.

iii. Three indentations were drilled on the machined surface of the outside face of the extension tube, to secure the lead pouring assembly to the steel top ring.

I.5 MILD STEEL BASE PLATES

To prevent the movement of concrete inside the mild steel cylinder and to seal the pore pressure of the heated concrete at the end away from the heat source, two types of base plates were designed.

1. Twelve clearance holes for 5/8 inch diameter screws were also drilled in each base plate, at the same central distance as the threaded holes of the bottom end of the steel cylinder (Section I.2).

2. A 50 inch diameter hole was drilled in the centre of the base plates used for one-end sealed specimens, to release the pore pressure of concrete to the atmosphere at the end away from heat. The base plates used for sealed and partially sealed specimens did not have a hole.

3. The surface of the base plates making contact with the metal "O" ring seals of the sealed specimens (Plate I.7) were polished (Section I.7).

Figure I.13 and Plate I.7 show both types of plates, and Table I.2 lists the type of base plate used for each specimen.

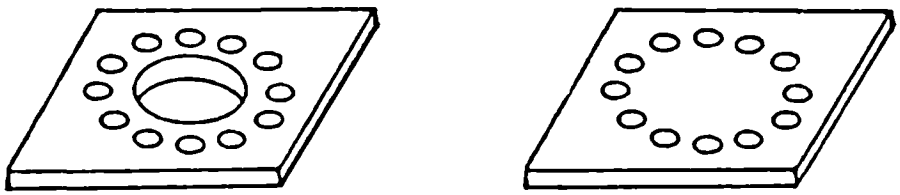

Figure I.13: Two types of base plates after machining.

LTS-1	LTS-2	LTS-3	LTS-4	LTS-5	LTS-7
(a)	(a)	(b)	(b)	(b)	(b)

(a) Base plate with a hole in the centre.
(b) Base plate without a hole in the centre.

Table I.2: Types of base plates used with the "LTS" specimens.

I.6 BOLTING OF THE ASSEMBLY

The limited space available for the bolt heads (Section I.4), dictated the use of hexagon cap head screws, to clamp the stainless steel diaphragm between the steel top ring and the top end of the steel cylinder, and to bolt the base plates to the bottom end of the steel cylinder, as shown in Figure I.2 and Plate I.1. High strength steel was selected as the material for the bolts, due to the presence of considerable forces on these bolts (e.g. thermal stresses and pore pressures). The bolts were capable of working in temperatures in excess of 600 ^{o}C.

Twelve bolts of 5/8 inch diameter used at each end of the cylinder were adequate for a safety factor greater than 2. The screws used for clamping together the steel top ring and the stainless steel diaphragm at the top end of the steel cylinder were 4.5 inches long, while 2.5 inch long screws bolted the base plate to the bottom end of the steel cylinder. Figure I.14 shows the two types of the bolts.

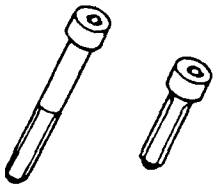

Figure I.14:
Two types of bolts used to bolt the assembly.

I.7 PRESSURE SEALING

In designing the pressure seals for pore pressures of 17-18 N/mm^2 (2500 psi) and temperature in excess of 400 ^{o}C, a number of options was considered. The combination of temperature and pressure limited the choice of sealing materials especially between the stainless steel diaphragm and the heated end of the steel cylinder. After carefully considering a few of the available seals, it was decided to use a metal seal at the heated end for all the specimens, and at both ends of the cylinder for sealed specimens. The end of the steel cylinder furthest away from the heat source was sealed by clamping an asbestos based gasket between the base plate and the cylinder.

Two metal seals were tested, i.e. a copper gasket, and a hollow metal "O" ring externally coated with silver and filled with gas at high pressure. The gasket was rejected, because it did not provide efficient sealing. The metal "O" ring (Figure I.15, Plate I.1) was selected, because it provided the best means of sealing the pressures at high temperatures. Table I.3 lists the 'O' ring specifications.

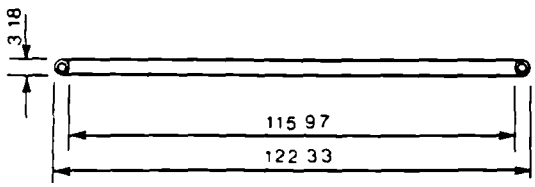

Figure I.15:
Metal "O" ring used for sealing.

Ring Material used was Stainless Steel Type 316	Ring Size mm			Plating or Coating	Recomended Torque Ft-Ibs	Working Temperature C
	o.d.	Tube	Wall			
	122.3	3.18	.508	Silver	150-160	800

Table I.3: Specifications for the metal "O" rings.

The metal "O" ring was placed inside a groove (Figure I.5), and clamped under a stainless steel diaphragm at the heated end of the cylinder for all the specimens, and under a base plate at the end away from heat for sealed specimens, as shown in Figure I.1. It was important that all machining marks were concentric with the line of seal, because the spiral or radial marks would form a leak path across the face of the seal. Although the silver coating on the external surface of the "O" ring reduced the need for polishing the machined surfaces to some extent, the metal surfaces in contact with the "O" rings were still ground (to a surface finish of 0.4064 microns).

A torque of 150-160 ft-lbs was applied to each bolt to achieve a satisfactory seal, and each "O" ring was tested after completing the assembly before casting concrete.

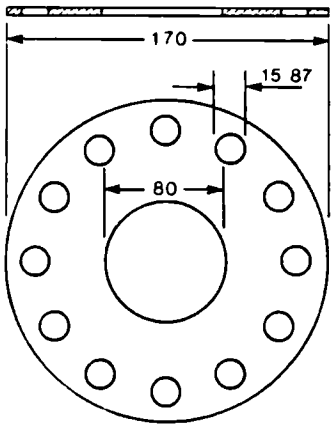

Figure I.16: Sealing gasket.

The asbestos based gasket's construction was such that it did not absorb moisture, and it was capable of working under a temperature of 250 ^{o}C. Twelve clearance holes (for 5/8 inch screws) and a hole in the centre were punched in the gasket, as shown in Figure I.16.

The sealing between the mild steel cylinder and the fittings attached to it (i.e. thermocouple glands and stud couplings) was provided by copper washers, as described in Section I.2.

I.8 SINTOX TUBE FOR READING DISPLACEMENT OF DIAPHRAGM AND ITS PROTECTION FROM MOLTEN LEAD

The central deflection of the stainless steel diaphragm was recorded by a transducing system (Chapter 4, Section 4.3.1). It was not possible to use this system directley on the diaphragm, due to the presence of molten lead and high temperature. The system was therefore mounted on an assembly which rested on top of three Sintox tubes. The diaphragm deflection was transferred to the transducer through a fourth Sintox tube, positioned between the transducer and the diaphragm (Chapter 4, Section 4.3.3 & 4.3.4).

The Sintox tube (6.35mm o.d., 3.17mm i.d., and 255mm long) was placed on top of a stainless steel ball located in the central indentation of the diaphragm, as shown in Figure I.17.

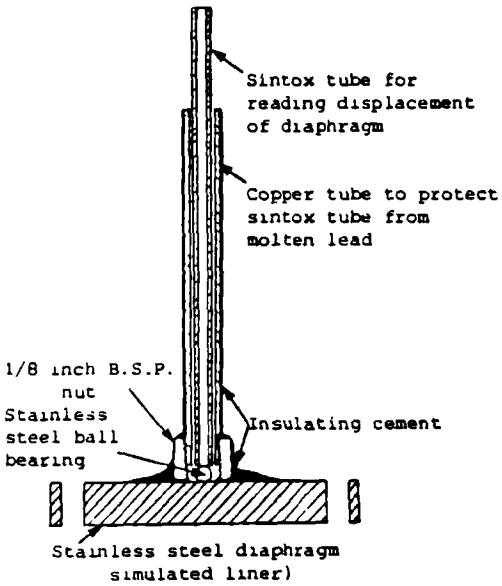

Figure I.17:

Cross-sectional view of a Sintox tube, the steel ball, and the copper tube screwed and cemented to a nut and the diaphragm.

The Sintox tube was selected for better thermal properties (e.g. deformation and thermal shock resistance, Table I.4) than the other materials.

Specific Heat at 25 °C	Thermal Conductivity 25-40 °C	Deformation Temperature	Thermal Shock
CGS Unit	CGS Unit	°C	°C
0.175	0.054	1450	160

Table I.4: Some of the thermal properties of the Sintox tubes.

To protect the Sintox tube from the splash of molten lead during the experiments, a brass nut was cemented to the diaphragm using a high temperature cement. A copper tube was screwed into the nut and these were completely covered with high temperature thermal insulating cement (Figure I.2 & I.17). A provision was made to introduce the thermocouples through the wall of the copper tube to measure the temperature of the Sintox tube, as described in Appendix IV.

I.9 LEAD POURING ASSEMBLY

The lead pouring assembly (Plate I.8) was designed:

- to assist in pouring the molten lead into the steel top ring
- to pour the molten lead out of the steel top ring, at the end of the calibration tests (Appendix IV), or during the main tests of the "LTS" in case of an emergency
- to attach the internal heater and the thermocouples (measuring the lead and steel diaphragm temperatures) to the assembly.

The following work was carried out to construct this assembly.

1. A mild steel tube (100mm i.d.,120mm o.d.) was machined to fit the top end of the steel top ring.
2. A mild steel funnel was made and welded to (1 inch i.d., 1.25 inch o.d.) a mild steel pipe.
3. To connect the funnel pipe to the steel tube, a clearance hole (to suit the external diameter of the pipe) was drilled through the wall of the tube, and the pipe was welded to the tube in alignment with the hole.
4. A hole was drilled in the steel tube and a mild steel pipe (2 inch i.d., 2.25 inch o.d.) was welded to the tube in alignment with this hole, to pour the molten lead out, as shown in Figure I.18 and Plate I.8.

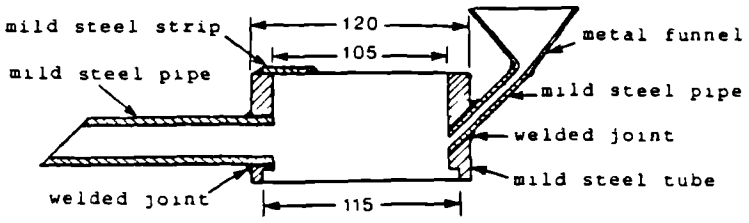

Figure I.18: Lead pouring assembly after machining and welding the components together.

5. Three holes were drilled and tapped for 4 BA screws through the steel tube wall, to secure the lead pouring assembly to the steel top ring. The positions where the screws came into contact with the top ring, an indentation was drilled on the outer surface of the top ring at each screw position (Section I.4).

6. An extra piece of steel strip was welded on top of the mild steel tube to prevent the spillage of molten lead while pouring the lead out of the test cell.

7. Two grooves were cut at the top of the steel tube, to introduce the internal spiral heater inside the top ring.

8. Three thermocouples were mounted on a steel strip (Plate I.8), to measure the temperature of the molten lead and the lead-diaphragm interface, and to control the thermostat of the internal spiral heater, as discussed in Chapter 3, Section 3.3.3. A piece was cut from the tube and a steel strip with the thermocouples attached to it was screwed to the outside wall of the steel tube of the lead pouring assembly.

9. To secure and protect the thermocouple leads (used to measure the Sintox tube temperature, Section I.8), a steel strip was screwed to the outside of the lead pouring assembly. Another piece of steel strip was used to clamp these leads between the two strips (Plate 3.9 of Chapter 3). Both the strips were thermally insulated with a high temperature insulation paper (Plate I.8).

10. All the internal surfaces of the lead pouring assembly were lined with high temperature thermal insulating cement (Plate I.8).

I.10 TEST RIG FOR HOLDING THE TEST CELL

A test rig (Plate I.9) was designed for the reasons given below:

i. To hold the mild steel cylinder while bolting, the stainless steel diaphragm, the mild steel top ring, and the base plate to the steel cylinder.

ii. To hold the test cell during the calibration and the testing of the "LTS". This was done to prevent the spillage of the molten lead accidently.

iii. To retrieve the molten lead from the mild steel top ring at the end of the calibration tests, as described in Appendix IV.

iv. To protect the deflection measuring system from vibrations and to provide stability during testing.

The test rig was bolted to the joints of the floor. The handles of the steel cylinder were clamped inside the arms of the test rig so that the test cell could be rotated through 180 degrees, to pour the molten lead out (Plate I.9). The molten lead was poured out of the steel top ring by tilting the test cell and pouring the lead out through the pipe welded on to the lead pouring assembly (Section I.9). The test rig was situated close to all the instruments.

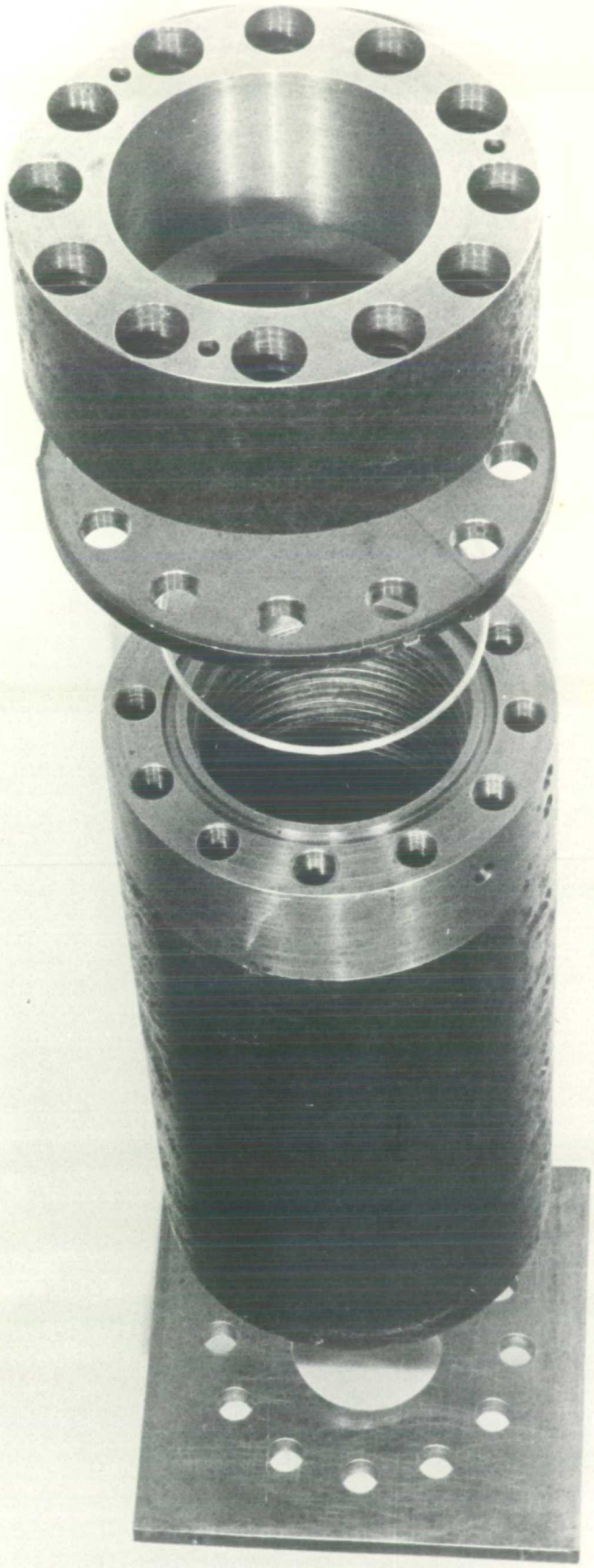

PLATE I.1: EXPLODED VIEW OF "LINER TEST SERIES" CELL

PLATE I.2 MILD STEEL CYLINDER AFTER MACHINING

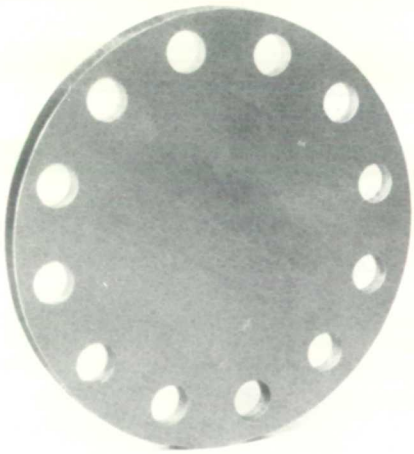

PLATE I.3
STAINLESS STEEL DIAPHRAGM,
BOTTOM SURFACE

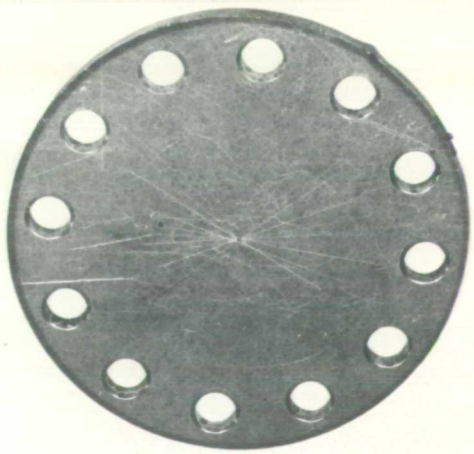

PLATE I.4
STAINLESS STEEL DIAPHRAGM,
TOP SURFACE

PLATE I.5: TOP VIEW OF MILD STEEL TOP RING

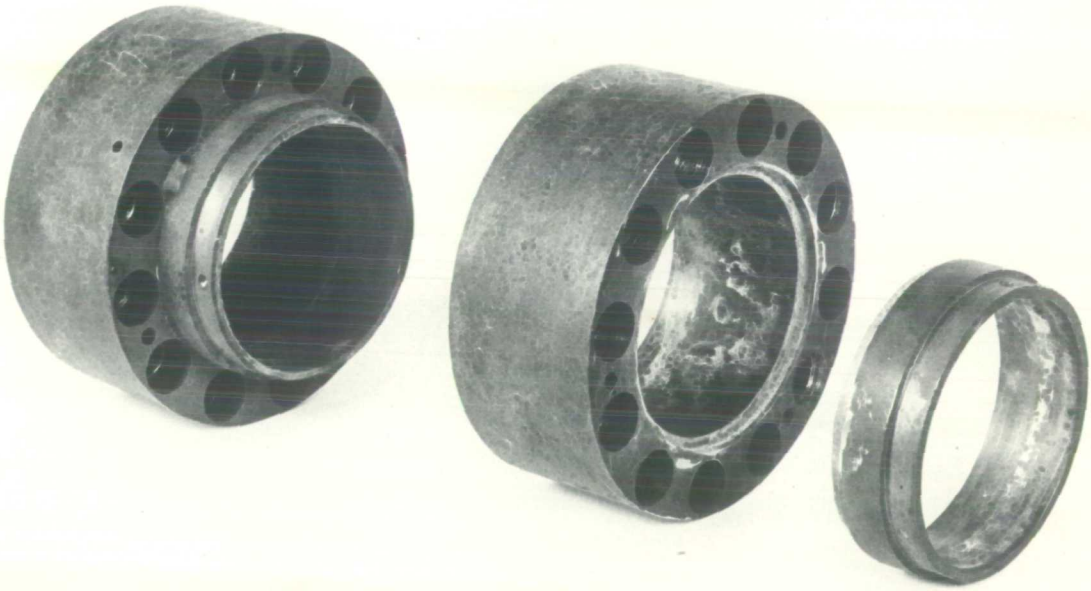

PLATE I.6: EXPLODED AND ISOMETRIC VIEW OF MILD STEEL TOP RING

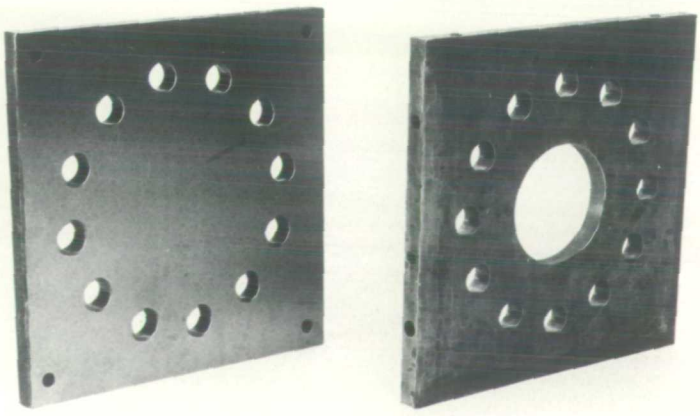

PLATE I.7: TWO TYPES OF BASE PLATES

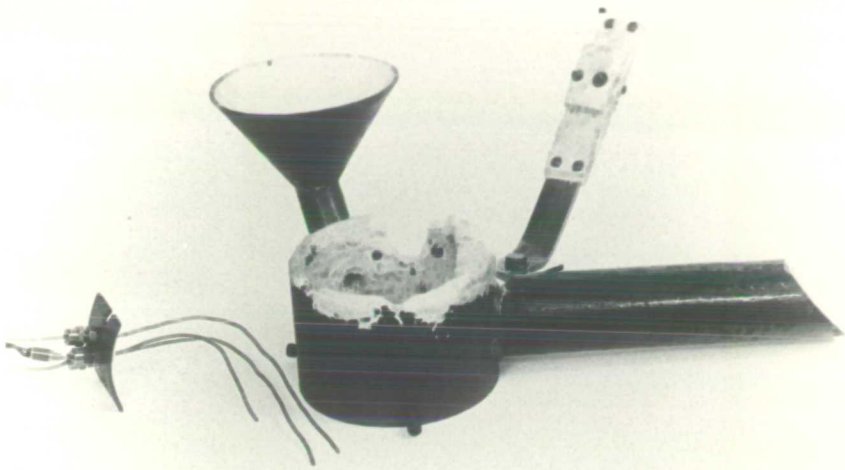

PLATE I.8: LEAD POURING ASSEMBLY

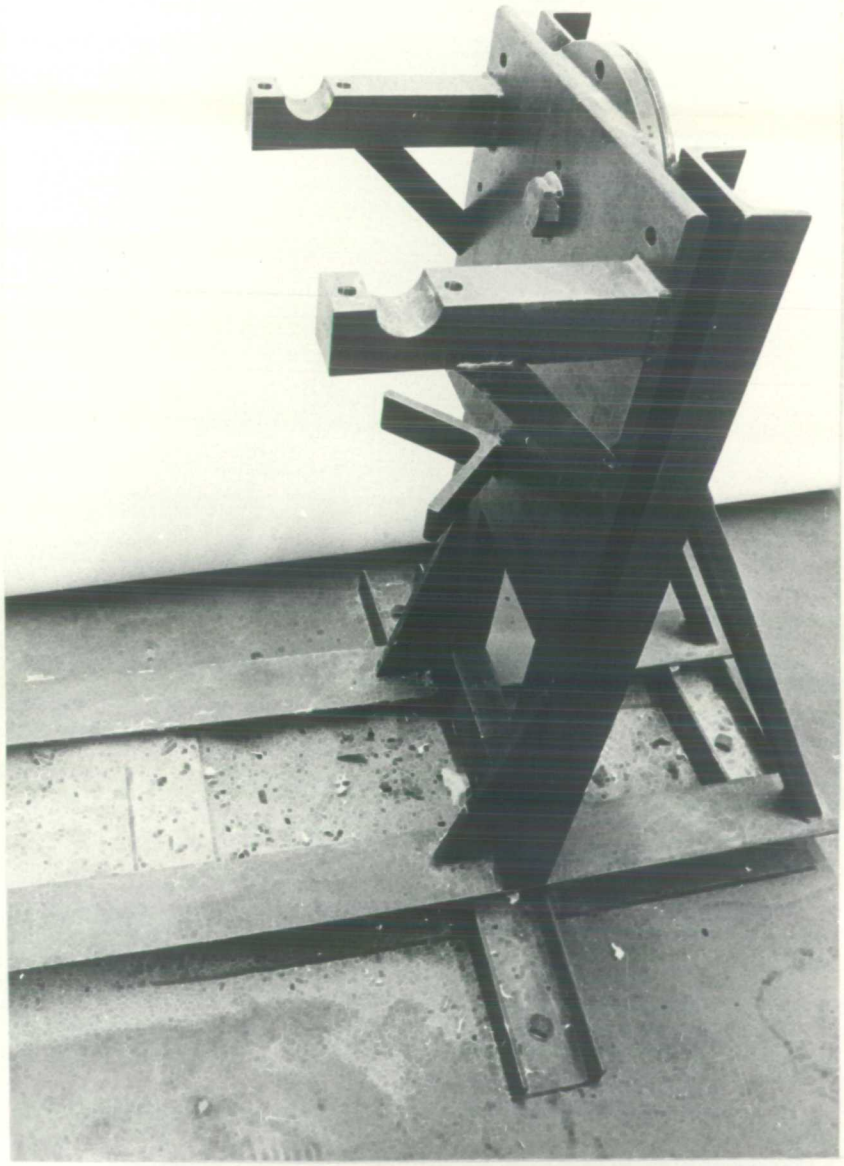

PLATE I.9: TEST RIG FOR HOLDING "LTS" CELL DURING TESTING

APPENDIX - II

DESIGN OF "RELEASE TEST SERIES"

II.1 INTRODUCTION

The "Release Test Series" was designed to monitor pore pressure (24-25 N/mm^2), temperature (400 ^oC) and weight loss of the concrete by periodically breaking the seal and allowing the moisture to escape. Good pressure sealing, robustness of the release valve, and the structural integrity and safety of the assembly were the main criteria for the design of the assembly. Numerous release procedures for the measurement of the weight loss necessitated the use of materials which could be used repeatedly without failure or deterioration. The weight loss measurements also dictated the assembly to be designed where no weight was lost other than the weight lost from the concrete due to the release of moisture. Therefore a complete metal assembly as shown in Figure II.1 and Plate II.1 was selected. The design, dimensions and machining procedures for each item used are explained below.

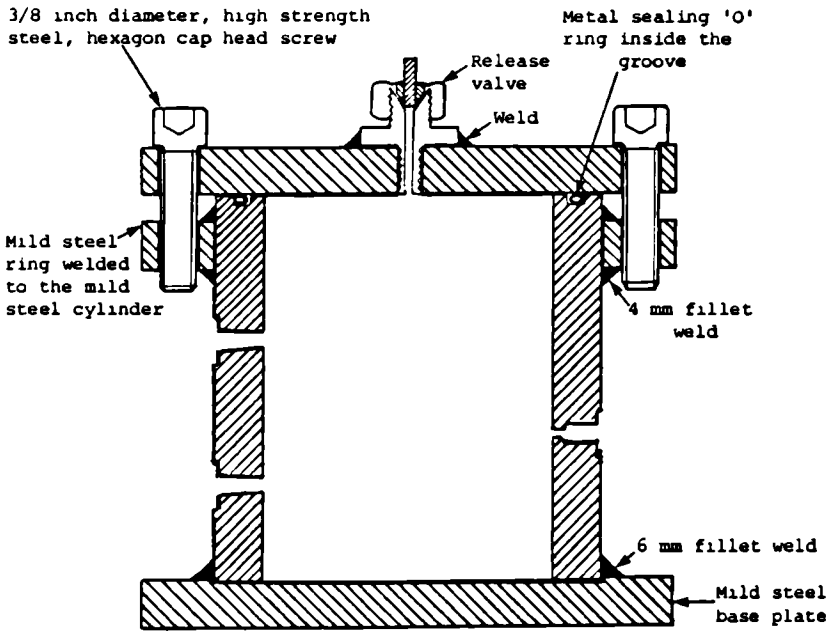

Figure II.1: Cross-sectional view of a typical "Release Test Series" cell, without instrumentation.

II.2 MILD STEEL CYLINDER FOR HOLDING CONCRETE

To achieve a safety factor greater than two at a pressure of 25 N/mm^2 and temperatures of 400 ^{o}C a mild steel cylinder (76.2mm i.d. x 101.6mm od. x 110.0mm long) was selected. The following preparation work was carried out on this cylinder:

1. Both ends of the cylinder were machined flat and a circular groove (Figure II.2) was machined at the top end. The groove was used to locate a metal "O" ring which was clamped under the steel disc to provide pressure sealing.

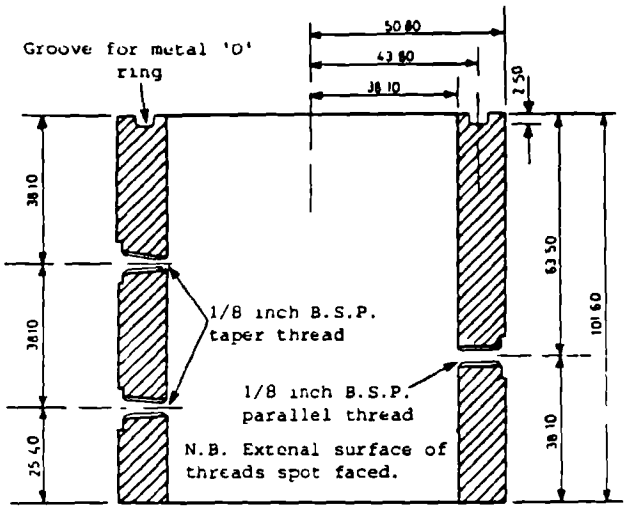

Figure II.2:
Mild steel cylinder after machining.

2. Two (1/8 inch B.S.P.) tapered threads were tapped through one side of the cylinder wall for thermocouple glands, and a (1/8 inch B.S.P.) parallel thread was tapped diametrically opposite the tapered threads for the pore pressure fitting, as shown in Figure II.2.

3. The surfaces around the threaded holes were spot faced to clamp a copper washer under each fitting to provide pressure sealing.

4. The wall thickness of the steel cylinder was not sufficient to provide the threads for bolting the top end disc to the cylinder. Therefore, a mild steel ring (100mm i.d., 140mm o.d. and 12.7mm thick) was machined to an internal diameter of 101.6mm to match the external diameter of the steel cylinder.

5. Twelve 3/8 inch Whitworth threads were tapped in the ring

(Figure II.3), and the ring was welded to the cylinder, as shown in Figure II.4 and Plate II.1. A 4mm fillet weld either side of the ring was considered adequate for the stresses induced due to the temperatures and the pore pressures.

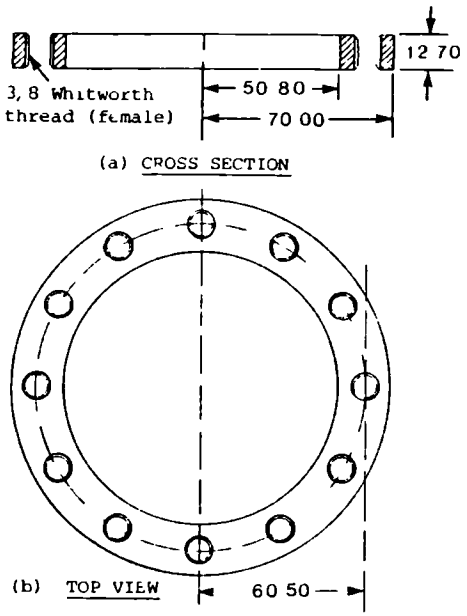

Figure II.3: Mild steel ring after machining.

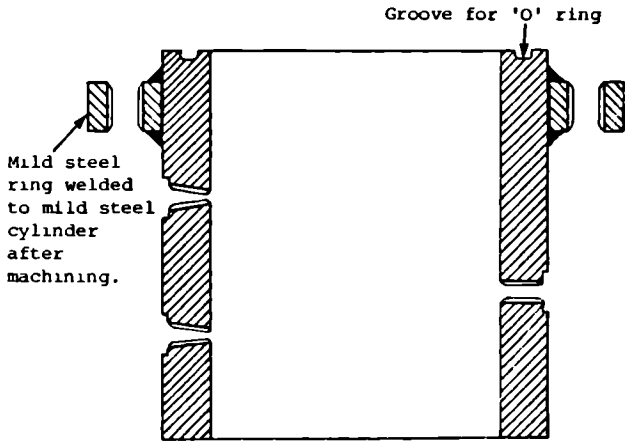

Figure II.4: Mild steel ring welded to mild steel cylinder.

6. A mild steel disc (140mm diameter x 12.7mm thick) was used as a base plate and a recess was machined in the plate as shown in Figure II.5. To provide the sealing at the bottom end of the cylinder, the steel cylinder was located and welded to the base plate (Figure II.6 & Plate II.1). The safe design for the fillet weld was 6mm in this case.

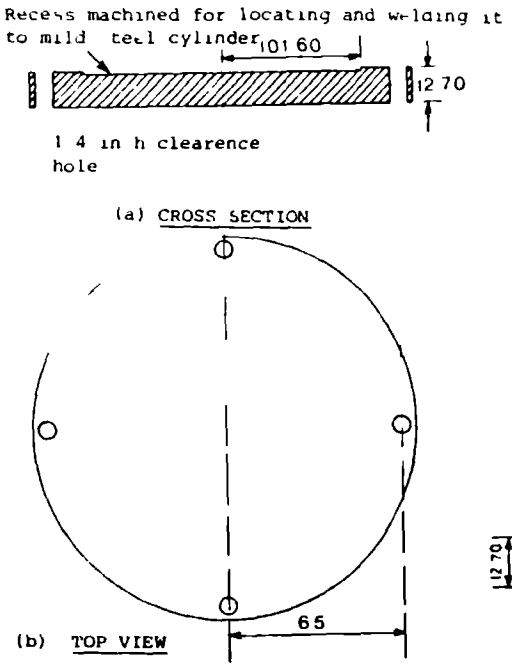

Figure II.5: Mild steel disc used as a base plate.

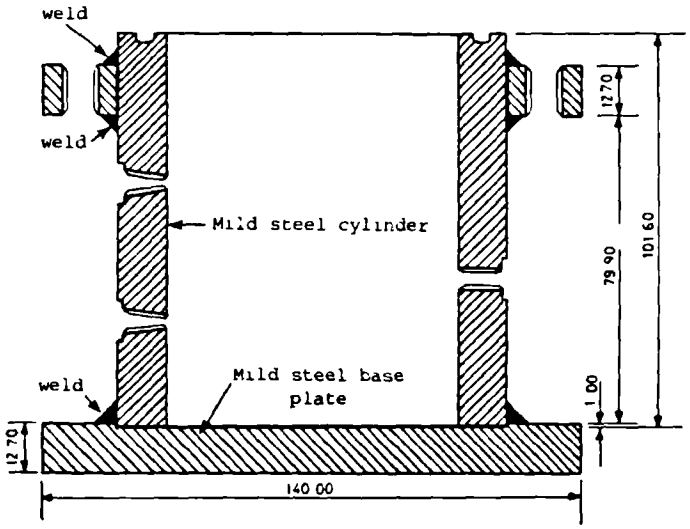

Figure II.6: Base plate welded to mild steel cylinder.

7. After all the machining and welding, the groove in the top end of the steel cylinder was ground.

II.3 MILD STEEL DISC FOR TOP END

A mild steel disc was used to seal the top end of the cylinder by compressing a metal "O" ring inside a groove under the disc (Section II.2).

The steel discs (140mm diameter and 15.0mm thick) were machined to a thickness of 12.7mm. Twelve clearance holes were drilled for 3/8 inch Whitworth bolts at the corresponding central distance, as the threads in the steel ring welded to the steel cylinder (Section II.2).

A hole was drilled and tapped (for 1/8 inch B.S.P. parallel threads) in the centre of the disc, to accommodate a pressure release valve as described in Section II.6. The release valve was screwed and welded to the steel disc to provide sealing between the valve and the disc.

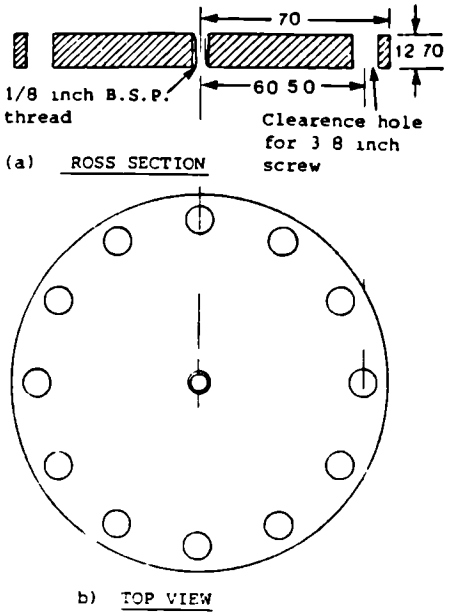

The lower surface of the disc making contact with the metal "O" ring was polished as specified by the manufacturers of the "O" ring (Section II.4). This was done to achieve good sealing between the steel disc and the steel cylinder .

Figure II.7, Plate II.1 & II.2 show the steel disc for top end.

Figure II.7: Mild steel disc for top end after machining.

II.4 PRESSURE SEALING

To seal the pore pressure of concrete at the top end of the steel cylinder at temperatures up to 400 ^{o}C, a metal "O" ring (Plate II.1) similar to the one described in Appendix I, Section I.7 was used. However, the size and the wall thickness of the "O" ring used here (Figure II.8 and Table II.1) was different to the size and the wall thickness of the ring used for the "LTS" specimen, as explained in Appendix I, Section I .7.

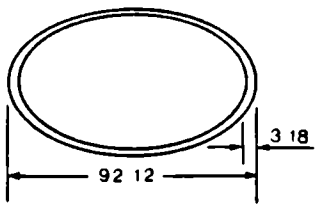

Figure II.8:
Metal "O" ring used for pressure sealing.

Ring Material used was Stainless Steel Type 316	Ring Size mm			Plating or Coating	Recomended Torque Ft-lbs	Working Temperature C
	o.d.	Tube	Wall			
	92.1	3.18	.254	Silver	30-40	800

Table II.1: "O" ring specifications for the "RTS" specimens.

The torque applied to each bolt was only 30-40 ft-lbs, because the wall thickness of the "O" ring tube here was smaller than the "O" rings used for the "LTS".

Once again the metal surfaces in contact with the "O" ring were polished (0.4064 microns), as explained in Appendix I, Section I.7.

Plate II.3 shows a metal "O" ring and Figure II.9 gives an enlarged cross-sectional view of the "O" ring inside the groove.

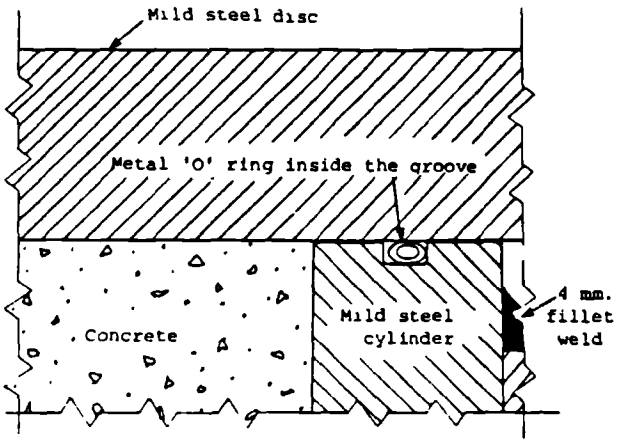

Figure II.9:
Enlarged cros-sectional view of a metal "O" ring inside the groove.

The sealing at the bottom end of the steel cylinder was provided by welding the base plate to the cylinder and each weld was tested for hydraulic pressure before casting the concrete.

Copper washers were used under the temperature and pressure fittings, to seal the pressure between the fittings and the steel cylinder.

The release valve was welded to the steel disc for the top end for pressure sealing between the valve and the disc (Section II.6).

II.5 BOLTING OF THE ASSEMBLY

High strength steel hexagon cap head screws (Plate II.1 and Figure II.1) were used to clamp the top end steel disc to the steel cylinder. Twelve 3/8 inch diameter screws were sufficient to take the stresses induced by the pore pressures of concrete and the test temperatures.

II.6 RELEASE VALVE FOR RELEASING PORE PRESSURE

A release valve was designed and located in the middle of the top end steel disc to release the pore pressures of the concrete during testing (Section II.3).

The valve was machined from 1 inch diameter mild steel rod. The bottom end of the release valve fitting was threaded for 1/8 inch B.S.P. male threads, while at the top end of the fitting a cone was machined at an angle of 60 degrees. The outer diameter around the cone was threaded for 1/4 inch B.S.P. threads (Figure II.10) and a 1/8 inch diameter hole was drilled through the centre of the fitting. Finally a blank nipple placed inside the cone and screwed under a 1/4 inch B.S.P. nut (Figure II.11, Plate II.4) provided the pressure seal at the cone end of the valve.

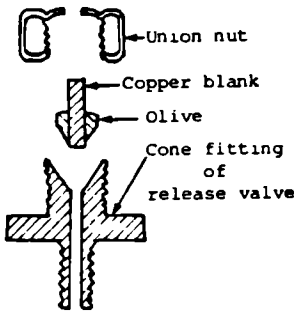

Figure II.10:
Cross-sectional view of a release valve.

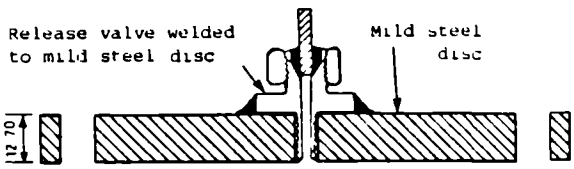

Figure II.11:
Release valve welded to a mild steel disc for top end.

Initially it was decided to use a copper washer for pressure sealing between the release valve and the steel disc. However, after testing this idea in a pilot test, the copper washer was rejected because on opening and closing the release valve frequently pressure leaked past the copper washer. It was therefore decided to weld the release valve to the steel disc. The welded connection provided satisfactory sealing as tested by further pilot tests. Plate II.4 and Figure II.11 show the release valve welded to the disc.

To use the fitting as a release valve the 1/4 inch B.S.P. nut was opened and moisture was allowed to escape before closing the nut again.

II.7 TEST RIG FOR HOLDING THE TEST CELL

A test rig was designed to:

- hold the test cell during testing,
- take the cell out from the furnace for weighing,
- protect the instrumentation from damage.

The following steps were taken to complete the test rig.

1. Two mild steel strips (1/16 inch thick) were bent and connected together by welding another short strip and a 1/4 inch diameter mild steel rod between them (Plate II.6).

2. The heads of two 1/4 inch bolts were welded on each strip.

3. Two clearance holes (for 1/4 inch bolts) were drilled in the two mild steel plates (1/4 inch thick), at the same centres as the welded bolts on each of the bent strips (Figure II.12).

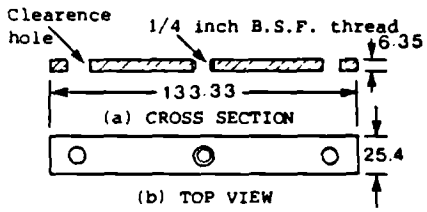

Figure II.12:
Mild steel plate after machining.

4. A 1/4 inch B.S.F. thread was tapped in the middle of each 1/4 inch plate (Figure II.12), and a 1/4 inch B.S.F. bolt was screwed in each thread.

5. A slot was machined in each 1/16 inch steel strip (Plate II.6), to position and hold the cooler, as shown in Plate II.5.

6. An aluminium angle strip was screwed to each end of the steel strip, to assist in lifting the test rig along with the specimen.

7. A ball valve (Chapter 3, Section 3.4.7) was introduced in the system:

- to connect the instruments positioned on the instrumentation

board to the small bore copper tube attached to the specimen.

- to remove the specimen for periodic weighing (Chapter 3, Section 3.4.7).

8. The valve was mounted vertically on an aluminium plate with the help of two "U" bolts. The aluminium plate holding the valve was screwed to another aluminium strip bent in "L" shape, which was then screwed to the test rig (Plate II.7).

9. Two (3/8 inch x 1/4 inch B.S.P.) parallel stud couplings were screwed to each end of the valve, with Dowty seals providing sealing for pressure between the valve and the couplings.

10. A small bore copper tube (with the soldered nipples and union nuts at either end of the tube) was used to connect the coupling at the bottom end of the valve to the fitting at the end of the small bore copper tube of the specimen (Plate II.7).

11. Two ball valves with a 1/4 inch x 1/4 inch B.S.P. brass stud couplings at each end were also attached to the test rig in a similar fashion as the valve described in (8) above. These valves were used to connect and circulate the cold water through the cooler (Chapter 4, Section 4. 2.4.1). Dowty seales were again used to seal the pressure between the couplings and the valves.

12. To connect the valves to the cooler, a high pressure nylon tube with compression fitting on each end was attached to the bottom end of each valve (Plate II.7). The other end of the nylon tubes were connected to the couplings on the cooler of the "RTS" specimen (Plate II.5).

To secure the test cell to the test rig, the cell was placed on the two mild steel strips, and the base plate of the cell was bolted between 1/16 inch thick steel strips and 1/4 inch thick steel plates (as described in 3. above) with the help of the welded bolts, and the nuts. Plate II.5 shows a "RTS" test cell clamped to the test rig.

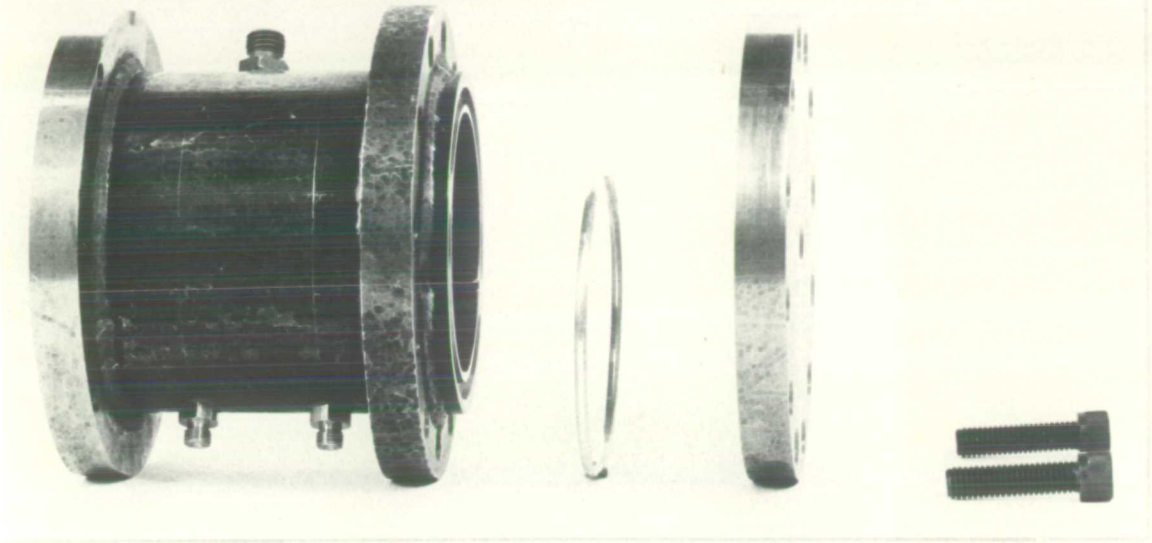

PLATE II.1 EXPLODED VIEW OF "RELEASE TEST SERIES" CELL

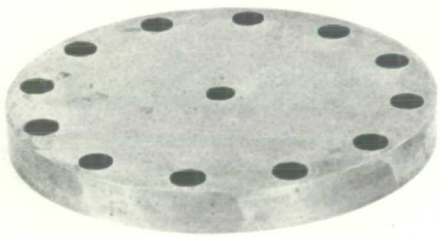

PLATE II.2: TOP END MILD STEEL DISC

PLATE II.3 METAL "O" RING

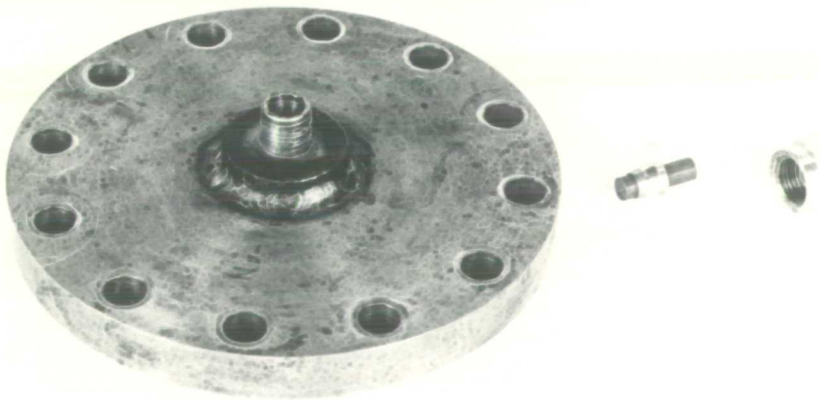

PLATE II.4: TOP END MILD STEEL DISC WITH RELEASE VALVE

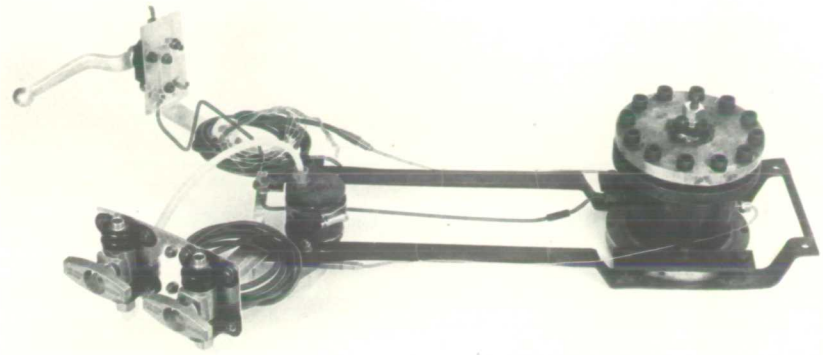

PLATE II.5: "RTS" SPECIMEN CLAMPED ON TEST RIG

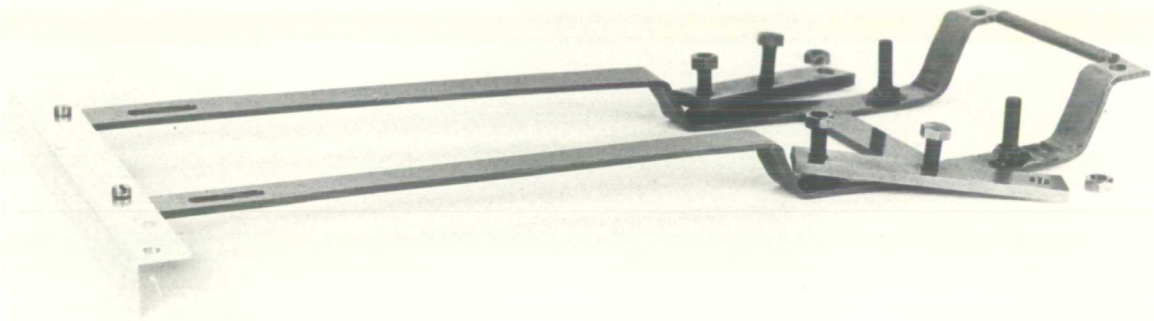

PLATE II.6: TEST RIG FOR HOLDING "RTS" SPECIMEN

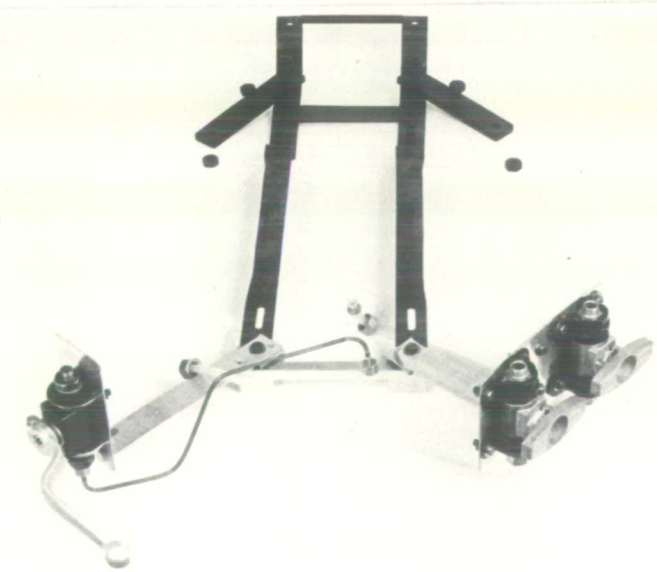

PLATE II.7: ALUMINUM STRIPS AND VALVES SCREWED TO THE TEST RIG

APPENDIX - III

PRESSURE/DEFLECTION CALIBRATION TEST

III.1 INTRODUCTION

After assembling the test cell and prior to the concrete casting in the cells, each stainless steel diaphragm was hydraulically pressurised to measure its deflections at room temperature. The data obtained from these calibrations was a reference datum, which provided a method of checking and varifying the deflection due to pore pressures from experimentally measured deflections in the final tests (Chapter 5, Section 5.3.3), as described in Appendix IV, Section IV.4.

The pressure/deflection calibrations data was compared against the theoretically calculated deflection of the diaphragm for a given pressure and known thickness of the diaphragm (Table III.1), and the typical values are shown in Figure III.1. Theoretical values were calculated by using the equation of Chapter 5, Section 5.3.4. The theoretical values above 10 N/mm^2 showed non-elastic behaviour. However, the maximum pressure recorded in the "LTS" series was less than 10 N/mm^2, therefore the curve above this value did not affect the resutlts for these series. These tests were also used to check the efficiency of the test cell, the joints, and the seals for pressure.

Test Category	LTS-1	LTS-2	LTS-3	LTS-4	LTS-5	LTS-6
Diaphragm Thickness mm	9.347	9.220	9.525	9.347	9.601	9.500

Table III.1: Thickness of the diaphragms for each "LTS" specimen.

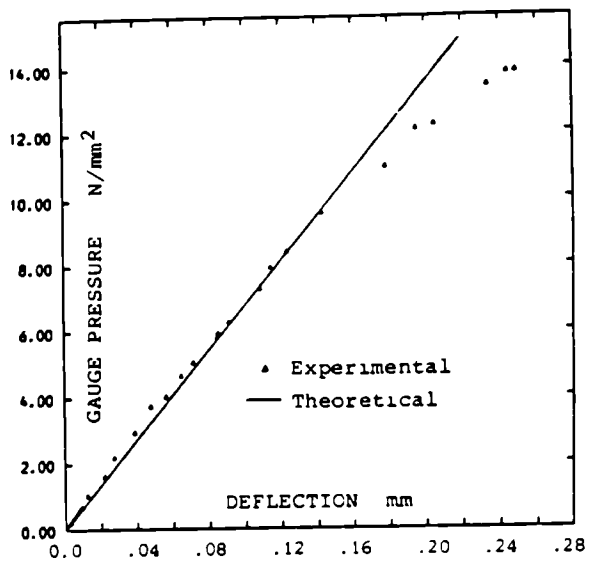

Figure III.1: Typical experimental and theoretical values of pressure against deflection for a diaphragm of the "LTS" cell.

III.2 EXPERIMENTAL SET UP AND TEST PROCEDURE

The experimental set up and test procedures are described below.

1. Each test cell was mounted on the test rig in the same way as the "LTS" specimens for the main tests (Chapter 3, Section 3.3.7).

2. The test cell was rotated through 180 degrees after clamping it to the test rig, to fill the cell with water and to clamp the base plate to the cylinder.
   Note: The base plate was not connected to the mild steel cylinder at this stage.

3. The pressure fitting at the end of the small bore copper tubes (Chapter 4, Section 4.2.5.2) used to connect the specimen to the instrumentation board were temporarily blocked. Water was filled in the cylinder through its bottom end.

4. A mild steel plate similar to the base plate of the sealed specimen of the "LTS" (Appendix I, Section I.5) was used at the bottom end of the cylinder. A rubber gasket provided the seal between the cylinder and the plate. A pressure fitting was screwed to the base plate (Figure III.2) to connect the hydraulic pump to the cell. P.T.F.E. tape was used to seal the pressure between the fitting and the base plate.

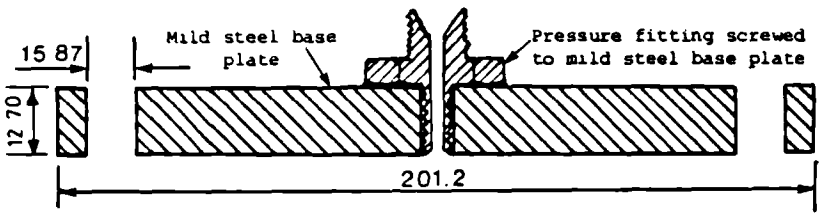

Figure III.2: Base plate with fitting attached to it.

5. Twelve clearance holes for the bolts and a hole for hydraulic pressure inlet were punched in the rubber gasket (Figure III.3).

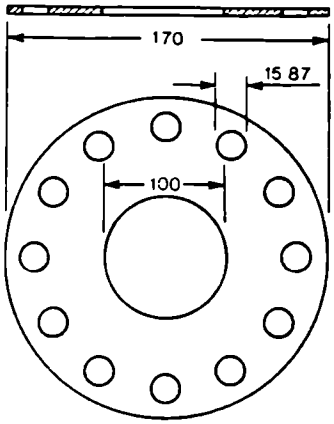

Figure III.3:
Rubber gasket used to seal the pressure.

6. After clamping the base plate to the cylinder, the test cell was rotated through 180 degrees, to get it back in the upright position again.

7. The hydraulic pump was connected to the cell through the fitting on the base plate.

8. The copper tube fitting (described in 3. above) nearest to the diaphragm was unblocked. A copper tube was screwed between the test cell and the instrumentation board, at the first transducer position (Chapter 3, Section 3.3.7 and Chapter 4, Section 4.2.7.1).

9. The pressure measuring system (Chapter 4, Section 4.2.6.1) was used to record the hydraulic pressure. However, the back pressure was not applied in these tests.

10. The deflection measuring assembly was set up in the same way as for the "LTS" (Chapter 3, Section 3.3.7), to measure the deflection of the diaphragm.

11. A hydraulic pressure was applied and the pressure and deflection were measured, by using a data logger and a chart recorder (Chapter 3, Section 3.4.7).

12. All the fitttings, seals and joints were checked while the cell was under pressure and any problems encountered were rectified. The test cell was re-tested and the test was not considered to be complete until all the components were performing satisfactorily.

To check the instrumentation and to minimise the error during testing, the pressure and deflection readings were repeated at least three times. Consistent readings were obtained on each occasion.

After completing the test, the base plate was detached from the cylinder and water was drained from the cell into a container. The test cell was then dried and prepared to cast concrete.

III.3 RESULTS

The results of the central deflection of the diaphragm against the pressure is plotted for each diaphragm in Figure III.4. A typical example of the theoretical and calibrated values described earlier in Section III.1 is shown in Figure III.1.

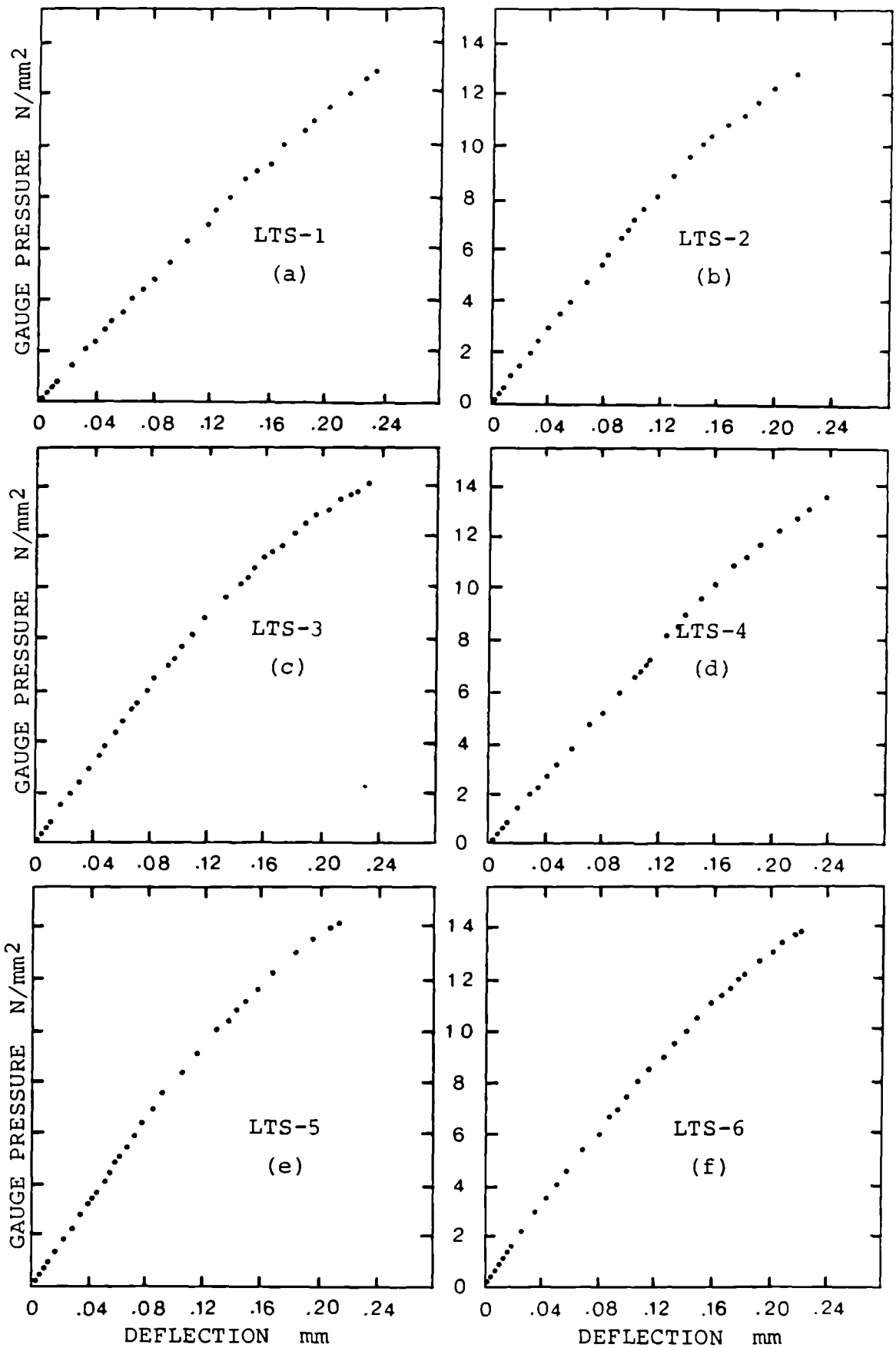

Figure III.4: Variation of diaphragm deflection with hydraulic pressure.

APPENDIX IV

PRESSURE/DEFLECTION SEPARATION FROM TEMPERATURE CORRECTION

IV.1 INTRODUCTION

The central deflection of the stainless steel diaphragm was monitored in the "Liner Test Series". The deflection which was experimentally measured resulted from the combined effects of the pore pressures of concrete and the thermal expansion of the Sintox tubes used for the measurement of deflection (Chapter 4, Section 4.3.3). It was therefore necessary to separate the deflection of the diaphragm due to the pressure from the thermal expansion of the Sintox tubes, or any other temperature effects. A series of calibration tests was carried out to experimentally determine each parameter. Finally, an empirical method was proposed to calculate the deflection due to the pressure generated inside the heated concrete of the "LTS" specimen. These calibration tests were divided into two main groups, Pressure/Deflection and Temperature/Deflection calibrations.

IV.1.1 PRESSURE/DEFLECTION CALIBRATION

The deflection of each stainless steel diaphragm of the "LTS" was measured under hydraulic pressure and room temperature, as discussed in Appendix III.

IV.1.2 TEMPERATURE/DEFLECTION CALIBRATION

The Temperature/Deflection calibrations were carried out:

1. To determine the experimental coefficient of thermal expansion for the central and outside Sintox tubes used to measure the diaphragm deflection (Chapter 4, Section 4.3.3).

2. To develop a theoretical method to analyse the deflection of the diaphragm which was recorded in the Temperature/Deflection calibration tests.

3. To separate the Pressure/Deflection of the diaphragm, from the Temperature/Deflection of the final test results of the "LTS" (Temperature/Pressure/Deflection), as described in Chapter 5, Section 5.3.3.

Two series of the experiments (Section IV.2 & IV.3) were performed and

an empirical method was developed to separate these deflections. The results obtained from the calibration tests were applied to the results of a "LTS" specimen and the deflections were separated as an example (Section IV.4).

IV.2 TESTS TO DETERMINE EXPERIMENTALLY THE COEFFICIENT OF THERMAL EXPANSION OF SINTOX TUBES

The following options were considered to determine experimentally the average coefficient of thermal expansion of Sintox tubes:

a. The Sintox tube was heated in a 2 inch diameter tube furnace and the temperature and expansion of the tube was recorded. This method was rejected because:

- The thermocouples were attached to the external surface of the tube and these thermocouples were only measuring the surface temperature.

- The temperature measurements did not represent the true temperature throughout the cross-section of the Sintox tube.

- The heating method used here did not correspond to the conditions used in the "LTS" tests.

b. A copper tube similar to the one used to protect the central Sintox tube (Appendix I, Section I.8) was cast in a concrete block and the test was set-up and performed as below:

- A spiral heating element was wrapped around the tube (Plate IV.1).

- The mild steel top ring (Appendix I, Section I.4) was placed on the concrete block

- The transducer assembly (Chapter 4, Section 4.3.2) was mounted on top of the Sintox tubes.

- The thermocouples used to measure the temperature (Chapter 4, Section 4.4) were attached to the Sintox tubes

- The external rope heater (Chapter 3, Section 3.3.3) was clamped to the top ring under a thermal insulation paper, as shown in Plate IV.2.

- The transducer and thermocouples were connected to the data logger and the chart recorder.

- Both the heaters were switched on.

- The expansion of the central Sintox tube was recorded and its coefficient of thermal expansion was evaluated.

This method was also rejected because the heating medium did not conform to the heating procedures used for the "LTS" tests.

c. It was therefore decided, to use the similar testing and heating techniques, as used for the "LTS" and the following experiment was performed.

IV.2.1 EXPERIMENTAL SET UP AND TEST PROCEDURE

A "LTS" cell (Chapter 3, Section 3.3.2) previously tested for Temperature/Pressure/Deflection test as a pilot test was used for this experiment. The pressure measuring positions were left unconnected, and the pressure seals of this test cell were broken to prevent the pore pressure generation in the heated concrete.

The heating (Chapter 3, Section 3.3.3) procedure and the temperature measuring techniques (Chapter 4, Section 4.4) were similar to all the main tests of the "LTS". However, in this test the expansion and the temperature distribution of the outside Sintox tubes were also measured for each tube independently.

To measure the expansion of each tube, the tranducer assembly (Chapter 4, Section 4.3.2) was modified and set up as below:

i. A transducer along with a displacement accessory was mounted in the centre of the assembly in the same way as for the "LTS".

ii. Three additional transducers and displacement accessories were screwed to the assembly, as shown in Figure IV.1.

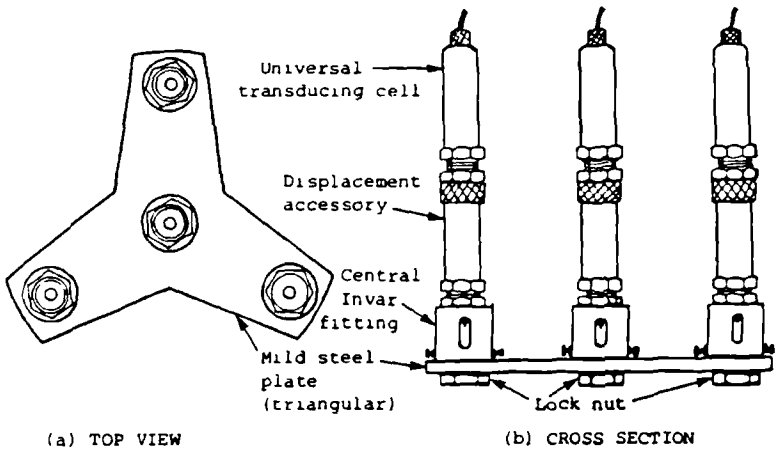

Figure IV.1: Transducers mounted on the modified transducer assembly.

To measure the deflection of the diaphragm the transducer assembly was located on top of the three outside Sintox tubes in the "LTS" (Chapter 3, Section 4.3.2). As the expansion of the outside tubes was also recorded in this test, it was necessary to design a system for carrying the transducer assembly. To achieve this, three Invar rods were screwed to the top ring and the transducer assembly was connected to these rods, as shown in Figure IV.2. In this way the inside and the outside Sintox tubes were free to expand under the thermal effect.

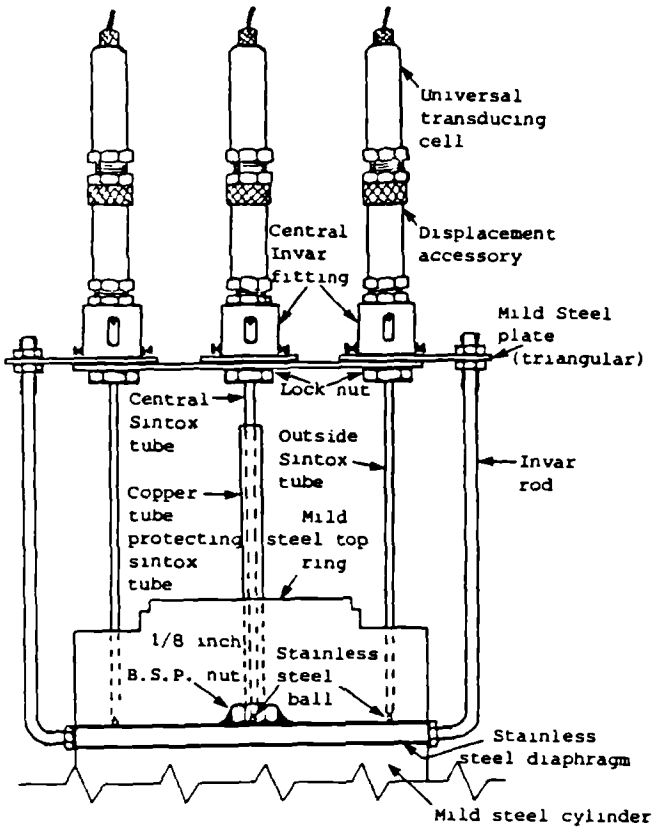

Figure IV.2:

Invar rods connecting the transducer assembly to the top ring.

An identical procedure was used to measure the central and the outside Sintox tubes temperature. The same procedure was also used for the "LTS" tests. Figure IV.3 shows the distance and positions on a Sintox tube for the measurement of temperatures.

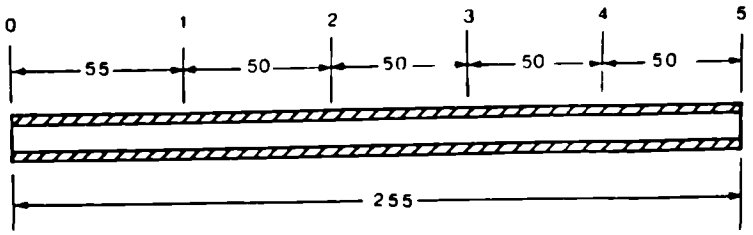

Figure IV.3: Temperature measuring positions on a Sintox Tube and the distance between the thermocouples.

The outside Sintox tubes between position 0 and 1 (55mm) were inside the holes in the mild steel top ring (which was drilled to accommodate the tube, as described in Appendix I, Section I.4). The top ring was externally covered with a rope heater and it was not possible to measure the temperature at position 0. Therefore the temperature measured at position 1 was assumed to be uniform over the length 0-1 (Figure IV.3) for a given time.

Similarly the 55mm length of inside Sintox tube between position 0-1 was inside a copper tube which was submerged in molten lead, and the first suitable position to measure the temperature was at position 1. The temperature measured at this position for the inside Sintox tube was again assumed to be uniform over the length 0-1, as described above.

IV.2.2 RESULTS AND THEORETICAL INTERPRETATION

An average coefficient of thermal expansion was evaluated for the inside and the outside Sintox tubes by incorporating the experimental data (i.e. the temperatures and the tube expansions) in the following equations.

$$d = \alpha \sum_{i=1}^{i=5} (\Delta T_i . L_i) \qquad \text{Equation IV.2.1}$$

or $$\alpha = d / \sum_{i=1}^{i=5} (\Delta T_i . L_i) \qquad \text{Equation IV.2.2}$$

where:

d = experimentally measured expansion of a Sintox tube.

α = the average coefficient of thermal expansion.

ΔT_i = the difference of temperatures between 2 times.

L_i = the distance between adjacent points.

Note: Suffix "c" and "os" to be used for the central and the outside tube values respectively (i.e. d_c, d_{os} etc.).

The term $(\Delta T_i . L_i)$ was evaluated by inserting ΔT_i and L_i from the experimental results. Figure IV.4 shows the difference of temperature (ΔT_i) between two times (t_o and t) against the distance (i.e. L_1, L_2 etc.) for a Sintox tube.

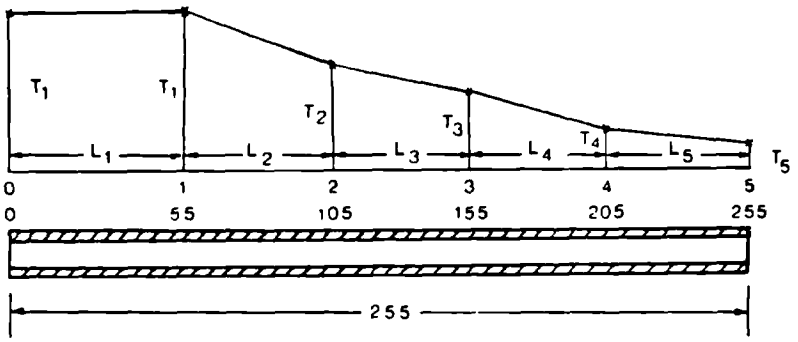

Figure IV.4: A typical graph of the temperature difference between two times (t_o and t) against the distance.

The average temperature of a Sintox tube was computed as the area under a curve similar to the curve in Figure IV.4 by using the following equations.

$$\sum_{i=1}^{i=5} \Delta T(t_1)\, L_i = \Delta T(t_1)\, \Delta L_1 + \int_{L_i=55}^{L=255} \Delta T_i \, dL \quad (i=2,3,4,5)$$

$$\sum_{i=1}^{i=5} \Delta T(t_i)\, L_i = \Delta T_1\, \Delta L_1 + \int_{L=55}^{L=255} \Delta T_i \, dL \quad (i=2,3,4,5) \qquad \text{Equation IV.2.3}$$

The results obtained from Equation IV.2.3 were incorporated in Equation IV.2.2 and the average coefficient of thermal expansion for the central (α_c) and the outside (α_{os}) Sintox tube was obtained (Figures IV.5).

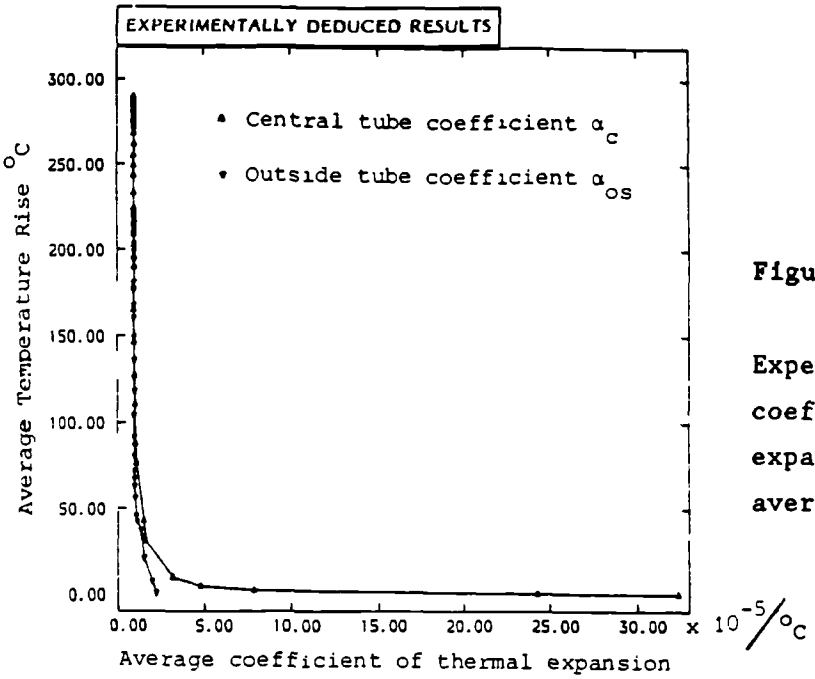

Figure IV.5:

Experimentally derived coefficient of thermal expansion against the average temperature.

These coefficients were used:

- to calculate the thermal expansions of the Sintox tubes.

- to compare the computed results of the tube expansion against the experimental results, as described in Section IV.3.

- to separate the pressure deflection from the thermal expansion of the Sintox tubes in the Temperature/Pressure/Deflection tests (Section IV.4).

IV.3 TEMPERATURE CORRECTION TEST TO BE USED AS A CALIBRATION TEST FOR SEPARATION OF STAINLESS STEEL DIAPHRAGM DEFLECTION

The temperature correction test was carried out:

i. To check the validity of the coeffecient of thermal expansion computed for the central and the outside Sintox tubes (Section IV.2.2).

ii. To compare the calculated thermal expansion of the central Sintox tube (with respect to the outer Sintox tubes) against the expansion measured in this experiment.

The experimental set-up described later in Section IV.3.1 was similar

to the set-up of the "LTS" without the presence of the pore pressures inside the heated concrete (Section IV.2.1).

IV.3.1 EXPERIMENTAL SET UP AND TEST PROCEDURE

A "LTS" specimen previously used for the expansion experiments (Section IV.2) was used here. The heating and the temperature measuring techniques were identical to the test described in Section IV.2.1 and the "LTS" experiments. The transducer and the displacement accessory were mounted in the transducer assembly and used in the same way as for the "LTS" described in Chapter 4, Section 4.3.2.

IV.3.2 RESULTS AND THEORETICAL INTERPRETATION

The measurements of the temperature, the time from the start of heating and the deflection of the diaphragm were recorded. The results were obtained by using the appropriate equations given below:

1. The average temperature for the central and the outside Sintox tube was calculated by inserting the experimental data in Equation IV.2.3.

2. The coeffecient of thermal expansion for the central and the outside tubes was obtained from Figure IV.5, by reading the values against the calculated values of the average temperaure from (1) above.

3. The expansion of the central (d_c) and the outside (d_{os}) Sintox tubes was calculated by modifying Equation IV.2.1 to:

$$d_c = -\alpha_{ci} \sum_{i=1}^{i=5} \Delta T_i \, L_i \qquad \text{Equation IV.3.2.1}$$

$$d_{os} = -\alpha_{osi} \sum_{i=1}^{i=5} \Delta T_i \, L_i \qquad \text{Equation IV.3.2.2}$$

4. The theoretical deflection at the centre of a fixed edge plate under a thermal gradient is zero (Roark et al, 1975). The steel diaphragm was bolted between the steel top ring and the steel cylinder in the "LTS" test cells, therefore the diaphragm would

behave like a fixed edge plate. The diaphragm deflection measured in this experiment (δ_R) was assumed to be from the expansion of the central Sintox tube with respect to the outside Sintox tubes (i.e. the temperature correction deflection due to the expansion of Sintox tube (δ_E), because there was no pressure exerted on the diaphragm.

$$\delta_R - \delta_E \qquad \text{Equation IV.3.2.3}$$

δ_R - the recorded diaphragm deflection
δ_E - the temperature correction deflection due to the expansion of Sintox tubes.

5. The deflection was measured by a single transducer resting on the central Sintox tube and the transducer assembly was resting on the three outside tubes, which were also expanding with respect to the inside tube (Section IV.3.1). The mode of expansion (or the recorded diaphragm deflection) of the Sintox tubes is diagramatically shown in Figure IV.6 , and the temperature correction deflection due to the expansion of the Sintox tubes can be calculated by using the following equation:

$$\delta_E = d_c - d_{os} \qquad \text{Equation IV.3.2.4}$$

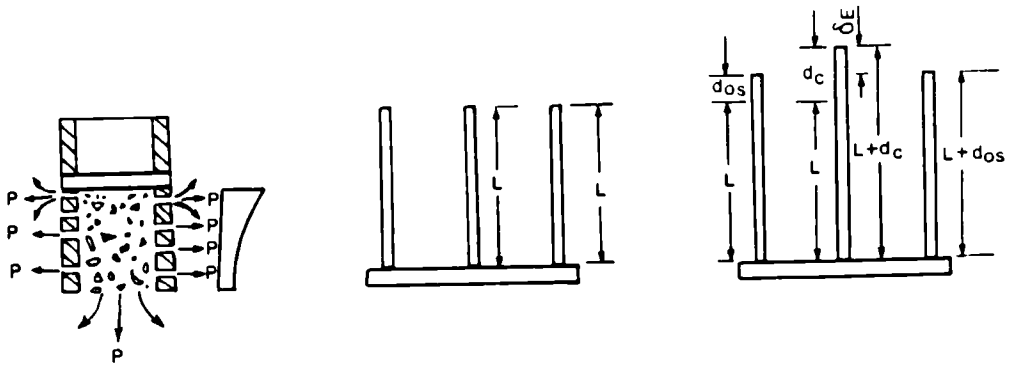

Figure IV.6: Diagramatic representation of the expansion of the Sintox tubes.

6. The values for δ_E were evaluated by substituting d_c and d_{os} values from (3) above. Figure IV.7 shows the experimental and theoretically calculated values plotted against time.

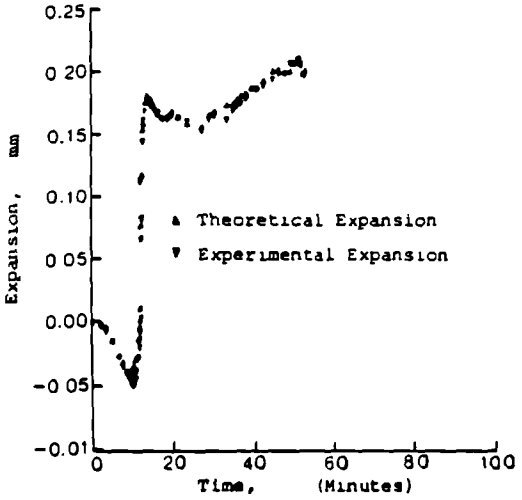

Figure IV.7:

Experimentally recorded and theoretically calculated expansion against time.

Comparison between the experimental and the theoretical values showed that the above procedure could be used to calculate the expansion of the Sintox tube for the experimental results of the "LTS" (Section IV.4). The pressure deflection of the diaphragm could be separated from the sintox tube expansion.

The average temperature rise against the time of heating for the Sintox tubes is shown in Figure IV.8 and Figure IV.9 shows the temperature for top and bottom end of the diaphragm against the time of heating.

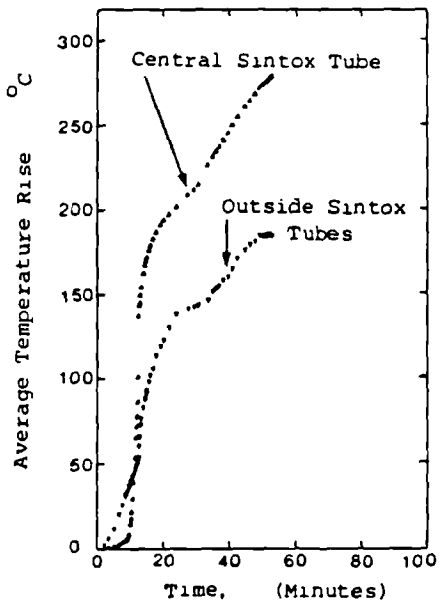

Figure IV.8: Average temperature rise against time.

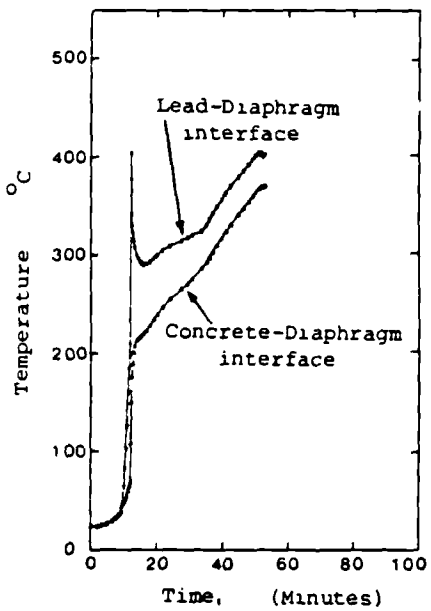

Figure IV.9: Diaphragm temperature against time.

IV.4 TEMPERATURE/PRESSURE/DEFLECTION TEST

The test procedure for the "LTS" tests is described in Chapter 3, Section 3.3.8, and the results obtained are analysed in Chapter 5, Section 5.3.3. The techniques to measure the temperature and the deflection for the "LTS" specimen were similar to the test explained in Section IV.3.1. However, the pore pressures generated in the heated concrete were also recorded for the experiments discussed here. These pressures exerted a force on the diaphragm and deflected it in the centre. The measured diaphragm deflection therefore consisted of a deflection due to the pore pressures, and the expansion of the Sintox tubes due to the temperature (Section IV.3.2). This combined effect is diagramatically shown in Figure IV.10 and represented by the following eqautions.

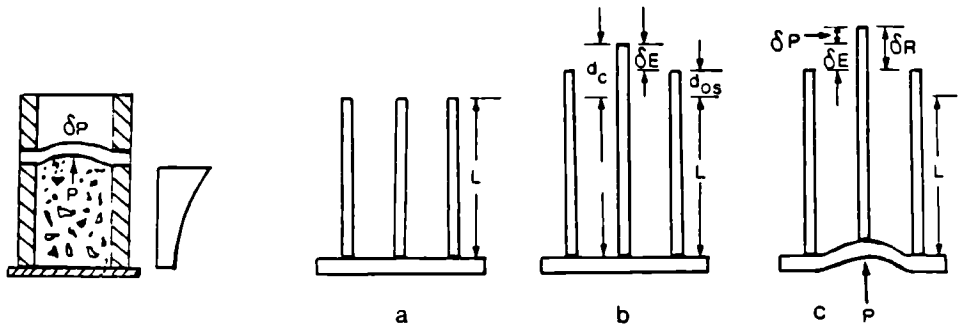

Figure IV.10: Diagramatic representation of the recorded diaphragm deflection δ_R.

$$\delta_R = \delta_E + \delta_P \qquad \text{Equation IV.4.1}$$

where:

δ_E and δ_R are same as before

δ_P = the pressure only deflection of the diaphragm

Re-arranging the above expression

$$\delta_P = \delta_R - \delta_E \qquad \text{Equation IV.4.2}$$

The temperatures, the pore pressures, the time from start of heating and the diaphragm deflection δ_R were experimentally recorded in the "LTS" experiments and δ_E was evaluated by the following method.

1-3. Same as 1. to 3. of Section IV.3.2.

4. The temperature correction deflection due to the expansion of the Sintox tube (δ_E) was computed by using Equation IV.3.2.4.

5. Finally the pressure only deflection of diaphragm δ_P was obtained inserting the experimentally recorded values δ_R and calculated results δ_E in Equation IV.4.2.

Figure IV.11 shows a typical graph of the recorded diaphragm deflection δ_R and the temperature correction deflection δ_E plotted against the time of heating. Comparing δ_R with δ_E it is seen that the recorded deflection values are greater than the calculated temperature correction values. The difference between the two values which is pressure only deflection (Figure IV.12) highlights the existence of pore pressures in the concrete adjacent to the diaphragm.

The pressure only deflection of the diaphragm deduced from the results as described above was checked with the pressure deflection from the Pressure/Deflection calibration results (Appendix III) of the relevant "LTS" specimen. This was done by interpolating the deflection values by knowing the pore pressure values which were obtained during the "LTS" test of the same specimen. Figures IV.12 to IV.16 show, the calculated values of δ_P as described above in this section, and the interpolated values from the Pressure/Deflection calibration tests (Appendix III).

The comparison between the experimentally deduced and the interpolated values shows good agreement with each other. The pressure only deflection of the diaphragm in the "LTS" could therefore be separated from the Temperature/Deflection or Sintox tube expansion confidently.

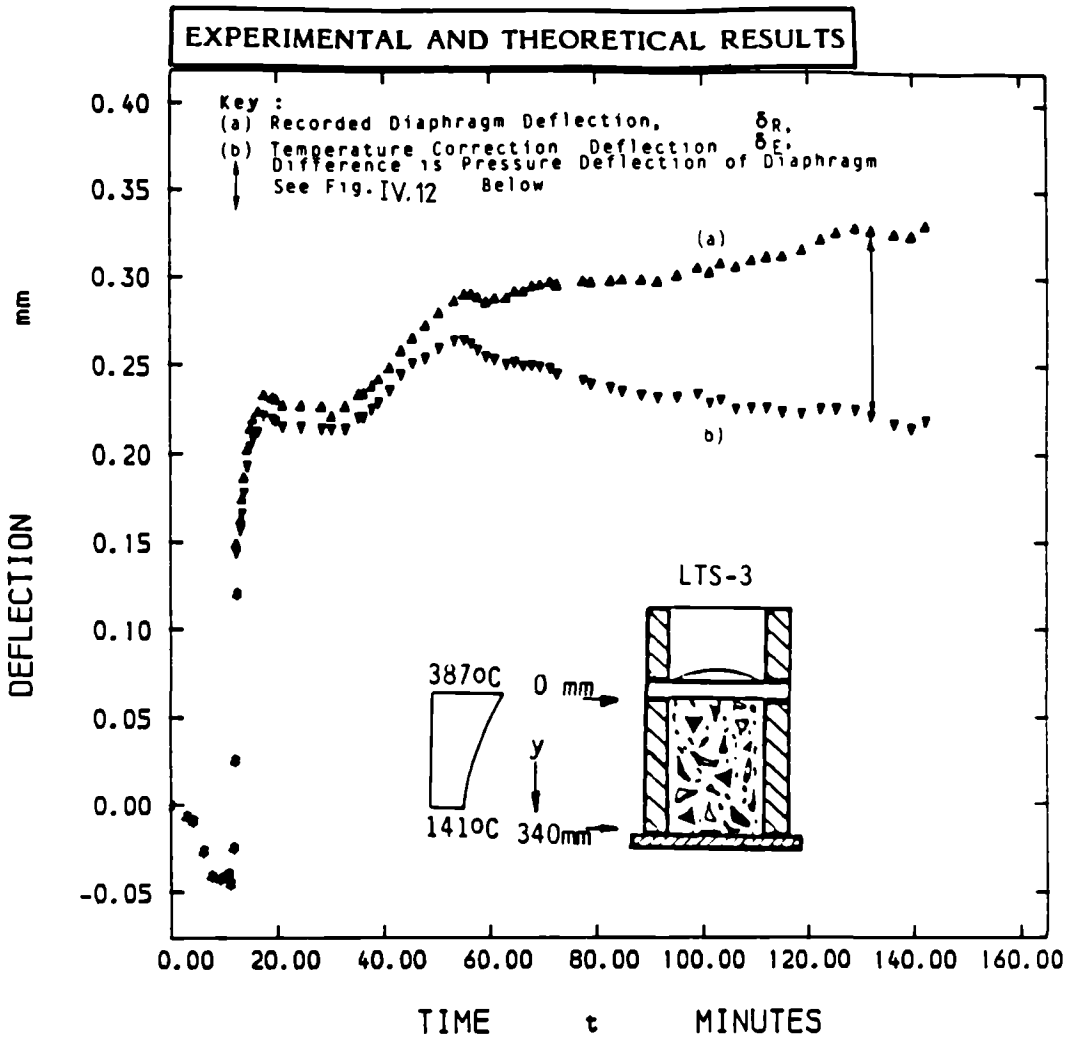

Figure IV.11 : :

Variation of Diaphragm Deflection, and Sintox Tubes Expansion, with Time from start of Heating
Specimen No: LTS-3

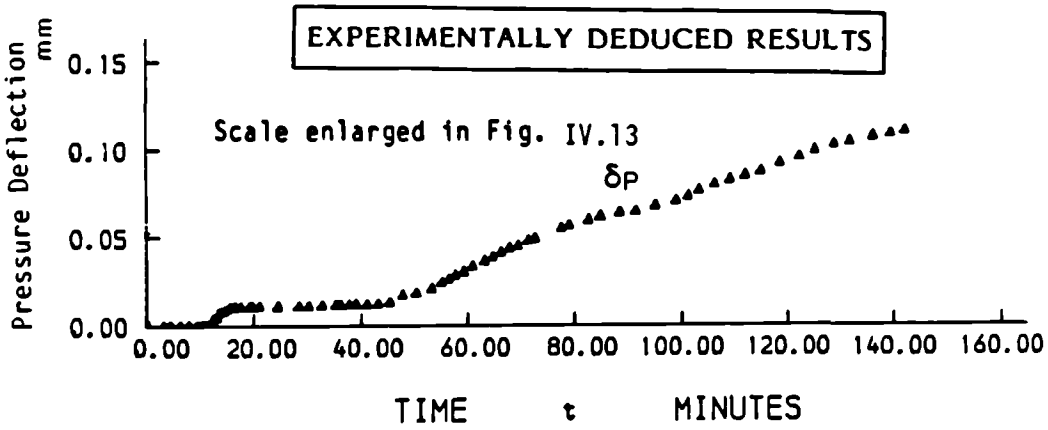

Figure IV.12 :
Pressure only Deflection of Diaphragm with Time from Start of Heating Specimen No: LTS-3

Note : $\delta_P = \delta_R - \delta_E$
δ_R = Recorded Diaphragm Deflection,
δ_E = Temperature Correction Deflection due to Expansion of Sintox Tubes

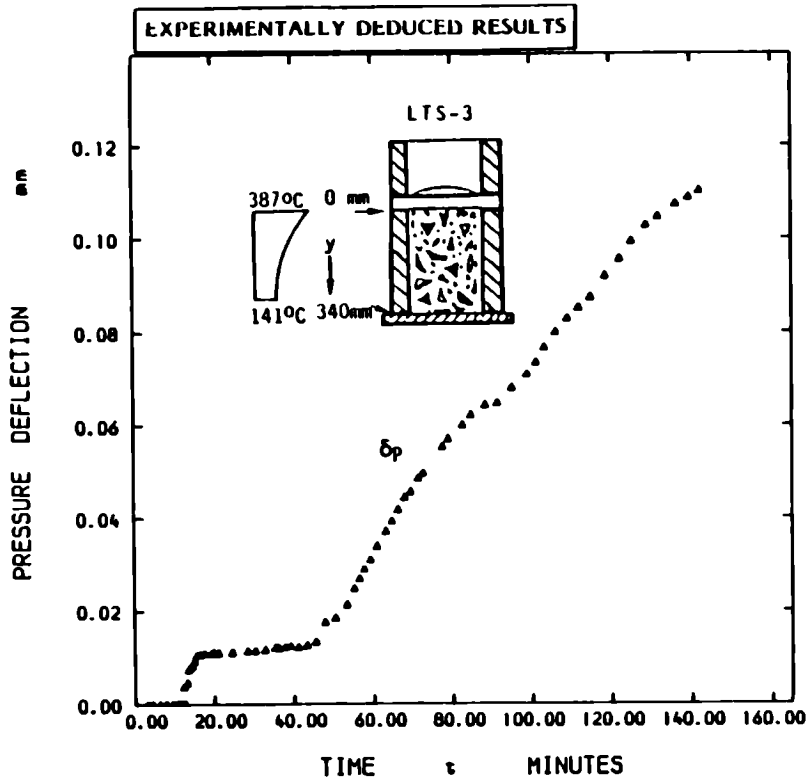

Figure IV.13 :

Pressure only Deflection of Diaphragm with Time from Start of Heating Specimen No: LTS-3

Note : $\delta_P = \delta_R - \delta_E$
δ_R = Recorded Diaphragm Deflection,
δ_E = Temperature Correction D[illegible]
Expans[illegible]

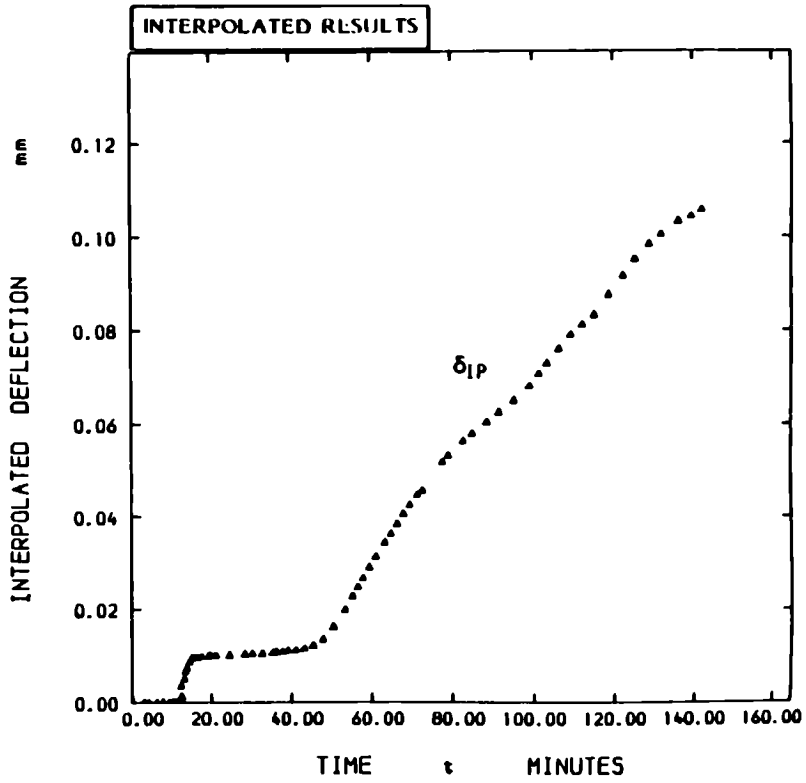

Figure IV.14 :

Diaphragm Deflection with Time from Start of Heating Specimen No: LTS-3

Note : Diaphragm Deflection, δ_{IP}, Derived from Pore Pressures, P1, and Interpolation from Pressure / Diaphragm Deflection Calibration Test

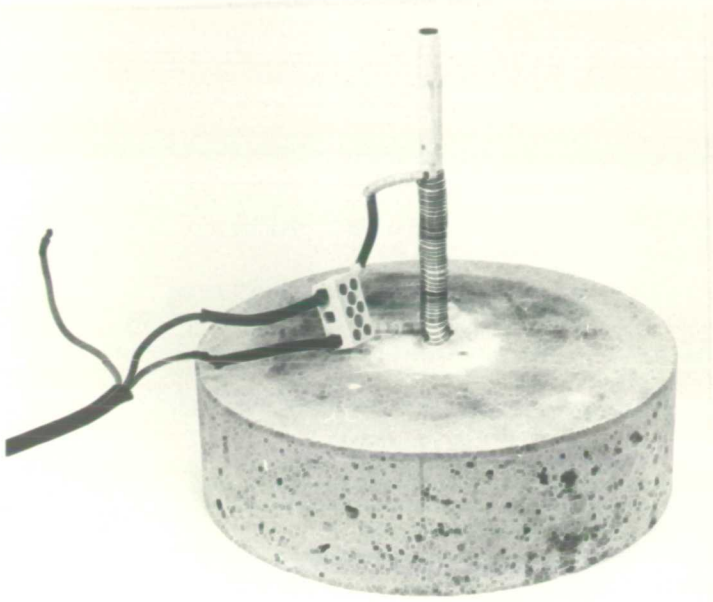

PLATE IV.1: COPPER TUBE CAST INSIDE CONCRETE BLOCK

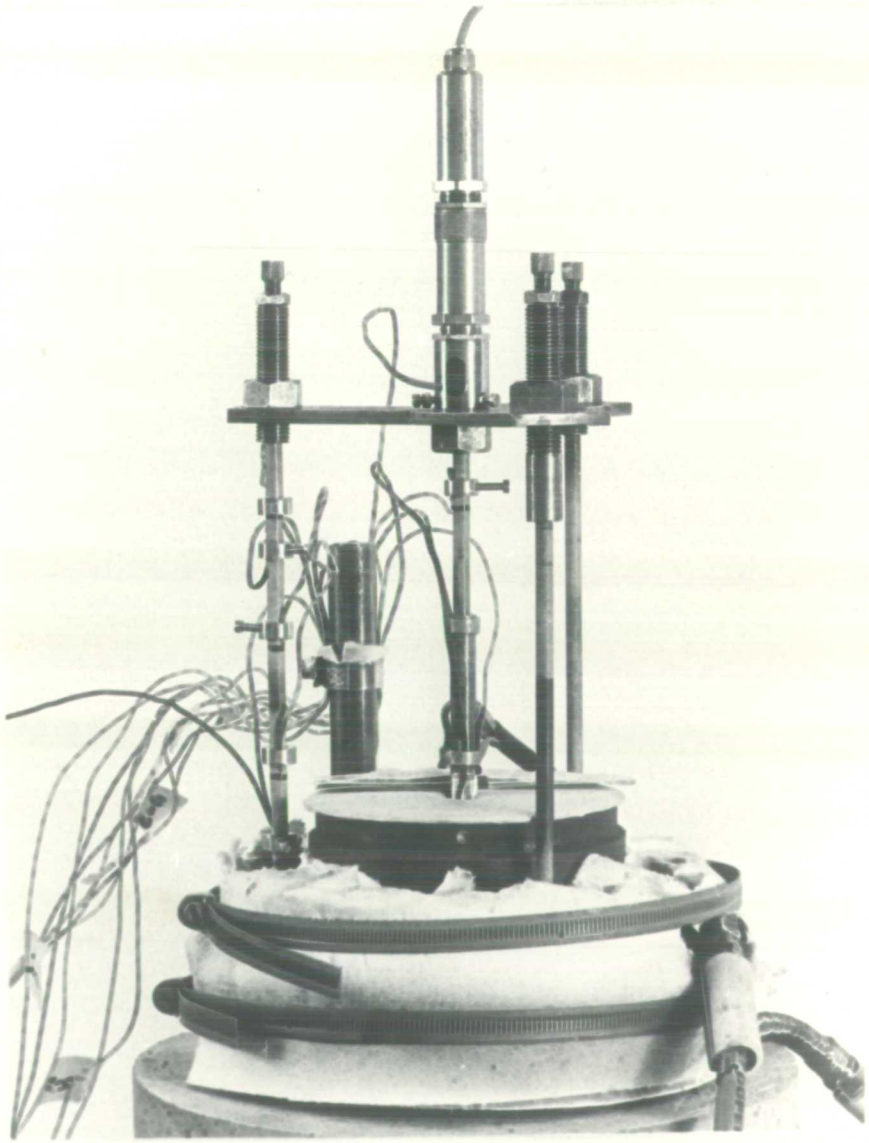

PLATE IV.2: SET UP FOR MEASURING SINTOX TUBE EXPANSION

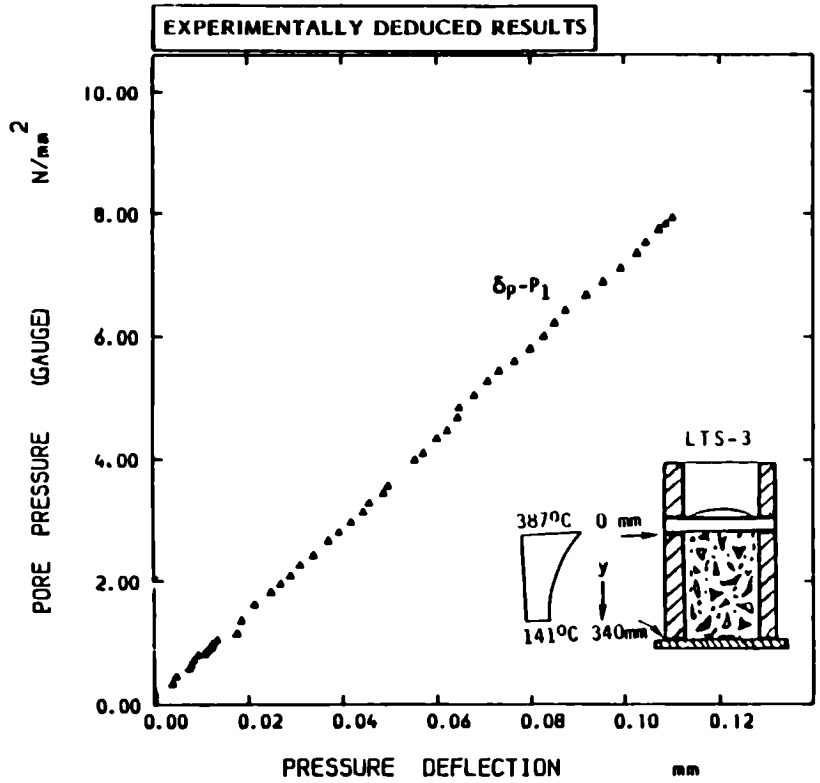

Figure IV.15 :

Variation of Pore Pressures with Pressure only Deflection of Diaphragm Specimen No: LTS-3

Note : $\delta_p = \delta_R - \delta_t$
δ_R - Recorded Diaphragm Deflection,
δ_t - Temperature Correction Deflection due to Expansion of Sintox Tubes,

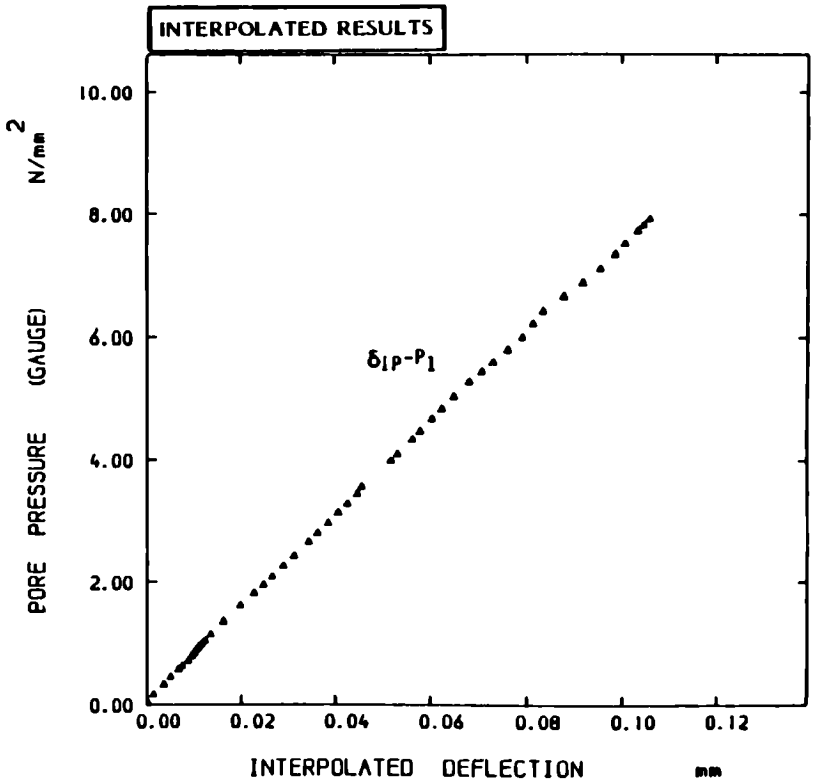

Figure IV.16 :

Part of Pressure / Diaphragm Deflection Calibration Curve for Comparison with Experimental Results of Figure IV.15

Note : Diaphragm Deflection, δ_{Ip}, Derived from Pore Pressures P_1 and Interpolation from Pressure / Diaphragm Deflection Calibration Test

APPENDIX - V

ABBREVIATIONS AND TERMS USED IN THIS THESIS

V.1 ABBREVIATIONS

The abbreviations used in this thesis are listed below and the symbols used in the equations are principally described in the relevant chapter or appendix.

ABBREVIATION	DEFINITION
BFS	Blast Furnace Slag
CT	Control Test
FBR	Fast Breeder Reactor
ipm	inert porous material
"LTS"	"Liner Test Series"
PCPV	Prestressed Concrete Pressure Vessel
PCRV	Prestressed Concrete Reactor Vessel
PFA	Pulverised Fuel Ash
PT	Pilot Test
"RTS"	Release Test Series"
SRPC	Sulphate Resisting Portland Cement
svp	saturation vapour pressure
UTC	Universal Transducing Cell

V.2 GLOSSARY OF TERMS

The definitions of a number of terms used in this thesis are described below. However, many other terms which need explanation are defined wherever they occur.

TERMS	MEANINGS
Cementitious Materials:	Blend of Sulphate Resisting Portland Cement and Cemsave used in 50/50 ratio.
Cemsave:	A trade name for Blast Furnace Slag
Sealed:	Sealed means pressure sealing of concrete from all sides avoiding any loss of pressure to the atmosphere.

Experimental Deflection: The central deflection of diaphragm directly recorded during the "LTS" experiments before applying any corrections.

Partially Sealed: Partially sealed is used in context with sealing of concrete when sealing is applied to all sides of concrete. However, due to inadequate sealing (i.e use of unsuitable sealing materials or leak in fittings and joints) restricted pressure loss is possible.

Note: For "Liner Test Series" the heated end and the sides of concrete specimen were sealed but the end away from heat was deliberately sealed with inferior sealing material to create partial sealing.

Pressure Deflection: The central deflection of diaphragm resulting from the pore pressures of concrete.

Sealing Conditions: Sealing of the concrete specimen whether during curing, testing or otherwise.

Temperature Correction: The correction applied to separate the central deflection of diaphragm due to thermal effects.

Test Age: The age of concrete on the testing day from the day it was cast.

Test Cell or Cell: The cell which is used for casting concrete for either "Liner Test Series" or "Release Test Series" experiments.

Test Rig: The mechanical rig used for supporting and protecting the test cell and instrumentation during testing

Unsealed or One-end Sealed:	Unsealed or one-end sealed refers to the pressure sealing condition of "Liner Test Series" specimen when the heated end and the sides of the concrete specimen are sealed and the end away from heat is not sealed.
% Wt. Loss:	The weight lost as the percentage of original weight of mix proportions (i.e. weight of mix water or weight of cementitious materials).

REFERENCES

BAKER, R.F.M. 1981. "About the cause of the resistance of blast furnace cement concrete to the alkali-silica reaction". Proceedings, 5th International Conference on Alkali-Aggregate Reactions in Concrete (Cape Town, 1981), National Building Research Institute, CSIR, Pretoria, 1981, 5252/29, pp.1-7.

BAZANT, Z.P., CHERN, J., and THONGUTHAI, W. 1981. "Finite element programme for moisture and heat transfer in heated concrete". Nuclear Engineering and Design, 68, pp.61-70, North-Holland Publishing Co.

BAZANT, Z.P., THONGUTHAI, W. 1978. "Pore pressure and drying of concrete at high temperature". Journal of the Engineering Mechanics Division - ASCE, Vol.104, No.EM5, October.

BAZANT, Z.P., THONGUTHAI, W. 1979. "Pore pressure in heated concrete walls". Magazine of Concrete Research: Vol.31, No.107.

BERTERO, V.V., POLIVKA, M. 1970. "Influence of thermal exposure on mechanical characteristics of concrete". ACI Seminar 'Concrete for Nuclear Reactors', Oct., Berlin, SP34-28.

BHATTY, M.S.Y., and GREENING, N. 1978. "Interaction of alkalis with hydrating and hydrated calcium silicates". Proceedings, 4th International Conference on Effects of Alkalis in Cement and Concrete, Purdue University, Pub. No.CE-MAT-1-78, pp.87-112.

BISHOP, A.W., HENKEL, J.D. 1962. "The measurement of soil properties in the triaxial test". Edward Arnold & Sons, London.

BOGUE, R.H., LERCH, W. 1934. "Hydration of Portland cement compounds". Industrial and Engineering Chemistry, pp.837-847, Vol.26, No.8.

BREMER, F. 1967. "Multi-layer (double-wall) prestressed concrete pressure vessels". Nuclear Eng. and Design, Vol.5, No.2.

BROWNE, R.D. 1967. "Properties of concrete in reactor vessels". Conference on Prestressed Concrete Pressure Vessels, 13-17 March, Institution of Civil Engineers, London.

BRUNAUER, S., COPELAND, L.E. 1964. "The chemistry of concrete". Scientific American, Vol.210, No.4.

BS 882, 1973. "Concrete aggregate from natural sources". British Standards Institution, London, Part 2.

CAMPBELL-ALLEN, D., DESAI, P.M. 1967. "The influence of aggregate on the behaviour of concrete at elevated temperature". Nuclear Engineering and Design, 6, pp.65-77.

CHAPMAN, D.A. 1976. "A study of the movement of moisture in and from concrete at elevated and non-uniform temperatures". Ph.D. Thesis, King's College, University of London.

CHAPMAN, D.A., ENGLAND, G.L. 1977. "The effect of moisture migration on shrinkage, pore pressure and other concrete properties". Conference on Structural Mechanics in Reactor Technology, San Francisco.

CHEMICAL ENGINEERS HANDBOOK 1973. 5th Edition, McGraw-Hill.

CHEUNG, F.B., BAKER, JR. L., BINGLE, J.D. 1976. "Diffusion of Heat in Concrete at Elevated Temperatures". Heat Transfer Division of The American Society of Mechanical Engineers, December 5.

CIVIL and MARINE LTD. Data Sheet 1. "An Introduction to Ground Granulated Blastfurnace Slag and Portland Blastfurnace Cement Concrete". London Road, West Thurrock, Grays, Essex, RM16 1NL.

CIVIL and MARINE LTD. 1985, Data Sheet 2. "Ground Granulated Blastfurnace Slag and Alkali-Aggregate Reaction". London Road, West Thurrock, Grays, Essex, RM16 1NL, May.

COPELAND, L.E. 1956. "Specific volume of evaporable water in hardened portland cement pastes". Journal ACI, Vol.27, No.8, April.

COPELAND, L.E., HAYES, J.C. 1953. "Determination of non-evaporable water in hardened portland cement paste". ASTM Bulletin No.194, December, pp.70-74.

CRISPINO, E. 1970. "Studies on the technology of concrete under thermal conditions". ACI Conference on Concrete for Nuclear Reactors, Berlin, Paper SP34-25.

DAIMON, M. 1980. "Mechanism and kinetics of slag cement hydration". Proceedings, 7th International Congress on the Chemistry of Cement (Paris 1980), Edition Septima, Vol.1, Principal paper III-2, pp.1-9.

DOUBLE, D.D. 1980. "Studies of the hydration of Portland cement". Proceedings of the International Congress on Admixtures, (London, April 16-17), Construction Press Ltd; Lancaster, London, New York.

ENGLAND, G.L., ROSS, A.D. 1970. "Shrinkage, moisture and pore pressure in heated concrete". ACI Seminar on Concrete for Nuclear Reactors, West Berlin, October 5-9, ACI Pub. No.34.

ENGLAND, G.L., SHARP, T.J. 1972. "Migration of Moisture and pore pressures in heated concrete". Proceedings of the First International Conference on Structural Mechanics in Reactor Technology, Berlin, Germany, 20-24 September, Vol.4-Part H.

ENGLAND, G.L., SKIPPER, M.E. 1973. "On the prediction of moisture movement in heated concrete". Reprints of the 2nd International Conference on Structural Mechanics in Reactor Technology, Berlin, Germany, 10-14 September, Vol.III-Part G-H.

FIELD, S.N. 1979. "Heysham II Nuclear Power Station Concrete Property Tests". Interim Report (R1) Covering Mix Trials, Mix Designs and Estimation of Pressure Vessel Concrete Properties, Taylor Woodrow Research Report, Report No. 014J/79/2141.

FIELD, S.N. 1979. "Heysham II Nuclear Power Station Concrete Property Tests". Report (R2) Covering Determination of Concrete Properties of Heysham II Pressure Vessel Mix, Taylor Woodrow Research Report (R2) No. 014J/80/2183.

GJORV, O.E., VENNESLAND, O. 1979. "Diffusion of chloride ions from sea water". Cement and Concrete Research, Vol.9, No.2, pp.229-238.

GREATHEAD, R.J. 1986. "Permeability of concrete containing Blast Furnace Slag as affected by Temperature, Moisture and Time". Ph.D. Thesis, King's College, University of London.

HANDBOOK of CHEMISTRY and PHYSICS. 1971-72. 53rd Edition, Published by Chemical Rubber Company, Cleveland, Ohio, U.S.A.

HARMATHY, T.Z. 1970. "Moisture and heat transport with particular reference to concrete". Division of Building Research, National Research Council of Canada, Highway Research Rec. Vol.342, pp.5-16.

HILSDORF, H.K. 1967. "A method to estimate the water content of concrete shields". Nuclear Engineering and Design, 6, pp.251-263, North-Holland Publishing Co.

HOGAN, F.J., MEUSEL, J.W. 1981. "The Evalution of Durability and Strength of a Ground Granulated Blast Furnace slag". Cement, Concrete, and Aggregates, Vol.3, No.1, pp.41-52.

HUANG, C.L.D., SIANG, H.H. 1983. "Effects of the thermal gradient on the moisture migration in a cylindrical concrete vessel". International J. Heat Mass Transfer, Vol.26, No.11, pp.1707-1710.

HUANG, C.L.D., SIANG, H.H., BEST, C.H. 1979. "Heat and moisture transfer in concrete slabs". International J. Heat Mass Transfer Vol.22, No.2, pp.257-266.

HUGHES, B.P., LOWE, I.R.G., and WALKER, J. 1966. "The diffusion of water in concrete at temperatures between 50 and 95 ^{o}C". British Journal of Applied Physics, Vol.17.

HUNDT, J., SCHIMMELWITZ, P. 1973. "Heat and moisture transfer in concrete under the effect of a temperature gradient". Paper H 6/1, 2nd. International Conference on Structural Mechanics in Reactor Technology, Berlin.

KAMP, C.L., ROELFSTRA, P.E., and WITTMANN, F.H. 1987. "Mechanism of moisture transfer through porous materials". Transactions of the 9th International Conference on Structural Mechanics in Reactor Technology, Lausanne, 17-21 August, Vol. H.

KAMP, C.L., ROELFSTRA, P.E., WITTMANN, F.H., MIHASHI, H. 1987. "Diffusion mechanism and drying of concrete at elevated temperatures". Transactions of the 9th International Conference on Structural Mechanics in Reactor Technology, Lausanne, 17-21 August, Vol. H.

KHOURY, G.A., GRAINGER, B.N., SULLIVAN, J.E. 1985. "Transient thermal strain of concrete: literature review, conditions within specimen and behaviour of individual constituents". Magazine of Concrete Research: Vol.37, No.132, September.

KORDINA, K., and SCHNEIDER, U. 1979. "Moisture Transport and Vapour Release of Concrete at Temperatures >100 ^{o}C". 5th International Conference on Structural Mechanics in Reactor Technology, Berlin, August, Paper H 1/5.

LANGTON, C.A., ROY, D.M. 1980. "Morphology and microstructure of cement paste/rock interfacial regions". Proceedings, 7th International Congress on the Chemistry of Cement (Paris 1980), Edition Septima, Vol.2, paper VII-127-133.

LANKARD, D.R., BIRKIMER, D.L., FONDRIEST, F.F., SNYDER, M.J. (1970). "Effects of Moisture Content on the Structural Properties of Portland Cement Concrete Exposed to Temperatures up to 500 ^{o}F". ACI Seminar 'Concrete for Nuclear Reactors', Oct., Berlin, SP 25-3.

LEA, F.M. 1970. "The chemistry of cement and concrete". Edward Arnold (Publishers) Ltd.

McDONALD, J.E. 1970. "An experimental study of moisture migration in concrete". ACI Seminar 'Concrete for Nuclear Reactors', Oct., Berlin SP34-35.

McDONALD, J.E. 1975. "Moisture migration in concrete". U.S. Army Engineer, Waterways Experimental Station, Tech. Rep. C-75-1, May.

METALS HANDBOOK. 1948. The American Society Of Metals, Ohio.

MUSKAT, M. 1937. "The flow of homogeneous fluids through porous media". McGraw Hill Co. Inc., New York.

NEVILLE, A.M. 1971. "Hardened concrete: Physical and Mechanical aspects". ACI Monograph Series.

NEVILLE, A.M. 1977. "Properties of concrete". Pitman Publishing.

PARKER, K.M., ROY, D.M. 1982. "Porosity, permeability and microstructure of Portland-Blast Furnace-Slag cement pastes". American Ceramic Society Bulletin, Vol.61, p.345.

PARKINSON, J.D. 1966. "The variation with time of water content and shrinkage of concrete subjected to thermal gradient". Ph.D. Thesis, King's College, University of London.

POITEVIN, P. 1970. "Water migration in concrete under a sustained temperature gradient". ACI Seminar 'Concrete for Nuclear Reactors' Oct. Berlin SP34-43.

POWERS, T.C. 1949. "The non-evaporable water content of hardened portland cement paste: its significance for concrete research and its method of determination". ASTM Bulletin No.158.

POWERS, T.C. 1958. "Structure and physical properties of hardened Portland cement paste". Journal of American Ceramic Society, Vol.41, pp.1-6, Jan.

POWERS, T.C. 1960. "Physical properties of cement paste". Proceedings of 4th International Symposium on the Chemistry of Cement, Washington, Paper V-1.

POWERS, T.C., BROWNYARD, T.L. 1947. "Studies of the Physical properties of hardened Portland cement paste". Journal ACI Vol.18, No.43, Nine Part Paper.

POWERS, T.C., COPELAND, L.E., HAYES, J.C., MANN, H.M. 1954. "Permeability of Portland cement paste". Journal ACI Vol.26, No.3.

REGOURD, M. 1980. "Structure and behaviour of slag cement hydrates". Proceedings, 7th International Congress on the Chemistry of Cement (Paris 1980), Edition Septima, Vol.I, III-2-18.

REGOURD, M., THOMASSIN, J.H., BAILLIF, P., TOURAY, J.C. 1983. "Blast-Furnace Slag hydration, surface analysis". Cement and Concrete Research, Vol.13, no. 4, pp.549-556.

REY, M. 1957. "Study of hydrated hydraulic binders by differential thermal analysis". Silicates Industriels, Vol.22, pp.533-540.

ROARK, R., YOUNG, J., WARREN, C. 1975. "Formulae for stress and strain". 5th Edition, McGraw-Hill, New York.

ROSS, A.D., ILLSTON, J.M., ENGLAND, G.L. 1965. "Short and long term deformation of concrete as influenced by its physical structure and state". International conference on the structure of concrete, London.

ROY, D.M., IDORN,G.M. 1982. "Hydration, structure and properties of blast furnace slag, cements, mortars and concrete". ACI Journal, Nov.-Dec, Technical Paper, Title No. 79-43.

SCHNEIDER, U., HERBST, H.J., DIEDERICHS, U. 1985. "Permeability and Porosity of Concrete at Elevated Temperature". Transactions of the 8th International Conference on Structural Mechanics in Reactor Technology, Brussel, Belgium, August 19-23, Vol. H.

SCHNEIDER, U., and HERBST, H.J. 1987. "Transport processes in thick concrete structures at high temperatures". Transactions of the 9th International Conference on Structural Mechanics in Reactor Technology, Lausanne, 17-21 August, Vol. H.

SCHNEIDER, U., HERBST, H.J. 1989. "Pressure Development in Heated Concrete Members". Transactions of the 10th International Conference on Structural Mechanics in Reactor Technology, Anaheim, California, USA, 14-18 August, Vol. H.

SEARS, F.W. 1953. "An introduction to thermodynamics, the kinetic theory of gases and statistical mechanics". Addison-Wesley Publishing Company.

SHARP, T.J. 1971. "The influence of elevated temperature on the physical behaviour of water in concrete". Ph.D. Thesis, King's College, University of London.

SMOLCZYK, H.G. 1975. "Investigation on the diffusion of Na-Ion in concrete". 6th International Congress on the Chemistry of Cement, Moscow.

SMOLCZYK, H.G. 1980. "Slag structure and identification of slags". Proceedings, 7th International Congress on the Chemistry of Cement (Paris 1980), Edition Septima, Vol.1, III-1/3-III-1/II.

STEAM TABLES, 1970. "U.K. Steam Tables in SI Units". Edward Arnold (Publishers) Ltd; London.

TAKEDA, T., NAKANE, S., and NAGAO, K. 1987. "Experimental studies on characteristics of concrete members subjected to high temperature". Transactions of the 9th International Conference on Structural Mechanics in Reactor Technology, Lausanne, 17-21 August, Vol. H.

TAYLOR, H.F.W. 1964. "The chemistry of cements". Volume 1, Academic Press, London and New York.

TIMOSHENKO, S.P. 1940. "Theory of plates and shells". McGraw-Hill, New York.

VERBECK, G.J.I. 1955. "Hardened concrete-pore structure" . ASTM SP. Tech. Publication, No.169, pp136-142.

WITTMANN, F.H., ROELFSTRA, P.E., and KAMP, C.L. 1988. "Drying of Concrete: An Application of the 3L-Approach". Nuclear Engineering and Design, 105(1988) 185-198, North-Holland Amsterdam.

ZANGLE, K., SADOUKI, H., WITTMANN, F.H. 1989. "Heat and Mass Transfer in a Concrete Pressure Vessel". Transactions of the 10th International Conference on Structural Mechanics in Reactor Technology, Anaheim, California, USA, 14-18 August, Vol. H.